UNIVERSIDAD DE GRANADA

Facultad de Ciencias

Departamento de Microbiología

IMPACTO DE LA COMUNIDAD MICROBIANA PRESENTE EN BENTONITAS SOBRE LOS PROCESOS BIOGEOQUÍMICOS DEL SISTEMA TERNARIO BENTONITA/MICROORGANISMO/RADIONUCLEIDO: IMPLICACIONES PARA EL CONCEPTO DE ALMACENAMIENTO GEOLÓGICO PROFUNDO DE RESIDUOS NUCLEARES

THE IMPACT OF BENTONITE MICROBIAL COMMUNITIES ON THE BIOGEOCHEMICAL PROCESSES AT BENTONITE/MICROBE/RADIONUCLIDE INTERFACE: IMPLICATIONS FOR DEEP GEOLOGICAL REPOSITORY OF NUCLEAR WASTES

Programa Oficial de Doctorado en Biología Fundamental y de Sistemas

Cristina Povedano Priego

Tesis Doctoral

Granada, 2019

Editor: Universidad de Granada. Tesis Doctorales
Autor: Cristina Povedano Priego
ISBN: 978-84-1117-320-9
URI: http://hdl.handle.net/10481/74720

INDICE

RESUMEN 13
SUMMARY 17
INTRODUCCIÓN 21
1. ENERGÍA NUCLEAR Y RESIDUOS GENERADOS 21
1.1. Tipos de residuos radiactivos y su gestión 22
2. ALMACENAMIENTO GEOLÓGICO PROFUNDO 24
3. DIVERSIDAD MICROBIANA EN EL MATERIAL DE RELLENO Y SELLADO DEL AGP 27
4. IMPACTO DE LA ACTIVIDAD MICROBIANA EN EL ALMACENAMIENTO GEOLÓGICO PROFUNDO 30
4.1. Biocorrosión de los contenedores metálicos 31
4.2. Alteración de la mineralogía de la bentonita por la actividad microbiana 32
4.3. Impacto de los microorganismos sobre la movilización de los radionucleidos: uranio y selenio 34
5. REFERENCIAS 41
OBJETIVOS 49
MATERIALS AND METHODS 51
1. BENTONITE SAMPLE COLLECTION 51
2. MINERALOGICAL CHARACTERIZATION OF THE BENTONITE SAMPLES 51
3. CHEMICAL CHARACTERIZATION OF BENTONITE 52
4. MICROSCOPIC ANALYSES 52
5. CHARACTERIZATION OF BENTONITE BACTERIAL DIVERSITY 54
5.1. Bioinformatics and statistical analyses 54
5.2. Network analysis 55
6. REFERENCES 55
CHAPTER I 57
1. ABSTRACT 59
2. GRAPHICAL ABSTRACT 60
3. INTRODUCTION 61
4. MATERIALS AND METHODS 63
4.1. Bentonite samples collection 63
4.2. Chemical characterization of bentonite pore water 64
4.3. Preparation of bentonite microcosms 64

4.4. Mineralogical characterization of the bentonite samples 65
4.5. Microcosms bacterial diversity characterization 66
4.6. Effect of the bentonite bacterial isolates on the chemical speciation of uranium in the presence of G2P 68
5. RESULTS AND DISCUSSION 69
5.1. Effect of uranyl nitrate and G2P on the geochemistry and mineralogy of the bentonite samples 69
5.2. Bentonite bacterial diversity changes induced by uranyl nitrate and G2P amendments 73
5.3. Impact of bacterial diversity changes on the biogeochemical processes under DGR concept 79
5.4. Impact of enriched bentonite bacterial isolates on the biogeochemical cycle of U in presence of G2P 84
6. ENVIRONMENTAL IMPLICATIONS 87
7. ACKNOWLEDGEMENTS 88
8. FUNDINGS SOURCES 88
9. REFERENCES 89
10. SUPPLEMENTARY MATERIAL 97
10.1. S1. Effect of bentonite bacterial isolates on the chemical speciation of uranium in presence of G2P 97
10.2. S2 Rarefaction curves 98
10.3. S3 Bacterial community composition at class level 98
10.4. Tables 99
10.5. Figures 100
10.6. References 104
10.7. Supplementary tables 105
CHAPTER II 119
1. ABSTRACT 121
2. INTRODUCTION 123
3. MATERIAL AND METHODS 125
3.1. Bentonite samples collection and microcosm establishment 125
3.2. Chemical and mineralogical characterization of anaerobic microcosms 126
3.3. Microscopic characterization of anaerobic microcosms 127
3.4. Microcosms bacterial diversity characterization 128
4. RESULTS AND DISCUSSION 130
4.1. Changes in the chemistry and mineralogy of the treated microcosms 130
4.2. Microscopic characterization of bentonite minerals in anaerobic microcosms 131

4.3. Changes in the bacterial diversity of anaerobic microcosms induced by uranyl nitrate and G2P 137
4.4. Impact of bacterial community changes on the biogeochemical processes under DGR conditions 143
5. ENVIRONMENTAL IMPLICATIONS OF BACTERIAL DIVERSITY OF ANAEROBIC MICROCOSMS IN THE DGR CONCEPT 148
6. ACKNOWLEDGEMENTS 150
7. FUNDINGS SOURCES 150
8. REFERENCES 150
9. SUPPLEMENTARY TABLES 159
CHAPTER III 175
1. ABSTRACT 177
2. INTRODUCTION 179
2.1. Background and applications 179
2.2. Comparison with other methods 180
3. EXPERIMENTAL DESIGN 182
3.1. Controls 186
4. MATERIALS 186
4.1. Sample 186
4.2. Reagents 186
4.3. Equipment 188
4.4. Reagent setup 189
4.5. Equipment setup 192
5. PROCEDURE 192
5.1. Sample pre-treatment (Steps 1-3). Timing: 15 min 192
5.2. Genomic DNA extraction protocol (Steps 4-28). Timing: 7 h 192
5.3. Quantification and quality assessment of extracted genomic DNA (Steps 29-30). Timing: 20 min 195
6. TIMING 196
7. TROUBLESHOOTING 197
8. ANTICIPATED RESULTS 198
9. ACKNOWLEDGEMENTS 202
10. AUTHOR CONTRIBUTIONS 202
11. COMPETING FINANCIAL INTERESTS 202
12. REFERENCES 202
CHAPTER IV 205
1. ABSTRACT 207

2. INTRODUCTION 209
3. MATERIAL AND METHODS 212
3.1. Bentonite compaction and anaerobic incubation 212
3.2. Characterization of the compacted bentonite bacterial diversity 215
3.3. Chemical, mineralogical and microscopic characterization of the compacted bentonite 216
4. RESULTS 217
4.1. Acetate amendment to bentonite and their compaction at different densities 217
4.2. Bacterial diversity in the acetate amended compacted bentonite under anaerobic conditions 218
4.3. Geochemical, mineralogical and microscopic characterization of the compacted bentonites 227
5. DISCUSSION 228
5.1. Effects of SRB and IRB on the biogeochemical processes in the DGR concept 232
6. ACKNOWLEDGEMENTS 235
7. REFERENCES 235
8. SUPPLEMENTARY TABLES 243
CHAPTER V 265
1. ABSTRACT 267
2. INTRODUCTION 269
3. MATERIAL AND METHODS 271
3.1. Bentonite sample collection 271
3.2. Preparation of water-saturated bentonite microcosms 272
3.3. Characterization of bacterial community in the water-saturated microcosms 275
3.4. Mineralogical and microscopic characterization of water-saturated bentonite microcosms and selenium nanoparticles 276
4. RESULTS 277
4.1. Changes in microbial diversity of saturated-bentonite microcosms induced by sodium selenite 277
4.2. Electron microscopic and spectroscopic characterization of the resulting products from Se(IV) reduction in water-saturated anaerobic microcosms 283
5. DISCUSSION 303
5.1. Impact of selenite on the microbial diversity of water-saturated bentonite 303
5.2. Effect of bentonite microbial communities on the chemical speciation of Se(VI) 305
6. REFERENCES 309
7. SUPPLEMENTARY TABLES 315
DISCUSIÓN GENERAL 321

1. REFERENCIAS 331
CONCLUSIONES 339
CONCLUSIONS 341

RESUMEN

El Almacenamiento Geológico Profundo (AGP) es una prioridad internacional, actualmente se considera como una de las opciones más seguras para el almacenamiento de residuos radiactivos de alta actividad. Este sistema multibarrera consiste en encapsular los residuos nucleares en contenedores metálicos (de hierro fundido, acero inoxidable o cobre), rodeados por bentonita compactada (barrera artificial) que se colocarán a varios cientos de metros de profundidad dentro de una roca hospedante (barrera natural). El uranio (U) y el selenio (Se) se consideran los radionucleidos más relevantes entre los residuos nucleares. Sus efectos nocivos sobre la estructura y las funciones del ecosistema dependen, en gran medida, de su movilidad y biodisponibilidad.

Los microorganismos pueden afectar potencialmente la especiación química de los radionucleidos y, en consecuencia, su migración sirviéndose de varios procesos tales como la biosorción, la biomineralización, la acumulación intracelular, y la biotranformación. En caso de que se produzca una fuga accidental de los elementos radiactivos que forman parte de los residuos nucleares, estos procesos pueden darse en el AGP y así controlar la movilización de los radionucleidos. Además, los microorganismos presentes en las bentonitas pueden producir un efecto en la estructura y la estabilidad de estas arcillas mediante la biotransformación de minerales que contienen hierro.

El buen funcionamiento del AGP está relacionado con un mejor conocimiento de los mecanismos de interacción entre los radionucleidos y los microorganismos que habitan las diferentes barreras del AGP. Por ello, se tomaron muestras de la formación geológica de bentonitas localizada en El Cortijo de Archidona (Almería, Spain). Esta bentonita se ha utilizado en todos los experimentos que se han desarrollado en esta Tesis Doctoral. En primer lugar, se elaboraron dos series de microcosmos tratados con nitrato de uranilo (U; 1,26 mM) y glicerol-2-fosfato (G2P, 10 mM). Una de las series fue incubada aeróbicamente y la otra en anaerobiosis durante 6 meses a temperatura ambiente. Los análisis por secuenciación del gen ARNr 16S de segunda generación (*Next Generation Sequencing* en inglés, NGS) reveló la presencia de diferentes comunidades bacterianas en los dos tipos de microcosmos. En los microcosmos

aeróbicos, las Actinobacterias y las Proteobacterias fueron los filos dominantes. El G2P y el nitrato indujeron el enriquecimiento de las bacterias implicadas en los ciclos biogeoquímicos del nitrógeno y del carbono (p. ej. *Azotobacter*), así como el uranio estimuló de forma significativa la presencia de bacterias sulfato-reductoras (*Desulfonauticus* y *Desulfomicrobium*) en los microcosmos correspondientes (U). La actinobacteria, *Amycolatopsis* se vio enriquecida en las bentonitas tratadas con una combinación de G2P y U. La capacidad de esta bacteria, junto con un consorcio procedente de la bentonita (*Bradyrhizobium-Rhizobium* y *Pseudomonas*), para precipitar el uranio en minerales de fosfatos de uranio (debido a la actividad fosfatasa), fue demostrada mediante técnicas dependientes de cultivo y microscopía electrónica de transmisión. Por su parte, los microcosmos anaeróbicos se caracterizaron por la presencia de 29 filos, entre ellos Proteobacteria, Bacteroidetes, Firmicutes y Verrucomicrobia. Se detectaron cepas bacterianas de gran relevancia ecológica en estos microcosmos, incluyendo por un lado las bacterias sulfato-reductoras (p. ej. *Desulfatiglans*), y las oxidadoras de azufre (p. ej. *Sulfurimonas* y *Thiobacillus*) que fueron identificadas en los microcosmos tratados con U, y, por otro lado, *Pseudomonas* y *Desulfovibrio* en los microcosmos tratados con U y G2P. Estas últimas, son conocidas por su capacidad para inmovilizar U como fosfatos U por biomineralización y reducción enzimática de U(VI) a U(IV), respectivamente. Además, las bacterias oxidadoras de Mn(II) probablemente pudieron afectar el ciclo biogeoquímico del Mn al concentrar e inmovilizar este elemento en las bentonitas produciendo la formación de óxidos de Mn(IV).

En esta tesis doctoral se desarrolló y propuso un protocolo optimizado que facilita la extracción de ADN de la bentonita. Dicho protocolo con mayores rendimientos basado en el método clásico de extracción con fenol:cloroformo en combinación con tratamientos previos de lisis mecánica y química, proporcionó suficiente ADN bacteriano (2-6 ng/µL) para realizar NGS y obtener datos válidos de la diversidad microbiana. Al ser considerado como el método más efectivo para la bentonita, en comparación con otros métodos basados en kits comerciales, este protocolo se utilizó en todos los experimentos que requerían de extracción de ADN, incluyendo la de bentonitas compactadas.

La bentonita compactada como material de relleno y sellado ha sido propuesta, comúnmente, para su uso en el AGP actuando como barrera artificial. Sin embargo, aún

se requiere profundizar en el conocimiento del comportamiento de dicha estructura después de su colocación en el repositorio, incluyendo el estudio de los microorganismos naturales de la bentonita, su supervivencia y movilidad. Por lo tanto, las muestras de bentonita no tratadas y tratadas con acetato se compactaron a dos densidades secas diferentes (1,5 y 1,7 g/cm^3) y se incubaron durante 24 meses en condiciones anaeróbicas a temperatura ambiente. La NGS demostró que los filos Actinobacteria y Proteobacteria fueron dominantes en estas muestras. Dentro de las Actinobacterias, *Arthrobacter* fue el género más abundante en las muestras de tiempo 0, y éste junto con *Pseudoarthrobacter* fueron dominantes tras 24 meses de incubación. Además, se obtuvieron resultados interesantes en cuanto a la microbiota de estas muestras pues se identificaron bacterias reductoras de Fe (p. ej. *Geobacillus*, *Thermicanus*, y *Stenotrophomonas*), oxidadoras de hierro (p. ej. *Thiobacillus*, *Syderoxidans*, y *Rhodobacter*), oxidadoras de azufre (p. ej. *Thiobacillus*, *Delftia*, *Sulfurifustis,* y *Sulfurimonas*) y sulfato-reductoras (p. ej. *Pseudomonas*, *Desulfuromonas*, *Desulfoporosinus*) que son conocidas por la utilización de acetato como fuente de carbono para su crecimiento.

En el futuro AGP, Se^{79} podría ser otro radioisótopo crítico debido a su actividad de larga vida media y su especiación química dependiente del estado de oxidación (VI, IV, 0 y -II). Por lo tanto, el impacto de Se(IV) sobre la diversidad microbiana de bentonita se ha estudiado aquí por primera vez, destacando la capacidad de algunos microorganismos para reducir este elemento a Se(0) e influir en su estructura. Los microcosmos de bentonitas de Cabo de Gata saturadas de agua se trataron con selenito, Se(IV), acetato, G2P, inoculados con un consorcio bacteriano BSPAS (formado por *Bacillus*, *Stenotrophomonas*, *Pseudomonas*, *Amycolatopsis*, y *Shewanella*) y fueron incubados anaeróbicamente durante 6 meses a temperatura ambiente. En este estudio, la NGS reveló la presencia de Bacteria (principalmente Firmicutes y Proteobacteria) y Archaea (principalmente *Methanosarcina*). *Pseudomonas* y *Stenotrophomonas* fueron identificadas en los microcosmos no inoculados con el consorcio BSPAS, junto con *Desulfosporosinus*, y géneros no-clasificado afiliados a *Desulfuromonadaceae*, Clostridia, and Firmicutes, todos ellos, probablemente, están implicados en la reducción del Se(VI) a Se elemental. Además, se observaron cambios en el color de la bentonita, de transparente a negro con una fase intermedia de color naranja a lo largo del tiempo de incubación. Se encontraron nanoestructuras de Se(0) en los microcosmos tratados

con Se(IV) confirmando la reducción de Se(IV) al selenio metálico. Las capas anaranjadas analizadas estaban compuestas por nanoesferas de Se amorfo o de fases cristalinas de Se monoclínico, mientras que los precipitados negros mostraron la estructura típica del selenio trigonal (la forma más estable de Se), cuando estaban presentes tanto las bacterias naturales de la bentonita como las inoculadas con el consorcio BSPAS. Estos resultados confirmaron un proceso de biotransformación de nanoesferas de Se amorfo/monoclínico a Se trigonal estable en las bentonitas tratadas con Se(IV).

En conjunto, los resultados obtenidos en esta Tesis Doctoral resaltan muchos aspectos del funcionamiento y la seguridad de los futuros DGR, por un lado, el papel que las comunidades microbianas desempeñarían afectando así las propiedades óptimas de cualquier tipo de bentonita (bentonita compactada y no compactada) y, por otro lado, los efectos que estas comunidades pueden tener al retener radionucleidos relevantes (U y Se) como resultado de alguna fuga accidental que pudiera tener lugar durante la larga vida útil del AGP. Finalmente, se muestran y analizan los efectos sobre los procesos biogeoquímicos en los que intervienen microorganismos que comprometen la seguridad del repositorio. En general, esta Tesis Doctoral proporciona nuevos conocimientos sobre el desarrollo de tratamientos apropiados de residuos, remediación y estrategias de gestión a largo plazo.

SUMMARY

Deep Geological Repository (DGR) is an international priority, currently considered as one of the safest options for the disposal of high-level radioactive wastes. This multi-barrier system consists of storing the spent fuel in canisters of cast iron, stainless steel, or copper, which will be emplaced several hundred meters underground, surrounded by compacted bentonite buffer (engineered barrier) within a host rock (natural geological barrier). Uranium (U) and Selenium (Se) are considered the most hazardous radionuclides among the nuclear wastes. Their harmful effects on the ecosystem structure and functions largely depend on their mobility and bioavailability.

Microorganisms can potentially affect the speciation of radionuclides, and in consequence their migration, through various processes including biosorption, biomineralization, bioaccumulation and biotransformation. These processes may occur in DGRs, in case any radioactive element leakage accidentally occurs from the nuclear wastes, controlling the radionuclide mobilization. In addition, indigenous microorganisms of bentonites may affect the structure and stability of these clays through Fe-containing mineral biotransformation.

A good performance of deep geological disposal of nuclear wastes is associated to the better understanding of radionuclide interactions with the natural microbes inhabiting the different DGR barriers. Therefore, bentonite was collected from geological formation in “El Cortijo de Archidona” (Almeria, Spain) and was used in all the experiments developed in this PhD Thesis. Firstly, two series of bentonite microcosms were amended with uranyl nitrate (U; 1.26 mM) and glycerol-2-phosphate (G2P, 10 mM). One set of samples was incubated aerobically and the other anaerobically both for 6 months at room temperature. Next generation 16S rRNA gene sequencing (NGS) revealed variable bacterial communities in both type of microcosms. In the aerobic microcosms, Actinobacteria and Proteobacteria were the most dominant phyla. G2P and nitrate stimulated the enrichment of bacteria involved in the nitrogen and carbon biogeochemical cycles (e.g. *Azotobacter*), as well as significant presence of sulfate-reducing bacteria (*Desulfonauticus* and *Desulfomicrobium*) in the U-treated microcosms. The actinobacteria *Amycolatopsis* was enriched in G2P-uranium amended bentonites. The capacity of this bacterium and a bentonite consortium (*Bradyrhizobium*-

Rhizobium and *Pseudomonas*) to precipitate U as U phosphate mineral phases, probably due to the phosphatase activity, was demonstrated through transmission electron microscope analysis and culture-dependent techniques. In turn, the anaerobic microcosms were characterized by the presence of 29 phyla such as Proteobacteria, Bacteroidetes, Firmicutes, and Verrucomicrobia. Interesting bacteria were detected in these microcosms including sulfate-reducing bacteria (e.g.: *Desulfatiglans*), sulfur-oxidizing bacteria (e.g.: *Sulfurimonas* and *Thiobacillus*) identified in the U microcosms, and *Pseudomonas* and *Desulfovibrio* in the U-G2P microcosms, known for their ability to immobilize U as U phosphates by biomineralization and enzymatic reduction of U(VI) to U(IV), respectively. Furthermore, Mn(II) oxidizing bacteria were likely able to affect the biogeochemical cycle of Mn by concentrating and immobilizing this element in the bentonites producing the formation of Mn(IV) oxides.

An optimized protocol that facilitates the extraction of higher DNA-yields from bentonite was developed and proposed in this PhD thesis. Based on the phenol:chloroform technique and combined with previous mechanical and chemical lyses it provided sufficient DNA (2-6 ng/µL) from Spanish bentonite to perform NGS and obtain valid microbial diversity data. Being considered as the most effective for bentonite (including the compacted one) in comparison to other commercial and kit-based methods, this house-made protocol was used for all DNA extractions from bentonite procedures in all the designed experiments.

Compacted bentonite-based sealing and backfilling materials are commonly proposed for the use in DGR as engineered barrier. However, an in-depth understanding of the behaviour of such structure after placement in the repository is still required, including the presence of native microorganisms, their survival and mobility. Thus, untreated and acetate-treated bentonite samples were compacted at two different dry densities (1.5 and 1.7 g/cm^3) and incubated for 24 months under anaerobic conditions at room temperature. NGS revealed the dominance of Actinobacteria and Proteobacteria. Only *Arthrobacter* dominated the bentonite in time 0, while also *Pseudoarthrobacter* was present in the 24-months compacted bentonite. Interestingly, iron-reducing bacteria (e.g. *Geobacillus*, *Thermicanus*, *Stenotrophomonas*) and iron-oxidizing bacteria (e.g. *Thiobacillus*, *Syderoxidans*, and *Rhodobacter*) as well as sulfur-oxidizing bacteria (e.g. *Thiobacillus*, *Delftia*, *Sulfurifustis,* and *Sulfurimonas*), and sulphate-reducing bacteria (e.g. *Pseudomonas*, *Desulfuromonas*, *Desulfoporosinus*) were detected in the compacted

bentonite. Also, bacteria (*Delftia*, *Paracoccus*, *Stenotrophomonas*, and *Thermicanus*) known to utilize acetate as a carbon source were enriched.

In the future DGR, Se^{79} could be another critical radioisotope due to its long half-life activity and chemistry controlled by the oxidation state (VI, IV, 0 and -II). Therefore, the impact of Se(IV) on the bentonite microbial diversity highlighting their capacity to reduce this element and to influence the structure of the biogenic Se(0) is studied here for the first time. Microcosms of water-saturated Spanish bentonites were treated with selenite, acetate, G2P, spiked with a bacterial consortium BSPAS (*Bacillus*, *Stenotrophomonas*, *Pseudomonas*, *Amycolatopsis*, and *Shewanella*), and incubated anaerobically for 6 months at room temperature. Here, the NGS revealed the presence of Bacteria (mainly Firmicutes and Proteobacteria) and Archaea (mainly *Methanosarcina*). *Pseudomonas* and *Stenotrophomonas* were also found in the non-spiked microcosms beside *Desulfosporosinus*, and unclassified genera affiliated to *Desulfuromonadaceae*, Clostridia, and Firmicutes, all of which are probably involved in the reduction of selenite to elemental Se. In addition, shifts in the color of bentonite, from transparent to black through an intermediate orange color were observed along the incubation time. Se(0) nanostructures were found in the selenite-treated microcosms confirming the reduction of Se(IV) to the elemental Se. The analyzed orange layers consisted of amorphous Se nanospheres or monoclinic crystalline phases, while the black precipitates showed the typical structure of trigonal selenium (the most stable form of Se), when both native and spiked bacteria were present. These results confirmed a biotransformation process of amorphous/monoclinic Se nanospheres to stable trigonal Se in the Se(IV)-treated bentonites.

Altogether the results of this PhD thesis would help to highlight many aspects of performance and safety of future DGRs, such as on one hand, the role that the microbial communities would play in affecting the optimal properties of any type of bentonite (compacted and uncompacted bentonite); and on another hand, the effects that these communities may have in retaining hazardous radionuclides (U and Se) resulting from any accidental leakage that could occur along the timeline of DGR lifespan. Finally, the effects on the biogeochemical processes in which microorganisms are involved compromising the safety of the repository are displayed and discussed. Overall, the findings of this PhD thesis would provide new insights on the development of appropriate waste treatments, remediation and long-term management strategies.

INTRODUCCIÓN

1. ENERGÍA NUCLEAR Y RESIDUOS GENERADOS

La energía nuclear es aquella que, contenida en el núcleo de un átomo, se puede obtener (liberar) mediante fusión y fisión nuclear. En la fusión nuclear los núcleos de los átomos son fusionados o combinados para formar un núcleo más grande generando una gran cantidad de energía. Sin embargo, en la fisión nuclear la energía se produce cuando el núcleo de un átomo pesado, al capturar un neutrón incidente, se divide en dos o más núcleos de átomos más ligeros. Ésta es la energía de la que se sirven las centrales nucleares para la producción de electricidad, utilizando la energía calorífica liberada para producir vapor (Consejo de Seguridad Nuclear, https://www.csn.es/).

El interés por la energía nuclear, que presentan tanto los países desarrollados como los que se encuentran en vía de desarrollo, deriva de la búsqueda de la reducción de la huella de carbono y del agotamiento de recursos (p. ej. combustibles fósiles) utilizados por la industria energética (Y. Li et al., 2014). El único elemento natural que se utiliza actualmente para la fisión nuclear en centrales nucleares es el uranio, ya que es altamente energético (un kilogramo de este radionúclido puede llegar a producir tanta energía como 10 toneladas de petróleo). A pesar de esta gran energía que se origina por esta vía para producir electricidad, estimándose que en el año 2013 más del 10% de la electricidad total mundial se producía en las centrales nucleares (un total de 435 a finales de ese mismo año), se generan a su vez grandes cantidades de residuos radiactivos (Martínez, 2015).

Según un informe de la Comisión Europea de 2017, los residuos radiactivos son aquellos materiales (forma sólida, líquida o gaseosa) a los que ya no se les puede atribuir ningún otro uso y cuya generación está asociada bien a la producción de electricidad en plantas nucleares o bien a usos no energéticos de materiales radiactivos (medicina, investigación, industria o agricultura). Estos residuos, atendiendo a sus propiedades radiológicas y su riesgo potencial, se pueden clasificar como de actividad muy baja, baja, media o alta, estimándose que alrededor del 90% de los residuos radiactivos generados en la Unión Europea son de actividad baja o muy baja.

1.1. Tipos de residuos radiactivos y su gestión

Todos los países generan desechos radiactivos, incluso aquellos que no disponen de centrales nucleares. Estos residuos, que deben ser eliminados, tienen varios orígenes, aunque la mayoría de ellos proviene de las centrales nucleares incluyendo elementos de combustible y otros materiales radiactivos (Martínez, 2015).

La Agencia Internacional de Energía Atómica (*International Atomic Energy Agency* [IAEA] en inglés) propuso un sistema de clasificación de los residuos radiactivos basado en los radionucleidos que contienen, sus vidas medias y los niveles de actividad (IAEA, 2009). La clasificación, que va desde residuos de muy baja a alta actividad, se describe a continuación:

a) **Residuos de muy baja actividad (RBBA)**. Son aquellos residuos que pueden derivar de materiales de la operación o desmantelamiento de instalaciones nucleares. También se incluyen los desechos que provienen de la extracción de minerales que contienen radionucleidos de forma natural. Para ellos no se requiere un alto nivel de aislamiento, pudiendo ser almacenados en vertederos con cierto control.

b) **Residuos de baja actividad (RBA).** Se trata de aquellos residuos que contienen suficiente cantidad de material radiactivo como para requerir un aislamiento de hasta cientos de años. Para su almacenamiento se precisa de instalaciones que pueden llegar a los 30 m de profundidad.

c) **Residuos de actividad intermedia (RAI).** Este tipo de residuos contiene compuestos de larga vida media y que podrían producir emisiones alfa. Por tanto, se requieren instalaciones situadas a profundidades que van desde decenas a varios cientos de metros, dependiendo de la gestión del país.

d) **Residuos de alta actividad (RAA).** Se definen así aquellos residuos que generan calor durante el proceso de decaimiento de su actividad y que contienen gran cantidad de material radiactivo de vida larga. Su confinamiento se debe producir a varios cientos de metros de profundidad, en una formación geológica estable, para conseguir la seguridad a largo

plazo. El combustible gastado procedente del núcleo de un reactor se incluye en los RAA.

Para los RBA y los RAI, el diseño de las instalaciones que aseguren los periodos de confinamiento y el aislamiento requeridos es una práctica real y viable con los materiales tecnológicos de los que se dispone actualmente (hormigones, aceros, etc.) (Astudillo Pastor, 2001). En Francia, los RBA y RAI, así como los desechos relacionados con el mantenimiento (ropa, herramientas, guantes, filtros, etc.) y la operación de instalaciones nucleares (residuos del tratamiento de efluentes gaseosos y líquidos), se vienen almacenando desde 1992 en ANDRA CSFMA (*Centre de stockage des déchets à faible et moyenne activité et à vie courte*) (National Academies of Sciences et al., 2017). En España, el Parlamento de la Nación tomó la decisión, en 1983, de crear una entidad pública, sin ánimo de lucro, que gestionara de forma integral y segura estos materiales. Con este fin, el Real Decreto 1522/1984 de 4 de julio autorizó la constitución de la Empresa Nacional de Residuos Radiactivos, S.A. (ENRESA; http://www.enresa.es/) ("Plan General de Residuos Radiactivos," 2006). El diseño y construcción de un almacenamiento para RBA y RAI en El Cabril (Córdoba) se llevó a cabo por ENRESA, estando operativo desde 1992 hasta nuestros días, y es considerado por la *Nuclear Regulatory Commission* (NRC) como una de las mejores instalaciones de almacenamiento de residuos radiactivos del mundo.

Figura 1. Instalación del almacén de Residuos de Baja-Intermedia Actividad situado en El Cabril (Córdoba) por ENRESA (Fotografía tomada de www.enresa.es).

La estimación del inventario total de residuos radiactivos en el territorio de la Unión Europea (UE) asciende a 3.313.000 m³, de los que alrededor del 70% están almacenados definitivamente y el 30% temporalmente. La composición principal de estos residuos es un 74% RBA, un 15% RBBA, un 10% RAI y un 0,2% de RAA (Publications Office of the European Union, 2017). Además, todo el combustible gastado presente en la UE se encuentra en almacenamiento temporal, debido a que, actualmente, no funciona en el mundo ninguna instalación civil de almacenamiento definitivo para ello. Sin embargo, la mayoría de los miembros de la UE que disponen de centrales nucleares activas tienen la voluntad de, en el futuro, almacenar su combustible gastado en un almacenamiento geológico profundo.

2. ALMACENAMIENTO GEOLÓGICO PROFUNDO

En las cinco últimas décadas se han sugerido muchas formas para tratar los residuos radiactivos de alta actividad, desde el vertido en el fondo oceánico hasta su envío, mediante cohetes, al espacio. Sin embargo, hoy en día hay consenso internacional en que la forma más apropiada es inmovilizándolos en forma de desechos y almacenándolos en un repositorio geológico diseñado a tal efecto (Vance and Begg, 2010). El potencial confinante de la geosfera se ha puesto de manifiesto en los yacimientos minerales, donde acumulaciones explotables de petróleo, gas, metales, etc. han permanecido confinados durante millones de años sin contacto con la atmósfera en lugares que cumplen con una serie de características geológicas, geoquímicas, estructurales e hidrogeológicas adecuadas (Astudillo Pastor, 2001).

Este concepto de Almacenamiento Geológico Profundo (AGP) fue acuñado en 1995 por la Agencia de Energía Nuclear (*Nuclear Energy Agency*, en inglés; NEA) definiéndolo como un sistema para aislar los residuos radiactivos de la biosfera durante períodos de tiempo extremadamente largos, asegurando que las sustancias radiactivas residuales que alcancen la biosfera tengan un nivel de actividad comparable al natural (Sellin and Leupin, 2013). El AGP se basa en un sistema formado por la combinación de barreras naturales y artificiales proporcionando el aislamiento de los residuos radiactivos de alta actividad durante, al menos, 100.000 años (Anderson et al., 2011):

- La barrera natural consiste en la propia formación geológica (roca hospedante) donde se sitúa el almacenamiento (Sellin and Leupin, 2013).
- Las barreras artificiales son aquellos materiales con los que se rodea a los residuos radiactivos. Entre ellos se incluyen los contenedores metálicos resistentes a la corrosión y los materiales de relleno y sellado (Anderson et al., 2011).

De esta manera, los residuos radiactivos se encontrarán encapsulados en contenedores metálicos (hierro fundido, acero inoxidable o cobre, según el diseño de cada país) que, después de haber sido rodeados de un material que les dará soporte (generalmente bentonita compactada), se situarán en un almacenamiento subterráneo excavado a cientos de metros de profundidad en una roca geológica estable de baja permeabilidad (Anderson et al., 2011; Lopez-Fernandez et al., 2018; Ojovan and Lee, 2014, 2005; Pedersen, 1999; Stroes-Gascoyne et al., 2007). En la Fig. 2 se muestra un esquema de la disposición del AGP.

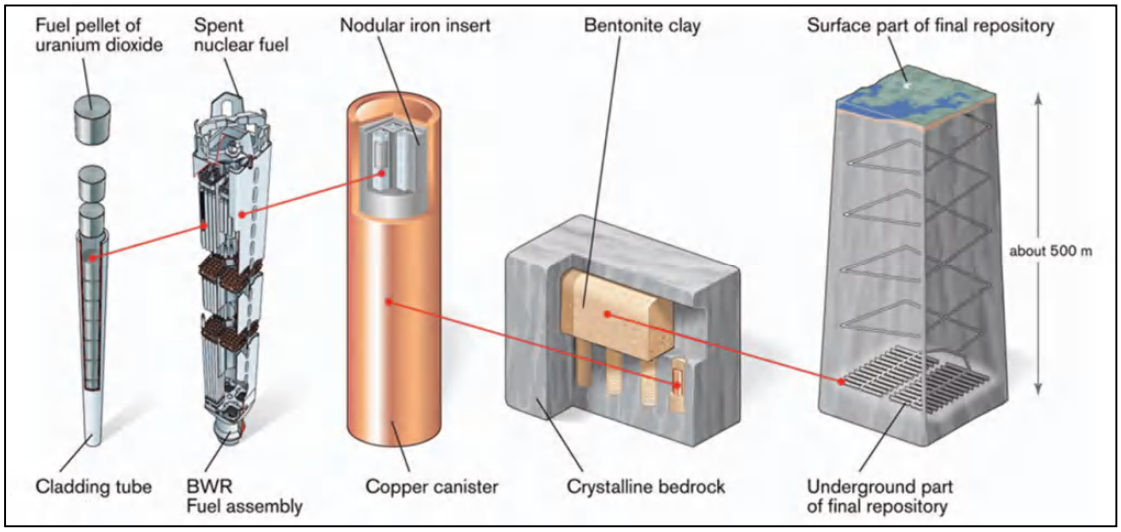

Figura 2. Esquema de las partes del sistema de Almacenamiento Geológico Profundo (AGP) en el que el combustible gastado es encapsulado en contenedores metálicos que se sitúan, rodeados de arcilla compactada, en agujeros de deposición en un sistema de túneles a unos 500 metros de profundidad en una roca hospedadora estable (Figura tomada de SKB, 2011).

El papel que juega la barrera natural geológica en el AGP es clave, ya que va a incidir en el funcionamiento de las demás barreras y a suministrar un elemento definitivo de seguridad a largo plazo (Astudillo Pastor, 2001). Se han estudiado diferentes tipos de roca hospedante para determinar el más adecuado para el AGP y se

han elegido tres tipos principales: roca cristalina (en Suecia y Finlandia, por ejemplo), roca sedimentaria como la arcilla (en Bélgica y Francia) y roca evaporítica como depósitos de sales (en Alemania) (Ojovan et al., 2019). En cuanto a la principal función de las barreras artificiales será la contención de los radionucleidos que contienen los residuos radiactivos de alta actividad. El material de relleno y sellado es el encargado de sellar la mayor parte de los espacios vacíos que se producen entre los contenedores y la roca hospedante y las galerías excavadas (Ojovan et al., 2019). La bentonita, o la mezcla de bentonita y arena, son la opción más preferible para este propósito (Sellin and Leupin, 2013).

Las arcillas, por tanto, se podrían utilizar tanto como roca hospedante como material para las barreras artificiales. Como roca hospedante las arcillas son, además, hidrogeológica, geoquímica y mecánicamente estables en escalas geológicas de tiempo, es decir, millones de años (Norris, 2017). Tenemos dos ejemplos de países, Suiza y Bélgica, que apuestan por la arcilla como roca hospedante para un almacenamiento de residuos radiactivos de baja y media actividad: *Opalinus Clay* (arcilla endurecida) en Suiza y *Boom Clay* (arcilla poco endurecida) en Bélgica (Norris, 2017; Lopez-Fernandez et al., 2014). Además, las propiedades de la bentonita (tipo de arcilla rica en esmectita) la convierten en el material más adecuado como barrera artificial del AGP (Pedersen et al., 2017). Algunas de esas características son: alta capacidad de adsorción, gran área superficial, impermeabilidad e hinchamiento cuando se hidrata (Perdrial et al., 2009). Este material, como principal función, podrá suministrar soporte mecánico y reducir la llegada de agua a los contenedores metálicos, y, además, tendrá la capacidad de retener los radionucleidos evitando su dispersión (Masurat et al., 2010). Está extensamente aceptado el uso de estas bentonitas en su forma compactada y utilizada en forma de bloques, creándose así espacios entre los contenedores y el material de sellado para facilitar la dispersión del calor generado por los residuos radiactivos. A largo plazo, estos espacios se sellarán completamente cuando la bentonita quede saturada por el agua, gracias a su propiedad de hinchamiento (Sellin and Leupin, 2013).

Las bentonitas han sido seleccionadas y extensamente estudiadas en España como material de relleno y sellado para un futuro almacenamiento de residuos radiactivos. Los primeros estudios dieron lugar a la selección de yacimientos de bentonita de la región de Cabo de Gata (Almería) y de la Cuenca Terciaria de Madrid (Toledo). Finalmente se seleccionó el yacimiento de Cortijo de Archidona (Almería), cuya

bentonita ha sido objeto de un gran número de investigaciones haciendo de ella una de las más intensivamente caracterizadas en sus aspectos mineralógico, térmico, hidráulico, mecánico, geoquímico y de alterabilidad (Villar et al., 2006). También se ha llevado a cabo el estudio de su comportamiento en el laboratorio, simulando las condiciones a las de un almacenamiento en condiciones reales a largo plazo, siendo el último de ellos el desarrollado en el proyecto internacional FEBEX, coordinado por ENRESA, y en el que participaron varias organizaciones europeas (Villar et al., 1998, 2002, 2006).

En la actualidad, mientras que países como Japón, Rusia, China e India optan por políticas de reprocesamiento de combustible gastado, tratando de reducir la producción de residuos radiactivos de alta actividad, la mayoría de naciones europeas, como Suecia y Finlandia, han priorizado el sistema directo de almacenamiento (Kim et al., 2011). Muchos de los estados miembros de la UE tienen previsto desarrollar instalaciones de almacenamiento geológico en las próximas décadas, pero hasta el momento solo Finlandia, Francia y Suecia han seleccionado los emplazamientos debido al gran reto que supone pasar de la fase de planificación a la de aplicación práctica. Globalmente, Finlandia es el primer país donde se ha iniciado la construcción de una instalación de almacenamiento geológico profundo, que se espera esté en funcionamiento en 2022, mientras que las de Francia y Suecia se prevé que comiencen a funcionar para 2030 (Comision europea, 2017).

3. DIVERSIDAD MICROBIANA EN EL MATERIAL DE RELLENO Y SELLADO DEL AGP

La presencia de comunidades microbianas activas en la barrera de bentonita es una de las cuestiones que se han de tener en cuenta debido a que los microorganismos puedan tener una influencia en las propiedades fisicoquímicas de las bentonitas y afectar, por tanto, su función como barrera artificial del AGP (Mulligan et al., 2009). Ya, en 1987, la microbiología entró a formar parte del programa científico sueco para el almacenamiento seguro de los RAA. El objetivo de este programa era entender cómo podrían interactuar los microorganismos subterráneos con el correcto funcionamiento del AGP (Pedersen, 1999).

A lo largo de los años se han llevado a cabo numerosos estudios acerca de los microorganismos presentes en diferentes tipos de arcillas como las arcillas *Opalinus Clay* (Suiza), *Boom Clay* (Bélgica), *Callovo-Oxfordian Clay* (Francia), y la bentonita comercial MX-80 (Canadá, Finlandia y Suecia) (Bengtsson and Pedersen, 2017, 2016; Grigoryan et al., 2018; Leupin et al., 2017; Stone et al., 2016a; Stroes-Gascoyne et al., 2007). Stroes-Gascoyne y colaboradores (2007) estudiaron la presencia de microorganismos autóctonos de la arcilla, en cuanto al tamaño y estructura de la comunidad microbiana en el núcleo de arcilla *Opalinus* del laboratorio subterráneo Mont Terri. Todos sus intentos de extraer ADN amplificable por PCR de las muestras de arcilla fallaron. Sin embargo, mediante técnicas de cultivo lograron resultados positivos para el crecimiento de bacterias reductoras de sulfato (BRS) y otras bacterias heterótrofas aeróbicas y anaeróbicas. Finalmente consiguieron aislar siete cepas bacterianas pertenecientes a *Sphingomonas* y *Alicyclobacillus*. Otro intento más reciente de extracción de ADN de la arcilla *Opalinus* puso de manifiesto la presencia de *Sphingomonas*, *Procabacteriaceae*, *Bdellovibrio*, *Ralstonia*, *Methylophilaceae*, y Rhizobiales (Bagnaud, 2015). Los fracasos de las técnicas independientes de cultivo para la identificación de la microbiota de la bentonita se suelen atribuir a su capacidad de hinchamiento, que impide que las soluciones utilizadas se mezclen bien con ella, y a su alta capacidad de intercambio iónico, que hace que los ácidos nucleicos se unan fuertemente a la arcilla dificultando así su extracción (Stone et al., 2016).

Recientemente, se ha conseguido obtener información acerca de la diversidad microbiana en bentonitas gracias a la secuenciación del gen del ARN ribosomal 16S. Grigoryan y colaboradores (2018), analizaron la estructura y la composición de las comunidades bacterianas de microcosmos que contenían la bentonita comercial MX-80 en su forma no compactada, obteniendo que Firmicutes y Proteobacteria (Gamma- y Deltaproteobacteria) eran los filos más abundantes representados por el 77% y el 22.6% de la población total bacteriana. A nivel de género destacaron la presencia de los géneros *Desulfosporosinus*, *Bacillus*, *Alkaliphilus*, *Tissierella* y *Desulfitobacterum* dentro del filo Firmicutes.

Las bentonitas españolas pertenecientes a la formación geológica localizada en Almería (en el sureste de España) han sido estudiadas también a nivel microbiológico (Fig. 3, A y B). De esta manera, mediante técnicas dependientes de cultivo, se aisló un alto número de cepas bacterianas pertenecientes a los géneros *Stenotrophomonas*, *Micrococcus*, *Arthrobacter*, *Kocuria*, *Sphingomonas*, *Bacillus*, y *Pseudomonas*, entre otros géneros, pertenecientes a los filos Proteobacteria, Actinobacteria y Firmicutes (Lopez-Fernandez et al., 2014). Sin embargo, no solo se ha demostrado la presencia de bacterias cultivables en estas bentonitas, sino que también se ha confirmado una alta diversidad bacteriana gracias al estudio del gen del ARN ribosomal 16S, mediante librerías de clones y secuenciación con Illumina. Esa gran diversidad está representada por diversos filos entre los que se encuentran, por orden de abundancia, Proteobacteria, Bacteroidetes, Acidobacteria, Actinobacteria y Chloroflexi (Fig. 3C). Algunos de los

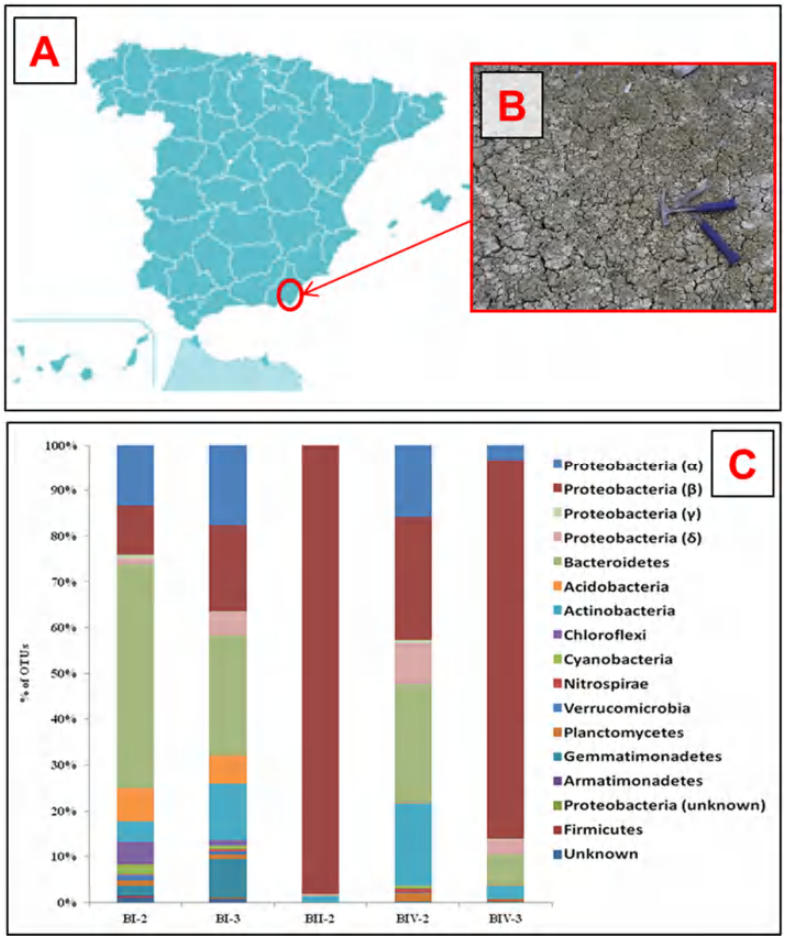

Figura 3. A) Localización de las formaciones geológicas de bentonitas seleccionadas como material de relleno y sellado para un futuro Almacenamiento Geológico Profundo. B) Bentonita española procedente de El Cortijo de Archidona (Almería). C) Diversidad bacteriana a nivel de filo de las muestras de bentonita analizadas. Las imágenes han sido modificadas de Lopez-Fernandez y colaboradores (2015).

géneros identificados han sido descritos por su capacidad para interactuar con hierro y diferentes metales pesados y radionucleidos, como es el caso de *Acidovorax*, *Ralstonia*, *Variovorax,* y *Sphingomonas* (Lopez-Fernandez et al., 2015).

Sin embargo, la forma en que se utilizarán las bentonitas en el AGP, en forma de bloques compactados de dimensiones determinadas y densidades secas, creará condiciones muy adversas para la actividad y la subsistencia de microorganismos autóctonos y alóctonos. Esas condiciones desfavorables vienen marcadas por la baja actividad de agua de la bentonita compactada y la presión de hinchamiento muy alta del orden de 7-8 MPa a plena saturación de agua (Ratto and Itavaara, 2012). A esto hay que añadir que el diámetro de poro promedio de la bentonita compactada está en el rango de 0,005-0,1 µm aproximadamente, siendo 0,02 µm el diámetro de mayor frecuencia (Stroes-Gascoyne et al., 2011). A pesar de estas condiciones desfavorables para el crecimiento microbiano, conocer la actividad microbiana y de su diversidad es esencial para evaluar la seguridad de los repositorios. De hecho, se espera que algunos microorganismos sobrevivan y mantengan la actividad metabólica en las bentonitas compactadas por su capacidad de crecimiento en los huecos y en las áreas menos comprimidas, como el espacio que se puede crear entre la bentonita y los contenedores metálicos, entre la bentonita y la roca hospedante e incluso entre los propios bloques de bentonita (Pedersen et al., 2000). Estas estructuras podrían albergar bacterias de pequeño tamaño (nanobacterias) y permitir una actividad microbiana. Además, bajo condiciones limitantes de fuentes de energía y situaciones de estrés fisicoquímico, algunos microorganismos son capaces de reducir considerablemente su tamaño y alterar su morfología y motilidad para aumentar su supervivencia (Ghuneim et al., 2018).

4. IMPACTO DE LA ACTIVIDAD MICROBIANA EN EL ALMACENAMIENTO GEOLÓGICO PROFUNDO

Dado que los microorganismos son ubicuos en todos los ambientes naturales, su impacto sobre la seguridad del AGP se ha estudiado ampliamente en varios tipos de bentonitas (Bengtsson and Pedersen, 2017; Leupin *et al.*, 2017; Lopez-Fernandez *et al.*, 2018; Pedersen *et al.*, 2017; Smart *et al.*, 2017). La actividad microbiana podría afectar la integridad y el rendimiento del almacenamiento a través de diferentes procesos, entre los que se incluyen la producción de gases como el CO_2, H_2 y CH_4, corrosión de los

contenedores metálicos debido a la producción de sulfuro por parte de bacterias reductoras de sulfato, y la alteración de las propiedades de la bentonita propiciada por la reducción del hierro estructural de la esmectita (Liu *et al.*, 2017; Pentráková *et al.*, 2013; Stone *et al.*, 2016; Stroes-Gascoyne *et al.*, 2010). Además, en caso de que se produjeran daños en los contenedores metálicos y se liberaran en consecuencia los radionucleidos contenidos, los microorganismos podrían controlar su especiación y movilidad a través de diferentes mecanismos como la biosorción, la acumulación intracelular, la biomineralización y la biorreducción (Lopez-Fernandez *et al.*, 2018).

4.1. Biocorrosión de los contenedores metálicos

Los contenedores metálicos son susceptibles de sufrir procesos de deterioro. La corrosión del metal por sulfuro es uno de los posibles procesos que podrían afectar las condiciones óptimas de los contenedores pudiendo causar su rotura prematura, lo que llevaría a la liberación de radionucleidos. La actividad microbiana de algunos grupos de bacterias puede contribuir a este tipo de degradación, como es el caso de las bacterias reductoras de sulfato. Por tanto, la producción de sulfuro microbiano podría afectar la seguridad del AGP al comprometer las funciones de aislamiento y contención de los contenedores (Bengtsson and Pedersen, 2017).

La corrosión es un proceso electroquímico donde se produce una transferencia de electrones desde el metal hacia otro aceptor de electrones, resultando en una liberación de iones metálicos y el deterioro del metal que conforman los contenedores. La aceleración de este proceso por parte de la actividad microbiana es lo que se denomina Corrosión Influenciada Microbiológicamente (CIM; *microbially influenced corrosión* en inglés). Este proceso es llevado a cabo principalmente por las bacterias sulfato-reductoras (BSR), bien por mecanismos directos o indirectos. Entre los mecanismos indirectos, la CIM se puede producir por el ataque del ácido sulfhídrico producido y por la adsorción de polímeros extracelulares bacterianos al metal. Entre los mecanismos directos están la eliminación de átomos de hidrógeno que se acumulan en la superficie del metal resultado de la corrosión y la captación de iones metálicos por parte de las propias células bacterianas (Meleshyn, 2014).

La evaluación de la seguridad de un futuro AGP se ha de realizar de manera conservadora teniendo en cuenta el peor de los escenarios. En lugares puntuales, la bentonita compactada podrá entrar en contacto con el agua subterránea que fluye por las fracturas que se crean en las rocas, lo que ofrecerá un suministro de sulfato, nutrientes y energía (como acetato o lactato) para el crecimiento de bacterias, entre ellas las BSR que con su actividad pueden producir grandes cantidades de sulfuro ocasionando, de esta manera, la corrosión de los contenedores metálicos (Fig. 4) (Masurat et al., 2010; Pedersen, 2010). En un estudio de Masurat y colaboradores (2010) demostraron la existencia de BSR en la bentonita comercial MX-80, incluso cuando ésta es desecada y cuando es sometida conjuntamente a altas temperaturas y salinidad.

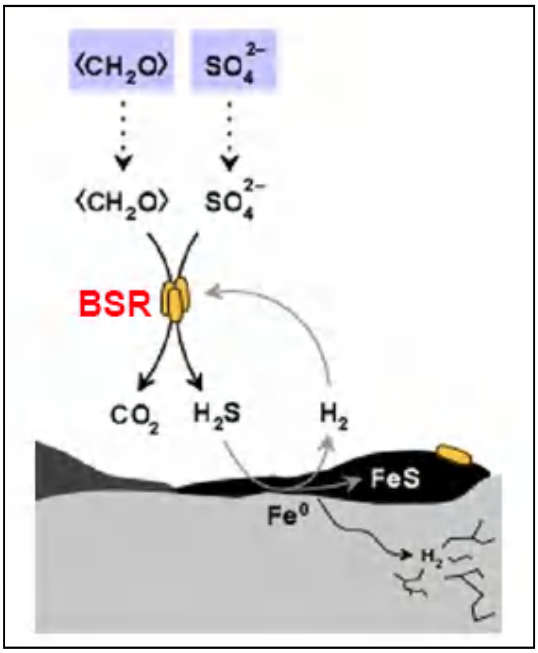

Figura 4. Ilustración esquemática de la corrosión de contenedores de hierro mediante la reducción de sulfato por las bacterias sulfato-reductoras (BSR) sirviéndose de un donador de electrones orgánico (p. ej. lactato o acetato). El ácido sulfhídrico (H_2S) producido por las bacterias reacciona con el hierro metálico para producir sulfuro ferroso (FeS). La imagen ha sido modificada de Enning y Garrelfs (2014).

4.2. Alteración de la mineralogía de la bentonita por la actividad microbiana

Como la función principal de la barrera artificial es inhibir o reducir la entrada de agua subterránea que podría corroer los contenedores metálicos y transportar compuestos contaminantes a la biosfera, es de vital importancia que la bentonita permanezca químicamente estable y mantenga su capacidad total de hinchamiento y sellado (Perdrial *et al.*, 2009).

De manera general, la bentonita está compuesta por filosilicatos de aluminio y es originada principalmente por la alteración de la ceniza volcánica. En su composición mineralógica participan diversos minerales, siendo la esmectita el mineral principal (montmorillonita) en un rango del 80-90%. La estructura de las esmectitas está formada por dos tipos de láminas estructurales: octaédrica y tetraédrica. En el caso concreto de la montmorillonita, las láminas se disponen en forma de sándwich: dos láminas de sílice tetraédrica con una lámina octaédrica intercalada. Las capas de arcilla tienen carga negativa, aunque se encuentran equilibradas por cationes intercambiables (ej. Na^{+}, K^{+}, y Ca^{2+}) en la capa intermedia (Fig. 5). Estos cationes absorben agua tras la hidratación, lo que resulta en una alta capacidad de hinchamiento y una muy baja conductividad hidráulica (Abdullahi y Audu, 2017).

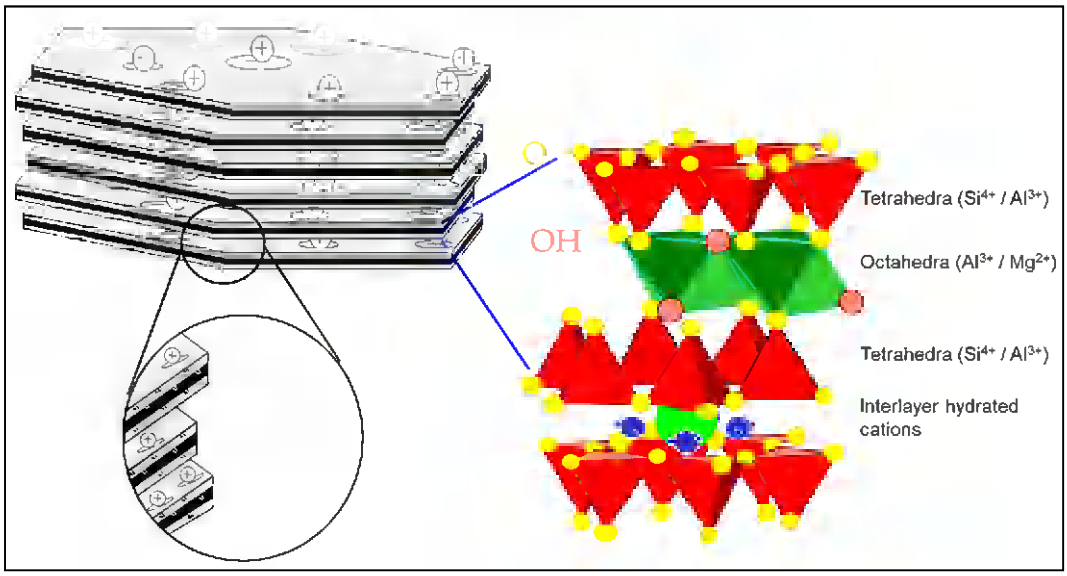

Figura 5. Representación esquemática de la estructura de la bentonita. Cada capa de esmectita está compuesta por dos capas tetraédricas y una octaédrica. Entre diferentes capas de esmectita se encuentran cationes que absorben agua cuando se hidratan (Imagen de YMERIS: www.imerys-additivesformetallurgy.com/our-resources/bentonite/).

Como se ha explicado anteriormente, en los últimos años se ha demostrado la existencia de una gran diversidad microbiana en diferentes bentonitas en todo el mundo (Grigoryan et al., 2018; Haynes et al., 2018; Lopez-Fernandez et al., 2018, 2015, 2014). Estos microorganismos interactúan con ellas a través de diversos mecanismos, entre los que se encuentran tanto la oxidación/reducción del hierro estructural como la disolución y precipitación de minerales mediante la producción de sideróforos y ácidos orgánicos (Dong, 2012). Por tanto, los procesos microbianos afectan el ciclo biogeoquímico del Fe

estructural de bentonitas (ej. la ilitización de la esmectita), principalmente debido a la actividad de bacterias reductoras de hierro, reduciendo el hierro estructural de férrico a ferroso. La transformación de esmectita a ilita (ilitización) inducida por la actividad microbiana es una consecuencia de la necesidad de los microorganismos de obtener energía a partir de la reducción del Fe(III) (Kim et al., 2019).

Hasta la fecha se han descrito una gran variedad de bacterias y arqueas capaces de reducir el Fe(III) a Fe(II) en las arcillas (Dong et al., 2009; Liu et al., 2012). Se ha descubierto que los microorganismos metanógenos (principalmente las arqueas) son menos eficientes para reducir el Fe(III) estructural que las bacterias hierro-reductoras y sulfato-reductoras (Dong, 2012). Kim y colaboradores (2019) descubrieron que la bacteria hierro-reductora *Shewanella oneidensis* MR-1 podía inducir la disolución de la esmectita a través de la reducción de Fe(III) estructural en la esmectita. En otro estudio, usando una combinación de microscopía electrónica (de transmisión y de barrido) y de difracción de rayos X, se demostró el papel que la actividad de *Thermoanaerobacter ethanolicus,* una bacteria termofílica reductora de metales aislada del subsuelo profundo, tenía sobre la ilitización de la esmectita rica en hierro (Zhang et al., 2007).

Esta reducción del Fe(III) presente en las bentonitas podría tener graves consecuencias en la seguridad del AGP puesto que la ilitización tiende a disminuir el área superficial, el espaciado interlaminar de la esmectita y la capacidad de hinchamiento cuando se hidratan. Otra consecuencia descrita es la disminución de la capacidad de adsorción de nutrientes y otros metales en el espacio interlaminar debido al colapso de las láminas de esmectita, aunque esto bien podría ser algo positivo, en la medida en que los radionucleidos se vieran atrapados cuando se produjera el colapso de la esmectita, debido a que reduciría su movilidad (Dong, 2012).

4.3. Impacto de los microorganismos sobre la movilización de los radionucleidos: uranio y selenio

En la mayoría de los casos, los RAA están compuestos fundamentalmente de combustible gastado procedente de las centrales nucleares, el cual contiene distintos radionucleidos entre los que destacan el uranio (el cual se usa como combustible en forma de pastillas de UO_2 enriquecidas en ^{235}U), transuránidos (plutonio y actínidos

minoritarios), productos de fisión (ej. Be, Ce, y Se) y productos de activación (ej. Ni, Mo, y Sr) (Astudillo Pastor, 2001). Por tanto, a parte del uranio, el selenio (concretamente el isótopo ^{79}Se) es uno de los radionucleidos que forman parte de los RAA pudiendo ser problemático para el AGP debido a la emisión de radiactividad en forma de partículas beta (Kang et al., 2011).

La movilidad del uranio en el medio ambiente depende de su especiación y su estado redox. En el medio natural, el U(VI) en condiciones aerobias se encuentra en forma de UO_2^{2+} a pH por debajo de 2.5, complejos de hidroxilo por debajo de pH 6.5, y como carbonato de uranilo a pH superior a 7 (Acharya, 2015). La toxicidad del selenio está relacionada con el estado de oxidación, siendo los oxianiones (selenato [Se(VI)] y selenito [Se(IV)] las formas más tóxicas de Se debido a su alta solubilidad y movilidad causando efectos nocivos en el entorno (Avendaño et al., 2016; Garbisu et al., 1996; Nancharaiah and Lens, 2015). Por otro lado, el selenio metálico [Se(0)] y seleniuros [Se(-II)] en los ambientes terrestres y acuáticos son las formas menos solubles e inmóviles y, por tanto, menos tóxicas (Avendaño et al., 2016).

Todos los escenarios planteados para el AGP sugieren que la liberación de radionucleidos durante el período de repositorio a largo plazo podría ser inevitable. En caso de fallo de los contenedores metálicos, a parte de la cualidad de las bentonitas de adsorber metales debido a su alta capacidad de cambio catiónico, los microorganismos también tienen un papel importante en la inmovilización de radionucleidos. Las interacciones entre los microorganismos y el radionucleido juegan un papel muy importante en el control de su movilidad en el medioambiente, inmovilizándolo para evitar su biodisponibilidad (Acharya, 2015). Las interacciones metal-microorganismo más interesantes que se pueden dar para la inmovilización de radionucleidos son: biosorción (Merroun et al., 2005; Pedersen, 1999; Stroes-Gascoyne et al., 2007), bioacumulación (Brookshaw et al., 2012), biotransformación por reducción (Brookshaw et al., 2012; Fresneda et al., 2018; Zhengji, 2010), y biomineralización (Merroun et al., 2011).

4.3.1. Biosorción

Se denomina biosorción a la adsorción pasiva de iones metálicos en la superficie de células microbianas, tanto vivas como muertas (incluyendo fragmentos celulares).

Las envolturas celulares bacterianas de bacterias Gram positivas y Gram negativas poseen una carga electronegativa que puede atraer cationes metálicos que se adsorben a la superficie, es decir, se trata de un proceso electrostático. En este proceso de sorción química están involucrados, principalmente, grupos carboxilo, amida, hidroxilo, fosfato y sulfhidrilo (Newsome et al., 2014).

A lo largo de los años, se han realizado varios estudios sobre la bioadsorción del uranio en células bacterianas. En el año 2005, Merroun y colaboradores encontraron que la capa S (una envuelta proteica que rodea la bacteria) de *Bacillus sphaericus* JG-A12 tenía la habilidad de fijar uranio y otros metales pesados debido a la presencia de grupos carboxilo y fosfato formando depósitos de U en la superficie celular (Fig. 6a). Esto también se pudo observar con otra especie de *Bacillus* (cepa dw-2) gracias a la microscopía electrónica de transmisión (*Transmission Electron Microscopy*, en inglés; TEM) que permitió la identificación de precipitados de U en forma de pequeñas agujas (Fig. 6b) (Zhao et al., 2016). La bioadsorción de U también se ha descrito en otras especies bacterianas, como es el caso de *Amycolatopsis*, perteneciente al grupo de las actinobacterias, que presenta grupos carboxilo, amida e hidroxilo a los que se uniría el uranio (Celik et al., 2018).

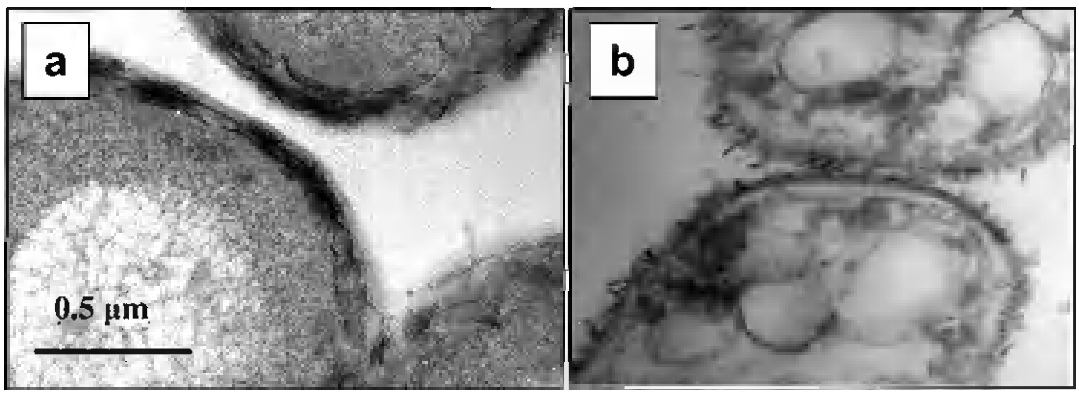

Figura 6. Ejemplos de biosorción de uranio en las células de a) *Bacillus sphaericus* JG-7B (Merroun et al., 2005) y b) *Bacillus* sp. dwc-2 (Zhao et al., 2016) donde se observa la presencia de uranio a nivel de la superficie celular. Imágenes modificadas a partir de las fuentes originales.

Recientemente, también se ha descrito la biosorción de selenio en células bacterianas. Se desconocía cómo los oxianiones de Se(IV) y Se(VI), con carga negativa, se podrían unir a las superficies de células microbianas con carga negativa. Sin embargo, en el estudio de Yu y colaboradores (2018) se describe el mecanismo de

adsorción de selenito en las células bacterianas de *B. subtilis* en el que los grupos sulfhidrilo de la envoltura celular tienen un papel importante. Una vez adsorbido en la bacteria, el selenito se reduce y forma compuestos organo-Se reducidos (R1S-Se-SR2) (Fig. 7). Puesto que los grupos sulfhidrilo forman parte de las envolturas celulares de una gran variedad de bacterias, este mecanismo podría ser adoptado por otros grupos bacterianos.

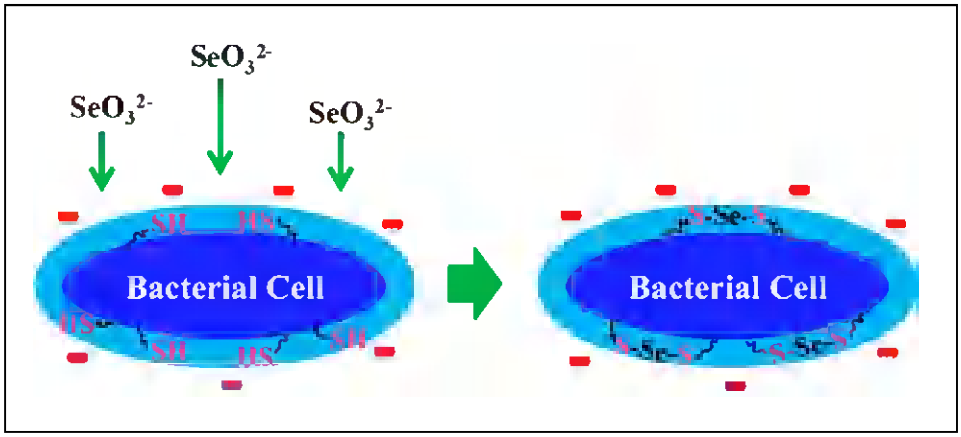

Figura 7. Mecanismo de adsorción de selenito en las células bacterianas mediado por grupos sulfhidrilo. Tras su adsorción el selenito se reduce y forma compuestos organo-Se reducidos (R1S-Se-SR2) (Imagen de Yu y colaboradores, 2018).

4.3.2. Bioacumulación

Las células bacterianas también pueden acumular intracelularmente una amplia variedad de metales, bien porque el metal es químicamente similar a un elemento esencial para el metabolismo de la bacteria, y entraría por los mecanismos de transporte, o bien por un aumento en la permeabilidad de la membrana causado por la toxicidad que produce un determinado metal (Fig. 8). Éste último proceso es el que se llevaría a cabo en el caso del uranio, ya que no se le ha encontrado ninguna función biológica (Newsome et al., 2014). Este mecanismo ha sido descrito para especies pertenecientes al género bacteriano *Pseudomonas* (Kazy et al., 2009; König et al., 2010).

Una vez dentro del espacio intracelular, los radionucleidos pueden ser secuestrados por proteínas (ej. metalotioneínas) y ligandos peptídicos, pequeños polímeros (ej. fitoquelatinas), y cuerpos de polifosfatos (Fig. 8) (Diep et al., 2018). En el caso de *Pseudomonas*, se ha podido observar la acumulación intracelular de depósitos

de uranio los cuales estaban compuestos por fosfatos de uranio cuya formación podría estar ligada a gránulos de polifosfato (Kazy et al., 2009).

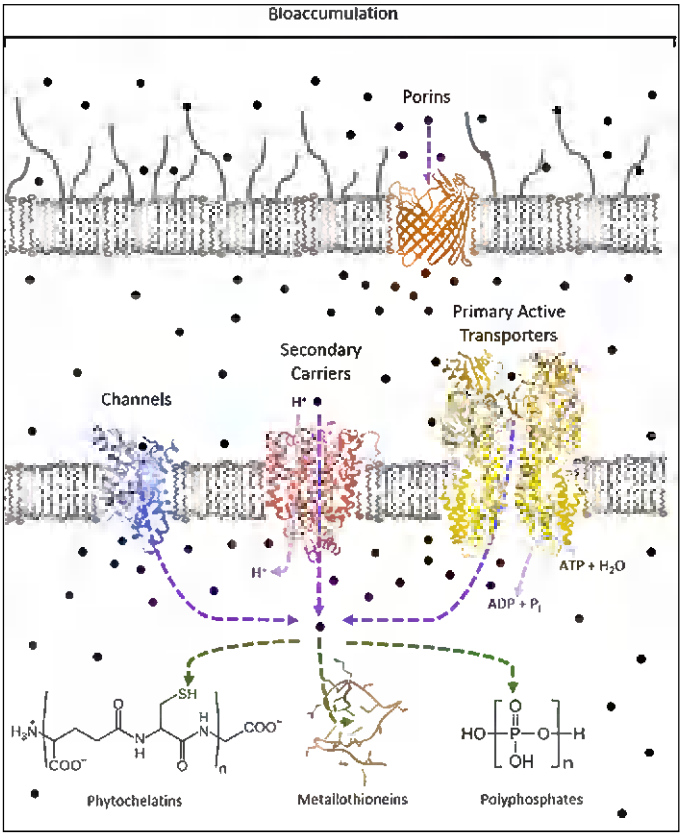

Figura 8. Esquema del proceso de bioacumulación de metales y radionucleidos dentro de las células. El primer paso es la entrada al citoplasma del metal o radionucleido, bien por cambios en la permeabilidad de la membrana o por transportadores de membrana. Una vez en el citoplasma, el metal o radionucleido es secuestrado por fitoquelatinas, metalotioneínas o polifosfatos (la imagen ha sido modificada de Diep y colaboradores (2018).

4.3.3. Biomineralización

La biomineralización es un proceso mediante el cual los microorganismos precipitan metales pesados sirviéndose de la producción de ligandos generados enzimáticamente como fosfatos, y sulfatos o bien carbonatos e hidróxidos en respuesta a condiciones alcalinas localizadas a nivel de la superficie celular (Newsome et al., 2014).

Las bacterias pueden llevar a cabo la biomineralización del uranio produciendo fosfatos de U(VI) insolubles, del grupo de la autunita, con alta estabilidad en condiciones oxidativas dentro de un amplio rango de valores de pH (Beazley et al.,

2011; Jroundi et al., 2007). La biomineralización del uranio se ve especialmente potenciada por la presencia de organofosfatos como el glicerol-2-fosfato (G2P) y el glicerol-3-fosfato (G3P). Estos compuestos estimulan la actividad de fosfatasas microbiana (ácida o alcalina) para liberar fosfatos inorgánicos, que interaccionarán con el radionucleido para dar lugar a la precipitación de fosfatos de uranio como mecanismo de desintoxicación (Beazley et al., 2011; Merroun et al., 2011). Este proceso se ha podido comprobar en varias bacterias. Un caso descrito por Yung y Jiao (2014), *Caulobacter crescentus* era capaz de precipitar fosfatos de uranio cristalinos, del grupo de la meta-autunita, a nivel de la superficie celular. Este proceso podría estar mediado por una fosfatasa alcalina inespecífica responsable de la producción de fosfatos inorgánicos en el periplasma que, a su vez, precipitan con U(VI) para formar minerales en la superficie celular (Fig. 9) (Yung and Jiao, 2014).

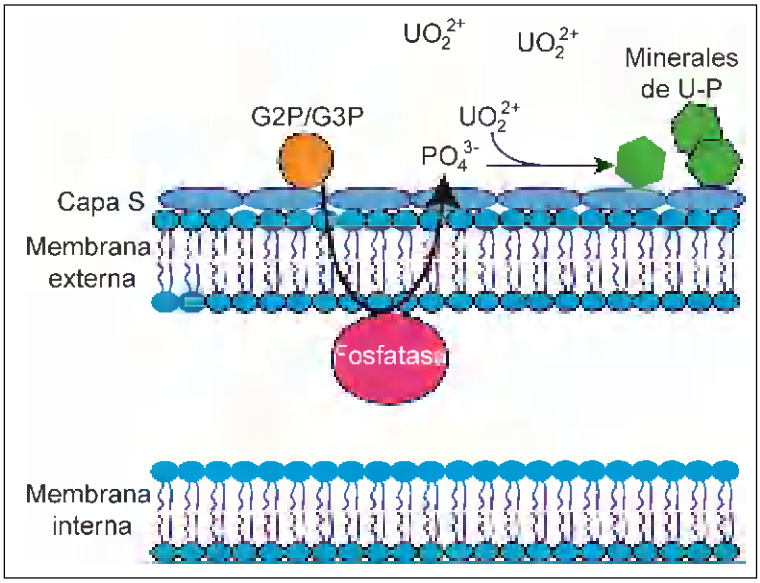

Figura 9. Esquema del proceso de biomineralización mediado por una fosfatasa periplasmática que libera fosfatos inorgánicos de una fuente orgánica para que puedan interaccionar con el U(VI) y dar lugar a la precipitación de fosfatos de uranio (biomineralización). Imagen de Yung y Jiao (2014).

En ambientes anaeróbicos también se puede producir la biomineralización. Por ejemplo, *Serratia* ha sido descrita por su capacidad de respirar/fermentar glicerol fosfato (fuente orgánica de fósforo) produciendo, en consecuencia, la precipitación de biominerales de fosfatos de uranio (Newsome et al., 2015).

4.3.4. Biotransformación por reducción

En ausencia de oxígeno, las bacterias son capaces de utilizar diferentes aceptores de electrones para obtener la energía requerida para el metabolismo. Los aceptadores de electrones energéticamente más favorables son el nitrato, manganeso(IV), hierro(III), sulfato y CO_2. Además, algunas bacterias pueden obtener energía de radionucleidos (ej. uranio) y de metaloides (ej. selenio) (Newsome et al., 2014).

La reducción microbiológica del uranio hexavalente [U(VI)] a uranio tetravalente [U(IV)] ha sido frecuentemente estudiada debido a su potencial papel en la inmovilización de uranio puesto que al reducirse los minerales resultantes de U(IV), como la uraninita, son menos solubles y, por tanto, menos móviles (Fig. 10). Este proceso ha sido descrito en varios grupos bacterianos: bacterias sulfato-reductoras (ej. *Desulfovibrio*), bacterias reductoras de hierro (ej. *Geobacter*), bacterias desnitrificantes (ej. *Pseudomonas*), y bacterias formadoras de esporas (e.g. *Clostridium*) (Chabalala and Chirwa, 2010; Cologgi et al., 2011; Gao and Francis, 2008; Stylo et al., 2015; Vecchia et al., 2010).

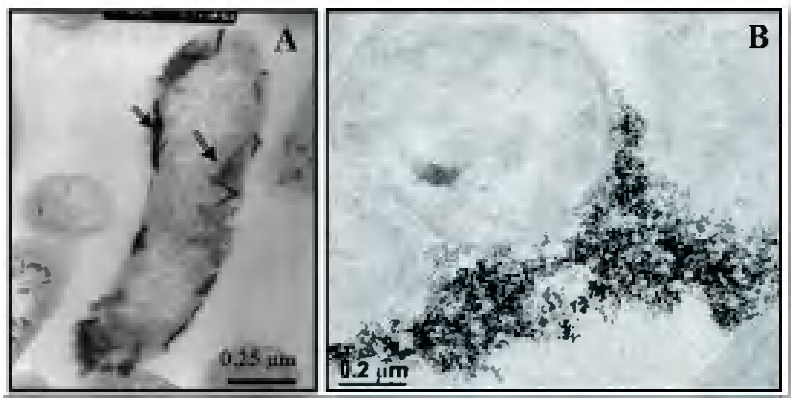

Figura 10. Fotografías, de microscopía electrónica de transmisión, de precipitados de uraninita producidos a partir de la reducción de uranio llevada a cabo por (A) *Desulfovibrio äspöensis* (Merroun and Selenska-Pobell, 2008) y (B) *Shewanella oneidensis* (Bernier-Latmani et al., 2010).

Además de la reducción del U(VI), algunas especies bacterianas son capaces de reducir los oxianiones de selenio. Las diferentes cepas bacterianas pueden reducir Se(IV) (selenito) y Se(VI) (selenato) a Se(0) menos tóxico originando la precipitación de nanopartículas de Se (SeNP) (Fresneda et al., 2018; Tan et al., 2016). La reducción del selenito está más ampliamente estudiada que la del selenato. Algunos de los estudios para determinar la reducción del Se(IV) se llevaron a cabo en cultivos de especies

bacterianas como *Stenotrophomonas bentonitica* (Fresneda et al., 2018; Ruiz-Fresneda et al., 2019), *Pseudomonas* spp. (Avendaño et al., 2016; Dwivedi et al., 2013; Hunter, 2014), *Shewanella oneidensis* (D.-B. Li et al., 2014) y *Pediococcus acidilactici* (Kousha et al., 2017), entre otros muchos.

Para determinar el mecanismo por el que se produce la reducción del selenito a selenio elemental, Tan y colaboradores (2016) utilizaron una cepa de *Streptomyces* en condiciones aeróbicas. Los resultados obtenidos indicaron que dicha reducción está mediada por el glutatión en el citoplasma celular sintetizándose SeNPs. Posteriormente, esas SeNPs son liberadas al espacio extracelular. Este mecanismo también se pudo confirmar en *S. bentonitica*, produciéndose SeNPs compuestas por Se(0) de tipo amorfo en el interior celular; sin embargo, las SeNPs analizadas en el espacio extracelular mostraron una forma trigonal del Se(0), la cual es cristalina y muy estable (Fresneda et al., 2018). Por lo tanto, se trata de un mecanismo con un gran potencial para conseguir la inmovilización de este metaloide.

5. REFERENCIAS

Abdullahi, S.L., Audu, A.A., 2017. Comparative analysis on chemical composition of bentonite clays obtained from Ashaka and tango deposits in Gombe State, Nigeria. ChemSearch Journal 8, 35-40–40.

Acharya, C., 2015. Microbial bioremediation of Uranium: an overview. BARC Newsletter 27–30.

Anderson, C., Johnsson, A., Moll, H., Pedersen, K., 2011. Radionuclide Geomicrobiology of the Deep Biosphere. Geomicrobiology Journal 28, 540–561. https://doi.org/10.1080/01490451.2010.507644

Anderson, C., Pedersen, K., Jakobsson, A.-M., 2006. Autoradiographic Comparisons of Radionuclide Adsorption Between Subsurface Anaerobic Biofilms and Granitic Host Rocks. Geomicrobiology Journal 23, 15–29. https://doi.org/10.1080/01490450500399946

Astudillo Pastor, J., 2001. El almacenamiento geológico profundo de los residuos radiactivos de alta actividad: principios básicos y tecnología.

Avendaño, R., Chaves, N., Fuentes, P., Sánchez, E., Jiménez, J.I., Chavarría, M., 2016. Production of selenium nanoparticles in Pseudomonas putida KT2440. Scientific Reports 6, 1–9. https://doi.org/10.1038/srep37155

Beazley, M.J., Martinez, R.J., Webb, S.M., Sobecky, P.A., Taillefert, M., 2011. The effect of pH and natural microbial phosphatase activity on the speciation of uranium in subsurface soils. Geochimica et Cosmochimica Acta 75, 5648–5663. https://doi.org/10.1016/j.gca.2011.07.006

Bengtsson, A., Pedersen, K., 2017. Microbial sulphide-producing activity in water saturated Wyoming MX-80, Asha and Calcigel bentonites at wet densities from 1500 to 2000kgm−3. Applied Clay Science 137, 203–212. https://doi.org/10.1016/j.clay.2016.12.024

Bengtsson, A., Pedersen, K., 2016. Microbial sulphate-reducing activity over load pressure and density in water saturated Boom Clay. Applied Clay Science 132–133, 542–551. https://doi.org/10.1016/j.clay.2016.08.002

Bernier-Latmani, R., Veeramani, H., Vecchia, E.D., Junier, P., Lezama-Pacheco, J.S., Suvorova, E.I., Sharp, J.O., Wigginton, N.S., Bargar, J.R., 2010. Non-uraninite Products of Microbial U(VI) Reduction. Environ. Sci. Technol. 44, 9456–9462. https://doi.org/10.1021/es101675a

Brookshaw, D.R., Pattrick, R.A.D., Lloyd, J.R., Vaughan, D.J., 2012. Microbial effects on mineral–radionuclide interactions and radionuclide solid-phase capture processes. Mineralogical Magazine 76, 777–806. https://doi.org/10.1180/minmag.2012.076.3.25

Celik, F., Camas, M., Kyeremeh, K., Sazak Camas, A., 2018. Microbial Sorption of Uranium Using Amycolatopsis sp. K47 Isolated from Uranium Deposits. Water Air Soil Pollut 229, 112. https://doi.org/10.1007/s11270-018-3766-5

Chabalala, S., Chirwa, E.M.N., 2010. Uranium(VI) reduction and removal by high performing purified anaerobic cultures from mine soil. Chemosphere 78, 52–55. https://doi.org/10.1016/j.chemosphere.2009.10.026

Cologgi, D.L., Lampa-Pastirk, S., Speers, A.M., Kelly, S.D., Reguera, G., 2011. Extracellular reduction of uranium via Geobacter conductive pili as a protective cellular mechanism. Proc Natl Acad Sci U S A 108, 15248–15252. https://doi.org/10.1073/pnas.1108616108

Diep, P., Mahadevan, R., Yakunin, A.F., 2018. Heavy Metal Removal by Bioaccumulation Using Genetically Engineered Microorganisms. Front. Bioeng. Biotechnol. 6. https://doi.org/10.3389/fbioe.2018.00157

Dong, H., 2012. Clay–Microbe Interactions and Implications for Environmental Mitigation. Elements 8, 113–118. https://doi.org/10.2113/gselements.8.2.113

Dong, H., Jaisi, D.P., Kim, J., Zhang, G., 2009. Microbe-clay mineral interactions. American Mineralogist 94, 1505–1519. https://doi.org/10.2138/am.2009.3246

Dwivedi, S., AlKhedhairy, A.A., Ahamed, M., Musarrat, J., 2013. Biomimetic Synthesis of Selenium Nanospheres by Bacterial Strain JS-11 and Its Role as a Biosensor for Nanotoxicity Assessment: A Novel Se-Bioassay. PLOS ONE 8, e57404. https://doi.org/10.1371/journal.pone.0057404

Enning, D., Garrelfs, J., 2014. Corrosion of Iron by Sulfate-Reducing Bacteria: New Views of an Old Problem. Appl. Environ. Microbiol. 80, 1226–1236. https://doi.org/10.1128/AEM.02848-13

Fresneda, M.A.R., Martín, J.D., Bolívar, J.G., Cantos, M.V.F., Bosch-Estévez, G., Moreno, M.F.M., Merroun, M.L., 2018. Green synthesis and biotransformation of amorphous Se nanospheres to trigonal 1D Se nanostructures: impact on Se mobility within the concept of radioactive waste disposal. Environ. Sci.: Nano 5, 2103–2116. https://doi.org/10.1039/C8EN00221E

Gao, W., Francis, A.J., 2008. Reduction of Uranium(VI) to Uranium(IV) by Clostridia. Appl. Environ. Microbiol. 74, 4580–4584. https://doi.org/10.1128/AEM.00239-08

Garbisu, C., Ishii, T., Leighton, T., Buchanan, B.B., 1996. Bacterial reduction of selenite to elemental selenium. Chemical Geology, Chemical And Biological Control On Mineral Growth And Dissolution Kinetics, American Chemical Society Meeting 132, 199–204. https://doi.org/10.1016/S0009-2541(96)00056-3

Ghuneim, L.-A.J., Jones, D.L., Golyshin, P.N., Golyshina, O.V., 2018. Nano-Sized and Filterable Bacteria and Archaea: Biodiversity and Function. Front Microbiol 9. https://doi.org/10.3389/fmicb.2018.01971

Grigoryan, A.A., Jalique, D.R., Medihala, P., Stroes-Gascoyne, S., Wolfaardt, G.M., McKelvie, J., Korber, D.R., 2018. Bacterial diversity and production of sulfide in microcosms containing uncompacted bentonites. Heliyon 4. https://doi.org/10.1016/j.heliyon.2018.e00722

Haynes, H.M., Pearce, C.I., Boothman, C., Lloyd, J.R., 2018. Response of bentonite microbial communities to stresses relevant to geodisposal of radioactive waste. Chemical Geology 501, 58–67. https://doi.org/10.1016/j.chemgeo.2018.10.004

Hunter, W.J., 2014. Pseudomonas seleniipraecipitans Proteins Potentially Involved in Selenite Reduction. Curr Microbiol 69, 69–74. https://doi.org/10.1007/s00284-014-0555-2

Jroundi, F., Merroun, M.L., Arias, J.M., Rossberg, A., Selenska-Pobell, S., González-Muñoz, M.T., 2007. Spectroscopic and Microscopic Characterization of Uranium Biomineralization in Myxococcus xanthus. Geomicrobiology Journal 24, 441–449. https://doi.org/10.1080/01490450701437651

Kang, M., Chen, F., Wu, S., Yang, Y., Bruggeman, C., Charlet, L., 2011. Effect of pH on Aqueous Se(IV) Reduction by Pyrite. Environ. Sci. Technol. 45, 2704–2710. https://doi.org/10.1021/es1033553

Kazy, S.K., D'Souza, S.F., Sar, P., 2009. Uranium and thorium sequestration by a Pseudomonas sp.: Mechanism and chemical characterization. Journal of Hazardous Materials 163, 65–72. https://doi.org/10.1016/j.jhazmat.2008.06.076

Kim, J., Dong, H., Yang, K., Park, H., Elliott, W.C., Spivack, A., Koo, T., Kim, G., Morono, Y., Henkel, S., Inagaki, F., Zeng, Q., Hoshino, T., Heuer, V.B., 2019. Naturally occurring, microbially induced smectite-to-illite reaction. Geology 47, 535–539. https://doi.org/10.1130/G46122.1

Kim, J.-S., Kwon, S.-K., Sanchez, M., Cho, G.-C., 2011. Geological storage of high level nuclear waste. KSCE J Civ Eng 15, 721–737. https://doi.org/10.1007/s12205-011-0012-8

König, H., Claus, H., Varma, A., 2010. Prokaryotic Cell Wall Compounds: Structure and Biochemistry. Springer Science & Business Media.

Kousha, M., Yeganeh, S., Keramat Amirkolaie, A., 2017. Effect of sodium selenite on the bacteria growth, selenium accumulation, and selenium biotransformation in Pediococcus acidilactici. Food Sci. Biotechnol. 26, 1013–1018. https://doi.org/10.1007/s10068-017-0142-y

Leupin, O.X., Bernier-Latmani, R., Bagnoud, A., Moors, H., Leys, N., Wouters, K., Stroes-Gascoyne, S., 2017. Fifteen years of microbiological investigation in Opalinus Clay at the Mont Terri rock laboratory (Switzerland). Swiss J Geosci 110, 343–354. https://doi.org/10.1007/s00015-016-0255-y

Li, D.-B., Cheng, Y.-Y., Wu, C., Li, W.-W., Li, N., Yang, Z.-C., Tong, Z.-H., Yu, H.-Q., 2014. Selenite reduction by Shewanella oneidensis MR-1 is mediated by fumarate reductase in periplasm. Sci Rep 4, 1–7. https://doi.org/10.1038/srep03735

Li, Y., Cao, H., Wang, S., Jin, Y., Li, D., Wang, X., Ding, Y., 2014. Load shifting of nuclear power plants using cryogenic energy storage technology. Applied Energy 113, 1710–1716. https://doi.org/10.1016/j.apenergy.2013.08.077

Liu, D., Dong, H., Bishop, M.E., Zhang, J., Wang, H., Xie, S., Wang, S., Huang, L., Eberl, D.D., 2012. Microbial reduction of structural iron in interstratified illite-smectite minerals by a sulfate-reducing bacterium. Geobiology 10, 150–162. https://doi.org/10.1111/j.1472-4669.2011.00307.x

Liu, G., Qiu, S., Liu, B., Pu, Y., Gao, Z., Wang, J., Jin, R., Zhou, J., 2017. Microbial reduction of Fe(III)-bearing clay minerals in the presence of humic acids. Scientific Reports 7, 45354. https://doi.org/10.1038/srep45354

Lopez-Fernandez, M., Cherkouk, A., Vilchez-Vargas, R., Jauregui, R., Pieper, D., Boon, N., Sanchez-Castro, I., Merroun, M.L., 2015. Bacterial Diversity in Bentonites, Engineered Barrier for Deep Geological Disposal of Radioactive Wastes. Microb Ecol 70, 922–935. https://doi.org/10.1007/s00248-015-0630-7

Lopez-Fernandez, M., Fernández-Sanfrancisco, O., Moreno-García, A., Martín-Sánchez, I., Sánchez-Castro, I., Merroun, M.L., 2014. Microbial communities in bentonite formations and their

interactions with uranium. Applied Geochemistry 49, 77–86. https://doi.org/10.1016/j.apgeochem.2014.06.022

Lopez-Fernandez, M., Vilchez-Vargas, R., Jroundi, F., Boon, N., Pieper, D., Merroun, M.L., 2018. Microbial community changes induced by uranyl nitrate in bentonite clay microcosms. Applied Clay Science, ACS - SI ICC 2017 XVI International Clay Conference – Clays, from the oceans to space 160, 206–216. https://doi.org/10.1016/j.clay.2017.12.034

Martínez, A.C., 2015. Review and international prospects of nuclear power in 2014, in: Energy and Geostrategy 2015, 2015, ISBN 978-84-9091-056-6, págs. 29-58. Presented at the Energy and Geostrategy 2015, Instituto Español de Estudios Estratégicos, pp. 29–58.

Masurat, P., Eriksson, S., Pedersen, K., 2010. Evidence of indigenous sulphate-reducing bacteria in commercial Wyoming bentonite MX-80. Applied Clay Science, Advanced smectitic clay research 47, 51–57. https://doi.org/10.1016/j.clay.2008.07.002

Meleshyn, A., 2014. Microbial processes relevant for the long-term performance of high-level radioactive waste repositories in clays. Geological Society, London, Special Publications 400, 179–194. https://doi.org/10.1144/SP400.6

Merroun, M.L., Nedelkova, M., Ojeda, J.J., Reitz, T., Fernández, M.L., Arias, J.M., Romero-González, M., Selenska-Pobell, S., 2011. Bio-precipitation of uranium by two bacterial isolates recovered from extreme environments as estimated by potentiometric titration, TEM and X-ray absorption spectroscopic analyses. Journal of Hazardous Materials 197, 1–10. https://doi.org/10.1016/j.jhazmat.2011.09.049

Merroun, M.L., Raff, J., Rossberg, A., Hennig, C., Reich, T., Selenska-Pobell, S., 2005. Complexation of Uranium by Cells and S-Layer Sheets of Bacillus sphaericus JG-A12. Appl. Environ. Microbiol. 71, 5532–5543. https://doi.org/10.1128/AEM.71.9.5532-5543.2005

Merroun, M.L., Selenska-Pobell, S., 2008. Bacterial interactions with uranium: an environmental perspective. J. Contam. Hydrol. 102, 285–295. https://doi.org/10.1016/j.jconhyd.2008.09.019

Mondani, L., Benzerara, K., Carrière, M., Christen, R., Mamindy-Pajany, Y., Février, L., Marmier, N., Achouak, W., Nardoux, P., Berthomieu, C., Chapon, V., 2011. Influence of Uranium on Bacterial Communities: A Comparison of Natural Uranium-Rich Soils with Controls. PLoS ONE 6, e25771. https://doi.org/10.1371/journal.pone.0025771

Mulligan, C., Yong, R., Fukue, M., 2009. Some effects of microbial activity on the evolution of clay-based buffer properties in underground repositories. Applied Clay Science 42, 331–335. https://doi.org/10.1016/j.clay.2008.03.002

Nancharaiah, Y.V., Lens, P.N.L., 2015. Ecology and Biotechnology of Selenium-Respiring Bacteria. Microbiol. Mol. Biol. Rev. 79, 61–80. https://doi.org/10.1128/MMBR.00037-14

National Academies of Sciences, E., Studies, D. on E. and L., Board, N. and R.S., Workshop, P.C. on L.-L.R.W.M. and D.A., 2017. Low-Level Radioactive Waste Management and Disposition: Background Information. National Academies Press (US).

Newsome, L., Morris, K., Lloyd, J.R., 2015. Uranium Biominerals Precipitated by an Environmental Isolate of Serratia under Anaerobic Conditions. PLOS ONE 10, e0132392. https://doi.org/10.1371/journal.pone.0132392

Newsome, L., Morris, K., Lloyd, J.R., 2014. The biogeochemistry and bioremediation of uranium and other priority radionuclides. Chemical Geology 363, 164–184. https://doi.org/10.1016/j.chemgeo.2013.10.034

Norris, S., 2017. Radioactive waste confinement: clays in natural and engineered barriers – introduction. Geological Society, London, Special Publications 443, 1–8. https://doi.org/10.1144/SP443.26

Ojovan, M.I., Lee, W.E., 2014. 20 - Nuclear Waste Disposal, in: An Introduction to Nuclear Waste Immobilisation (Second Edition). Elsevier, Oxford, pp. 321–335. https://doi.org/10.1016/B978-0-08-099392-8.00020-6

Ojovan, M.I., Lee, W.E., 2005. Chapter 19 - Nuclear Waste Disposal, in: An Introduction to Nuclear Waste Immobilisation. Elsevier, Oxford, pp. 269–287. https://doi.org/10.1016/B978-008044462-8/50021-1

Ojovan, M.I., Lee, W.E., Kalmykov, S.N., 2019. Chapter 22 - Nuclear Waste Disposal, in: Ojovan, M.I., Lee, W.E., Kalmykov, S.N. (Eds.), An Introduction to Nuclear Waste Immobilisation (Third Edition). Elsevier, pp. 415–432. https://doi.org/10.1016/B978-0-08-102702-8.00022-4

Pedersen, K., 2010. Analysis of copper corrosion in compacted bentonite clay as a function of clay density and growth conditions for sulfate-reducing bacteria. J. Appl. Microbiol. 108, 1094–1104. https://doi.org/10.1111/j.1365-2672.2009.04629.x

Pedersen, K., 1999. Subterranean microorganisms and radioactive waste disposal in Sweden. Engineering Geology 52, 163–176. https://doi.org/10.1016/S0013-7952(99)00004-6

Pedersen, K., Bengtsson, A., Blom, A., Johansson, L., Taborowski, T., 2017. Mobility and reactivity of sulphide in bentonite clays – Implications for engineered bentonite barriers in geological repositories for radioactive wastes. Applied Clay Science 146, 495–502. https://doi.org/10.1016/j.clay.2017.07.003

Pedersen, K., Motamedi, M., Karnland, O., Sandén, T., 2000. Mixing and sulphate-reducing activity of bacteria in swelling, compacted bentonite clay under high-level radioactive waste repository conditions. Journal of Applied Microbiology 89, 1038–1047. https://doi.org/10.1046/j.1365-2672.2000.01212.x

Pentráková, L., Su, K., Pentrák, M., Stucki, J.W., 2013. A review of microbial redox interactions with structural Fe in clay minerals. Clay Minerals 48, 543–560. https://doi.org/10.1180/claymin.2013.048.3.10

Perdrial, J.N., Warr, L.N., Perdrial, N., Lett, M.-C., Elsass, F., 2009. Interaction between smectite and bacteria: Implications for bentonite as backfill material in the disposal of nuclear waste. Chemical Geology 264, 281–294. https://doi.org/10.1016/j.chemgeo.2009.03.012

Plan General de Residuos Radiactivos [WWW Document], 2006. URL http://www.enresa.es/esp/inicio/conozca-enresa/plan-general-de-residuos-radiactivos (accessed 12.10.19).

Publications Office of the European Union, 2017. COM/2017/0236 final, REPORT FROM THE COMMISSION TO THE COUNCIL AND THE EUROPEAN PARLIAMENT on progress of implementation of Council Directive 2011/70/EURATOM and an inventory of radioactive waste and spent fuel present in the Community's territory and the future prospects [WWW Document]. URL https://op.europa.eu:443/en/publication-detail/-/publication/a7fb4e4c-3954-11e7-a08e-01aa75ed71a1/language-en (accessed 12.9.19).

Ratto, M., Itavaara, M., 2012. Microbial activity in bentonite buffers. Literature study (No. VTT-TECHNOLOGY--20). VTT Technical Research Centre of Finland.

Ruiz-Fresneda, M.A., Gomez-Bolivar, J., Delgado-Martin, J., Abad-Ortega, M. del M., Guerra-Tschuschke, I., Merroun, M.L., 2019. The Bioreduction of Selenite under Anaerobic and Alkaline Conditions Analogous to Those Expected for a Deep Geological Repository System. Molecules 24, 3868. https://doi.org/10.3390/molecules24213868

Sellin, P., Leupin, O.X., 2013. The Use of Clay as an Engineered Barrier in Radioactive-Waste Management a Review. Clays Clay Miner. 61, 477–498. https://doi.org/10.1346/CCMN.2013.0610601

Smart, N.R., Reddy, B., Rance, A.P., Nixon, D.J., Frutschi, M., Bernier-Latmani, R., Diomidis, N., 2017. The anaerobic corrosion of carbon steel in compacted bentonite exposed to natural Opalinus Clay porewater containing native microbial populations. Corrosion Engineering, Science and Technology 52, 101–112. https://doi.org/10.1080/1478422X.2017.1315233

Stone, W., Kroukamp, O., Moes, A., McKelvie, J., Korber, D.R., Wolfaardt, G.M., 2016a. Measuring microbial metabolism in atypical environments: Bentonite in used nuclear fuel storage. J. Microbiol. Methods 120, 79–90. https://doi.org/10.1016/j.mimet.2015.11.006

Stone, W., Kroukamp, O., Moes, A., McKelvie, J., Korber, D.R., Wolfaardt, G.M., 2016b. Measuring microbial metabolism in atypical environments: Bentonite in used nuclear fuel storage. J. Microbiol. Methods 120, 79–90. https://doi.org/10.1016/j.mimet.2015.11.006

Stroes-Gascoyne, S., Hamon, C.J., Maak, P., 2011. Limits to the use of highly compacted bentonite as a deterrent for microbiologically influenced corrosion in a nuclear fuel waste repository. Physics and Chemistry of the Earth, Parts A/B/C, Clays in Natural & Engineered Barriers for Radioactive Waste Confinement 36, 1630–1638. https://doi.org/10.1016/j.pce.2011.07.085

Stroes-Gascoyne, S., Hamon, C.J., Maak, P., Russell, S., 2010. The effects of the physical properties of highly compacted smectitic clay (bentonite) on the culturability of indigenous microorganisms. Applied Clay Science, Advanced smectitic clay research 47, 155–162. https://doi.org/10.1016/j.clay.2008.06.010

Stroes-Gascoyne, S., Schippers, A., Schwyn, B., Poulain, S., Sergeant, C., Simonoff, M., Le Marrec, C., Altmann, S., Nagaoka, T., Mauclaire, L., McKenzie, J., Daumas, S., Vinsot, A., Beaucaire, C., Matray, J.-M., 2007. Microbial Community Analysis of Opalinus Clay Drill Core Samples from the Mont Terri Underground Research Laboratory, Switzerland. Geomicrobiology Journal 24, 1–17. https://doi.org/10.1080/01490450601134275

Stylo, M., Neubert, N., Roebbert, Y., Weyer, S., Bernier-Latmani, R., 2015. Mechanism of Uranium Reduction and Immobilization in Desulfovibrio vulgaris Biofilms. Environ. Sci. Technol. 49, 10553–10561. https://doi.org/10.1021/acs.est.5b01769

Tan, Y., Yao, R., Wang, R., Wang, D., Wang, G., Zheng, S., 2016. Reduction of selenite to Se(0) nanoparticles by filamentous bacterium Streptomyces sp. ES2-5 isolated from a selenium mining soil. Microbial Cell Factories 15, 157. https://doi.org/10.1186/s12934-016-0554-z

Vance, E.R., Begg, B.D., 2010. 9 - Immobilisation of spent nuclear fuel and high-level radioactive waste for safe disposal in geological repository systems, in: Ahn, J., Apted, M.J. (Eds.), Geological Repository Systems for Safe Disposal of Spent Nuclear Fuels and Radioactive Waste, Woodhead Publishing Series in Energy. Woodhead Publishing, pp. 261–285. https://doi.org/10.1533/9781845699789.3.261

Vecchia, E.D., Veeramani, H., Suvorova, E.I., Wigginton, N.S., Bargar, J.R., Bernier-Latmani, R., 2010. U(VI) reduction by spores of Clostridium acetobutylicum. Research in Microbiology, Special issue on the biology of spore-formers 161, 765–771. https://doi.org/10.1016/j.resmic.2010.08.001

Villar, M.V., Cuevas, J., Leguey, S., Caballero, E., Huertas, F.J., Delgado, A., Fernández-Soler, J.M., Astudillo, J., 2006. The study of Spanish clays for their use as sealing materials in nuclear waste repositories: 20 years of progress. Journal of Iberian Geology 32, 15–36.

Yu, Q., Boyanov, M.I., Liu, J., Kemner, K.M., Fein, J.B., 2018. Adsorption of Selenite onto Bacillus subtilis: The Overlooked Role of Cell Envelope Sulfhydryl Sites in the Microbial Conversion of Se(IV). Environ. Sci. Technol. 52, 10400–10407. https://doi.org/10.1021/acs.est.8b02280

Yung, M.C., Jiao, Y., 2014. Biomineralization of Uranium by PhoY Phosphatase Activity Aids Cell Survival in Caulobacter crescentus. Appl Environ Microbiol 80, 4795–4804. https://doi.org/10.1128/AEM.01050-14

Zhang, G., Dong, H., Kim, J., Eberl, D.D., 2007. Microbial reduction of structural Fe3+ in nontronite by a thermophilic bacterium and its role in promoting the smectite to illite reaction. American Mineralogist 92, 9. https://doi.org/10.2138/am.2007.2498

Zhao, C., Liu, J., Li, X., Li, F., Tu, H., Sun, Q., Liao, J., Yang, J., Yang, Y., Liu, N., 2016. Biosorption and bioaccumulation behavior of uranium on Bacillus sp. dwc-2: Investigation by Box-Behenken design method. Journal of Molecular Liquids 221, 156–165. https://doi.org/10.1016/j.molliq.2016.05.085

Zhengji, Y., 2010. Microbial removal of uranyl by sulfate reducing bacteria in the presence of Fe (III) (hydr)oxides. Journal of Environmental Radioactivity 101, 700–705. https://doi.org/10.1016/j.jenvrad.2010.04.009

OBJETIVOS

En esta Tesis Doctoral se han establecido unos objetivos en base al estudio de la bentonita y la diversidad microbiana presente en ella, ya que este tipo de arcilla ha sido seleccionado como el material de relleno y sellado más adecuado para el establecimiento del Almacenamiento Geológico Profundo (AGP) de residuos radiactivos de alta actividad (RAA). Se precisa, por tanto, de un estudio exhaustivo de las implicaciones derivadas de la actividad de microorganismos sobre la estabilidad de la bentonita y la movilización los radionucleidos críticos para la seguridad de los AGPs.

Por consiguiente, los objetivos específicos para el desarrollo de la presente Tesis Doctoral son:

1. Optimizar y desarrollar un método de extracción de ADN microbiano, eficiente y reproducible, a partir de muestras de bentonita.

2. Investigar el efecto del uranio y del glicerol-2-fosfato (G2P) sobre la química, mineralogía y diversidad microbiana de los microcosmos de bentonita bajo condiciones aerobias y anaerobias.

3. Determinar el impacto potencial de la microbiota presente en la bentonita sobre la especiación química del uranio, en presencia y en ausencia de G2P, bajo condiciones aerobias y anaerobias.

4. Estudiar el efecto de la compactación de las bentonitas sobre la diversidad microbiana, así como el papel de ésta en la estabilidad y seguridad del AGP.

5. Determinar los posibles cambios producidos en la diversidad microbiana de la bentonita por la presencia de selenito, y la biotransformación de éste empleando una metodología multidisciplinar.

MATERIALS AND METHODS

In this chapter, it is exposed the Material and Methods in common with all the studies developed in the different specific Chapters that compound this PhD Thesis. Included here, techniques and characterization like bentonite sample collection, mineralogical and chemical characterization of the bentonite samples, microscopic analyses, and bentonite bacterial diversity analyses (bioinformatics and statistical analyses). More detailed information about the establishment of the different experiments (bentonite microcosms and compacted blocks) and specific techniques can be found in the Material and Methods section of each chapter (Chapters I-V).

1. BENTONITE SAMPLE COLLECTION

Bentonite samples were collected at a depth of 80 cm from "El Cortijo de Archidona" deposit in Almeria (Spain). While very pure and with exceptional colloidal properties (Villar et al., 2006), these bentonites have been well characterized from mineralogical, geochemical and mechanical point of view. The collection of the samples was performed in sterile containers under aseptic conditions and were stored at 4 ºC until further use.

2. MINERALOGICAL CHARACTERIZATION OF THE BENTONITE SAMPLES

The mineralogy of the solid bentonite was determined by X-Ray Diffraction (XRD) before and after the different treatments. A PANalytical X'Pert Pro diffractometer equipped with an X'Celerator solid-state detector, a spinning sample stage, a Ni filter, and 0.25º divergence slit was used. X-ray powder diffraction patterns were recorded using random oriented mounts with CuKα radiation (λ = 1.5405 Å), operated at 45 kV and 40 mA, scanned from 4 to 70 °2θ. Powder samples were deposited in zero-background silicon sample holders for analysis. Mineral phases were

identified by comparison with JCPDS powder spectra (Joint Committee on Powder Diffraction Standards).

3. CHEMICAL CHARACTERIZATION OF BENTONITE

Trace element composition of the Spanish bentonite pore water (PW) was carried out using Inductively Coupled Plasma-Mass Spectrometry (ICP-MS) by NexION 300D spectrometer. Composition of major elements of the bentonite was determined in duplicate by X-ray fluorescence (XRF) spectroscopy (Philips Magix Pro, PW-2440).

The pH of each sample was measured in triplicate according to the method developed by Stone et al., (2016), where a 1:15 bentonite:$CaCl_2$-buffer ratio were used. $CaCl_2$ buffer resulted to be suitable for this analysis. For the pH measurement, Crison pH-meter (MicropH, 2002) was standardized against pH 4.00, and 7.02 commercial reference solutions. The reported accuracy was of ± 0.02 pH units.

4. MICROSCOPIC ANALYSES

High-Resolution Transmission Electron Microscope (HRTEM, Philips CM 200) at an acceleration voltage of 200 kV and also High-Angle Annular Dark Field Scanning Transmission Electron Microscope (HAADF-STEM, FEI TITAN G2 80–300) at an acceleration voltage of 300 kV and MegaViewIII camera under standard operating conditions with liquid nitrogen anticontaminator in place (Fig. 1). Energy Dispersive X-ray Spectroscopy (EDX) microanalysis was performed at 300 kV using a spot size of 7 nm and a live counting time of 20 s. Samples were dispersed in ethanol by sonication and then deposited on carbon-coated copper grids for observation. In addition, Selected-Area Electron Diffraction (SAED) and HRTEM combined with Fast Fourier Transform (FFT) were used for the characterization of some precipitates.

Figure 1. High-Angle Annular Dark Field-Scanning Transmission Electron Microscope (HAADF-STEM) FEI TITAN G2-80-300 located at "Centro de Instrumentación Científica" (University of Granada) (https://cic.ugr.es/servicios-y-unidades/ficha.php?codServicio=6&unidad=28#).

Variable Pressure Field Emission Scanning Electron Microscopy (VP-FESEM), a Zeiss SUPRA40VP equipped with SE (InLens) and BSE detectors was used to provide morphological and chemical characterizations, respectively (Fig. 2). For elemental analysis, EDX detector was a 50 mm^2 silicon drift detector XMAX enabling detection of elements with $Z4 \geq$ (Be) and high-count rates. In addition, this model is equipped with Raman spectrometer *Renishaw In Via* fitted with a Nd:YAG 532 nm laser and a near infrared diode 785 nm laser, with 500 mW and 100 mW as maximum powers, respectively (Guerra and Cardell, 2015).

Figure 2. Variable Pressure Field Emission Scanning Electron Microscope (VP-FESEM) Zeiss SUPRA40VP equipped with SE (InLens) and BSE detectors. This microscope is located at "Centro de Instrumentación Científica" in the University of Granada (https://cic.ugr.es/servicios-y-unidades/ficha.php?codServicio=6&unidad=49).

5. CHARACTERIZATION OF BENTONITE BACTERIAL DIVERSITY

All DNA extractions from bentonite samples were carried out with a house-made and optimized DNA extraction protocol described in detail in Povedano-Priego et al. (2019) (Chapter 1 and 3). The extracted total DNA was quantified on Qubit 3.0 Fluorometer (Life Technology), and stored at -20 °C until extractions from all samples were finished and ready for sequencing.

The V3–V4 region of the 16S rRNA gene from each sample was amplified by a two-step PCR using the bacterial primers 341F (5'-CCTACGGGNGGCWGCAG- 3') and 805R (5'-GACTACHVGGGTATCTAATCC- 3'). In some cases, the V5-V6 regions of the 16S rRNA gene were amplified using the primers 807F (5'-ACGACGCTCTTCCGATCTGGATTAGATACCCBRGTAGTC-3') and 1050R (5'-GACGTGTGCTCTTCCGATCTAGYTGDCGACRRCCRTGCA-3'). Illumina MiSeq was used to sequence the purified amplicon-barcode-primer complexes. Then, sample-specific barcodes were used for reads demultiplexing and separation.

5.1. Bioinformatics and statistical analyses

Operational Taxonomic Units (OTUs, at 97 % identity) were detected by the QIIME v. 1.8 pipeline and were identified using UCLUST (Edgar, 2010) and classified using the SILVA 119 QIIME 16S database (Quast et al., 2013). Finally, clustered and annotated OTUs were analyzed in Explicet 2.10.5 for the stacked bars construction. Alpha- and beta-diversity indices were determined by R software. One-way ANOVA test, using a significance level of 0.05, was used to look for significant differences in the alpha diversity between the samples. Principal Coordinate Analysis (PCoA) was constructed using QIIME and PAST3 v. 3.18. Heatmaps were made using the heatmap.2 function in the R gplots v. 3.0.1.1 package and included only taxa at ≥1% relative abundance in all samples/replicates.

5.2. Network analysis

Pearson's correlation index between selected genera were calculated using 'phyloseq' 'MASS' and 'reshape2' packages of R software. A valid co-occurrence was selected as a strong correlation if the Pearson's correlation coefficient was ≥0.9. Correlation networks between genera were constructed and visualized in the Cytoscape software v.3.7.2 (Shannon et al., 2003).

6. REFERENCES

Edgar, R.C., 2010. Search and clustering orders of magnitude faster than BLAST. Bioinformatics 26, 2460–2461. https://doi.org/10.1093/bioinformatics/btq461

Guerra, I., Cardell, C., 2015. Optimizing use of the structural chemical analyser (variable pressure FESEM-EDX raman spectroscopy) on micro-size complex historical paintings characterization. Journal of Microscopy 260, 47–61. https://doi.org/10.1111/jmi.12265

Quast, C., Pruesse, E., Yilmaz, P., Gerken, J., Schweer, T., Yarza, P., Peplies, J., Glöckner, F.O., 2013. The SILVA ribosomal RNA gene database project: improved data processing and web-based tools. Nucleic Acids Res. 41, D590-596. https://doi.org/10.1093/nar/gks1219

Shannon, P., Markiel, A., Ozier, O., Baliga, N.S., Wang, J.T., Ramage, D., Amin, N., Schwikowski, B., Ideker, T., 2003. Cytoscape: a software environment for integrated models of biomolecular interaction networks. Genome Res. 13, 2498–2504. https://doi.org/10.1101/gr.1239303

Stone, W., Kroukamp, O., Moes, A., McKelvie, J., Korber, D.R., Wolfaardt, G.M., 2016. Measuring microbial metabolism in atypical environments: Bentonite in used nuclear fuel storage. J. Microbiol. Methods 120, 79–90. https://doi.org/10.1016/j.mimet.2015.11.006

Villar, M.V., Cuevas, J., Leguey, S., Caballero, E., Huertas, F.J., Delgado, A., Fernández-Soler, J.M., Astudillo, J., 2006. The study of Spanish clays for their use as sealing materials in nuclear waste repositories: 20 years of progress. Journal of Iberian Geology 32, 15–36.

CHAPTER I

Shifts in bentonite bacterial community and mineralogy in response to uranium and glycerol-2-phosphate exposure

Cristina Povedano-Priego[1], Fadwa Jroundi[1*], Margarita Lopez-Fernandez[2], Iván Sánchez-Castro[1], Inés Martin-Sánchez[1], F. Javier Huertas[3], Mohamed L. Merroun[1]

[1]Department of Microbiology, University of Granada, Campus Fuentenueva s/n 18071, Granada, Spain. ppriego@ugr.es; fadwa@ugr.es; sanchezcastro@ugr.es; inesms@ugr.es; merroun@ugr.es.

[2]Institute of Resource Ecology, Helmholtz-Zentrum Dresden-Rossendorf, Bautzner Landstraße 400, 01328 Dresden, Germany. m.lopez-fernandez@hzdr.de

[3]Instituto Andaluz de Ciencias de la Tierra, CSIC – University of Granada, 18100 Granada, Spain. javierhuertas@ugr.es

Este capítulo ha sido publicado en la revista internacional Science of the Total Environment (10.1016/j.scitotenv.2019.07.228): **Povedano-Priego, C.**, Jroundi, F., Lopez-Fernandez, M., Sánchez-Castro, I., Martin-Sánchez, I., Huertas, F.J., Merroun, M.L., 2019. Shifts in bentonite bacterial community and mineralogy in response to uranium and glycerol-2-phosphate exposure. Sci. Total Environ. 692:219-232.

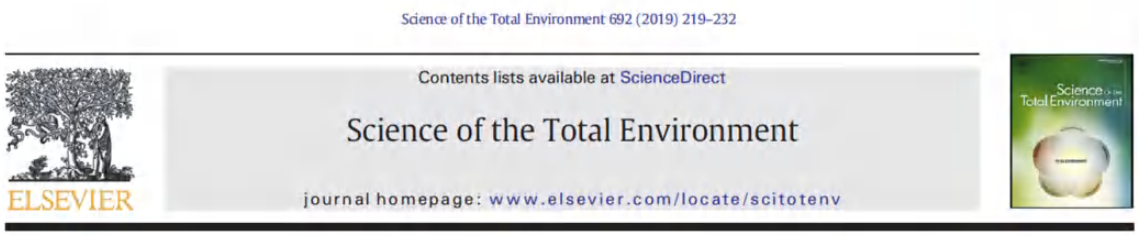

Shifts in bentonite bacterial community and mineralogy in response to uranium and glycerol-2-phosphate exposure

Cristina Povedano-Priego [a], Fadwa Jroundi [a,*], Margarita Lopez-Fernandez [b], Iván Sánchez-Castro [a], Inés Martin-Sánchez [a], F. Javier Huertas [c], Mohamed L. Merroun [a]

[a] Department of Microbiology, University of Granada, Campus Fuentenueva s/n, 18071 Granada, Spain
[b] Institute of Resource Ecology, Helmholtz-Zentrum Dresden-Rossendorf, Bautzner Landstraße 400, 01328 Dresden, Germany
[c] Instituto Andaluz de Ciencias de la Tierra, CSIC – University of Granada, 18100 Granada, Spain

1. ABSTRACT

The multi-barrier deep geological repository system is currently considered as one of the safest option for the disposal of high-level radioactive wastes. Indigenous microorganisms of bentonites, may affect the structure and stability of these clays through Fe-containing minerals biotransformation and radionuclides mobilization. The present work aimed to investigate the behavior of bentonite and its bacterial community in the case of a uranium leakage from the waste containers. Hence, bentonite microcosms were amended with uranyl nitrate (U) and glycerol-2-phosphate (G2P) and incubated aerobically for 6 months. Next generation 16S rRNA gene sequencing revealed that the bacterial populations of all treated microcosms were dominated by Actinobacteria and Proteobacteria, accounting for more than 50% of the community. Additionally, G2P and nitrate had a remarkable effect on the bacterial diversity of bentonites by the enrichment of bacteria involved in the nitrogen and carbon biogeochemical cycles (e.g. *Azotobacter*). A significant presence of sulfate-reducing bacteria such as *Desulfonauticus* and *Desulfomicrobium* were detected in the U-treated microcosms. The actinobacteria *Amycolatopsis* was enriched in G2P-uranium amended bentonites. High Annular Angle Dark-Field Scanning Transmission Electron Microscopy analyses showed the capacity of *Amycolatopsis* and a bentonite consortium formed by *Bradyrhizobium-Rhizobium* and *Pseudomonas* to precipitate U as U phosphate mineral phases, probably due to the phosphatase activity. The different amendments did not affect the mineralogy of the bentonite pointing to a high structural stability. These results would help to predict the impact of microbial processes on the biogeochemical cycles of elements (N and U) within the bentonite barrier under repository relevant conditions and to determine the changes in the microbial community induced by a uranium release.

Keywords: deep geological repository, bentonite, bacterial diversity, uranium, glycerol-2-phosphate, microscopy

2. GRAPHICAL ABSTRACT

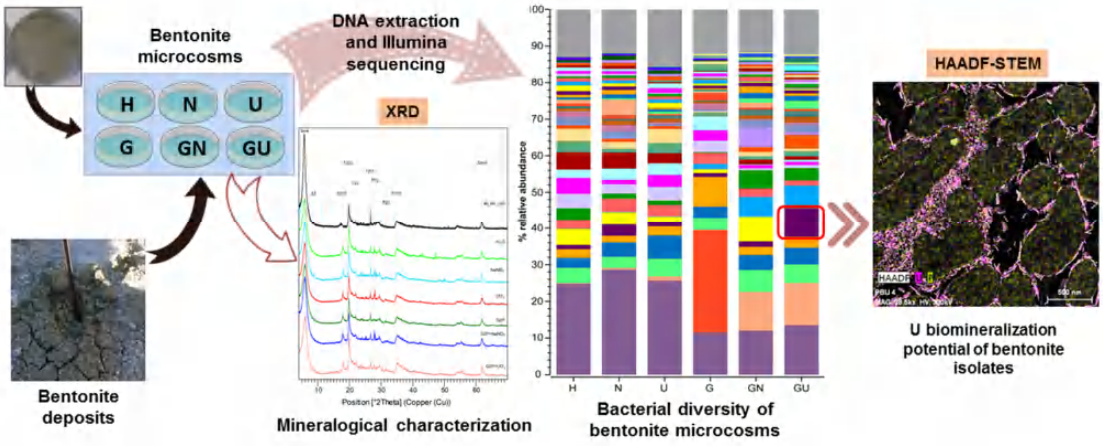

3. INTRODUCTION

Several countries have been working to determine the best option for the containment of spent fuel and other high-level radioactive wastes. These wastes must be stored safely for at least 100,000 years until their radiotoxicity decrease to levels similar to those of natural uranium (Anderson et al., 2011). While their construction around the world is still in progress (Pedersen et al., 2017), deep geological repositories (DGR) are an internationally accepted solution for such long-term radioactive wastes storage. The universal disposal concept involves a multi-barrier system, which comprises storing the spent fuel in canisters of cast iron, stainless steel, or copper (depending on the design of each country). These canisters will be emplaced several hundred meters underground, surrounded by compacted bentonite clay buffer (engineered barrier) within a host rock (natural geological barrier) (Anderson et al., 2011). Bentonites, rich in montmorillonite, are the most suitable material for the engineered barriers in DGR (Pedersen et al., 2017) due to their high adsorption capacity, large surface area, impermeability and swelling properties when hydrated (Perdrial et al., 2009). Furthermore, bentonite would provide mechanical support and reduce water inflow to the canisters, in addition to the capacity of holding and retarding the dispersion of radionuclides (Masurat et al., 2010). In Spain, bentonite formations from Almeria have been selected as the engineered barrier reference material for the future Spanish DGR (Villar et al., 2006).

Safety of DGR could be altered not only by physical and chemical parameters but also by microbial activities, since high microbial diversity has been reported in different bentonites (Bengtsson and Pedersen, 2017; Lopez-Fernandez et al., 2018b; Perdrial et al., 2009). Microbial activity may affect directly or indirectly the integrity and performance of the repository, through different processes: 1) gas production such as CO_2, CH_4 or H_2 by methanogens (Stroes-Gascoyne et al., 2010); 2) sulfide generation by sulfate-reducing bacteria, resulting in the corrosion of the canisters (Stone et al., 2016); and 3) bentonite alteration by reduction of structural Fe(III) in smectite (Liu et al., 2017; Pentráková et al., 2013). However, microorganisms could also control the speciation and migration of radionuclides (Lopez-Fernandez et al., 2018a).

In case of a canister failure, when radionuclides would be released and migrate through the repository, microorganisms may interact with these elements through different processes including biosorption (Pedersen, 1999), reduction (Brookshaw et al.,

2012), biomineralization (Merroun et al., 2011), and bioaccumulation (Brookshaw et al., 2012). This circumstance would occur in the long terms when anaerobic conditions were established, but it would be also worthy to study this potential situation in the presence of O_2 which would be present and slowly consumed during the first years (King et al., 2017) or even first decades (Pedersen, 1999) after repository closure. Several studies have described many microorganisms influencing the speciation of radionuclides such as uranium, through a reduction process, generating insoluble U(IV) as uraninite phase (Cologgi et al., 2014). These microorganisms include sulfate-reducing bacteria (e.g., *Desulfovibrio* spp.), iron-reducing bacteria (e.g., *Geobacter* spp.), denitrifiers (e.g., *Pseudomonas* spp.), and spore-forming species (e.g., *Clostridium* spp., *Anaeromyxobacter* spp.) (Cologgi et al., 2014). However, the microbial reduction of U(VI) can be diminished or completely inhibited by the presence of nitrate, which may be used as a competing and more energetically favorable electron acceptor for microorganisms (Xu et al., 2017). Bacteria can also facilitate uranium biomineralization producing insoluble U(VI) phosphates of the autunite group (Beazley et al., 2011; Jroundi et al., 2007) with high stability towards oxidative conditions over a wide range of pH values (Salome et al., 2017). Biomineralization of uranium is particularly enhanced by the presence of organophosphates such as glycerol-2-phosphate (G2P) and glycerol-3-phosphate (G3P) (Martinez et al., 2014). Many microbes are able to metabolize glycerol generating precursors (G2P, G3P, etc.) needed for the synthesis of special cellular components such as lipids (e.g. phospholipids of the plasma membrane) and cell walls (Yeh et al., 2008). Hence, G2P and G3P are usually present as cell wall compounds or within the bacterial and fungal cell extracts (Martinez et al., 2014). In DGR concept, glycerol may derive from the oxidation of glucose through the glycolytic route or from the hydrolysis of teichoic acids, which contain glycerol-phosphate repeating units (Weidenmaier and Peschel, 2008). G2P stimulates microbial phosphatase activity to release inorganic phosphates, which are employed either as essential nutrient or for U(VI) precipitation as a detoxification mechanism (Beazley et al., 2011). Several bacteria have the capacity for uranium biomineralization by phosphatase activity such as *Rahnella*, *Bacillus*, *Serratia*, *Caulobacter*, *Aeromonas*, and also indigenous bacterial community from the U.S. Department of Energy (DOE) Oak Ridge site (Martinez et al., 2014; Newsome et al., 2015). Since bacteria are able to affect the speciation and mobility of uranium in the environment, radionuclides may in turn modify the structure of the bacterial community, enriching those with high uranium

tolerance capacity. Some studies reported changes in the indigenous bacterial community of soils after the addition of U(VI) (Geissler and Selenska-Pobell, 2005; Lopez-Fernandez et al., 2018b) and G2P (Newsome et al., 2015). Accordingly, it is of great importance to consider the influence of G2P on both the bacterial diversity and the uranium speciation, in case uranium was released from the DGR canisters.

This study aimed to investigate the effect of uranyl nitrate and G2P on: 1) the mineralogy and structure of Spanish bentonites, and 2) the bacterial community composition of these clays. Our research hypotheses point out the fact that (1) uranium would affect the structure and composition of the bacterial community in bentonite, enhancing the abundance of bacteria with U-tolerance capacities and also (2) the bacterial community would influence the speciation of uranium through its immobilization by U biomineralization leading to the formation of highly insoluble uranium phosphate phases. These hypotheses were verified in bentonite microcosms treated with uranium, where G2P was added as a carbon and phosphate source to stimulate the growth of bacteria, since the organic carbon and phosphorus contents in Spanish bentonite are very low (Lopez-Fernandez et al., 2015). Moreover, the ability of natural bacterial isolates, enriched from G2P-U-treated bentonite, to precipitate this radionuclide was also evaluated. The implications of the obtained results on the safety of deep geological disposal of radioactive wastes are highlighted.

4. MATERIALS AND METHODS

4.1.Bentonite samples collection

Bentonite samples were collected at a depth of 80 cm from “El Cortijo de Archidona” deposit in Almeria (Spain). While very pure and with exceptional colloidal properties (Villar et al., 2006), these bentonites have been mineralogically, geochemically, and mechanically well characterized. Sample collection was performed in January 2016 under aseptic conditions in sterile containers, which were stored at 4 ºC until further use.

4.2.Chemical characterization of bentonite pore water

Determination of the trace element composition of the Spanish bentonite pore water (PW) was carried out using Inductively Coupled Plasma-Mass Spectrometry (ICP-MS) by NexION 300D spectrometer. Bentonite PW was extracted by shaking (at 180 rpm) one gram of bentonite in 100 mL sterile distilled water during 24 h at 28 ºC and then filtering the liquid phase using sterile filters of 0.45 μm pore-size. Composition of major elements of the bentonite was determined in duplicate by X-ray fluorescence (XRF) spectroscopy (Philips Magix Pro, PW-2440).

The pH of each sample was measured in triplicate according to the method used by Stone et al. (2016). Briefly, one gram of bentonite was mixed with 15 mL $CaCl_2$ (0.01 M) at 1:15 bentonite:solvent ratio and the pH was measured using a Crison pH-meter (MicropH, 2002) standardized against pH 4.00, and 7.02 commercial reference solutions. The reported accuracy was of ± 0.02 pH units. The main advantage of the measurements of soil pH in 0.01 M $CaCl_2$ buffer is the elimination of the interferences from suspension effects and variable salt contents.

4.3. Preparation of bentonite microcosms

Microcosms were prepared in sterile plastic plates (9 cm diameter, 1 cm depth) containing each 40 g of aseptically grinded bentonite (Fig. S1). Bentonite in plates were amended with different solutions: 1) sodium nitrate solution (2.7 mM) was used as nitrate-controls (N); 2) uranyl nitrate solution (1.26 mM) for U-treated bentonite (U); 3) G2P solution (10 mM) for bentonite treated with organic phosphate source (G); 4) a combined solution of G2P and sodium nitrate was used as organic phosphate-nitrate interaction controls (GN); 5) a combined solution of G2P and uranyl nitrate as uranium-G2P-treated bentonite (GU); and 6) sterile distilled water (H) was used as control for N and G microcosms (Table 1, Fig. S1). Stock solution and working solution of uranyl nitrate was prepared as described in Lopez-Fernandez et al. (2018b). The stock solution was sterilized by filtration through 0.22 μm pore-size nitrocellulose filter and stored at 4 ºC until used. All working solutions were filtrated and homogenously added to each bentonite-containing plate until complete saturation of clays was reached. Treatments were performed in triplicate (a total of 18 individual microcosms) and incubated in

darkness at room temperature under aerobic conditions in a tightly closed system where O_2 levels were gradually depleted during the six months of incubation. This incubation time is too short considering DGR concept, thus 10 mM G2P solution was used in order to accelerate the microbial processes on the bentonite, stimulating thus the growth of bacteria with the ability of using glycerol as an electron donor. To prevent desiccation of the microcosms during incubation, the plates were tightly closed with parafilm and two water-filled recipients were placed beside as humidity support to maintain moisture conditions.

Table 1. Identification of the different aerobic microcosms treated with: distilled water (H; dH_2O), sodium nitrate (N; $NaNO_3$), uranyl nitrate (U; $UO_2(NO_3)_2$), glycerol-2-phosphate (G; G2P), G2P-sodium nitrate (GN; G2P+ $NaNO_3$), and G2P-uranyl nitrate (GU; G2P+ $UO_2(NO_3)_2$). The concentrations expressed as mM refer to the concentration of each component in each experimental solution (one per treatment).

Sample	Treatment	Concentration (mM)
H	dH_2O	-
N	$NaNO_3$	2.7
U	$UO_2(NO_3)_2$	1.26
G	G2P	10
GN	G2P+ $NaNO_3$	10 (G2P); 2.7 ($NaNO_3$)
GU	G2P+ $UO_2(NO_3)_2$	10 (G2P); 1.26 [$UO_2(NO_3)_2$]

4.4. Mineralogical characterization of the bentonite samples

The mineralogy of the solid bentonite microcosms was determined by X-Ray Diffraction (XRD) before (time 0) and 6 months after the different treatments. A PANalytical X'Pert Pro diffractometer equipped with an X'Celerator solid-state detector, a spinning sample stage, a Ni filter, and 0.25º divergence slit was used. X-ray powder diffraction patterns were recorded using random oriented mounts with CuKα radiation (λ = 1.5405 Å), operated at 45 kV and 40 mA, scanned from 4 to 70 °2θ. Powder samples were deposited in zero-background silicon sample holders for analysis.

Mineral phases were identified by comparison with JCPDS powder spectra (Joint Committee on Powder Diffraction Standards).

Additional microstructural features of the bentonite microcosms before and after treatments were determined using High-Resolution Transmission Electron Microscope (HRTEM, Philips CM 200) at an acceleration voltage of 200 kV and also High-Angle Annular Dark Field Scanning Transmission Electron Microscope (HAADF-STEM, FEI TITAN G2 80–300) at an acceleration voltage of 300 kV and MegaViewIII camera under standard operating conditions with liquid nitrogen anticontaminator in place. Energy Dispersive X-ray Spectroscopy (EDX) microanalysis was performed at 300 kV using a spot size of 7 nm and a live counting time of 20 s. Samples were dispersed in ethanol by sonication and then deposited on carbon-coated copper grids for observation.

4.5. Microcosms bacterial diversity characterization

4.5.1. DNA extraction from bentonite microcosms

To study the microbial diversity of the bentonite microcosms (H, N, U, G, GN, and GU) after six months of incubation, total DNA was extracted from 18 treated microcosms (3 bentonite-containing plates per treatment). Each replicate (0.3 g) was mixed with glass beads (≈ 0.3 g) of different diameters in a sterile screw-cap tube and resuspended by energetic vortexing in 400 µL of Na_2HPO_4 (0.12 M, pH 8.0). Then, 600 µL of lysis buffer [Tris-HCl (100 mM, pH 8.0); EDTA (100 mM, pH 8.0); NaCl (100 mM); polyvinylpyrrolidone (PVP, 1%); and SDS (2%)], 24 µL freshly made lysozyme (10 mg/mL), and 2.5 µL proteinase K (20 mg/mL) were added to each tube. Mechanical lysis was performed using a FastPrep® FP120 at a speed of 5.5 m s^{-1} for 45 s, two times with an intermittent cooling on ice for 5 min. Samples were incubated at two different temperatures: first, at 37 ºC for 30 min and after that at 60 ºC for 45 min and then centrifuged at 14,000 × g for 5 min at room temperature. The supernatants were collected in new 15-mL Falcon tubes and the bentonite pellets were mixed again with 1 mL of lysis buffer and disrupted another two times by FastPrep. After centrifugation, supernatants were transferred to the previously used 15-mL tubes and a series of washing steps were performed using one volume of phenol:chloroform:isoamyl alcohol (PCI-25:24:1, pH 8), one volume of phenol:chloroform (PC-1:1), and one volume of

chloroform followed by centrifugation at 1,500 × g for 10 min at 4 ºC. DNA was precipitated by adding one volume of cold-isopropanol and 1:10 volume of 3 M sodium acetate (pH 5), incubating for 1 hour at -80 ºC and centrifuging at 5,000 × g for 30 min at 4 ºC. The pellets were washed with 80% cold-ethanol and then dissolved in 35 µL Tris (5 mM, pH 8.5)-TE buffer [Tris-HCl (10 mM, pH 8.0) and EDTA (1 mM)]. Finally, the extracted total DNA was quantified on Qubit 3.0 Fluorometer (Life Technology), and stored at -20 °C until extractions from all microcosms were finished, and ready for sequencing.

4.5.2. Amplification and sequencing of the samples

16S rRNA gene Illumina libraries were constructed and sequenced at LGC Genomics (Berlin, Germany, http://www.lgcgroup.com/). DNA extracted from each microcosm was amplified using bacterial 16S rRNA gene primers: 341F (5'-TCC TAC GGG NGG CWG CAG-3') and 785R (5'-GAC TAC HVG GGT ATC TAA KCC-3') (Klindworth et al., 2013). These primers are appropriate for amplifying the V3-V4 hypervariable region, detecting a broad range of bacterial taxa. To study the diversity of both bacteria and archaea, the V5-V6 region should be amplified as it was reported in the previous work of Lopez-Fernandez et al. (2018b). Libraries construction was performed as described in Carlsen et al., (2012). Illumina MiSeq was used to sequence the purified amplicon-barcode-primer complexes. Then, sample-specific barcodes were used for reads demultiplexing and separation.

4.5.3. Bioinformatics and bacterial diversity analyses

After quality controls, paired-end reads were combined and clustered into Operational Taxonomic Units (OTUs, at 97% identity) through the QIIME v. 1.8 pipeline. OTUs were identified using UCLUST (Edgar, 2010) and classified using the SILVA 119 QIIME 16S database (Quast et al., 2013). Finally, clustered and annotated OTUs were analyzed in Explicet 2.10.5 for the stacked bars construction representing triplicates average.

Similarity between taxa identities and their abundances in bentonite microcosms were evaluated using beta-diversity indices by R software. At OTU level, bacterial community composition was analyzed through the use of weighted UniFrac distance

measured in QIIME and PAST3 v. 3.18 and the output visualized with Principal Coordinate Analysis (PCoA). Specific differences in the communities structure were further visualized in a heatmap made using the heatmap.2 function in the R gplots v. 3.0.1.1 package (Warnes et al., 2019) and included only taxa at ≥1% relative abundance in all samples/replicates.

Raw sequences for this study were deposited in the NCBI sequence read archive (SRA) under the accession number PRJNA523116.

4.5.4. Statistical analyses of bacterial diversity

Significant differences in phyla relative abundance ($p < 0.05$) between the different samples were determined using one-way ANOVA test after normalization of all counts. In addition, alpha diversity (Shannon H index) was calculated based on rarefied data to the lowest sample size (6782 counts) and bootstrapped 100 times. Then, one-way ANOVA test, using a significance level of 0.05, was used to look for significant differences in the alpha diversity between the samples.

4.6. Effect of the bentonite bacterial isolates on the chemical speciation of uranium in the presence of G2P

This batch assay consisted in a number of acid-washed glass Erlenmeyer flasks representing different treatments where uranium (1.26 mM), *Amycolatopsis ruanii* (one of the most abundant genera in the studied samples) in addition to bentonite PW indigenous bacterial strains (*Bradyrhizobium-Rhizobium* and *Pseudomonas,* BRP), and G2P (5 mM) as organic phosphate source were combined. Fifteen mL of bentonite-extracted and filtered porewater (PW) were used as incubation medium in all cases. PW plays a major role in buffering the solutions as bentonite does, leading to constant pH in the batch experiment. The bacterial strain *Amycolatopsis ruanii* NCIMB14711 was purchased from NCIMB culture collection (https://www.ncimb.com/) and cultivated as indicated by the provider. Uranium was obtained from the stock solution of uranyl nitrate (0.1 M). The main treatment (T1) included the bacterial strain *A. ruanii*, U, BRP, and G2P. Additional treatments including *A. ruanii*/bacterial consortium and U (T2), *A. ruanii*/bacterial consortium and G2P (T3), and bacterial consortium, U plus G2P (T4)

were also considered to determine the effect of these components. Control treatments only with bacterial consortium and U (T5), *A. ruanii*/bacterial consortium (T6) and bacterial consortium (T7) were included (Table S3). Either *A. ruanii* and G2P-U, nor *A. ruanii* and U controls would provide key information for further interpretation since BRP would be commonly occurring in the natural environment.

In the case of *A. ruanii*, initial biomass concentration was adjusted to 0.5 (optical density at a wavelength of 600 nm) for all *A. ruanii*-containing treatments. Bacterial cells grown to mid-exponential phase in LB medium were washed twice in saline solution and the pellets used for the different treatments. Incubations were always conducted for 48 h under controlled temperature conditions (28 ºC) and continuous shaking (165 rpm) to maintain optimal oxic conditions.

Once incubations were completed, 5 mL from flasks corresponding to treatments including *A. ruanii*/enriched bentonite bacterial consortium were recovered for the phosphatase activity quantification. Additionally, 10 mL from all flasks were centrifuged at 10,000 × g for 10 min at 4 ºC and supernatants were stored at 4 ºC for further determination of the dissolved uranium and inorganic phosphates in solution. Aseptic techniques were followed during assembly and sub-sampling of all treatments. All treatments were conducted in triplicate and all subsequent analyses utilized all replicates data from each respective treatment for statistics.

Determination of the phosphatase activity, dissolved uranium, inorganic phosphates as well as the STEM-HAADF/EDX analyses were performed as described in detail in the supplementary material (S1).

5. RESULTS AND DISCUSSION

5.1. Effect of uranyl nitrate and G2P on the geochemistry and mineralogy of the bentonite samples

Chemical analyses of the bentonite samples prior to incubation (time 0) indicated a composition similar to that of the bentonites from "Serrata de Níjar" zone (Caballero et al., 2005) (Table S1). The dominant oxides were SiO_2 (61.85 ± 3.59%), Al_2O_3 (15.41 ± 1.41%), and F_2O_3 (3.39 ± 0.21%). These results were consistent with those of the

bentonites BI-2 and BI-3 collected from the surface at "El Cortijo de Archidona" deposit (Almeria) during March 2011 (Lopez-Fernandez et al., 2015).

The pH values of the bentonite samples (untreated and treated for 0 and 6 months) determined in 0.01 M $CaCl_2$ solution were alkaline ranging between 7.9 and 9.79 (Table S2). To avoid interferences due to bentonite swelling capacity in the pH measurement, a 15:1 buffer:soil ratio was used. According to Stone et al., (2016), pH measurements are more efficient using $CaCl_2$ than distilled water, since $CaCl_2$ buffer reduce the impact of electrolytes others than H^+ and OH^-. An alkaline pH is expected for the untreated bentonite, due to the buffer capacity of the bentonite itself (Rozalen et al., 2009). As shown in table (S2), after incubation pH values were less alkaline in all treatments in comparison with those of time 0. No significant differences in pH were observed among the several microcosms samples, irrespective of the amendment. The most important change occurs between the sample at time 0 (9.79) and after 6 months (7.9-8.3). Fernandez Díaz (2004) observed the solution pH of "El Cortijo de Archidona" bentonite decreased during incubation experiments (lixiviation). The behavior was attributed to dissolution of calcite in minor amount (approximately 0.6 wt%) and ion exchange reactions between bentonite (Na) and solution (Ca). CO_2 produced during bacterial metabolism might also contribute to pH reduction.

The XRD semi-quantitative estimation of the mineralogical composition of the bentonite sample at time 0 indicated that smectite (montmorillonite) was the dominant mineral phase (91%), beside other minority mineral phases such as quartz (4%), phyllosilicates (2%), and plagioclase (2%) (Fig. 1). In addition to mineral identified by XRD, other bentonite contains minor amount of other minerals as calcite (Fernández Díaz, 2004). After six months of incubation, the mineralogy of treated-bentonites (H, N, U, G, GN and GU) was similar to the original samples, indicating the stability of the bentonite's mineralogy. However, small variations on the intensity of some peaks were probably due to the expected alterations of accompanying minerals. HRTEM results were in agreement with those obtained by XRD, showing that smectites were the dominant phase. Chemical analysis of clay crystals obtained by EDX revealed peaks for Si, Al, Mg, O, Ca, K, and Fe corresponding to the typical elemental composition of montmorillonite (data not shown).

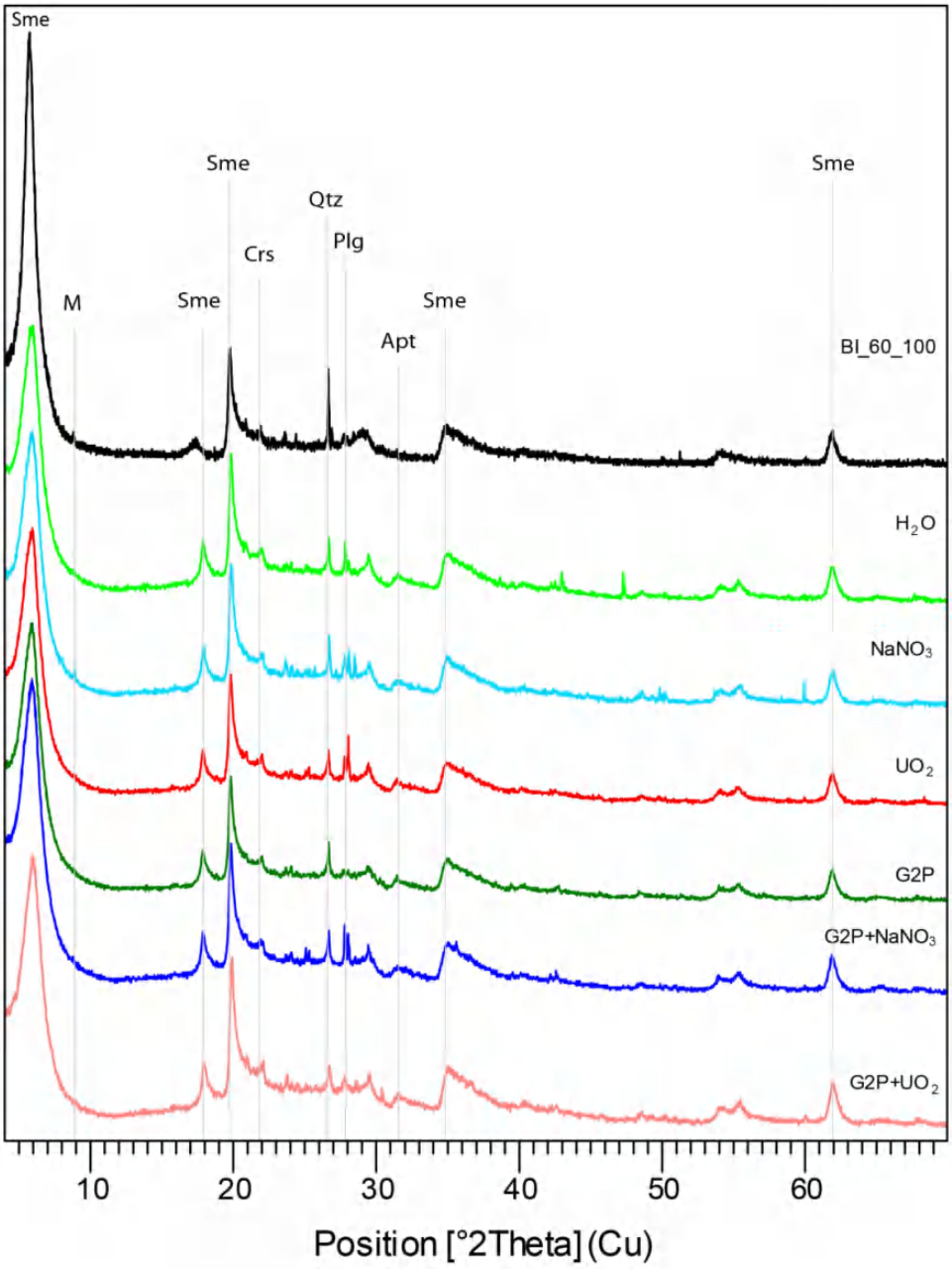

Figure 1. X-ray Diffraction (XRD) patterns of bentonite microcosm samples treated with: distilled water (H_2O), sodium nitrate ($NaNO_3$), uranyl nitrate (UO_2), glycerol-2-phosphate (G2P), glycerol-nitrate (G2P + $NaNO_3$), and glycerol-uranyl-nitrate (G2P + UO_2). Sme: smectite, M: mica, Crs: cristobalite, Qtz: quartz, Plg: plagioclase and Apt, apatite.

XRD and HRTEM analyses showed no illitization process, a transformation of smectite-to-illite resulting in a drop of swelling and adsorption capacity (Dong, 2012). This is important for the correct performance of the bentonite in the DGR because physical and chemical properties must be preserved in long-term disposals. It is crucial that smectites remain chemically stable since structural changes in the bentonite could

result in severe consequences for the safety conditions (Perdrial et al., 2009). However, after six months of incubation a very low alteration of these minerals was observed, probably originated by the interaction between the bentonite and the aqueous solutions resulting in smectite dissolution (Cappelli et al., 2018; Huertas et al., 2001).

EDX analysis revealed the presence of different phases such as amorphous silica (SiO_2) as individual particles and adsorbed on smectite flakes. As expected, evidence of precipitation of cristobalite (polymorph of silica) was found (data not shown). However, Huertas et al. (2001) reported that the dissolution rates would be lower under the repository conditions. Interestingly, a particular mineral structure composed of P, Ca and Cl was found. This composition might be related to calcium phosphate such as apatite (chlorapatite), although no crystalline nature was obtained by performing electron diffraction (Fig. 2). Apatite was also identified in the XRD patterns (Fig. 1).

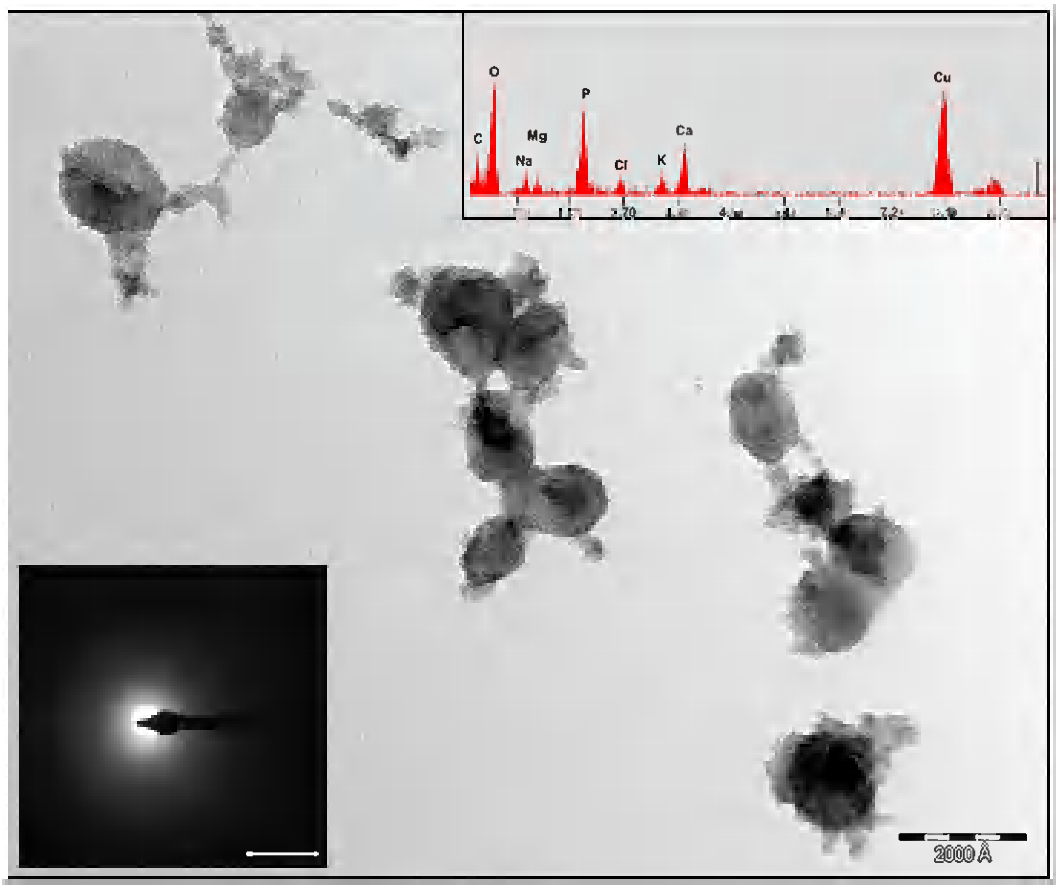

Figure 2. High Resolution Transmission Electron Microscopy (HRTEM) analysis of calcium phosphate particles found in the water-treated microcosms. Energy Dispersive (EDX) spectrum and Selected Area Diffraction Electron (SAED) pattern of one of the particles are included. Bar scale: 0.2 Å.

The presence of apatite in the bentonite could contribute to the uranium removal by a co-precipitation of U(VI) with Ca-P minerals (Shelobolina et al., 2009). Several studies demonstrated the immobilization of U by hydroxyapatite (e.g. Simon et al., 2008). In our study, the use of the state of the art HAADF-STEM technique provided some weak U speciation data in the GU sample due to different factors: such as low concentration of U, incubation time, and type of microcosms, among others. Indeed, U associated with Si from bentonites with some P contributions was observed. In Fig. S2, EDX spectrum (E) and maps (B, C, and D) from the electron-dense deposits (A) showed presence of U, Ca, and P, which could be due to U-P precipitates associated with Ca.

5.2. Bentonite bacterial diversity changes induced by uranyl nitrate and G2P amendments

Total DNA of bentonite microcosms was extracted and sequenced by Illumina approach, giving detailed information about the bacterial diversity of each sample. Two replicates (H3 and G3) were discarded due to their great differences compared to the

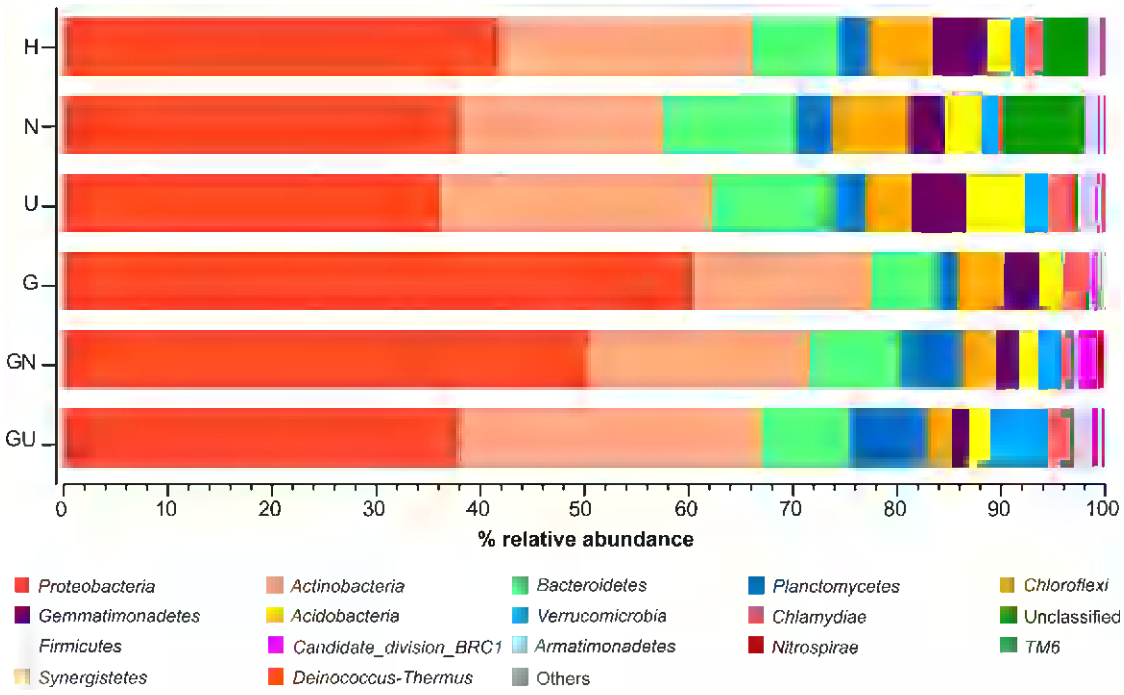

Figure 3. Relative abundances of phyla in all treated bentonite microcosms averaging triplicates (except for H and G which were in duplicates). (H) Distilled water, (N) sodium nitrate, (U) uranyl nitrate, (G) glycerol-2-phosphate (G2P), (GN) G2P and sodium nitrate, and (GU) G2P and uranyl nitrate.

others under exactly the same experimental conditions.

After normalization, a mean of 24,708 sequences per sample was annotated. Rarefaction curves (Fig. S3) and values of Good's coverage (>98% in all cases) indicated that sufficient sequencing depth was obtained to well represent the bacterial community in our study but not enough to adequately detect all phylotypes in the microcosms. Normalization by relative abundance final count values was used instead. This has been described as more accurate than rarefying (McMurdie and Holmes, 2013). A number of 4,952 OTUs were classified into phylum (94% of phylotypes), class (86% of phylotypes), order (71% of phylotypes), family (54% phylotypes) and genus (34% phylotypes) levels.

The obtained OTUs were taxonomically related to 29 different bacterial phyla including Actinobacteria, Bacteroidetes, Chloroflexi, Gemmatimonadetes, Planctomycetes, Proteobacteria, Verrucomicrobia, and Candidate Divisions (BRC1, TM7, TM6, OD1, and TA06) (Fig. 3). In all microcosms, the bacterial diversity was

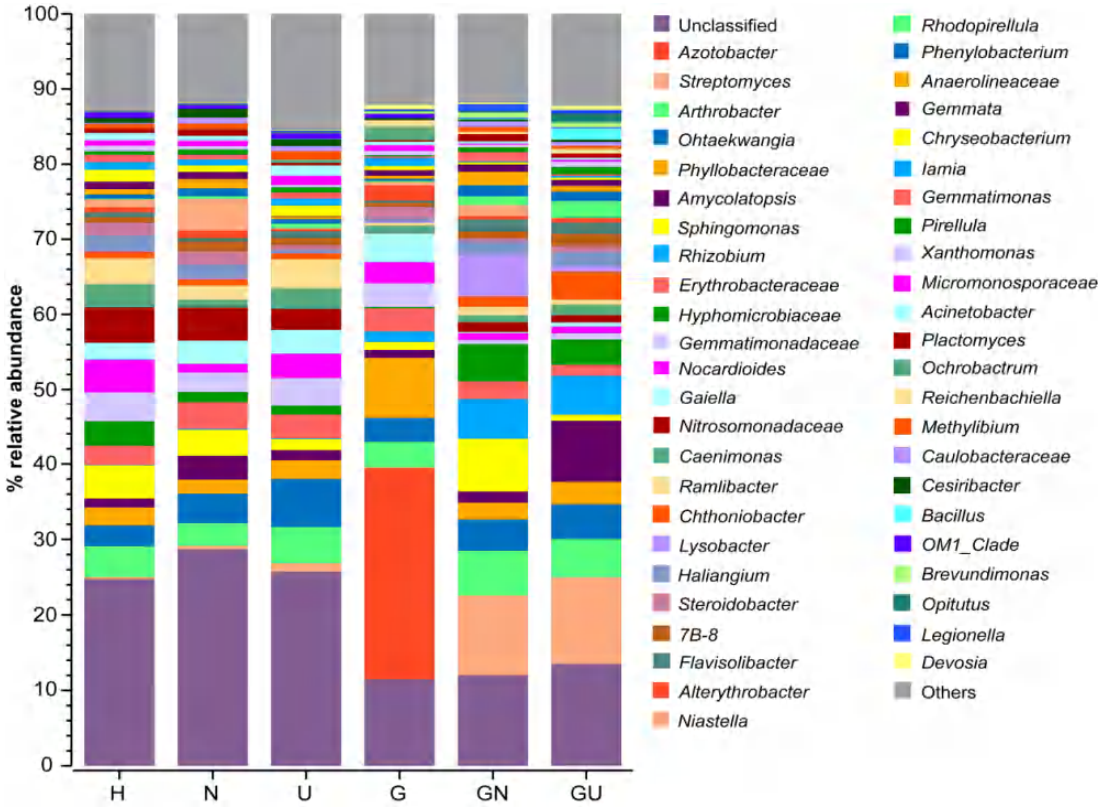

Figure 4. Structure of the bacterial community of the treated bentonite microcosms at genus level represented only by dominant OTUs with > 0.3 % of relative abundance and averaging triplicates (except for H and G which were in duplicates).

dominated by Proteobacteria (mainly Gamma-, Alpha-, and Deltaproteobacteria) and Actinobacteria representing both together 58-78% of the population (Fig. 3). For more details about bacterial diversity at class level, refer to the Supplementary material S3, Fig. S4, and Supplementary Table 5. At genus level in all microcosms, identification of bacterial groups revealed the presence of 558 genera, being *Azotobacter* (7.8%) the most abundant genus followed by *Streptomyces* (5.8%), *Arthrobacter* (4.6%), *Ohtaekwangia* (4.2%), and *Amycolatopsis* (3.41%) (Fig. 4). *Azotobacter* was only detected in G microcosms where it accounted for 40% of the population, probably due to the capacity of some *Azotobacter* spp. to use glycerol as a carbon source for their growth only under nitrogen-free conditions (Yoneyama et al., 2015).

In general, G microcosms revealed a different bacterial community composition. Based on the Shannon index (Fig. 5) and other diversity indices (data not shown), the

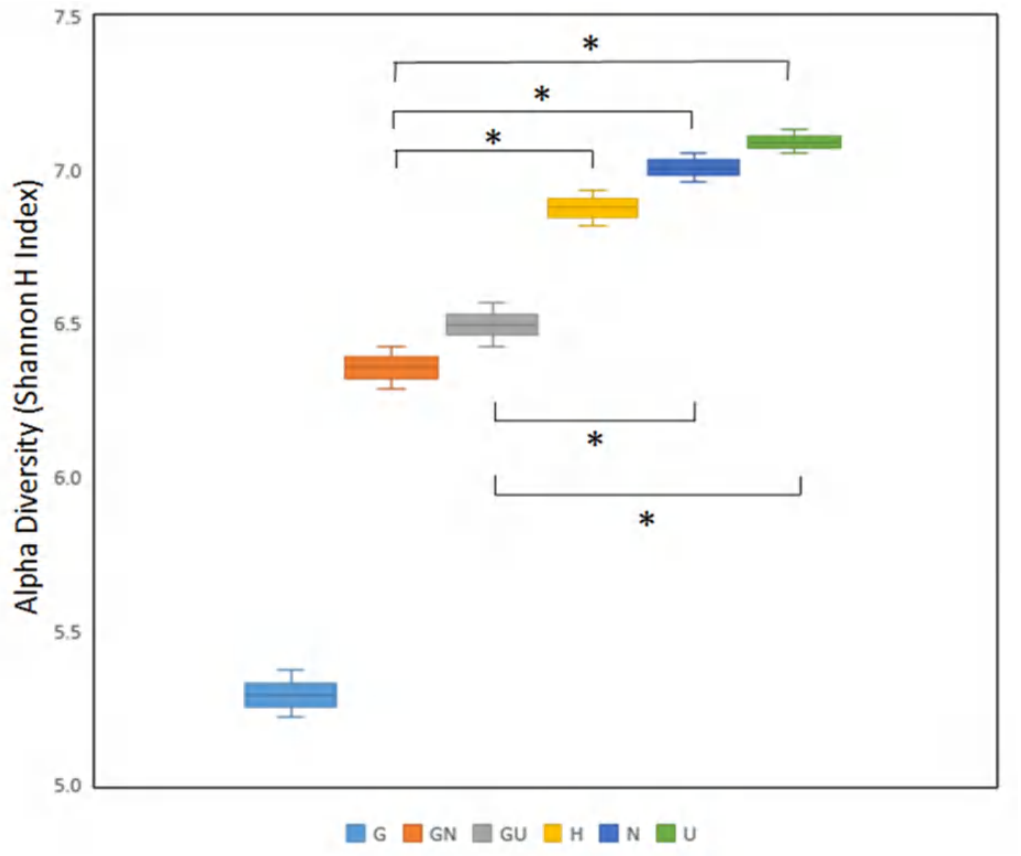

Figure 5. Alpha diversity plot showing Shannon H values based on all OTUs obtained for the different treated microcosm samples averaging triplicates (n=3 per treatment), the vertical bars represents standard errors. Values marked with a star represent the statistically different Shannon H alpha diversities between the samples. One-way ANOVA test ($p<0.05$, n=3 per treatment) was used. (H) Distilled water, (N) sodium nitrate, (U) uranyl nitrate, (G) G2P, (GN), G2P and sodium nitrate, and (GU) G2P and uranyl nitrate.

structure of bacterial populations of G microcosms was also different to that of the other studied microcosms. Comparing the effect of G2P and U treatments, the relative abundance at genus level throughout the sample sets demonstrated significant variations as shown in the heatmap plot (Fig. 6). G microcosms were clearly different from the rest of the treatments, which were divided into two clusters: G2P-treated microcosms (GN1, GN2, GN3, GU1, GU2, and GU3) and non-G2P-treated microcosms (H1, H2, N1, N2, N3, U1, U2, and U3). The PCoA of the relative abundance at genus level showed a clear separation between different treatments (Fig. 7), supporting the results obtained by the heatmap.

If considering only the non-G2P-treated microcosms [water-treated (H), nitrate-treated (N) and uranium-treated (U) microcosms], these were mainly dominated by Proteobacteria with an average of 39, 38 and 36% in H-, N- and U-treated microcosms, respectively (Fig. 3), being Alphaproteobacteria (≈ 20%) and Betaproteobacteria (≈ 12%) the most abundant classes. However, according to Lopez-Fernandez et al. (2018) the bacterial community in superficial Spanish bentonites was dominated by Firmicutes (70%) in the H, N and U treatments. The difference in the results obtained here may be explained by the fact that despite of being similar bentonite from "El Cortijo de Archidona", the bacterial diversity could be influenced by sampling characteristics such as depth and zone, and in fact the samples analyzed in this study were collected from 80 cm depth. Actinobacteria was the second more abundant phylum (23, 19, and 26%), followed by Bacteroidetes (8, 13, and 12%), Chloroflexi (6, 7, and 4%), Gemmatimonadetes (≈ 5%), and Acidobacteria (2, 3, and 6%). The phylum Bacteroidetes, whose members are nitrate reducers, was increased by the addition of sodium nitrate similarly to what occurred in a uranium mining waste soil sample (Geissler and Selenska-Pobell, 2005). At genus level, *Ohtaekwangia* (2.4, 3.9, and 6.4%), *Arthrobacter* (4.5, 3, and 4.8%), *Sphingomonas* (4.8, 3.4, and 1.5%), *Ramlibacter* (3.1, 1.9, and 3.9%), unclassified *Nitrosomonadaceae* (4.8, 4.4, and 2.8%), *Gemmatimonadaceae* (4, 2.6, and 3.8%) and *Erythrobacteraceae* (≈ 3% in all three microcosms) were the most abundant genera in H, N and U microcosms, respectively (Fig. 4). Interestingly, *Arthrobacter* was slightly increased in U-treated microcosms, demonstrating a possible uranium tolerance capacity.

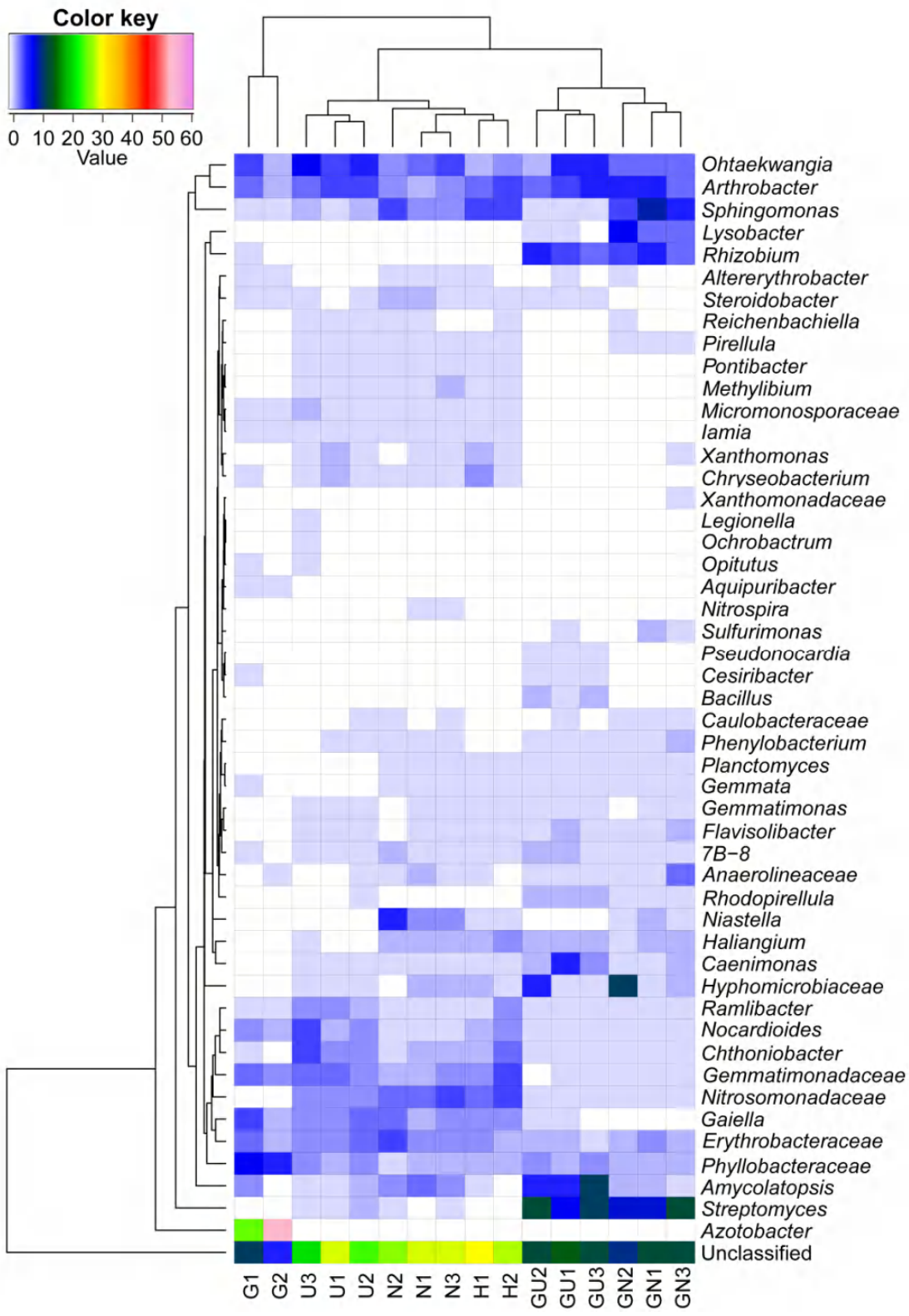

Figure 6. Heatmap based on the relative abundance of the genera with an average abundance of 1 % in bentonite microcosm samples showing triplicates (except in H and G with duplicates). The relative abundance of each genus was shown by different colors.

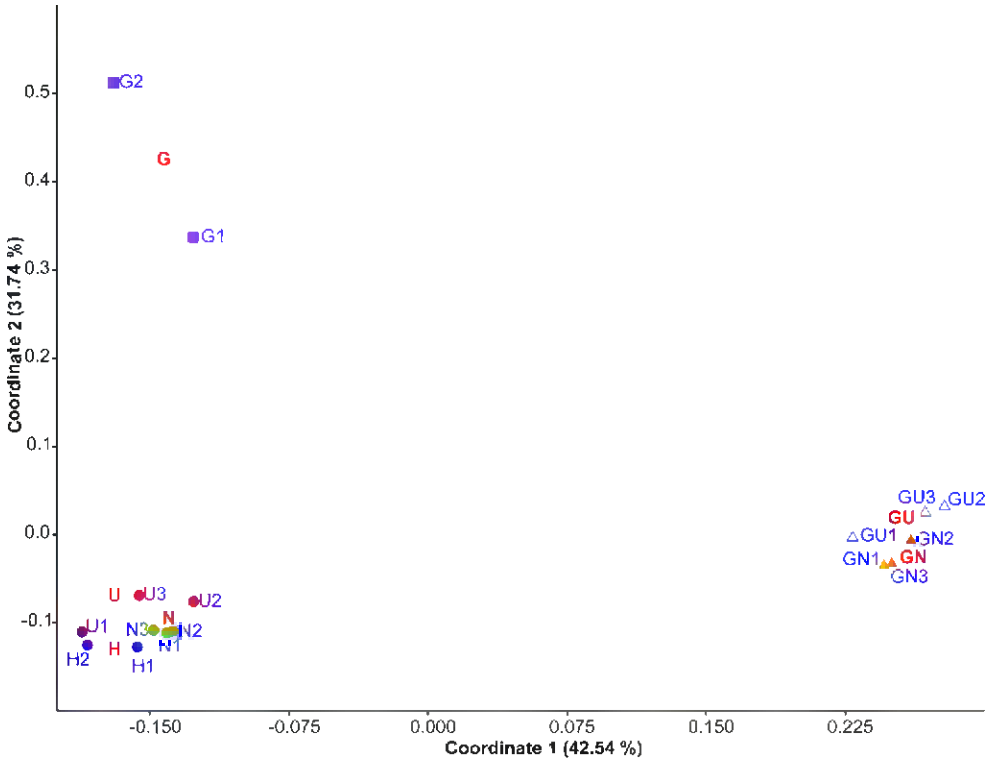

Figure 7. Principal component analysis (PCoA) plot comparing the bacterial community structure at genus level of the different treated samples showing triplicates (except in H and G with duplicates). The percentage of variation explained by Coordinate 1 and Coordinate 2 are indicated in the axis.

Concerning all G2P-treated microcosms [G2P (G), G2P/sodium nitrate (GN), and G2P/uranyl nitrate (GU) treatments], the highest bacterial diversity was shown in GN- and GU-microcosms in comparison with all studied microcosms, according to the assessment by Shannon index (H), while the lowest was that of G treatment (Fig. 5). This high bacterial diversity might probably be due to their amendments with more than two chemical compounds: G2P and nitrates (for GN); and G2P, nitrates, and U (for GU). Here, the bacterial diversity was dominated by Proteobacteria (63, 50.5, and 38.2% in G, GN, and GU, respectively), enhanced by the presence of G2P (except in co-existence with uranium), being Alphaproteobacteria (17, 32 and 25%, respectively) and Gammaproteobacteria (44, 9 and 5%, respectively) the most abundant classes. *Azotobacter* was the principal contributor to the relative abundance of Gammaproteobacteria in G samples. The second most abundant phylum was Actinobacteria accounting for 16.8, 21.3, and 28.8% of G, GN and GU bacterial communities, followed by Bacteroidetes (6.1, 8.8 and 8.6%), Planctomycetes (1.7, 5.6, and 7.4%) and Chloroflexi (4.0, 3.3, and 2.3%) (Fig. 4). The most abundant genera were *Streptomyces* (0.2, 10.6, and 11.5%), *Arthrobacter* (3, 6, and 5%), *Amycolatopsis* (1.5,

1.5, and 8%), *Rhizobium* (0.7, 5.4, and 5.3%), *Sphingomonas* (0.9, 7, and 0.8%), and unclassified genera related to the families *Phyllobacteraceae* (6.7, 2.2, and 3%), *Hyphomicrobiaceae* (0.3, 5, and 3.4%) and *Erythrobacteraceae* (3, 2.3, and 1.4%) (Fig. 4). *Rhizobium* species, which are known for their capacity to reduce nitrate and to use glycerol as a carbon source (Spain and Krumholz, 2012), showed to be significantly abundant in microcosms that contain both sodium or uranyl nitrate and G2P, according to the One-Way ANOVA ($p < 0.05$) test.

5.3. Impact of bacterial diversity changes on the biogeochemical processes under DGR concept

To highlight the effects of G2P, uranium and nitrate amendments on the bentonite bacterial community, One-Way ANOVA ($p \leq 0.01$, n=3 except n=2 for G and H) statistical analysis was performed. Comparing all treatments together, significant differences in the OTU abundance at phylum level were found only for Candidate division BRC1, Fusobacteria, Nitrospirae, Planctomycetes, Proteobacteria, and Verrucomicrobia (Supplementary Table 1). At genus level, significant differences in the relative abundance ($p \leq 0.005$) were obtained for genera like *Azotobacter*, *Streptomyces*, *Phyllobacteraceae*, *Sphingomonas*, *Rhizobium*, *Lysobacter*, *Flavisolibacter*, and *Brevundimonas* (Supplementary Table 2).

5.3.1. Effect of nitrate amendment on the bentonite bacterial diversity

In order to determine the effect of nitrate on the structure and composition of the bacterial community, N-treated (N) and G2P-N-treated (GN) microcosms were compared with their respective controls (H and G microcosms). Nitrate can occur in the DGR during the repository construction as a consequence of the blasting activity, which lead to the accumulation of nitrates on rock surfaces and in the groundwater (Kutvonen et al., 2015). It is well known that nitrates, and other N compounds, enhance the activity of microbes involved in the biogeochemical cycle of N, which in turn may affect the corrosion of the containers and the consequent radionuclide mobilization (Kutvonen et al., 2015). Nitrates may enhance the diversity and activity of nitrate reducing bacteria, which essentially form N_2 or denitrification intermediates depending on the pH of the

medium (concrete or clay-rich rock) and the type of microbial strains present in the environment (Ollivier et al., 2011).

The results obtained in this work indicated that the addition of nitrate to the studied microcosms led to the enrichment of bacteria involved in the biogeochemical cycle of nitrogen (e.g. nitrate reducing, nitrogen fixing bacteria). Thus, comparing both G2P-nitrate and G2P-treated samples, the statistical analysis showed that the presence of organisms such as *Streptomyces*, *Sphingomonas*, *Rhizobium*, *Flavisolibacter*, *Niastella*, *Planctomyces*, *Nitrospira,* and *Bradyrhizobium*, which are commonly identified within nitrate reducing bacteria, was more significant ($p \leq 0.015$) in GN microcosms (Supplementary Table 3). *Niastella* accounted for 4.2% in N-microcosms and it was statistically more abundant in the GN sample than in H controls (1.2%). *Niastella* and *Flavisolibacter*, members of the *Chitinophagaceae* family, have been reported to play a major role in denitrification processes generating N_2 (Lai et al., 2016; Nishizawa et al., 2014). The released N_2, in turn, can be used by *Rhizobium* and *Bradyrhizobium* to produce ammonium (Safonov et al., 2018; Zahran, 1999). Hence, Safonov et al. (2018) found that some *Rhizobium* strains were able to reduce nitrates to nitrite and/or nitrogen. Some *Nitrospira* spp., in addition to being a nitrite-oxidizing bacteria, have the capacity to reduce nitrate coupled with H_2 oxidation, as it was previously reported for *N. moscoviensis* (Koch et al., 2015).

The enrichment of nitrogen fixing-bacteria within the phyla Armatimonadetes, Verrumicrobia, Planctomycetes, and Nitrospirae, was mainly detected in nitrate treated microcosms (N and GN samples in comparison to their respective controls) (Fig. 3). The relative abundance of Armatimonadetes in N samples was significantly higher than in H microcosms (Supplementary Table 4). These organisms have been shown to have a prevalence under carbon and nitrogen free conditions, which indicates a N_2 fixing capacity (Tamez-Guerra et al., 2017). Verrucomicrobia, Planctomycetes, and Nitrospirae (highly represented by *Nitrospira*, a nitrite-oxidizing bacteria) were highly enriched in GN in comparison with G samples. Members of both Verrucomicrobia and Planctomycetes have been described to be capable of fixing nitrogen (Chiang et al., 2018; Delmont et al., 2018).

The presence of nitrate reducing bacteria seems to have a high relevance since there is no net U(VI) reduction until nitrate is completely reduced. Nitrate serves as a

competing and thermodynamically more suitable electron acceptor for metal-reducing bacteria in nitrate-metal co-contaminated environments (Safonov et al., 2018; Spain and Krumholz, 2012). Once nitrate is depleted, U(VI) and Fe(III) are reduced simultaneously (Finneran et al., 2002).

5.3.2. Effect of G2P amendment on the bentonite bacterial diversity

The G2P amendment to the microcosms resulted in significant changes in the indigenous bacterial communities (Fig. 3 and 4). Significant differences ($p < 0.025$) in the relative abundance between G and H microcosms were found, being Proteobacteria and Armatimonadetes more abundant in G microcosms than in H controls; whilst Verrucomicrobia showed lower abundance in G samples. In addition, the statistical analysis ($p \leq 0.025$) of G2P-nitrate (GN) and nitrate (N) microcosms showed that Actinobacteria, Planctomycetes, Verrucomicrobia, Chlamydiae, and Nitrospirae were significantly more abundant in presence of G2P (Supplementary Table 4).

Within the 155 genera analyzed by the ANOVA test ($p < 0.05$; n=2), 25 of them such as *Azotobacter*, *Glycomyces*, *Nocardioides*, *Gaiella*, and unclassified genera affiliated to *Phyllobacteraceae*, and *Erythrobacteraceae* were significantly enhanced in G microcosms in comparison with the controls (H). In contrast, *Pontibacter, Pautilibacter*, and *Acidiferrobacter*, among others, showed a lower abundance in G than in H microcosms (Supplementary Table 3). The significantly higher (ANOVA test, $p < 0.05$; n=3) abundance of *Streptomyces*, *Arthrobacter*, *Rhizobium*, *Phenylobacterium, Planctomyces*, and *Brevundimonas*, among others, in GN and GU microcosms in comparison with their controls (N, and U, respectively) may be due to the ability of these enriched genera to use G2P as carbon and phosphorus sources. Actually, glycerol is one of the best carbon sources used by *Streptomyces* spp. for growth and antibiotic production (Lee et al., 2017). In addition, *Arthrobacter* cells are able to grow on glycerol through the activity of glycerol kinase (*GlpK*) and glycerol-3-phosphate dehydrogenase (*GlpD*), producing dihydroxyacetone phosphate that enters glycolysis cycle, leading to the formation of pyruvate (Husserl et al., 2012; Niewerth et al., 2012). Then, pyruvate can be fermented to several end products (e.g. lactate and acetate) by different fermentation routes, which stimulate the growth of iron-reducing and sulfate-reducing bacteria (Bengtsson and Pedersen, 2017; Kostka et al., 2002). These bacterial groups play a major role in the biogeochemical cycle of S, Fe and U (Barton et al.,

2015; Rickard, 2012), which could affect the stability of bentonites and other DGR components. In addition, genera such as *Sphingomonas*, *Nitrospira*, and *Bradyrhizobium* were significantly ($p \leq 0.001$) more representative in GN than in N microcosms, and *Amycolatopsis*, *Xanthomonas*, *Bacillus*, and *Opitutus* were significantly ($p < 0.02$) more abundant in GU than in U microcosms. The difference in the relative abundance of *Amycolatopsis* and *Bacillus* could be explained by their ability to degrade G2P through their phosphatase activity releasing orthophosphates needed for the biomineralization of such radionuclide (Merroun et al. 2011; Zucchi et al., 2012).

5.3.3. Effect of uranium on the bentonite bacterial diversity

According to ANOVA ($p<0.05$, n=3 per treatment), significant differences on the structure and composition of the microbial populations of the U amended microcosms were observed. For instance, Chlamydiae phylum was statistically more abundant in uranyl nitrate microcosms (U) than in nitrate controls (N) (Supplementary Table 4). Verrucomicrobia showed higher relative abundance in G2P-uranyl-nitrate microcosms (GU) than in G2P-nitrate controls (GN). It is well known that *Verrucomicrobia and Chlamydia* belong to *Planctomycetes-Verrucomicrobia-Chlamydia* super-phylum, which was described to be present in potentially-toxic metal polluted soils (Hemmat-Jou et al., 2018). According to Li et al., (2018), Chlamydiae was enriched from 4.8 to 17.1% in groundwater contaminated with U(VI), where bioreduction of this radionuclide to U(IV) and its subsequent immobilization were stimulated by intermittent ethanol injections as an electron donor. Moreover, uranium positively influenced the presence of *Chlamydia* in U contaminated stream water located in the Department of Energy reservation in Oak Ridge, at concentrations ranging between 175 and 268.4 mg/L (Vishnivetskaya et al., 2011).

In contrast, the presence of U in the studied bentonite microcosms negatively affected the presence of some specific phyla. Particularly, Nitrospirae and Candidate division BRC1 were significantly more abundant ($p < 0.05$) in GN than in GU microcosms (Supplementary Table 4). These phyla are probably more sensitive to the toxic effect of uranium than others.

In the case of genera enriched in presence of U, the statistical analysis of ANOVA ($p < 0.05$, n=3 per treatment) revealed that *Colwellia*, *Noviherbaspirillum*, *Burkholderia*,

Nitriliruptor, *Rhodoplanes*, *Desulfonauticus,* and *Desulfomicrobium* were more abundant in the U compared to the N microcosms (Supplementary Table 3). Several *Burkholderia* spp. were isolated from uranium contaminated environments exhibiting high tolerance to this radionuclide (Pathak et al., 2017). In fact, *B. arbores* was shown to display phosphatase activity in presence of uranyl-carbonate under acidic and alkaline conditions leading to the immobilization of U through the formation of U phosphates (Acharya, 2015). The sulfate reducing *Desulfomicrobium* was also reported to immobilize U(VI) via enzymatic reduction to insoluble U(IV) species (Converse et al., 2013). While *Colwellia* was enhanced in U-contaminated sediments due to the amendment with acetate (Xu et al., 2017), *Rhodoplanes* was actually found in a uranium mining-impacted wetland (Wang et al., 2014).

Among the 155 genera analyzed by ANOVA ($p < 0.05$, n=3 per treatment), 20 of them such as *Amycolatopsis*, *Chthoniobacter, Xanthomonas, Bacillus, Opitutus,* and *Devosia*, among others, were significantly more abundant in GU microcosms than in GN controls (Supplementary Table 3). *Xanthomonas* was stimulated by the presence of high uranium concentrations in a U contaminated groundwater (Cho et al., 2012). The enrichment of genera like *Bacillus* was not surprising since strains of this genus were reported to affect the biogeochemical cycle of U interacting through different mechanisms that include biosorption, bioaccumulation or biomineralization (Merroun et al., 2011; Merroun and Selenska-Pobell, 2008). In addition, uranium was found to be immobilized by intracellular polyphosphate bodies formed by microorganisms such as *Bacillus* (Zhao et al., 2016). Accordingly, *B. mucilaginosus* and *B. sphaericus* JG-7B were described to precipitate U as U phosphate mineral phases (Huang et al., 2017, Merroun et al. 2011). Moreover, it has been previously demonstrated that *Bacillus* sp. BII-C3, a strain isolated from Spanish microcosms treated with uranyl nitrate, was able to extracellularly precipitate U-phosphate minerals (Lopez-Fernandez et al., 2018b).

In GU microcosms, *Amycolatopsis* was highly enriched in comparison with the controls. These microorganisms were reported to efficiently interact with uranium through biosorption at their cell surface (Celik et al., 2018). Another likely known mechanism to cope with the toxicity of U is through biomineralization, based on the phosphatase activity that is induced by the presence of G2P as organic phosphate source. Interestingly, phosphatase activity was previously described for members of *Amycolatopsis* (Camas et al., 2013; Zucchi et al., 2012).

5.4. Impact of enriched bentonite bacterial isolates on the biogeochemical cycle of U in presence of G2P

Sequences corresponding to the genus *Amycolatopsis* were significantly enriched in the microcosms treated with uranium and G2P, as shown above (Fig. 4). In the present study, we conducted experiments to evaluate the U biomineralization potential of a consortium using G2P. The consortium consisted of *A. ruanii* NCIMB14711 and two indigenous bacterial strains (*Bradyrhizobium-Rhizobium* and *Pseudomonas*) from bentonite PW. In order to imitate environmental conditions, we used bentonite extracted PW as background culture medium. Culture dependent and molecular techniques revealed the presence of *Bradyrhizobium-Rhizobium* and *Pseudomonas* (referred to hereafter as BRP) as the main components of the bentonite PW. For clarification, the BRP will be omitted from the text and will be integrated in the concept of PW since this consortium is PW naturally occurring microbes. We quantified the effect of the different treatments on the i) amounts of inorganic phosphate (P_i) released as results of degradation of G2P; ii) phosphatase activity and iii) U removal rates. In addition, STEM-HAADF and EDX analyses were applied to investigate the cellular localization of U accumulates and to identify their chemical composition.

The amounts (in mg/L) of P_i released in solution by the cell biomass of the different treatments are presented in Figure S3. T3 presented the highest concentrations of P_i in solution (100.54 mg/L), 4 to 10 fold increase than those of other treatments (T1, T2 and T4) where the P_i concentration ranged between 6 and 27 mg/L. The low P_i levels in the latter samples were likely due to the U since this radionuclide form insoluble complexes with Pi leading to its removal from the solution (no U is available in T3). The control samples (T5, T6 and T7) exhibited background levels of P_i. The high P_i levels in T3 were associated with high phosphatase activity expressed by the bacterial cells (Fig. S5). Moderate phosphatase activity was exhibited by the bacterial cells in presence of U (T2) and U plus G2P (T1) (Fig. S6). Presence of Pi in treatments where G2P was not amended (T2 and T6) might be explained by the release of this phosphorus by *A. ruanii* cells from lysed dead cells. Regarding U removal, maximum values (88%) were obtained when *A. ruanii* and BRP were incubated in PW with presence of G2P (Fig. S7). However, this effect should be attributed mainly to BRP, since the values of U precipitation in the control treatments (in the absence of *A. ruanii*) were 83 and 67%.

The U immobilization potential of *A. ruanii* and the BRP consortium was estimated by the use of a combination of STEM-HAADF and EDX analysis. In addition, the effect of G2P on this process was also studied. TEM micrographs of thin sections of cells treated with U without/with G2P are presented in Figs. 8 and 9. The cellular localization of U accumulates was affected by G2P. While electron-dense precipitates were both observed at the cell surface and extracellularly in T2 (Fig. 8A and 9A), and they were composed of U and P as the EDX element-distribution maps revealed (Fig 8B, 8C, 8D). G2P amended samples (T1) showed similar precipitates but also exhibited intracellular amorphous needle-like fibrils deposits (Fig. 9E). EDX element-distribution maps revealed that in both cases, the U deposits located at the cell walls as well as in the intracellular and extracellular spaces presented U and P signals (Fig. 9B, 9C, 9D, 9F, 9G and 9H). In the case of T2, P could come from cell death releasing phosphorylated cell components which could be used for phosphatases to

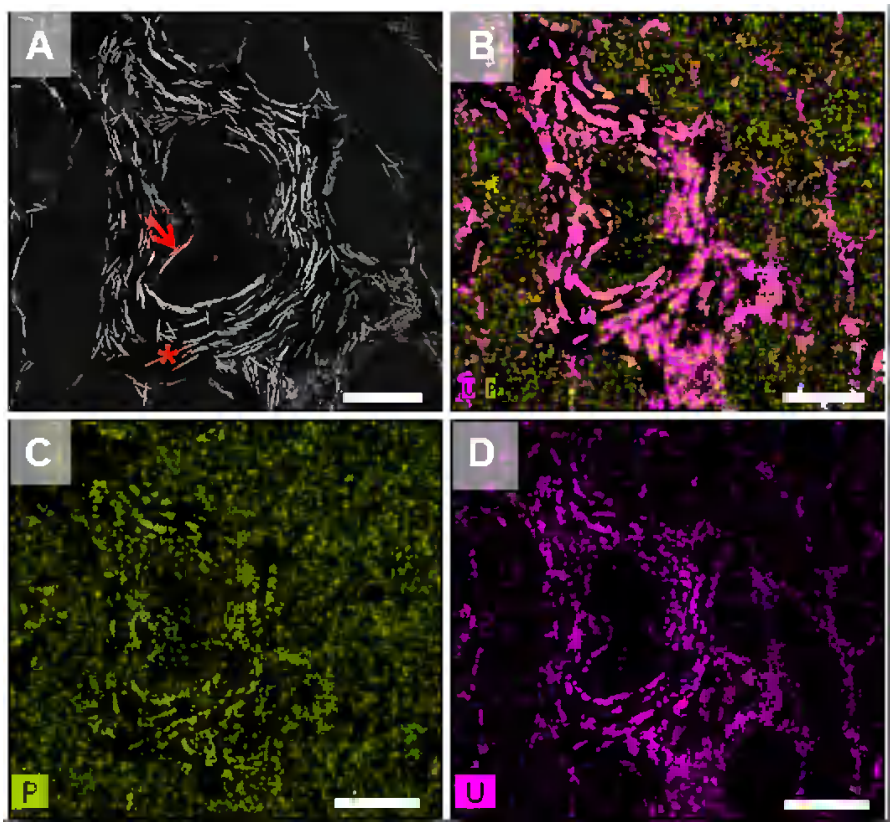

Figure 8. Scanning Transmission Electron Microscopy-High-Angle Annular Dark-Field imaging (STEM-HAADF) micrographs of thin sections of *Amycolatopsis ruanii*/ bacterial consortium (*Bradyrhizobium-Rhizobium* and *Pseudomonas*, BRP) cells treated with uranium (A) and the corresponding EDX maps showing the distribution of P (C), U (D), and P + U (B). Extracellular U-P precipitates (asterisk) and deposits located at the cell walls (arrow) were shown (A). Bar scale: 500 nm.

precipitate U. Maybe due to the low concentration of organic phosphates in T2, intracellular U-P precipitates could not be formed as in T1 where high concentration of G2P was added.

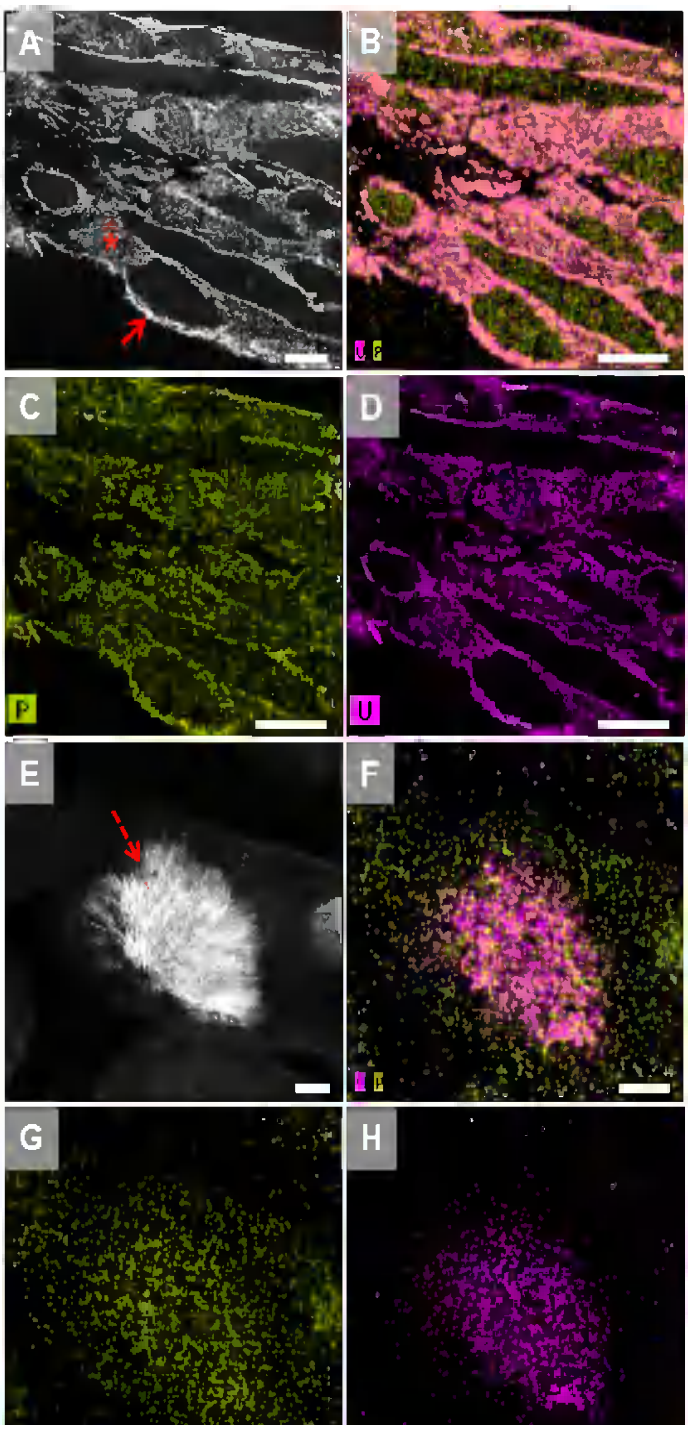

Figure 9. Scanning Transmission Electron Microscopy-High-Angle Annular Dark-Field imaging (STEM-HAADF) micrographs of thin sections of *Amycolatopsis ruanii*/ bacterial consortium (*Bradyrhizobium-Rhizobium* and *Pseudomonas*, BRP) cells treated with uranium and glycerol-2-phosphate (G2P) showing U-P deposits at cell wall level (arrow), extra- (asterisk) and intracellular (dashed arrow) uranium phosphates precipitates (A and E), and their corresponding EDX maps with the distribution of P (C and G), U (D and H), and P + U (B and F). Bar scale: 500 nm (A); 800 nm (B-D); 100 nm (E-H).

These results agree with those showing high U removal capacity of about 83-88%, as it was shown above (Fig. S7). Moreover, significant phosphatase activity was observed in both samples (Fig. S6), releasing P_i and precipitating this radionuclide as U phosphate mineral phases (Fig. S5). The intracellular U deposits observed in the sample treated with G2P could be due to the ability of the cells to uptake G2P degrading it through the phosphatase activity and releasing inorganic phosphates. This leads to the biomineralization of U phosphates intracellularly, which was not observed in cells where G2P was absent. Many bacterial isolates interacting with U and G2P were described by their ability to use glycerol as organic carbon source (Zhao et al., 2016; Huang et al., 2017, Merroun et al. 2011). Several works described the ability of *Pseudomonas* and *Amycolotopsis* to interact with uranium. For example, Celik et al., (2018) reported the ability of *Amycolatopsis* sp. K47 to sorb U at the cell surface, while *Pseudomonas* spp. were demonstrated to precipitate U as U phosphates, as a result of their phosphatase activity (Choudhary and Sar, 2011).

6. ENVIRONMENTAL IMPLICATIONS

The Deep Geological Repository is a promising multi-barrier system for the management and storage of high-level radioactive wastes. Bentonite, as part of the DGR engineered-barrier, might play a relevant role in the retention of radionuclides in case of a metal containers damage. Thus, it is important that bentonite maintains its physicochemical and mineralogical properties, which could be affected by bentonite microbial processes. In the present work, we described the bentonite bacterial shifts that occurred by the addition of uranyl nitrate and G2P, an organic phosphate source known to enhance the enrichment of microorganisms with U(VI) biomineralization potential. No significant changes in the mineralogy of the bentonite were observed indicating the high stability of these clays; even with the changes occurred in the structure and composition of the bacterial populations. Amendments with uranyl nitrate and G2P induced bacterial diversity changes with enrichment of bacteria involved in the biogeochemical cycle of U and N. Denitrifiers (*Niastella*, *Nitrospira*) and N_2-fixing bacteria (*Azotobacter*, *Streptomyces*, *Rhizobium*, and *Bradyrhizobium*) were enriched in the nitrate-amended bentonite. In presence of uranium and G2P, the relative abundance

of bacteria with U immobilization potential, through reduction (e.g. *Desulfomicrobium*) or biomineralization (*Burkholderia, Bacillus, Amycolatopsis,* etc.), has been increased.

The biomineralization potential of *A. ruanii* and the bentonite natural consortium formed by *Bradyrhizobium-Rhizobium-Pseudomonas* was demonstrated using STEM-HAADF analyses. Phosphatase activity on G2P leads to orthophosphate release for the precipitation of stable insoluble U phosphates. The results presented here may have several implications for the long-term disposal of radioactive wastes in the DGR. Microorganisms from bentonite could precipitate uranium phosphate phases, being more resistant to oxidative remobilization, and having the potential for preventing the transport and mobilization of U from the canisters in case of a leakage of this radionuclide.

7. ACKNOWLEDGEMENTS

We acknowledge the assistance of María del Mar Abad Ortega, and Concepción Hernández-Castillo (Microscopy Service, Centro de Instrumentación Científica, University of Granada, Spain).

8. FUNDINGS SOURCES

This work was funded by the ERDF-financed Grant CGL2014-59616-R (80% funding by FEDER), (Ministerio de Ciencia e Innovación, España) as well as by an FPU 14/04263 ("Formación de Profesorado Universitario") grant to the first author from the Spanish Ministry (Ministerio de Educación Cultura y Deporte, MECD).

9. REFERENCES

Acharya, C., 2015. Microbial bioremediation of Uranium: an overview. BARC Newsletter 27–30.

Anderson, C., Johnsson, A., Moll, H., Pedersen, K., 2011. Radionuclide geomicrobiology of the deep biosphere. Geomicrobiology Journal 28, 540–561. https://doi.org/10.1080/01490451.2010.507644

Barton, L.L., Tomei-Torres, F.A., Xu, H., Zocco, T., 2015. Metabolism of metals and metalloids by the sulfate-reducing bacteria, in: Saffarini, D. (Ed.), Bacteria-metal interactions. Springer International Publishing, Cham, pp. 57–83. https://doi.org/10.1007/978-3-319-18570-5_4

Beazley, M.J., Martinez, R.J., Webb, S.M., Sobecky, P.A., Taillefert, M., 2011. The effect of pH and natural microbial phosphatase activity on the speciation of uranium in subsurface soils. Geochimica et Cosmochimica Acta 75, 5648–5663. https://doi.org/10.1016/j.gca.2011.07.006

Bengtsson, A., Pedersen, K., 2017. Microbial sulphide-producing activity in water saturated Wyoming MX-80, Asha and Calcigel bentonites at wet densities from 1500 to 2000 kg m^{-3}. Applied Clay Science 137, 203–212. https://doi.org/10.1016/j.clay.2016.12.024

Brookshaw, D.R., Pattrick, R.A.D., Lloyd, J.R., Vaughan, D.J., 2012. Microbial effects on mineral–radionuclide interactions and radionuclide solid-phase capture processes. Mineralogical Magazine 76, 777–806. https://doi.org/10.1180/minmag.2012.076.3.25

Caballero, E., Cisneros, C.J. de, Huertas, F.J., Huertas, F., Pozzuoli, A., Linares, J., 2005. Bentonites from Cabo de Gata, Almería, Spain: a mineralogical and geochemical overview. Clay Minerals 40, 463–480. https://doi.org/10.1180/0009855054040184

Camas, M., Sahin, N., Sazak, A., Spröer, C., Klenk, H.-P., 2013. *Amycolatopsis magusensis* sp. nov., isolated from soil. Int. J. Syst. Evol. Microbiol. 63, 1254–1260. https://doi.org/10.1099/ijs.0.042770-0

Cappelli, C., Yokoyama, S., Cama, J., Huertas, F.J., 2018. Montmorillonite dissolution kinetics: Experimental and reactive transport modeling interpretation. Geochimica et Cosmochimica Acta 227, 96–122. https://doi.org/10.1016/j.gca.2018.01.039

Carlsen, T., Aas, A.B., Lindner, D., Vrålstad, T., Schumacher, T., Kauserud, H., 2012. Don't make a mistake: is tag switching an overlooked source of error in amplicon pyrosequencing studies? Fungal Ecology 5, 747–749. https://doi.org/10.1016/j.funeco.2012.06.003

Celik, F., Camas, M., Kyeremeh, K., Sazak Camas, A., 2018. Microbial sorption of uranium using *Amycolatopsis* sp. K47 isolated from uranium deposits. Water Air Soil Pollut 229, 112. https://doi.org/10.1007/s11270-018-3766-5

Chiang, E., Schmidt, M.L., Berry, M.A., Biddanda, B.A., Burtner, A., Johengen, T.H., Palladino, D., Denef, V.J., 2018. Verrucomicrobia are prevalent in north-temperate freshwater lakes and display class-level preferences between lake habitats. PLOS ONE 13, e0195112. https://doi.org/10.1371/journal.pone.0195112

Cho, K., Zholi, A., Frabutt, D., Flood, M., Floyd, D., Tiquia, S.M., 2012. Linking bacterial diversity and geochemistry of uranium-contaminated groundwater. Environmental Technology 33, 1629–1640. https://doi.org/10.1080/09593330.2011.641036

Choudhary, S., Sar, P., 2011. Uranium biomineralization by a metal resistant *Pseudomonas aeruginosa* strain isolated from contaminated mine waste. Journal of Hazardous Materials 186, 336–343. https://doi.org/10.1016/j.jhazmat.2010.11.004

Cologgi, D.L., Speers, A.M., Bullard, B.A., Kelly, S.D., Reguera, G., 2014. Enhanced uranium immobilization and reduction by *Geobacter sulfurreducens* biofilms. Appl. Environ. Microbiol. 80, 6638–6646. https://doi.org/10.1128/AEM.02289-14

Converse, B.J., Wu, T., Findlay, R.H., Roden, E.E., 2013. U(VI) Reduction in sulfate-reducing subsurface sediments amended with ethanol or acetate. Appl. Environ. Microbiol. 79, 4173–4177. https://doi.org/10.1128/AEM.00420-13

Delmont, T.O., Quince, C., Shaiber, A., Esen, Ö.C., Lee, S.T., Rappé, M.S., McLellan, S.L., Lücker, S., Eren, A.M., 2018. Nitrogen-fixing populations of Planctomycetes and Proteobacteria are abundant in surface ocean metagenomes. Nature Microbiology 3, 804. https://doi.org/10.1038/s41564-018-0176-9

Dong, H., 2012. Clay–microbe interactions and implications for environmental mitigation. Elements 8, 113–118. https://doi.org/10.2113/gselements.8.2.113

Edgar, R.C., 2010. Search and clustering orders of magnitude faster than BLAST. Bioinformatics 26, 2460–2461. https://doi.org/10.1093/bioinformatics/btq461

Fernández-Díaz, A.M., 2004. Caracterización y modelización del agua intersticial de materiales arcillosos: estudio de la bentonita de Cortijo de Archidona. PhD Thesis. Universidad Autónoma de Madrid Editorial CIEMAT, 505.

Finneran, K.T., Anderson, R.T., Nevin, K.P., Lovley, D.R., 2002. Potential for bioremediation of uranium-contaminated aquifers with microbial U(VI) reduction. Soil and Sediment Contamination: An International Journal 11, 339–357. https://doi.org/10.1080/20025891106781

Geissler, A., Selenska-Pobell, S., 2005. Addition of U(VI) to a uranium mining waste sample and resulting changes in the indigenous bacterial community. Geobiology 3, 275–285. https://doi.org/10.1111/j.1472-4669.2006.00061.x

Hemmat-Jou, M.H., Safari-Sinegani, A.A., Mirzaie-Asl, A., Tahmourespour, A., 2018. Analysis of microbial communities in heavy metals-contaminated soils using the metagenomic approach. Ecotoxicology 27, 1281–1291. https://doi.org/10.1007/s10646-018-1981-x

Huang, W., Cheng, W., Nie, X., Dong, F., Ding, C., Liu, M., Li, Z., Hayat, T., Alharbi, N.S., 2017. Microscopic and spectroscopic insights into uranium phosphate mineral precipitated by *Bacillus mucilaginosus*. ACS Earth Space Chem. 1, 483–492. https://doi.org/10.1021/acsearthspacechem.7b00060

Huertas, F.J., Caballero, E., Jiménez de Cisneros, C., Huertas, F., Linares, J., 2001. Kinetics of montmorillonite dissolution in granitic solutions. Applied Geochemistry 16, 397–407. https://doi.org/10.1016/S0883-2927(00)00049-4

Husserl, J., Hughes, J.B., Spain, J.C., 2012. Key enzymes enabling the growth of *Arthrobacter* sp. Strain JBH1 with nitroglycerin as the sole source of carbon and nitrogen. Appl Environ Microbiol 78, 3649–3655. https://doi.org/10.1128/AEM.00006-12

Jroundi, F., Merroun, M.L., Arias, J.M., Rossberg, A., Selenska-Pobell, S., González-Muñoz, M.T., 2007. Spectroscopic and microscopic characterization of uranium biomineralization in *Myxococcus xanthus*. Geomicrobiology Journal 24, 441–449. https://doi.org/10.1080/01490450701437651

Klindworth, A., Pruesse, E., Schweer, T., Peplies, J., Quast, C., Horn, M., Glöckner, F.O., 2013. Evaluation of general 16S ribosomal RNA gene PCR primers for classical and next-generation sequencing-based diversity studies. Nucleic Acids Res 41, e1–e1. https://doi.org/10.1093/nar/gks808

Koch, H., Lücker, S., Albertsen, M., Kitzinger, K., Herbold, C., Spieck, E., Nielsen, P.H., Wagner, M., Daims, H., 2015. Expanded metabolic versatility of ubiquitous nitrite-oxidizing bacteria from the genus *Nitrospira*. Proc Natl Acad Sci USA 112, 11371–11376. https://doi.org/10.1073/pnas.1506533112

Kostka, J.E., Dalton, D.D., Skelton, H., Dollhopf, S., Stucki, J.W., 2002. Growth of iron(III)-reducing bacteria on clay minerals as the sole electron acceptor and comparison of growth yields on a variety of oxidized iron forms. Appl Environ Microbiol 68, 6256–6262. https://doi.org/10.1128/AEM.68.12.6256-6262.2002

Kutvonen, H., Rajala, P., Carpén, L., Bomberg, M., 2015. Nitrate and ammonia as nitrogen sources for deep subsurface microorganisms. Front. Microbiol. 6. https://doi.org/10.3389/fmicb.2015.01079

Lai, C.-Y., Zhong, L., Zhang, Y., Chen, J.-X., Wen, L.-L., Shi, L.-D., Sun, Y.-P., Ma, F., Rittmann, B.E., Zhou, C., Tang, Y., Zheng, P., Zhao, H.-P., 2016. Bioreduction of chromate in a methane-based membrane biofilm reactor. Environ. Sci. Technol. 50, 5832–5839. https://doi.org/10.1021/acs.est.5b06177

Lee, B.-R., Bhatia, S.K., Song, H.-S., Kim, J., Kim, W., Park, H., Yoon, J.-J., Park, S.-H., Hwang, D., Kim, B.-G., Yang, Y.-H., 2017. The role of NdgR in glycerol metabolism in *Streptomyces coelicolor*. Bioprocess Biosyst Eng 40, 1573–1580. https://doi.org/10.1007/s00449-017-1813-z

Li, B., Wu, W.-M., Watson, D.B., Cardenas, E., Chao, Y., Phillips, D.H., Mehlhorn, T., Lowe, K., Kelly, S.D., Li, P., Tao, H., Tiedje, J.M., Criddle, C.S., Zhang, T., 2018. Bacterial community shift and coexisting/coexcluding patterns revealed by network analysis in a uranium-contaminated site after bioreduction followed by reoxidation. Appl. Environ. Microbiol. 84, e02885-17. https://doi.org/10.1128/AEM.02885-17

Liu, G., Qiu, S., Liu, B., Pu, Y., Gao, Z., Wang, J., Jin, R., Zhou, J., 2017. Microbial reduction of Fe(III)-bearing clay minerals in the presence of humic acids. Scientific Reports 7, 45354. https://doi.org/10.1038/srep45354

Lopez-Fernandez, M., Cherkouk, A., Vilchez-Vargas, R., Jauregui, R., Pieper, D., Boon, N., Sanchez-Castro, I., Merroun, M.L., 2015. Bacterial diversity in bentonites, engineered barrier for deep geological disposal of radioactive wastes. Microb Ecol 70, 922–935. https://doi.org/10.1007/s00248-015-0630-7

Lopez-Fernandez, M., Romero-González, M., Günther, A., Solari, P.L., Merroun, M.L., 2018a. Effect of U(VI) aqueous speciation on the binding of uranium by the cell surface of *Rhodotorula mucilaginosa*, a natural yeast isolate from bentonites. Chemosphere 199, 351–360. https://doi.org/10.1016/j.chemosphere.2018.02.055

Lopez-Fernandez, M., Vilchez-Vargas, R., Jroundi, F., Boon, N., Pieper, D., Merroun, M.L., 2018b. Microbial community changes induced by uranyl nitrate in bentonite clay microcosms. Applied Clay Science, ACS - SI ICC 2017 XVI International Clay Conference – Clays, from the oceans to space 160, 206–216. https://doi.org/10.1016/j.clay.2017.12.034

Martinez, R.J., Wu, C.H., Beazley, M.J., Andersen, G.L., Conrad, M.E., Hazen, T.C., Taillefert, M., Sobecky, P.A., 2014. Microbial community responses to organophosphate substrate additions in contaminated subsurface sediments. PLOS ONE 9, e100383. https://doi.org/10.1371/journal.pone.0100383

Masurat, P., Eriksson, S., Pedersen, K., 2010. Evidence of indigenous sulphate-reducing bacteria in commercial Wyoming bentonite MX-80. Applied Clay Science, Advanced smectitic clay research 47, 51–57. https://doi.org/10.1016/j.clay.2008.07.002

McMurdie, P.J., Holmes, S., 2013. phyloseq: an R package for reproducible interactive analysis and graphics of microbiome census data. PLoS ONE 8, e61217. https://doi.org/10.1371/journal.pone.0061217

Merroun, M.L., Nedelkova, M., Ojeda, J.J., Reitz, T., Fernández, M.L., Arias, J.M., Romero-González, M., Selenska-Pobell, S., 2011. Bio-precipitation of uranium by two bacterial isolates recovered from extreme environments as estimated by potentiometric titration, TEM and X-ray absorption spectroscopic analyses. Journal of Hazardous Materials 197, 1–10. https://doi.org/10.1016/j.jhazmat.2011.09.049

Merroun, M.L., Selenska-Pobell, S., 2008. Bacterial interactions with uranium: an environmental perspective. J. Contam. Hydrol. 102, 285–295. https://doi.org/10.1016/j.jconhyd.2008.09.019

Newsome, L., Morris, K., Trivedi, D., Bewsher, A., Lloyd, J.R., 2015. Biostimulation by glycerol phosphate to precipitate recalcitrant uranium(IV) phosphate. Environ. Sci. Technol. 49, 11070–11078. https://doi.org/10.1021/acs.est.5b02042

Niewerth, H., Schuldes, J., Parschat, K., Kiefer, P., Vorholt, J.A., Daniel, R., Fetzner, S., 2012. Complete genome sequence and metabolic potential of the quinaldine-degrading bacterium *Arthrobacter* sp. Rue61a. BMC Genomics 13, 534. https://doi.org/10.1186/1471-2164-13-534

Nishizawa, T., Quan, A., Kai, A., Tago, K., Ishii, S., Shen, W., Isobe, K., Otsuka, S., Senoo, K., 2014. Inoculation with N_2-generating denitrifier strains mitigates N_2O emission from agricultural soil fertilized with poultry manure. Biol Fertil Soils 50, 1001–1007. https://doi.org/10.1007/s00374-014-0918-7

Ollivier, J., Töwe, S., Bannert, A., Hai, B., Kastl, E.-M., Meyer, A., Su, M.X., Kleineidam, K., Schloter, M., 2011. Nitrogen turnover in soil and global change. FEMS Microbiology Ecology 78, 3–16. https://doi.org/10.1111/j.1574-6941.2011.01165.x

Pathak, A., Chauhan, A., Stothard, P., Green, S., Maienschein-Cline, M., Jaswal, R., Seaman, J., 2017. Genome-centric evaluation of *Burkholderia* sp. strain SRS-W-2-2016 resistant to

high concentrations of uranium and nickel isolated from the Savannah River Site (SRS), USA. Genom Data 12, 62–68. https://doi.org/10.1016/j.gdata.2017.02.011

Pedersen, K., 1999. Subterranean microorganisms and radioactive waste disposal in Sweden. Engineering Geology 52, 163–176. https://doi.org/10.1016/S0013-7952(99)00004-6

Pedersen, K., Bengtsson, A., Blom, A., Johansson, L., Taborowski, T., 2017. Mobility and reactivity of sulphide in bentonite clays – Implications for engineered bentonite barriers in geological repositories for radioactive wastes. Applied Clay Science 146, 495–502. https://doi.org/10.1016/j.clay.2017.07.003

Pentráková, L., Su, K., Pentrák, M., Stucki, J.W., 2013. A review of microbial redox interactions with structural Fe in clay minerals. Clay Minerals 48, 543–560. https://doi.org/10.1180/claymin.2013.048.3.10

Perdrial, J.N., Warr, L.N., Perdrial, N., Lett, M.-C., Elsass, F., 2009. Interaction between smectite and bacteria: Implications for bentonite as backfill material in the disposal of nuclear waste. Chemical Geology 264, 281–294. https://doi.org/10.1016/j.chemgeo.2009.03.012

Quast, C., Pruesse, E., Yilmaz, P., Gerken, J., Schweer, T., Yarza, P., Peplies, J., Glöckner, F.O., 2013. The SILVA ribosomal RNA gene database project: improved data processing and web-based tools. Nucleic Acids Res. 41, D590-596. https://doi.org/10.1093/nar/gks1219

Rickard, D., 2012. Chapter 3 - Sedimentary iron biogeochemistry, in: Rickard, D. (Ed.), Developments in sedimentology, sulfidic sediments and sedimentary rocks. Elsevier, pp. 85–119. https://doi.org/10.1016/B978-0-444-52989-3.00003-9

Rozalén, M., Brady, P.V., Huertas, F.J., 2009. Surface chemistry of K-montmorillonite: ionic strength, temperature dependence and dissolution kinetics. J Colloid Interface Sci 333, 474–484. https://doi.org/10.1016/j.jcis.2009.01.059

Safonov, A.V., Babich, T.L., Sokolova, D.S., Grouzdev, D.S., Tourova, T.P., Poltaraus, A.B., Zakharova, E.V., Merkel, A.Y., Novikov, A.P., Nazina, T.N., 2018. Microbial community and in situ bioremediation of groundwater by nitrate removal in the zone of a radioactive waste surface repository. Front. Microbiol. 9. https://doi.org/10.3389/fmicb.2018.01985

Salome, K.R., Beazley, M.J., Webb, S.M., Sobecky, P.A., Taillefert, M., 2017. Biomineralization of U(VI) phosphate promoted by microbially-mediated phytate hydrolysis in contaminated soils. Geochimica et Cosmochimica Acta 197, 27–42. https://doi.org/10.1016/j.gca.2016.10.008

Shelobolina, E.S., Konishi, H., Xu, H., Roden, E.E., 2009. U(VI) Sequestration in hydroxyapatite produced by microbial glycerol-3-phosphate metabolism. Appl. Environ. Microbiol. 75, 5773–5778. https://doi.org/10.1128/AEM.00628-09

Simon, F.G., Biermann, V., Peplinski, B., 2008. Uranium removal from groundwater using hydroxyapatite. Applied Geochemistry 23, 2137–2145. https://doi.org/10.1016/j.apgeochem.2008.04.025

Spain, A.M., Krumholz, L., 2012. Cooperation of three denitrifying bacteria in nitrate removal of acidic nitrate- and uranium-contaminated groundwater. Geomicrobiology Journal 29, 830–842. https://doi.org/10.1080/01490451.2011.635757

Stone, W., Kroukamp, O., Moes, A., McKelvie, J., Korber, D.R., Wolfaardt, G.M., 2016. Measuring microbial metabolism in atypical environments: Bentonite in used nuclear fuel storage. J. Microbiol. Methods 120, 79–90. https://doi.org/10.1016/j.mimet.2015.11.006

Stroes-Gascoyne, S., Hamon, C.J., Maak, P., Russell, S., 2010. The effects of the physical properties of highly compacted smectitic clay (bentonite) on the culturability of indigenous microorganisms. Applied Clay Science 47, 155–162. https://doi.org/10.1016/j.clay.2008.06.010

Tamez-Guerra, P., Zuñiga-Sanchez, J.O., Orozco-Flores, A.A., Valadez-Lira, J.A., Rodriguez-Padilla, C., Cañizares-Villanueva, R.O., Gomez-Flores, R., 2017. Prevalence of Proteobacteria and Armatimonadetes phyla in a photobioreactor under carbon- and nitrogen-free production process. Fermentation Technology 6, 1–4. https://doi.org/10.4172/2167-7972.1000142

Villar, M.V., Cuevas, J., Leguey, S., Caballero, E., Huertas, F.J., Delgado, A., Fernández-Soler, J.M., Astudillo, J., 2006. The study of Spanish clays for their use as sealing materials in nuclear waste repositories: 20 years of progress. Journal of Iberian Geology 32, 15–36.

Vishnivetskaya, T.A., Mosher, J.J., Palumbo, A.V., Yang, Z.K., Podar, M., Brown, S.D., Brooks, S.C., Gu, B., Southworth, G.R., Drake, M.M., Brandt, C.C., Elias, D.A., 2011. Mercury and other heavy metals influence bacterial community structure in contaminated Tennessee streams. Appl. Environ. Microbiol. 77, 302–311. https://doi.org/10.1128/AEM.01715-10

Wang, Y., Bagnoud, A., Suvorova, E., McGivney, E., Chesaux, L., Phrommavanh, V., Descostes, M., Bernier-Latmani, R., 2014. Geochemical control on uranium(IV) mobility in a mining-impacted wetland. Environ. Sci. Technol. 48, 10062–10070. https://doi.org/10.1021/es501556d

Warnes, G.R., Bolker, B., Bonebakker, L., Gentleman, R., Liaw, W.H.A., Lumley, T., Maechler, M., Magnusson, A., Moeller, S., Schwartz, M., Venables, B., 2019. gplots: Various R Programming Tools for Plotting Data.

Weidenmaier, C., Peschel, A., 2008. Teichoic acids and related cell-wall glycopolymers in Gram-positive physiology and host interactions. Nature Reviews Microbiology 6, 276–287. https://doi.org/10.1038/nrmicro1861

Xu, J., Veeramani, H., Qafoku, N.P., Singh, G., Riquelme, M.V., Pruden, A., Kukkadapu, R.K., Gartman, B.N., Hochella, M.F., 2017. Efficacy of acetate-amended biostimulation for uranium sequestration: Combined analysis of sediment/groundwater geochemistry and bacterial community structure. Applied Geochemistry 78, 172–185. https://doi.org/10.1016/j.apgeochem.2016.12.024

Yeh, J.I., Chinte, U., Du, S., 2008. Structure of glycerol-3-phosphate dehydrogenase, an essential monotopic membrane enzyme involved in respiration and metabolism. PNAS 105, 3280–3285. https://doi.org/10.1073/pnas.0712331105

Yoneyama, F., Yamamoto, M., Hashimoto, W., Murata, K., 2015. Production of polyhydroxybutyrate and alginate from glycerol by *Azotobacter vinelandii* under nitrogen-free conditions. Bioengineered 6, 209–217. https://doi.org/10.1080/21655979.2015.1040209

Zahran, H.H., 1999. *Rhizobium*-legume symbiosis and nitrogen fixation under severe conditions and in an arid climate. Microbiol Mol Biol Rev 63, 968–989.

Zhao, C., Liu, J., Li, X., Li, F., Tu, H., Sun, Q., Liao, J., Yang, J., Yang, Y., Liu, N., 2016. Biosorption and bioaccumulation behavior of uranium on *Bacillus* sp. dwc-2: Investigation by Box-Behenken design method. Journal of Molecular Liquids 221, 156–165. https://doi.org/10.1016/j.molliq.2016.05.085

Zucchi, T.D., Tan, G.Y.A., Bonda, A.N.V., Frank, S., Kshetrimayum, J.D., Goodfellow, M., 2012. *Amycolatopsis granulosa* sp. nov., *Amycolatopsis ruanii* sp. nov. and *Amycolatopsis thermalba* sp. nov., thermophilic Actinomycetes isolated from arid soils. Int. J. Syst. Evol. Microbiol. 62, 1245–1251. https://doi.org/10.1099/ijs.0.031039-0

10.SUPPLEMENTARY MATERIAL

10.1. S1. Effect of bentonite bacterial isolates on the chemical speciation of uranium in presence of G2P

10.1.1. Phosphatase activity measurements

Determination of phosphatase activity was based on the procedure of German et al. (2011) using 4 methylumbelliferone (MUB)-phosphate di-Na salt (4-MUB-P). The maximum substrate concentration in the assay (300 µM) was selected based on previous optimization experiments (unpublished data). Cells contained in 10 mL of each sample were recovered, washed with saline solution, and re-dissolved in 5 mL of Na-perclorate (pH 5). Cell suspensions (200 µl) and MUB standards (0.16 µM, 0.625 µM, 1.25 µM and 2.5 µM) dissolved in Na-perclorate buffer were used to calculate the emission and quench coefficients for each sample respectively. Microplates were read at 360 nm excitation and 465 nm emission (NanoQuant modelo Infinite M200 Pro), and cells phosphatase activity was calculated as µmol 4-MUB-P g^{-1} cells h^{-1}. Calculations were performed according to German et al. (2011).

10.1.2. Determination of dissolved uranium and inorganic phosphates

ICP-MS was used to determine U concentration in the supernatant of each replicate. Three mL of sample were acidified (4 % HNO_3) before measurements.

Ammonium molybdate and potassium antimony tartrate react in an acid medium with orthophosphate to form a heteropoly acid – phosphomolybdic acid – that is reduced to intensely coloured molybdenum blue by ascorbic acid. Absorbance of the (blue) solution is measured at 850 nm after exactly 30 min.

10.1.3. STEM/HAADF/EDX analyses

To determine the ability of *A. ruanii/*enriched bentonite bacterial consortium to precipitate uranium, STEM analyses were performed. Cells coming from T2 and T4 treatments were processed for microscopic analysis. Samples were prepared according to the method described in Merroun et al. (2005) and further examined under STEM-HAADF (FEI TITAN G2 80–300).

10.2. S2 Rarefaction curves

Rarefaction curves were determined using the VEGAN v. 2.4-6 package in R v. 3.4.3.

10.3. S3 Bacterial community composition at class level

The 4,952 OTUs were taxonomically related to 29 different bacterial phyla including *Proteobacteria*, *Actinobacteria*, *Bacteroidetes*, *Planctomycetes*, *Chloroflexi*, *Gemmatimonadetes*, *Verrucomicrobia,* and Candidate Division (BRC1, TM7, TM6, OD1, and TA06). Significant differences ($p \leq 0.01$) in the OTU abundance at phylum level between the different treatments were found only for the bacterial phyla Candidate division BRC1, *Fusobacteria*, *Nitrospirae*, *Planctomycetes*, *Proteobacteria,* and *Verrucomicrobia*.

In order to determine the effect of nitrate in the bacterial community, nitrate-treated (N) and G2P-nitrate-treated (GN) microcosms were compared with their respective controls (H and G microcosm). Regarding classes, significantly higher abundances ($p \leq 0.018$) in GN microcosms were shown in *Deltaproteobacteria*, *Sphingobacteria*, *Holophagae*, and *Nitrospira* versus G samples. However, several classes seemed to be negatively affected in presence of nitrate showed by their relative abundance were significantly more abundant ($p=0.001$) in G than in GN microcosms such as *Armatimonadia*, *Gammaproteobacteria*, and *Thermoleophilia* (Fig. S4) and similarly *Betaproteobacteria* and *Acidimicrobia* were more representative in H than N microcosms.

Studying the effect of uranium in the community, presence of *Nitriliruptoria* (belonging to *Actinobacteria*), P2-11E, JG30-KF-CM66, and B085 classes (all affiliated with the *Chloroflexi*) was significantly different in U microcosms comparing with N-controls (Fig. S4). The statistical analysis of *Bacilli* ($p=0.015$), *Chlamydiae* ($p=0.035$), *Phycisphaerae* ($p=0.031$), *Opitutae* ($p=0.001$) and *Spartobacteria* ($p=0.03$), both affiliated to *Verrucomicrobia* phylum, showed that their relative abundances were significantly higher in GU microcosms than in GN controls. *Holophagae* and *Nitrospira* were more represented in GN samples versus GU.

Concerning the effect of glycerol-2-phosphate, at the class level, *Gammaproteobacteria* (p=0.000) and *Armatimonadia* (p=0.000) were the most dominant showing significantly higher abundance in G microcosms than in water-controls. *Alphaproteobacteria* (p=0.005), *Phycisphaera* (p=0.035), *Holophagae* (p=0.011) and *Nitrospira* (p=0.000) were more abundant in GN samples versus N microcosms. However, *Acidimicrobia,* and *TK10* (*Chloroflexi*) were lower in treatments with G2P (G and GN microcosms) than in their controls (H and N samples, respectively). Several classes such as *Alphaproteobacteria* (p=0.014), *Actinobacteria* (p=0.01), *Deltaproteobacteria* (p=0.005), *Sphingobacteria* (p=0.006), *Spartobacteria* (p=0.009), *Phycisphaerae* (p=0.001), and *Bacilli* (p=0.011), among others, differed significantly between samples being more abundant in GU samples than in microcosms treated only with uranium. In contrast, *Acidimicrobia* (p=0.013) and *Clostridia* (p=0.036), and several classes affiliated to *Chloroflexi* (JG30-KF-CM66, P2-11E, and S085) were significantly more abundant in U microcosms (Fig. S4).

10.4. Tables

Table S1. Chemical composition of major elements of two bentonite samples before incubation (time 0) determined by XRF spectroscopy. Values are in wt %, except Zr in ppm.

Elements	SiO_2	Al_2O_3	Fe_2O_3	MnO	MgO	CaO	Na_2O	K_2O	TiO_2	P_2O_5	Zr	LOI	SUMA
BI-1	64.38	14.41	3.24	0.02	4.11	2.04	1.11	0.99	0.22	0.05	155	8.71	99.28
BI-2	59.31	16.4	3.54	0.02	4.94	1.84	1.14	0.62	0.24	0.05	190.7	11.27	99.37

Table S2. pH values of the different microcosms measured in a calcium chloride suspension. H: distilled water, N: sodium nitrate, U: uranyl nitrate, G: G2P, GN: G2P and sodium nitrate, and GU: G2P and uranyl nitrate.

	Time 0	**After 6 months of incubation**					
		H	N	U	G	GN	GU
$CaCl_2$	9.79 ± 0.15	8.31 ± 0.08	8.14 ± 0.07	8.18 ± 0.09	8.11 ± 0.03	8.10 ± 0.07	7.90 ± 0.13

Table S3. Identification of the different treatments in the batch experiment.

Treatment ID	Treatment composition
T1	PW (BRP) + *Amycolatopsis ruanii* + U + G2P
T2	PW (BRP) + *A. ruanii* + U
T3	PW (BRP) + *A. ruanii* + G2P
T4	PW (BRP) + U + G2P
T5	PW (BRP) + U
T6	PW (BRP) + *A. ruanii*
T7	PW (BRP)

PW (bentonite porewater), BRP (bacterial consortium = *Bradyrhizobium-Rhizobium* and *Pseudomonas*), U (uranium; 1.26 mM), G2P (glycerol 2-phosphate; 5 mM)

10.5. Figures

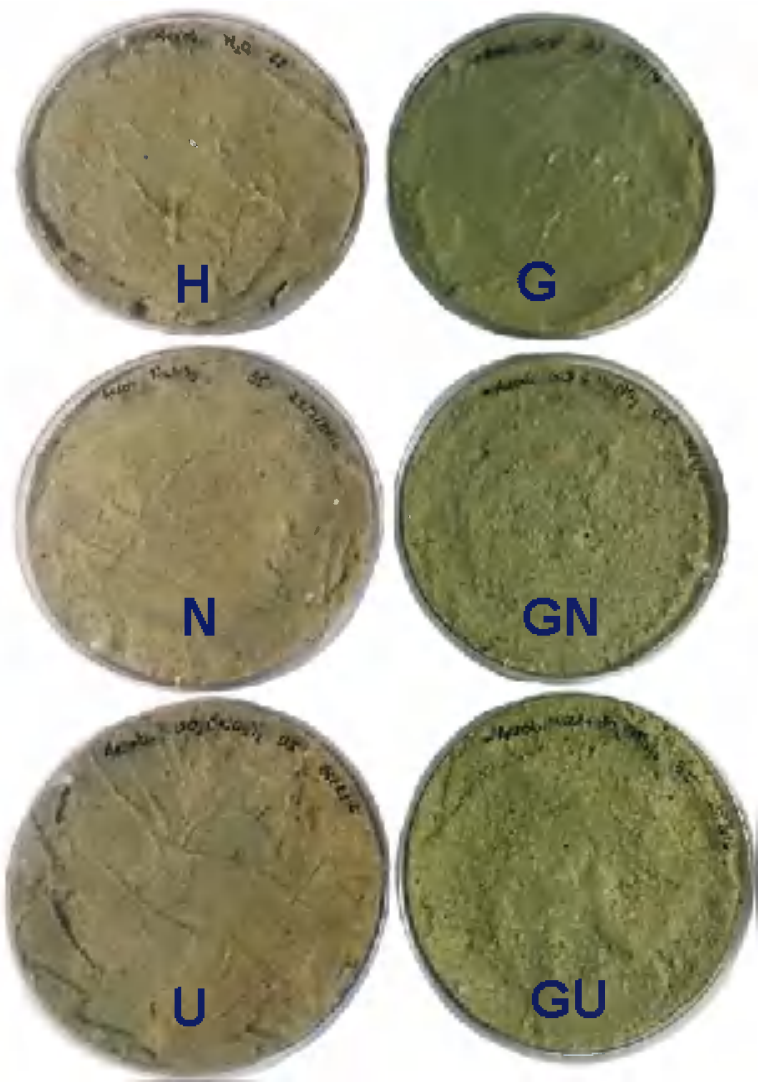

Figure S1. Plates of bentonite microcosms treated with distilled water (H), sodium nitrate (N), uranyl nitrate (U), glycerol-2-phosphate (G2P; G), G2P and sodium nitrate (GN), and G2P and uranyl nitrate (GU) after six months of incubation under aerobic conditions.

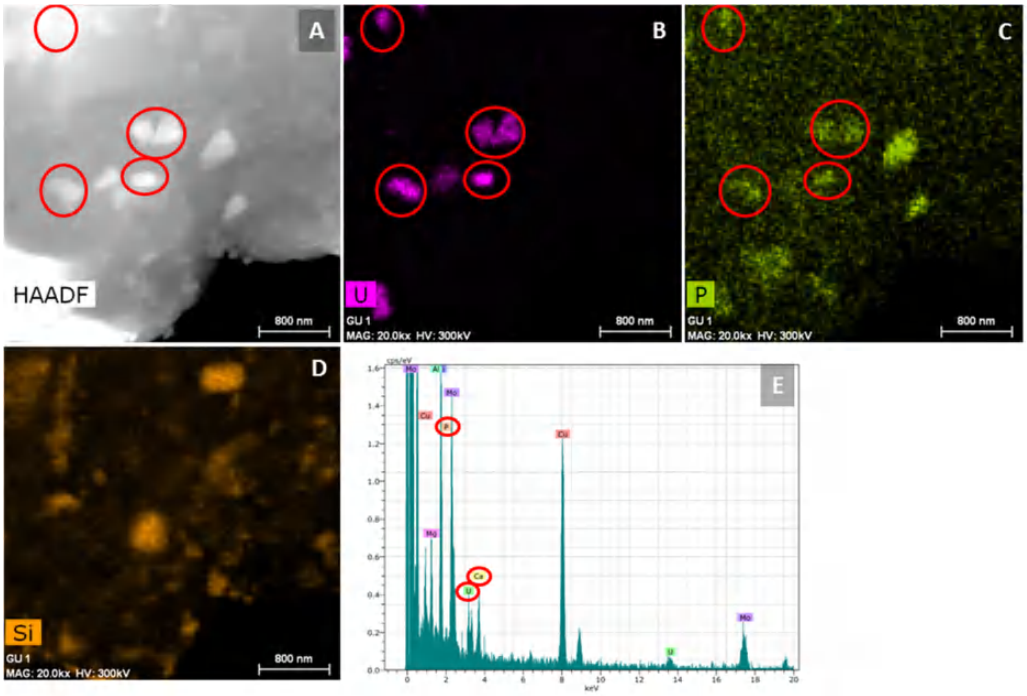

Figure S2. HAADF/STEM image (A) and EDX maps (B, C and D) showing Si from bentonite, U precipitates and a weak signal of P. EDX spectrum (E) showed a U, P and Ca composition of electron-dense deposits.

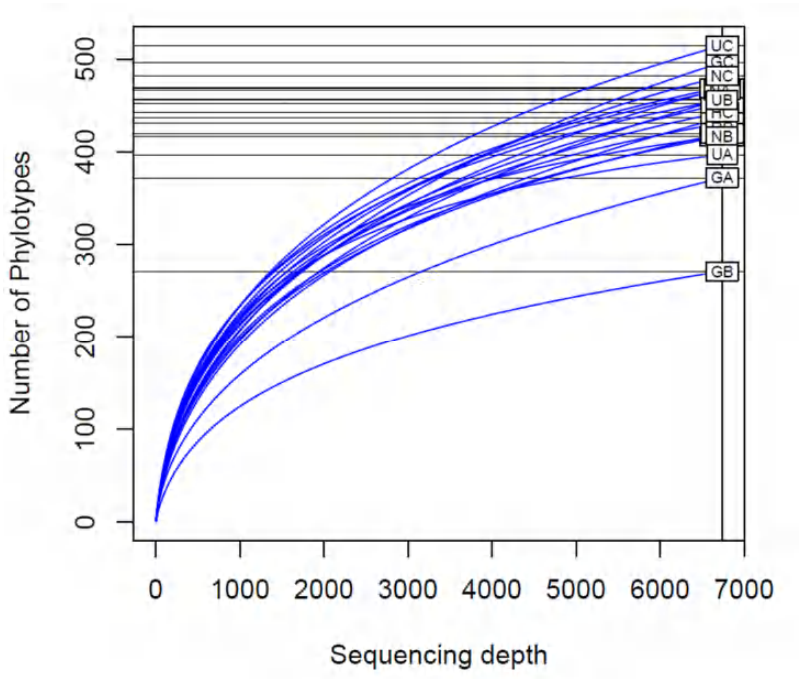

Figure S3. Rarefaction curves portraying the number of phylotypes against sequencing depth of each sample. HA, HB, HC: H microcosms; NA, NB, NC: N microcosms; UA, UB, UC: U microcosms; GA, GB, GC: G microcosms; GNA, GNB, GNC: GN microcosms, GUA, GUB, GUC: GU microcosms.

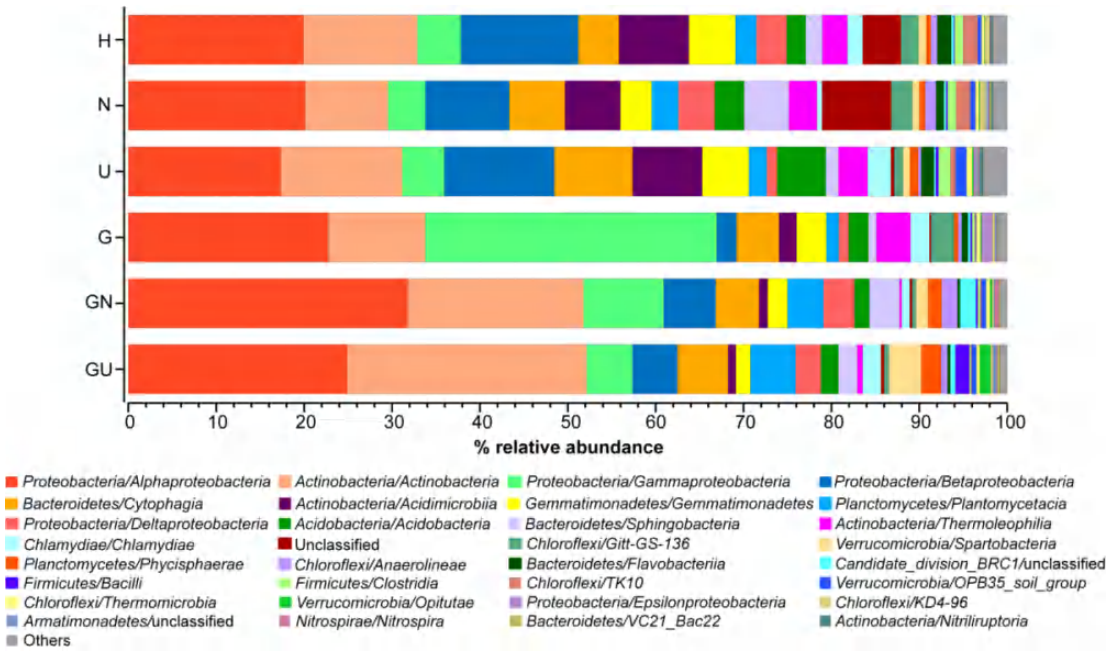

Figure S4. Relative abundance at class level in all treated bentonite microcosms. (H) Distilled water, (N) sodium nitrate, (U) uranyl nitrate, (G) G2P, (GN) G2P and sodium nitrate, and (GU) G2P and uranyl nitrate.

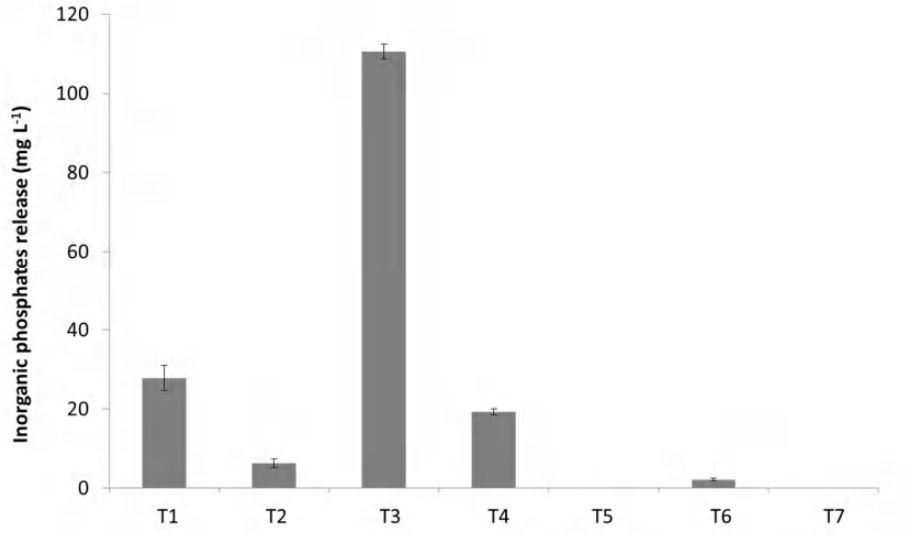

Figure S5. Dissolved inorganic phosphates determination. T1: pore water (PW) + uranium (U) + *Amycolatopsis ruanii*/bacterial consortium (*Bradyrhizobium-Rhizobium* and *Pseudomonas*, BRP) + glycerol-2-phosphate (G2P); T2: PW + U + *A. ruanii*/BRP; T3: PW + *A. ruanii*/BRP + G2P; T4: PW + BRP + U + G2P; T5: PW + BRP + U; T6: PW + *A. ruanii*/BRP; T7: PW + BRP. Error bars represent one standard deviation of the mean (n = 3).

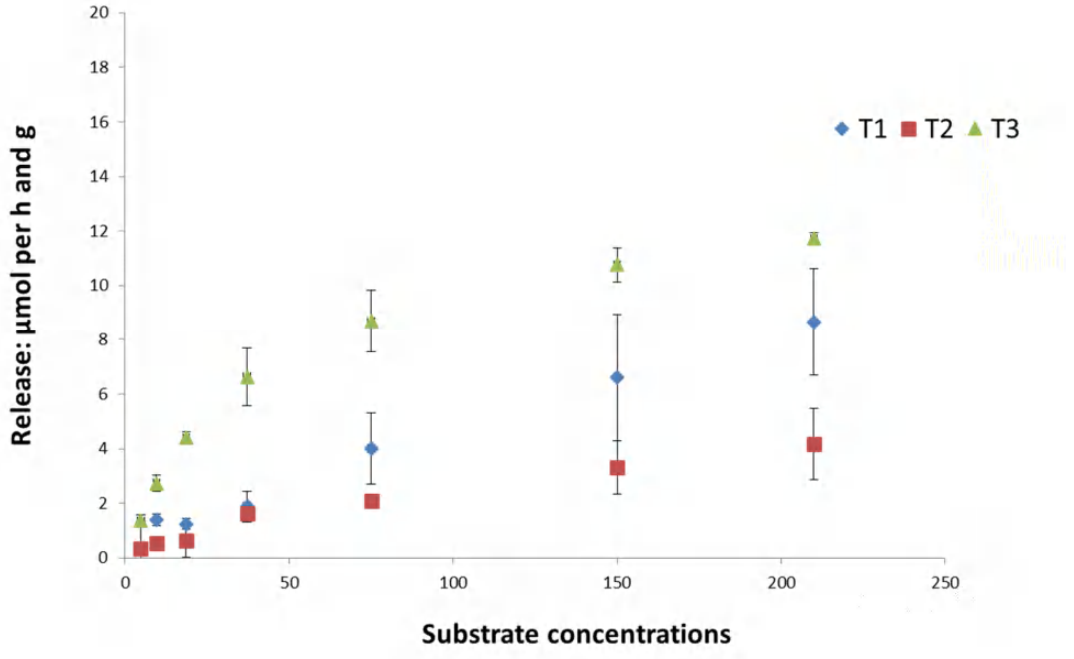

Figure S6. Phosphatase activity measured for all samples including *Amycolatopsis ruanii* cells. Phosphatase activity expressed as µmoles of 4-MUB-P per gram of dry biomass of *A. ruanii* and hour. T1: pore water (PW) + uranium (U) + *A. ruanii*/bacterial consortium (*Bradyrhizobium-Rhizobium* and *Pseudomonas*, BRP) + glycerol-2-phosphate (G2P); T2: PW + U + *A. ruanii*/BRP; T3: PW + *A. ruanii*/BRP + G2P; 4-MUB, 4-methylumbelliferone. Error bars represent one standard deviation of the mean (n = 3).

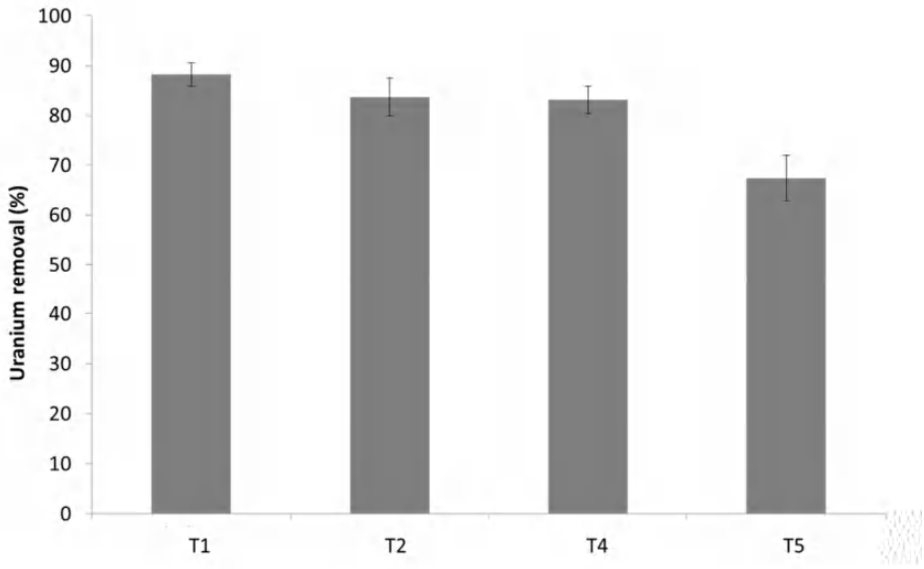

Figure S7. Removal of U(VI) from incubation medium. T1: pore water (PW) + uranium (U) + *Amycolatopsis ruanii*/bacterial consortium (*Bradyrhizobium-Rhizobium* and *Pseudomonas*, BRP) + glycerol-2-phosphate (G2P); T2: PW + U + *A. ruanii*/BRP; T4: PW + BRP + U + G2P; T5: PW + BRP + U. Error bars represent one standard deviation of the mean (n = 3).

10.6. References

German DP, Weintraub MN, Grandy AS, Lauber CL, Rinkes ZL, Allison SD (2011). Optimization of hydrolytic and oxidative enzyme methods for ecosystem studies. Soil Biology and Biochemistry 43, 1387-1397

Merroun ML, Raff J, Rossberg A, Hennig C, Reich T, Selenska-Pobell S, 2005. Complexation of Uranium by Cells and S-Layer Sheets of Bacillus sphaericus JG-A12. Applied and Environmental Microbiology 71, 5532–5543

10.7.Supplementary tables

Supplementary Table 1. Bacterial phyla of bentonite microcosms and their corresponding p-values. One-way ANOVA test, using a significance level of 0.05, was used to look for significant differences in the alpha diversity between the samples. Coloured cells represent p-value < 0.05.

Phyla	p value
Acidobacteria	0.165
Actinobacteria	0.087
Armatimonadetes	0.107
Bacteroidetes	0.33
Caldiserica	0.458
Candidate_division_BRC1	0
Candidate_division_JS1	0.458
Candidate_division_OD1	0.645
Candidate_division_TM7	0.034
Chlamydiae	0.074
Chlorobi	0.181
Chloroflexi	0.152
Cyanobacteria	0.527
Deinococcus-Thermus	0.419
Elusimicrobia	0.643
Fibrobacteres	0.458
Firmicutes	0.09
Fusobacteria	0.01
Gemmatimonadetes	0.073
Lentisphaerae	0.458
Nitrospirae	0
NPL-UPA2	0.571
Planctomycetes	0.003
Proteobacteria	0
SM2F11	0.458
Spirochaetae	0.571
Synergistetes	0.469
TA06	0.458
Tenericutes	0.458
Thermodesulfobacteria	0.347
TM6	0.264
unclassified	0.003
Verrucomicrobia	0.008

Supplementary Table 2. Bacterial families/genera of bentonite microcosms and their corresponding p-values. One-way ANOVA test, using a significance level of 0.05, was used to look for significant differences in the alpha diversity between all samples. Red values represent p-value < 0.05.

Families/Genera	p-value	Families/Genera	p-value
Unclassified	0.897	*Methylibium*	0.451
Azotobacter	0.000	*Reichenbachiella*	0.005
Streptomyces	0.001	*Bacillus*	0.053
Arthrobacter	0.110	OM1_clade	0.019
Ohtaekwangia	0.309	*Legionella*	0.169
Amycolatopsis	0.101	*Brevundimonas*	0.003
Phyllobacteraceae	0.001	*Sulfurimonas*	0.285
Sphingomonas	0.003	*Pseudonocardia*	0.163
Rhizobium	0.000	*Opitutus*	0.003
Erythrobacteraceae	0.054	*Devosia*	0.008
Hyphomicrobiaceae	0.437	*Pontibacter*	0.021
Gemmatimonadaceae	0.007	*Parachlamydiaceae*	0.065
Nocardioides	0.028	*Skermanella*	0.060
Gaiella	0.009	AKIW1012	0.175
Nitrosomonadaceae	0.042	*Comamonadaceae*	0.105
Chthoniobacter	0.049	*Defluviicoccus*	0.020
Ramlibacter	0.359	*Sphingomonadaceae*	0.241
Caenimonas	0.288	*Pseudomonas*	0.310
Lysobacter	0.004	DUNssu044	0.163
Haliangium	0.008	*Pseudonocardiaceae*	0.145
Steroidobacter	0.011	*Aquipuribacter*	0.000
Altererythrobacter	0.408	DA111	0.004
7B-8	0.015	*Colwellia*	0.110
Flavisolibacter	0.005	*Procabacter*	0.023
Rhodopirellula	0.007	*Oxalobacteraceae*	0.192
Phenylobacterium	0.021	*Clostridium_sensu_stricto_7*	0.582
Niastella	0.000	*Glycomyces*	0.000
Anaerolineaceae	0.240	*Microvirga*	0.128
Gemmata	0.052	*Nordella*	0.167
Chryseobacterium	0.353	*Aquicella*	0.097
Iamia	0.028	*Planctomycetaceae*	0.036
Gemmatimonas	0.001	*Sandaracinus*	0.000
Pirellula	0.055	Pir4_lineage	0.018
Planctomyces	0.023	*Xanthomonadaceae*	0.061
Acinetobacter	0.480	*Paucimonas*	0.021
Xanthomonas	0.086	*Sandaracinaceae*	0.157
Micromonosporaceae	0.079	*Noviherbaspirillum*	0.172
Ochrobactrum	0.373	*Nitrospira*	0.000
Caulobacteraceae	0.215	*Rhodocytophaga*	0.001
Cesiribacter	0.554	*Burkholderia*	0.235
Rubellimicrobium	0.543	*Acidiferrobacter*	0.074
Paracoccus	0.006	*Geodermatophilus*	0.083
Bosea	0.006	*Truepera*	0.380

Caldilineaceae	0.945	NS11-12_marine_group	0.311
Herpetosiphon	0.224	JG34-KF-361	0.315
Bradyrhizobium	0.000	*Acidimicrobiaceae*	0.765
Pseudorhodoferax	0.001	*Staphylococcus*	0.208
Ilumatobacter	0.223	*Desulfonauticus*	0.236
Belnapia	0.208	*Actinotalea*	0.114
Thalassobaculum	0.102	EF100-94H03	0.443
Sphingobacteriaceae	0.012	TK34	0.228
Bdellovibrio	0.022	*Blastococcus*	0.001
Phycisphaera	0.059	*Rhizobacter*	0.255
CL500-29_marine_group	0.000	*Kribbella*	0.057
Cytophaga	0.028	KCM-B-15	0.072
Rhodobacteraceae	0.881	*Promicromonospora*	0.696
Xanthomonadales_Incertae_Sedis	0.013	*Proteus*	0.172
Roseomonas	0.142	*Lachnospiraceae*	0.257
Microbacteriaceae	0.000	PRD01a011B	0.555
Marmoricola	0.454	*Desulfuromonas*	0.149
Enhydrobacter	0.323	*Inquilinus*	0.605
Propionibacterium	0.868	*Desulfovibrio*	0.037
Thermovirga	0.458	*Bauldia*	0.265
FFCH16767	0.241	Family_XVIII	0.358
mle1-27	0.001	*Candidatus_Odyssella*	0.603
Nitriliruptor	0.017	*Euzebya*	0.057
Nannocystis	0.183	*Desulfomicrobium*	0.132
Microbacterium	0.000	*Phaselicystis*	0.004
Rhodoplanes	0.082	*Massilia*	0.913
Pedomicrobium	0.114	*Enterobacteriaceae*	0.387
Kocuria	0.253	*Escherichia-Shigella*	0.811
Luteimonas	0.083	*Singulisphaera*	0.079
Hydrotalea	0.216	*Microlunatus*	0.006
Peredibacter	0.004	*Ralstonia*	0.631
Holosporaceae	0.052	M05-Pitesti	0.411
Pseudoxanthomonas	0.037	*Sorangium*	0.041
Hamadaea	0.001	*Solirubrobacter*	0.001
I-10	0.306	D05-2	0.161
Geminicoccus	0.032	*Loktanella*	0.328
Cytophagaceae	0.236	JG37-AG-20	0.062
Chitinophagaceae	0.105	*Nocardia*	0.104
Cystobacteraceae	0.003	*Vibrio*	0.563
Coxiella	0.247	RB446	0.234
Chitinophaga	0.596	SM1A02	0.036
Patulibacter	0.213	*Methylophaga*	0.059
envOPS_17	0.444	*Hymenobacter*	0.000
Clostridium_sensu_stricto_3	0.405	*Pseudoalteromonas*	0.146
Ellin6055	0.314	*Streptococcus*	0.755
Pseudospirillum	0.630	*Rubrobacter*	0.204
Parvibaculum	0.239	*Bacteroides*	0.089
Oleiphilus	0.071	*Micrococcaceae*	0.447

Hyphomicrobium	0.765	*Clostridium_sensu_stricto_16*	0.087
Novosphingobium	0.022	*Methylobacteriaceae*	0.249
Byssovorax	0.001	*Pelagibius*	0.496
Rhodothermaceae	0.112	*Reyranella*	0.039
Flavobacteriaceae	0.660	0319-6G20	0.143
Geobacillus	0.492	MNG7	0.185
Methylocystis	0.101	*Marinobacter*	0.152
Lactobacillus	0.435	MNC12	0.182
Streptomycetaceae	0.166	*Acetobacteraceae*	0.354

Supplementary Table 3. Bacterial families/genera of bentonite microcosms and their corresponding p-values. Multiple comparison using DMS test and a significance level of 0.05 were used to look for significant differences in the alpha diversity between pair of samples. Coloured cellsrepresent p-value < 0.05: blue for H, light green for G, orange for N, green for GN, purple for U, and light purple for GU.

Families/Genera	**Multiple comparisons between pair of samples**														
	G-GN	**G-GU**	**G-H**	**G-N**	**G-U**	**GN-GU**	**GN-H**	**GN-N**	**GN-U**	**GU-H**	**GU-N**	**GU-U**	**H-N**	**H-U**	**N-U**
Unclassified	0.991	0.411	0.546	0.752	0.941	0.354	0.502	0.716	0.925	0.866	0.564	0.402	0.726	0.556	0.786
Azotobacter	0.000 G	0.000 G	0.000 G	0.000 G	0.000 G	1.000	1.000	1.000	1.000	1.000	1.000	1.000	1.000	1.000	1.000
Streptomyces	0.007 GN	0.001 GU	0.975	0.993	0.881	0.261	0.007 GN	0.004 GN	0.005 GN	0.001 GU	0.001 GU	0.001 GU	0.965	0.854	0.875
Arthrobacter	0.351	0.233	0.524	0.268	0.478	0.752	0.120	0.037 GN	0.084	0.074	0.021 GU	0.048 GU	0.662	0.988	0.637
Ohtaekwangia	0.856	0.439	0.225	0.302	0.633	0.293	0.246	0.337	0.740	0.050	0.060	0.177	0.748	0.376	0.520
Amycolatopsis	0.912	0.046 GU	0.731	0.912	0.754	0.023 GU	0.790	1.000	0.820	0.024 GU	0.023 GU	0.016 GU	0.790	0.949	0.820
Phyllobacteraceae	0.000 G	0.002 G	0.000 G	0.000 G	0.000 G	0.227	0.315	0.290	0.462	0.052	0.037	0.067	0.953	0.715	0.732
Sphingomonas	0.001 GN	0.860	0.353	0.837	0.753	0.000 GN	0.007 GN	0.001 GN	0.000 GN	0.240	0.670	0.876	0.412	0.194	0.563
Rhizobium	0.003 GN	0.001 GU	0.489	0.461	0.458	0.606	0.001 GN	0.000 GN	0.000 GN	0.000 GU	0.000 GU	0.000 GU	0.983	0.988	0.995
Erythrobacteraceae	0.049 G	0.010 G	0.010 G	0.008 G	0.008 G	0.311	0.228	0.264	0.273	0.748	0.910	0.929	0.825	0.808	0.981
Hyphomicrobiaceae	0.115	0.456	0.899	0.890	0.921	0.312	0.144	0.107	0.099	0.541	0.495	0.469	0.999	0.968	0.965
Gemmatimonadaceae	0.000 G	0.001 G	0.014 G	0.001 G	0.009 G	0.332	0.071	0.279	0.050	0.294	0.902	0.255	0.344	0.980	0.305
Nocardioides	0.005 G	0.004 G	0.011 G	0.003 G	0.039 G	0.895	0.872	0.604	0.227	0.781	0.697	0.185	0.534	0.347	0.098
Gaiella	0.000 G	0.001 G	0.005 G	0.004 G	0.006 G	0.573	0.231	0.176	0.106	0.469	0.403	0.261	0.978	0.760	0.757
Nitrosomonadaceae	0.072	0.090	0.004 H	0.007 N	0.050 U	0.884	0.066	0.153	0.816	0.053	0.121	0.706	0.511	0.094	0.220
Chthoniobacter	0.391	0.010 GU	0.761	0.806	0.795	0.030 GU	0.591	0.487	0.497	0.018 GU	0.009 GU	0.009 GU	0.930	0.941	0.988
Ramlibacter	0.501	0.771	0.285	0.639	0.067	0.665	0.602	0.815	0.161	0.370	0.840	0.078	0.469	0.434	0.110
Caenimonas	0.459	0.518	0.696	0.147	0.976	0.139	0.749	0.391	0.427	0.293	0.031 GU	0.452	0.284	0.690	0.115
Lysobacter	0.002 GN	0.645	0.913	0.904	0.869	0.002 GN	0.001 GN	0.001 GN	0.001 GN	0.563	0.519	0.488	1.000	0.964	0.960
Haliangium	0.023 GN	0.004 GU	0.162	0.356	0.651	0.258	0.327	0.084	0.006 GN	0.062	0.011 GU	0.001 GU	0.508	0.060	0.140
Steroidobacter	0.002 G	0.031 G	0.003 G	0.012 G	0.001 G	0.074	0.968	0.192	0.876	0.098	0.564	0.057	0.226	0.920	0.150
Altererythrobacter	0.140	0.271	0.186	0.113	0.048 G	0.634	0.962	0.886	0.484	0.705	0.538	0.251	0.860	0.500	0.574
7B-8	0.582	0.011 GU	0.585	0.653	0.563	0.017 GU	0.263	0.276	0.221	0.004 GU	0.002 GU	0.002 GU	0.880	0.984	0.883
Flavisolibacter	0.016 GN	0.005 GU	0.980	0.795	0.830	0.441	0.016 GN	0.005 GN	0.013 GN	0.005 GU	0.001 GU	0.003 GU	0.774	0.851	0.597

Rhodopirellula	0.135	0.002 GU	0.974	0.970	0.781	0.020 GU	0.127	0.106	0.164	0.002 GU	0.001 GU	0.002 GU	0.942	0.755	0.789
Phenylobacterium	0.047 GN	0.018 GU	0.777	0.870	0.821	0.553	0.027 GN	0.041 GN	0.019 GN	0.011 GU	0.014 GU	0.007 GU	0.637	0.933	0.663
Niastella	0.000 GN	0.304	0.095	0.000 N	0.239	0.000 GN	0.001 GN	0.066	0.000 GN	0.011 H	0.000 N	0.854	0.000 N	0.008 H	0.000 N
Anaerolineaceae	0.155	0.698	0.573	0.990	0.473	0.232	0.055	0.114	0.029 GN	0.324	0.656	0.229	0.545	0.916	0.431
Gemmata	0.655	0.579	0.438	0.298	0.033 G	0.901	0.208	0.112	0.008 GN	0.175	0.091	0.007 GU	0.836	0.144	0.156
Chryseobacterium	0.431	0.575	0.214	0.609	0.988	0.793	0.046 H	0.749	0.389	0.070	0.955	0.542	0.076	0.173	0.580
Iamia	0.002 G	0.004 G	0.055	0.010 G	0.021 G	0.680	0.111	0.321	0.152	0.202	0.550	0.286	0.435	0.727	0.622
Gemmatimonas	0.000 GN	0.953	0.176	0.981	0.499	0.000 GN	0.005 GN	0.000 GN	0.001 GN	0.129	0.927	0.415	0.147	0.392	0.467
Pirellula	0.225	0.010 GU	0.744	0.646	0.611	0.056	0.376	0.380	0.410	0.017 GU	0.011 GU	0.013 GU	0.919	0.878	0.954
Planctomyces	0.009 GN	0.045 GU	0.522	0.390	0.787	0.309	0.030 GN	0.025 GN	0.003 GN	0.149	0.151	0.017 GU	0.867	0.338	0.218
Acinetobacter	0.532	0.817	0.422	0.698	0.406	0.657	0.149	0.788	0.121	0.275	0.860	0.245	0.217	0.962	0.187
Xanthomonas	0.547	0.176	0.615	0.225	0.197	0.042 GU	0.957	0.471	0.417	0.071	0.012 GU	0.010 GU	0.485	0.435	0.924
Micromonosporaceae	0.008 G	0.015 G	0.045 G	0.024 G	0.141	0.690	0.447	0.485	0.087	0.680	0.759	0.167	0.889	0.386	0.268
Ochrobactrum	0.968	0.927	0.945	0.943	0.127	0.955	0.972	0.973	0.086	0.988	0.982	0.078	0.996	0.112	0.081
Caulobacteraceae	0.048 GN	0.059	0.766	0.323	0.321	0.890	0.084	0.205	0.206	0.104	0.253	0.254	0.497	0.495	0.997
Cesiribacter	0.718	0.767	0.967	0.220	0.593	0.467	0.751	0.090	0.326	0.733	0.288	0.787	0.205	0.563	0.417
Methylibium	0.062	0.194	0.433	0.291	0.128	0.444	0.254	0.294	0.630	0.629	0.761	0.771	0.832	0.462	0.554
Reichenbachiella	0.0178 G	0.425	0.004 G	0.002 G	0.002 G	0.049 GU	0.231	0.154	0.204	0.008 GU	0.004 GU	0.005 GU	0.918	0.954	0.858
Bacillus	0.775	0.016 GU	0.994	0.998	0.968	0.016 GU	0.769	0.748	0.784	0.016 GU	0.009 GU	0.010 GU	0.995	0.961	0.963
OM1_clade	0.002 G	0.003 G	0.065	0.013 G	0.076	0.634	0.076	0.201	0.029 U	0.154	0.400	0.067	0.466	0.776	0.267
Legionella	0.161	0.508	0.483	0.512	0.587	0.375	0.043 GN	0.034 GN	0.043 GN	0.168	0.158	0.193	0.907	0.818	0.898
Brevundimonas	0.016 GN	0.008 GU	0.681	0.633	0.682	0.649	0.008 GN	0.004 GN	0.004 GN	0.004 GU	0.002 GU	0.002 GU	0.977	0.967	0.938
Sulfurimonas	0.772	0.797	0.791	0.772	0.133	0.971	1.000	1.000	0.056	0.974	0.971	0.059	1.000	0.082	0.056
Pseudonocardia	0.026 G	0.024 G	0.042 G	0.022 G	0.030 G	0.963	0.948	0.927	0.921	0.916	0.963	0.885	0.883	0.981	0.849
Opitutus	0.742	0.001 GU	0.748	0.797	0.871	0.001 GU	0.500	0.516	0.585	0.001 GU	0.000 GU	0.000 GU	0.923	0.849	0.916
Devosia	0.042 G	0.811	0.007 G	0.005 G	0.006 G	0.042 GU	0.203	0.197	0.223	0.006 GU	0.004 GU	0.005 GU	0.903	0.845	0.934
Pontibacter	0.792	0.928	0.047 H	0.135	0.012 U	0.694	0.021 H	0.060	0.004 U	0.038 H	0.117	0.008 U	0.415	0.586	0.145
Parachlamydiaceae	0.509	0.030 GU	0.805	0.563	0.871	0.065	0.693	0.182	0.364	0.048 GU	0.006 GU	0.013 GU	0.402	0.666	0.640
Skermanella	0.471	0.006 GU	0.232	0.344	0.169	0.012 GU	0.533	0.791	0.433	0.064	0.020 GU	0.050 GU	0.696	0.933	0.598
AKIW1012	0.278	0.209	0.629	0.552	0.574	0.831	0.122	0.077	0.082	0.088	0.053	0.057	0.946	0.972	0.971
Comamonadaceae	0.075	0.024 GU	0.176	0.589	0.743	0.476	0.705	0.142	0.095	0.318	0.042 GU	0.027 GU	0.324	0.237	0.810
Defluviicoccus	0.041 GN	0.003 GU	0.282	0.263	0.620	0.108	0.296	0.223	0.067	0.023 GU	0.012 GU	0.003 GU	0.953	0.480	0.469
Sphingomonadaceae	0.327	0.315	0.914	0.100	0.049 U	0.977	0.384	0.403	0.205	0.371	0.418	0.214	0.122	0.060	0.640
Pseudomonas	0.954	0.104	0.910	0.898	0.951	0.066	0.947	0.937	0.895	0.085	0.058	0.083	0.997	0.853	0.833

DUNssu044	0.409	0.112	0.034 H	0.092	0.029 U	0.346	0.097	0.289	0.090	0.365	0.898	0.395	0.425	0.880	0.466
Pseudonocardiaceae	0.949	0.063	0.767	0.655	0.728	0.036 GU	0.794	0.667	0.646	0.036 GU	0.017 GU	0.081	0.901	0.505	0.381
Aquipuribacter	0.000	0.000	0.000	0.000	0.000	0.729	0.579	0.781	0.228	0.393	0.535	0.132	0.756	0.579	0.342
DA111	0.071	0.061	0.001 H	0.003 N	0.823	0.925	0.016 H	0.071	0.073	0.018 H	0.083	0.062	0.299	0.001 H	0.002 N
Colwellia	0.957	0.957	0.960	0.957	0.038 U	1.000	1.000	1.000	0.021 U	1.000	1.000	0.021 U	1.000	0.034 U	0.021 U
Procabacter	0.015 GN	0.083	0.876	0.773	0.976	0.280	0.011 GN	0.005 GN	0.009 GN	0.062	0.032 GU	0.060	0.906	0.840	0.722
Oxalobacteraceae	0.887	0.056	0.973	0.914	0.272	0.048 GU	0.858	0.970	0.282	0.052	0.045 GU	0.290	0.884	0.258	0.267
*Clostridium_sensu_stricto_*	0.714	0.436	0.365	0.594	0.833	0.638	0.187	0.850	0.861	0.094	0.777	0.521	0.143	0.237	0.716
Glycomyces	0.000 G	0.000 G	0.000 G	0.000 G	0.000 G	0.709	0.218	0.170	0.142	0.128	0.092	0.076	0.993	0.913	0.910
Microvirga	0.229	0.072	0.948	0.619	0.953	0.432	0.205	0.073	0.202	0.063	0.018 GU	0.054	0.670	0.896	0.535
Nordella	0.172	0.639	0.045 G	0.059	0.061	0.295	0.326	0.478	0.493	0.071	0.095	0.099	0.717	0.701	0.981
Aquicella	0.423	0.022 GU	0.910	0.879	0.560	0.062	0.358	0.464	0.799	0.017 GU	0.017 GU	0.040 GU	0.783	0.482	0.628
Planctomycetaceae	0.661	0.041 GU	0.409	0.410	0.494	0.011 GU	0.633	0.658	0.780	0.008 GU	0.005 GU	0.007 GU	0.935	0.819	0.869
Sandaracinus	0.000 GN	0.028 GU	0.252	0.177	0.145	0.000 GN	0.000 GN	0.000 GN	0.000 GN	0.003 GU	0.001 GU	0.001 GU	0.909	0.809	0.887
Pir4_lineage	0.003 GN	0.017 GU	0.405	0.488	0.194	0.269	0.015 GN	0.005 GN	0.019 GN	0.087	0.038 GU	0.134	0.820	0.670	0.469
Xanthomonadaceae	0.019 GN	0.527	0.969	0.973	0.950	0.038 GN	0.018 GN	0.010 GN	0.010 GN	0.501	0.458	0.440	0.993	0.984	0.975
Paucimonas	0.454	0.005 GU	0.948	0.848	0.714	0.011 GU	0.497	0.530	0.663	0.006 GU	0.004 GU	0.005 GU	0.905	0.768	0.844
Sandaracinaceae	0.305	0.490	0.333	0.029 N	0.974	0.693	0.974	0.132	0.269	0.700	0.068	0.462	0.182	0.305	0.018 N
Noviherbaspirillum	0.862	0.446	0.494	0.987	0.051	0.302	0.362	0.860	0.023 U	0.987	0.386	0.142	0.446	0.180	0.031 U
Nitrospira	0.000 GN	0.029 GU	0.660	0.695	0.479	0.001 GN	0.000 GN	0.000 GN	0.000 GN	0.067	0.037 GU	0.069	0.929	0.816	0.719
Rhodocytophaga	0.002 GN	0.000 GU	0.000 G	0.000 G	0.000 G	0.172	0.039 GN	0.190	0.039 GN	0.313	0.948	0.388	0.288	0.804	0.355
Burkholderia	0.869	0.869	0.880	0.869	0.092	1.000	1.000	1.000	0.046 U	1.000	1.000	0.046 U	1.000	0.069	0.046 U
Rubellimicrobium	0.729	0.981	0.824	0.341	0.478	0.680	0.558	0.161	0.680	0.826	0.301	0.415	0.471	0.347	0.081
Paracoccus	0.023 GN	0.004 GU	0.885	0.921	0.767	0.301	0.018 GN	0.011 GN	0.024 GN	0.003 GU	0.002 GU	0.004 GU	0.953	0.651	0.660
Bosea	0.010 G	0.009 G	0.002 G	0.000 G	0.002 G	0.966	0.164	0.044 GN	0.260	0.174	0.048 GU	0.277	0.592	0.673	0.295
Caldilineaceae	0.943	0.591	0.694	0.928	0.971	0.498	0.719	0.856	0.968	0.342	0.617	0.523	0.604	0.693	0.888
Herpetosiphon	0.020 G	0.042 G	0.149	0.108	0.135	0.647	0.323	0.297	0.237	0.551	0.543	0.450	0.957	0.933	0.878
Bradyrhizobium	0.000 GN	0.237	0.954	0.610	0.859	0.000 GN	0.000 GN	0.000 GN	0.000 GN	0.260	0.074	0.138	0.568	0.810	0.709
Pseudorhodoferax	0.002 GN	0.572	0.478	0.439	0.439	0.000 GN	0.000 GN	0.000 GN	0.000 GN	0.828	0.808	0.808	1.000	1.000	1.000
Ilumatobacter	0.252	0.242	0.732	0.403	0.482	0.975	0.140	0.709	0.055	0.134	0.686	0.052	0.237	0.738	0.103
Belnapia	0.530	0.141	0.815	0.428	0.470	0.313	0.383	0.130	0.913	0.092	0.022 GU	0.364	0.586	0.335	0.109
Thalassobaculum	0.227	0.500	0.024 G	0.029 G	0.056	0.527	0.133	0.187	0.353	0.050	0.065	0.134	0.720	0.461	0.666
Sphingobacteriaceae	0.069	0.003 GU	0.940	0.941	0.469	0.073	0.080	0.053	0.183	0.004 GU	0.002 GU	0.006 GU	0.993	0.519	0.466

Bdellovibrio	0.535	0.006 GU	0.973	0.951	0.883	0.011 GU	0.559	0.532	0.595	0.007 GU	0.004 GU	0.004 GU	0.980	0.912	0.923
Phycisphaera	0.384	0.017 GU	0.904	0.852	0.655	0.056	0.321	0.247	0.626	0.014 GU	0.007 GU	0.024 GU	0.956	0.565	0.483
CL500-29_marine_group	0.004 G	0.000 G	0.000 G	0.000 G	0.000 G	0.121	0.001 GN	0.001 GN	0.001 GN	0.008 GU	0.014 GU	0.008 GU	0.548	0.732	0.768
Cytophaga	0.076	0.058	0.173	0.510	0.102	0.862	0.005 H	0.177	0.843	0.004 H	0.134	0.710	0.045 H	0.007 H	0.241
Rhodobacteraceae	0.341	0.275	0.498	0.365	0.296	0.867	0.822	0.955	0.911	0.708	0.823	0.955	0.861	0.746	0.867
Xanthomonadales	0.043 GN	0.007 GU	0.606	0.674	0.717	0.257	0.114	0.062	0.013 GN	0.019 GU	0.008 GU	0.002 GU	0.884	0.361	0.388
Roseomonas	0.057	0.136	0.026 G	0.020 G	0.024 G	0.569	0.488	0.511	0.589	0.241	0.233	0.278	0.914	0.829	0.904
Microbacteriaceae	0.000 G	0.000 G	0.000 G	0.000 G	0.000	0.687	0.448	0.128	0.054	0.273	0.064	0.027 GU	0.502	0.273	0.615
Marmoricola	0.440	0.101	0.601	0.648	0.149	0.289	0.836	0.717	0.416	0.253	0.167	0.792	0.906	0.355	0.250
Enhydrobacter	0.128	0.123	0.919	0.092	0.170	0.978	0.154	0.824	0.846	0.148	0.846	0.824	0.111	0.202	0.678
Propionibacterium	0.684	0.875	0.495	0.421	0.684	0.530	0.730	0.649	1.000	0.371	0.289	0.530	0.950	0.730	0.649
Thermovirga	1.000	1.000	1.000	1.000	0.145	1.000	1.000	1.000	0.108	1.000	1.000	0.108	1.000	0.145	0.108
FFCH16767	0.153	0.043 GU	0.455	0.442	0.763	0.407	0.502	0.422	0.196	0.172	0.120	0.048 GU	0.960	0.600	0.596
mle1-27	0.009 GN	0.017 G	0.312	0.098	0.208	0.000 GN	0.001 GN	0.000 GN	0.000 GN	0.125	0.282	0.125	0.525	0.861	0.604
Nitriliruptor	0.481	0.621	0.109	0.621	0.017 U	0.809	0.024 H	0.195	0.002 U	0.035 H	0.281	0.004 U	0.186	0.374	0.025 U
Nannocystis	0.044 GN	0.671	0.793	0.402	0.898	0.064	0.073	0.143	0.022 GN	0.890	0.635	0.539	0.575	0.678	0.286
Microbacterium	0.000 G	0.000 G	0.000 G	0.000 G	0.000 G	0.330	0.161	0.236	0.878	0.563	0.818	0.407	0.707	0.200	0.296
Rhodoplanes	0.605	0.054	0.346	0.560	0.017 U	0.094	0.594	0.940	0.026 U	0.296	0.107	0.459	0.640	0.104	0.029 U
Pedomicrobium	0.016 GN	0.076	0.067	0.535	0.090	0.333	0.535	0.031 GN	0.282	0.794	0.165	0.907	0.139	0.716	0.199
Kocuria	0.235	0.048 GU	0.845	0.657	0.199	0.294	0.321	0.388	0.905	0.069	0.072	0.348	0.816	0.275	0.330
Luteimonas	0.154	0.044 GU	0.895	0.746	0.876	0.412	0.122	0.062	0.153	0.034 GU	0.014 GU	0.037 GU	0.857	0.764	0.593
Hydrotalea	0.377	0.563	0.188	0.874	0.434	0.723	0.033 H	0.252	0.081	0.057	0.415	0.145	0.196	0.480	0.483
Peredibacter	0.498	0.004 GU	0.228	0.732	0.498	0.007 GU	0.061	0.265	0.147	0.000 GU	0.001 GU	0.001 GU	0.316	0.498	0.702
Holosporaceae	0.772	0.025 GU	0.702	0.676	0.923	0.026 GU	0.483	0.434	0.666	0.012 GU	0.006 GU	0.012 GU	1.000	0.747	0.719
Pseudoxanthomonas	0.671	0.016 GU	0.735	0.732	0.711	0.021 GU	0.956	0.398	0.382	0.031 GU	0.005 GU	0.004 GU	0.480	0.464	0.975
Hamadaea	0.000 G	0.000 G	0.000 G	0.000 G	0.001 G	0.814	0.861	0.969	0.178	0.972	0.845	0.122	0.888	0.171	0.167
I-10	0.986	0.249	0.562	0.482	0.471	0.195	0.537	0.444	0.433	0.089	0.054	0.052	0.943	0.929	0.984
Geminicoccus	0.016 G	0.020 G	0.004 G	0.004 G	0.004 G	0.904	0.293	0.364	0.364	0.250	0.307	0.307	0.801	0.801	1.000
Cytophagaceae	0.502	0.233	0.328	0.523	0.640	0.053	0.677	0.969	0.815	0.038 GU	0.056	0.079	0.652	0.534	0.846
Chitinophagaceae	0.136	0.025 GU	0.812	0.958	0.333	0.290	0.205	0.110	0.513	0.040 GU	0.017 GU	0.103	0.835	0.471	0.307
Cystobacteraceae	0.312	0.012 G	0.041 G	0.016 G	0.009 G	0.001 GN	0.005 GN	0.001 GN	0.001 GN	0.626	0.847	0.847	0.751	0.511	0.700
Coxiella	0.479	0.202	0.557	0.506	0.691	0.041 GU	0.945	0.959	0.722	0.069	0.044 GU	0.075	0.982	0.802	0.760
Chitinophaga	0.533	0.672	0.362	0.395	0.422	0.254	0.697	0.790	0.834	0.169	0.169	0.185	0.878	0.838	0.955

Patulibacter	0.901	1.000	0.043 H	0.885	0.514	0.890	0.037 H	0.982	0.552	0.029 H	0.872	0.466	0.038 H	0.092	0.567
envOPS_17	0.251	0.166	0.942	0.587	0.925	0.766	0.282	0.479	0.172	0.189	0.322	0.106	0.642	0.862	0.479
Acidiferrobacter	0.132	0.902	0.041 H	0.053	0.677	0.076	0.372	0.549	0.205	0.022 H	0.027 N	0.549	0.713	0.057	0.076
Geodermatophilus	0.018 G	0.008 G	0.024 G	0.010 G	0.030 G	0.609	0.950	0.709	0.744	0.692	0.888	0.408	0.786	0.723	0.488
Truepera	0.718	0.773	0.767	0.520	0.073	0.936	0.971	0.747	0.098	0.971	0.687	0.086	0.745	0.126	0.166
NS11-12_marine_group	0.242	0.179	0.893	0.794	0.695	0.826	0.193	0.301	0.095	0.141	0.218	0.066	0.683	0.806	0.470
JG34-KF-361	1.000	0.906	0.128	0.559	0.194	0.895	0.099	0.514	0.151	0.082	0.436	0.122	0.254	0.681	0.400
Acidimicrobiaceae	0.203	0.608	0.251	0.470	0.470	0.373	0.978	0.509	0.509	0.438	0.808	0.808	0.572	0.572	1.000
Staphylococcus	0.032 G	0.034 G	0.055	0.035 G	0.032 G	0.975	0.917	0.963	1.000	0.939	0.988	0.975	0.950	0.917	0.963
Desulfonauticus	1.000	1.000	1.000	1.000	0.072	1.000	1.000	1.000	0.048 U	1.000	1.000	0.048 U	1.000	0.072	0.048 U
Actinotalea	0.759	0.343	0.285	0.169	0.280	0.465	0.151	0.072	0.134	0.049 GU	0.020 GU	0.038 GU	0.813	0.925	0.712
EF100-94H03	0.948	0.746	0.300	0.284	0.312	0.665	0.284	0.261	0.290	0.157	0.132	0.149	0.948	0.897	0.942
TK34	0.807	0.588	0.184	0.238	0.200	0.386	0.218	0.288	0.239	0.060	0.070	0.056	0.764	0.851	0.899
Blastococcus	0.000 G	0.001 G	0.000 G	0.000 G	0.000 G	0.264	0.570	0.526	0.449	0.131	0.096	0.702	1.000	0.225	0.179
Rhizobacter	0.846	0.070	0.978	0.992	0.878	0.069	0.822	0.819	0.964	0.067	0.046 GU	0.063	0.984	0.854	0.855
Kribbella	0.073	0.026 GU	0.839	0.711	0.901	0.511	0.106	0.099	0.038 GU	0.038 GU	0.031 GU	0.012 GU	0.882	0.729	0.583
KCM-B-15	0.061	0.025 GU	0.879	0.411	0.911	0.578	0.081	0.190	0.049 GU	0.034 GU	0.076	0.018 GU	0.508	0.956	0.425
Promicromonospora	0.192	0.338	0.369	0.239	0.721	0.670	0.721	0.873	0.276	0.981	0.789	0.492	0.830	0.523	0.347
Proteus	0.154	0.118	0.509	0.175	0.175	0.856	0.048 H	0.928	0.928	0.034 H	0.785	0.785	0.052	0.052	1.000
Lachnospiraceae	0.753	0.486	0.147	0.516	0.753	0.665	0.068	0.291	1.000	0.035 H	0.150	0.665	0.320	0.068	0.291
PRD01a011B	0.256	0.223	0.525	0.432	0.888	0.916	0.641	0.676	0.163	0.576	0.602	0.137	0.925	0.407	0.307
Desulfuromonas	0.409	0.642	0.062	0.277	0.156	0.165	0.181	0.755	0.471	0.020 H	0.099	0.048 U	0.277	0.461	0.677
Inquilinus	0.600	0.903	0.328	0.447	0.715	0.473	0.126	0.167	0.329	0.341	0.473	0.785	0.746	0.470	0.651
Desulfovibrio	0.655	0.655	0.006 H	0.095	0.655	1.000	0.007 H	0.154	1.000	0.007 H	0.154	1.000	0.079	0.007 H	0.154
Bauldia	0.748	0.217	0.388	0.609	0.609	0.295	0.217	0.360	0.360	0.044 GU	0.066	0.066	0.654	0.654	1.000
Family_XVIII	0.720	0.720	0.925	0.488	0.185	1.000	0.797	0.251	0.073	0.797	0.251	0.073	0.428	0.157	0.450
Candidatus_Odyssella	0.836	0.205	0.965	0.962	0.962	0.230	0.799	0.776	0.776	0.190	0.147	0.147	1.000	1.000	1.000
Euzebya	0.830	0.830	0.441	0.412	0.020 G	1.000	0.297	0.257	0.008 U	0.297	0.257	0.008 U	0.981	0.089	0.059
Desulfomicrobium	0.170	0.170	0.207	0.170	0.477	1.000	1.000	1.000	0.033 U	1.000	1.000	0.033 U	1.000	0.051	0.033 U
Phaselicystis	0.554	0.001 GU	1.000	1.000	0.842	0.002 GU	0.554	0.509	0.658	0.001 GU	0.001 GU	0.001 GU	1.000	0.842	0.824
Massilia	0.483	0.568	0.926	0.406	0.406	0.880	0.546	0.880	0.880	0.637	0.763	0.763	0.463	0.463	1.000

Supplementary Table 4. Bacterial phyla of bentonite microcosms and their corresponding p-values. Multiple comparison using DMS test and a significance level of 0.05 were used to look for significant differences in the alpha diversity between pair of samples. Coloured cells represent p-value < 0.05: blue for H, light green for G, orange for N, green for GN, purple for U, light purple for GU .

Phyla	Multiple comparisons between pair of samples														
	G-GN	G-GU	GN-GU	GN-H	GN-N	GN-U	GU-H	GU-N	GU-U	H-N	H-U	N-U	G-H	G-N	G-U
Acidobacteria	0.086	0.661	0.366	0.083	0.782	0.199	0.196	0.349	0.816	0.402	0.102	0.202	0.042 G	0.101	0.838
Actinobacteria	0.761	0.400	0.331	0.078	0.019 GN	0.065	0.177	0.120	0.161	0.265	0.771	0.415	0.162	0.061	0.133
Armatimonadetes	0.036 G	0.737	0.240	0.017 GN	0.327	0.795	0.182	0.260	0.233	0.007 N	0.213	0.484	0.019 G	0.044 G	0.039 G
Bacteroidetes	0.943	0.618	0.566	0.044 GN	0.119	0.198	0.211	0.286	0.304	0.568	0.594	0.968	0.154	0.278	0.329
Caldiserica	0.374	NA	0.374	0.374	0.374	0.374	NA	NA	NA	NA	NA	NaN	NA	NA	NA
Candidate_division_BRC1	0.003 GN	0.315	0.021 GN	0.001 GN	0.001 GN	0.000 GN	0.102	0.080	0.070	0.702	0.520	0.737	0.284	0.194	0.157
Candidate_division_JS1	0.374	0.374	NA	NA	NA	NaN	NA	NA	NA	NA	NA	NaN	0.374	0.374	0.374
Candidate_division_OD1	0.374	0.689	0.355	0.374	NA	0.145	0.481	0.355	0.747	0.374	0.391	0.145	0.638	0.374	0.863
Candidate_division_TM7	0.130	0.080	0.309	0.117	0.117	0.117	0.056	0.056	0.056	NA	NA	NaN	0.132	0.132	0.132
Chlamydiae	0.145	0.818	0.109	0.850	0.025 GN	0.249	0.185	0.052	0.207	0.306	0.672	0.032 U	0.200	0.083	0.229
Chlorobi	0.277	0.403	0.192	0.374	0.374	NaN	0.236	0.212	0.192	0.678	0.374	0.374	0.446	0.349	0.277
Chloroflexi	0.074	0.105	0.893	0.702	0.719	0.34	0.672	0.683	0.556	0.975	0.268	0.324	0.151	0.198	0.031 G
Cyanobacteria	0.643	0.407	0.609	0.238	0.345	0.872	0.223	0.275	0.718	0.374	0.261	0.346	0.158	0.374	0.573
Deinococcus-Thermus	0.964	0.565	0.726	0.507	0.699	0.323	0.106	0.212	0.218	0.621	0.455	0.372	0.396	0.636	0.304
Elusimicrobia	0.374	0.374	NA	0.374	0.374	NaN	0.374	0.374	NA	0.561	0.374	0.374	0.678	0.795	0.374
Fibrobacteres	NA	NA	NA	NA	NA	0.374	NA	NA	0.374	NA	0.374	0.374	NA	NA	0.374
Firmicutes	0.307	0.196	0.144	0.413	0.384	0.221	0.177	0.155	0.230	0.614	0.534	0.301	0.774	0.441	0.720
Fusobacteria	0.205	0.026 G	0.374	0.374	0.374	0.374	NA	NA	NA	NA	NA	NaN	0.026 G	0.026 G	0.026 G
Gemmatimonadetes	0.018 G	0.084	0.977	0.112	0.392	0.567	0.453	0.651	0.659	0.109	0.859	0.352	0.074	0.021 G	0.164
Lentisphaerae	0.374	0.374	NA	NA	NA	NaN	NA	NA	NA	NA	NA	NaN	0.374	0.374	0.374
Nitrospirae	0.000 GN	0.098	0.034 GN	0.001 GN	0.001 GN	0.001 GN	0.156	0.151	0.254	0.914	0.317	0.208	0.261	0.001 N	0.044 U
NPL-UPA2	0.374	0.374	1.000	0.374	0.374	0.374	0.374	0.374	0.374	NA	NA	NaN	NA	NA	NA
Planctomycetes	0.01 GN	0.073	0.255	0.001 GN	0.007 GN	0.003 GN	0.050 GU	0.056	0.050	0.786	0.912	0.746	0.240	0.450	0.265
Proteobacteria	0.041 G	0.052	0.694	0.049 GN	0.023 GN	0.033 GN	0.173	0.094	0.115	0.388	0.530	0.902	0.001 G	0.001 G	0.001 G
SM2F11	NA	NA	NA	NA	NA	0.374	NA	NA	0.374	NA	0.374	0.374	NA	NA	0.374
Spirochaetae	0.374	0.374	NA	NA	NA	0.374	NA	NA	0.374	NA	0.374	0.374	0.374	0.374	1.000
Synergistetes	0.374	0.374	NA	NA	NA	0.326	NA	NA	0.326	NA	0.326	0.326	0.374	0.374	0.398
TA06	NA	0.374	0.374	NA	NA	NaN	0.374	0.374	0.374	NA	NA	NaN	NA	NA	NA
Tenericutes	NA	NA	NA	0.374	NA	NaN	0.374	NA	NA	0.374	0.374	NaN	0.374	NA	NA

Thermodesulfobacteria	0.307	0.307	NA	NA	NA	0.374	NA	NA	0.374	NA	0.374	0.374	0.307	0.307	0.414
TM6	0.316	0.328	0.817	0.941	0.172	0.344	0.756	0.033 GU	0.096	0.215	0.412	0.067	0.311	0.240	0.263
unclassified	0.678	0.252	0.310	0.122	0.010 N	0.143	0.154	0.013 N	0.136	0.468	0.109	0.008 N	0.118	0.009 N	0.408
Verrucomicrobia	0.000 GN	0.062	0.136	0.001 GN	0.003 GN	0.049 GN	0.076	0.075	0.090	0.860	0.381	0.365	0.023 H	0.099	0.075

Supplementary Table 5. Bacterial classes of bentonite microcosms and their corresponding p-values. Multiple comparison using DMS test and a significance level of 0.05 were used to look for significant differences in the alpha diversity between pair of samples. Coloured cells represent p-value < 0.05: blue for H, light green for G, orange for N, green for GN, purple for U, light purple for GU.

Classes	**Multiple comparisons between pair of samples**														
	G-GN	**G-GU**	**GN-GU**	**GN-H**	**GN-N**	**GN-U**	**GU-H**	**GU-N**	**GU-U**	**H-N**	**H-U**	**N-U**	**G-H**	**G-N**	**G-U**
Acidimicrobiia	0.241	0.250	0.979	0.003 H	0.041 N	0.030 U	0.003 H	0.043 N	0.031 U	0.091	0.121	0.847	0.032 H	0.415	0.328
Acidobacteria	0.303	0.936	0.288	0.640	0.927	0.172	0.168	0.252	0.735	0.699	0.102	0.149	0.183	0.269	0.824
Actinobacteria	0.597	0.069	0.127	0.150	0.103	0.169	0.012 GU	0.006 GU	0.010 GU	0.966	0.819	0.762	0.376	0.315	0.454
Alphaproteobacteria	0.166	0.368	0.551	0.011 GN	0.005 GN	0.005 GN	0.029 GU	0.014 GU	0.014 GU	0.927	0.918	0.990	0.174	0.120	0.118
Anaerolineae	0.155	0.698	0.231	0.055	0.114	0.029 GN	0.325	0.657	0.231	0.546	0.918	0.433	0.575	0.992	0.476
Ardenticatenia	1.000	0.205	0.161	0.514	0.902	1.000	0.514	0.195	0.161	0.585	0.514	0.902	0.550	0.912	1.000
Armatimonadia	0.000 G	0.000 G	0.352	0.672	0.812	0.812	0.672	0.251	0.481	0.527	0.832	0.636	0.000 G	0.000 G	0.000 G
Bacilli	0.879	0.034 GU	0.015 GU	0.791	0.810	0.872	0.016 GU	0.010 GU	0.011 GU	0.960	0.904	0.937	0.704	0.714	0.767
Bacteroidia	0.741	0.583	0.335	0.005 H	0.057	0.712	0.024 H	0.281	0.541	0.131	0.009 H	0.107	0.015 H	0.144	1.000
BD7-11	0.140	0.605	0.260	1.000	1.000	1.000	0.310	0.260	0.260	1.000	1.000	1.000	0.174	0.140	0.140
Betaproteobacteria	0.179	0.130	0.826	0.882	0.548	0.824	0.961	0.416	0.999	0.495	0.960	0.415	0.175	0.395	0.130
Caldilineae	0.943	0.591	0.498	0.719	0.856	0.968	0.342	0.617	0.523	0.604	0.693	0.888	0.694	0.928	0.971
Caldisericia	0.188	1.000	0.145	0.188	0.145	0.145	1.000	1.000	1.000	1.000	1.000	1.000	1.000	1.000	1.000
Candidate_division_OD1_unclassified	1.000	0.204	0.160	0.642	1.000	0.349	0.400	0.160	0.604	0.642	0.698	0.349	0.671	1.000	0.400
Chlamydiae	0.204	0.427	0.035 GU	0.518	0.444	0.577	0.160	0.009 GU	0.091	0.197	0.880	0.200	0.544	0.065	0.419
Chlorobi_unclassified	1.000	1.000	1.000	1.000	0.145	1.000	1.000	0.145	1.000	0.188	1.000	0.145	1.000	0.188	1.000
Chlorobia	0.863	0.065	0.031 GU	0.730	1.000	1.000	0.088	0.031 GU	0.031 GU	0.730	0.730	1.000	0.874	0.863	0.863
Chloroflexi_unclassified	0.208	0.851	0.226	0.528	0.289	0.101	0.628	0.867	0.617	0.736	0.359	0.507	0.541	0.736	0.793
Chloroflexia	0.020 G	0.039 G	0.682	0.345	0.334	0.258	0.554	0.567	0.455	0.935	0.935	0.856	0.137	0.094	0.123
Chthonomonadetes	0.034 G	0.034 G	1.000	1.000	1.000	1.000	1.000	1.000	1.000	1.000	1.000	1.000	0.049 G	0.034 G	0.034 G
Clostridia	0.291	0.254	0.917	0.056	0.329	0.044 U	0.048 H	0.283	0.036 U	0.243	0.926	0.229	0.362	0.848	0.364
Coriobacteriia	0.002 G	0.002 G	1.000	0.209	0.341	1.000	0.209	0.341	1.000	0.664	0.209	0.341	0.034 G	0.011 G	0.002 G
Cyanobacteria	0.008 G	0.029 G	0.433	1.000	0.433	0.433	0.482	1.000	1.000	0.482	0.482	1.000	0.013 G	0.029 G	0.029 G
Cytophagia	0.609	0.608	0.264	0.405	0.520	0.934	0.083	0.094	0.234	0.790	0.446	0.574	0.231	0.287	0.559

Dehalococcoidia	0.664	1.000	0.628	0.664	0.341	0.628	1.000	0.165	1.000	0.209	1.000	0.165	1.000	0.209	1.000
Deinococci	0.866	0.686	0.792	0.674	0.763	0.134	0.514	0.574	0.087	0.879	0.330	0.217	0.817	0.919	0.228
Deltaproteobacteria	0.018 GN	0.017 GU	0.977	0.145	0.091	0.005 GN	0.139	0.087	0.005 GU	0.930	0.132	0.114	0.280	0.273	0.704
Elusimicrobia	1.000	1.000	1.000	0.512	0.160	1.000	0.512	0.160	1.000	0.512	0.512	0.160	0.549	0.204	1.000
Epsilonproteobacteria	0.821	0.809	0.987	0.964	0.960	0.065	0.976	0.973	0.063	1.000	0.086	0.059	0.804	0.786	0.135
Erysipelotrichia	1.000	0.194	0.150	0.685	1.000	1.000	0.352	0.150	0.150	0.685	0.685	1.000	0.711	1.000	1.000
Fibrobacteria	1.000	1.000	1.000	1.000	1.000	0.145	1.000	1.000	0.145	1.000	0.188	0.145	1.000	1.000	0.188
Firmicutes_unclassified	0.228	0.678	0.362	0.755	0.182	0.182	0.605	0.643	0.643	0.359	0.359	1.000	0.400	1.000	1.000
Flavobacteriia	0.442	0.593	0.786	0.048 H	0.739	0.382	0.073	0.950	0.540	0.081	0.182	0.581	0.215	0.632	0.988
Fusobacteriia	0.136	0.015 G	0.177	0.224	0.177	0.177	1.000	1.000	1.000	1.000	1.000	1.000	0.023 G	0.015 G	0.015 G
Gammaproteobacteria	0.000 G	0.000 G	0.659	0.313	0.236	0.261	0.526	0.439	0.479	0.951	0.999	0.946	0.000 G	0.000 G	0.000 G
Gemmatimonadetes	0.045 G	0.043 G	0.978	0.604	0.598	0.568	0.588	0.616	0.550	0.331	0.995	0.282	0.141	0.020 G	0.109
Gitt-GS-136	0.001 G	0.002 G	0.577	0.270	0.165	0.905	0.529	0.379	0.659	0.867	0.315	0.199	0.009 G	0.007 G	0.001 G
Holophagae	0.011 GN	0.767	0.003 GN	0.004 GN	0.011 GN	0.002 GN	0.812	0.511	0.791	0.414	1.000	0.363	0.628	0.767	0.596
Ignavibacteria	1.000	0.188	0.145	1.000	1.000	1.000	0.188	0.145	0.145	1.000	1.000	1.000	1.000	1.000	1.000
JG30-KF-CM66	0.915	0.750	0.636	0.276	0.879	0.011 U	0.491	0.746	0.025 U	0.335	0.130	0.014 U	0.363	0.977	0.023 U
KD4-96	0.461	0.919	0.475	0.861	0.486	0.213	0.639	0.986	0.065	0.650	0.201	0.067	0.604	0.907	0.079
Ktedonobacteria	1.000	1.000	1.000	1.000	0.350	0.148	1.000	0.350	0.148	0.401	0.191	0.569	1.000	0.401	0.191
MACA-EFT26	1.000	0.235	0.188	1.000	1.000	0.496	0.235	0.188	0.496	1.000	0.541	0.496	1.000	1.000	0.541
MB-A2-108	1.000	1.000	1.000	1.000	1.000	0.145	1.000	1.000	0.145	1.000	0.188	0.145	1.000	1.000	0.188
Melainabacteria	0.404	0.194	0.572	0.404	0.353	1.000	0.194	0.151	0.572	1.000	0.404	0.353	1.000	1.000	0.404
Negativicutes	0.131	0.131	1.000	0.819	0.318	0.275	0.819	0.318	0.275	0.497	0.443	0.918	0.227	0.497	0.555
Nitriliruptoria	0.447	0.560	0.837	0.011 H	0.061	0.000 U	0.015 U	0.087	0.000 U	0.249	0.049 U	0.003 U	0.060	0.300	0.001 U
Nitrospira	0.000 GN	0.028 GU	0.001 GN	0.000 GN	0.000 GN	0.000 GN	0.078	0.038 GU	0.093	0.865	0.767	0.604	0.591	0.674	0.383
NPL-UPA2_unclassified	0.341	0.341	1.000	0.341	0.290	0.290	0.341	0.290	0.290	1.000	1.000	1.000	1.000	1.000	1.000
OM190	0.623	0.254	0.449	0.682	0.736	0.467	0.286	0.283	0.154	0.913	0.805	0.691	0.940	0.848	0.869
OPB35_soil_group	0.096	0.032 GU	0.481	0.314	0.259	0.571	0.117	0.082	0.886	0.991	0.144	0.105	0.494	0.461	0.040 U
OPB54	0.664	1.000	0.628	0.664	0.628	0.341	1.000	1.000	0.165	1.000	0.209	0.165	1.000	1.000	0.209
Opitutae	0.758	0.001 GU	0.001 GU	0.524	0.540	0.621	0.001 GU	0.000 GU	0.000 GU	0.929	0.843	0.903	0.761	0.807	0.892
P2-11E	0.730	0.698	0.961	0.468	0.311	0.000 U	0.443	0.290	0.000 U	0.846	0.003 U	0.002 U	0.723	0.562	0.002 U
Phycisphaerae	0.131	0.003 GU	0.031 GU	0.040 GN	0.035 GN	0.071	0.001 GU	0.001 GU	0.001 GU	0.865	0.597	0.686	0.532	0.604	0.874
Pla4_lineage	1.000	1.000	1.000	0.034 H	1.000	1.000	0.034 H	1.000	1.000	0.034 H	0.034 H	1.000	0.049 H	1.000	1.000
Planctomycetacia	0.132	0.009 GU	0.111	0.119	0.087	0.060	0.008 GU	0.004 GU	0.003 GU	0.993	0.776	0.744	0.956	0.959	0.731
Planctomycetes_unclassified	0.616	0.616	1.000	1.000	0.153	1.000	1.000	0.153	1.000	0.197	1.000	0.153	0.646	0.408	0.616
Rubrobacteria	0.052	0.109	0.633	0.297	0.526	0.044 U	0.524	0.873	0.101	0.618	0.362	0.132	0.338	0.137	0.886
S085	0.251	0.644	0.427	0.608	0.542	0.099	0.837	0.848	0.025 U	0.973	0.057	0.034 U	0.544	0.528	0.017 U
SAR202_clade	0.625	0.058	0.097	0.196	0.286	1.000	0.806	0.497	0.097	0.713	0.196	0.286	0.115	0.162	0.625
SHA-26	0.341	0.341	1.000	0.341	0.290	0.290	0.341	0.290	0.290	1.000	1.000	1.000	1.000	1.000	1.000

SM2F11_unclassified	1.000	1.000	1.000	1.000	1.000	0.145	1.000	1.000	0.145	1.000	0.188	0.145	1.000	1.000	0.188
Spartobacteria	0.391	0.010 GU	0.030 GU	0.591	0.487	0.497	0.018 GU	0.009 GU	0.009 GU	0.930	0.941	0.988	0.761	0.806	0.795
Sphingobacteriia	0.002 GN	0.014 GU	0.213	0.005 GN	0.054	0.001 GN	0.036 GU	0.416	0.006 GU	0.127	0.486	0.023 N	0.635	0.052	0.856
Spirochaetes	1.000	1.000	1.000	1.000	1.000	0.145	1.000	1.000	0.145	1.000	0.188	0.145	1.000	1.000	0.188
SPOTSOCT00m83	0.121	0.846	0.125	0.121	0.125	0.087	0.846	1.000	0.828	0.846	1.000	0.828	1.000	0.846	1.000
Subgroup_22	1.000	1.000	1.000	1.000	1.000	0.145	1.000	1.000	0.145	1.000	0.188	0.145	1.000	1.000	0.188
Synergistia	1.000	1.000	1.000	1.000	1.000	0.108	1.000	1.000	0.108	1.000	0.145	0.108	1.000	1.000	0.145
TA06_unclassified	1.000	0.188	0.145	1.000	1.000	1.000	0.188	0.145	0.145	1.000	1.000	1.000	1.000	1.000	1.000
TakashiAC-B11	1.000	1.000	1.000	1.000	1.000	0.145	1.000	1.000	0.145	1.000	0.188	0.145	1.000	1.000	0.188
Thermodesulfobacteria	0.353	0.353	1.000	1.000	1.000	0.177	1.000	1.000	0.177	1.000	0.224	0.177	0.395	0.353	0.752
Thermoleophilia	0.001 G	0.001 G	0.587	0.183	0.186	0.110	0.374	0.410	0.260	0.875	0.894	0.746	0.009 G	0.004 G	0.006 G
Thermomicrobia	0.705	0.872	0.808	0.041 GN	0.050	0.289	0.028 GU	0.033 GU	0.201	0.737	0.211	0.293	0.032 G	0.038 G	0.194
TK10	0.927	0.911	0.983	0.009 H	0.013 N	0.547	0.008 H	0.012 N	0.533	0.590	0.022 H	0.037 N	0.016 H	0.026 N	0.653
unclassified	1.000	0.188	0.145	1.000	1.000	1.000	0.188	0.145	0.145	1.000	1.000	1.000	1.000	1.000	1.000
VC21_Bac22	0.406	0.313	0.056	0.788	0.926	0.960	0.052	0.066	0.052	0.725	0.822	0.887	0.321	0.452	0.382
Verrucomicrobiae	0.905	0.129	0.075	0.564	0.805	0.340	0.039 GU	0.049 GU	0.014 GU	0.719	0.770	0.471	0.527	0.735	0.333

CHAPTER II

Evolution of bacterial community and mineralogy of Spanish bentonite microcosms in response to uranium and glycerol-2-phosphate exposure under anaerobic conditions

Cristina Povedano-Priego[1], Fadwa Jroundi[1], Margarita Lopez-Fernandez[2], Inés Martin-Sánchez[1], F. Javier Huertas[3], Mark Dopson[4], Mohamed L. Merroun[1]

[1]Department of Microbiology, Faculty of Sciences, University of Granada, Granada, Spain. ppriego@ugr.es; fadwa@ugr.es; sanchezcastro@ugr.es; inesms@ugr.es; merroun@ugr.es.

[2]Institute of Resource Ecology, Helmholtz-Zentrum Dresden-Rossendorf, Dresden, Germany. m.lopez-fernandez@hzdr.de

[3]Instituto Andaluz de Ciencias de la Tierra, CSIC – University of Granada, Granada, Spain. javierhuertas@ugr.es

[4]Centre for Ecology and Evolution in Microbial Model Systems (EEMiS), Linnaeus University, Kalmar, Sweden. mark.dopson@lnu.se

1. ABSTRACT

The requirement for Deep Geological Repositories (DGR) is an international priority. Among nuclear wastes, uranium (U) is considered the most hazardous radionuclide, and its harmful effects on the ecosystem structure and functions largely depend on its mobility and bioavailability. Microorganisms can potentially affect the speciation of radionuclides and in consequence their migration, through various processes including biosorption, biomineralization, bioaccumulation and biotransformation. These processes may occur in DGRs, if any radioactive element were accidentally leaked from the nuclear wastes into the environment.

A good performance of deep geological disposal of nuclear wastes is associated to the better understanding of radionuclide interactions with the natural microbes inhabiting the different DGR barriers. In order to simulate a situation where the mobilization of radionuclides from the repository to the bentonite buffer may occur, bentonite microcosms from a geological formation from Almeria (Spain), amended with uranyl nitrate (1.26 mM) and glycerol-2-phosphate (G2P, 10 mM), were studied. These microcosms were incubated during six months under anaerobic conditions at room temperature. The Spanish bentonites have been largely studied from mineralogical, geochemical, mechanical and alterability criteria as they were selected as a reference buffer material for the future Spanish DGR. After incubation, DNA from all samples were extracted and bacterial diversity analyses were carried out following Next Generation Sequencing (NGS) based on Illumina, determining the changes occurring in the structure and composition of the bacterial community present in these samples after 6 months.

Our results showed the presence of 29 bacterial phyla such as Proteobacteria, Bacteroidetes, Firmicutes, and Verrucomicrobia. Among the 258 different genera found in all anaerobic microcosms, dominant genera such as *Desulfatiglans* (a sulfate-reducing bacterium), and sulfur-oxidizing bacteria (*Sulfurimonas* and *Thiobacillus*) were identified in the U microcosms, while Pseudomonas and *Desulfovibrio*, were the most abundant genera in the U-G2P microcosms. Both are described for their ability to immobilize U as U phosphates through biomineralization (by *Pseudomonas*) and by enzymatic reduction of U(VI) to U(IV) (by *Desulfovibrio*).

Interestingly, many changes occurred also at the macroscopic level showed by the presence of brown spots localized both on the surface and within the bentonite microcosms. Scanning electron microscopy analyses of these spots revealed the probable formation of Mn(IV) oxides likely through the activity of Mn(II) oxidizing bacteria. This could affect the biogeochemical cycle of Mn concentrating and immobilizing this element in the bentonites. But, on other hand, XRD analyses determined that the different amendments did not affect the mineralogy of the bentonite pointing to a high structural stability.

The outputs of this study would help to predict the impact of microbial processes on the DGR long-term performance as well as to develop appropriate waste treatments, remediation and long-term management strategies.

Keywords: bentonite, bacterial diversity, uranium, glycerol-2-phosphate, uranium reduction, deep geological repository

2. INTRODUCTION

The Deep Geological Repository (DGR) is the internationally accepted option by many countries for the storage and management of highly-radioactive wastes (Grigoryan et al., 2018), although their construction is still in progress worldwide (Pedersen et al., 2017). The universal disposal concept involves a multi-barrier system that comprises storing the spent fuel in canisters made of cast iron, stainless steel, or copper, depending on the DGR design in each country (Anderson et al., 2011; Bengtsson and Pedersen, 2017). These canisters must generally be surrounded by another engineered barrier system consisting of a highly-compacted bentonite clay (Grigoryan et al., 2018). Bentonites, rich in montmorillonite, are the most suitable backfill materials for the DGR since they have a high swelling capacity, plasticity, low permeability and high sorption ability for radionuclide retardation (Masurat et al., 2010; Missana et al., 2003). In Spain, bentonite formation from "El Cortijo de Archidona" (Almeria) has been mineralogically well studied and selected as the engineered barrier reference material for the future Spanish DGR (Villar et al., 2006).

Since microorganisms are ubiquitous in all environments, their inferences on the DGR safety have been extensively studied in various types of bentonites (Bengtsson and Pedersen, 2017; Leupin et al., 2017; Lopez-Fernandez et al., 2018; Pedersen et al., 2017; Smart et al., 2017). Microbial activity could affect the integrity and performance of the repository, through different processes including microbial gas production (Stroes-Gascoyne et al., 2010), containers corrosion influenced by sulfate-reducing bacteria (Stone et al., 2016), and alteration of bentonite mineralogy by the reduction of structural Fe(III) in smectite (Liu et al., 2017; Pentráková et al., 2013). Furthermore, in case of a canister failure, microorganisms could control the speciation and mobility of radionuclides through different mechanisms such as biosorption, intracellular accumulation, biomineralization, and bioreduction (Lopez-Fernandez et al., 2018; Povedano-Priego et al., 2019).

Several studies were conducted to investigate the impact of bentonite microbial populations on uranium mobilization and the effects that have this radionuclide on the bacterial diversity in these clays under aerobic conditions (Lopez-Fernandez et al., 2018; Povedano-Priego et al., 2019). The results revealed the enrichment of bacterial populations involved in U biomineralization as U-phosphate mineral phases through

phosphatase activity (e.g. *Bacillus*). However, biomineralization of uranium has been described to be greatly enhanced by the presence of organophosphates such as glycerol-2-phosphate (G2P) and glycerol-3-phosphate (G3P) (Martinez et al., 2014). Thus, Povedano-Priego et al. (2019) have focused on the effects of uranium and G2P treatment under aerobic conditions, where G2P was acting as a substrate for phosphatase enzymes. These authors reported the release of inorganic phosphates leading to uranium precipitation (biomineralization). In spite of these interesting results, in the DGR concept oxygen, introduced during construction and canister emplacement, has been demonstrated to remain up to two years, after which its consumption will be relatively rapid due to microbial activity, corrosion processes or mineral oxidation (King et al., 2017; Payer et al., 2019). Therefore and because of the prevalence of a long-term anoxic phase in the DGR concept, bentonite microbial diversity studies need to be addressed under anaerobic conditions.

Radionuclide-microorganism interaction mechanisms could occur under anaerobic and reducing environments. Bioreduction of U(VI) to a less soluble U(IV) has frequently been studied; as various groups of bacteria have the capacity to enzymatically reduce U(VI) (Newsome et al., 2014a) including sulfate-reducing bacteria (e.g. *Desulfovibrio*), iron-reducing bacteria (e.g. *Geobacter*), denitrifiers (e.g. *Pseudomonas*), and spore-forming species (e.g. *Clostridium*) (Chabalala and Chirwa, 2010; Cologgi et al., 2011; Gao and Francis, 2008; Stylo et al., 2015; Vecchia et al., 2010). The dominant product of microbial uranium reduction was often reported to be uraninite mineral (desirable for its stability against oxidation), however other non-uraninite minerals have been recently identified as bioreduced uranium such as ningyoite [$CaU(PO_4)_2$] produced by *Thermoterrabacterium ferrireducens* and *Desulfotomaculum reducens*, and monomeric U(IV) by *Shewanella oneidensis* (Alessi et al., 2012; Bernier-Latmani et al., 2010; Newsome et al., 2014a). However, these bioreduced U(IV) can be reoxidized to U(VI), especially in the presence of nitrate and/or other oxidant agents (e.g. Fe(III)) (Xu et al., 2017). As nitrate is an energetically favorable terminal electron acceptor, its presence in the environment could diminish or totally inhibit U(VI) reduction (Xu et al., 2017). Therefore, it is highly important to consider the impact of nitrates on the biogeochemical cycle of U under DGR relevant conditions.

While microorganisms can affect the speciation and mobility of radionuclides in the environment, uranium may influence the bacterial community enriching those with high U-tolerance. In addition, anaerobic conditions could influence the bacterial diversity enhancing the growth of nitrate-, manganese(IV)-, iron-, and sulfate-reducing bacteria (Newsome et al., 2014a). Different studies reported changes in the indigenous bacterial community of soils/bentonites in presence of U(VI), and that of uranium-containing samples amended with G2P (Lopez-Fernandez et al., 2018; Newsome et al., 2015; Povedano-Priego et al., 2019). Hence, it is of great importance to consider the influence of G2P on both the bacterial diversity and the uranium speciation, in case uranium was released from the DGR canisters to the biosphere. In accordance, it can be hypothesized that under anaerobic conditions uranium would affect the bentonite bacterial community structure, enhancing the abundance of U-tolerant bacteria; also, that such a bacterial community will influence the uranium speciation through well-known interaction mechanisms (e.g. biomineralization, bioreduction).

This work was aimed to investigate the effect of uranyl nitrate and G2P on: 1) the mineralogy and structure of bentonites, and 2) the bacterial community composition of these clays. The outputs of this study would help to predict the impact of microbial processes on the DGR long-term performance when anaerobic conditions would be established. This is important due to the need for keeping the safety conditions that are global concern, and the particular compromise for the fulfilling of the knowledge of the DGR in situ conditions.

3. MATERIAL AND METHODS

3.1. Bentonite samples collection and microcosm establishment

Bentonite samples from El Cortijo de Archidona (Almeria, Spain) were collected as described in Povedano-Priego et al. (2019). These bentonites have been selected for their good properties as backfilling and sealing material for the future high-level radioactive waste repository. In this study, these bentonites were used for the establishment of anaerobic microcosms following the steps for their preparation previously described in detail in Povedano-Priego et al. (2019) (Fig. 1A). We treated the

bentonite microcosms with: 1) uranyl nitrate to observe the effect of uranium after incubation (U samples), 2) glycerol-2-phosphate (G2P) and uranyl nitrate to determine the effect of uranium in presence of an organic phosphate source (GU samples). In addition, distilled water (H samples), sodium nitrate (N samples) and G2P (G samples) solutions were added to the bentonite and used as different controls.

Treatments were performed in triplicate (a total of 18 individual microcosms) and incubated in darkness at room temperature under anaerobic conditions for six months. To stablish the anaerobic conditions, containing-microcosms plates were introduced in an anaerobic jar (BBL™ GasPak™ Anaerobic Systems) where anaerobiosis generator sacs (AnaeroGen™, Thermo Scientific) were introduced (Fig. 1B). After incubation, samples were stored at -20 ºC until further use.

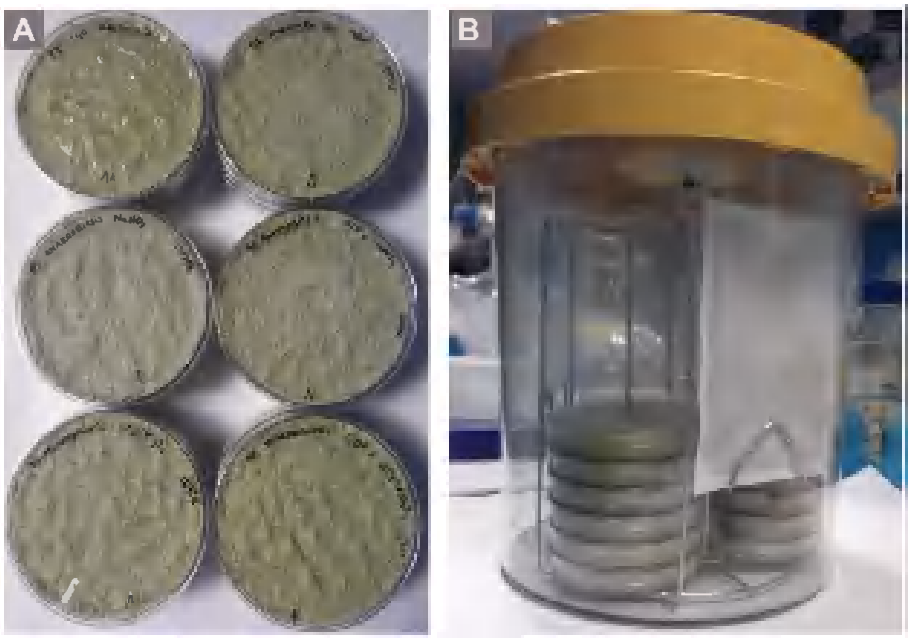

Figure 1. (A) Different treated microcosms prepared for the experiment previous to incubation. (B) Anaerobic jar containing bentonite microcosms and anaerobiosis generator sacs.

3.2. Chemical and mineralogical characterization of anaerobic microcosms

The pH of each sample was measured in triplicate according to the method developed by Stone et al., (2016), where a 1:15 bentonite:$CaCl_2$-buffer ratio was used. For the pH measurement a Crison pH-meter (MicropH, 2002) was standardized against

pH 4.00, and 7.02 commercial reference solutions. The reported accuracy was of ± 0.02 pH units.

The mineralogy of the solid bentonite microcosms was determined by X-Ray Diffraction (XRD) 6 months after the different treatments. A PANalytical X'Pert Pro diffractometer equipped with a X'Celerator solid-state detector, a spinning sample stage, a Ni filter, and 0.25º divergence slit was used (Instituto Andaluz de Ciencias de la Tierra, CSIC-University of Granada, Spain). X-ray powder diffraction patterns were recorded using random oriented mounts with CuKα radiation (λ = 1.5405 Å), operated at 45 kV and 40 mA, scanned from 4 to 70 °2θ. Powder samples were deposited in zero-background silicon sample holders for analysis. Mineral phases were identified by comparison with JCPDS powder spectra (Joint Committee on Powder Diffraction Standards).

3.3. Microscopic characterization of anaerobic microcosms

Microstructural features of the bentonite microcosms after treatments were determined using a High-Angle Annular Dark Field Scanning Transmission Electron Microscope (HAADF-STEM) FEI TITAN G2 80–300 at an acceleration voltage of 300 kV and MegaViewIII camera under standard operating conditions with liquid nitrogen anticontaminator in place (Centro de Instrumentación Científica, Universidad de Granada, Spain). Energy Dispersive X-ray Spectroscopy (EDX) microanalysis was performed at 300 kV using a spot size of 7 nm and a live counting time of 20 s. Samples were dispersed in ethanol and then deposited on carbon-coated copper grids for observation.

After six months of anaerobic incubation, brown spots in the surface of the microcosms were analyzed using Variable Pressure Field Emission Scanning Electron Microscopy (VP-FESEM) *ZeissSupra 40VP* equipped with SE (InLens) and BSE detectors to provide morphological and chemical images, respectively. For elemental analysis, the EDX detector used was a 50 mm^2 silicon drift detector XMAX enabling detection of elements with $Z4 \geq$ (Be) and high-count rates. For the mounting of samples, conductive double coated carbon tape was used as adhesive in the stubs.

3.4. Microcosms bacterial diversity characterization

3.4.1. DNA extraction from bentonite microcosms

To study the microbial diversity of the anaerobic microcosms (H, N, U, G, GN, and GU) after six months of incubation, total DNA was extracted from 18 treated microcosms. Each replicate (0.3 g) was mixed with glass beads (≈ 0.3 g) of different diameters in a sterile screw-cap tube and mixed by energetic vortexing in 400 µL of Na_2HPO_4 (0.12 M, pH 8.0). Afterwards, 600 µL of lysis buffer [Tris-HCl (100 mM, pH 8.0); EDTA (100 mM, pH 8.0); NaCl (100 mM); polyvinylpyrrolidone (PVP, 1%); and SDS (2%)], 24 µL freshly made lysozyme (10 mg/mL), and 2.5 µL proteinase K (20 mg/mL) were added to each tube for the chemical lysis. Mechanical lysis was performed twice using a FastPrep® FP120 at a speed of 5.5 m s−1 for 45 s. Samples were firstly incubated at 37 ºC for 30 min followed by an incubation at 60 ºC for 45 min. After a centrifugation at 14,000 × g for 5 min at room temperature, the supernatants were collected in new 15-mL tubes and bentonite pellets were mixed again with 1 mL of lysis buffer and disrupted another two times by FastPrep. After centrifugation, the second supernatants were transferred to the 15-mL tubes and a series of washing steps were performed using one volume of phenol:chloroform:isoamyl alcohol (PCI-25:24:1, pH 8), one volume of phenol:chloroform (PC-1:1), and one volume of chloroform and centrifuged at 1,500 × g for 10 min at 4 ºC. DNA was precipitated by adding one volume of cold-isopropanol and 1:10 volume of sodium acetate (3 M, pH 5) and incubating for 1 hour at -80 ºC. After incubation, tubes were centrifuged at 5,000 × g for 30 min at 4 ºC. The pellets were resuspended with 1 mL of 80 % cold-ethanol and centrifuged at 10,000 × *g* for 5 min at 4 ºC. Then, pellets were dissolved in 35 µL Tris (5 mM, pH 8.5)-TE buffer [Tris-HCl (10 mM, pH 8.0) and EDTA (1 mM)]. Finally, the concentration of the extracted total DNA was measured on a Qubit 3.0 Fluorometer (Life Technology) and stored at -20 °C until extractions from all microcosms were finished and ready for sequencing.

3.4.2. Amplification and sequencing of the samples

The V3–V4 region of the 16S rRNA gene from each microcosm was amplified by a two-step PCR using bacterial primers 341F (5'-CCTACGGGNGGCWGCAG- 3') and 805R (5'-GACTACHVGGGTATCTAATCC- 3') (Herlemann et al., 2011) to detect a

broad range of bacterial taxa following the PCR protocol described in (Hugerth et al., 2014). 16S rRNA gene Illumina libraries were constructed at Centre for Ecology and Evolution in Microbial model Systems (Linnaeus University, Sweden) and sequencing was performed at Science for Life Laboratory (Sweden) on the Illumina MiSeq platform (2 × 300 bp pair-end reads). Sample-specific barcodes were used for reads demultiplexing and separation.

3.4.3. Bioinformatics and bacterial diversity analyses

After quality controls, paired-end reads were combined and clustered into Operational Taxonomic Units (OTUs) at 97% similarity threshold. OTUs were identified using UCLUST (Edgar, 2010) and classified using the SILVA 132 database (Quast et al., 2013). Finally, clustered and annotated OTUs were analyzed in Explicet 2.10.5 (Robertson et al., 2013) for the relative abundance stacked bars construction representing triplicates average, as this has been found to be more accurate than rarefying (McMurdie and Holmes 2013).

Alpha diversity (Shannon H index) was calculated to the lowest sample size (67) and bootstrapped 100 times. Similarity between taxa identities and their relative abundances in anaerobic bentonite microcosms were evaluated using beta-diversity indices by R software. Specific differences in the bacterial community structure were further visualized in a heatmap using the heatmap.2 function in the R gplots v. 3.0.1.1 package (Warnes et al., 2019) and including only taxa at ≥ 1% relative abundance in all samples. At OTU level, microbial community composition was analyzed using weighted UniFrac distance measured in QIIME and PAST3 v. 3.18 and the output visualized with Principal Coordinate Analysis (PCoA).

3.4.4. Statistical analyses of bacterial diversity

Significant differences in taxa relative abundance ($p < 0.05$) between the different samples were determined using one-way ANOVA test after normalization of all counts. In addition, one-way ANOVA Tukey posthoc test was used to test for significant differences in relative taxa abundance ($p < 0.05$) between the six microcosm treatments for the total community. To look for significant differences in the alpha diversity

between the samples, one-way ANOVA test, using a significance level of 0.05, was used.

4. RESULTS AND DISCUSSION

4.1. Changes in the chemistry and mineralogy of the treated microcosms

Chemical analyses of bentonite samples prior to incubation (time 0) were described and discussed in detail in Povedano-Priego et al. (2019). The dominant oxides were SiO_2 (61.85 ± 3.59%), Al_2O_3 (15.41 ± 1.41%), Fe_2O_3 (3.39 ± 0.21%) (Data not shown).

The measured pH values of the bentonite samples (untreated and acetate treated for 0 and 6 months) using 0.01 M $CaCl_2$ solution were alkaline ranging between 7.53 and 10.02 (Table 1). The use of $CaCl_2$ for pH measurements in soils was implemented by Stone et al. (2016) who showed the capacity of this solution to reduce the impact of other electrolytes different from H^+ and OH^-. As shown in Table 1, pH values of bentonites were less alkaline in all treatments after 6 months in comparison with those of time 0 (except for H sample). No significant differences in pH were observed among the treated microcosms, while H microcosms with a value of 10.02 were significantly more alkaline than the others. In these anaerobic microcosms, pH values were slightly lower than in those incubated aerobically with the same treatments (Povedano-Priego et al., 2019), where they ranged between 7.9 and 9.31.

This decrease in the pH during incubation experiments of bentonite from "El Cortijo de Archidona" was previously demonstrated in a lixiviation process (Díaz-Fernández, 2004). The dissolution of calcite in minor amounts (≈0.6 wt%) and ion exchange reactions between bentonite (Na) and solution (Ca) could contribute to this process. Moreover, this decrease in the slightly alkaline pH could be further explained by the protonation/deprotonation reactions of the smectite under anaerobic conditions (Nessa et al., 2007). In addition, carbon dioxide and organic acids produced by the anaerobic bacterial metabolism might also contribute to the mentioned pH decrease. Anaerobic bacteria such as *Clostridium* spp. may produce some of these organic acids during the fermentation process, resulting in the release of butyrate and acetate as

fermentative products (Luo et al., 2019). Besides, fermentation of glycerol by some bacteria may also be taken into consideration for the production of organic acids mainly formate, and in minor amounts, acetate (Temudo et al., 2008). Recently, Patil et al. (2016) described the production of acetate and formate from glycerol fermentation by the strictly anaerobic bacterium *Anaerobium acetethylicum*.

Table 1. pH values of the treated microcosms measured in a calcium chloride solution. H: distilled water, N: sodium nitrate, U: uranyl nitrate, G: G2P, GN: G2P and sodium nitrate, and GU: G2P and uranyl nitrate.

	Time 0	After 6 months of anaerobic incubation					
		H	N	U	G	GN	GU
$CaCl_2$	9.79	10.02	7.53	7.73	7.67	7.79	8.04

Standard errors: 0.02-0.04

The XRD semi-quantitative estimation of the mineralogical composition of the bentonite sample at time 0 was similar to that described in Povedano-Priego et al. (2019). After six months of incubation, the mineralogy of treated-bentonites (H, N, U, G, GN and GU) showed no remarkable differences in comparison to time 0 (Fig. 2). XRD spectra revealed peaks of smectite (montmorillonite) being the dominant mineral phase, beside other minority mineral phases such as quartz, mica, cristobalite, and plagioclase (Fig. 2).

4.2. Microscopic characterization of bentonite minerals in anaerobic microcosms

After six months of anaerobic incubation, the low dissolution of smectite observed using STEM analysis was probably originated by the interaction between the bentonite and the aqueous solutions (Cappelli et al., 2018; Huertas et al., 2001). In addition to smectite, STEM and EDX analyses revealed the presence of different accompanying mineral phases such as amorphous silica (SiO_2) (as both individual particles and adsorbed to smectite flakes), phosphate mineral (monazite-Ce and monazite-La), and calcite (Fig. 3A, B, C, respectively). However, no U mineral phases were identified in the U treated samples, probably due to the low metal concentration assayed and the method of the sample preparation.

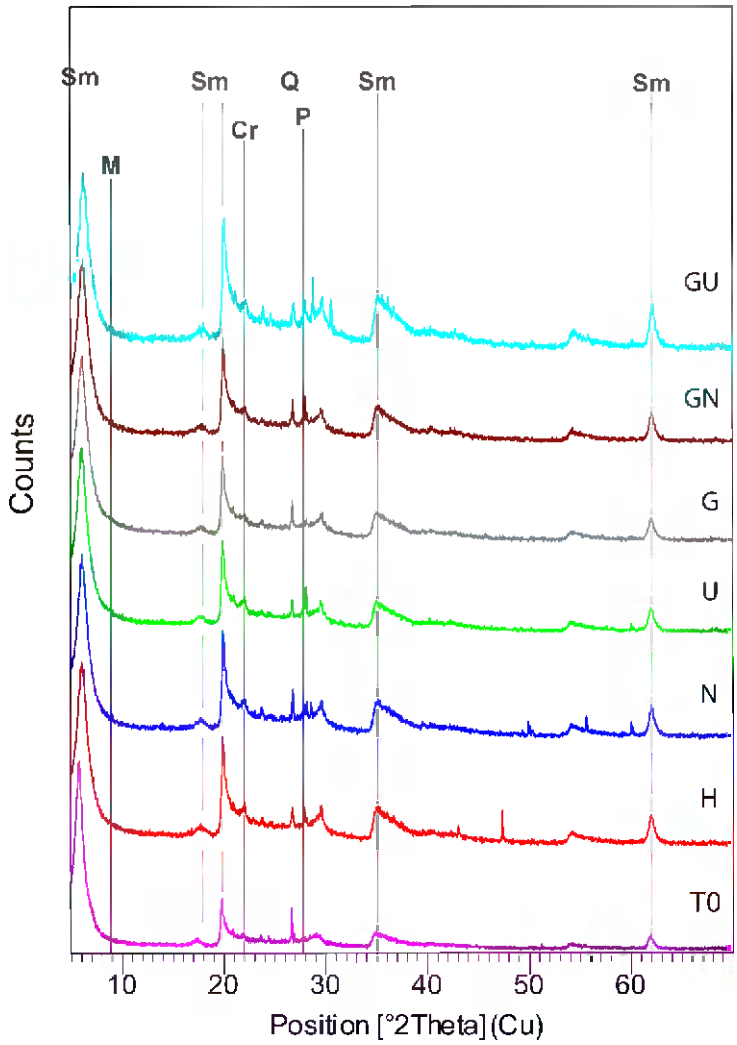

Figure 2. X-ray Diffraction (XRD) patterns of bentonite microcosm samples treated with: distilled water (H), sodium nitrate (N), uranyl nitrate (U), glycerol-2-phosphate (G), glycerol-nitrate (GN), and glycerol-uranyl-nitrate (GU). Sm: smectite, M: mica, Cr: cristobalite, Q: quartz, Plg: plagioclase and Apt, apatite.

HAADF-STEM and EDX analyses revealed the presence of a bright mineral structure, which could be identified as an iron sulfide (Fe, S) accompanied by smectite (Si, Al, Mg, Ca) in the U treated microcosms (Fig. 3D). This iron sulfide may probably occur in form of pyrite (FeS_2), as an accessory mineral in the bentonite. Pyrite would act as a sulfide source to corrode copper canisters compromising thus the safety of the DGR. Nevertheless, it was previously reported that corrosion of Cu-canisters by pyrite may differ depending on the bentonite barrier, which was not tested neither confirmed in all different type of bentonites and also because of its low solubility to produce hydrogen sulfide (HS^-) (Kaufhold et al., 2017). On the other hand, bentonites have been described for their high microbial diversity, including sulfate reducing bacteria (SRB) (Lopez-Fernandez et al., 2015; Svensson et al., 2011). These SRB produce sulfide

whose oxidation is coupled with ferric iron mineral reduction. The resultant ferrous iron could react with free sulfides producing iron sulfide (Pedersen et al., 2017). Therefore, the iron sulfides observed in these samples is assumed to be originated by

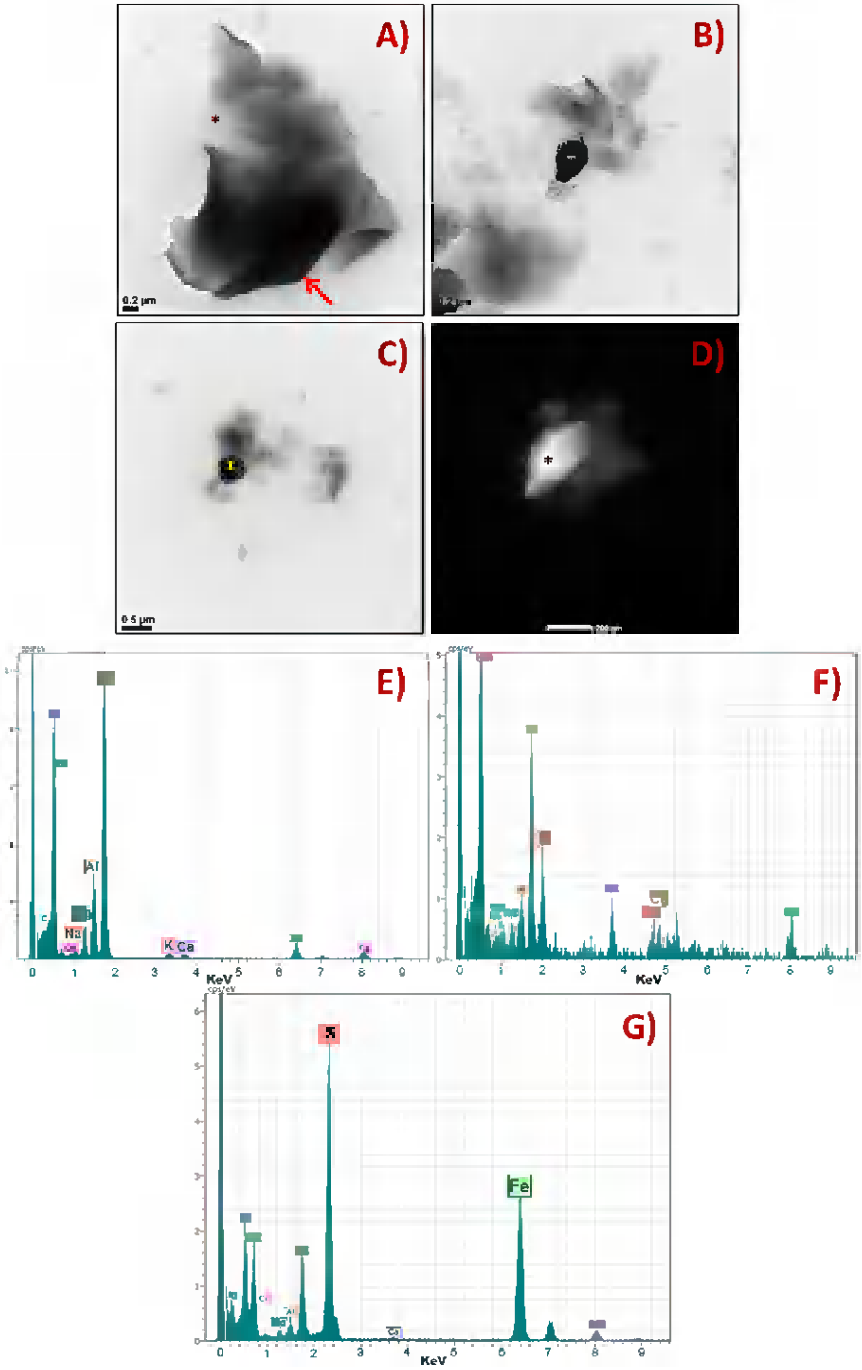

Figure 3. High Resolution Transmission Electron Microscopy (HRTEM) micrographs (A, B, and C), and Scanning Transmission Electron Microscopy-High-Angle Annular Dark-Field (STEM-HAADF) imaging (D) of minerals in the anaerobic bentonite microcosms. Smectite (A, arrow), amorphous silica (A, asterisk), Ce- and La-monazite (B, asterisk), calcite (C, asterisk), and pyrite (D, asterisk) are shown. EDX spectra indicate the composition of smectite (E), monazite (F), and pyrite (G).

microbiological and/or geochemical processes. In the present study, we identified several indigenous bacteria belonging to the SRB group such as *Desulfovibrio*, *Desulfatiglans*, and *Desulfobulbaceae* family, all of which may contribute to the formation of pyrite in the bentonite microcosms. A bioreduction by SRB of structural ferric iron of smectite to ferrous iron concomitant with the oxidation of sulfide to elemental sulfur would lead to the bentonite destabilization at long term in the DGRs (Liu et al., 2012; Pedersen et al., 2017).

4.2.1. Analyses of brown spots in the bentonite microcosms

Brown spots different in color, size and quantity were observed in all treated microcosms under anaerobic conditions (Fig. 4). Among these macroscopic characteristics, the spots color varied in the samples between a darker color (black) in the non-G2P treated samples (H, N and U) and orange brown in the G2P-treated microcosms (G, GN and GU). The largest brown spots were identified in GU microcosms while nearly unappreciated ones were observed in U-treated samples. Wide

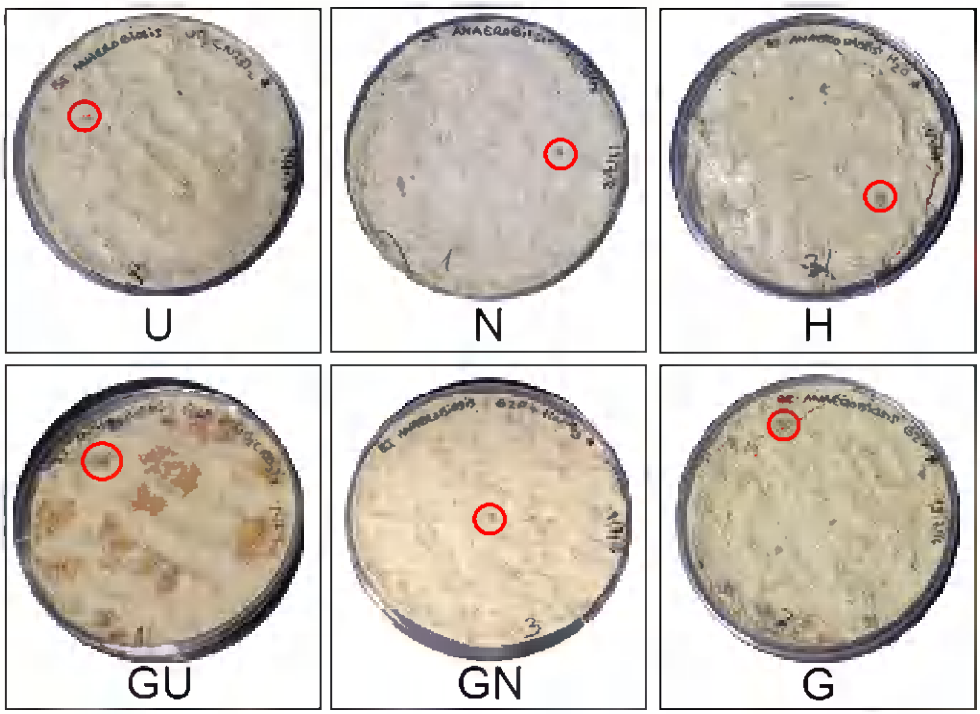

Figure 4. Plates of bentonite microcosms showing different brown spots after six months incubation under anaerobic conditions. The microcosms were treated with uranyl nitrate (U), sodium nitrate (N), distilled water (H), G2P- uranyl nitrate (GU), G2P-sodium nitrate (GN), and G2P (G). The brown spots are indicated by a red circle in the microcosms.

range of sizes was in turn observed in the other samples. In general, the number of spots in the surface was highly different between the treatments, being GN microcosms with more detected spots in the whole treated area (Fig. 4).

In order to provide more information about the chemical and mineralogical nature of these colored spots, VP-FESEM and EDX analyses were performed. As shown in the figures obtained by secondary electrons, typical leaf-like morphology of smectites was observed (Fig. 5A, E). However, analyses by backscattered electron mode highlighted some areas with high atomic number being brighter than others (Fig. 5B, F in arrows). When analyzing the composition of these areas, EDX spectra revealed high peaks of Mn and O in addition to the ones corresponding to smectites (Si, Al, Mg, Na), although no U mineral phases were identified in the U treated samples (Fig. 5A). EDX spectrum and maps showed the elemental distribution in the bentonite particles of Mn and Si, which associated with the brighter areas and the smectite, respectively (Fig. 5C, D, G, H). These findings probably correspond to Mn oxides attached to bentonite. On one hand, sorption of Mn in bentonites has previously been reported in several works (Al-Jariri and Khalili, 2010; Dolinská et al., 2015; Iskander et al., 2011). As an example, Iskander et al. (2011) reported that the amount of Mn adsorbed ranged between 9.83% and 33.24% of the total Mn added. On the other hand, although structural properties could be affected, bentonite provides an efficient surface for the Mn oxides due to their large surface area (Dolinská et al., 2015). These precipitates could also correspond to Mn(IV) oxides, recently denoted for being dark brown colored (Kitjanukit et al., 2019). In addition, Liu et al., (2018) reported that reoxidation of Mn(II) to Mn(IV) may occur, although Mn(II)-oxidizing bacteria are aerobic and the limiting O_2 conditions affect their activity. Moreover, fungi are described for their ability to oxidize Mn(II) forming MnO_2 mineral phases (Santelli et al., 2011). By means of culture dependent techniques several fungal strains were isolated from the U treated bentonites, which could play a role in the oxidation of Mn(II) (Data not shown). In addition, VP-FESEM images (Fig. 4G) revealed the presence of fungal mycelia associated with MnO_2. Meanwhile, there is however still a lack of information in the literature concerning oxidation of Mn(II) to Mn(IV) under anaerobic conditions. Therefore, more research is further required about this process and the origin of these deep brown precipitates in bentonite microcosms under anaerobic conditions.

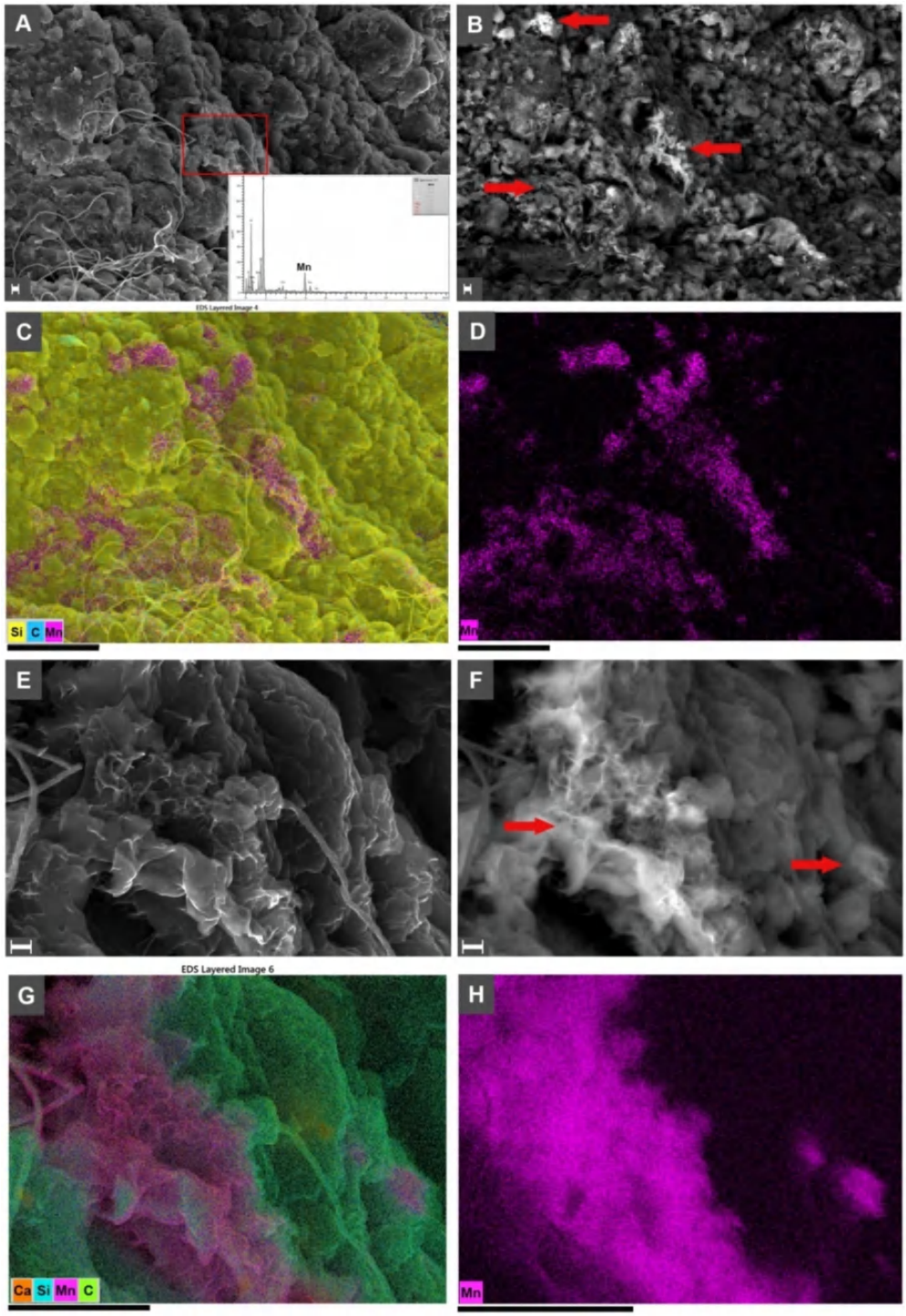

Figure 5. VP-FESEM and EDX map images of brown spots in anaerobic treated microcosms. Images shown in secondary electrons with the InLens detector of the bentonite samples (A and E) and images shown in backscattered electrons with the AsB detector (B and F). Red square area in A was amplified in E and F. Bright areas with high atomic number are indicated by arrows in B and F. C) and D) EDX layered maps corresponding to images A and B with represented Si, C, and Mn signals (C) and only with Mn signal (D). G) and H) EDX layered maps corresponding to images E and F with represented Ca, Si, C, and Mn signals (G) and only with Mn signal (H). Scale bar represents 2 µm in A and B, 25 µm in C and D, 1 µm in E and F, and 10 µm in G and H.

4.3. Changes in the bacterial diversity of anaerobic microcosms induced by uranyl nitrate and G2P

Total DNA of bentonite microcosms were extracted and sequenced by Illumina platform, providing information about the complete structure and composition of the bacterial community of each sample. One replicate of each treatment was discarded for its great deviation from the other replicates under the same experimental conditions, being not representative of the community structure. Values of Good's coverage index, indicating whether a sufficient sequencing depth was achieved to well represent the bacterial community, are shown in Table 2. Normalization by relative abundance final count values was used, being more accurate than rarefying (McMurdie and Holmes, 2013).

A mean of 3715 sequences per sample was annotated obtaining a number of 790 OTUs classified into phylum (93.9% of phylotypes), class (89.1% of phylotypes), order (87.9% of phylotypes), family (76.1% phylotypes), and genus (42.2% phylotypes) levels. Richness, evenness and diversity of the samples were calculated using the traditional diversity indices (Shannon, Shannon's evenness, and Simpson). According to the ShannonD and SimpsonD indices, a high bacterial diversity was found and a nearly uniform distribution of OTUs was reached in all microcosms (ShannonE) (Table 2).

Table 2. Alpha-diversity indices of anaerobic bentonite microcosms. Richness index (S), diversity indices (ShannonD, and SimpsonD), evenness index (ShannonE), and Good's coverage values are shown.

Sample	S	ShannonD	ShannonE	SimpsonD	Good's coverage
H	71.1	549.5	0.89	0.97	0.78
N	81	575.9	0.91	0.98	0.70
U	84.2	575.6	0.90	0.98	0.67
G	39	413.9	0.78	0.91	0.89
GN	45	428.3	0.78	0.91	0.86
GU	31	41.8	0.84	0.93	0.94

The annotated OTUs were taxonomically related to 29 different bacterial phyla including Proteobacteria, Bacteroidetes, Epsilonbacteraeota, Cyanobacteria, Firmicutes, Zixibacteria, Verrucomicrobia, Chloroflexi, Spirochaetes, and Planctomycetes, among

others (Fig. 6). Considering all microcosms, Proteobacteria (mainly Gamma- and Deltaproteobacteria) was found to be the dominant phylum representing 46.7-72.9% of the total community, followed by Bacteroidetes (mainly Bacteroidia) with a mean of 13.92% (Figs. 6 and 7). Whilst in this study Actinobacteria were represented by only 0.61% of the bacterial community, this phylum was identified as one of the most abundant groups in the aerobic bentonite microcosms treated with uranium and glycerol-2-phosphate (Povedano-Priego et al., 2019). This remarkable difference may be explained by the fact that most representatives of Actinobacteria are aerobic microorganisms while some genera have had to adapt to the anaerobic conditions such as the marine Actinobacteria (Anandan et al., 2016) which could explain the low percentage in relative abundance of this phylum in anaerobic microcosms. At genus level, annotation of phylotypes revealed the presence of 258 genera, being *Sulfurimonas* (6.7%), *Desulfatiglans* (5.9%), *Clostridium* (3.9%), and *Candidatus Electrothrix* (3.8%) the most abundant genera, beside unclassified genera belonging to *Desulfobacteraceae* (6.1%) and *Flavobacteraceae* (2.4%) (Fig. 8). The presence of these strictly anaerobic bacteria mainly *Desulfatiglans* and *Clostridium* was notably higher in the anaerobic

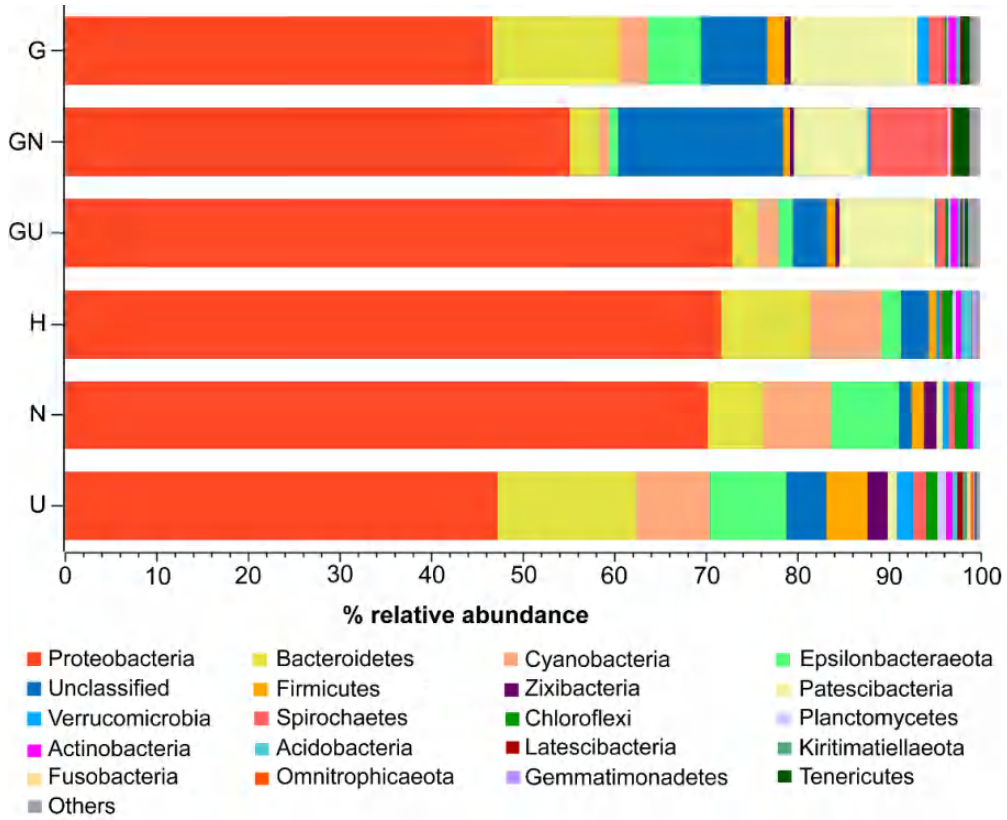

Figure 6. Relative abundances of phyla in all treated bentonite microcosms averaging duplicates. (H) Distilled water, (N) sodium nitrate, (U) uranyl nitrate, (G) glycerol-2-phosphate (G2P), (GN) G2P and sodium nitrate, and (GU) G2P and uranyl nitrate treated samples (cut-off > 0.15% of total).

microcosms. However, in the previous aerobic microcosms no presence of such genera were detected (Povedano-Priego et al., 2019).

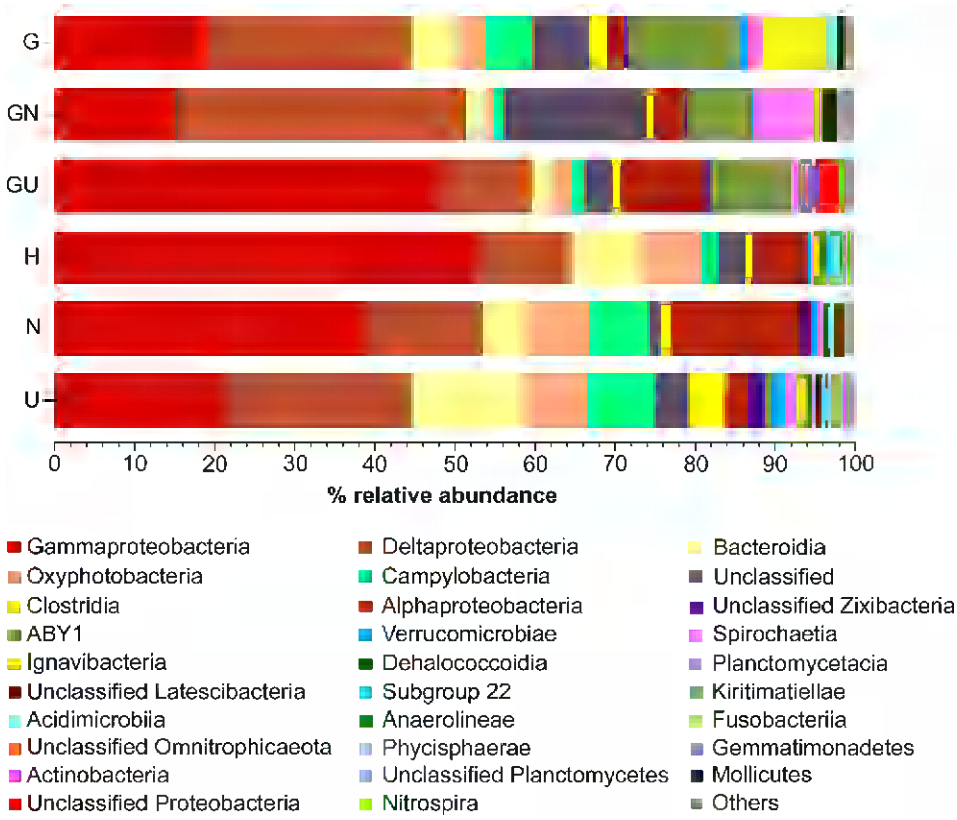

Figure 7. Relative abundances of the bacterial classes in all treated bentonite microcosms, averaging duplicates. (H) Distilled water, (N) sodium nitrate, (U) uranyl nitrate, (G) glycerol-2-phosphate (G2P), (GN) G2P and sodium nitrate, and (GU) G2P and uranyl nitrate treated samples (cut-off > 0.12% of total).

Considering the bacterial diversity distribution along the communities of the anaerobic microcosms, GU samples were the most different to that of the other studied microcosms. PCoA analysis showed considerable differences between treatments, being GU microcosms separated from the rest of samples, and these were divided into two different clusters: G2P-treated samples (G2, G3, GN1, and GN3), and non-G2P-treated-samples (H1, H2, N1, N2, U2 and U3) (Fig. 9). Therefore, the concomitance of uranium and G2P had a pronounced effect on the bacterial community of the bentonite microcosms. In addition, heatmap construction supported the clustering of the treated microcosms showed by the aforementioned PCoA, being the main involved genera *Ralstonia*, *Pseudomonas*, *Marinobacter*, *Desulfovibrio*, *Sulfuritalea,* unclassified *Desulfobulbaceae,* and *Candidatus Falkowbacteria* (Fig. 10).

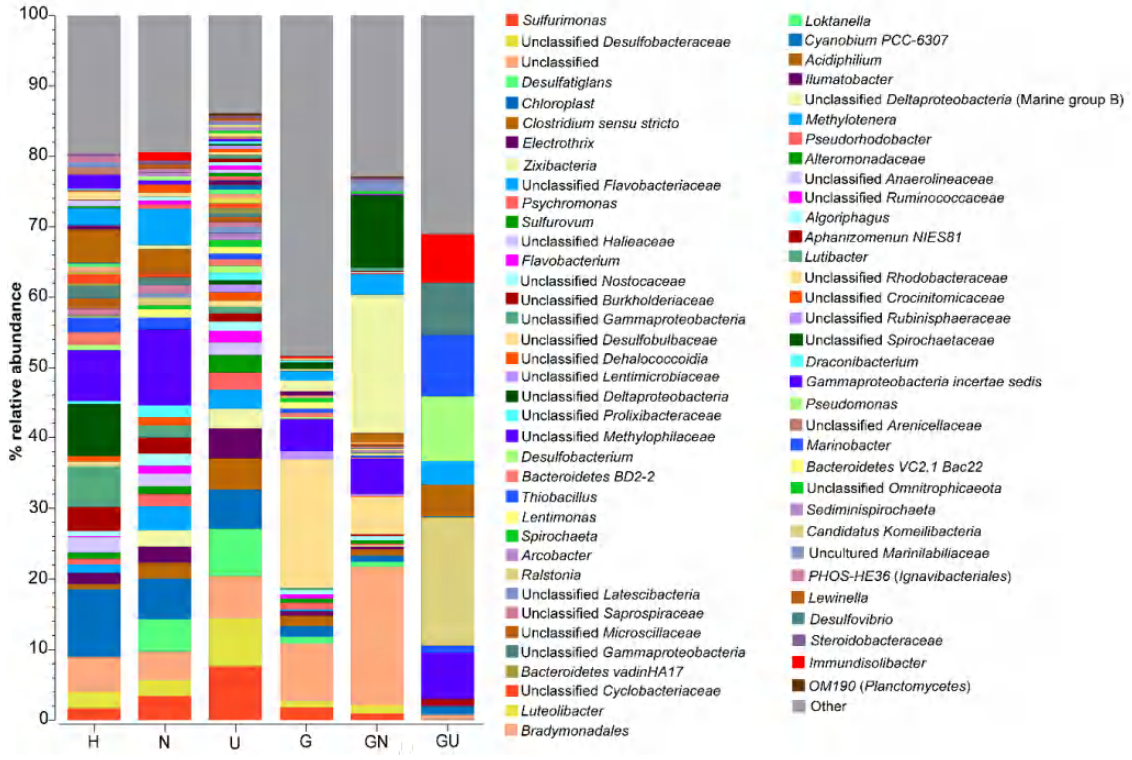

Figure 8. Structure of the bacterial community of the different treated bentonite microcosms at genus level represented by dominant OTUs with > 0.3% of relative abundance and averaging duplicates. (H) Distilled water, (N) sodium nitrate, (U) uranyl nitrate, (G) glycerol-2-phosphate (G2P), (GN) G2P and sodium nitrate, and (GU) G2P and uranyl nitrate treatments.

Regarding the non-G2P-treated microcosms (water-treated (H), nitrate-treated (N) and uranium-treated (U) microcosms), these were mainly dominated by Proteobacteria with an average of 71.6, 70.3 and 47.3% in H-, N- and U-treated microcosms, respectively (Fig. 6), being Gammaproteobacteria (52.8, 39.2, and 21.3%) and Deltaproteobacteria (11.8, 14.2, and 23.3%) the most abundant classes (Fig. 7). Other occurrent phyla were Bacteroidetes (9.8, 6.1, and 15.2%), Cyanobacteria (7.8, 7.4, and 8.1%), Epsilonbacteraeota (2.2, 7.4, and 8.4%), and Firmicutes (0.8, 1.4, 4.6%); and their corresponding classes Bacteroidia (8.8, 6.1, and 14.1%), Oxyphotobacteria (7.8, 7.4, 8%), Campylobacteria (2.2, 7.4, and 8.4%), and Clostridia (0.8, 1.4, 4.6%), respectively (Figs. 6 and 7). At genus level, *Sulfurimonas* (1.7, 3.4, and 7.6%), unclassified *Desulfobacteraceae* (2.4, 2.3, and 6.8%), *Desulfatiglans* (0.1, 4.6, and 6.7%), *Clostridium* (0.8, 2.3, and 4.5%), *Candidatus Electrothrix* (1.6, 2.3, and 4.2%), and unclassified *Flavobacteraceae* (1.2, 3.4, and 2.7%) were the most abundant genera in H, N and U microcosms, respectively (Fig. 8). Being strict or facultative anaerobic bacteria, these microorganisms are known for their successful growth under anaerobic

conditions (Bernardet and Nakagawa, 2006; Hung et al., 2011; Kuever, 2014; Takai et al., 2006; Xie and Müller, 2018).

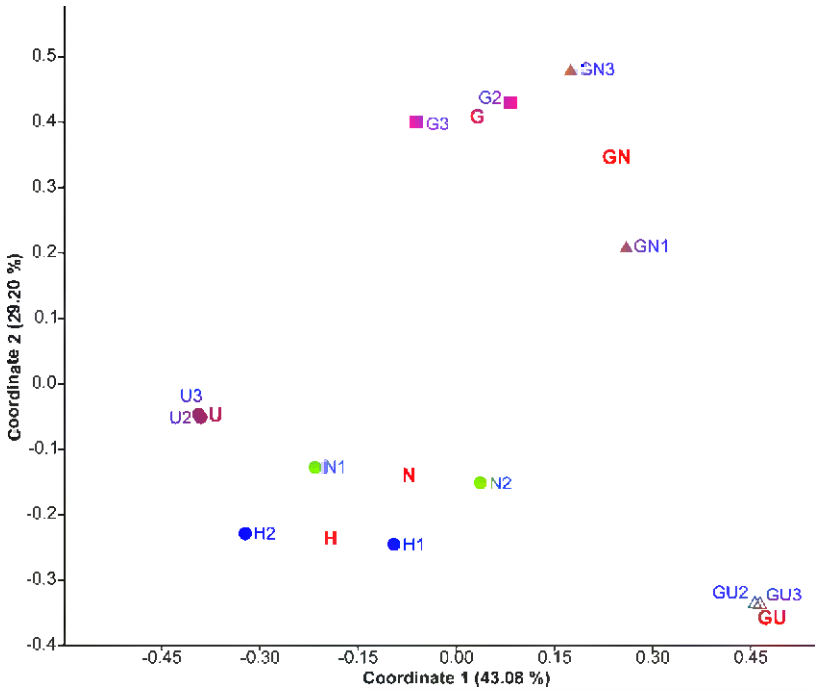

Figure 9. Principal Component Analysis (PCoA) plot comparing the bacterial community structure at genus level of the different treated microcosms (showing duplicates). The percentage of variation explained by Coordinate 1 and Coordinate 2 is indicated in the axes.

Concerning all G2P-treated microcosms (G2P (G), G2P/sodium nitrate (GN), and G2P/uranyl nitrate (GU) treatments), some differences with respect to the non-G2P-treated samples were observed. Here, like in the H, N and U microcosms, Proteobacteria was the predominant phylum in the community represented by 46.7, 55.2, and 72.9% in G, GN and GU microcosms, respectively (Fig. 6). Belonging to Proteobacteria, Gamma- (25.4, 36.1, and 11.34%) and Delta- (19.2, 15.1, and 48.3%) and Alphaproteobacteria (2.1, 4, and 10.7%) were the most abundant classes (Fig. 7). The second most abundant phylum was, however, Patescibacteria accounting for 13.9, 8, and 10.5% of G, GN and GU bacterial communities, respectively, followed by Bacteroidetes (13.9, 3.1, and 2.8%), Spirochaetes (1.7, 8.5, and 1%), and Cyanobacteria (3.2, 1.1, and 2.2%) (Fig. 6). The corresponding classes of these phyla, ABY1 (Patescibacteria; 13.9, 8, and 10.2%), Bacteroidia (6.2, 2.6, and 2.7%), Spirochaetia (1.7, 7.4, and 0.8%), and Oxyphotobacteria (3.2, 1.1, and 2.2%) were the most represented with more than 2% of the total community (Fig. 7). Visualizing the stacked bars with the relative abundances

of genera in Fig. 8, the most different bacterial community was shown in GU microcosms with respect to the other treatments. *Ralstonia* (18.2%), *Pseudomonas* (9.2%), *Marinobacter* (8.8%), *Desulfovibrio* (7.4%), *Immundisolibacter* (6.9%), and *Sulfuritalea* (4.6%) were the most abundant genera in GU microcosms but no presence (or negligible) of such genera were detected in controls (G and GN) (Fig. 8). In

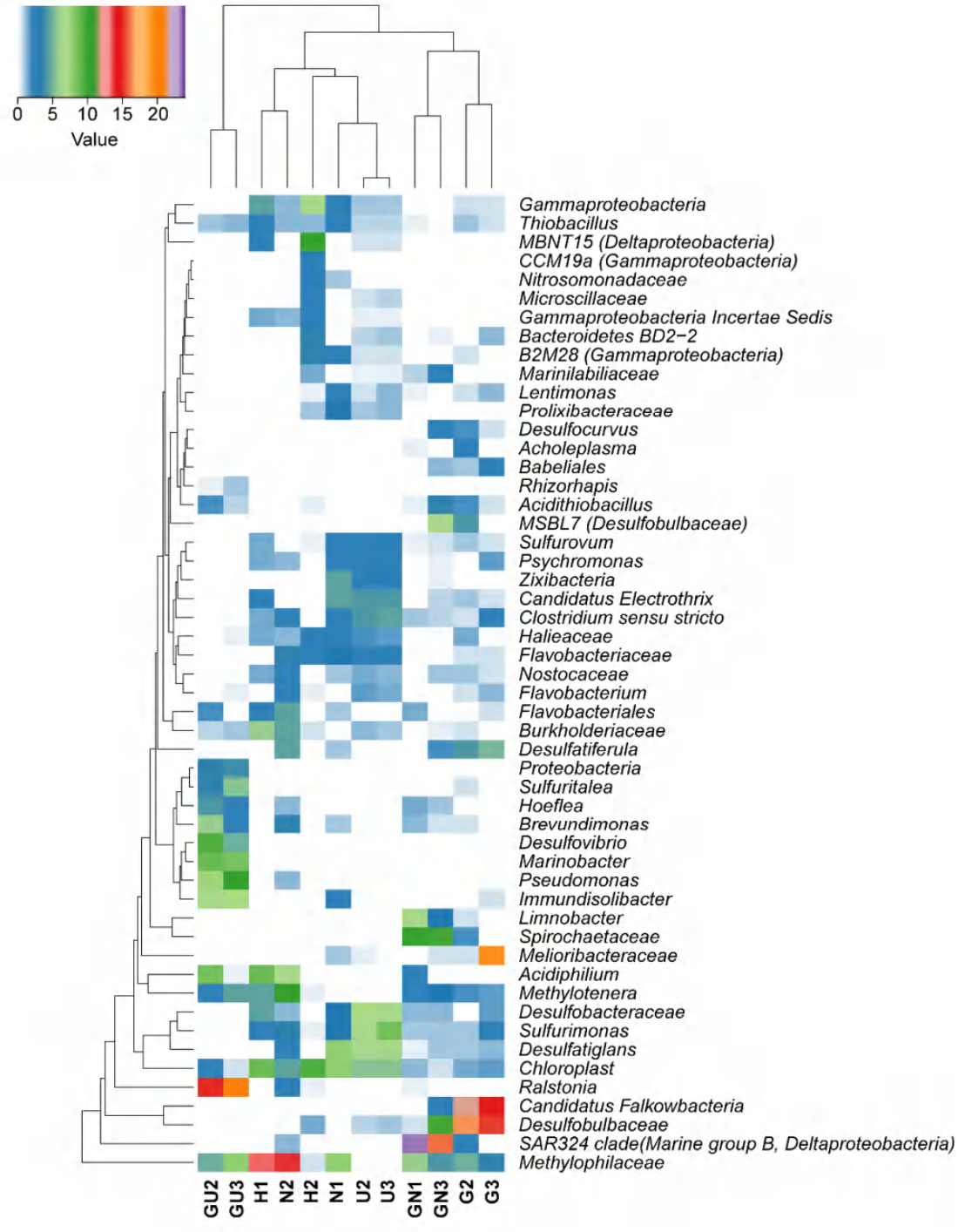

Figure 10. Heatmap of the relative abundance at the genus level, and the clustering based on Manhattan distance and average linkage for both columns and rows throughout the sample set. The relative abundance of each genus was shown by different colors indicated in the color bar.

addition, unclassified Deltaproteobacteria (Marine group B; 1.51, and 19.8%), *Desulfobulbaceae* (18.1, and 5.3%), *Spirochaetaceae* (0.9, and 10.3%), *Candidatus Falkowbacteria* (20.9, and 1.4%) and *Methylophilaceae* (4.5, and 5%) have been detected with higher relative abundance in G and GN microcosms than in the others (Fig. 8).

4.4. Impact of bacterial community changes on the biogeochemical processes under DGR conditions

To determine the effects of G2P, uranium, and nitrate treatments on the bentonite bacterial community, One-Way ANOVA ($p \leq 0.05$, n=2) statistical analyses were performed. Comparing all samples, significant differences in the OTU relative abundance at phylum level were found for Cyanobacteria, Firmicutes, Spirochaetes, as the most represented (>1% of relative abundance) (Supplementary Table 1). Regarding the classes, Deltaproteobacteria, Oxyphotobacteria, Clostridia, Fusobacteriia, Leptospirae, and Oligosphaeria, with at least 0.1% of relative abundance, were significantly different (Supplementary Table 2). At genus level, significant differences in the relative abundance were obtained for 28 genera (including unclassified bacteria) with 1% in at least one sample such as *Ralstonia*, *Pseudomonas*, *Desulfovibrio*, *Marinobacter*, *Sulfurimonas*, *Desulfatiglans*, unclassified genus belonging to Marine Group B (Deltaproteobacteria), *Candidatus Falkowbacteria,* and *Desulfobulbaceae*, among others (Supplementary Table 3).

4.4.1. Effect of nitrate on the bentonite bacterial diversity in the anaerobic microcosms

In order to study the effects that could have nitrates on the structure and composition of the bacterial community, both N- and GN-treated microcosms were compared with their respective controls (H and G microcosms, respectively). Nitrate can be reduced to N_2 through anaerobic processes like denitrification, acting as an alternative electron acceptor, when oxygen is fully consumed by heterotrophic microorganisms (Kutvonen et al., 2015). In the DGRs, during the construction the introduction of different nitrogen compounds such as nitrate may enhance the growth of microorganisms that could corrode the canisters and release radionuclides resulting in

severe consequences for the safety of nuclear wastes (Kutvonen et al., 2015; Rajala et al., 2015).

Interestingly, in this study the phylum Spirochaetes, represented by the family *Spirochaetaceae*, was the only one with a significant abundance in GN samples ($p<0.045$) (Fig. 6, Supplementary Table 4). This group of bacteria encompasses members described for their capacity to anaerobically reduce nitrates to nitrites such as *Spirochaeta aurantia*, and *Spirochaeta halophila* (Leschine and Paster, 2015). Furthermore, recently, Saad et al., (2017) reported a strong effect of a nitrate treatment on the microbial community of marine sediments, favoring the development of fermentative bacteria like *Spirochaeta* species. Several microorganisms described for their nitrate reduction capacity were detected here in the anaerobic microcosms. Comparing both G2P-nitrate and G2P-samples, both Unclassified Deltaproteobacteria Marine Group B ($p<0.002$), and *Limnobacter* ($p<0.022$) were significantly represented in GN microcosms (Supplementary table 5). *Limnobacter* accounting for 5% of relative abundance in GN, have been found to utilize nitrate or nitrite as a nitrogen source through nitrate/nitrite reduction (Chen et al., 2016). *Flavobacterium* and other unclassified members belonging to *Flavobacteriaceae* were more abundant in microcosms containing nitrate like N and U samples. This family includes species capable of nitrate reduction such as *Flavobacterium denitrificans* (Broman et al., 2017; Sun et al., 2009). These nitrate reducing bacteria could affect positively the uranium reduction since U(VI) reduction could not happen until total reduction of nitrate and these bacteria contributes to this process (Safonov et al., 2018). In addition, some denitrifying bacteria could oxidize the previously immobilized U(IV) into soluble U(VI) using nitrate as terminal electron acceptor (Wu et al., 2010).

4.4.2. Effect of glycerol-2-phosphate on the bacterial diversity in the anaerobic bentonite microcosms

The G2P amendment to the microcosms resulted in significant changes in the indigenous bacterial communities (Figs. 6, 7, and 78). At phylum level, only Spirochaetes was significantly enriched in GN ($p=0.027$) in comparison to H microcosms, and the same occurred with Deltaproteobacteria at class level. However, in our previous work using aerobic microcosms, more significant differences between G2P-treated and non-G2P-treated microcosms were found (Povedano-Priego et al.,

2019). This greatest effect of G2P under aerobic conditions could be due to the fact that the oxidative utilization of glycerol by microbes is more favorable when oxygen is available. The reduced nature of glycerol makes it difficult for bacteria to assimilate under reducing conditions (Kang et al., 2014). Nevertheless, some bacteria are able to utilize glycerol anaerobically as carbon source for their growth such as *Escherichia coli* and members of Clostridia (*Clostridium* spp. and *Anaerobium acetethylicum*), among others, producing ethanol, hydrogen, formate, butyrate and acetic acids (Biebl, 2001; Patil et al., 2016). At genus level, 15 out of 100 statistically analyzed genera (> 1% of relative abundance in at least one sample) were found to be significantly more abundant in G2P-treated samples than in controls, including *Pseudomonas*, *Desulfovibrio*, *Marinobacter*, *Limnobacter*, *Desulfatiferula*, *Hoeflea*, *Candidatus Falkowbacteria*, and some unclassified genera (belonging to *Desulfobulbaceae*, *Lentimicrobiaceae*, and Deltaproteobacteria Marine Group B), among others (Fig. 8, Supplementary table 5). An outstanding fact was the presence of members of *Desulfovibrio* in these microcosms since several species of this genus have been described for their ability to utilize glycerol as electron donor (Ben Ali Gam et al., 2018; Qatibi et al., 1998). This bacterium is able to oxidize glycerol to acetate in presence of sulfate as terminal electron acceptor, although glycerol is difficult to be used as a carbon source in anaerobic conditions (Qatibi et al., 1998). The resulting acetate could be used as an energy source by other groups of bacteria such as the iron-reducing bacteria from the family *Geobacteraceae*. In fact members of this family have been often detected with high abundance in subsurface environments after stimulation of concomitant U(VI) and Fe(III) reduction by the addition of acetate as electron donor (Petrie et al., 2003).

4.4.3. Effect of uranium on the bacterial diversity in the anaerobic bentonite microcosms

According to Tukey post-hoc test ($p<0.05$, n=2 per treatment), significant differences in the microbial communities of the U-containing microcosms were observed. For instance, the phylum Firmicutes was statistically more abundant (4.6%) in uranyl nitrate microcosms (U) than in nitrate controls (N) (1.4%) (Supplementary Tables 1 and 7). Members of Firmicutes have been previously detected in U-contaminated sites (Khan et al., 2013; Lopez-Fernandez et al., 2018; Povedano-Priego et al., 2019). According to Khan et al., (2013), Firmicutes was well represented with

24% of the total bacterial population in uranium mine tailings-water interface. In addition, in a similar study to the present one, Firmicutes was found to be dominant in uranyl nitrate-treated bentonite microcosms under aerobic conditions (Lopez-Fernandez et al., 2018). Lentisphaera, Thermotogae and Candidate bacterial phylum BRC1 were also significantly identified in U samples but with minor relative abundance (Supplementary Tables 1 and 7). Lentisphaera belong to *Planctomycetes-Verrucomicrobia-Chlamydia* super-phylum, which was described to be distributed in heavy metal polluted soils (Hemmat-Jou et al., 2018; Yilmaz et al., 2016; Youssef and Elshahed, 2014).

Analyzing the bacterial community in the uranium-treated microcosms, the presence of the classes Leptospirae (belonging to Spirochaetes), and Clostridia (affiliated with the Firmicutes) were significantly higher in U samples in comparison to N-controls (Supplementary Table 8). Clostridia class is known for their extensive prevalence in sediments, soils and even radioactive wastes, and for playing a key role in the reduction of soluble U(VI) to insoluble U(IV) species (Francis and Dodge, 2008, Newsome et al. 2014a). Furthermore, the genus *Clostridium* was found to be highly and significantly abundant in U microcosms with 4.5% of relative abundance (Supplementary Tables 3 and 9). Gao and Francis (2008) reported the ability to reduce U(VI) to U(IV) in a nitrate independent process of several species of *Clostridium* previously exposed to uranyl nitrate under anaerobic conditions. This was in disagreement with what reported other authors about the fact that nitrate can act as an oxidizer of U(VI) through different mechanisms: 1) abiotic oxidation by intermediates denitrification such as nitrite, 2) direct oxidation coupled to nitrate reduction by bacteria, or 3) oxidation by Fe(III) produced through oxidation (denitrification) (Newsome et al., 2014a). Moreover, in presence of H_2 not only vegetative cells but also spores of *Clostridium* are able to reduce U(VI) producing a U(IV) precipitate (Vecchia et al., 2010).

In addition to *Clostridium*, *Sulfurimonas*, *Desulfatiglans*, *Hyphomonas* and unclassified *Lentimicrobiaceae* were significantly abundant ($p<0.045$) in U microcosms in comparison to controls. *Sulfurimonas* contributes to the formation of sulfate by oxidation of sulfide by the complete reduction of nitrate to N_2 (nitrate comes from uranyl nitrate) (Handley et al., 2013). This microorganism also possesses proteins that could play a role in heavy metal tolerance (Han and Perner, 2015). The generated

sulfate may be used by sulfate-reducing bacteria (SRB) such as *Desulfatiglans* (Jochum et al., 2018).

Among the 100 genera of the bacterial community in G2P-uranium-treated microcosms analyzed by Tukey post-hoc test ($p<0.05$, n=2 per treatment), *Ralstonia* (18.2%), *Pseudomonas* (9.2%), *Marinobacter* (8.8%), *Desulfovibrio* (7.4%), *Immundisolibacter* (6.9%), *Sulfuritalea* (4.6%), *Hyphomonas* (1.4%), *Pseudoalteromonas* (1.2%) were significantly more abundant in GU microcosms than in GN controls (Supplementary Table 9). *Ralstonia* was enhanced in N-treated microcosms due to its capacity to use nitrate as terminal electron acceptor (Lopez-Fernandez et al., 2018). In addition, they have previously been isolated from uranium contaminated sites (Brzoska and Bollmann, 2016; Salome et al., 2013). The denitrifying *Pseudomonas* species are well-known for their capacity to interact with uranium through different mechanisms such as biosorption, intracellular accumulation, biomineralization and bioreduction contributing to the immobilization of U (Chabalala and Chirwa, 2010; D'Souza et al., 2006; Hu et al., 1996; Kazy et al., 2009, 2008; Newsome et al., 2014b). These processes would be positive for the safety of DGRs, in case any radioactive element would be accidentally leaked from nuclear wastes into the bentonite barrier. The biosorption of uranium was described in *P. aeruginosa* and *P. fluorescens* in several studies where cell surface-bound uranium was detected in the entire outer membrane-peptidoglycan-plasma membrane complex (Hu et al., 1996; Merroun et al., 2005). In addition to the biosorption using the whole cell, extracellular polysaccharide (EPS) excreted by *P. aeruginosa* is able to bind U through carboxylic groups (Kazy et al., 2008). Other previously described uranium-*Pseudomonas* interaction mechanisms were the bioaccumulation mediated by the increase of membrane permeability, which allows metal diffusion inside the cells (Kazy et al., 2009; König et al., 2010). Besides, uranium can be sequestered within the cells as crystalline U-phosphates through biomineralization process (Choudhary and Sar, 2011; Kazy et al., 2009). In turn, under anaerobic and reducing conditions, *Pseudomonas* spp. have the capacity to reduce soluble U(VI) to more insoluble form U(IV) (Chabalala and Chirwa, 2010; Newsome et al., 2015, 2014b). Therefore, *Pseudomonas* is a remarkably interesting genus in DGR concept for their aforementioned abilities to interact and immobilize uranium.

In addition to *Pseudomonas*, also *Desulfovibrio* has been extensively studied for their capacity to reduce hexavalent uranium (Heidelberg et al., 2004; Lovley et al., 1993; Payne et al., 2002; Stylo et al., 2015). *Desulfovibrio* is a SRB well known for their capacity to reduce not only sulfate but also iron and nitrate (Li et al., 2017; Payne et al., 2002). The mechanism to reduce U(VI) seems to be related to the cytochrome c_3 (identified as a U(VI) reductase), although no exclusively; a complex c-type cytochrome network in the periplasm could provide electrons for the U(VI) reduction (Heidelberg et al., 2004; Newsome et al., 2014a).

5. ENVIRONMENTAL IMPLICATIONS OF BACTERIAL DIVERSITY OF ANAEROBIC MICROCOSMS IN THE DGR CONCEPT

Microbial activity could affect the integrity and performance of the repository through different processes such as 1) container corrosion influenced by sulfate-reducing bacteria (Stone et al., 2016), 2) alteration of bentonite mineralogy by the reduction of structural Fe(III) in smectite (Liu et al., 2017; Pentráková et al., 2013), and 3) changing the speciation and mobility of radionuclides (e.g. uranium). In the present study, no significant changes in the mineralogy of the bentonite were observed indicating the high stability of these clays; however brown spots in the microcosms were observed probably consisting of Mn(IV) precipitates may be produced by the microbial activity.

One of the concerns in the DGR is the introduction of nitrate because its assimilation by nitrate-reducing bacteria could produce the reoxidation of reduced U(IV) into the more soluble U(VI) coupled to nitrate reduction (Wu et al., 2010). To further visualize statistically significant taxa in all anaerobic microcosms, LEfSe (LDA Effect Size) analysis was performed. In Fig. 10, significant taxa related to nitrate treatment were shown in green (for GN) or light blue (for N). Some of the nitrate reducers were found significant in these samples such as *Spirochaetacea* family (GN), *Limnobacter* (GN) and *Brevundimonas* (N).

In addition, glycerol is a parameter to take into account in terms of its possible utilization as a carbon source by diverse microorganisms such as *Desulfovibrio* (Qatibi

et al., 1998). This glycerol could be transformed to other carbon compounds such as acetate, which could be utilized mainly for the growth of iron-reducing bacteria and some SRB (Petrie et al., 2003). These iron-reducing bacteria have been found to produce concomitant U(VI) and Fe(III) reduction, while SRB have been studied for their capacities to reduce soluble U(VI) to a more insoluble and less toxic U(IV) (Lovley et al., 1993; Spear et al., 2000). We found *Desulfovibrio* with significant presence in GU microcosms indicating that their abundance was enhanced by glycerol utilization and also by uranium tolerance mechanisms (e.g. bioreduction) (Fig. 11).

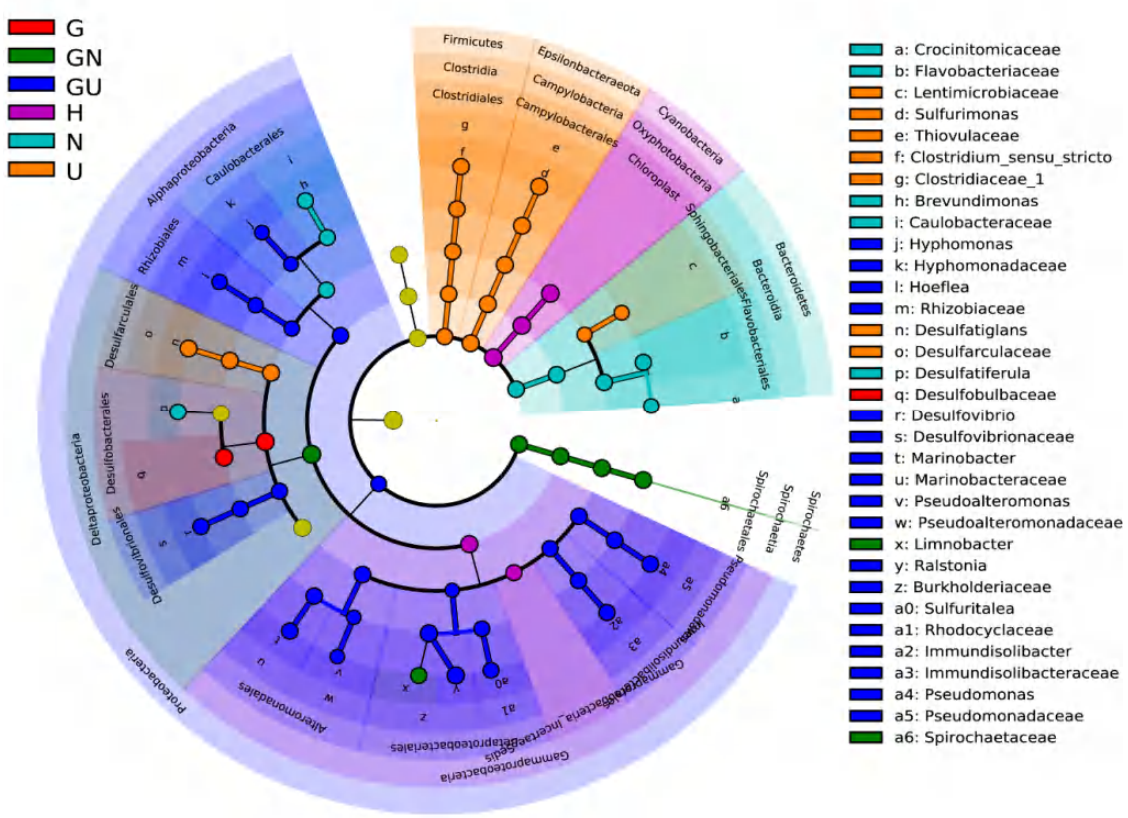

Figure 10. Cladogram showing differentially abundant taxonomic levels in each treatment with an LDA score > 2.0, $p < 0.05$. Significant taxa of G, GN, GU, H, N and U microcosms are represented in red, dark green, blue, purple, light green and orange, respectively. Family and genus taxonomic levels are shown in the legend.

As mentioned before, GU-treatment showed to encompass more significant taxa such as *Desulfovibrio*, *Pseudomonas*, *Ralstonia*, *Marinobacter*, among others (Fig. 11). LefSe plot also highlighted the significant abundance of *Clostridium*, *Sulfurimonas*, and *Desulfatiglans* in U microcosms. These bacteria may have a key role in the DGR concept. They are involved in the biogeochemical cycle of U due to their capacities to interact with this radionuclide through different mechanisms such as biosorption,

intracellular accumulation, biomineralization and bioreduction, depleting the toxic U(VI) from the environment (Gao and Francis, 2008; Kazy et al., 2009; Newsome et al., 2014a).

6. ACKNOWLEDGEMENTS

We acknowledge the assistance of María del Mar Abad Ortega (STEM technician), Isabel Guerra Tschuschke (VP-FESEM technician), and Concepción Hernández-Castillo (preparation of samples for microscopic analyses), members of Centro de Instrumentación Científica (University of Granada, Spain).

7. FUNDINGS SOURCES

This work was funded by the ERDF-financed Grant CGL2014-59616-R (80% funding by FEDER), (Ministerio de Ciencia e Innovación, España) as well as by an FPU 14/04263 ("Formación de Profesorado Universitario") grant to the first author from the Spanish Ministry (Ministerio de Educación Cultura y Deporte, MECD).

8. REFERENCES

Alessi, D.S., Uster, B., Veeramani, H., Suvorova, E.I., Lezama-Pacheco, J.S., Stubbs, J.E., Bargar, J.R., Bernier-Latmani, R., 2012. Quantitative separation of monomeric U(IV) from UO_2 in products of U(VI) reduction. Environ. Sci. Technol. 46, 6150–6157. https://doi.org/10.1021/es204123z

Al-Jariri, J.S., Khalili, F., 2010. Adsorption of Zn(II), Pb(II), Cr(III) and Mn(II) from water by Jordanian bentonite. Desalination and Water Treatment 21, 308–322. https://doi.org/10.5004/dwt.2010.1623

Anandan, R., Dharumadurai, D., Manogaran, G.P., 2016. An introduction to Actinobacteria. Actinobacteria - basics and biotechnological applications. https://doi.org/10.5772/62329

Anderson, C., Johnsson, A., Moll, H., Pedersen, K., 2011. Radionuclide geomicrobiology of the deep biosphere. Geomicrobiology Journal 28, 540–561. https://doi.org/10.1080/01490451.2010.507644

Ben Ali Gam, Z., Thioye, A., Cayol, J.-L., Joseph, M., Fauque, G., Labat, M., 2018. Characterization of *Desulfovibrio salinus* sp. nov., a slightly halophilic sulfate-reducing bacterium isolated from a saline lake in Tunisia. Int. J. Syst. Evol. Microbiol. 68, 715–720. https://doi.org/10.1099/ijsem.0.002567

Bengtsson, A., Pedersen, K., 2017. Microbial sulphide-producing activity in water saturated Wyoming MX-80, Asha and Calcigel bentonites at wet densities from 1500 to 2000 kg·m^{-3}. Applied Clay Science 137, 203–212. https://doi.org/10.1016/j.clay.2016.12.024

Bernardet, J.-F., Nakagawa, Y., 2006. An introduction to the family *Flavobacteriaceae*, in: Dworkin, M., Falkow, S., Rosenberg, E., Schleifer, K.-H., Stackebrandt, E. (Eds.), The Prokaryotes: Volume 7: Proteobacteria: Delta, Epsilon Subclass. Springer New York, New York, NY, pp. 455–480. https://doi.org/10.1007/0-387-30747-8_16

Bernier-Latmani, R., Veeramani, H., Vecchia, E.D., Junier, P., Lezama-Pacheco, J.S., Suvorova, E.I., Sharp, J.O., Wigginton, N.S., Bargar, J.R., 2010. Non-uraninite Products of Microbial U(VI) Reduction. Environ. Sci. Technol. 44, 9456–9462. https://doi.org/10.1021/es101675a

Biebl, H., 2001. Fermentation of glycerol by *Clostridium pasteurianum* −batch and continuous culture studies. J. Ind. Microbiol. Biotechnol. 27, 18–26. https://doi.org/10.1038/sj/jim/7000155

Broman, E., Jawad, A., Wu, X., Christel, S., Ni, G., Lopez-Fernandez, M., Sundkvist, J.-E., Dopson, M., 2017. Low temperature, autotrophic microbial denitrification using thiosulfate or thiocyanate as electron donor. Biodegradation 28, 287–301. https://doi.org/10.1007/s10532-017-9796-7

Brzoska, R.M., Bollmann, A., 2016. The long-term effect of uranium and pH on the community composition of an artificial consortium. FEMS Microbiol. Ecol. 92. https://doi.org/10.1093/femsec/fiv158

Cappelli, C., Yokoyama, S., Cama, J., Huertas, F.J., 2018. Montmorillonite dissolution kinetics: Experimental and reactive transport modeling interpretation. Geochimica et Cosmochimica Acta 227, 96–122. https://doi.org/10.1016/j.gca.2018.01.039

Chabalala, S., Chirwa, E.M.N., 2010. Uranium(VI) reduction and removal by high performing purified anaerobic cultures from mine soil. Chemosphere 78, 52–55. https://doi.org/10.1016/j.chemosphere.2009.10.026

Chen, Y., Feng, X., He, Y., Wang, F., 2016. Genome analysis of a *Limnobacter* sp. identified in an anaerobic methane-consuming cell consortium. Front. Mar. Sci. 3. https://doi.org/10.3389/fmars.2016.00257

Choudhary, S., Sar, P., 2011. Uranium biomineralization by a metal resistant *Pseudomonas aeruginosa* strain isolated from contaminated mine waste. J. Hazard. Mater. 186, 336–343. https://doi.org/10.1016/j.jhazmat.2010.11.004

Cologgi, D.L., Lampa-Pastirk, S., Speers, A.M., Kelly, S.D., Reguera, G., 2011. Extracellular reduction of uranium via *Geobacter* conductive pili as a protective cellular mechanism. Proc Natl Acad Sci U S A 108, 15248–15252. https://doi.org/10.1073/pnas.1108616108

Díaz-Fernández, A.M., 2004. Caracterización y modelización del agua intersticial de materiales arcillosos: estudio de la bentonita de Cortijo de Archidona. PhD Thesis. Universidad Autónoma de Madrid Editorial CIEMAT, 505.

Dolinská, S., Schütz, T., Znamenáčková, I., Lovas, M., Vaculíková, L., 2015. Bentonite modification with manganese oxides and its characterization. Inzynieria Mineralna 2015, 213–218.

D'Souza, S.F., Sar, P., Kazy, S.K., Kubal, B.S., 2006. Uranium Sorption by *Pseudomonas* Biomass Immobilized in Radiation Polymerized Polyacrylamide Bio-Beads. Journal of Environmental Science and Health, Part A 41, 487–500. https://doi.org/10.1080/10934520500428377

Edgar, R.C., 2010. Search and clustering orders of magnitude faster than BLAST. Bioinformatics 26, 2460–2461. https://doi.org/10.1093/bioinformatics/btq461

Francis, A.J., Dodge, C.J., 2008. Bioreduction of uranium(VI) complexed with citric acid by Clostridia affects its structure and solubility. Environ. Sci. Technol. 42, 8277–8282. https://doi.org/10.1021/es801045m

Gao, W., Francis, A.J., 2008. Reduction of uranium(VI) to uranium(IV) by Clostridia. Appl. Environ. Microbiol. 74, 4580–4584. https://doi.org/10.1128/AEM.00239-08

Geissler, A., Selenska-Pobell, S., 2005. Addition of U(VI) to a uranium mining waste sample and resulting changes in the indigenous bacterial community. Geobiology 3, 275–285. https://doi.org/10.1111/j.1472-4669.2006.00061.x

Grigoryan, A.A., Jalique, D.R., Medihala, P., Stroes-Gascoyne, S., Wolfaardt, G.M., McKelvie, J., Korber, D.R., 2018. Bacterial diversity and production of sulfide in microcosms containing uncompacted bentonites. Heliyon 4. https://doi.org/10.1016/j.heliyon.2018.e00722

Han, Y., Perner, M., 2015. The globally widespread genus *Sulfurimonas*: versatile energy metabolisms and adaptations to redox clines. Front. Microbiol. 6. https://doi.org/10.3389/fmicb.2015.00989

Handley, K.M., VerBerkmoes, N.C., Steefel, C.I., Williams, K.H., Sharon, I., Miller, C.S., Frischkorn, K.R., Chourey, K., Thomas, B.C., Shah, M.B., Long, P.E., Hettich, R.L., Banfield, J.F., 2013. Biostimulation induces syntrophic interactions that impact C, S and N cycling in a sediment microbial community. ISME J 7, 800–816. https://doi.org/10.1038/ismej.2012.148

Heidelberg, J.F., Seshadri, R., Haveman, S.A., Hemme, C.L., Paulsen, I.T., Kolonay, J.F., Eisen, J.A., Ward, N., Methe, B., Brinkac, L.M., Daugherty, S.C., Deboy, R.T., Dodson, R.J., Durkin, A.S., Madupu, R., Nelson, W.C., Sullivan, S.A., Fouts, D., Haft, D.H., Selengut, J., Peterson, J.D., Davidsen, T.M., Zafar, N., Zhou, L., Radune, D., Dimitrov, G., Hance, M., Tran, K., Khouri, H., Gill, J., Utterback, T.R., Feldblyum, T.V., Wall, J.D., Voordouw, G., Fraser, C.M., 2004. The genome sequence of the anaerobic, sulfate-reducing bacterium *Desulfovibrio vulgaris* Hildenborough. Nat Biotechnol 22, 554–559. https://doi.org/10.1038/nbt959

Hemmat-Jou, M.H., Safari-Sinegani, A.A., Mirzaie-Asl, A., Tahmourespour, A., 2018. Analysis of microbial communities in heavy metals-contaminated soils using the metagenomic approach. Ecotoxicology 27, 1281–1291. https://doi.org/10.1007/s10646-018-1981-x

Herlemann, D.P., Labrenz, M., Jürgens, K., Bertilsson, S., Waniek, J.J., Andersson, A.F., 2011. Transitions in bacterial communities along the 2000 km salinity gradient of the Baltic Sea. ISME J 5, 1571–1579. https://doi.org/10.1038/ismej.2011.41

Hu, M.Z.-C., Norman, J.M., Faison, B.D., Reeves, M.E., 1996. Biosorption of uranium by *Pseudomonas aeruginosa* strain CSU: Characterization and comparison studies. Biotechnology and Bioengineering 51, 237–247. https://doi.org/10.1002/(SICI)1097-0290(19960720)51:2<237::AID-BIT14>3.0.CO;2-J

Huertas, F.J., Caballero, E., Jiménez de Cisneros, C., Huertas, F., Linares, J., 2001. Kinetics of montmorillonite dissolution in granitic solutions. Applied Geochemistry 16, 397–407. https://doi.org/10.1016/S0883-2927(00)00049-4

Hugerth, L.W., Wefer, H.A., Lundin, S., Jakobsson, H.E., Lindberg, M., Rodin, S., Engstrand, L., Andersson, A.F., 2014. DegePrime, a program for degenerate primer design for broad-taxonomic-range PCR in microbial ecology studies. Appl. Environ. Microbiol. 80, 5116–5123. https://doi.org/10.1128/AEM.01403-14

Hung, C.-H., Chang, Y.-T., Chang, Y.-J., 2011. Roles of microorganisms other than *Clostridium* and *Enterobacter* in anaerobic fermentative biohydrogen production systems – A review. Bioresource Technology, Special Issue: Biofuels-III: Biohydrogen 102, 8437–8444. https://doi.org/10.1016/j.biortech.2011.02.084

Iskander, A.L., Khald, E.M., Sheta, A.S., 2011. Zinc and manganese sorption behavior by natural zeolite and bentonite. Annals of Agricultural Sciences 56, 43–48. https://doi.org/10.1016/j.aoas.2011.05.002

Jochum, L.M., Schreiber, L., Marshall, I.P.G., Jørgensen, B.B., Schramm, A., Kjeldsen, K.U., 2018. Single-cell genomics reveals a diverse metabolic potential of uncultivated *Desulfatiglans*-related

Deltaproteobacteria widely distributed in marine sediment. Front. Microbiol. 9. https://doi.org/10.3389/fmicb.2018.02038

Kang, T.S., Korber, D.R., Tanaka, T., 2014. Metabolic engineering of a glycerol-oxidative pathway in *Lactobacillus panis* PM1 for utilization of bioethanol thin stillage: Potential to produce platform chemicals from glycerol. Appl. Environ. Microbiol. 80, 7631–7639. https://doi.org/10.1128/AEM.01454-14

Kaufhold, S., Dohrmann, R., Gröger-Trampe, J., 2017. Reaction of native copper in contact with pyrite and bentonite in anaerobic water at elevated temperature. Corrosion Engineering, Science and Technology 52, 349–358. https://doi.org/10.1080/1478422X.2017.1292201

Kazy, S.K., D'Souza, S.F., Sar, P., 2009. Uranium and thorium sequestration by a *Pseudomonas* sp.: Mechanism and chemical characterization. Journal of Hazardous Materials 163, 65–72. https://doi.org/10.1016/j.jhazmat.2008.06.076

Kazy, S.K., Sar, P., D'Souza, S.F., 2008. Studies on uranium removal by the extracellular polysaccharide of a *Pseudomonas aeruginosa* strain. Bioremediation Journal 12, 47–57. https://doi.org/10.1080/10889860802052870

Khan, N.H., Bondici, V.F., Medihala, P.G., Lawrence, J.R., Wolfaardt, G.M., Warner, J., Korber, D.R., 2013. Bacterial diversity and composition of an alkaline uranium mine tailings-water interface. J Microbiol. 51, 558–569. https://doi.org/10.1007/s12275-013-3075-z

King, F., Hall, D.S., Keech, P.G., 2017. Nature of the near-field environment in a deep geological repository and the implications for the corrosion behaviour of the container. Corrosion Engineering, Science and Technology 52, 25–30. https://doi.org/10.1080/1478422X.2017.1330736

Kitjanukit, S., Takamatsu, K., Okibe, N., 2019. Natural attenuation of Mn(II) in metal refinery wastewater: Microbial community structure analysis and isolation of a new Mn(II)-oxidizing bacterium *Pseudomonas* sp. SK3. Water 11, 507. https://doi.org/10.3390/w11030507

König, H., Claus, H., Varma, A., 2010. Prokaryotic Cell Wall Compounds: Structure and Biochemistry. Springer Science & Business Media.

Kuever, J., 2014. The Family Desulfobacteraceae, in: Rosenberg, E., DeLong, E.F., Lory, S., Stackebrandt, E., Thompson, F. (Eds.), The Prokaryotes: Deltaproteobacteria and Epsilonproteobacteria. Springer Berlin Heidelberg, Berlin, Heidelberg, pp. 45–73. https://doi.org/10.1007/978-3-642-39044-9_266

Kutvonen, H., Rajala, P., Carpén, L., Bomberg, M., 2015. Nitrate and ammonia as nitrogen sources for deep subsurface microorganisms. Front. Microbiol. 6. https://doi.org/10.3389/fmicb.2015.01079

Leschine, S., Paster, B.J., 2015. Spirochaeta, in: Bergey's Manual of Systematics of Archaea and Bacteria. American Cancer Society, pp. 1–18. https://doi.org/10.1002/9781118960608.gbm01248

Leupin, O.X., Bernier-Latmani, R., Bagnoud, A., Moors, H., Leys, N., Wouters, K., Stroes-Gascoyne, S., 2017. Fifteen years of microbiological investigation in Opalinus Clay at the Mont Terri rock laboratory (Switzerland). Swiss J Geosci 110, 343–354. https://doi.org/10.1007/s00015-016-0255-y

Li, X.-X., Yang, T., Mbadinga, S.M., Liu, J.-F., Yang, S.-Z., Gu, J.-D., Mu, B.-Z., 2017. Responses of microbial community composition to temperature gradient and carbon steel corrosion in production water of petroleum reservoir. Front. Microbiol. 8. https://doi.org/10.3389/fmicb.2017.02379

Liu, D., Dong, H., Bishop, M.E., Zhang, J., Wang, H., Xie, S., Wang, S., Huang, L., Eberl, D.D., 2012. Microbial reduction of structural iron in interstratified illite-smectite minerals by a sulfate-reducing bacterium. Geobiology 10, 150–162. https://doi.org/10.1111/j.1472-4669.2011.00307.x

Liu, G., Qiu, S., Liu, B., Pu, Y., Gao, Z., Wang, J., Jin, R., Zhou, J., 2017. Microbial reduction of Fe(III)-bearing clay minerals in the presence of humic acids. Scientific Reports 7, 45354. https://doi.org/10.1038/srep45354

Liu, W., Langenhoff, A.A.M., Sutton, N.B., Rijnaarts, H.H.M., 2018. Biological regeneration of manganese(IV) and iron(III) for anaerobic metal oxide-mediated removal of pharmaceuticals from water. Chemosphere 208, 122–130. https://doi.org/10.1016/j.chemosphere.2018.05.097

Lopez-Fernandez, M., Cherkouk, A., Vilchez-Vargas, R., Jauregui, R., Pieper, D., Boon, N., Sanchez-Castro, I., Merroun, M.L., 2015. Bacterial diversity in bentonites, engineered barrier for Deep Geological Disposal of radioactive wastes. Microb Ecol 70, 922–935. https://doi.org/10.1007/s00248-015-0630-7

Lopez-Fernandez, M., Vilchez-Vargas, R., Jroundi, F., Boon, N., Pieper, D., Merroun, M.L., 2018. Microbial community changes induced by uranyl nitrate in bentonite clay microcosms. Applied Clay Science, ACS - SI ICC 2017 XVI International Clay Conference – Clays, from the oceans to space 160, 206–216. https://doi.org/10.1016/j.clay.2017.12.034

Lovley, D.R., Roden, E.E., Phillips, E.J.P., Woodward, J.C., 1993. Enzymatic iron and uranium reduction by sulfate-reducing bacteria. Marine Geology, Marine Sediments, Burial, Pore Water Chemistry, Microbiology and Diagenesis 113, 41–53. https://doi.org/10.1016/0025-3227(93)90148-O

Luo, H., Zheng, P., Xie, F., Yang, R., Liu, L., Han, S., Zhao, Y., Bilal, M., 2019. Co-production of solvents and organic acids in butanol fermentation by *Clostridium acetobutylicum* in the presence of lignin-derived phenolics. RSC Adv. 9, 6919–6927. https://doi.org/10.1039/C9RA00325H

Martinez, R.J., Wu, C.H., Beazley, M.J., Andersen, G.L., Conrad, M.E., Hazen, T.C., Taillefert, M., Sobecky, P.A., 2014. Microbial community responses to organophosphate substrate additions in contaminated subsurface sediments. PLOS ONE 9, e100383. https://doi.org/10.1371/journal.pone.0100383

Masurat, P., Eriksson, S., Pedersen, K., 2010. Evidence of indigenous sulphate-reducing bacteria in commercial Wyoming bentonite MX-80. Applied Clay Science, Advanced smectitic clay research 47, 51–57. https://doi.org/10.1016/j.clay.2008.07.002

McMurdie, P.J., Holmes, S., 2013. phyloseq: an R package for reproducible interactive analysis and graphics of microbiome census data. PLoS ONE 8, e61217. https://doi.org/10.1371/journal.pone.0061217

Merroun, M.L., Raff, J., Rossberg, A., Hennig, C., Reich, T., Selenska-Pobell, S., 2005. Complexation of uranium by cells and S-layer sheets of *Bacillus sphaericus* JG-A12. Appl. Environ. Microbiol. 71, 5532–5543. https://doi.org/10.1128/AEM.71.9.5532-5543.2005

Missana, T., Alonso, U., Turrero, M.J., 2003. Generation and stability of bentonite colloids at the bentonite/granite interface of a deep geological radioactive waste repository. J. Contam. Hydrol. 61, 17–31. https://doi.org/10.1016/S0169-7722(02)00110-9

Mondani, L., Benzerara, K., Carrière, M., Christen, R., Mamindy-Pajany, Y., Février, L., Marmier, N., Achouak, W., Nardoux, P., Berthomieu, C., Chapon, V., 2011. Influence of uranium on bacterial communities: A comparison of natural uranium-rich soils with controls. PLoS ONE 6, e25771. https://doi.org/10.1371/journal.pone.0025771

Nessa, S., Idemitsu, K., Yamasaki, Y., Inagaki, Y., Arima, T., 2007. Measurement of pH of the compacted bentonite under the reducing condition. Memoirs of the Faculty of Engineering, Kyushu University, 67:15–31.

Newsome, L., Morris, K., Lloyd, J.R., 2014a. The biogeochemistry and bioremediation of uranium and other priority radionuclides. Chemical Geology 363, 164–184. https://doi.org/10.1016/j.chemgeo.2013.10.034

Newsome, L., Morris, K., Shaw, S., Trivedi, D., Lloyd, J.R., 2015. The stability of microbially reduced U(IV); impact of residual electron donor and sediment ageing. Chemical Geology 409, 125–135. https://doi.org/10.1016/j.chemgeo.2015.05.016

Newsome, L., Morris, K., Trivedi, D., Atherton, N., Lloyd, J.R., 2014b. Microbial reduction of uranium(VI) in sediments of different lithologies collected from Sellafield. Applied Geochemistry 51, 55–64. https://doi.org/10.1016/j.apgeochem.2014.09.008

Patil, Y., Junghare, M., Müller, N., 2016. Fermentation of glycerol by *Anaerobium acetethylicum* and its potential use in biofuel production. Microb Biotechnol 10, 203–217. https://doi.org/10.1111/1751-7915.12484

Payer, J.H., Finsterle, S., Apps, J.A., Muller, R.A., 2019. Corrosion performance of engineered barrier system in deep horizontal drillholes. Energies 12, 1491. https://doi.org/10.3390/en12081491

Payne, R.B., Gentry, D.M., Rapp-Giles, B.J., Casalot, L., Wall, J.D., 2002. Uranium reduction by *Desulfovibrio desulfuricans* Strain G20 and a cytochrome c_3 mutant. Appl Environ Microbiol 68, 3129–3132. https://doi.org/10.1128/AEM.68.6.3129-3132.2002

Pedersen, K., Bengtsson, A., Blom, A., Johansson, L., Taborowski, T., 2017. Mobility and reactivity of sulphide in bentonite clays – Implications for engineered bentonite barriers in geological repositories for radioactive wastes. Applied Clay Science 146, 495–502. https://doi.org/10.1016/j.clay.2017.07.003

Pentráková, L., Su, K., Pentrák, M., Stucki, J.W., 2013. A review of microbial redox interactions with structural Fe in clay minerals. Clay Minerals 48, 543–560. https://doi.org/10.1180/claymin.2013.048.3.10

Petrie, L., North, N.N., Dollhopf, S.L., Balkwill, D.L., Kostka, J.E., 2003. Enumeration and characterization of iron(III)-reducing microbial communities from acidic subsurface sediments contaminated with uranium(VI). Appl. Environ. Microbiol. 69, 7467–7479. https://doi.org/10.1128/aem.69.12.7467-7479.2003

Povedano-Priego, C., Jroundi, F., Lopez-Fernandez, M., Sánchez-Castro, I., Martin-Sánchez, I., Huertas, F.J., Merroun, M.L., 2019. Shifts in bentonite bacterial community and mineralogy in response to uranium and glycerol-2-phosphate exposure. Science of The Total Environment 692, 219–232. https://doi.org/10.1016/j.scitotenv.2019.07.228

Qatibi, A.I., Bennisse, R., Jana, M., Garcia, J.-L., 1998. Anaerobic degradation of glycerol by *Desulfovibrio fructosovorans* and *D. carbinolicus* and evidence for glycerol-dependent utilization of 1,2-propanediol. Curr. Microbiol. 36, 283–290.

Quast, C., Pruesse, E., Yilmaz, P., Gerken, J., Schweer, T., Yarza, P., Peplies, J., Glöckner, F.O., 2013. The SILVA ribosomal RNA gene database project: improved data processing and web-based tools. Nucleic Acids Res 41, D590–D596. https://doi.org/10.1093/nar/gks1219

Rajala, P., Carpén, L., Vepsäläinen, M., Raulio, M., Sohlberg, E., Bomberg, M., 2015. Microbially induced corrosion of carbon steel in deep groundwater environment. Front Microbiol 6. https://doi.org/10.3389/fmicb.2015.00647

Robertson, C.E., Harris, J.K., Wagner, B.D., Granger, D., Browne, K., Tatem, B., Feazel, L.M., Park, K., Pace, N.R., Frank, D.N., 2013. Explicet: graphical user interface software for metadata-driven management, analysis and visualization of microbiome data. Bioinformatics 29, 3100–3101. https://doi.org/10.1093/bioinformatics/btt526

Saad, S., Bhatnagar, S., Tegetmeyer, H.E., Geelhoed, J.S., Strous, M., Ruff, S.E., 2017. Transient exposure to oxygen or nitrate reveals ecophysiology of fermentative and sulfate-reducing benthic microbial populations. Environ Microbiol 19, 4866–4881. https://doi.org/10.1111/1462-2920.13895

Safonov, A.V., Babich, T.L., Sokolova, D.S., Grouzdev, D.S., Tourova, T.P., Poltaraus, A.B., Zakharova, E.V., Merkel, A.Y., Novikov, A.P., Nazina, T.N., 2018. Microbial community and in situ bioremediation of groundwater by nitrate removal in the zone of a radioactive waste surface repository. Front. Microbiol. 9. https://doi.org/10.3389/fmicb.2018.01985

Salome, K.R., Green, S.J., Beazley, M.J., Webb, S.M., Kostka, J.E., Taillefert, M., 2013. The role of anaerobic respiration in the immobilization of uranium through biomineralization of phosphate minerals. Geochimica et Cosmochimica Acta 106, 344–363. https://doi.org/10.1016/j.gca.2012.12.037

Santelli, C.M., Webb, S.M., Dohnalkova, A.C., Hansel, C.M., 2011. Diversity of Mn oxides produced by Mn(II)-oxidizing fungi. Geochimica et Cosmochimica Acta 75, 2762–2776. https://doi.org/10.1016/j.gca.2011.02.022

Smart, N.R., Reddy, B., Rance, A.P., Nixon, D.J., Frutschi, M., Bernier-Latmani, R., Diomidis, N., 2017. The anaerobic corrosion of carbon steel in compacted bentonite exposed to natural Opalinus Clay porewater containing native microbial populations. Corrosion Engineering, Science and Technology 52, 101–112. https://doi.org/10.1080/1478422X.2017.1315233

Spear, J.R., Figueroa, L.A., Honeyman, B.D., 2000. Modeling reduction of uranium U(VI) under variable sulfate concentrations by sulfate-reducing bacteria. Applied and Environmental Microbiology 66, 3711–3721. https://doi.org/10.1128/AEM.66.9.3711-3721.2000

Stone, W., Kroukamp, O., Moes, A., McKelvie, J., Korber, D.R., Wolfaardt, G.M., 2016. Measuring microbial metabolism in atypical environments: Bentonite in used nuclear fuel storage. J. Microbiol. Methods 120, 79–90. https://doi.org/10.1016/j.mimet.2015.11.006

Stroes-Gascoyne, S., Hamon, C.J., Maak, P., Russell, S., 2010. The effects of the physical properties of highly compacted smectitic clay (bentonite) on the culturability of indigenous microorganisms. Applied Clay Science 47, 155–162. https://doi.org/10.1016/j.clay.2008.06.010

Stroes-Gascoyne, S., Schippers, A., Schwyn, B., Poulain, S., Sergeant, C., Simonoff, M., Le Marrec, C., Altmann, S., Nagaoka, T., Mauclaire, L., McKenzie, J., Daumas, S., Vinsot, A., Beaucaire, C., Matray, J.-M., 2007. Microbial community analysis of Opalinus Clay drill core samples from the Mont Terri underground research laboratory, Switzerland. Geomicrobiology Journal 24, 1–17. https://doi.org/10.1080/01490450601134275

Stylo, M., Neubert, N., Roebbert, Y., Weyer, S., Bernier-Latmani, R., 2015. Mechanism of uranium reduction and immobilization in *Desulfovibrio vulgaris* biofilms. Environ. Sci. Technol. 49, 10553–10561. https://doi.org/10.1021/acs.est.5b01769

Sun, H., Yang, Q., Peng, Y., Shi, X., Wang, S., Zhang, S., 2009. Nitrite accumulation during the denitrification process in SBR for the treatment of pre-treated landfill leachate. Chinese Journal of Chemical Engineering 17, 1027–1031. https://doi.org/10.1016/S1004-9541(08)60312-2

Svensson, D., Dueck, A., Nilsson, U., Olsson, S., Sandén, T., Lydmark, S., Jägerwall, S., Pedersen, K., Hansen, S., 2011. Alternative buffer material – Status of the ongoing laboratory investigation of reference materials and test package 1. SKB Technical Report. Swedish Nuclear Fuel & Waste Management Co 1–146.

Takai, K., Suzuki, M., Nakagawa, S., Miyazaki, M., Suzuki, Y., Inagaki, F., Horikoshi, K., 2006. *Sulfurimonas paralvinellae* sp. nov., a novel mesophilic, hydrogen- and sulfur-oxidizing chemolithoautotroph within the Epsilonproteobacteria isolated from a deep-sea hydrothermal vent polychaete nest, reclassification of *Thiomicrospira denitrificans* as *Sulfurimonas*

denitrificans comb. nov. and emended description of the genus *Sulfurimonas*. International Journal of Systematic and Evolutionary Microbiology, 56, 1725–1733. https://doi.org/10.1099/ijs.0.64255-0

Temudo, M.F., Poldermans, R., Kleerebezem, R., Loosdrecht, M.C.M. van, 2008. Glycerol fermentation by (open) mixed cultures: A chemostat study. Biotechnology and Bioengineering 100, 1088–1098. https://doi.org/10.1002/bit.21857

Vecchia, E.D., Veeramani, H., Suvorova, E.I., Wigginton, N.S., Bargar, J.R., Bernier-Latmani, R., 2010. U(VI) reduction by spores of *Clostridium acetobutylicum*. Research in Microbiology, Special issue on the biology of spore-formers 161, 765–771. https://doi.org/10.1016/j.resmic.2010.08.001

Villar, M.V., Cuevas, J., Leguey, S., Caballero, E., Huertas, F.J., Delgado, A., Fernández-Soler, J.M., Astudillo, J., 2006. The study of Spanish clays for their use as sealing materials in nuclear waste repositories: 20 years of progress. Journal of Iberian Geology 32, 15–36.

Wu, W.-M., Carley, J., Green, S.J., Luo, J., Kelly, S.D., Nostrand, J.V., Lowe, K., Mehlhorn, T., Carroll, S., Boonchayanant, B., Löfller, F.E., Watson, D., Kemner, K.M., Zhou, J., Kitanidis, P.K., Kostka, J.E., Jardine, P.M., Criddle, C.S., 2010. Effects of nitrate on the stability of uranium in a bioreduced region of the subsurface. Environ. Sci. Technol. 44, 5104–5111. https://doi.org/10.1021/es1000837

Xie, X., Müller, N., 2018. Enzymes involved in the anaerobic degradation of phenol by the sulfate-reducing bacterium *Desulfatiglans anilini*. BMC Microbiol. 18, 93. https://doi.org/10.1186/s12866-018-1238-0

Xu, J., Veeramani, H., Qafoku, N.P., Singh, G., Riquelme, M.V., Pruden, A., Kukkadapu, R.K., Gartman, B.N., Hochella, M.F., 2017. Efficacy of acetate-amended biostimulation for uranium sequestration: Combined analysis of sediment/groundwater geochemistry and bacterial community structure. Applied Geochemistry 78, 172–185. https://doi.org/10.1016/j.apgeochem.2016.12.024

Yilmaz, P., Yarza, P., Rapp, J.Z., Glöckner, F.O., 2016. Expanding the world of marine bacterial and archaeal clades. Front Microbiol 6. https://doi.org/10.3389/fmicb.2015.01524

Youssef, N.H., Elshahed, M.S., 2014. The Phylum Planctomycetes, in: Rosenberg, E., DeLong, E.F., Lory, S., Stackebrandt, E., Thompson, F. (Eds.), The Prokaryotes: Other major lineages of Bacteria and the Archaea. Springer Berlin Heidelberg, Berlin, Heidelberg, pp. 759–810. https://doi.org/10.1007/978-3-642-38954-2_155

9. SUPPLEMENTARY TABLES

Supplementary Table 1. Bacterial phyla of anaerobic microcosms and their corresponding relative abundances (%) in each treatment.

Phlya	Anaerobic microcosms					
	G (%)	GN (%)	GU (%)	H (%)	N (%)	U (%)
Proteobacteria	46.70	55.23	72.93	71.69	70.27	47.28
Bacteroidetes	13.86	3.11	2.83	9.81	6.08	15.18
Cyanobacteria	3.20	1.12	2.23	7.75	7.43	8.05
Epsilonbacteraeota	5.76	1.04	1.62	2.17	7.43	8.36
Unclassified	7.25	17.98	3.64	3.04	1.35	4.35
Firmicutes	1.92	0.78	0.96	0.80	1.35	4.55
Zixibacteria	0.64	0.43	0.46	0.00	1.35	2.18
Patescibacteria	13.86	8.04	10.48	0.00	0.68	1.02
Verrucomicrobia	1.28	0.35	0.15	0.36	0.68	1.75
Spirochaetes	1.71	8.47	0.96	0.22	0.68	1.46
Chloroflexi	0.21	0.00	0.30	1.19	1.35	1.20
Planctomycetes	0.21	0.26	0.30	0.36	0.00	1.00
Actinobacteria	0.85	0.00	0.76	0.54	0.68	0.62
Acidobacteria	0.43	0.00	0.30	1.09	0.68	0.56
Latescibacteria	0.21	0.00	0.15	0.00	0.00	0.58
Kiritimatiellaeota	0.00	0.00	0.15	0.18	0.00	0.48
Fusobacteria	0.00	0.00	0.00	0.00	0.00	0.45
Omnitrophicaeota	0.00	0.26	0.00	0.00	0.00	0.26
Gemmatimonadetes	0.00	0.00	0.15	0.40	0.00	0.17
Tenericutes	0.85	1.82	0.30	0.00	0.00	0.12
Nitrospirae	0.00	0.00	0.76	0.36	0.00	0.08
LCP-89	0.00	0.00	0.00	0.00	0.00	0.09
Lentisphaerae	0.00	0.00	0.00	0.00	0.00	0.08
Dependentiae	1.07	1.12	0.51	0.00	0.00	0.00
BRC1	0.00	0.00	0.00	0.00	0.00	0.05
Thermotogae	0.00	0.00	0.00	0.00	0.00	0.05
Margulisbacteria	0.00	0.00	0.00	0.00	0.00	0.03
Dadabacteria	0.00	0.00	0.00	0.04	0.00	0.01
Armatimonadetes	0.00	0.00	0.05	0.00	0.00	0.00

Supplementary Table 2. Bacterial classes of anaerobic microcosms and their corresponding relative abundances (%) in each treatment.

Classes	Anaerobic microcosms					
	G (%)	GN (%)	GU (%)	H (%)	N (%)	U (%)
Gammaproteobacteria	19.19	15.13	48.33	52.75	39.19	21.30
Deltaproteobacteria	25.37	36.13	11.34	11.77	14.19	23.28
Bacteroidia	6.18	2.59	2.68	8.76	6.08	14.07
Oxyphotobacteria	3.20	1.12	2.23	7.75	7.43	7.98
Campylobacteria	5.76	1.04	1.62	2.17	7.43	8.36
Unclassified	7.25	17.89	3.49	3.04	1.35	4.23
Clostridia	1.92	0.78	0.96	0.80	1.35	4.55
Alphaproteobacteria	2.13	3.98	10.68	7.17	16.22	2.69
unclassified Zixibacteria	0.64	0.43	0.46	0.00	1.35	2.18
ABY1	13.86	8.04	10.22	0.00	0.00	0.93
Verrucomicrobiae	1.28	0.35	0.15	0.36	0.68	1.75
Spirochaetia	1.71	7.35	0.81	0.22	0.68	1.35
Ignavibacteria	7.68	0.52	0.15	1.05	0.00	1.11
Dehalococcoidia	0.21	0.00	0.15	0.51	0.68	0.78
Planctomycetacia	0.21	0.00	0.30	0.33	0.00	0.56
unclassified Latescibacteria	0.21	0.00	0.15	0.00	0.00	0.58
Subgroup_22	0.21	0.00	0.15	0.76	0.00	0.45
Kiritimatiellae	0.00	0.00	0.15	0.18	0.00	0.48
Acidimicrobiia	0.85	0.00	0.35	0.40	0.68	0.43
Anaerolineae	0.00	0.00	0.15	0.47	0.68	0.41
Fusobacteriia	0.00	0.00	0.00	0.00	0.00	0.45
unclassified Omnitrophicaeota	0.00	0.26	0.00	0.00	0.00	0.26
Phycisphaerae	0.00	0.00	0.00	0.00	0.00	0.22
Gemmatimonadetes	0.00	0.00	0.15	0.40	0.00	0.17
Actinobacteria	0.00	0.00	0.35	0.11	0.00	0.19
unclassified Planctomycetes	0.00	0.26	0.00	0.00	0.00	0.20
Mollicutes	0.85	1.82	0.30	0.00	0.00	0.12
unclassified Proteobacteria	0.00	0.00	2.58	0.00	0.68	0.00
Nitrospira	0.00	0.00	0.76	0.36	0.00	0.08
unclassified Bacteria	0.00	0.09	0.15	0.00	0.00	0.12
Leptospirae	0.00	0.00	0.00	0.00	0.00	0.10
unclassified LCP-89	0.00	0.00	0.00	0.00	0.00	0.09
Oligosphaeria	0.00	0.00	0.00	0.00	0.00	0.08
Acidobacteriia	0.00	0.00	0.15	0.04	0.00	0.06
Melainabacteria	0.00	0.00	0.00	0.00	0.00	0.07
Babeliae	1.07	1.12	0.51	0.00	0.00	0.00
Gracilibacteria	0.00	0.00	0.00	0.00	0.68	0.05
unclassified BRC1	0.00	0.00	0.00	0.00	0.00	0.05
uncultured Spirochaetes	0.00	1.12	0.15	0.00	0.00	0.00
Thermotogae	0.00	0.00	0.00	0.00	0.00	0.05
unclassified Margulisbacteria	0.00	0.00	0.00	0.00	0.00	0.03

Parcubacteria	0.00	0.00	0.25	0.00	0.00	0.02
Holophagae	0.21	0.00	0.00	0.18	0.00	0.02
KD4-96	0.00	0.00	0.00	0.22	0.00	0.01
OM190	0.00	0.00	0.00	0.04	0.00	0.02
Thermoanaerobaculia	0.00	0.00	0.00	0.07	0.00	0.02
Aminicenantia	0.00	0.00	0.00	0.00	0.00	0.01
Subgroup_17	0.00	0.00	0.00	0.04	0.00	0.01
Thermoleophilia	0.00	0.00	0.05	0.04	0.00	0.01
Saccharimonadia	0.00	0.00	0.00	0.00	0.00	0.01
Dadabacteriia	0.00	0.00	0.00	0.04	0.00	0.01
Lentisphaeria	0.00	0.00	0.00	0.00	0.00	0.01
Fimbriimonadia	0.00	0.00	0.05	0.00	0.00	0.00
Subgroup_18	0.00	0.00	0.00	0.00	0.68	0.00
V2072-189E03	0.00	0.00	0.00	0.00	0.00	0.01

Supplementary Table 3. Bacterial families/genera of anaerobic microcosms and their corresponding relative abundances (%) in each treatment.

Families/Genera	**Anaerobic microcosms**					
	G (%)	**GN (%)**	**GU (%)**	**H (%)**	**N (%)**	**U (%)**
Sulfurimonas	1.81	0.98	0.00	1.69	3.43	7.60
Desulfobacteraceae	0.91	1.17	0.06	2.37	2.29	6.81
Unclassified	8.16	19.57	0.67	4.87	4.00	5.94
Desulfatiglans	0.91	0.68	0.00	0.08	4.57	6.72
Chloroplast	1.51	0.88	1.17	9.49	5.71	5.53
Clostridium_sensu_stricto	1.51	0.88	0.00	0.76	2.29	4.46
Candidatus_Electrothrix	0.60	0.39	0.00	1.57	2.29	4.24
Zixibacteria	0.00	0.20	0.00	0.00	2.29	2.80
Flavobacteriaceae	0.30	0.00	0.00	1.21	3.43	2.67
Psychromonas	0.91	0.20	0.06	0.80	1.71	2.56
Sulfurovum	0.60	0.49	0.06	0.88	1.14	2.47
Halieaceae	0.00	0.00	0.00	2.17	1.71	1.78
Flavobacterium	0.60	0.00	0.11	0.12	1.14	1.65
Nostocaceae	0.60	0.59	0.00	0.76	1.71	1.37
Burkholderiaceae	0.00	0.29	0.89	3.38	2.29	1.15
Gammaproteobacteria	0.30	0.00	0.00	5.79	1.71	0.91
Desulfobulbaceae	18.13	5.28	0.00	0.64	0.00	0.91
Dehalococcoidia/GIF9	0.00	0.10	0.00	0.76	1.14	1.17
Lentimicrobiaceae	1.21	0.29	0.00	0.00	0.00	1.09
Prolixibacteraceae	0.00	0.00	0.00	0.44	1.71	1.05
Deltaproteobacteria/MBNT15	0.00	0.00	0.00	7.36	0.00	0.60
Methylophilaceae	4.53	4.99	6.55	7.32	10.86	0.04
Desulfobacterium	0.30	0.00	0.00	0.80	0.00	1.00
*Bacteroidetes*_ BD2-2	0.60	0.20	0.00	1.77	0.00	0.91
Thiobacillus	0.60	0.29	1.00	2.09	1.71	0.82
Spirochaeta_2	0.60	0.10	0.00	0.04	0.57	0.96
Lentimonas	0.91	0.29	0.00	0.12	1.14	0.94
Arcobacter	0.00	0.29	0.00	0.00	0.00	0.94
Ralstonia	0.00	0.29	18.16	0.12	1.14	0.03
Latescibacteria	0.00	0.10	0.00	0.00	0.57	0.86
Saprospiraceae	0.00	0.10	0.00	0.97	1.14	0.78
Microscillaceae	0.00	0.20	0.06	1.45	0.00	0.66
Gammaproteobacteria B2M28	0.00	0.10	0.00	1.77	1.14	0.63
Luteolibacter	0.00	0.10	0.00	0.24	0.00	0.69
Bacteroidetes_vadinHA17	0.00	0.00	0.00	0.36	0.00	0.68
Cyclobacteriaceae	0.00	0.20	0.00	1.33	0.57	0.61
unclassified Bradymonadales	0.30	0.10	0.00	0.80	0.00	0.64
Loktanella	0.00	0.00	0.00	0.40	0.00	0.65
Cyanobium_PCC-6307	0.00	0.00	0.11	0.16	0.00	0.63
Acidiphilium	0.00	1.17	4.44	4.75	3.43	0.04
Ilumatobacter	0.60	0.10	0.00	0.52	0.00	0.54
Pseudorhodobacter	0.00	0.20	0.00	0.04	0.57	0.54
Methylotenera	1.51	2.94	3.33	2.45	5.14	0.11
Deltaproteobacteria/SAR324_clade	1.51	19.77	0.00	0.00	0.57	0.00
Ruminococcaceae	0.00	0.00	0.00	0.00	0.57	0.53
Alteromonadaceae	0.00	0.00	0.00	0.28	0.00	0.51

Anaerolineaceae	0.00	0.00	0.00	0.76	0.00	0.48
Algoriphagus	0.00	0.10	0.00	0.04	0.57	0.51
Aphanizomenon NIES81	0.00	0.10	0.00	0.04	0.00	0.49
Lutibacter	0.00	0.49	0.00	0.00	0.00	0.48
Rhodobacteraceae	0.30	0.00	0.00	1.17	0.57	0.41
Crocinitomicaceae	0.00	0.00	0.00	0.12	1.14	0.48
Rubinisphaeraceae	0.00	0.00	0.00	0.12	0.00	0.47
Spirochaetaceae	0.91	10.27	0.00	0.00	0.00	0.19
Draconibacterium	0.30	0.00	0.00	0.20	0.00	0.45
Gammaproteobacteria_Incertae_Sedis	0.00	0.10	0.00	1.97	0.57	0.32
Pseudomonas	0.00	0.00	9.16	0.00	0.57	0.00
Arenicellaceae	0.00	0.10	0.00	1.05	0.00	0.36
Marinobacter	0.00	0.00	8.83	0.00	0.00	0.00
Sediminispirochaeta	0.00	0.00	0.00	0.00	0.57	0.42
Bacteroidetes_VC2.1_Bac22	0.00	0.00	0.00	0.00	0.00	0.41
Omnitrophicaeota	0.00	0.39	0.00	0.00	0.00	0.40
Candidatus_Komeilibacteria	0.30	0.00	0.06	0.00	0.00	0.39
Marinilabiliaceae	0.00	1.47	0.00	0.76	0.00	0.30
Lewinella	0.00	0.00	0.00	0.00	0.57	0.37
Ignavibacteriales/PHOS-HE36	0.00	0.20	0.00	0.80	0.57	0.31
Steroidobacteraceae	0.00	0.20	0.00	0.32	0.57	0.33
Desulfovibrio	0.00	0.00	7.38	0.00	0.00	0.00
Planctomycetes/OM190	0.00	0.20	0.00	0.04	0.00	0.34
Immundisolibacter	0.30	0.00	6.89	0.00	1.14	0.00
Phycisphaeraceae/CL500-3	0.00	0.00	0.00	0.00	0.00	0.31
Melioribacteraceae	11.48	0.39	0.00	0.00	0.57	0.20
Sulfuritalea	0.00	0.00	4.55	0.00	0.00	0.10
Geopsychrobacter	0.00	0.00	0.00	0.08	0.00	0.28
Gemmatimonadaceae	0.00	0.00	0.00	0.64	0.00	0.25
Desulfuromonadaceae	0.00	0.00	0.00	0.00	0.00	0.27
Thiotrichaceae	0.00	0.00	0.00	0.36	0.00	0.25
unclassified *Acidobacteria*	0.00	0.10	0.00	1.01	0.00	0.20
Nitrosomonadaceae	0.00	0.00	0.00	1.25	0.57	0.20
Rhodoferax	0.00	0.10	0.00	0.00	0.00	0.26
Roseibacillus	0.00	0.00	0.00	0.00	0.57	0.26
Colwellia	0.00	0.00	0.00	0.84	0.57	0.21
Gammaproteobacteria CCM19a	0.00	0.00	0.00	1.17	0.00	0.18
Ulvibacter	0.00	0.00	0.00	0.84	0.00	0.20
Brevundimonas	0.00	0.88	4.50	0.00	2.29	0.00
Unclasified Chitinophagales	0.00	0.10	0.00	0.00	0.00	0.25
Gallionellaceae	0.00	0.10	0.56	0.04	0.00	0.22
Kiritimatiellaceae	0.00	0.00	0.00	0.28	0.00	0.22
Desulfobacteraceae/Sva0081	0.00	0.10	0.00	0.44	0.57	0.20
Hoeflea	0.00	1.17	3.28	0.00	0.57	0.05
Candidatus_Falkowbacteria	20.85	1.37	0.00	0.04	0.00	0.02

Supplementary Table 4. Bacterial phyla of bentonite microcosms and their corresponding p-values. One-way ANOVA test, using a significance level of 0.05, was used to look for significant differences in the alpha diversity between the samples. Red values represent p-value < 0.05.

Phyla	**p-value**
Proteobacteria	0.405
Bacteroidetes	0.227
Epsilonbacteraeota	0.081
Cyanobacteria	0.023
Unclassified	0.047
Firmicutes	0.044
Zixibacteria	0.391
Verrucomicrobia	0.342
Spirochaetes	0.010
Chloroflexi	0.175
Planctomycetes	0.742
Patescibacteria	0.452
Actinobacteria	0.786
Latescibacteria	0.474
Acidobacteria	0.690
Omnitrophicaeota	0.329
Gemmatimonadetes	0.579
Kiritimatiellaeota	0.168
Nitrospirae	0.223
Tenericutes	0.361
Fusobacteria	0.041
LCP-89	0.102
Lentisphaerae	0.023
BRC1	0.023
Thermotogae	0.023
Dependentiae	0.228
Margulisbacteria	0.035
Dadabacteria	0.502
Armatimonadetes	0.458

Supplementary Table 5. Bacterial classes of bentonite microcosms and their corresponding p-values. One-way ANOVA test, using a significance level of 0.05, was used to look for significant differences in the alpha diversity between the samples. Red values represent p-value < 0.05.

Classes	p-value	Classes	p-value
Deltaproteobacteria	0.006	Fusobacteriia	0.041
Gammaproteobacteria	0.148	Leptospirae	0.023
Bacteroidia	0.103	Oligosphaeria	0.023
Unclassified	0.161	Melainabacteria	0.030
Campylobacteria	0.081	Acidobacteriia	0.614
Oxyphotobacteria	0.023	Parcubacteria	0.039
Clostridia	0.044	Gracilibacteria	0.473
Verrucomicrobiae	0.342	KD4-96	0.470
Spirochaetia	0.073	Thermotogae	0.023
Dehalococcoidia	0.512	Holophagae	0.592
Ignavibacteria	0.492	Thermoanaerobaculia	0.611
Planctomycetacia	0.873	Babeliae	0.228
ABY1	0.444	Dadabacteriia	0.502
Anaerolineae	0.739	Thermoleophilia	0.574
Acidimicrobiia	0.821	Aminicenantia	0.139
Gemmatimonadetes	0.579	Saccharimonadia	0.319
Phycisphaerae	0.248	Subgroup_17	0.588
OM190	0.063	Lentisphaeria	0.042
Subgroup_22	0.507	V2072-189E03	0.458
Actinobacteria	0.278	Fimbriimonadia	0.458
Kiritimatiellae	0.168	Subgroup_18	0.459
Nitrospira	0.223	Subgroup_6	0.458
Mollicutes	0.361		

Supplementary Table 6. Bacterial families/genera of bentonite microcosms and their corresponding p-values. One-way ANOVA test, using a significance level of 0.05, was used to look for significant differences in the alpha diversity between the samples. Red values represent p-value < 0.05.

Families/Genera	p-value	Families/Genera	p-value
Deltaproteobacteria_SAR324_clade	0.001	*Acholeplasma*	0.520
Candidatus_Falkowbacteria	0.001	*Desulfocurvus*	0.381
Ralstonia	0.000	Unclassified *Nostocaceae*	0.216
Unclassified *Melioribacteraceae*	0.467	*Flavobacterium*	0.243
Unclassified *Desulfobulbaceae*	0.007	Unclassified Babeliales	0.088
Unclassified *Methylophilaceae*	0.346	Gammaproteobacteria|CCM19a	0.507
Unclassified *MBNT15*	0.109	*Lentimonas*	0.544
Unclassified *Spirochaetaceae*	0.000	Unclassified *Marinilabiliaceae*	0.223
Pseudomonas	0.000	*Arenimonas*	0.413

Methylotenera	0.754	Acidobacteria|unclassified	0.531
Unclassified Chloroplast	0.001	Unclassified *Anaerolineaceae*	0.452
Desulfovibrio	0.007	*Ignavibacteriales|PHOS-HE36*	0.695
Acidiphilium	0.750	*Woeseia*	0.174
Marinobacter	0.000	Unclassified Bradymonadales	0.394
Sulfurimonas	0.004	*Dehalococcoidia|GIF9*	0.091
Desulfatiglans	0.022	*Desulfobacterium*	0.158
Unclassified *Desulfobacteraceae*	0.037	Unclassified *Saprospiraceae*	0.062
Immundisolibacter	0.000	Unclassified *Cyclobacteriaceae*	0.109
Limnobacter	0.011	Unclassified *Rhodobacteraceae*	0.136
Unclassified Gammaproteobacteria	0.002	Unclassified *Arenicellaceae*	0.070
MSBL7 *(Desulfobulbaceae)*	0.581	*Ulvibacter*	0.284
Unclassified *Burkholderiaceae*	0.652	*Colwellia*	0.502
Brevundimonas	0.040	Sphingobacteriales|AKYH767	0.208
Sulfuritalea	0.001	*Methylobacter*	0.498
Desulfatiferula	0.030	*Acidocella*	0.550
Unclassified Flavobacteriales	0.514	*Nitrospira*	0.127
Clostridium_sensu_stricto	0.006	*Hyphomonas*	0.000
Candidatus_Electrothrix	0.218	*Ignavibacterium*	0.508
Unclassified Zixibacteria	0.216	Unclassified *Lentimicrobiaceae*	0.000
Hoeflea	0.010	Desulfuromonadales|Sva1033	0.503
Proteobacteria	0.000	*Sulfuricurvum*	0.071
Gammaproteobacteria|B2M28	0.697	Unclassified *Gemmatimonadaceae*	0.492
Acidithiobacillus	0.373	*Pseudoalteromonas*	0.000
Bacteroidetes_BD2-2	0.584	Unclassified *Sandaracinaceae*	0.507
Unclassified *Flavobacteriaceae*	0.018	Unclassified Betaproteobacteriales	0.001
Unclassified *Prolixibacteraceae*	0.504	*Spirochaeta_2*	0.400
Thiobacillus	0.182	Unclassified *Steroidobacteraceae*	0.654
Unclassified *Halieaceae*	0.066	*Latescibacteria*	0.240
Unclassified *Microscillaceae*	0.517	*Pseudorhodobacter*	0.392
Psychromonas	0.088	Unclassified *Crocinitomicaceae*	0.000
Sulfurovum	0.166	*Nitrosomonadaceae*	0.591
Gammaproteobacteria_Incertae_Sedis	0.026		

Supplementary Table 7. Bacterial phyla of bentonite anaerobic microcosms and their corresponding p-values. Multiple comparison using Tukey test, and a significance level of 0.05 was used to look for significant differences in the alpha diversity between pair of samples. Coloured cells represent p-value < 0.05: green for GN, and purple for U.

Phyla	Multiple comparisons between pair of samples														
	G-GN	G-GU	GN-GU	GN-H	GN-N	GN-U	GU-H	GU-N	GU-U	H-N	H-U	N-U	G-H	G-N	G-U
Proteobacteria	0.995	0.545	0.826	0.890	0.994	0.997	1.000	0.980	0.574	0.993	0.660	0.916	0.631	0.898	1.000
Bacteroidetes	0.521	0.416	1.000	0.860	0.834	0.396	0.766	0.735	0.306	1.000	0.947	0.960	0.986	0.991	1.000
Epsilonbacteraeota	0.564	0.633	1.000	0.999	0.395	0.142	1.000	0.456	0.171	0.582	0.239	0.976	0.759	0.999	0.898
Cyanobacteria	0.886	0.986	0.998	0.080	0.190	0.056	0.160	0.351	0.114	0.993	1.000	0.969	0.389	0.691	0.293
Unclassified	0.285	0.933	0.068	0.060	0.081	0.088	1.000	1.000	1.000	1.000	1.000	1.000	0.909	0.959	0.968
Firmicutes	0.914	0.910	1.000	1.000	0.962	0.064	1.000	0.960	0.063	0.918	0.048	0.226	0.848	1.000	0.294
Zixibacteria	1.000	1.000	1.000	0.998	0.906	0.581	0.997	0.929	0.624	0.726	0.372	0.985	0.984	0.972	0.732
Verrucomicrobia	0.922	0.742	0.998	1.000	0.943	0.517	0.992	0.781	0.313	0.974	0.604	0.944	0.961	1.000	0.960
Spirochaetes	0.044	0.994	0.018	0.009	0.027	0.030	0.998	1.000	1.000	0.987	0.981	1.000	0.936	1.000	1.000
Chloroflexi	1.000	1.000	0.999	0.399	0.399	0.539	0.571	0.571	0.720	1.000	1.000	1.000	0.484	0.484	0.632
Planctomycetes	1.000	1.000	1.000	1.000	1.000	0.740	1.000	1.000	0.814	1.000	0.880	0.777	1.000	1.000	0.799
Patescibacteria	0.985	1.000	0.999	0.920	0.940	0.953	0.763	0.798	0.824	1.000	1.000	1.000	0.605	0.645	0.675
Actinobacteria	0.725	1.000	0.818	0.975	0.974	0.970	0.995	0.996	0.997	1.000	1.000	1.000	0.981	0.982	0.985
Latescibacteria	0.900	0.976	0.999	1.000	0.909	0.616	0.994	0.980	0.788	0.826	0.499	0.989	0.813	1.000	0.991
Acidobacteria	0.998	1.000	0.999	0.704	0.810	0.987	0.875	0.941	1.000	1.000	0.958	0.987	0.901	0.957	1.000
Omnitrophicaeota	0.650	1.000	0.650	0.650	0.650	1.000	1.000	1.000	0.626	1.000	0.626	0.626	1.000	1.000	0.626
Gemmatimonadetes	1.000	0.988	0.988	0.620	1.000	0.984	0.915	0.988	1.000	0.620	0.930	0.984	0.620	1.000	0.984
Kiritimatiellaeota	1.000	0.953	0.953	0.929	1.000	0.202	1.000	0.953	0.588	0.929	0.642	0.202	0.929	1.000	0.202
Nitrospirae	1.000	0.278	0.359	0.920	1.000	1.000	0.868	0.278	0.380	0.848	0.934	1.000	0.848	1.000	1.000
Tenericutes	0.934	0.980	0.610	0.421	0.414	0.484	0.999	0.999	1.000	1.000	1.000	1.000	0.899	0.894	0.937
Fusobacteria	1.000	1.000	1.000	1.000	1.000	0.070	1.000	1.000	0.070	1.000	0.070	0.070	1.000	1.000	0.070
LCP-89	1.000	1.000	1.000	1.000	1.000	0.153	1.000	1.000	0.153	1.000	0.153	0.153	1.000	1.000	0.153
Lentisphaerae	1.000	1.000	1.000	1.000	1.000	0.042	1.000	1.000	0.042	1.000	0.042	0.042	1.000	1.000	0.042

BRC1	1.000	1.000	1.000	1.000	1.000	0.043	1.000	1.000	0.043	1.000	0.043	0.043	1.000	1.000	0.043
Thermotogae	1.000	1.000	1.000	1.000	1.000	0.042	1.000	1.000	0.042	1.000	0.042	0.042	1.000	1.000	0.042
Dependentiae	1.000	0.912	0.901	0.472	0.472	0.472	0.956	0.956	0.956	1.000	1.000	1.000	0.489	0.489	0.489
Margulisbacteria	1.000	1.000	1.000	1.000	1.000	0.060	1.000	1.000	0.060	1.000	0.060	0.060	1.000	1.000	0.060
Dadabacteria	1.000	1.000	1.000	0.560	1.000	0.999	0.560	1.000	0.999	0.560	0.763	0.999	0.560	1.000	0.999
Armatimonadetes	1.000	0.538	0.538	1.000	1.000	1.000	0.538	0.538	0.538	1.000	1.000	1.000	1.000	1.000	1.000

Supplementary Table 8. Bacterial classes of bentonite anaerobic microcosms and their corresponding p-values. Multiple comparison using Tukey test, and a significance level of 0.05 was used to look for significant differences in the alpha diversity between pair of samples. Coloured cells represent p-value < 0.05: green for GN, and purple for U.

Classes	**Multiple comparisons between pair of samples**														
	G-GN	**G-GU**	**GN-GU**	**GN-H**	**GN-N**	**GN-U**	**GU-H**	**GU-N**	**GU-U**	**H-N**	**H-U**	**N-U**	**G-H**	**G-N**	**G-U**
Deltaproteobacteria	0.459	0.225	0.010	0.012	0.026	0.352	1.000	0.993	0.304	0.997	0.348	0.579	0.259	0.459	1.000
Gammaproteobacteria	1.000	0.473	0.332	0.247	0.788	0.999	1.000	0.951	0.528	0.886	0.413	0.940	0.365	0.910	1.000
Bacteroidia	0.946	0.888	1.000	0.679	0.591	0.146	0.573	0.487	0.109	1.000	0.821	0.887	0.988	0.968	0.485
Unclassified	0.293	0.845	0.886	0.250	0.949	0.239	0.792	1.000	0.775	0.681	1.000	0.662	1.000	0.744	1.000
Campylobacteria	0.564	0.633	1.000	0.999	0.395	0.142	1.000	0.456	0.171	0.582	0.239	0.976	0.759	0.999	0.898
Oxyphotobacteria	0.886	0.986	0.998	0.079	0.190	0.059	0.159	0.350	0.120	0.993	1.000	0.974	0.388	0.690	0.307
Clostridia	0.914	0.910	1.000	1.000	0.962	0.064	1.000	0.960	0.063	0.918	0.048	0.226	0.848	1.000	0.294
Verrucomicrobiae	0.922	0.742	0.998	1.000	0.943	0.517	0.992	0.781	0.313	0.974	0.604	0.944	0.961	1.000	0.960
Spirochaetia	0.224	0.995	0.102	0.066	0.155	0.154	1.000	1.000	1.000	0.994	0.994	1.000	0.967	1.000	1.000
Dehalococcoidia	0.999	1.000	1.000	0.926	0.666	0.641	0.974	0.784	0.762	0.992	0.989	1.000	0.990	0.854	0.835
Ignavibacteria	0.551	0.496	1.000	1.000	1.000	1.000	1.000	1.000	1.000	1.000	1.000	1.000	0.626	0.583	0.640
Planctomycetacia	0.998	0.998	0.957	0.944	0.973	0.829	1.000	1.000	0.999	1.000	0.999	0.997	0.996	0.999	0.962

ABY1	0.985	0.999	0.999	0.920	0.918	0.951	0.783	0.781	0.839	1.000	1.000	1.000	0.607	0.604	0.674
Anaerolineae	1.000	1.000	1.000	0.879	0.902	0.984	0.940	0.955	0.996	1.000	0.998	0.999	0.828	0.856	0.967
Acidimicrobiia	0.734	0.964	0.990	0.994	0.926	0.990	1.000	0.999	1.000	0.998	1.000	0.999	0.951	0.997	0.963
Gemmatimonadetes	1.000	0.988	0.988	0.620	1.000	0.984	0.915	0.988	1.000	0.620	0.930	0.984	0.620	1.000	0.984
Phycisphaerae	0.728	0.728	1.000	1.000	1.000	0.404	1.000	1.000	0.404	1.000	0.463	0.404	0.788	0.728	0.990
OM190	0.173	1.000	0.173	0.298	0.173	0.998	0.999	1.000	0.322	0.999	0.508	0.322	0.999	1.000	0.322
Subgroup_22	0.998	1.000	1.000	0.586	1.000	0.927	0.724	0.998	0.978	0.496	0.978	0.871	0.810	0.991	0.993
Actinobacteria	0.986	0.713	0.366	0.988	0.998	0.955	0.698	0.202	0.815	0.896	1.000	0.799	1.000	0.886	1.000
Kiritimatiellae	1.000	0.953	0.953	0.929	1.000	0.202	1.000	0.953	0.588	0.929	0.642	0.202	0.929	1.000	0.202
Nitrospira	1.000	0.278	0.359	0.920	1.000	1.000	0.868	0.278	0.380	0.848	0.934	1.000	0.848	1.000	1.000
Mollicutes	0.934	0.980	0.610	0.421	0.414	0.484	0.999	0.999	1.000	1.000	1.000	1.000	0.899	0.894	0.937
Fusobacteriia	1.000	1.000	1.000	1.000	1.000	0.070	1.000	1.000	0.070	1.000	0.070	0.070	1.000	1.000	0.070
Leptospirae	1.000	1.000	1.000	1.000	1.000	0.042	1.000	1.000	0.042	1.000	0.042	0.042	1.000	1.000	0.042
Oligosphaeria	1.000	1.000	1.000	1.000	1.000	0.042	1.000	1.000	0.042	1.000	0.042	0.042	1.000	1.000	0.042
Melainabacteria	1.000	1.000	1.000	1.000	1.000	0.054	1.000	1.000	0.054	1.000	0.054	0.054	1.000	1.000	0.054
Acidobacteriia	1.000	0.981	0.981	1.000	0.627	1.000	0.997	0.939	0.997	0.747	1.000	0.757	1.000	0.627	1.000
Parcubacteria	1.000	0.055	0.055	0.997	1.000	0.999	0.116	0.055	0.096	0.997	1.000	0.999	0.997	1.000	0.999
Gracilibacteria	1.000	1.000	1.000	1.000	0.539	1.000	1.000	0.539	1.000	0.539	1.000	0.626	1.000	0.539	1.000
KD4-96	1.000	1.000	1.000	0.538	1.000	1.000	0.538	1.000	1.000	0.538	0.600	1.000	0.538	1.000	1.000
Thermotogae	1.000	1.000	1.000	1.000	1.000	0.042	1.000	1.000	0.042	1.000	0.042	0.042	1.000	1.000	0.042
Holophagae	0.783	0.783	1.000	0.851	1.000	1.000	0.851	1.000	1.000	0.851	0.900	1.000	1.000	0.783	0.842
Thermoanaerobaculia	0.908	1.000	0.908	0.998	0.908	0.979	0.726	1.000	1.000	0.726	0.875	1.000	0.726	1.000	1.000
Babeliae	1.000	0.912	0.901	0.472	0.472	0.472	0.956	0.956	0.956	1.000	1.000	1.000	0.489	0.489	0.489
Dadabacteriia	1.000	1.000	1.000	0.560	1.000	0.999	0.560	1.000	0.999	0.560	0.763	0.999	0.560	1.000	0.999
Thermoleophilia	1.000	0.670	0.670	0.949	1.000	1.000	0.986	0.670	0.734	0.949	0.971	1.000	0.949	1.000	1.000
Aminicenantia	1.000	1.000	1.000	1.000	1.000	0.199	1.000	1.000	0.199	1.000	0.199	0.199	1.000	1.000	0.199
Saccharimonadia	1.000	1.000	1.000	0.655	1.000	0.603	0.655	1.000	0.603	0.655	1.000	0.603	0.655	1.000	0.603
Subgroup_17	1.000	0.916	0.916	0.715	1.000	1.000	0.997	0.916	0.952	0.715	0.787	1.000	0.715	1.000	1.000

Lentisphaeria	1.000	1.000	1.000	1.000	1.000	0.071	1.000	1.000	0.071	1.000	0.071	0.071	1.000	1.000	0.071
V2072-189E03	1.000	1.000	1.000	1.000	1.000	0.538	1.000	1.000	0.538	1.000	0.538	0.538	1.000	1.000	0.538
Fimbriimonadia	1.000	0.538	0.538	1.000	1.000	1.000	0.538	0.538	0.538	1.000	1.000	1.000	1.000	1.000	1.000
Subgroup_18	1.000	1.000	1.000	1.000	0.538	1.000	1.000	0.538	1.000	0.538	1.000	0.540	1.000	0.538	1.000
Subgroup_6	1.000	1.000	1.000	0.538	1.000	1.000	0.538	1.000	1.000	0.538	0.538	1.000	0.538	1.000	1.000

Supplementary Table 9. Bacterial families/genera of bentonite microcosms and their corresponding p-values. Multiple comparison using DMS test and a significance level of 0.05 were used to look for significant differences in the alpha diversity between pair of samples. Coloured cells represent p-value < 0.05: blue for H, orange for G, red for N, green for GN, dark purple for U, and light purple for GU.

Families/Genera	**Multiple comparisons between pair of samples**														
	G-GN	**G-GU**	**GN-GU**	**GN-H**	**GN-N**	**GN-U**	**GU-H**	**GU-N**	**GU-U**	**H-N**	**H-U**	**N-U**	**G-H**	**G-N**	**G-U**
Deltaproteobacteria_SAR324_clade	0.002	0.987	0.001	0.001	0.001	0.001	1.000	1.000	1.000	1.000	1.000	1.000	0.985	0.998	0.985
Candidatus_Falkowbacteria	0.002	0.001	0.984	0.984	0.982	0.983	1.000	1.000	1.000	1.000	1.000	1.000	0.001	0.001	0.001
Ralstonia	1.000	0.000	0.000	1.000	0.994	1.000	0.000	0.001	0.000	0.988	1.000	0.981	1.000	0.978	1.000
Unclassified *Melioribacteraceae*	0.553	0.518	1.000	1.000	1.000	1.000	1.000	1.000	1.000	1.000	1.000	1.000	0.518	0.568	0.536
Unclassified *Desulfobulbaceae*	0.057	0.009	0.471	0.591	0.471	0.635	1.000	1.000	0.999	1.000	1.000	0.999	0.011	0.009	0.012
Unclassified *Methylophilaceae*	1.000	0.992	0.999	0.997	0.754	0.832	1.000	0.894	0.675	0.933	0.613	0.248	0.980	0.642	0.916
Unclassified MBNT15	1.000	1.000	1.000	0.142	1.000	1.000	0.142	1.000	1.000	0.142	0.190	1.000	0.142	1.000	1.000
Unclassified *Spirochaetaceae*	0.000	0.635	0.000	0.000	0.000	0.000	1.000	1.000	0.999	1.000	0.999	0.999	0.635	0.635	0.792
Pseudomonas	1.000	0.001	0.001	1.000	0.988	1.000	0.001	0.001	0.001	0.990	1.000	0.989	1.000	0.988	1.000
Methylotenera	0.999	0.996	1.000	1.000	0.977	0.945	1.000	0.991	0.908	0.948	0.976	0.658	1.000	0.896	0.993
Unclassified Chloroplast	0.981	1.000	0.998	0.002	0.019	0.036	0.002	0.028	0.054	0.169	0.084	0.984	0.003	0.037	0.071
Desulfovibrio	1.000	0.011	0.011	1.000	1.000	1.000	0.011	0.011	0.011	1.000	1.000	1.000	1.000	1.000	1.000

Acidiphilium	0.999	0.876	0.964	0.958	0.992	0.999	1.000	1.000	0.880	1.000	0.867	0.950	0.863	0.947	1.000
Marinobacter	1.000	0.000	0.000	1.000	1.000	1.000	0.000	0.000	0.000	1.000	1.000	1.000	1.000	1.000	1.000
Sulfurimonas	0.941	0.539	0.932	0.982	0.337	0.007	0.652	0.124	0.003	0.626	0.012	0.057	1.000	0.740	0.014
Desulfatiglans	1.000	0.981	0.997	0.999	0.202	0.065	1.000	0.125	0.042	0.134	0.044	0.898	0.988	0.260	0.084
Unclassified *Desulfobacteraceae*	1.000	0.993	0.970	0.964	0.973	0.065	0.677	0.703	0.030	1.000	0.151	0.143	0.911	0.927	0.052
Immundisolibacter	0.997	0.001	0.000	1.000	0.614	1.000	0.000	0.001	0.000	0.614	1.000	0.614	0.997	0.821	0.997
Limnobacter	0.022	1.000	0.017	0.017	0.017	0.017	1.000	1.000	1.000	1.000	1.000	1.000	1.000	1.000	1.000
Unclassified Gammaproteobacteria	0.968	0.978	1.000	0.002	0.292	0.783	0.002	0.313	0.813	0.011	0.005	0.868	0.003	0.607	0.992
MSBL7 *(Desulfobulbaceae)*	0.997	0.908	0.716	0.716	0.716	0.718	1.000	1.000	1.000	1.000	1.000	1.000	0.908	0.908	0.909
Unclassified *Burkholderiaceae*	1.000	0.999	1.000	0.701	0.910	0.998	0.838	0.976	1.000	0.995	0.888	0.990	0.688	0.901	0.997
Brevundimonas	0.990	0.067	0.125	0.962	0.801	0.962	0.053	0.481	0.053	0.424	1.000	0.424	1.000	0.521	1.000
Sulfuritalea	0.997	0.003	0.002	1.000	1.000	1.000	0.002	0.002	0.002	1.000	1.000	1.000	0.997	0.997	1.000
Desulfatiferula	0.119	0.048	0.951	0.951	0.630	0.952	1.000	0.279	1.000	0.279	1.000	0.280	0.048	0.628	0.048
Unclassified Flavobacteriales	1.000	0.997	1.000	0.991	0.699	0.996	0.999	0.787	0.984	0.930	0.904	0.475	0.956	0.566	1.000
Clostridium_sensu_stricto	0.968	0.422	0.785	1.000	0.420	0.015	0.868	0.103	0.005	0.346	0.012	0.121	0.923	0.783	0.030
Candidatus_Electrothrix	1.000	0.995	1.000	0.970	0.833	0.270	0.907	0.713	0.204	0.997	0.566	0.790	0.995	0.923	0.350
unclassified Zixibacteria	1.000	1.000	1.000	1.000	0.640	0.433	1.000	0.563	0.371	0.563	0.371	0.997	1.000	0.563	0.371
Hoeflea	0.458	0.013	0.095	0.458	0.907	0.500	0.013	0.033	0.014	0.916	1.000	0.942	1.000	0.916	1.000
Unclassified Proteobacteria	1.000	0.000	0.000	1.000	1.000	1.000	0.000	0.000	0.000	1.000	1.000	1.000	1.000	1.000	1.000
Gammaproteobacteria B2M28	1.000	1.000	1.000	0.737	0.952	0.997	0.735	0.951	0.997	0.991	0.919	0.998	0.794	0.974	0.999
Acidithiobacillus	0.978	1.000	0.989	0.558	0.486	0.493	0.844	0.776	0.783	1.000	1.000	1.000	0.884	0.822	0.829
Bacteroidetes_BD2-2	0.999	0.992	1.000	0.700	1.000	0.978	0.607	1.000	0.944	0.607	0.962	0.944	0.864	0.992	0.999
Unclassified *Flavobacteriaceae*	0.977	0.985	1.000	0.561	0.032	0.088	0.591	0.034	0.094	0.209	0.559	0.918	0.887	0.066	0.188
Unclassified *Prolixibacteraceae*	1.000	1.000	1.000	0.996	0.590	0.885	0.996	0.590	0.885	0.815	0.987	0.985	0.996	0.590	0.885
Thiobacillus	0.965	0.996	0.809	0.171	0.342	0.950	0.611	0.902	0.998	0.984	0.422	0.729	0.393	0.692	1.000
Unclassified *Halieaceae*	0.873	0.939	1.000	0.106	0.248	0.212	0.133	0.310	0.266	0.965	0.985	1.000	0.352	0.704	0.633
Unclassified *Microscillaceae*	1.000	1.000	1.000	0.680	1.000	0.990	0.602	1.000	0.971	0.560	0.927	0.956	0.560	1.000	0.956
Psychromonas	0.931	0.873	1.000	0.956	0.417	0.115	0.908	0.347	0.095	0.808	0.283	0.835	1.000	0.851	0.315
Sulfurovum	0.999	0.925	0.991	0.993	0.951	0.228	0.872	0.734	0.122	0.999	0.401	0.538	1.000	0.996	0.342

Gammaproteobacteria_Incertae_Sedis	1.000	1.000	1.000	0.036	0.870	0.993	0.032	0.821	0.984	0.118	0.063	0.989	0.029	0.772	0.969
Nitrosomonadaceae	1.000	1.000	1.000	0.637	0.973	1.000	0.637	0.973	1.000	0.942	0.768	0.996	0.637	0.973	1.000
Acholeplasma	0.773	0.562	0.997	0.997	0.997	0.999	1.000	1.000	1.000	1.000	1.000	1.000	0.562	0.562	0.605
Desulfocurvus	1.000	0.629	0.677	0.677	0.677	0.677	1.000	1.000	1.000	1.000	1.000	1.000	0.629	0.629	0.629
Unclassified *Nostocaceae*	0.999	0.792	0.912	0.999	0.501	0.784	0.793	0.179	0.333	0.649	0.906	0.990	1.000	0.650	0.907
Flavobacterium	0.842	0.914	1.000	1.000	0.607	0.302	1.000	0.706	0.371	0.692	0.361	0.974	0.906	0.995	0.827
Unclassified Babeliales	0.422	0.120	0.845	0.845	0.845	0.845	1.000	1.000	1.000	1.000	1.000	1.000	0.120	0.120	0.120
Gammaproteobacteria|CCM19a	1.000	1.000	1.000	0.559	1.000	1.000	0.559	1.000	1.000	0.559	0.703	1.000	0.559	1.000	1.000
Lentimonas	0.967	0.838	0.997	1.000	0.833	0.928	1.000	0.627	0.759	0.728	0.848	1.000	0.912	0.997	1.000
Unclassified *Marinilabiliaceae*	0.258	1.000	0.306	0.811	0.258	0.446	0.862	1.000	0.999	0.794	0.968	0.993	0.794	1.000	0.993
Arenimonas	0.691	0.992	0.431	0.463	0.431	0.605	1.000	1.000	0.999	1.000	1.000	0.999	0.996	0.992	1.000
Unclassified Acidobacteria	1.000	1.000	1.000	0.653	1.000	1.000	0.564	1.000	0.999	0.564	0.749	0.999	0.564	1.000	0.999
Unclassified *Anaerolineaceae*	1.000	1.000	1.000	0.560	1.000	0.912	0.560	1.000	0.912	0.560	0.966	0.912	0.560	1.000	0.912
PHOS-HE36 (Ignavibacteriales)	0.999	1.000	0.999	0.883	0.984	1.000	0.731	0.913	0.992	0.997	0.944	0.997	0.731	0.913	0.992
Woeseia	1.000	1.000	1.000	0.679	0.309	1.000	0.567	0.243	0.998	0.951	0.771	0.376	0.567	0.243	0.998
Unclassified Bradymonadales	0.997	0.981	1.000	0.613	1.000	0.809	0.502	1.000	0.699	0.502	0.998	0.699	0.827	0.981	0.957
GIF9 Dehalococcoidia	1.000	1.000	1.000	0.683	0.295	0.274	0.568	0.230	0.214	0.938	0.919	1.000	0.568	0.230	0.214
Desulfobacterium	0.784	0.784	1.000	0.470	1.000	0.271	0.470	1.000	0.271	0.470	0.993	0.271	0.984	0.784	0.840
Unclassified *Saprospiraceae*	0.998	0.975	1.000	0.252	0.145	0.435	0.183	0.106	0.324	0.995	0.993	0.899	0.393	0.231	0.635
Unclassified *Cyclobacteriaceae*	1.000	0.983	0.993	0.163	0.900	0.860	0.091	0.667	0.612	0.478	0.529	1.000	0.186	0.937	0.905
Unclassified *Rhodobacteraceae*	0.972	0.972	1.000	0.135	0.725	0.877	0.135	0.725	0.877	0.591	0.432	0.999	0.301	0.978	0.999
Unclassified *Arenicellaceae*	0.999	1.000	0.999	0.130	0.999	0.930	0.089	1.000	0.802	0.089	0.354	0.802	0.089	1.000	0.802
Ulvibacter	1.000	1.000	1.000	0.334	1.000	0.992	0.334	1.000	0.992	0.334	0.569	0.992	0.334	1.000	0.992
Colwellia	1.000	1.000	1.000	0.604	0.863	0.998	0.604	0.863	0.998	0.992	0.811	0.976	0.604	0.863	0.998
AKYH767 (Sphingobacteriales)	1.000	1.000	1.000	0.254	1.000	0.999	0.254	1.000	0.999	0.254	0.369	0.999	0.254	1.000	0.999
Methylobacter	1.000	1.000	1.000	0.560	1.000	1.000	0.560	1.000	1.000	0.560	0.608	1.000	0.560	1.000	1.000
Acidocella	1.000	0.999	1.000	0.692	1.000	1.000	0.735	0.999	0.999	0.580	0.582	1.000	0.580	1.000	1.000
Nitrospira	1.000	0.160	0.211	0.804	1.000	1.000	0.712	0.160	0.225	0.682	0.830	0.999	0.682	1.000	0.999
Hyphomonas	1.000	0.000	0.000	1.000	1.000	0.012	0.000	0.000	0.000	1.000	0.012	0.012	1.000	1.000	0.012

Ignavibacterium	1.000	1.000	1.000	0.560	1.000	0.999	0.560	1.000	0.999	0.560	0.712	0.999	0.560	1.000	0.999
Unclassified *Lentimicrobiaceae*	0.001	0.000	0.189	0.189	0.189	0.002	1.000	1.000	0.000	1.000	0.000	0.000	0.000	0.000	0.450
Sva1033 (Desulfuromonadales)	1.000	1.000	1.000	0.560	1.000	1.000	0.560	1.000	1.000	0.560	0.649	1.000	0.560	1.000	1.000
Sulfuricurvum	1.000	0.109	0.109	1.000	0.621	1.000	0.109	0.598	0.110	0.621	1.000	0.627	1.000	0.621	1.000
Unclassified *Gemmatimonadaceae*	1.000	1.000	1.000	0.560	1.000	0.979	0.560	1.000	0.979	0.560	0.881	0.979	0.560	1.000	0.979
Pseudoalteromonas	1.000	0.000	0.000	1.000	1.000	1.000	0.000	0.000	0.000	1.000	1.000	1.000	1.000	1.000	1.000
Unclassified *Sandaracinaceae*	1.000	1.000	1.000	0.560	1.000	0.996	0.560	1.000	0.996	0.560	0.789	0.996	0.560	1.000	0.996
Unclassified Betaproteobacteriales	1.000	0.001	0.001	1.000	1.000	1.000	0.001	0.001	0.001	1.000	1.000	1.000	1.000	1.000	1.000
Spirochaeta_2	0.907	0.828	1.000	1.000	0.918	0.529	1.000	0.843	0.435	0.918	0.529	0.948	0.907	1.000	0.956
Unclassified *Steroidobacteraceae*	0.993	1.000	0.993	0.999	0.900	0.999	0.951	0.666	0.937	0.976	1.000	0.984	0.951	0.666	0.937
Latescibacteria	0.998	0.981	1.000	1.000	0.774	0.399	1.000	0.639	0.301	0.639	0.301	0.962	0.981	0.929	0.579
Pseudorhodobacter	0.989	1.000	0.989	0.998	0.852	0.893	1.000	0.569	0.622	0.657	0.712	1.000	1.000	0.569	0.622
Unclassified *Crocinitomicaceae*	1.000	1.000	1.000	0.569	0.000	0.014	0.569	0.000	0.014	0.000	0.077	0.003	0.569	0.000	0.014
Algoriphagus	1.000	1.000	1.000	1.000	0.730	0.816	1.000	0.584	0.676	0.729	0.816	1.000	1.000	0.584	0.676
Sediminispirochaeta	0.980	0.980	1.000	1.000	0.628	0.840	1.000	0.628	0.840	0.656	0.863	0.997	0.986	0.925	0.995
TRA3-20 (Betaproteobacteriales)	1.000	1.000	1.000	0.986	0.615	1.000	0.986	0.615	1.000	0.897	0.997	0.697	0.986	0.615	1.000
Granulicella	1.000	1.000	1.000	1.000	0.560	1.000	1.000	0.560	1.000	0.589	1.000	0.560	1.000	0.560	1.000
Thioprofundum	1.000	1.000	1.000	1.000	0.567	1.000	1.000	0.567	1.000	0.686	1.000	0.567	1.000	0.567	1.000
Ilumatobacter	0.885	0.795	1.000	0.918	1.000	0.912	0.838	1.000	0.831	0.838	1.000	0.831	1.000	0.795	1.000
Unclassified *Ruminococcaceae*	1.000	1.000	1.000	1.000	0.563	0.606	1.000	0.563	0.606	0.594	0.637	1.000	1.000	0.563	0.606
Desulfobacteraceae	1.000	1.000	1.000	0.939	0.873	1.000	0.903	0.822	0.998	1.000	0.985	0.952	0.864	0.773	0.995
Filomicrobium	1.000	0.966	0.966	1.000	0.655	1.000	0.992	0.960	0.974	0.765	1.000	0.679	1.000	0.655	1.000
Lewinella	1.000	1.000	1.000	1.000	0.560	0.838	1.000	0.560	0.838	0.560	0.838	0.990	1.000	0.560	0.838
Roseibacillus	0.977	0.977	1.000	1.000	0.633	0.970	1.000	0.633	0.970	0.662	0.978	0.946	0.984	0.933	1.000
Bacteria	1.000	1.000	1.000	1.000	0.559	0.991	1.000	0.559	0.991	0.559	0.991	0.829	1.000	0.559	0.991
SB-5 (Bacteroidales)	0.998	0.978	1.000	1.000	0.782	1.000	1.000	0.643	0.999	0.671	0.999	0.818	0.985	0.936	0.999
Pseudohongiella	1.000	1.000	1.000	1.000	0.568	0.999	1.000	0.568	0.999	0.691	1.000	0.738	1.000	0.568	0.999

Unclassified *Gemmataceae*	1.000	1.000	1.000	1.000	0.560	1.000	1.000	0.560	1.000	0.560	1.000	0.653	1.000	0.560	1.000
NS11-12_marine_group (Sphingobacteriales)	1.000	1.000	1.000	1.000	0.559	1.000	1.000	0.559	1.000	0.559	1.000	0.637	1.000	0.559	1.000
Desulfurivibrio	1.000	0.842	0.842	1.000	0.782	1.000	0.842	1.000	0.842	0.782	1.000	0.782	1.000	0.782	1.000

CHAPTER III

Efficient, robust, and fast DNA extraction method from compacted bentonite: New insights for deep geological repository concept

Fadwa Jroundi[1], Cristina Povedano-Priego[1], Margarita Lopez-Fernandez[2, 3], Mark Dopson[2], Mohamed L. Merroun[1]

[1]Department of Microbiology, Faculty of Science, University of Granada, Granada, Spain. fadwa@ugr.es, ppriego@correo.ugr.es, merroun@ugr.es

[2]Centre for Ecology and Evolution in Microbial Model Systems (EEMiS), Linnaeus University, Kalmar, Sweden. margarita.lopezfernandez@lnu.se, mark.dopson@lnu.se

[3]Current address: Institute of Resource Ecology, Helmholtz-Zentrum Dresden-Rossendorf, Bautzner Landstraße 400, 01328 Dresden, Germany. m.lopez-fernandez@hzdr.de

1. ABSTRACT

Compacted bentonites have been selected as one of the best materials for sealing and backfilling clay in Deep Geological Repositories. However, they are highly challenging systems to nucleic acid extractions due to that cells and debris are strongly adsorbed to smectite and other particles. In addition, the high cation content in bentonites (e.g. Mg, Fe) reduces the efficiency of conventional DNA extraction methods. Here, we provide an optimized protocol that facilitates the extraction of higher DNA-yields from compacted bentonite. Based on the phenol:chloroform technique and combined with previous mechanical and chemical lyses, our protocol provides sufficient DNA (2-6 ng/μL) from Spanish compacted bentonite to perform Next Generation Sequencing and obtain valid microbial diversity data. Moreover, based on recovery efficiency in terms of yield DNA and requiring only eight hours, this protocol can be considered as the most effective for compacted bentonite in comparison to other non-commercial kit-based methods.

2. INTRODUCTION

2.1. Background and applications

Deep geological repositories (DGRs) are one of the internationally accepted long-term solutions for disposal of high level radioactive wastes (Alexander and McKinley, 2011; Lopez-Fernandez et al., 2018). Many countries including Spain, Finland, Canada, Sweden, and United States are studying these DGRs (Briggs et al., 2017). One option is to place the nuclear wastes within metallic containers resistant to corrosion that is surrounded by a compacted bentonite clay buffer to create an engineered system located approximately 400-500 m underground within a low permeability host rock (e.g.: clays or crystalline rock) that serves as a natural barrier (Briggs et al., 2017; Pedersen, 1999). Bentonites are swelling clays with high sorption capacity resulting in a very low hydraulic conductivity (Perdrial et al., 2009) making them the best candidate for the backfill or sealing material in the engineered barrier for a high-level nuclear waste repository (Lopez-Fernandez et al., 2015). This multi-barrier system is expected to maintain its integrity for at least 100,000 years (Anderson et al., 2011) making its safe design a critical challenge.

Besides the physical and chemical challenges of such a long-term DGR, biogeochemical activity of indigenous and introduced microorganisms might compromise the repository's safety (Lopez-Fernandez et al., 2018; Meleshyn, 2011). First, the metallic containers can be corroded, cracked, or affected by microbial activities (Bengtsson and Pedersen, 2017) while secondly, the bentonite clay geochemistry can be influenced by the introduced microorganisms during the repository construction and operation (Liu et al., 2017). Therefore, assessment of microbial communities in such geological material is vital for future radioactive waste management all over the world (Stroes-Gascoyne et al., 2010).

Compacted bentonites are characterized by the creation of very harsh conditions. The amount of free water is very low and the swelling pressure is very high ranging between 7 to 8 MPa at full water saturation (Ratto and Itavaara, 2012). In addition, the average pore diameter of compacted bentonite is in the range of approximately 0.005-0.1 µm, with 0.02 µm as the most frequently measured pore size (Stroes-Gascoyne et al., 2011). Despite the challenging conditions created for microbial growth, an

assessment of microbial activities is essential for safety assessments of the DGR concept.

DNA extraction from bentonite is the first and most important step to explore the microbiology of such an extreme environment. The challenge is to extract genomic DNA from this material despite its swelling characteristic by controlling the mixture of bentonite with the lysis buffers and the complete release of bacterial cells from the bentonite matrix. In fact, some studies attribute the failure of culture-independent techniques for the identification of bentonite microbiota due to these complexities, and impose culture-based approaches in DGR microbiology (Stone et al., 2016). Instead, only few studies successfully obtained low quantities of DNA from non-compacted bentonite samples (Lopez-Fernandez et al., 2015) and microcosms (Lopez-Fernandez et al., 2018). Nevertheless, compacted bentonites are characterized by a stronger binding capacity than the non-compacted ones, due to their inherent ion exchange properties. The latter are fundamental to the buffers performance and potentially interfere with the nucleic acids extraction because of charge-based complexing (Stone et al., 2016). This imposes several challenges to standard DNA extraction techniques and requires the development and standardization of a DNA extraction protocol that produces high-quality community DNA that is free from inhibitors and able to be amplified by PCR. Thus, here we provide an optimized protocol that allows the extraction of high DNA yields from compacted bentonites to perform Next Generation Sequencing (NGS). In addition, this protocol may be adapted to extract genomic DNA from low-biomass environmental samples such as aquatic samples or marine sediments.

2.2. Comparison with other methods

Several commercial DNA extraction kits such as the DNeasy PowerSoil Kit (Qiagen), FastDNA™ SPIN kit for soil (MP Biomedicals), and HigherPurity™ Soil DNA isolation kit (Canvax) were employed in our laboratory to extract DNA from compacted bentonite samples with no success. Thus, in this protocol we have included several key modifications in sample pre-treatment, mechanical and chemical lyses, and DNA extraction procedures. We show that such modifications and optimizations have greatly improved the DNA extraction efficiency from compacted bentonite samples. By using this protocol, sufficient genomic DNA (few to tens ng) is extracted from

compacted bentonite for high-throughput sequencing. As an example, we recently used this protocol to study the bacterial communities of Spanish bentonite, where genomic DNA was extracted from aerobically treated microcosms for 16S rRNA gene sequencing. The purpose was to characterize the structure and composition of these bentonite bacterial communities and we succeeded in identifying almost 1,500 bacterial operational taxonomic units (Povedano-Priego et al., 2019).

Several steps including cell detachment from clay particles, cell lysis, DNA precipitation, and DNA purification are required for a successful DNA extraction from environmental samples. Cell lysis plays an important role and can be performed using different treatments (Gupta et al., 2017) with bead beating being widely used for both lysis and breaking soil aggregates (Lombard et al., 2011; Shehadul Islam et al., 2017). In this study, better extraction efficiency was obtained using a sodium phosphate buffer, vortexing, and a mechanical treatment for separating the cells from the clay particles. In addition, physical cell lysis was combined with enzymatic lysis to obtain higher DNA efficiency. Enzymatic lysis was implemented by using proteinase K (20 mg/mL) and lysozyme (10 mg/mL) while the mechanical lysis was achieved by bead beating using FastPrep. After cell lysis, the released DNA may strongly interact with bentonite particles. Therefore, a Na_2HPO_4 buffer was employed for DNA desorption from the bentonite particles, which is affected by monovalent cations such as Na^+ and its use is commonly required for an effective DNA extraction from soil (Lombard et al., 2011).

Here, we describe a fast, economical, and reproducible protocol to obtain high-quality microbial community DNA from low-biomass systems, especially compacted bentonite. The method consistently permits the isolation of DNA of satisfactory size and quality for high-throughput sequencing analyses and is based on introducing several modifications to the well-known phenol-chloroform extraction method. The protocol outlines the steps for bentonite compaction, sample pre-treatment for cell separation from clay particles, DNA extraction from the compacted bentonite, quantification and quality assessment of extracted genomic DNA, and validation of the protocol by Illumina amplification and sequencing.

3. EXPERIMENTAL DESIGN

Non-compacted bentonite, collected in aseptic conditions from Cabo de Gata, Almeria, Spain, is compacted at a dry density of 1.5 g/cm^3 (Fig. 1) at "Centro de Investigaciones Energéticas, Medioambientales y Tecnológicas" (CIEMAT, Madrid). For the compaction procedure, non-compacted bentonite is weighted and placed in a cylindrical-steel mold followed by a hydraulic press (Fig. 2).

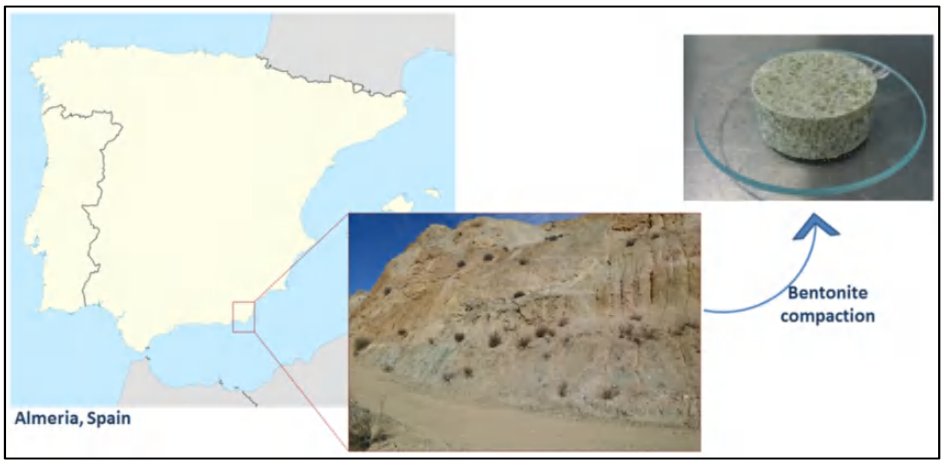

Figure 1. Geographical location of the clay sampling site in Almeria (South-East Spain) and a photograph of the compacted bentonite at a dry density of 1.5 g/cm^3 (30 mm of diameter and 12.1 mm of height).

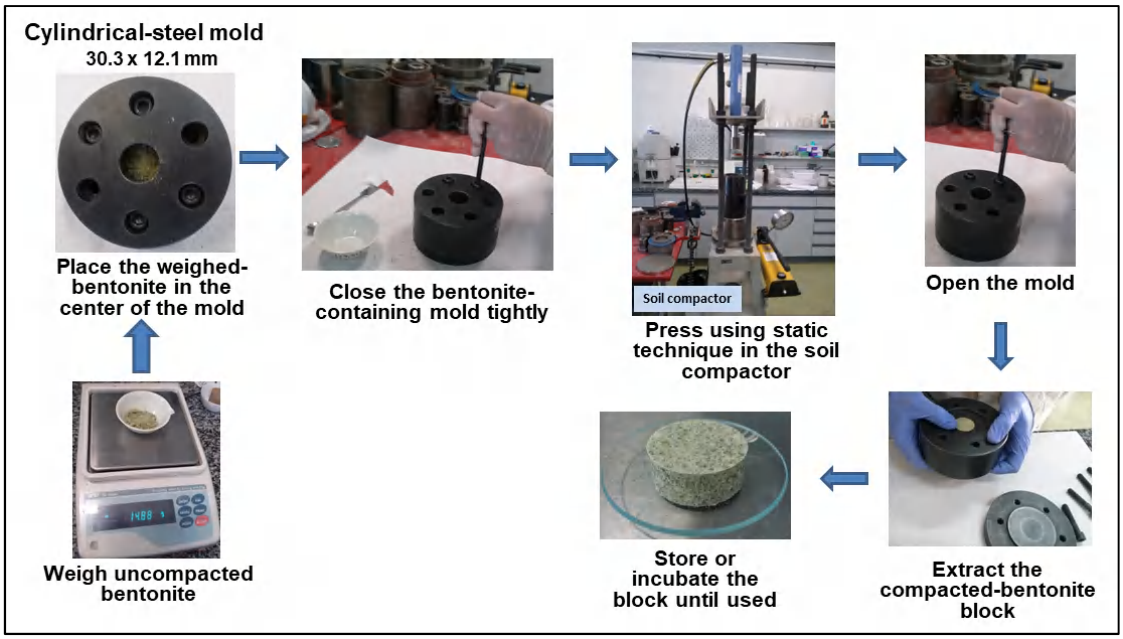

Figure 2. Bentonite compaction workflow.

Sample pre-treatment (Steps 1-3). This protocol begins with a pre-treatment of the samples after the compaction of bentonite and an incubation period. The blocks are broken in small fragments using an aseptic mortar and ground until a mixture of homogeneous powder is obtained (Fig. 3). This step is critical due to the impermeable nature of bentonites that limits the penetration of solutions into the whole clay matrix. However, for slurry samples, marine sediments, or water samples collected on filters, this step can be omitted.

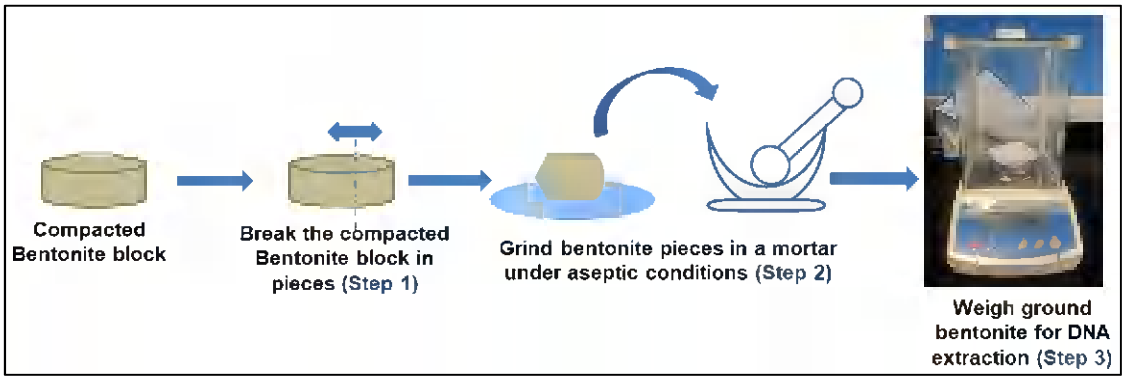

Figure 3. Sample pre-treatment workflow (Steps 1-3).

Mechanical and chemical lyses (Steps 4-16). A sterilized glass bead (size 3-5 mm) and 0.25 g of 0.3 mm diameter sterilized glass beads are added to a sterile 2 mL screw-cap microcentrifuge tube (SampleBead tube). Then, 0.3 g of ground compacted bentonite are added to each SampleBead tube (Fig. 4) and resuspended in 400 µL of Na_2HPO_4 (0.12 M pH 8.0) prior to mixing. We recommend vortexing at maximum speed during 1-2 min. The addition of Na_2HPO_4 buffer is an optimized step. In bentonite samples, DNA strongly interacts with the clay particles and Na_2HPO_4 is used to allow DNA desorption and thus, to improve the yield of extracted DNA but this step can be omitted with other types of samples. Afterwards, chemical lysis is achieved by adding 600 µL of lysis buffer (100 mM Tris-HCl [pH 8.0]; 100 mM EDTA [pH 8.0]; 100 mM NaCl; 1% polyvinylpyrrolidone [PVP]; and 2% SDS), 10 mg/mL freshly made lysozyme, and 20 mg/mL proteinase K. Lysozyme participates in the bacterial cell wall breakdown and proteinase K contributes to the degradation of proteins and nucleases that could affect the DNA molecules. Mechanical lysis of the cells is performed twice using a FastPrep® FP120 at a speed of 5.5 $m \cdot s^{-1}$ for 45 s. Between each Fastprep step, we recommend placing the tubes on ice for the 5 min pause recommended by the

manufacturer (MP Biomedicals). Afterwards, samples are incubated at 37 ºC for 30 min and at 60 ºC for 45 min. Supernatants are collected after centrifugation at 14,000 × *g* for 5 min at room temperature and transferred into 15 mL sterile tubes containing 1.5 g of vacuum grease previously prepared or ordered by the user such as MaXtract High Density Tubes (Qiagen). To ensure the collection of all DNA liberated from the cells, it is very useful to perform a second cycle of FastPrep after adding 1 mL of lysis buffer to the 2 mL SampleBead tube. This additional step allows the collection of the possible DNA molecules that could be still trapped in the bentonite sample. Supernatants from the second centrifugation are mixed with those obtained at the first FastPrep cycle (Fig. 4).

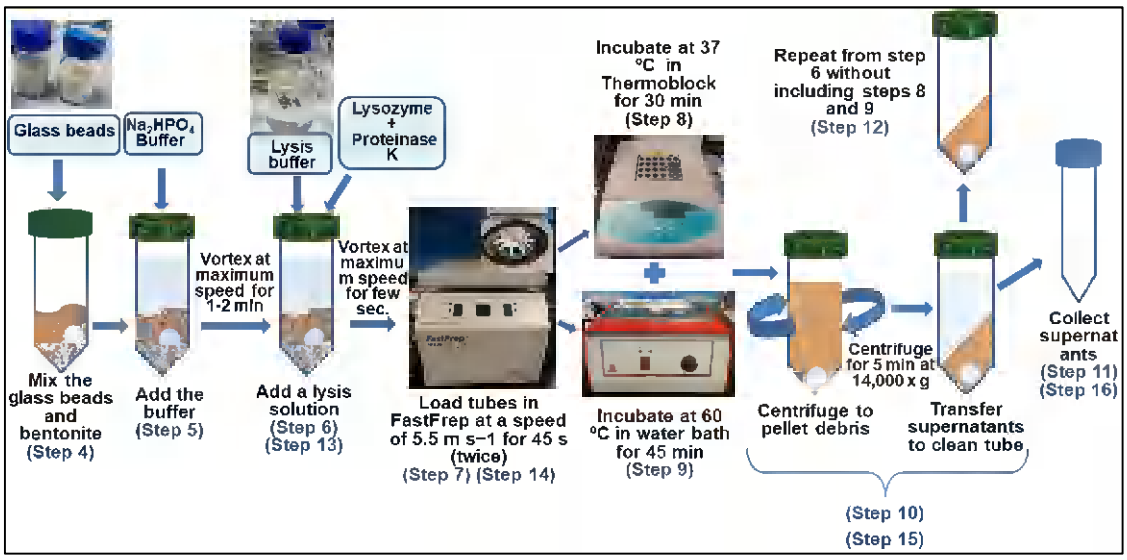

Figure 4. Mechanical and chemical lysis workflow (Steps 4-16).

DNA extraction and purification (Steps 17-28): supernatants are transferred to a previously prepared Phase Lock tube as shown in Fig. 5 and one volume of phenol:chloroform:isoamyl alcohol (PCI, 25:24:1, pH 8.0) is added and mixed thoroughly by gently inverting. Then, samples are centrifuged for 10 min at 1500 × *g* at 4 ºC and the aqueous phase is washed by adding another equal volume of phenol:chloroform (PC, 1:1, pH 8.0) and centrifuged as before. Sometimes, the resulting DNA could be contaminated by phenol residues coming from the previous steps. To avoid phenol contamination, we recommend including an additional washing step that consists of adding an equal volume of chloroform in the tubes and centrifuging

them under the same conditions. All the above steps should be performed in a fume hood cabinet and wearing safety gloves, goggles, and laboratory coat.

After centrifugation, supernatants are transferred to new 15 mL tubes and DNA is precipitated by adding one volume of ice-cold isopropanol and 0.1 volume of 3 M sodium acetate (pH 5.2) prior incubation for 1 h 30 min at -80 ºC. The protocol can be paused here, and the tubes stored overnight at -20 ºC. However, we observed lower efficiency in collecting clean and high-quality DNA after overnight incubation. The genomic DNA is then pelleted by centrifugation at 5000 × *g* for 30 min at 4 ºC and the resulting pellets are washed with 1 mL 80% cold ethanol followed by centrifugation at 10,000 × *g* for 5 min at 4 ºC. The ethanol should be carefully aspirated to avoid disturbing the pellet and then, dried at 37 ºC until all ethanol is evaporated. This step ensures that no ethanol is carried over during the DNA elution, which might interfere with the elution reaction. Total DNA is resuspended in 35 µL Tris (5 nM, pH 8.5)-TE buffer (10 mM Tris-HCl [pH 8.0] and 1 mM EDTA) or nuclease-free water. We highly recommend pre-warming the solution to approximately 60 ºC. This temperature facilitates the resuspension of the dried DNA pellet. The extracted genomic DNA is stored at -20 °C until further processing. Triplicate extractions from each sample should be performed to examine possible variations on the results.

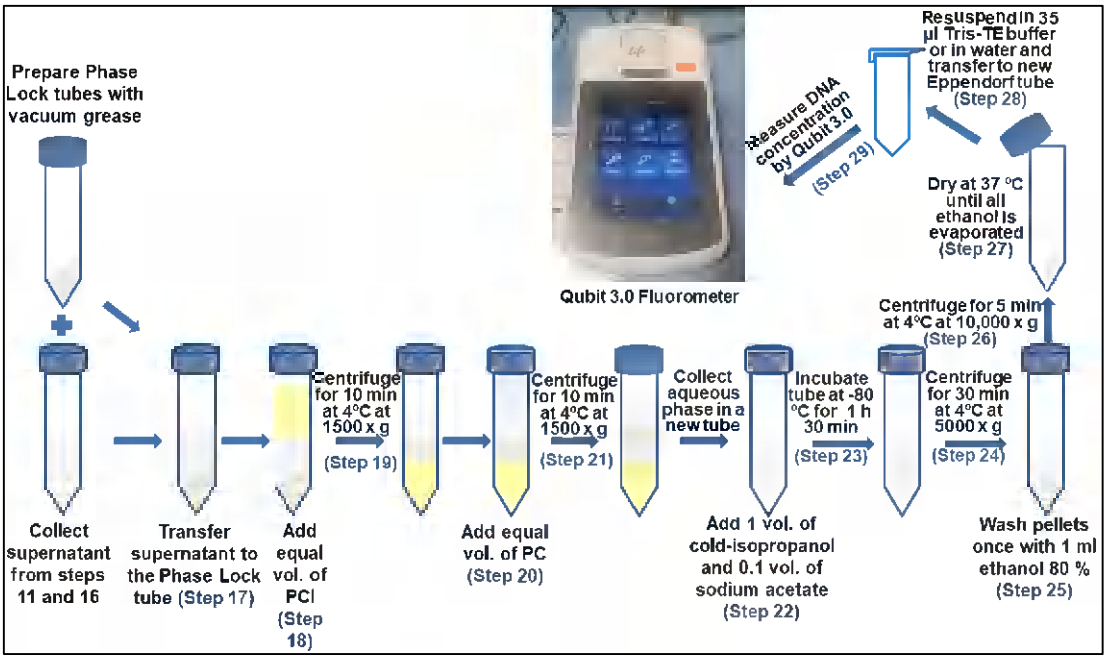

Figure 5. DNA extraction, purification, and quantification workflow (Steps 17-29).

Quantification and quality assessment of extracted genomic DNA (Steps 29-30): The extracted genomic DNA should be checked for concentration and quality before further analyses. The concentration of the extracted metagenomic DNA of such environmental samples is usually below the detection limit of common DNA quantification instruments such as the NanoDrop Spectrophotometer (Thermo Scientific). Therefore, we recommend using a fluorescent double-stranded DNA (dsDNA)-binding dye assay on the Qubit Fluorometer (Life Technologies). This instrument enables sensitive quantification of small amounts dsDNA in solution with a detection limit of 10-100 pg/µL. Moreover, in some cases low concentrations of DNA do not allow visualization on a normal agarose gel. Quality of the extracted DNA can be checked with a NanoDrop spectrophotometer expecting an A260/A280 ratio of ~1.8 for highly pure DNA.

3.1. Controls

When designing an experiment, it is crucial to consider suitable controls. Therefore, negative controls must be included, such as DNA extraction of the reagents used with no added bentonite sample. Accordingly, it is possible to assess possible DNA contamination introduced during the extraction procedure.

4. MATERIALS

4.1. Sample

- Compacted bentonite (Spanish bentonite collected from Cabo de Gata, Almeria, Spain or any type of compacted bentonite).

4.2. Reagents

- Glass beads (size 0.5 mm, e.g. Sigma-Aldrich, cat. no. Z250465 and size ~5 mm, Sigma-Aldrich, cat. no. 18406)
- Na_2HPO_4 (0.12 M, pH 8.0; Sigma-Aldrich, cat. no. S7907)

- EDTA (100 mM [pH 8.0]; Amresco, cat. no. 0322)
- NaOH (5N; Scharlab, cat. no. SO04200500)
- NaCl (100 mM; Scharlau, cat. no. SO02241000)
- Polyvinylpyrrolidone [PVP] (1% wt/vol; Sigma-Aldrich, cat. no. P5288)
- SDS (2% wt/vol; Sigma-Aldrich, cat. no. L6026)
- Tris-HCl (100 mM, pH 8.0; Amresco, cat. no. 0497)
- Phenol:chloroform:isoamyl alcohol (25:24:1, pH 8.0, Acros Organics, cat. no. 327115000)
    - Caution: This reagent is hazardous if ingested, inhaled or if it comes into contact with the skin or eyes. Wear safety goggles, gloves, and a laboratory coat when handling this reagent and work in a fume hood.
- Phenol (pH 8.0; Amresco, cat. no. 0945)
    - Caution: This reagent is hazardous if ingested, inhaled or if it comes into contact with the skin or eyes. Wear safety goggles, gloves, and a laboratory coat when handling this reagent and work in a fume hood.
- Chloroform (Carlo Erba, cat. no. 438601)
    - Caution: Chloroform is hazardous if ingested or inhaled. Causes serious skin and eyes irritations. Wear safety goggles, protective gloves, and a laboratory coat when handling this reagent and work in a fume hood.
- Proteinase K (20 mg mL^{-1}; US Biological, cat. no. P9100)
    - Critical: Proteinase K must be added just before each use. Shake gently as mixing too vigorously produces foam.
- Lysozyme (10 mg mL^{-1}; Sigma-Aldrich, cat. no. L6876)
- Isopropanol (Scharlau, cat. no. AL03121000)
    - Caution: Both the liquid and the vapor forms of isopropanol are flammable. This reagent is hazardous if ingested, inhaled, or if it comes in contact with skin and eyes. Wear safety glasses, protective gloves, and a laboratory coat when handling this reagent and work in a fume hood.
- Sodium acetate (3 M, pH 5.2; VWR Chemicals, cat. no. 443894K)

- Absolute ethanol (J.T. Baker, cat. no. 8025)
    - Caution: This reagent is highly flammable. Use it with caution and away from flame and store it in a fireproof cabinet.
- Qubit dsDNA high-sensitivity (HS) assay kit (Life Technologies, cat. no. Q32854)
    - Caution: This kit should be treated as a potential mutagen since it contains dyes that bind nucleic acid. Some of the reagents contain dimethyl sulfoxide (DMSO). Be careful using the kit.
- Acetic acid glacial (Scharlau, cat. no. AC03442500).
    - Caution: This reagent is hazardous if ingested, inhaled, or if it comes in contact with skin and eyes. Wear safety glasses, protective gloves, and a laboratory coat when handling this reagent and work in a fume hood.
- Hydrochloric acid (Scharlau, cat. no. AC07411000).
    - Caution: This reagent is corrosive to metals and hazardous if ingested, inhaled, or if it comes in contact with skin and eyes. Wear safety glasses, protective gloves, and a laboratory coat when handling this reagent and work in a fume hood.

4.3. Equipment

- Precision balance (e.g., Alkali Scientific Inc., cat. no. W3200).
- Biosafety cabinet (e.g., Biosafety Cabinet Bio II A, Telstar, cat. no. 20741107600).
- Fume Hood (e.g., Basic Laboratory Fume Hoods, Labconco, cat. no. 3646-00)
- Autoclave (e.g., Presoclave II, SELECTA, cat. no. 4002136)
- FastPrep® FP120 Cell Disrupter (e.g. MP Biomedicals FastPrep -24™ Instrument, cat. no. MP116004500).
- Refrigerated centrifuge with rotor and adapters for 15/50 mL tubes (e.g., Centrifuge 5804 R; Eppendorf, cat. no. 5805000327).

- Microcentrifuge (e.g., Centrifuge 5424; Eppendorf, cat. no. 5424000010).
- Water thermostatic bath (e.g., Bunsen, cat. no. 1611).
- pH meter (e.g., pHmeter Basic 20, Crison/Hach, cat. no. LPV2000.98.0002).
- Refrigerator, 4 °C (e.g., Isotemp general-purpose series laboratory refrigerators; Fisher Scientific, cat. no. 11670236).
- Ultra-low-temperature freezer (e.g., Ultra Low Freezer, Upright −86 °C; Thermo Scientific™ Revco™ UxF, cat. no. UXF50086A).
- Qubit 3.0 Fluorometer (Life Technologies, cat. no. Q33216).
- Qubit® assay tubes (Life Technologies, cat. no. Q32856).
- Vortexer ZX3 (e.g., VELP Scientifica, cat. no. VEL F20220176).
- High vacuum grease (Dow Corning, cat. no. Z273554).
- Microcentrifuge tubes (e.g. 2 mL screw-cap microcentrifuge tube, Sigma-Aldrich, cat. no. CLS430917).
- Centrifuge tubes (e.g. 15 mL clean centrifuge tubes, Corning Inc., cat. no. 352196).
- Pipettors (e.g., LABMATE PRO pipettes, 0.5–10, 20–200, 100–1,000 µL and 500-5,000 µL; HTL, cat. nos. 5662, 5665, 5666 and 5668).
- Sterile pipette tips (e.g., HTL. Racks pipette tips, 0.1–10, 2–200, 100–1,000, 500-5,000 µL, cat. nos. 30011, 30201, 31001 and 35001).
- Spectrophotometer (e.g., NanoDrop 2000; Fisher Scientific, cat. no. ND-2000).
- Thermoblock (e.g. AccuBlock™ Digital Dry Baths, Labnet International, Inc., cat. no. D1100).

4.4. Reagent setup

- Ethanol solution for DNA washing, 80% (vol/vol)
    - Dilute absolute ethanol to an 8:10 ratio in MilliQ ultrapure water and store at -20 ºC. This solution can be stored in a closed container for up to 4 weeks before use.

- Isopropanol solution for DNA precipitation
    - Store the solution at – 20 ºC to be cold before use.
- Tris-HCl (1 M; pH 8.0)
    - Add 12.1 g of Tris to 50 mL of MilliQ water and dissolve gently by shaking, adjusting pH to 8.0 with hydrochloric acid. Adjust the volume to 100 mL with MilliQ water. Store at room temperature for one year.
- Tris-HCl (0.18 M; pH 8.0)
    - Add 8.5 g of Tris to 100 mL of MilliQ water and dissolve gently by shaking. Adjust pH to 8.0 with hydrochloric acid. Adjust the volume to 300 mL with MilliQ. Prepare a sufficient volume, autoclave, and store at room temperature maximum for one year.
- EDTA (0.5 M; pH 8.0)
    - Add 21.9 g of EDTA to 60 mL of MilliQ water and dissolve gently by shaking. Adjust pH to 8.0 with sodium hydroxide (5N). Adjust the volume to 150 mL with MilliQ. Autoclave, and store at room temperature for a maximum of six months.
- Sodium hydroxide (5N)
    - Add 20 g of sodium hydroxide to 100 mL of MilliQ water. Dissolve by shaking gently. Store at room temperature for maximum one year.
        - Caution: When dissolved in water, an exothermic reaction is produced and irritates skin, eyes, and mucous. Thus, the use of gloves and goggles are recommended.
- NaCl (0.5 M)
    - Add 5.9 g of NaCl to 100 mL of MilliQ water and dissolve gently by shaking. Adjust the volume to 200 mL with MilliQ water. Prepare a sufficient volume, autoclave, and store at room temperature for maximum one year.
- DNA extraction buffer (100 mM Tris-HCl [pH 8.0]; 100 mM EDTA [pH 8.0]; 100 mM NaCl; 1% polyvinylpyrrolidone [PVP]; and 2% SDS):

- Add 285 ml of 0.18 M Tris-HCl (pH 8.0), 100 ml of 0.5 M EDTA (pH 8.0), 100 mL of 0.5 M NaCl, 10 g of SDS, and 5 g PVP. Mix and bring the volume to 500 mL with MilliQ water. Filter and autoclave the solution. This buffer is stable at room temperature (~20 °C) for one year.

- Phenol:chloroform 1:1
  - Combine 50 ml of phenol (pH 8.0), and 50 mL of chloroform in a brown glass bottle (or a clear bottle covered with foil). Store the solution at 4 °C for up to one month.
    - Caution: When using organic solvent such as phenol or chloroform, work under a fume hood to prevent inhalation of the vapors and take special care wearing protective gloves.
    - Critical: The pH of phenol is very important; to extract DNA phenol pH should be basic (buffered with Tris), an acidic pH degrades DNA and thus it may be entrapped in the wrong organic phase due to improper phase separation. Furthermore, phenol oxidizes by a free radical process, indicated by a pinkish color. Do not use oxidized phenol, as no DNA will be obtained.

- Tris-EDTA (TE) buffer
  - Add 1 mL of 1 M Tris-HCl (pH 8.0) and 0.2 mL of 0.5 EDTA (pH 8.0) to 98.8 mL of MilliQ water. Filter and autoclave the solution. Store the solution in a glass bottle at room temperature for one year.

- Tris (5 mM; pH 8.5)
  - Add 0.3 g of Tris to 100 mL of MilliQ water. Shake gently and adjust the pH to 8.5 using hydrochloric acid. Complete the volume to 500 mL with MilliQ water. Filter and autoclave the solution. Store the solution in a glass bottle at room temperature for one year.

- Tris (5 nM, pH 8.5)-TE buffer
  - Add 1 µL of Tris (5 mM; pH 8.5) to 1 L of Tris-EDTA buffer under sterile conditions. Store the solution in a glass bottle at room temperature for more than one year.

- DNA precipitation salt solution
    - Add 24.6 g of sodium acetate to 60 mL of MilliQ water and dissolve gently by shaking. Adjust pH to 5.2 with acetic acid glacial. Adjust the volume to 100 mL with MilliQ water. Prepare a sufficient volume, autoclave, and store at room temperature for one year.

4.5. Equipment setup

- Phase-Lock tubes preparation
    - Add 20 g of high vacuum grease into 20 mL sterile syringe and autoclave. In a safety cabin/sterile conditions, distribute 1.5 g/tube of grease in clean sterile 15 mL tubes. Centrifuge the tubes at 5000 × *g* for 10 min. Store prepared tubes at room temperature until use.

5. PROCEDURE

5.1. Sample pre-treatment (Steps 1-3). Timing: 15 min

1- Break the compacted bentonite block into pieces with hammer and chisel.

2- Using an ethanol-cleaned mortar and pestle, grind the bentonite pieces under aseptic conditions until a mixture of homogeneous particle size is obtained.

3- Weigh the necessary amount of bentonite for DNA extraction.

5.2. Genomic DNA extraction protocol (Steps 4-28). Timing: 7 h

Mechanical and chemical lyses (Steps 4-16). Timing: 3 h

Steps 4-6 should be carried out in a decontaminated biosafety cabinet.

4- Place one sterilized glass bead (size 3-5 mm) and 0.25 g of 0.3 mm diameter sterilized glass beads together with 0.3 g of compacted and grinded bentonite in a 2 mL screw-cap microcentrifuge tube (SampleBead tube).

TROUBLESHOOTING

5- Add 400 µL of Na_2HPO_4 (0.12 M pH 8.0) into the SampleBead tube, screw the lid on tightly, and vortex at maximum speed for 1-2 min to completely mix the bentonite with the buffer.

6- Add 600 µL of lysis buffer, 24 µL freshly made lysozyme (10 mg/mL) and 2 µL proteinase K (20 mg/mL) to each SampleBead tube and vortex briefly for a few seconds.

7- Place the SampleBead tubes in a FastPrep machine and then perform the bead beating at a speed of 5.5 m s^{-1} for 45 s. Cool the SampleBead tubes for 5 min on ice and then repeat the bead beating at the same conditions.

8- Place the SampleBead tubes in a thermoblock and incubate at 37 ºC for 30 min.

9- Place the SampleBead tubes in a water bath and incubate at 60 ºC for 45 min.

Critical step: Screw the cap of the SampleBead tubes tightly to make sure that the tubes do not dry up when heated in the water bath at 60 °C.

10- Centrifuge the SampleBead tubes at 14,000 × *g* for 5 min at room temperature.

Critical step: The centrifuge speed should not exceed 14,000 × *g* or it may damage the SampleBead tubes and cause the liquid to escape.

11- Transfer the supernatant from each SampleBead tube to a clean 15 mL tube and store at 4 ºC.

12- For SampleBead tubes repeat the procedure from step 6 but without the incubation steps (excluding steps 8 and 9).

13- Add 1 mL of lysis buffer to each SampleBead tube and vortex at maximum speed for few seconds.

TROUBLESHOOTING

14- Load the tubes in a FastPrep and perform the bead beating as in step 7.

15- Centrifuge the SampleBead tubes at 14,000 × *g* for 5 min at room temperature.

16- Collet the supernatants in the tubes from step 11 and discard the SampleBead tubes.

Critical step: Aspirate the supernatant completely from the SampleBead tube including some foam that may be formed at the bottom, but without disturbing the mixture clay debris/beads.

DNA extraction and purification (Steps 17-28). Timing: 4 h

17- Transfer the supernatants to the previously prepared Phase Lock tubes.

Critical step: Prepare the Phase Lock tubes with vacuum grease in advance and use them in this step. The use of these Phase Lock tubes facilitates the complete separation of the organic and aqueous phases and prevents the loss of the aqueous phase where the DNA is located.

18- Add one volume of phenol:chloroform:isoamyl alcohol (PCI, 25:24:1, pH 8.0) to the supernatants. Mix thoroughly by inverting the tubes.

Critical step: This step should be performed in a fume hood and wearing safety goggles, gloves, and a laboratory coat.

19- Centrifuge the tubes at 1500 × *g* for 10 min at 4 ºC.

TROUBLESHOOTING

20- Add one volume of phenol:chloroform (PC, 1:1, pH 8.0) to each tube and mix thoroughly by inverting.

Critical step: This step should be performed in a fume hood and wearing safety goggles, gloves, and a laboratory coat.

TROUBLESHOOTING

21- Centrifuge the tubes at 1500 × *g* for 10 min at 4 ºC.

TROUBLESHOOTING

22- Collect aqueous phase in a new clean tube and add one volume of cold-isopropanol and 0.1 volume of sodium acetate (3 M, pH 5.2). Mix gently by inverting.

Critical step: Collet the aqueous phase completely without any contact with the organic phase entrapped under the grease.

23- Incubate the tubes at -80 ºC for 1 h 30 min.

Pause point: Tubes can be stored overnight at -20 ºC.

24- Centrifuge the tubes at 5000 × *g* for 30 min at 4 ºC and discard the supernatants without disturbing the pellets.

TROUBLESHOOTING

25- Add an aliquot of 1 mL of 80% (vol/vol) cold-ethanol to rinse the pellet and then discard the ethanol by aspiration.

Critical step: Make sure all ethanol is removed and the pellet is not disturbed.

26- Centrifuge the tubes at 10,000 × *g* for 5 min, and then discard the ethanol by aspiration.

Critical step: Make sure all ethanol is removed and pellet not disturbed.

27- Dry the tubes in an electric stove at 37 ºC until ethanol is completely evaporated.

Critical step: Do not over dry the pellets by increasing the temperature, as this can substantially affect the DNA recovery efficiency.

TROUBLESHOOTING

Pause point: Tubes could be placed in an electric stove overnight to ensure the complete ethanol evaporation.

28- Remove the tubes from the stove. Add an aliquot of 35 µL of Tris-TE buffer or DNase free water to each tube and pipette gently to mix. Transfer the DNA sample from the 15 mL tube into a 1.5 mL nuclease-free Eppendorf tube.

Critical step: The use of 35 µL instead of a higher volume of water for elution results in sufficient DNA concentration for downstream analysis and sequencing.

TROUBLESHOOTING

5.3. Quantification and quality assessment of extracted genomic DNA (Steps 29-30). Timing: 20 min

29- Pipette 2 µL of the eluate from each tube and quantify the DNA concentration using a Qubit 3.0 fluorometer with the dsDNA HS assay kit.

TROUBLESHOOTING

30- Quality of the extracted DNA can be checked with a NanoDrop spectrophotometer expecting an A260/A280 ratio of ~1.8 for highly pure DNA.

Pause Point: The extracted genomic DNA can be stored at −20 °C or −80 °C indefinitely until further processing, although repeated freeze-thawing of the sample is not recommended.

6. TIMING

This protocol takes approximately 7.58 h to complete the DNA extraction. Step 23 could make the process longer if the overnight incubation is necessary.

Steps 1-3, sample pretreatment: 15 min

Steps 4-16, mechanical and chemical lysis: 3 h

Steps 17-28, DNA extraction and purification: 4 h

Steps 29-30, quantification and quality assessment of extracted genomic DNA: 20 min

7. TROUBLESHOOTING

Troubleshooting advice can be found in Table 1.

Table 1. Troubleshooting table and recommendations

Step	Problem	Possible reason	Solution
4	None or too little extracted genomic DNA	Insufficient quantity of material	Increase the amount of ground bentonite for DNA extraction. Use more tubes and respect the quantities used in each 2 mL screw-tap tube presented in this protocol
13	DNA concentration is too low	Volume of solutions is too high	Reduce the volume of lysis buffer to 700-800 µL in the second-cycle FastPrep
19, 21	Failure in phase separation	The high vacuum grease in the Phase Lock tubes breaks	Distribute more than 1.5 g/tube in the Phase Lock tubes
20	Pink color in the supernatants	Phenol solution is oxidized	Check the pH of the phenol solutions, which should be basic using the Tris-buffer
24	DNA pellet is contaminated with excessive salt DNA pellet is negligible	The incubation time at -80ºC is exceeded The incubation time at -80 ºC is not enough	Decrease the time of incubation in Step 28 Increase the time of incubation in Step 28
27	DNA degradation	DNA-pellets over dried by increasing the temperature	Extend the time of drying at 37 ºC but do not increase the temperature
28	Difficult pellet resuspension	Pellet may contain contaminant salt	Use Tris-TE buffer pre-warmed to 65 ºC
28	DNA is too diluted	The volume used to resuspend the DNA is too high	Reduce the volume of elution solution from 35 µL to 20-25 µL
29	Reduced DNA recovery efficiency	DNA is bound to bentonite particles	To improve the yield of extracted DNA use more volume of Na_2HPO_4 for DNA desorption from bentonite and vortex for a longer time in Step 10

8. ANTICIPATED RESULTS

This protocol describes the steps to isolate high quality and high-yield DNA from compacted bentonite, as summarized in Figs. 3-5. Using this protocol, we have obtained DNA concentrations ranging between 2 and 6 ng/µL from compacted bentonite samples (Table 2; Fig. 6); a suitable concentration for PCR amplifications and for further sequencing by Illumina platform. Figure 7A shows phylum-level bacterial diversity in compacted bentonite using this DNA extraction protocol. As expected, high bacterial diversity was obtained for all treated compacted bentonite samples. Triplicate extractions from each sample were performed to examine possible variations in the results of DNA obtained. As expected, similar ranges of DNA concentrations were obtained for each sample (see Fig. 6 for compacted bentonite samples). Moreover, this protocol was used in our previous study of the bacterial diversity in aerobic microcosms using Spanish bentonite in presence of uranium and glycerol-2-phosphate (Povedano-Priego et al., 2019). The DNA extraction was successful, and the analysis of bacterial community could be performed. Figure 7B shows an example of the high bacterial diversity obtained by NGS using Illumina platform for non-compacted bentonite incubated as microcosms with different treatments.

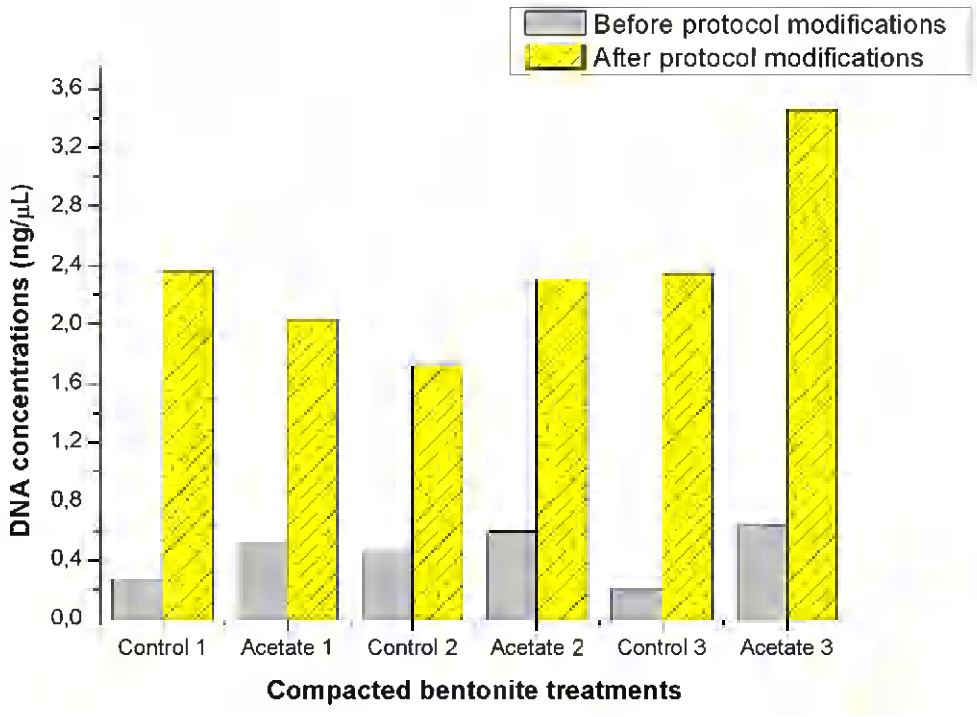

Figure 6. DNA concentrations (ng/µL) of control and acetate-treated compacted bentonite at 1.5 g/cm^3 after six months of incubation.

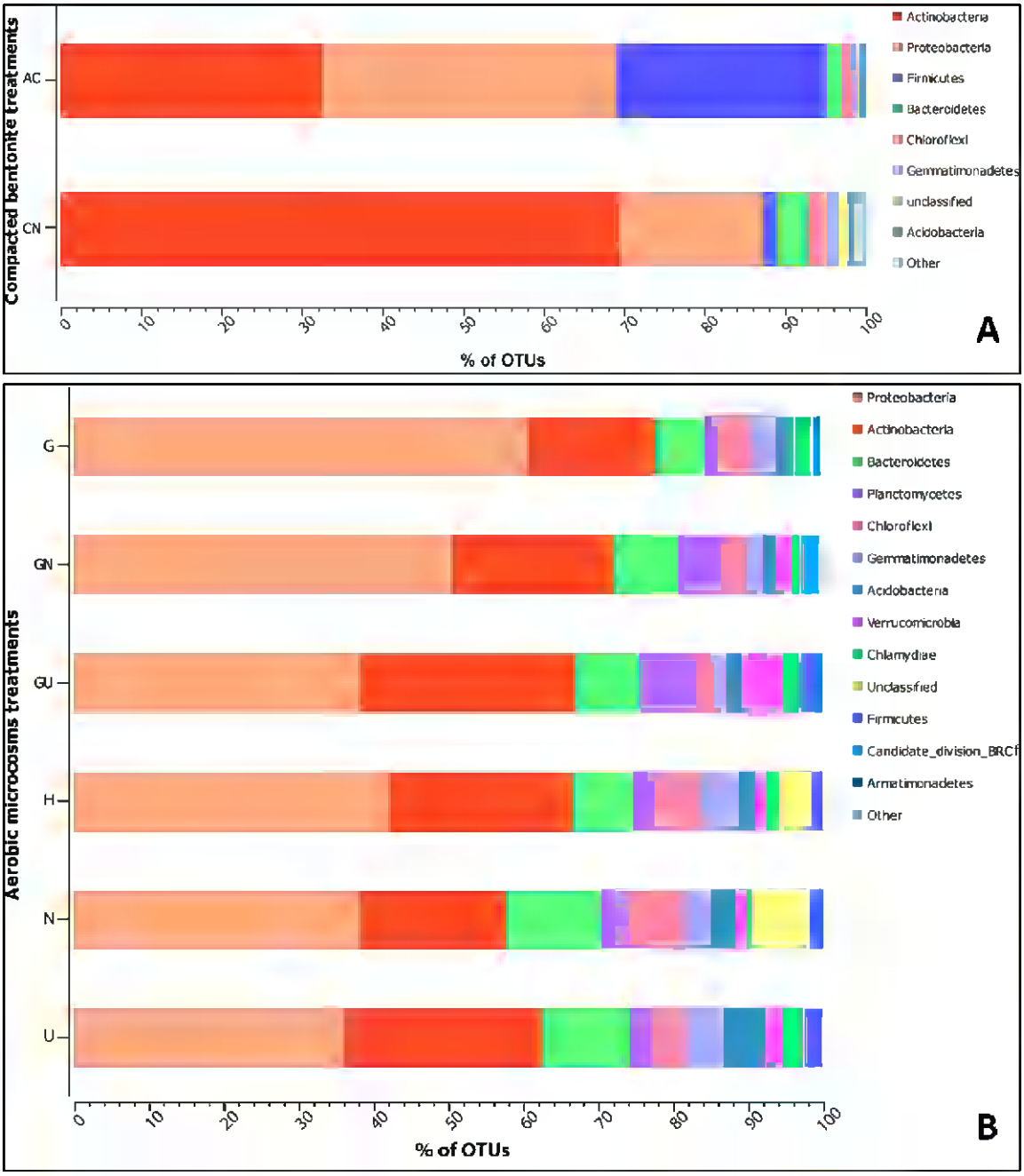

Figure 7. Phylum-level diversity of bacterial community in bentonite samples. A) In the control (CN) and acetate-treated (AC) compacted bentonite. B) In bentonite microcosms treated with distilled water (H), sodium nitrate (N), uranyl nitrate (CN), glycerol-2-phosphate (G), sodium nitrate with glycerol-2-phosphate (GN) and uranyl nitrate with glycerol-2-phosphate (GU) after six months of incubation under aerobic conditions.

We validated our method by extracting genomic DNA from many different and complex environmental samples, including non-compacted Spanish bentonites (Povedano-Priego et al., 2019), marine sediments from the Mediterranean Sea (Jroundi et al., 2019), and from subterranean groundwater (data not shown). In these cases, we obtained excellent yields of DNA with concentrations ranging from 3 ng/µL to 40 ng/µL (Table 2). Figure 8 shows an example of downstream applications of this protocol for DNA extraction from marine sediments and groundwater samples. Besides, 16S rRNA gene analyses of all these samples revealed a high microbial diversity and similar patterns in all triplicates of each sample (data not shown).

Finally, this protocol demonstrated to be particularly useful for extracting DNA from many complex environments and it is especially successful in isolating high-quality and high-yield DNA from compacted bentonite. This successful finding should facilitate the exploration and identification of the microbial community occurring within these low-biomass bentonite environments for applications in nuclear waste management.

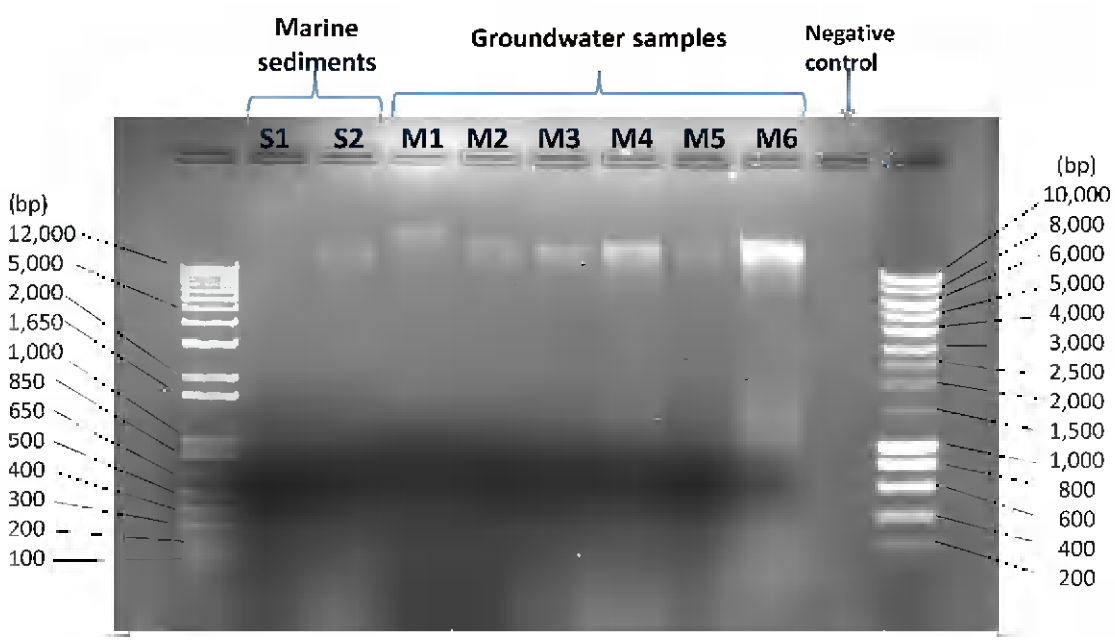

Figure 8. Example of DNA quality and integrity from marine sediments and groundwater samples. Agarose gel electrophoresis of genomic DNA to verify that there is no DNA degradation resulting in a DNA ladder.

Table 2: DNA extracted from various environmental samples by different extraction methods

Sample type	Material quantity	Volume (µL)	Conc. (ng/µL)	DNA quantity (ng)	Extraction and purification method
Groundwater M1	1.5 L	50	8.16	408.0	Lysis buffer, lysozyme, proteinase K, PCI, PC
Groundwater M2	1.5 L	50	10.00	500.0	Lysis buffer, lysozyme, proteinase K, PCI, PC
Groundwater M3	1.5 L	50	8.95	447.5	Lysis buffer, lysozyme, proteinase K, PCI, PC
Uncompacted bentonite H	1.5 g	35	2.27	79.5	Lysis buffer, lysozyme, proteinase K, PCI, PC
Uncompacted bentonite G	1.5 g	35	4.52	158.2	Lysis buffer, lysozyme, proteinase K, PCI, PC
Uncompacted bentonite N	1.5 g	35	4.45	155.8	Lysis buffer, lysozyme, proteinase K, PCI, PC
Marine sediment S1R1	1.5 g	40	3.08	123.2	(Lysis buffer) x 2, lysozyme, proteinase K, PCI, PC
Marine sediment S1R2	1.5 g	40	3.14	125.6	(Lysis buffer) x 2, lysozyme, proteinase K, PCI, PC
Marine sediment S1R3	1.5 g	40	1.18	47.2	(Lysis buffer) x 2, lysozyme, proteinase K, PCI, PC
Marine sediment S2R1	1.5 g	40	1.64	65.6	(Lysis buffer) x 2, lysozyme, proteinase K, PCI, PC
Marine sediment S2R2	1.5 g	40	3.07	122.8	(Lysis buffer) x 2, lysozyme, proteinase K, PCI, PC
Marine sediment S2R3	1.5 g	40	1.23	49.2	(Lysis buffer) x 2, lysozyme, proteinase K, PCI, PC
Compacted bentonite 1.5C	4.5 g	35	2.34	81.9	(Lysis buffer) x 2, lysozyme, proteinase K, PCI, PC
Compacted bentonite 1.5A	4.5 g	35	2.31	80.9	(Lysis buffer) x 2, lysozyme, proteinase K, PCI, PC
Compacted bentonite 1.7C	4.5 g	35	5.16	180.6	(Lysis buffer) x 2, lysozyme, proteinase K, PCI, PC
Compacted bentonite 1.7A	4.5 g	35	6.00	210.0	(Lysis buffer) x 2, lysozyme, proteinase K, PCI, PC

Lysis buffer= Tris-HCl, EDTA, NaCl, PVP, SDS
PCI= Phenol:Choroform:Isoamyl alcohol (25:24:1)
PC= Phenol:Choroform (1:1)

9. ACKNOWLEDGEMENTS

This work was supported by project CGL2014-59616-R and grant FPU 14/04263 from "Ministerio de Educación Cultura y Deporte" to Povedano-Priego and Swedish Research Council grant 2018-04311 to Dopson.

10. AUTHOR CONTRIBUTIONS

F.J. and C.P.P. wrote the manuscript with inputs from the other authors. F.J., C.P.P., and M.L.F. designed the protocol and implemented the modifications for optimizing the method. F.J. and C.P.P. performed the experiments and analyzed the data. M.D. contributed and supervised the modifications of the method. M.L.M. conceived the study and led the project. All authors contributed to reviewing the manuscript.

11. COMPETING FINANCIAL INTERESTS

The authors declare no competing financial interests.

12. REFERENCES

Alexander, W.R., McKinley, L., 2011. Deep Geological Disposal of Radioactive Waste. Elsevier.

Anderson, C., Johnsson, A., Moll, H., Pedersen, K., 2011. Radionuclide geomicrobiology of the deep biosphere. Geomicrobiology Journal 28, 540–561. https://doi.org/10.1080/01490451.2010.507644

Bengtsson, A., Pedersen, K., 2017. Microbial sulphide-producing activity in water saturated Wyoming MX-80, Asha and Calcigel bentonites at wet densities from 1500 to 2000 kg·m^{-3}. Applied Clay Science 137, 203–212. https://doi.org/10.1016/j.clay.2016.12.024

Briggs, S., McKelvie, J., Sleep, B., Krol, M., 2017. Multi-dimensional transport modelling of corrosive agents through a bentonite buffer in a Canadian deep geological repository. Science of The Total Environment 599–600, 348–354. https://doi.org/10.1016/j.scitotenv.2017.04.242

Gupta, P., Manjula, A., Rajendhran, J., Gunasekaran, P., Vakhlu, J., 2017. Comparison of metagenomic DNA extraction methods for soil sediments of high elevation Puga Hot Spring in Ladakh, India to explore bacterial diversity. Geomicrobiology Journal 34, 289–299. https://doi.org/10.1080/01490451.2015.1128995

Jroundi, F., Martinez-Ruiz, F., Merroun, M.L., Gonzalez-Muñoz, M.T., 2019. Exploring bacterial community composition in Mediterranean deep-sea sediments and their role in heavy metal accumulation. Science of The Total Environment 135660. https://doi.org/10.1016/j.scitotenv.2019.135660

Liu, G., Qiu, S., Liu, B., Pu, Y., Gao, Z., Wang, J., Jin, R., Zhou, J., 2017. Microbial reduction of Fe(III)-bearing clay minerals in the presence of humic acids. Scientific Reports 7, 45354. https://doi.org/10.1038/srep45354

Lombard, N., Prestat, E., Elsas, V., Dirk, J., Simonet, P., 2011. Soil-specific limitations for access and analysis of soil microbial communities by metagenomics. FEMS Microbiol Ecol 78, 31–49. https://doi.org/10.1111/j.1574-6941.2011.01140.x

Lopez-Fernandez, M., Cherkouk, A., Vilchez-Vargas, R., Jauregui, R., Pieper, D., Boon, N., Sanchez-Castro, I., Merroun, M.L., 2015. Bacterial diversity in bentonites, engineered barrier for Deep Geological Disposal of radioactive wastes. Microb. Ecol. 70, 922–935. https://doi.org/10.1007/s00248-015-0630-7

Lopez-Fernandez, M., Vilchez-Vargas, R., Jroundi, F., Boon, N., Pieper, D., Merroun, M.L., 2018. Microbial community changes induced by uranyl nitrate in bentonite clay microcosms. Applied Clay Science, ACS - SI ICC 2017 XVI International Clay Conference – Clays, from the oceans to space 160, 206–216. https://doi.org/10.1016/j.clay.2017.12.034

Meleshyn, A., 2011. Microbial processes relevant for long-term performance of radioactive waste repositories in clays, GRS. Ges. für Anlagen- und Reaktorsicherheit (GRS), Köln.

Pedersen, K., 1999. Subterranean microorganisms and radioactive waste disposal in Sweden. Engineering Geology 52, 163–176. https://doi.org/10.1016/S0013-7952(99)00004-6

Perdrial, J.N., Warr, L.N., Perdrial, N., Lett, M.-C., Elsass, F., 2009. Interaction between smectite and bacteria: Implications for bentonite as backfill material in the disposal of nuclear waste. Chemical Geology 264, 281–294. https://doi.org/10.1016/j.chemgeo.2009.03.012

Povedano-Priego, C., Jroundi, F., Lopez-Fernandez, M., Sánchez-Castro, I., Martin-Sánchez, I., Huertas, F.J., Merroun, M.L., 2019. Shifts in bentonite bacterial community and mineralogy in response to uranium and glycerol-2-phosphate exposure. Science of The Total Environment 692, 219–232. https://doi.org/10.1016/j.scitotenv.2019.07.228

Ratto, M., Itavaara, M., 2012. Microbial activity in bentonite buffers. Literature study (No. VTT-TECHNOLOGY – 20). VTT Technical Research Centre of Finland.

Shehadul Islam, M., Aryasomayajula, A., Selvaganapathy, P.R., 2017. A review on macroscale and microscale cell lysis methods. Micromachines (Basel) 8. https://doi.org/10.3390/mi8030083

Stone, W., Kroukamp, O., Moes, A., McKelvie, J., Korber, D.R., Wolfaardt, G.M., 2016. Measuring microbial metabolism in atypical environments: Bentonite in used nuclear fuel storage. J. Microbiol. Methods 120, 79–90. https://doi.org/10.1016/j.mimet.2015.11.006

Stroes-Gascoyne, S., Hamon, C.J., Maak, P., 2011. Limits to the use of highly compacted bentonite as a deterrent for microbiologically influenced corrosion in a nuclear fuel waste repository. Physics and Chemistry of the Earth, Parts A/B/C, Clays in Natural & Engineered Barriers for Radioactive Waste Confinement 36, 1630–1638. https://doi.org/10.1016/j.pce.2011.07.085

Stroes-Gascoyne, S., Hamon, C.J., Maak, P., Russell, S., 2010. The effects of the physical properties of highly compacted smectitic clay (bentonite) on the culturability of indigenous microorganisms. Applied Clay Science, Advanced smectitic clay research 47, 155–162. https://doi.org/10.1016/j.clay.2008.06.010

CHAPTER IV

Bacterial diversity of compacted bentonite at two different densities: influence on the safety conditions in the Deep Geological Repository of radioactive wastes

Cristina Povedano-Priego[1], Fadwa Jroundi[1], Rojina Shrestha[2], Inés Martin-Sánchez[1], María Victoria Villar[3], Jana Steinova[2], Merroun Mohamed L.[1]

[1]Departmento de Microbiología, Facultad de Ciencias, University of Granada, Granada, Spain. ppriego@correo.ugr.es, fadwa@ugr.es, merroun@ugr.es

[2] Institute for Nanomaterials, Advanced Technologies and Innovation, Technical University of Liberec, Liberec, Czech Republic. rojina.shrestha@tul.cz, jana.steinova@tul.cz

[3]Centro de Investigaciones Energéticas, Medioambientales y Tecnológicas (CIEMAT), Madrid, Spain. mv.villar@ciemat.es

1. ABSTRACT

Compacted bentonite-based materials are often considered as suitable sealing and backfilling material for Deep Geological Repository (DGR) of radioactive wastes. Several studies have been performed to characterize compacted bentonite and their physical properties (e.g. density, pore size, etc.). However, an in-depth understanding of their behaviour after placement in the repository is still required, including the impact of the microbial activity under DGR conditions. These studies should cover, among other topics, the presence of indigenous microorganisms and their survival and mobility in the compacted clay-based buffer materials. The study of microbial diversity of the Spanish bentonite is the key starting point to determine whether the indigenous microbes can produce corrosion of the metal containers, to transform the Fe-containing minerals and/or to affect the mobility and migration of radionuclides from repositories to the biosphere.

In the present chapter, untreated and acetate-treated bentonite samples were compacted at two different dry densities (1.5 and 1.7 g/cm^3) and incubated for 24 months under anaerobic conditions at room temperature. Acetate was used as an electron donor to stimulate the growth of iron-reducing bacteria (IRB). By using Illumina sequencing, it was demonstrated that the structure of the bacterial community before and after 24 months of anaerobic incubation of compacted bentonite remained dominated by Actinobacteria and Proteobacteria. Actinobacteria were mainly represented by *Pseudoarthrobacter* and *Arthrobacter* in the 24-months compacted bentonite while only *Arthrobacter* dominated the bentonite in time 0. Bacteria described for their role in biogeochemical cycle of Fe were found such as the IRB (e.g. *Geobacillus*, *Thermicanus*, *Stenotrophomonas*) and iron-oxidizing bacteria (e.g. *Thiobacillus*, *Syderoxidans*, and *Rhodobacter*). The presence of some bacteria involved in the geochemical cycle of S such as sulfur-oxidizing bacteria (e.g. *Thiobacillus*, *Delftia*, *Sulfurifustis,* and *Sulfurimonas*), and sulphate-reducing bacteria (e.g. *Pseudomonas*, *Desulfuromonas*, *Desulfoporosinus*) were also detected. Finally, some of the found bacteria were described for their capacity to utilize acetate as a carbon source for their growth such as *Delftia*, *Paracoccus*, *Stenotrophomonas*, and *Thermicanus*. In addition, scanning Electron Microscopy (SEM) analyses of the compacted bentonites revealed the formation of pores of 0.2 µm and cracks that can host several nanobacteria or spores, allowing thus their subsistence. These SEM analyses beside the microbial

diversity results are highlighting the effects of the compaction on the bentonite properties and on the indigenous microbiota.

Altogether the results of this study would help to highlight on one hand the role that the microbial communities play in affecting the optimal properties of compacted bentonites and on another hand the effects that these compaction densities may have on the bacterial diversity of the bentonite. Finally, the effects on the biogeochemical processes in which microorganisms are involved compromising the safety of the repository has been discussed.

2. INTRODUCTION

Many countries including Spain, Finland, Canada, Sweden, and United States are studying Deep Geological Repositories (DGRs) for the disposal of high level radioactive wastes (Alexander and McKinley, 2011; Briggs et al., 2017; Lopez-Fernandez et al., 2018b). DGR consists in introducing these radioactive wastes in corrosion-resistant metal containers (e.g. copper or stainless steel) surrounded by a compacted bentonite buffer to create an engineered system. The whole system would be emplaced at approximately 400-500 m underground within a low permeability host rock (Briggs et al., 2017; Pedersen, 1999). This multi-barrier system is expected to maintain its integrity for at least 100,000 years (Anderson et al., 2011). Bentonites are swelling clays with high sorption capacity resulting in a very low hydraulic conductivity (Perdrial et al., 2009) and making them the best candidate for the backfilling and sealing material in the engineered barrier (Lopez-Fernandez et al., 2015). As the main function of bentonites is to protect the canisters and reduce the migration of radionuclides to the biosphere, it is of vital importance that these bentonites remain chemically stable (Perdrial et al., 2009).

Bentonites would be utilized in the form of compacted blocks of determined dimensions and dry densities, but this is meant to create very harsh conditions for the activity and subsistence of indigenous and allochthonous microorganisms (Lopez-Fernandez et al., 2018b). Under compaction, bentonite water activity is very low and the swelling pressure is very high in the order of 7-8 MPa at full water saturation (Ratto and Itavaara, 2012). Moreover, the average pore diameter of compacted bentonite is in the range of approximately 0.005-0.1 µm, with 0.02 µm as the most frequently measured pore size (Stroes-Gascoyne et al., 2011). Despite these challenging conditions created against the microbial growth, evaluation of the microbial activity and diversity is essential for the safety assessments in the DGR concept.

It was reported that the microbial activity could not severely affect disposal conditions while the emplaced compacted bentonite maintains a uniform high dry density. The compaction of bentonite would reduce the microbial activity (but not necessary eliminates viable microorganisms) because of the deficiency of nutrients, water activity and restricted pore spaces (Perdrial et al., 2009; Stroes-Gascoyne et al., 2011). However, some microorganisms are expected to survive and maintain the

metabolic activity in compacted bentonites by their development in the gaps and in the less compressed areas such as the canisters-bentonite blocks interphase and fractures (Pedersen et al., 2000a). In the last years, several studies were focused on studying the behavior of added bacteria or the bacterial culturability and isolation in highly compacted bentonite (Jalique et al., 2016; Masurat et al., 2010; Pedersen et al., 2017, 2000a, 2000b; Stroes-Gascoyne et al., 2011). Masurat et al. (2010) demonstrated the bacterial survival capacity of both the indigenous and the colonizing bacteria from groundwater in compacted bentonite, although sulfate-reducing bacteria (SRB) producing copper sulfide decreased with the increasing bentonite density. Furthermore, Chi Fru and Athar (2008) recovered bacterial isolates from highly compacted bentonite saturated with groundwater. Jalique et al., (2016) also isolated Gram-positive spores-forming bacteria from compacted bentonite and concluded that this spore adaptation strategy could facilitate their survival in such a harsh environment.

SRB have been extensively studied due to their impact on the safety performance of DGR inducing the corrosion of metal canisters through generation of sulfide under anaerobic conditions (Bengtsson and Pedersen, 2017; Grigoryan et al., 2018; Necib et al., 2017; Pedersen, 2010; Pedersen et al., 2000a). Many SRB use a variety of electron donors such as lactate, acetate or hydrogen to reduce sulfate to sulfides, which in turn corrode the metal canisters (Pedersen, 2010). Bengtsson and Pedersen (2017) observed the occurrence of Cu_xS in the copper discs embedded in the compacted bentonite. They related this to the production of sulfide, although the consumption of sulfate was higher than the products of its reduction. Thus, some of the sulfide could be immobilized in the bentonite and unable to reach the surface of the hypothetical canisters, because of the presence of ferrous iron and resulting in iron sulfide precipitation (Bengtsson and Pedersen, 2016; Stone et al., 2016a). This was in accordance with the study of Pedersen (2010) reporting that sulfide corrosion of the canisters in DGR would depend on the diffusion of sulfide to reach the canisters, SRB growth conditions, and the presence of ferrous iron.

Structural Fe(III) reduction by iron reducing bacteria (IRB) in bentonites is another concern in the DGR concept due to the resulting alterations in the bentonites chemistry and the loss of their suitable properties as buffer material (Haynes et al., 2018). It has previously been proved that IRB were able to reduce the Fe(III) sheet silicates i.e. structural Fe(III) of smectites (Rickard, 2012). The reduction of this ferric

to ferrous iron in smectites could produce the decrease of surface area, water swelling, interlayer spacing, as well as hydraulic conductivity (Dong, 2012). A broad variety of IRB have been used to reduce Fe(III) in clay minerals such as *Shewanella putrefaciens*, *Geobacter metallireducens*, *Pseudomonas* spp., and *Bacillus* spp., among others (Dong et al., 2009; Pentráková et al., 2013; Perdrial et al., 2009). Lopez-Fernandez et al. (2015) isolated several bacterial strains implicated in the transformation of structural iron such as clones affiliated to *Pseudomonas*, *Ralstonia*, and *Bacillus*, from Spanish bentonite collected in the south-east of Spain. Recently, Haynes et al. (2018) identified an extensive IRB community in several bentonites, through selective growth media, including both Gram-negative bacteria (e.g. *Geobacter*) and Gram-positive spore-forming bacteria (e.g. *Bacillus*, *Desulfosporosinus*). Exposure of bentonite to pressure and heat stresses showed the dominance of Gram-positive bacteria whose subsistence in these harsh conditions were probably enhanced by their thicker cell walls and their capacity to spore formation (Haynes et al., 2018). Accordingly, a wide range of microorganism could survive the prevalence conditions in the DGR and therefore more studies on simulating the conditions of the radioactive waste repository are further required.

In previous works, the structure and composition of the bacterial community of Spanish bentonite was characterized (Lopez-Fernandez et al., 2018a, 2015; Povedano-Priego et al., 2019). However, the bacterial diversity occurring in highly compacted bentonite under DGR relevant conditions has remained largely overlooked and yet might help highlight some of the mentioned issues on the DGR safety. In the present study, 16S gene sequencing of the bacterial community in Spanish compacted bentonite was performed to determine the prevalent indigenous bacteria in compaction conditions. The aims of this work is to investigate the impact of microbial community on biogeochemical processes in DGR related to: 1) the structural Fe(III) bentonite transformations through the stimulation of the activity of iron-reducing bacteria supplying an electron donor (e.g. acetate), under repository relevant conditions; and 2) the impact of bentonite compaction at different dry densities (1.5 and 1.7 g/cm^3) on the diversity and activity of iron-reducing bacteria. Our findings may help in understanding the effects of compaction on the biogeochemical processes within the bentonite buffer on DGR concept as well as in developing appropriate waste treatment and long-term management strategies.

3. MATERIAL AND METHODS

3.1. Bentonite compaction and anaerobic incubation

3.1.1. Bentonite collection and pre-treatment

Bentonites were collected from "El Cortijo de Archidona" (Almeria, Spain) as it was described in Povedano-Priego et al. (2019). In the laboratory, bentonites were placed in a laminar flow cabinet to air dry during 72 h and facilitate the grinding of the samples in order to have a homogenous mixture of small particle size of bentonites. Afterwards, the grinded bentonite samples were treated with sodium acetate (30 mM) as electron donor to stimulate the growth of iron-reducing and sulfate-reducing bacteria. A control treatment consisting of the addition of distillated water was also conducted. The treatments were carried out spraying the solutions on bentonites under sterile conditions.

3.1.2. Compaction process and incubation

Bentonites were intended to be compacted at two different dry densities: 1.5 and 1.7 g/cm^3. To determine the water content in the bentonite (bentonite could not dry completely with the air drying), the hygroscopic water content was calculated using the following equation:

$$w\ (\%) = \left(\frac{M_w}{M_s}\right) \times 100$$

Being "M_w" the bentonite mass prior to desiccation and "M_s" the bentonite mass after desiccation. The hygroscopic water content of the studied bentonites was 12 %.

For the compaction, a cylindrical-steel mold with a diameter of 30.3 x 12.3 mm was used to obtain a pill of compacted bentonite given a volume of 8.81 cm^3. The amount of bentonite needed to obtain the different densities was calculated as follows: First, if considering the dry density:

$$d = M_s/V$$

Where "d" is the dry density, "M_s" is the dry mass and "V" is the volume of the mold.

For 1.5 g/cm^3:

$$M_s = 1.5\ \frac{g}{cm^3} \times 8.81\ cm^3 = 13.215\ g$$

For 1.7 g/cm^3:

$$M_s = 1.7\ \frac{g}{cm^3} \times 8.81\ cm^3 = 14.977\ g$$

But bentonites were not completely dry, thus the real densities must be calculated considering the wet mass of bentonites (considering the bentonite water content) as follows:

$$M_w = M_s \times \left(1 + \frac{w}{100}\right)$$

For 1.5 g/cm^3:

$$M_w = 13.215\ g \times \left(1 + \frac{12}{100}\right) = 14.8\ g$$

For 1.7 g/cm^3:

$$M_w = 14.977\ g \times \left(1 + \frac{12}{100}\right) = 16.77\ g$$

The compaction process was carried out in the Centro de Investigaciones Energéticas, Medioambientales y Tecnológicas (CIEMAT, Madrid) under aseptic conditions. The needed amount of bentonite was placed in the mold, which was tightly closed and a mean pressure of 79.88 and 279.57 kg/cm^2 was applied with a workshop press to obtain a bentonite block with densities of 1.5 and 1.7 g/cm^3, respectively (Fig. 1).

To establish anaerobic conditions, the compacted bentonite blocks were introduced in an anaerobic jar with anaerobiosis generator sacs (AnaeroGen™, Thermo Scientific) and were then incubated for 24 months under dark conditions. When the incubation time finished the samples were stored at -20 °C until used.

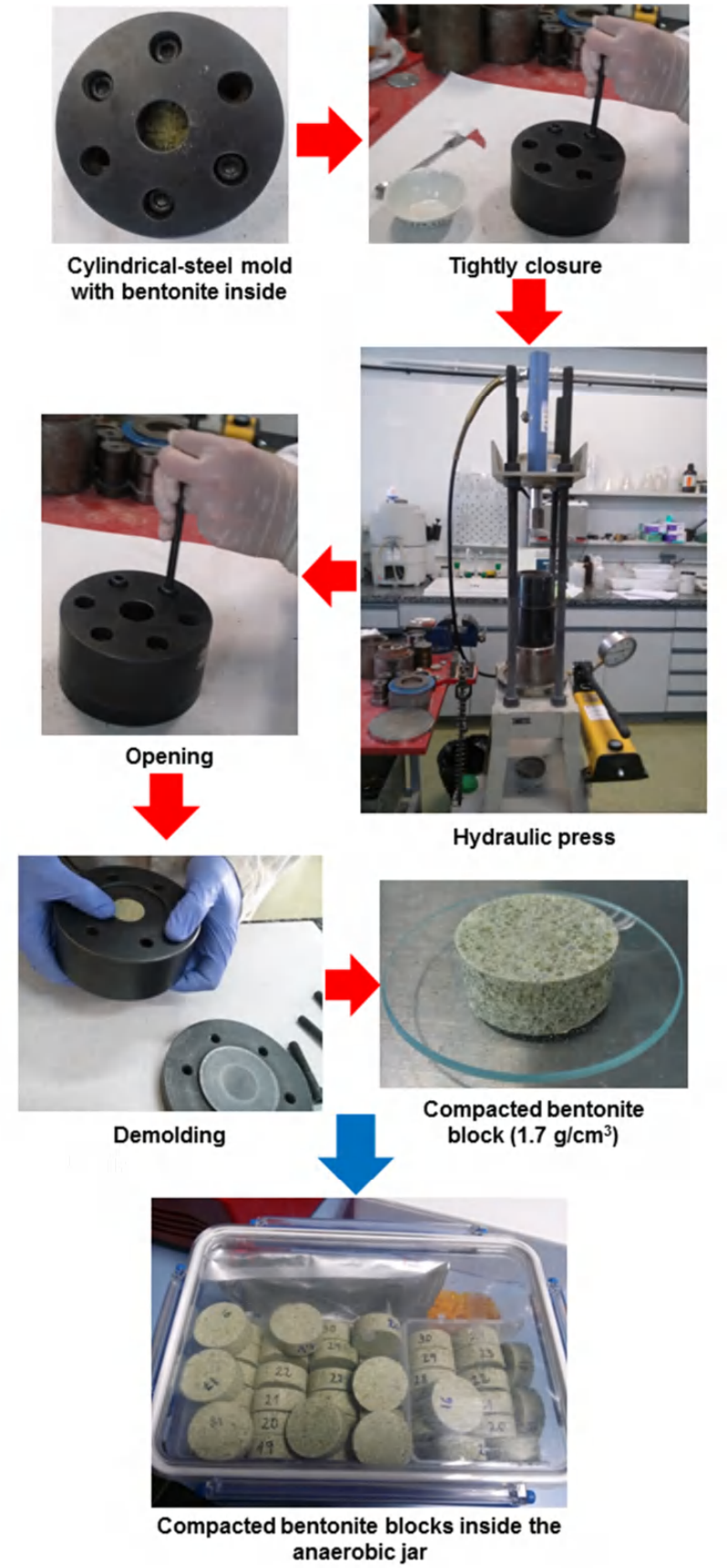

Figure 1. Workflow of the compaction process, resulting in a compacted block of 1.7 g/cm^3 density.

3.2. Characterization of the compacted bentonite bacterial diversity

3.2.2. DNA extraction from compacted bentonite

The DNA extraction from compacted bentonite is a challenging procedure because of their high binding capacity caused by the ion exchange properties (charge-based complexing) that potentially interferes with the nucleic acid extraction (Stone et al., 2016b). In addition, the microbial cells could be attached to clay particles, which demands efficient procedure to separate the cells from clay. We therefore used an optimized extraction protocol, where 400µL of Na_2HPO_4 (0.12 M pH 8.0) was added to 0.3 g of bentonite sample to allow DNA and cell desorption, beside a mechanical and chemical lyses of cells. The protocol used for DNA extraction from bentonite blocks of 1.5 and 1.7 g/cm^3 has been described in detail in Chapter III of this PhD thesis.

3.2.3. Library preparation and sequencing

The extracted DNA was further concentrated and purified using a Zymo research kit according to manufacturer's instruction and the concentration was measured on Qubit 2.0 fluorimeter (Life Technologies, MA, USA). Two consecutive PCR reactions were performed for each sample with the use of normal and bar code fusion primers for the library preparation. The primers used for amplification of variable V4 region of 16S rRNA gene were 530F (Dowd et al., 2008) and 802R (Claesson et al., 2010). Moreover, the size of the amplicon was kept below 400 bp to cover the maximum microbial diversity (Němeček et al., 2017).

The first PCR conditions were as follows: one cycle at 95 °C for 3 min; 15 cycles at 98 °C for 20 s, 50 °C for 15 s, and 72 °C for 45 s; and a final extension step at 72 °C for 1 min. The second PCR reaction was performed as follows: 95 °C for 3 min; 38 cycles at 98 ° for 20 s, 50 °C for 15 s, and 72 °C for 45 s; and a final extension step at 72 °C for 1 min. A gel-electrophoresis was used to check the quality of the library product. Additionally, the PCR products were purified using the Agencourt Ampure XP system (Beckman Coulter, Brea, CA, USA), and the concentration was measured using Qubit 2.0 fluorimeter. Then, the barcode-tagged amplicons from the different samples were mixed in equimolar concentrations. Sequencing of the amplicons was performed on an Ion Torrent Personal Genome Machine using the Ion PGM Hi-Q Sequencing Kit

with the Ion 314 Chip following the manufacturer's instruction (Thermo Fisher Scientific).

3.2.4. Bioinformatics and bacterial diversity analyses

Raw reads were split to samples using Mothur software (Schloss et al., 2009). Poor quality reads were trimmed and filtered. Similarly, chimeric sequences were detected by UCHIME (Edgar, 2013) and then removed. SILVA v.123 database with a bootstrap value set at 80 % was used for the classification of the sequences. For the clustering of the sequences into Operational Taxonomic Units (OTUs), a cut-off value of 97 % was applied. Cluster analysis was performed using 'vegan' package in the R statistical software (Oksanen et al., 2019).

Clustered and annotated OTUs were analyzed using Explicet 2.10.5 (Robertson et al., 2013) for the construction of relative abundance stacked bars, representing triplicate average. Alpha diversity indices were calculated to the lowest sample size (53,926) and bootstrapped 100 times. Taxa with ≤ 1 % relative abundance were visualized as heatmap made using the heatmap.2 function in the R gplots v. 3.0.1.1 and RColorBrewer packages (Warnes et al., 2019). The data comprising the relative abundances of genus taxonomic level were used to construct sample-similarity matrices by the Bray-Curtis algorithm, where samples were ordinated by Principal Coordinate Analysis using Past 3 (Hammer et al., 2001). Bacterial genera in compacted bentonite at densities of 1.5 and 1.7 g/cm^3 were used for network analyses, respectively. Pearson's correlation index between selected genera were calculated using 'phyloseq' 'MASS' and 'reshape2' packages of R software. A valid co-occurrence was selected as a strong correlation if the Pearson's correlation coefficient (ρ) was greater than 0.95. Correlation networks between genera in samples with different compaction densities were constructed and visualized in the Cytoscape software v.3.7.2 (Shannon et al., 2003).

3.3. Chemical, mineralogical and microscopic characterization of the compacted bentonite

The pH of compacted bentonite samples was measured in triplicate as described in Povedano-Priego et al., (2019). Before measurement, blocks were ground in a sterile

mortar and introduced in a 50 mL tubes containing the corresponding volume of 0.01 M $CaCl_2$ to establish 1:15 bentonite:solvent ratio.

After 24 months of incubation, the profile of the compacted bentonite blocks was analyzed using Variable Pressure Field Emission Scanning Electron Microscopy (VP-FESEM) ZeissSupra 40VP equipped with SE (InLens) and BSE detectors to provide morphological and chemical characterizations.

4. RESULTS

4.1. Acetate amendment to bentonite and their compaction at different densities

Spanish bentonite previously treated with sodium acetate (A) and distilled water (C) was compacted at two different dry densities (1.5 and 1.7 g/cm^3) and incubated anaerobically for 24 months. The experimental conditions of the elaborated and analyzed samples are summarized in the Table 1. After the 24-month anaerobic incubation of the compacted bentonite, no macroscopic changes were observed in comparison to those of time 0 (Fig. 2). However, while the 1.5 g/cm^3 of density blocks were shown to be easily hand-broken, those of 1.7 g/cm^3 required specific tools to be fragmented.

Table 1. Experimental conditions of the analyzed bentonite samples.

Sample ID	Replicates	Compaction (g/cm^3)	Carbon source (Acetate, mM)	Incubation time (months)
A	2*	0	30	0
C	2*	0	0	0
1.5A	3	1.5	30	24
1.5C	3	1.5	0	24
1.7A	2*	1.7	30	24
1.7C	3	1.7	0	24

*One of the replicates was discarded after diversity analyses

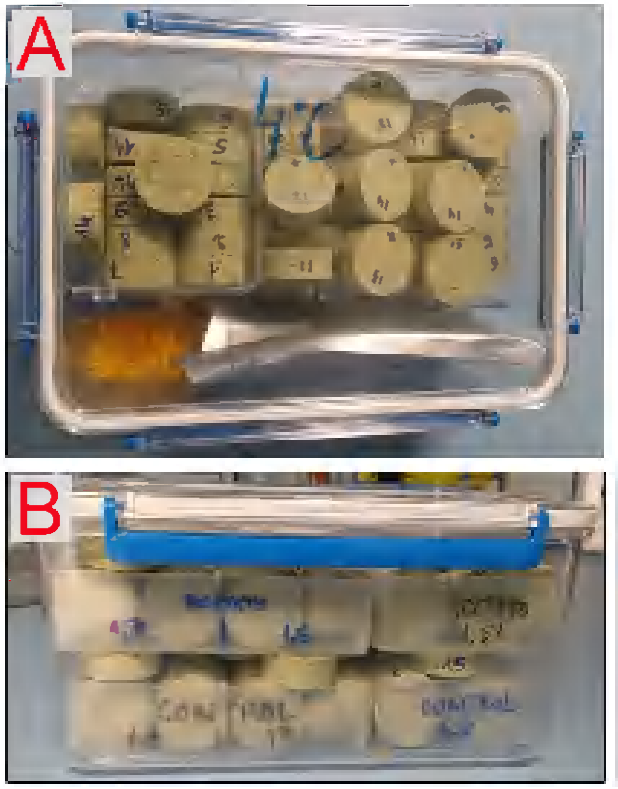

Figure 2. Acetate-treated and control compacted bentonite blocks at 1.5 and 1.7 g/cm^3 dry density after 24 months of anaerobic incubation. A) Top view of the anaerobic box. B) Side view of the anaerobic box where the position of acetate-treated and control blocks was shown.

4.2. Bacterial diversity in the acetate amended compacted bentonite under anaerobic conditions

Total DNA was extracted from both the untreated (control) and the acetate-treated compacted bentonite at 1.5 and 1.7 g/cm^3 before (time 0 samples) and after the anaerobic incubation (24-month samples). Afterwards, the extracted DNA was sequenced by Illumina MiSeq platform, providing information about the composition and structure of the microbial community of the studied samples. One of the replicates of samples A, C, and 1.7A were discarded due to the great deviations in their bacterial diversity in comparison to the other two replicates of the same sample. Good's coverage index, indicative of sufficient sequencing depth, was performed and are shown in Table 2.

A total of 303,053 bacterial reads were annotated obtaining a number of 1383 OTUs classified into phylum (99% of phylotypes), class (99% of phylotypes), order (91% of phylotypes), family (85% phylotypes), and genus (80% phylotypes) levels.

Richness, evenness and diversity of all the samples were calculated using diversity indices (Shannon, Shannon's evenness, and Simpson). The results indicated a high bacterial diversity in the bentonite samples at time 0 and after 24 months of incubation (according to ShannonD and SimpsonD indices) and a relatively uniform distribution of OTUs (according to ShannonE index) (Table 2).

Table 2. Alpha-diversity indices of compacted bentonite samples, before (A, and C) and after 24 months of incubation (1.5A, 1.5C, 1.7A, and 1.7C). Richness index (S), diversity indices (ShannonD, and SimpsonD), evenness index (ShannonE), and Good's coverage values are shown.

	S	ShannonD	ShannonE	SimpsonD	Good's coverage
A*	2357	8.77	0.78	0.98	0.999
C*	2431	9.13	0.81	0.99	1
1.5A**	361	5.11	0.60	0.87	0.999
1.5C**	323	5.13	0.62	0.89	0.999
1.7A**	283	5.16	0.63	0.90	0.999
1.7C**	306	5.36	0.65	0.92	0.999

*cutoff size: 261,435
**cutoff size: 53,926

Bacterial diversity analyses showed at both phylum and genus levels no significant differences between untreated and acetate-treated bentonites, neither between the different compaction densities (1.5 g/cm^3 and 1.7 g/cm^3) after 24 months of anaerobic incubation (Supplementary tables 1 and 2). In addition, no well-separated clusters were exhibited between treatments as shown by the PCoA analysis at genus level, which is probably due to the similarity of the bacterial composition of the bentonite samples (Fig. 3). Therefore, no clear segregations in community structure among all groups were observed. However, and in order to screen for genera that indicates some variances between the samples a heatmap was performed (Fig. 4). The acetate-treated compacted bentonite 1.5A_1 and 1.7A_1 were shown to be singular in comparison to the others and their replicates, mainly because of the high presence of *Thermicanus*, *Bacillus*, *Stenotrophomonas*, and *Delftia*, among others. These bacteria are known to be capable of utilizing acetate as carbon source for their growth (Gößner et al., 1999; Jangir et al., 2016; Sajjad et al., 2016; Sánchez-Castro et al., 2017).

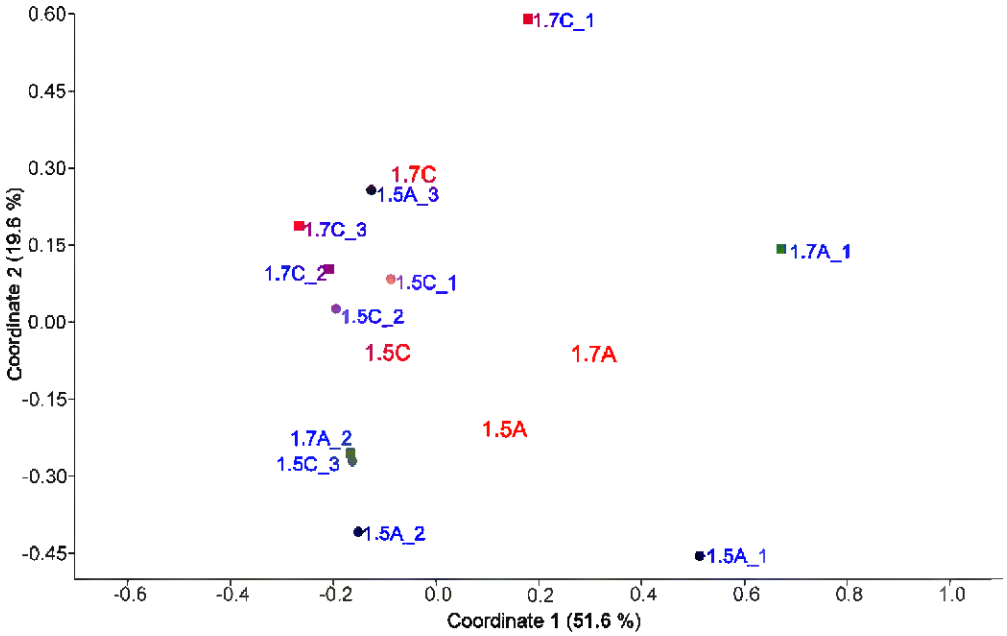

Figure 3. Principal Component Analysis (PCoA) plot comparing the bacterial community structure at genus level of the different acetate-treated and control compacted bentonite samples showing triplicates (except for 1.7A). 1.5C: control bentonite at 1.5 g/cm^3 density, 1.5A: acetate-treated bentonite at 1.5 g/cm^3 density, 1.7C: control bentonite at 1.7 g/cm^3 density, 1.7A: acetate-treated bentonite at 1.7 g/cm^3 density. The percentage of variation explained by Coordinate 1 and Coordinate 2 is indicated in the axis.

4.2.1. Effect of bentonite compaction on the bacterial diversity under anaerobic conditions

At time 0, Actinobacteria (≈50%) and Proteobacteria (≈30%) were the most abundant phyla representing together approximately 70% of the total bacterial community, followed by Bacteroidetes (7-8%), and Firmicutes (2 and 6% in A and C samples), Chloroflexi (2%), and Planctomycetes (1%) (Fig. 5A, and Supplementary Table 3). No significant changes in the bacterial diversity at the phylum level of all compacted bentonites after 24 months of anaerobic incubation were observed. Actinobacteria (≈60% in the 1.5 g/cm^3 density and 50% in the 1.7 g/cm^3 density), and Proteobacteria (≈20%) accounted for approximately 80% of the total community (Fig. 5B, and Supplementary table 4). In the 24-months samples, however, some differences with respect to time 0 were found, as for instance for Firmicutes and Chloroflexi, which were more abundant, and also for Bacteroidetes (≈4%) with a less relative abundance than in time 0 (Fig. 5B). In addition, a slight difference in the relative abundance of Firmicutes was observed between the acetate-treated and the untreated compacted

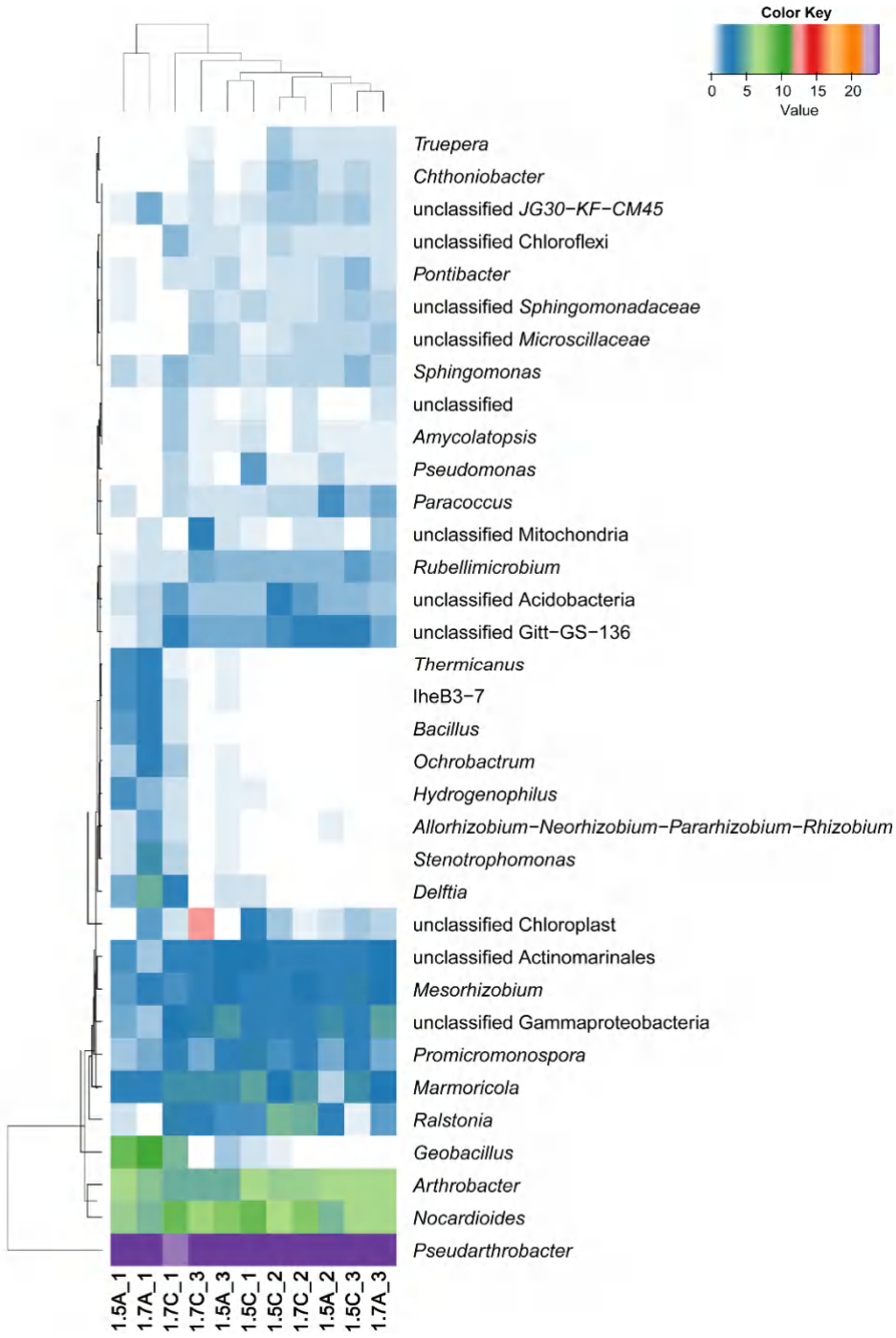

Figure 4. Heatmap of the relative abundance at the genus level in the compacted bentonites (1.5C, 1.5A, and 1.7C in triplicates, and 1.7A in duplicates), and the clustering based on Manhattan distance and average linkage for both columns and rows throughout the sample set. The relative abundance of each genus was shown by different colors indicated in the color bar.

bentonite after incubation, accounting for 0.7 and 2.8% in 1.5C and 1.7C, and 5.8 and 9.3% in 1.5A and 1.7A, respectively (Fig. 5B, and Supplementary Table 4). This could possibly be due to the capacity of Firmicutes to form spores whose smaller size made them able to resist the compaction conditions.

Regarding the class level, Actinobacteria was shown to be dominant in all cases represented by ≈50%, followed by Gamma- and Alphaproteobacteria with more than 8% of relative abundance (Fig. 6, Supplementary tables 5 and 6). Betaproteobacteria was also abundant at time 0 with 7% of relative abundance while in turn it was highly reduced in the 24-month compacted bentonites (Fig. 6A). This group was mainly represented by *Oxalicibacterium* and *Ramlibacter*; both are aerobic bacteria (Lee et al., 2014; Sahin et al., 2009). After the anaerobic incubation, in the untreated-acetate samples the presence of Betaproteobacteria was limited to *Ralstonia* (2%), whose members are able to grow under anaerobic conditions (Schwartz et al., 2003; Swanner et al., 2011). Cytophagia, Sphingobacteriia, Bacilli, and Deltaproteobacteria were represented by at least 2% of the bacterial community in both the acetate-treated and the control compacted bentonite samples (Supplementary Table 6). A remarkable difference was found between untreated and acetate-treated samples regarding the Bacilli class, which was more abundant in acetate-treated compacted bentonites (6 and 9% in 1.5A and 1.7A, respectively) than in the controls (0.6 and 3% in 1.5C and 1.7C, respectively) (Fig 6, and Supplementary Table 6).

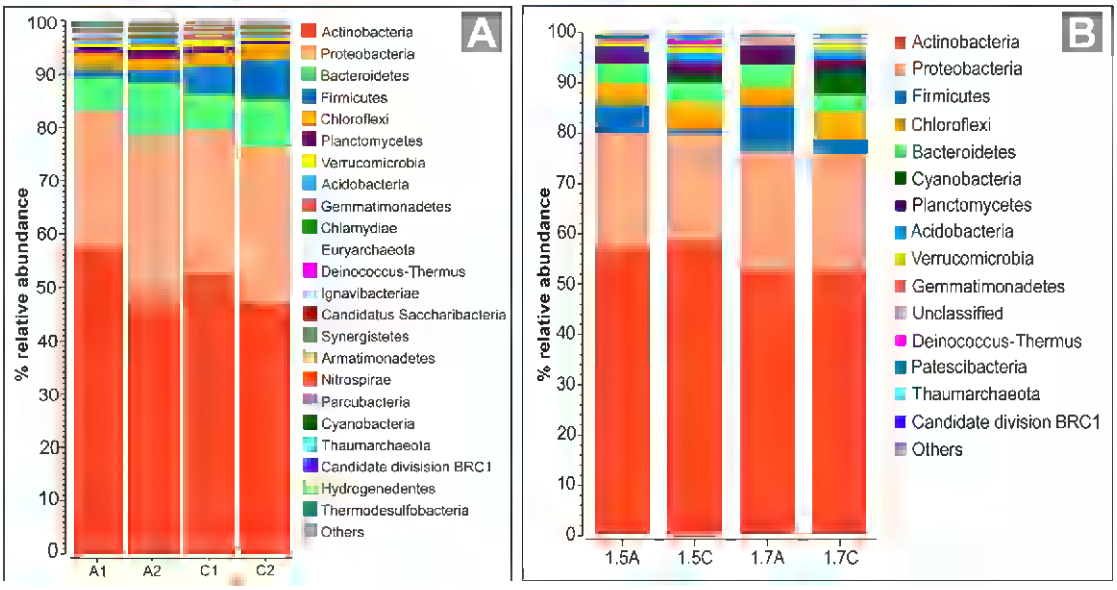

Figure 5. Relative abundance of phyla in bentonite samples at time 0 (A) and after 24 months of anaerobic incubation (B) averaging triplicates (duplicates in 1.7A sample). C: control bentonite, A: acetate-treated bentonite; 1.5C: control bentonite at 1.5 g/cm^3 density, 1.5A: acetate-treated bentonite at 1.5 g/cm^3 density, 1.7C: control bentonite at 1.7 g/cm^3 density, 1.7A: acetate-treated bentonite at 1.7 g/cm^3 density.

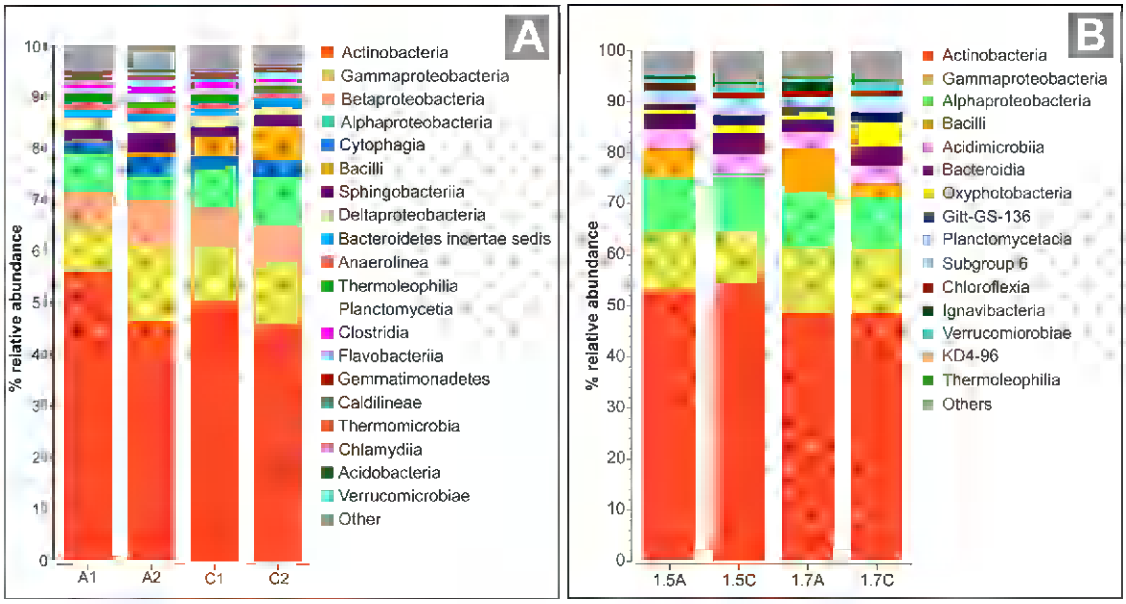

Figure 6. Relative abundance of classes in bentonite sample at time 0 (A) and after 24 months of anaerobic incubation (B) averaging triplicates (duplicates in 1.7A sample). C: control bentonite, A: acetate-treated bentonite; 1.5C: control bentonite at 1.5 g/cm^3 density, 1.5A: acetate-treated bentonite at 1.5 g/cm^3 density, 1.7C: control bentonite at 1.7 g/cm^3 density, 1.7A: acetate-treated bentonite at 1.7 g/cm^3 density.

At genus level, no significant differences have been found between the different treatments (Supplementary Tables 1 and 2). At time 0, the dominant genus was *Arthrobacter* with 25% and 18% of relative abundance in untreated (C) and acetate-treated (A) samples, respectively (Fig. 7A, Supplementary Table 7). With a lower presence in the community, *Nocardioides* was the second detected genus with approximately 7% of the total population, followed by *Methylogaea* (≈4%), *Candidatus Carsonella* (≈3%), *Promicromonospora* (≈3%), *Conexibacter* (2.5%), *Dermabacter* (2.4%), *Bacillus* (0.3% and 3.3% in A and C samples, respectively), *Ohktaekwangia* (1.4%), and *Chitinimonas* (1.4%), among others (Fig. 7A, Supplementary Table 7). Among these, several bacteria were identified to be involved in biogeochemical cycle of many elements (e.g. sulfur, iron, etc.) in the A and C samples; mainly 1) bacteria related to S cycle such as sulfate-reducing bacteria (e.g. *Desulfoglaeba*, *Desulfovirga*, *Desulfovermiculus*), sulfur-reducing bacteria (e.g. *Pseudomonas*, *Desulfuromonas*), and sulfur-oxidizing bacteria (e.g. *Sulfurimonas*, *Thiobacillus*, *Thioclava*); and 2) bacteria related to Fe cycle, such as Fe(III)-reducing bacteria (e.g. *Aciditerrimonas*, *Anaeromyxobacter*, *Desulfuromonas*), and Fe(II)-oxidizing bacteria (e.g. *Thiobacillus*, *Syderoxydans*, *Rhodobacter*, *Sphaerotilus*, *Leptospirillium*) were mentioned as the most

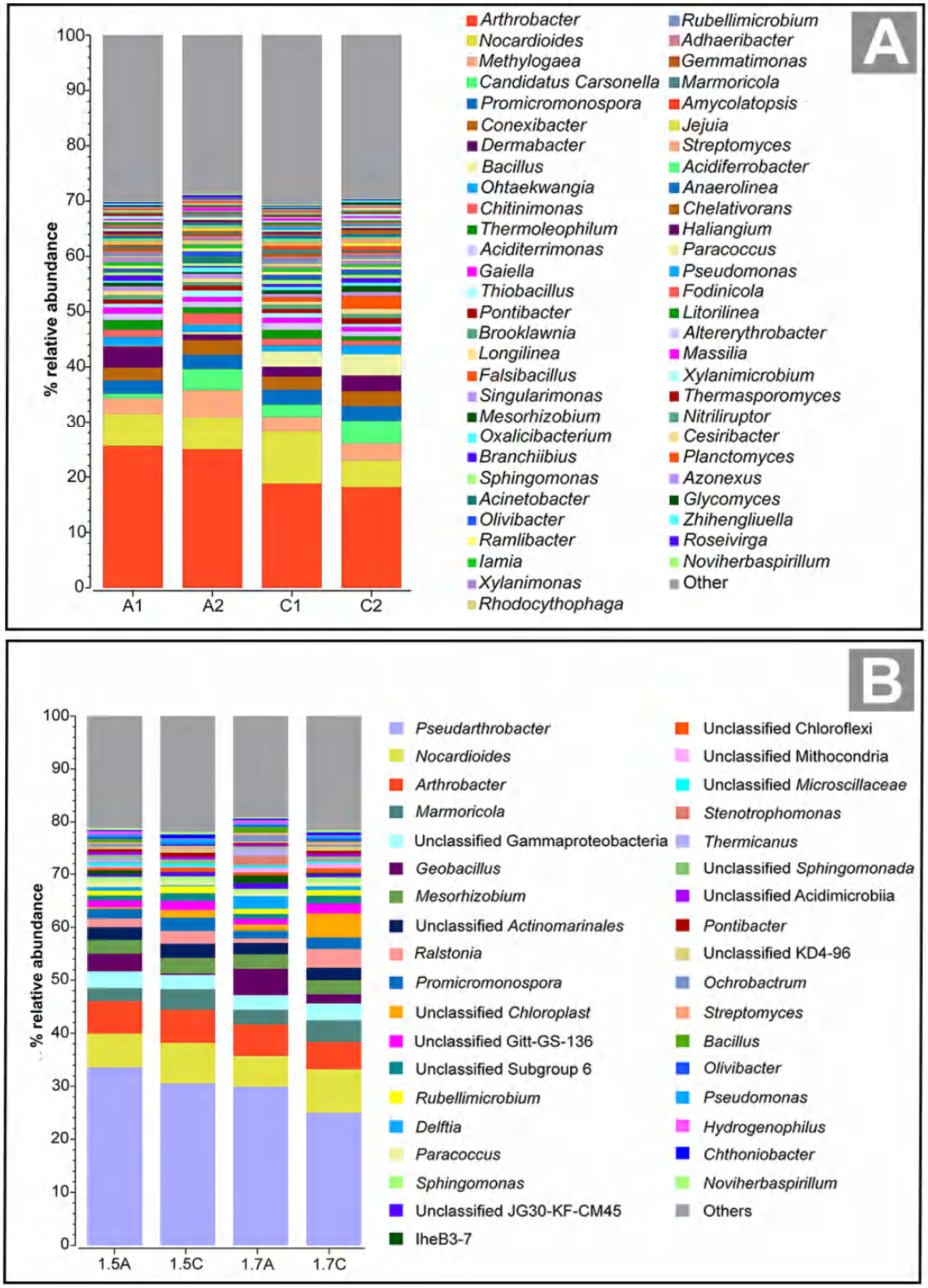

Figure 7. Relative abundance of genera in bentonite sample at time 0 (A) and after 24 months of anaerobic incubation (B) averaging triplicates (duplicates in 1.7A sample). C: control bentonite, A: acetate-treated bentonite; 1.5C: control bentonite at 1.5 g/cm^3 density, 1.5A: acetate-treated bentonite at 1.5 g/cm^3 density, 1.7C: control bentonite at 1.7 g/cm^3 density, 1.7A: acetate-treated bentonite at 1.7 g/cm^3 density.

relevant (Davidova et al., 2006; Emerson et al., 2010; Finster et al., 1994; Tian et al., 2017). Furthermore, some bacteria capable of acetate oxidation were also detected such as *Desulfuromonas* and *Pseudomonas*, both of which are able to grow utilizing acetate as a sole carbon source (Finster et al., 1994; Yang et al., 2019).

However, after the incubation period, the bacterial community at genus level was slightly different from time 0. In this case, the dominant genus was *Pseudarthrobacter* with 30% of relative abundance (30.6, 33.6, 25, and 29.9% in 1.5C, 1.5A, 1.7C and 1.7A, respectively), while *Arthrobacter* was represented by only 6% of the total community (Fig. 7B, Supplementary Table 8). *Nocardoides* maintained the 7% of relative abundance and the second abundant genus. The following genera with higher sequence counts were *Marmoricola* (3.2%), *Geobacillus* (3-5% in 1.5A and 1.7A, and 0.25-1.8% in 1.5C and 1.7C, respectively), *Mesorhizobium* (2.7%), *Ralstonia* (2.1%), and *Promicromonospora* (1.9%) (Fig. 7B, Supplementary Table 8). In addition, several genera involved in the S biogeochemical cycle were also detected after the incubation period such as sulfur oxidizers (e.g. *Delftia*, *Paracoccus*, *Mesorhizobium, Sulfurifustis*), sulfate-reducing bacteria (e.g. *Pseudomonas, Desulfuromonas, Desulfovibrio,* and *Desulfosporosinus*) and iron-reducing bacteria (e.g. *Geobacillus*, *Stenotrophomonas, Thermicanus,* and *Ralstonia*). All of these mentioned genera were enriched in the 24 months compacted bentonite samples in comparison to those of time 0 (Supplementary Tables 7 and 8).

4.2.2. Comparison of co-occurrence networks between compacted 1.5 and 1.7 g/cm^3 bentonite

Co-occurrence networks were constructed based on strong correlations ($\rho \geq 0.95$) between the relative abundance of the genera in compacted bentonites. These networks consist of 60 nodes and 127 edges in the 1.5 g/cm^3 samples, and 77 nodes and 340 edges in 1.7 g/cm^3 samples. Therefore, the latter is a complex community due to the higher number of nodes and edges (Figs. 8 and 9). Topological parameters of the performed networks are shown in Supplementary Table 9. The correlations identified were mostly positive in both networks (Figs. 8 and 9).

Betweenness centrality values were used to determine the relevance of a node for its capacity to hold together the nodes with which it could interact. In the compacted 1.5

g/cm^3 bentonite network, the genera with the highest values of betweenness centrality were *Streptococcus* (1.0), *Pirellula* (1.0), *Promicromonospora* (0.83), and unclassified *Microtrichales* (0.83) (Fig. 8, Supplementary Table 10). In one of the clusters, *Mesorhizobium* (0.5) was the most relevant for the other nodes included in the same cluster. However, in the cluster where *Bacillus* (0.12), *Geobacillus* (0.03), *Stenotrophomonas* (0.08) and *Gemmatimonas* (0.16) were included almost none of them was highlighted but they established many connections between each other, which is indicative of keystone genera.

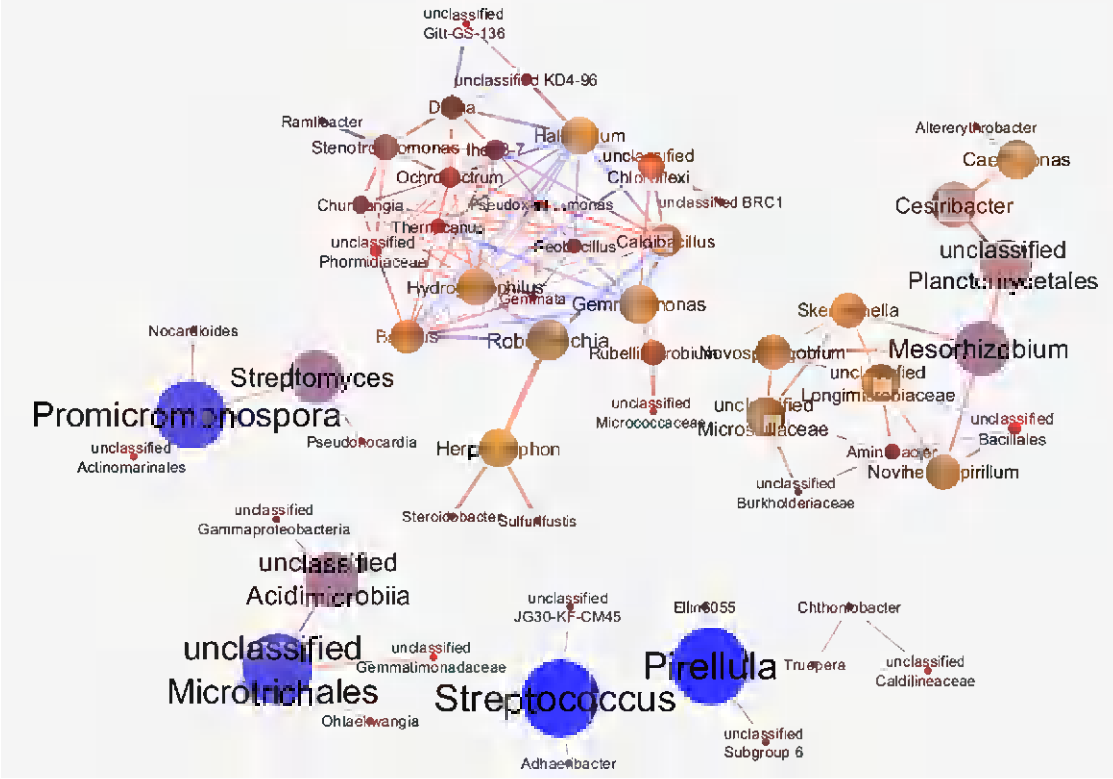

Figure 8. Co-occurrence network of bentonite at the density 1.5 g/cm^3. The connections were established based on strong (Pearson's $\rho \geq 0.95$) correlations. The colors of the edges correspond to positive (red) and negative (blue) correlations. Color and size of the nodes are related to the betweenness centrality values (the higher the bluer).

In the compacted 1.7 g/cm^3 bentonite, the genera with the highest values of betweenness centrality were unclassified Chloroflexi (0.35), *Pontibacter* (0.34), unclassified Gitt-GS-136 (Chloroflexi; 0.34), and unclassified Planctomycetales (0.30), followed by IheB3-7 (*Melioribacteraceae*) and *Pseudoxanthomonas* with 0.22 and 0.23, respectively (Fig. 9, Supplementary Table 11). In this network, all the nodes are connected to each other resulting in a single cluster where IheB3-7, *Pararhizobium*-

Rhizobium, *Adheribacter*, *Bifidobacterium*, *Chungangia*, *Bacillus*, *Stenotrophomonas* were directly connected with more than 15 nodes (Fig. 9).

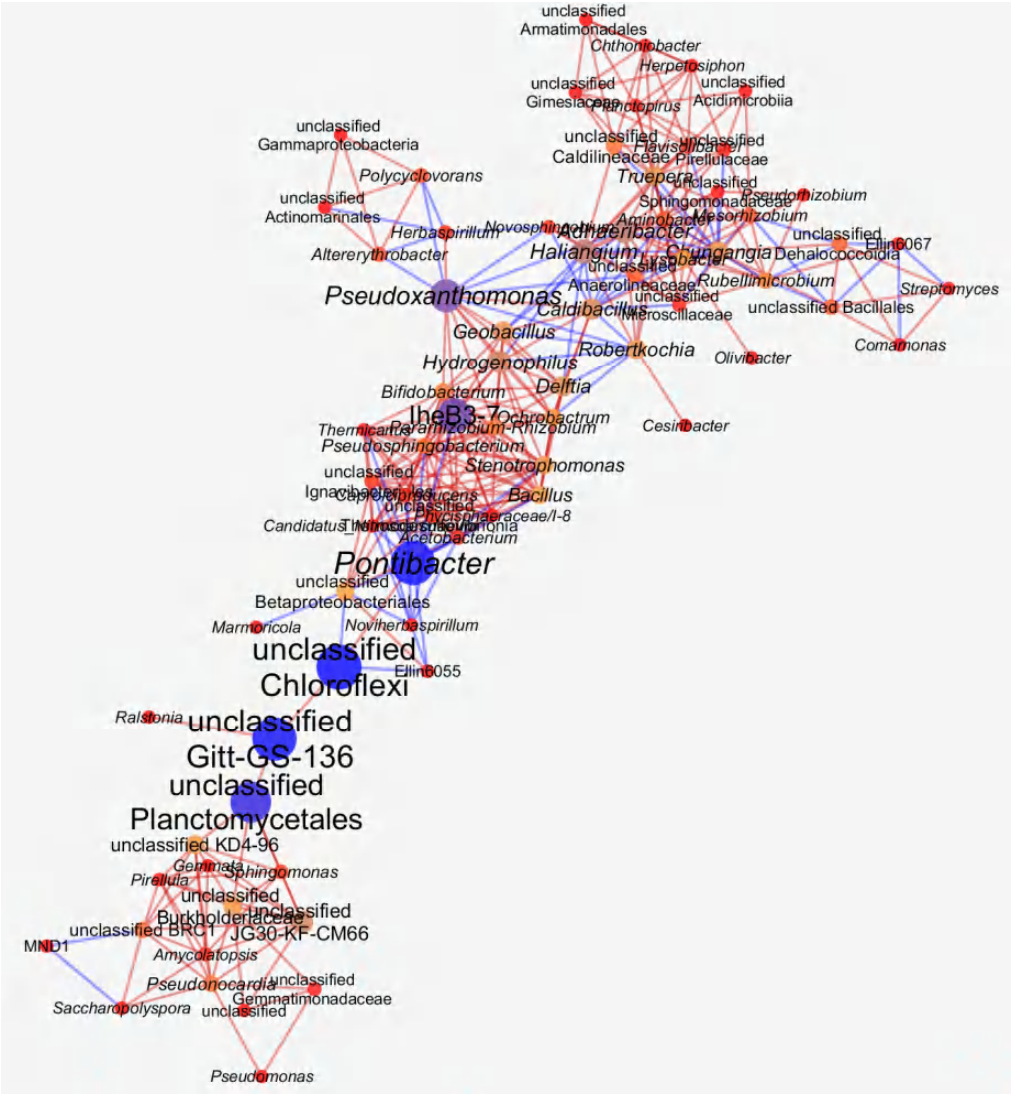

Figure 9. Co-occurrence network interactions of bentonite at the density 1.7 g/cm^3. The connections were established based on strong (Pearson's $\rho \geq 0.95$) correlation. The colors of the edges correspond to positive (red) and negative (blue) correlations. Color and size of the nodes are related to the betweenness centrality values (the higher the bluer).

4.3. Geochemical, mineralogical and microscopic characterization of the compacted bentonites

Geochemical analyses of the bentonite samples prior to incubation (time 0) were described in Povedano-Priego et al. (2019). The dominant oxides were SiO_2 (61.85 ± 3.59%), Al_2O_3 (15.41 ± 1.41%), and F_2O_3 (3.39 ± 0.21%) (Data not shown).

The measured pH values of the bentonite samples (acetate-treated and control for 0 and 24 months) using 0.01 M $CaCl_2$ solution were alkaline ranging between 7.90 and 9.79 (Table 3). As shown in Table XX, after incubation pH values decreased less than one unit in all treatments in comparison with those of time 0. No significant differences in pH were observed between the two dry densities of the compacted bentonites.

Table 3. pH values of the compacted bentonite before and after 24 months of anaerobic incubation measured in a calcium chloride suspension. C: control bentonite; 1.5A: acetate-treated bentonite at 1.5 g/cm^3 density, 1.5C: control bentonite at 1.5 g/cm^3 density, 1.7A: acetate-treated bentonite at 1.7 g/cm^3 density, 1.7C: control bentonite at 1.7 g/cm^3 density.

	Time 0	After 24 months of anaerobic incubation			
	C	**1.5A**	**1.5C**	**1.7A**	**1.7C**
$CaCl_2$	9.79 ± 0.15	8.06 ± 0.05	8.03 ± 0.03	7.90 ± 0.05	8.02 ± 0.05

VP-FESEM analyses of the cross-section profile of the compacted bentonites after 24 months of incubation were performed. A study of the surface was performed scanning an area of approximately 1 cm^3, obtaining images at low magnification of the compacted bentonites (Fig 10A and B). Several pores, cracks, and small fissures in the bentonite aggregates were observed (Fig. 10C and D). At high magnification, the typical leaf-like morphology of smectites in addition to detailed pores and cracks was observed (Fig. 10E and F).

5. DISCUSSION

Compacted bentonite may be used as sealing and backfilling material for the disposal of radioactive wastes. The compaction of this clay at a suitable dry density would protect the metal containers against corrosion, ensure a controlled transport of solutes, and retard the dispersion and mobilization of radionuclides (Masurat et al., 2010; Stroes-Gascoyne et al., 2011). In the DGR system, the compacted bentonites will possess a low water activity ranging between 10 and 17% at the beginning of the disposal establishment, very high swelling pressure and a pore size average of about 0.02 µm (Pedersen et al., 2000a; Ratto and Itavaara, 2012; Stroes-Gascoyne et al.,

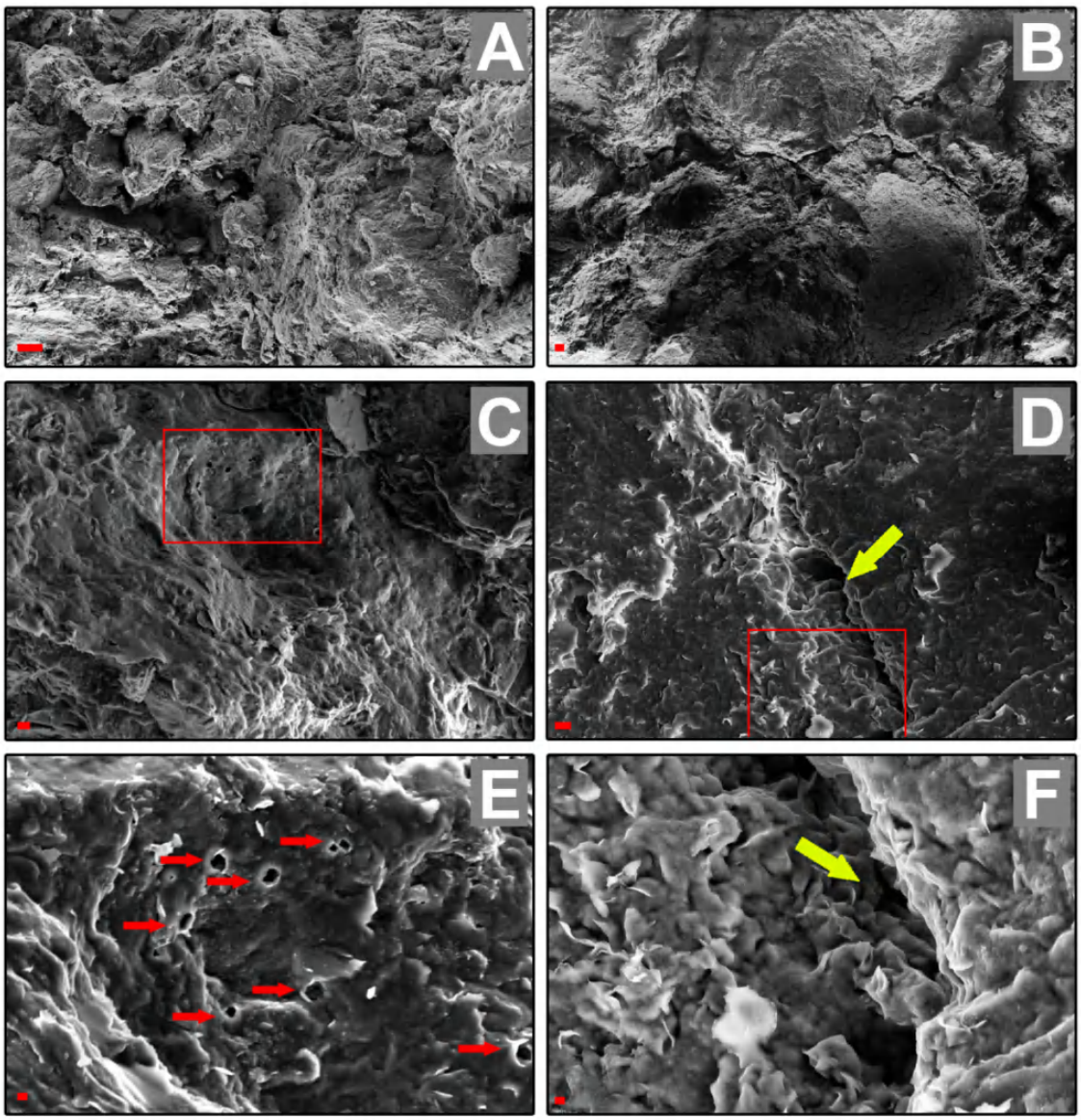

Figure 10. VP-FESEM images of compacted bentonite at 1.5 g/cm^3 density (A, C, and E) and 1.7 g/cm^3 density (B, D, and F). Images shown in secondary electrons with the InLens detector of the bentonites (D, E, and F) and images shown in secondary-backscattered electron mixing mode (A, B, C). Arrows indicate pores (red) and cracks (yellow) in D, E and F. Scale bar represents 10 µm in A and B, 1 µm in C and D, and 200 nm in E and F. Red squares in C and D were amplified in E and F, respectively.

2011). These characteristics would lead to the development of very harsh conditions for the activity and subsistence of both indigenous and introduced microorganisms in the bentonite buffer (Lopez-Fernandez et al., 2018b). It was reported that microbial activities could not affect severely disposal conditions if the emplaced compacted bentonite maintains an uniform high dry density (Stroes-Gascoyne et al., 2011).

Several studies, however, reported the probable presence of slots in the bentonite-canisters and bentonite-rock interfaces and between different bentonite blocks. These

structures could be filled with groundwater from rock fractures promoting the growth of microorganisms (Pedersen et al., 2000a). The metabolic activity of these living microbes in the compacted bentonite barrier would have the potential to adversely affect waste container corrosion rates and properties of the bentonite itself (Haynes et al., 2018).

In the present study, blocks of bentonites compacted at both dry densities (1.5 and 1.7 g/cm^3) presented some slots and pores as it was shown by VP-SEM analysis. These structures could host small-sized bacteria (e.g. nanobacteria) and allow a microbial activity. In fact, under energy limitations and physicochemical stress conditions, microorganisms could considerably decrease their size, and alter their morphology and motility to increase survivability (Ghuneim et al., 2018). Some bacteria have been reported to have the capacity to reduce their size under different starvation conditions: for example *Sphingomonas alaskensis* whose diameter and length were reduced from 0.8 µm and 2-3 µm, respectively, on nutrient-rich medium to 0.2-0.5 µm and 0.5-3 µm, respectively, under low-nutrient conditions; *Staphylococcus aureus* showed 40 % reduction in size; and *Pseudomonas syringae* reduced its size by 50 % from culture media to plant leaves (Chien et al., 2012; Ghuneim et al., 2018; Monier and Lindow, 2003). These bacteria with the capacity to adapt their size depending on the environmental conditions were identified here in the compacted bentonite before and after 24 months of anaerobic incubation, represented by *Sphingomonas* (0.6 and 0.8% on average, respectively) and *Pseudomonas* (0.4 and 0.45% on average, respectively).

In the last decade, researchers have been studying 1) the behavior of added bacteria in compacted bentonite or 2) the bacterial isolation and culturability from highly compacted bentonite (Jalique et al., 2016; Pedersen et al., 2017, 2000b, 2000a; Stroes-Gascoyne et al., 2011). To the best of our knowledge, therefore, this is the first study describing the effect of compaction density on the structure and composition of natural bacterial populations in compacted bentonite (without adding any cultivable bacteria prior to incubation). Acetate treated Spanish bentonites were compacted at two different dry densities (1.5 and 1.7 g/cm^3) and incubated anaerobically for 24 months. Sodium acetate was used as electron donor to stimulate the growth of indigenous iron-reducing (IRB) and sulfate-reducing bacteria (SRB). Therefore, the main objectives of the present study were: 1) to investigate the effects of density compaction of bentonite on the bacterial diversity of these clays, and 2) to assess the effect of amendment of

acetate (as electron donor) on the diversity of iron- and sulfate-reducing bacteria and their impact on the mineralogy of the bentonite.

The present study revealed that the bentonite bacterial diversity slightly decreased after 24 months of incubation regardless of the type of treatment (compaction density and acetate treatment) performed, as it was shown by Shannon's diversity index with values of approximately 9 and 5 for time 0 and after 24 months of incubation, respectively. This finding supports the hypothesis that high compaction of the bentonite affects the behavior of natural microorganisms and reduces the bacterial diversity in the community. However, no significant differences in the bacterial community structures between 1.5 and 1.7 g/cm^3 compacted bentonites were observed, which indicates that both dry densities showed the same effect on the subsistence of indigenous bacteria, although Stroes-Gascoyne et al. (2010, 2011) reported that the culturability of bacteria was reduced with compaction and was lower as the dry densities were increased.

The bacterial community of the 0 and 24 months incubated compacted bentonite remained dominated by Actinobacteria and Proteobacteria in all treatments. Actinobacteria were mainly represented by *Arthrobacter* at time 0 and *Arthrobacter* and *Pseudarthrobacter* at 24 months, both affiliated to the *Micrococcaceae* family and known for being mostly obligate aerobes although some are facultatively anaerobic and have developed alternative strategies to survive in oxygen limitation conditions by fermenting organic molecules such as organic acids, sugar, amino acids, among others (Busse and Wieser, 2014; Eschbach et al., 2003). *Nocardioides* also contributed with a mean of approximately 7 % in the bacterial community and, despite of being an Actinobacteria, they can live both in aerobic and anaerobic environments (Kutcherov and Kolesnikov, 2013). Proteobacteria was mostly represented by Gamma- and Alpha-proteobacteria in all samples, and also by Betaproteobacteria in time 0 samples. Within the Gammaproteobacteria, sequences belonging to *Pseudomonas* were detected in all samples, *Acidiferrobacter* in time 0 samples, and *Stenotrophomonas*, and *Sulfurifustis* in the 24-month anaerobically incubated compacted bentonites.

5.1. Effects of SRB and IRB on the biogeochemical processes in the DGR concept

IRB and SRB activities are of particular concern in the DGR concept. SRB could produce sulphide leading to the corrosion of the containers under anaerobic conditions (Grigoryan et al., 2018), while IRB are able to reduce the Fe(III) sheet silicates (i.e. structural Fe(III) of smectites) which could produce destabilization of bentonites and the loss of their suitable properties, affecting thus the safety performance of the DGR (Rickard, 2012).

Acetate is one of the electron donors used by these groups of bacteria (Rickard, 2012; van den Brand et al., 2014). In the present study, acetate seems to have no effect on the bacterial diversity since no significant differences were detected between untreated and acetate-treated compacted bentonite after 24 months of anaerobic incubation. However, we have found in the acetate-treated samples several bacteria with the capacity to grow using acetate as electron donor such as *Delftia*, *Paracoccus*, *Stenotrophomonas*, *Thermicanus, Desulfuromonas* and *Pseudomonas* (Finster et al., 1994; Gößner et al., 1999; Jangir et al., 2016; Sajjad et al., 2016; Sánchez-Castro et al., 2017; Yang et al., 2019). Assimilation of acetate is performed via tricarboxylic acid cycle in most bacteria including *Paracoccus* (Petushkova and Tsygankov, 2017). Interestingly, *Thermicanus*, a facultatively anaerobic bacterium, which can oxidize acetate under O_2-limiting conditions (Gößner et al., 1999). Low levels of oxygens trapped in the pores and cracks generated during the highly compacted blocks manufacturing could support the use of acetate by *Thermicanus* (Alonso and Ledesma, 2005).

One of the concerns in the DGR concept is the corrosion of the canisters, which are required to remain intact until the radioactivity of the wastes decay to natural background levels. Therefore, it is especially important to consider the diversity of indigenous sulfate-reducing bacteria (SRB) in the compacted bentonite. SRB couple the oxidation of organic acids (e.g. acetate) with the reduction of sulfate to hydrogen sulfide which could corrode the metal canisters (Pedersen, 2010). In this study, compacted bentonites were amended with acetate as an electron donor to stimulate the growth of IRB and SRB. Several genera of SRB are able to use this organic acid for their growth including *Desulfobacter* genus, Chrysiogenetes phylum and Halanaerobiales

(Clostridia) (Timmers et al., 2018; van den Brand et al., 2014). Low levels of sulfur and sulfate reducing bacterial populations belonging to *Desulfuromonas*, and *Desulfosporosinus* with the ability to generate sulfides were identified in our compacted bentonite samples. This production of sulfide occurred under anaerobic conditions by dissimilatory sulfate/sulfur reduction with the complete or incomplete oxidation of an electron donor (lactate, acetate) (Loka Bharathi, 2008). Sequences belonging to *Desulfosporosinus* have been detected in a study where compacted bentonite saturated with groundwater and amended with lactate was performed (Chi Fru and Athar, 2008). The sulfur-oxidizing bacteria (SOB) could use nitrate as alternative electron acceptor, when oxygen is restricted, to oxidize sulfide or metal-sulfides producing sulfite or sulfate depending of the enzymatic pathway (Poser et al., 2014). In our study, several sulfur-oxidizing bacteria were found after 24-month incubation such as *Delftia*, *Paracoccus*, *Mesorhizobium*, *Thiobacillus* and *Sulfurifustis* countering the activity of the sulfate-reducing bacteria (Huber et al., 2016; Poser et al., 2014; Quentmeier et al., 2003).

Regarding the Iron-reducing bacteria (IRB), these can oxidize acetate to CO_2 with the reduction of Fe(III) acting as the sole electron acceptor (Rickard, 2012). In the DGR environment, one of the most abundant electron acceptor is the structural Fe(III) from the smectite octahedral layer in bentonite, thus IRB could play a key role in bentonite alteration (Esnault et al., 2010). Microbial processes affect the biogeochemical cycle of structural Fe of bentonites (e.g. illitization of smectite). These processes are mediated by the activity of Fe-reducing bacteria, which are ubiquitous in the environment (Gates et al., 1993).

The illitization process could lead to: 1) increase of the layer charge, 2) prevent clay expansion upon hydration, 2) water releasing, and 4) changes in the hydraulic conductivity (Dong, 2012; Dong et al., 2009). Kostka et al. (2002) reported the growth of IRB (*Shewanella oneidensis*) using the iron bound in smectite as the sole electron acceptor. In addition, a combination of TEM and XDR were applied to report the ability of *Shewanella oneidensis* strain MR-1 to promote the dissolution of smectite through reduction of structural Fe(III) in smectite (Kim et al., 2004). In the present study, several IRB were found after 24 months in the acetate treated compacted bentonite such as *Geobacillus*, *Pseudomonas*, *Stenotrophomonas*, *Bacillus* and *Thermicanus*. These bacterial strains are able to reduce Fe(III) (Brooke, 2012; Gößner et al., 1999; Valencia-

Cantero and Peña-Cabriales, 2014). Some *Bacillus* members were described for the ferric iron reduction in anaerobic conditions such as *B. subterraneus* (a facultatively anaerobic bacterium) and *B. infernus* (a strictly anaerobic bacterium) utilizing Fe(III) as electron acceptor (Kanso et al., 2002).

Instead, *Pseudomonas* have been described for its potential to reduce Fe(III) through respiratory metabolisms (Kooli et al., 2018). Moreover, *Pseudomonas* has been described to form biofilm in carbon steel surfaces and utilize the Fe^0 as electron donor for respiration causing corrosion (Jia et al., 2017) and it could therefore adversely alter the carbon steel containers used in deep geological disposal of radioactive wastes. However, a recent study using *P. aeruginosa* concluded that the corrosion of copper material by SRB was inhibited to some extent probably due to the production of extracellular polymeric substance (EPS) by *P. aeruginosa*, changing the properties of the substrate and negatively affecting the activity of SRB (Xiaodong et al., 2019). Therefore, the impact of *Pseudomonas* on the stability of canisters depends upon the nature of these containers. In addition, *Pseudomonas* exhibited high tolerance to heavy metal and radionuclides such as uranium through different mechanisms (biosorption, accumulation, biomineralization), playing a key role in the radionuclide speciation and fate in case of canister rupture (Choudhary and Sar, 2011; Kazy et al., 2009, 2008). On the other hand, *Stenotrophomonas* and *Acidiferrobacter* have been reported to promote iron reduction under anaerobic conditions which could be detrimental for the structural stability of smectites (Hallberg et al., 2011; Ivanov et al., 2005; Valencia-Cantero et al., 2007).

In the light of these findings, the bacterial community of compacted bentonite was decreased over time of incubation because of the compaction effect at two different densities. However, neither significant differences between 1.5 and 1.7 g/cm^3 dry densities, nor between untreated and acetate-treated samples were observed. Despite of being a tough environment for the subsistence of microorganisms, an overly complex bacterial community was found where both detrimental and neutral bacteria for the safety of DGR are in coexistence. The bacterial diversity results of the present study showed the presence of bacterial groups related to the sulfur and iron biogeochemical cycles, which could be enriched by the addition of acetate. However, no differences in bacterial composition of the community were observed between acetate-treated and untreated compacted bentonites. This could be explained by the short incubation time (2

years), which seems to be insufficient to detect an enhancement of the IRB and SRB communities. Long-term incubation under anaerobic conditions of compacted bentonite could lead to the enrichment of these groups of bacteria, altering the stability of bentonites (by structural iron reduction) and inducing the metal canister corrosion (by sulfide production). Therefore, further deep studies performing long-term incubation (e.g. at least 10 years) and providing efficient electron donors (e.g. lactate and acetate) and terminal electron acceptors, such as sulfate for SRB, are required for a better understanding of the implications of SRB and IRB in the DGR concept.

6. ACKNOWLEDGEMENTS

We acknowledge the assistance of Isabel Guerra Tschuschke (VP-FESEM technician), and Concepción Hernández-Castillo (preparation of samples for microscopic analyses), members of Centro de Instrumentación Científica (University of Granada, Spain).

7. REFERENCES

Alexander, W.R., McKinley, L., 2011. Deep geological disposal of radioactive waste. Elsevier.

Alonso, E.E., Ledesma, A., 2005. Advances in understanding engineered clay barriers: Proceedings of the International Symposium on Large Scale Field Tests in Granite, Sitges, Barcelona, Spain, 12-14 November 2003. CRC Press.

Anderson, C., Johnsson, A., Moll, H., Pedersen, K., 2011. Radionuclide geomicrobiology of the deep biosphere. Geomicrobiology Journal 28, 540–561. https://doi.org/10.1080/01490451.2010.507644

Bengtsson, A., Pedersen, K., 2017. Microbial sulphide-producing activity in water saturated Wyoming MX-80, Asha and Calcigel bentonites at wet densities from 1500 to 2000kgm−3. Applied Clay Science 137, 203–212. https://doi.org/10.1016/j.clay.2016.12.024

Bengtsson, A., Pedersen, K., 2016. Microbial sulphate-reducing activity over load pressure and density in water saturated Boom Clay. Applied Clay Science 132–133, 542–551. https://doi.org/10.1016/j.clay.2016.08.002

Briggs, S., McKelvie, J., Sleep, B., Krol, M., 2017. Multi-dimensional transport modelling of corrosive agents through a bentonite buffer in a Canadian deep geological repository. Science of The Total Environment 599–600, 348–354. https://doi.org/10.1016/j.scitotenv.2017.04.242

Brooke, J.S., 2012. *Stenotrophomonas maltophilia*: An emerging global opportunistic pathogen. Clinical Microbiology Reviews 25, 2–41. https://doi.org/10.1128/CMR.00019-11

Busse, H.-J., Wieser, M., 2014. The Genus *Arthrobacter*, in: Rosenberg, E., DeLong, E.F., Lory, S., Stackebrandt, E., Thompson, F. (Eds.), The Prokaryotes: Actinobacteria. Springer, Berlin, Heidelberg, pp. 105–132. https://doi.org/10.1007/978-3-642-30138-4_204

Chi Fru, E., Athar, R., 2008. In situ bacterial colonization of compacted bentonite under deep geological high-level radioactive waste repository conditions. Appl Microbiol Biotechnol 79, 499–510. https://doi.org/10.1007/s00253-008-1436-z

Chien, A.-C., Hill, N.S., Levin, P.A., 2012. Cell size control in bacteria. Curr. Biol. 22, R340-349. https://doi.org/10.1016/j.cub.2012.02.032

Choudhary, S., Sar, P., 2011. Uranium biomineralization by a metal resistant *Pseudomonas aeruginosa* strain isolated from contaminated mine waste. J. Hazard. Mater. 186, 336–343. https://doi.org/10.1016/j.jhazmat.2010.11.004

Claesson, M.J., Wang, Q., O'Sullivan, O., Greene-Diniz, R., Cole, J.R., Ross, R.P., O'Toole, P.W., 2010. Comparison of two next-generation sequencing technologies for resolving highly complex microbiota composition using tandem variable 16S rRNA gene regions. Nucleic Acids Res. 38, e200. https://doi.org/10.1093/nar/gkq873

Davidova, I.A., Duncan, K.E., Choi, O.K., Suflita, J.M., 2006. *Desulfoglaeba alkanexedens* gen. nov., sp. nov., an n-alkane-degrading, sulfate-reducing bacterium. International Journal of Systematic and Evolutionary Microbiology, 56, 2737–2742. https://doi.org/10.1099/ijs.0.64398-0

Dong, H., 2012. Clay–microbe interactions and implications for environmental mitigation. elements 8, 113–118. https://doi.org/10.2113/gselements.8.2.113

Dong, H., Jaisi, D.P., Kim, J., Zhang, G., 2009. Microbe-clay mineral interactions. American Mineralogist 94, 1505–1519. https://doi.org/10.2138/am.2009.3246

Dowd, S.E., Callaway, T.R., Wolcott, R.D., Sun, Y., McKeehan, T., Hagevoort, R.G., Edrington, T.S., 2008. Evaluation of the bacterial diversity in the feces of cattle using 16S rDNA bacterial tag-encoded FLX amplicon pyrosequencing (bTEFAP). BMC Microbiol. 8, 125. https://doi.org/10.1186/1471-2180-8-125

Edgar, R.C., 2013. UPARSE: highly accurate OTU sequences from microbial amplicon reads. Nat. Methods 10, 996–998. https://doi.org/10.1038/nmeth.2604

Emerson, D., Fleming, E.J., McBeth, J.M., 2010. Iron-oxidizing bacteria: An environmental and genomic perspective. Annual Review of Microbiology 64, 561–583. https://doi.org/10.1146/annurev.micro.112408.134208

Eschbach, M., Möbitz, H., Rompf, A., Jahn, D., 2003. Members of the genus *Arthrobacter* grow anaerobically using nitrate ammonification and fermentative processes: anaerobic adaptation of aerobic bacteria abundant in soil. FEMS Microbiology Letters 223, 227–230. https://doi.org/10.1016/S0378-1097(03)00383-5

Esnault, L., Libert, M., Bildstein, O., Jullien, M., Mustin, C., 2010. Clay-iron reducing bacteria interaction in deep geological environment: Experimental and modeling approach. Presented at the Water-Rock Interaction - Proceedings of the 13th International Conference on Water-Rock Interaction, WRI-13, pp. 939–942.

Finster, K., Bak, F., Pfennig, N., 1994. *Desulfuromonas acetexigens* sp. nov., a dissimilatory sulfur-reducing eubacterium from anoxic freshwater sediments. Arch. Microbiol. 161, 328–332. https://doi.org/10.1007/BF00303588

Ghuneim, L.-A.J., Jones, D.L., Golyshin, P.N., Golyshina, O.V., 2018. Nano-sized and filterable Bacteria and Archaea: Biodiversity and function. Front Microbiol 9. https://doi.org/10.3389/fmicb.2018.01971

Gößner, A.S., Devereux, R., Ohnemüller, N., Acker, G., Stackebrandt, E., Drake, H.L., 1999. *Thermicanus aegyptius* gen. nov., sp. nov., isolated from oxic soil, a fermentative microaerophile that grows commensally with the thermophilic acetogen *Moorella thermoacetica*. Appl Environ Microbiol 65, 5124–5133.

Grigoryan, A.A., Jalique, D.R., Medihala, P., Stroes-Gascoyne, S., Wolfaardt, G.M., McKelvie, J., Korber, D.R., 2018. Bacterial diversity and production of sulfide in microcosms containing uncompacted bentonites. Heliyon 4. https://doi.org/10.1016/j.heliyon.2018.e00722

Hallberg, K.B., Hedrich, S., Johnson, D.B., 2011. *Acidiferrobacter thiooxydans*, gen. nov. sp. nov.; an acidophilic, thermo-tolerant, facultatively anaerobic iron- and sulfur-oxidizer of the family *Ectothiorhodospiraceae*. Extremophiles 15, 271–279. https://doi.org/10.1007/s00792-011-0359-2

Hammer, O., Harper, D.A.T., Ryan, P.D., 2001. PAST: Paleontological statistics software package for education and data analysis. Palaeontologia Electronica 4, 1–9.

Haynes, H.M., Pearce, C.I., Boothman, C., Lloyd, J.R., 2018. Response of bentonite microbial communities to stresses relevant to geodisposal of radioactive waste. Chemical Geology 501, 58–67. https://doi.org/10.1016/j.chemgeo.2018.10.004

Huber, B., Herzog, B., Drewes, J.E., Koch, K., Müller, E., 2016. Characterization of sulfur oxidizing bacteria related to biogenic sulfuric acid corrosion in sludge digesters. BMC Microbiol 16. https://doi.org/10.1186/s12866-016-0767-7

Ivanov, V., Stabnikov, V., Zhuang, W.Q., Tay, J.H., Tay, S.T.L., 2005. Phosphate removal from the returned liquor of municipal wastewater treatment plant using iron-reducing bacteria. J. Appl. Microbiol. 98, 1152–1161. https://doi.org/10.1111/j.1365-2672.2005.02567.x

Jalique, D.R., Stroes-Gascoyne, S., Hamon, C.J., Priyanto, D.G., Kohle, C., Evenden, W.G., Wolfaardt, G.M., Grigoryan, A.A., McKelvie, J., Korber, D.R., 2016. Culturability and diversity of microorganisms recovered from an eight-year old highly-compacted, saturated MX-80 Wyoming bentonite plug. Applied Clay Science 126, 245–250. https://doi.org/10.1016/j.clay.2016.03.022

Jangir, Y., French, S., Momper, L.M., Moser, D.P., Amend, J.P., El-Naggar, M.Y., 2016. Isolation and characterization of electrochemically active subsurface *Delftia* and *Azonexus* species. Front. Microbiol. 7. https://doi.org/10.3389/fmicb.2016.00756

Jia, R., Yang, D., Xu, D., Gu, T., 2017. Anaerobic corrosion of 304 stainless steel caused by the *Pseudomonas aeruginosa* biofilm. Front Microbiol 8. https://doi.org/10.3389/fmicb.2017.02335

Kanso, S., Greene, A.C., Patel, B.K.C., 2002. *Bacillus subterraneus* sp. nov., an iron- and manganese-reducing bacterium from a deep subsurface Australian thermal aquifer. International Journal of Systematic and Evolutionary Microbiology, 52, 869–874. https://doi.org/10.1099/00207713-52-3-869

Kazy, S.K., D'Souza, S.F., Sar, P., 2009. Uranium and thorium sequestration by a *Pseudomonas* sp.: Mechanism and chemical characterization. Journal of Hazardous Materials 163, 65–72. https://doi.org/10.1016/j.jhazmat.2008.06.076

Kazy, S.K., Sar, P., D'Souza, S.F., 2008. Studies on uranium removal by the extracellular polysaccharide of a *Pseudomonas aeruginosa* strain. Bioremediation Journal 12, 47–57. https://doi.org/10.1080/10889860802052870

Kim, J., Dong, H., Seabaugh, J., Newell, S.W., Eberl, D.D., 2004. Role of microbes in the smectite-to-illite reaction. Science 303, 830–832. https://doi.org/10.1126/science.1093245

Kooli, W.M., Comensoli, L., Maillard, J., Albini, M., Gelb, A., Junier, P., Joseph, E., 2018. Bacterial iron reduction and biogenic mineral formation for the stabilisation of corroded iron objects. Sci Rep 8, 1–11. https://doi.org/10.1038/s41598-017-19020-3

Kostka, J.E., Dalton, D.D., Skelton, H., Dollhopf, S., Stucki, J.W., 2002. Growth of iron(III)-reducing bacteria on clay minerals as the sole electron acceptor and comparison of growth yields on a variety of oxidized iron forms. Appl Environ Microbiol 68, 6256–6262. https://doi.org/10.1128/AEM.68.12.6256-6262.2002

Kutcherov, V., Kolesnikov, A., 2013. Hydrocarbon. BoD – Books on Demand.

Lee, H.J., Lee, S.H., Lee, S.-S., Lee, J.S., Kim, Y., Kim, S.-C., Jeon, C.O., 2014. *Ramlibacter solisilvae* sp. nov., isolated from forest soil, and emended description of the genus *Ramlibacter*. Int. J. Syst. Evol. Microbiol. 64, 1317–1322. https://doi.org/10.1099/ijs.0.058396-0

Loka Bharathi, P.A., 2008. Sulfur Cycle, in: Jørgensen, S.E., Fath, B.D. (Eds.), Encyclopedia of Ecology. Academic Press, Oxford, pp. 3424–3431. https://doi.org/10.1016/B978-008045405-4.00761-8

Lopez-Fernandez, M., Cherkouk, A., Vilchez-Vargas, R., Jauregui, R., Pieper, D., Boon, N., Sanchez-Castro, I., Merroun, M.L., 2015. Bacterial diversity in bentonites, engineered barrier for deep geological disposal of radioactive wastes. Microb. Ecol. 70, 922–935. https://doi.org/10.1007/s00248-015-0630-7

Lopez-Fernandez, M., Romero-González, M., Günther, A., Solari, P.L., Merroun, M.L., 2018a. Effect of U(VI) aqueous speciation on the binding of uranium by the cell surface of *Rhodotorula mucilaginosa*, a natural yeast isolate from bentonites. Chemosphere 199, 351–360. https://doi.org/10.1016/j.chemosphere.2018.02.055

Lopez-Fernandez, M., Vilchez-Vargas, R., Jroundi, F., Boon, N., Pieper, D., Merroun, M.L., 2018b. Microbial community changes induced by uranyl nitrate in bentonite clay microcosms. Applied Clay Science, ACS - SI ICC 2017 XVI International Clay Conference – Clays, from the oceans to space 160, 206–216. https://doi.org/10.1016/j.clay.2017.12.034

Masurat, P., Eriksson, S., Pedersen, K., 2010. Evidence of indigenous sulphate-reducing bacteria in commercial Wyoming bentonite MX-80. Applied Clay Science, Advanced smectitic clay research 47, 51–57. https://doi.org/10.1016/j.clay.2008.07.002

Monier, J.-M., Lindow, S.E., 2003. *Pseudomonas syringae* responds to the environment on leaves by cell size reduction. Phytopathology 93, 1209–1216. https://doi.org/10.1094/PHYTO.2003.93.10.1209

Necib, S., Diomidis, N., Keech, P., Nakayama, M., 2017. Corrosion of carbon steel in clay environments relevant to radioactive waste geological disposals, Mont Terri rock laboratory (Switzerland). Swiss J Geosci 110, 329–342. https://doi.org/10.1007/s00015-016-0259-7

Němeček, J., Dolinová, I., Macháčková, J., Špánek, R., Ševců, A., Lederer, T., Černík, M., 2017. Stratification of chlorinated ethenes natural attenuation in an alluvial aquifer assessed by hydrochemical and biomolecular tools. Chemosphere 184, 1157–1167. https://doi.org/10.1016/j.chemosphere.2017.06.100

Oksanen, J., Blanchet, F.G., Friendly, M., Kindt, R., Legendre, P., McGlinn, D., Minchin, P.R., O'Hara, R.B., Simpson, G.L., Solymos, P., Stevens, M.H.H., Szoecs, E., Wagner, H., 2019. vegan: Community Ecology Package.

Pedersen, K., 2010. Analysis of copper corrosion in compacted bentonite clay as a function of clay density and growth conditions for sulfate-reducing bacteria. J. Appl. Microbiol. 108, 1094–1104. https://doi.org/10.1111/j.1365-2672.2009.04629.x

Pedersen, K., 1999. Subterranean microorganisms and radioactive waste disposal in Sweden. Engineering Geology 52, 163–176. https://doi.org/10.1016/S0013-7952(99)00004-6

Pedersen, K., Bengtsson, A., Blom, A., Johansson, L., Taborowski, T., 2017. Mobility and reactivity of sulphide in bentonite clays – Implications for engineered bentonite barriers in geological repositories for radioactive wastes. Applied Clay Science 146, 495–502. https://doi.org/10.1016/j.clay.2017.07.003

Pedersen, K., Motamedi, M., Karnland, O., Sandén, T., 2000a. Mixing and sulphate-reducing activity of bacteria in swelling, compacted bentonite clay under high-level radioactive waste repository conditions. Journal of Applied Microbiology 89, 1038–1047. https://doi.org/10.1046/j.1365-2672.2000.01212.x

Pedersen, K., Motamedi, M., Karnland, O., Sanden, T., 2000b. Cultivability of microorganisms introduced into a compacted bentonite clay buffer under high-level radioactive waste repository conditions. Engineering geology 58, 149–161.

Pentráková, L., Su, K., Pentrák, M., Stucki, J.W., 2013. A review of microbial redox interactions with structural Fe in clay minerals. Clay Minerals 48, 543–560. https://doi.org/10.1180/claymin.2013.048.3.10

Perdrial, J.N., Warr, L.N., Perdrial, N., Lett, M.-C., Elsass, F., 2009. Interaction between smectite and bacteria: Implications for bentonite as backfill material in the disposal of nuclear waste. Chemical Geology 264, 281–294. https://doi.org/10.1016/j.chemgeo.2009.03.012

Petushkova, E.P., Tsygankov, A.A., 2017. Acetate metabolism in the purple non-sulfur bacterium *Rhodobacter capsulatus*. Biochemistry Moscow 82, 587–605. https://doi.org/10.1134/S0006297917050078

Poser, A., Vogt, C., Knöller, K., Ahlheim, J., Weiss, H., Kleinsteuber, S., Richnow, H.-H., 2014. Stable sulfur and oxygen isotope fractionation of anoxic sulfide oxidation by two different enzymatic pathways. Environ. Sci. Technol. 48, 9094–9102. https://doi.org/10.1021/es404808r

Povedano-Priego, C., Jroundi, F., Lopez-Fernandez, M., Sánchez-Castro, I., Martin-Sánchez, I., Huertas, F.J., Merroun, M.L., 2019. Shifts in bentonite bacterial community and mineralogy in response to uranium and glycerol-2-phosphate exposure. Science of The Total Environment 692, 219–232. https://doi.org/10.1016/j.scitotenv.2019.07.228

Quentmeier, A., Hellwig, P., Bardischewsky, F., Grelle, G., Kraft, R., Friedrich, C.G., 2003. Sulfur oxidation in *Paracoccus pantotrophus*: interaction of the sulfur-binding protein SoxYZ with the dimanganese SoxB protein. Biochem. Biophys. Res. Commun. 312, 1011–1018. https://doi.org/10.1016/j.bbrc.2003.11.021

Ratto, M., Itavaara, M., 2012. Microbial activity in bentonite buffers. Literature study (No. VTT-TECHNOLOGY–20). VTT Technical Research Centre of Finland.

Rickard, D., 2012. Chapter 3 - Sedimentary iron biogeochemistry, in: Rickard, D. (Ed.), Developments in sedimentology, sulfidic sediments and sedimentary rocks. Elsevier, pp. 85–119. https://doi.org/10.1016/B978-0-444-52989-3.00003-9

Robertson, C.E., Harris, J.K., Wagner, B.D., Granger, D., Browne, K., Tatem, B., Feazel, L.M., Park, K., Pace, N.R., Frank, D.N., 2013. Explicet: graphical user interface software for metadata-driven management, analysis and visualization of microbiome data. Bioinformatics 29, 3100–3101. https://doi.org/10.1093/bioinformatics/btt526

Sahin, N., Portillo Guisado, M. del C., Kato, Y., Schumann, P., 2009. Description of *Oxalicibacterium horti* sp. nov. and *Oxalicibacterium faecigallinarum* sp. nov., new aerobic, yellow-pigmented, oxalotrophic bacteria.

Sajjad, W., Bhatti, T.M., Hasan, F., Khan, S., Badshah, M., 2016. Characterization of sulfur-oxidizing bacteria isolated from acid mine drainage and black shale samples. Pakistan Journal of Botany 48, 1253–1262.

Sánchez-Castro, I., Ruiz-Fresneda, M.A., Bakkali, M., Kämpfer, P., Glaeser, S.P., Busse, H.J., López-Fernández, M., Martínez-Rodríguez, P., Merroun, M.L., 2017. *Stenotrophomonas bentonitica* sp. nov., isolated from bentonite formations. Int. J. Syst. Evol. Microbiol. 67, 2779–2786. https://doi.org/10.1099/ijsem.0.002016

Schloss, P.D., Westcott, S.L., Ryabin, T., Hall, J.R., Hartmann, M., Hollister, E.B., Lesniewski, R.A., Oakley, B.B., Parks, D.H., Robinson, C.J., Sahl, J.W., Stres, B., Thallinger, G.G., Horn, D.J.V., Weber, C.F., 2009. Introducing mothur: Open-source, platform-independent, community-supported software for describing and comparing microbial communities. Appl. Environ. Microbiol. 75, 7537–7541. https://doi.org/10.1128/AEM.01541-09

Schwartz, E., Henne, A., Cramm, R., Eitinger, T., Friedrich, B., Gottschalk, G., 2003. Complete nucleotide sequence of pHG1: a *Ralstonia eutropha* H16 megaplasmid encoding key enzymes of H(2)-based ithoautotrophy and anaerobiosis. J. Mol. Biol. 332, 369–383. https://doi.org/10.1016/s0022-2836(03)00894-5

Shannon, P., Markiel, A., Ozier, O., Baliga, N.S., Wang, J.T., Ramage, D., Amin, N., Schwikowski, B., Ideker, T., 2003. Cytoscape: a software environment for integrated models of biomolecular interaction networks. Genome Res. 13, 2498–2504. https://doi.org/10.1101/gr.1239303

Stone, W., Kroukamp, O., Moes, A., McKelvie, J., Korber, D.R., Wolfaardt, G.M., 2016a. Measuring microbial metabolism in atypical environments: Bentonite in used nuclear fuel storage. J. Microbiol. Methods 120, 79–90. https://doi.org/10.1016/j.mimet.2015.11.006

Stone, W., Kroukamp, O., Moes, A., McKelvie, J., Korber, D.R., Wolfaardt, G.M., 2016b. Measuring microbial metabolism in atypical environments: Bentonite in used nuclear fuel storage. J. Microbiol. Methods 120, 79–90. https://doi.org/10.1016/j.mimet.2015.11.006

Stroes-Gascoyne, S., Hamon, C.J., Maak, P., 2011. Limits to the use of highly compacted bentonite as a deterrent for microbiologically influenced corrosion in a nuclear fuel waste repository. Physics and Chemistry of the Earth, Parts A/B/C, Clays in Natural & Engineered Barriers for Radioactive Waste Confinement 36, 1630–1638. https://doi.org/10.1016/j.pce.2011.07.085

Stroes-Gascoyne, S., Hamon, C.J., Maak, P., Russell, S., 2010. The effects of the physical properties of highly compacted smectitic clay (bentonite) on the culturability of indigenous microorganisms. Applied Clay Science 47, 155–162. https://doi.org/10.1016/j.clay.2008.06.010

Swanner, E.D., Nell, R.M., Templeton, A.S., 2011. *Ralstonia* species mediate Fe-oxidation in circumneutral, metal-rich subsurface fluids of Henderson mine, CO. Chemical Geology 284, 339–350. https://doi.org/10.1016/j.chemgeo.2011.03.015

Tian, H., Gao, P., Chen, Z., Li, Yanshu, Li, Yan, Wang, Y., Zhou, J., Li, G., Ma, T., 2017. Compositions and abundances of sulfate-reducing and sulfur-oxidizing microorganisms in water-flooded petroleum reservoirs with different temperatures in China. Front Microbiol 8. https://doi.org/10.3389/fmicb.2017.00143

Timmers, P.H.A., Vavourakis, C.D., Kleerebezem, R., Damsté, J.S.S., Muyzer, G., Stams, A.J.M., Sorokin, D.Y., Plugge, C.M., 2018. Metabolism and occurrence of methanogenic and sulfate-reducing syntrophic acetate oxidizing communities in haloalkaline environments. Front Microbiol 9, 3039. https://doi.org/10.3389/fmicb.2018.03039

Valencia-Cantero, E., Hernández-Calderón, E., Velázquez-Becerra, C., López-Meza, J.E., Alfaro-Cuevas, R., López-Bucio, J., 2007. Role of dissimilatory fermentative iron-reducing bacteria in Fe uptake by common bean (*Phaseolus vulgaris* L.) plants grown in alkaline soil. Plant Soil 291, 263–273. https://doi.org/10.1007/s11104-007-9191-y

Valencia-Cantero, E., Peña-Cabriales, J.J., 2014. Effects of iron-reducing bacteria on carbon steel corrosion induced by thermophilic sulfate-reducing consortia. J. Microbiol. Biotechnol. 24, 280–286. https://doi.org/10.4014/jmb.1310.10002

van den Brand, T.P.H., Roest, K., Brdjanovic, D., Chen, G.H., van Loosdrecht, M.C.M., 2014. Influence of acetate and propionate on sulphate-reducing bacteria activity. J. Appl. Microbiol. 117, 1839–1847. https://doi.org/10.1111/jam.12661

Warnes, G.R., Bolker, B., Bonebakker, L., Gentleman, R., Liaw, W.H.A., Lumley, T., Maechler, M., Magnusson, A., Moeller, S., Schwartz, M., Venables, B., 2019. gplots: Various R Programming Tools for Plotting Data.

Xiaodong, Z., Yan, C., Jing, S., Jie, Y., Jie, L., Dongyu, S., Shuai, W., 2019. Influence of *Pseudomonas aeruginosa* and sulfate-reducing bacteria composite on the corrosion behaviour of brass. Int. J. Electrochem. Sci. 6468–6477. https://doi.org/10.20964/2019.07.19

Yang, S., Li, S., Jia, X., 2019. Production of medium chain length polyhydroxyalkanoate from acetate by engineered *Pseudomonas putida* KT2440. J Ind Microbiol Biotechnol 46, 793–800. https://doi.org/10.1007/s10295-019-02159-5

8. SUPPLEMENTARY TABLES

Supplementary Table 1. Bacterial phyla of compacted bentonite after 24 months of anaerobic incubation and their corresponding p-values. One-way ANOVA test, using a significance level of 0.05, was used to look for significant differences in the alpha diversity between the samples. Red values represent p-value < 0.05.

Phyla	p-value
Actinobacteria	0.339
Proteobacteria	0.706
Firmicutes	0.585
Chloroflexi	0.524
Bacteroidetes	0.987
Cyanobacteria	0.545
Planctomycetes	0.748
Acidobacteria	0.480
Gemmatimonadetes	0.881
Verrucomicrobia	0.454
unclassified	0.369
Deinococcus-Thermus	0.434
Patescibacteria	0.609
BRC1	0.294
Thaumarchaeota	0.492
Armatimonadetes	0.604
Nitrospirae	0.209
Dadabacteria	0.974
Epsilonbacteraeota	0.663
Hydrogenedentes	0.414
Nitrospinae	0.652
Eukaryota	0.709
FBP	0.614
Fusobacteria	0.651
Chlamydiae	0.797
Elusimicrobia	0.054
Nanoarchaeaeota	0.629
Dependentiae	0.510
Diapherotrites	0.510
Euryarchaeota	0.736
Fibrobacteres	0.510
Omnitrophicaeota	0.510
PAUC34f	0.510
Spirochaetes	0.510
WOR-1	0.510

Supplementary Table 2. Bacterial families/genera of compacted bentonite after 24 months of anaerobic incubation and their corresponding p-values. One-way ANOVA test, using a significance level of 0.05, was used to look for significant differences in the alpha diversity between the samples. Red values represent p-value < 0.05.

Families/Genera	**p-value**	**Families/Genera**	**p-value**
Pseudarthrobacter	0.224	unclassified Frankiales	0.128
Nocardioides	0.157	*Robertkochia*	0.772
Arthrobacter	0.352	*Polycyclovorans*	0.920
Marmoricola	0.193	*Chungangia*	0.668
Geobacillus	0.613	*Herbaspirillum*	0.546
unclassified Gammaproteobacteria	0.949	unclassified Planctomycetales	0.391
Mesorhizobium	0.937	*Aminobacter*	0.843
unclassified Actinomarinales	0.841	*Truepera*	0.433
Ralstonia	0.361	*Gaiella*	0.347
Promicromonospora	0.530	*Saccharopolyspora*	0.436
unclassified Chloroplast	0.572	unclassified *Anaerolineaceae*	0.911
unclassified Gitt-GS-136	0.416	unclassified Alphaproteobacteria	0.162
Delftia	0.459	unclassified *Burkholderiaceae*	0.454
unclassified Subgroup 6	0.353	unclassified *Micrococcaceae*	0.475
Rubellimicrobium	0.693	*Ellin6067*	0.920
Paracoccus	0.912	*Planctopirus*	0.781
Sphingomonas	0.405	*Caldibacillus*	0.645
IheB3-7	0.423	*Herpetosiphon*	0.715
unclassified Acidimicrobiia	0.772	*Myceligenerans*	0.928
Stenotrophomonas	0.274	unclassified BRC1	0.283
unclassified JG30-KF-CM45	0.357	unclassified Microtrichales	0.552
unclassified Chloroflexi	0.290	*Adhaeribacter*	0.847
Thermicanus	0.391	*Lysobacter*	0.648
Ochrobactrum	0.491	*Phycisphaeraceae* I-8	0.412
unclassified Mitochondria	0.454	unclassified Gemmatimonadaceae	0.950
Bacillus	0.473	unclassified *Gimesiaceae*	0.818
unclassified *Microscillaceae*	0.995	unclassified JG30-KF-CM66	0.268
Pontibacter	0.450	unclassified *Longimicrobiaceae*	0.515
Streptomyces	0.842	unclassified *Pirellulaceae*	0.822
unclassified *Sphingomonadaceae*	0.611	*Altererythrobacter*	0.507
unclassified KD4-96	0.267	*Glycomyces*	0.527
Hydrogenophilus	0.642	Ellin6055	0.078
Olivibacter	0.937	*Haliangium*	0.544
Pseudomonas	0.619	*Kocuria*	0.759
Noviherbaspirillum	0.432	*Novosphingobium*	0.908
Pararhizobium-Rhizobium	0.396	*Pseudorhizobium*	0.790
unclassified	0.367	unclassified Armatimonadales	0.502
Amycolatopsis	0.257	*Gemmata*	0.505
MND1	0.578	*Pseudonocardia*	0.488
Cesiribacter	0.444	unclassified Bacillales	0.957

Chthoniobacter	0.485	*Flavisolibacter*	0.882
Skermanella	0.953	*Rehaibacterium*	0.280
Caenimonas	0.397	unclassified *Caldilineaceae*	0.577
Porphyrobacter	0.984	*Pseudosphingobacterium*	0.177
Gemmatimonas	0.716	*Pseudoxanthomonas*	0.537
Nitrosomonadaceae oc32	0.579	*Belnapia*	0.451
Ramlibacter	0.342	*Cytophaga*	0.401
unclassified *Ilumatobacteraceae*	0.596	*Luteolibacter*	0.265
unclassified *Nitriliruptoraceae*	0.704	*Pirellula*	0.209
Microvirga	0.563	*Sulfurifustis*	0.637

Supplementary Table 3. Bacterial phyla of compacted bentonite at time 0 and their corresponding relative abundances (%) in each treatment.

Phlya	**Compacted bentonite at time 0**			
	A1 (%)	**A2 (%)**	**C1 (%)**	**C2 (%)**
Actinobacteria	57.78	47.73	52.21	46.90
Proteobacteria	25.36	30.34	27.71	29.60
Bacteroidetes	6.53	10.34	6.40	8.87
Firmicutes	1.34	2.39	5.00	7.28
Chloroflexi	2.80	2.12	2.60	2.80
Planctomycetes	1.14	1.77	1.32	0.76
Verrucomicrobia	0.73	1.02	0.79	0.62
Acidobacteria	0.48	0.77	0.49	0.48
Gemmatimonadetes	0.56	0.36	0.59	0.29
Chlamydiae	0.11	0.52	0.30	0.28
Euryarchaeota	0.52	0.15	0.30	0.02
Candidatus Saccharibacteria	0.14	0.34	0.18	0.28
Deinococcus-Thermus	0.28	0.17	0.24	0.20
Ignavibacteriae	0.18	0.23	0.14	0.26
Armatimonadetes	0.12	0.13	0.22	0.21
Synergistetes	0.32	0.17	0.17	0.08
Nitrospirae	0.26	0.18	0.13	0.12
Parcubacteria	0.20	0.19	0.15	0.11
Cyanobacteria	0.16	0.08	0.09	0.12
Thaumarchaeota	0.12	0.11	0.07	0.11
BRC1	0.06	0.17	0.11	0.04
Hydrogenedentes	0.15	0.06	0.11	0.07
Thermodesulfobacteria	0.12	0.10	0.10	0.03
candidate division WPS-1	0.08	0.11	0.07	0.08
candidate division WPS-2	0.06	0.11	0.09	0.03
Aquificae	0.08	0.09	0.03	0.01
Microgenomates	0.05	0.10	0.02	0.01
Tenericutes	0.00	0.00	0.08	0.18
Deferribacteres	0.04	0.07	0.02	0.04
Fibrobacteres	0.02	0.01	0.12	0.04
Thermotogae	0.10	0.01	0.05	0.02
Candidatus Calescamantes	0.03	0.01	0.02	0.00
Crenarchaeota	0.06	0.00	0.01	0.00
Elusimicrobia	0.03	0.01	0.03	0.01
Nitrospinae	0.00	0.03	0.01	0.04
Omnitrophica	0.02	0.00	0.05	0.00

Supplementary Table 4. Bacterial phyla of compacted bentonite after 24 months of anaerobic incubation and their corresponding relative abundances (%) in each treatment.

Phlya	**Relative abundances in compacted bentonite after 24 months of incubation (%)**										
	1.5A_1	**1.5A_2**	**1.5A_3**	**1.5C_1**	**1.5C_2**	**1.5C_3**	**1.7A_1**	**1.7A_3**	**1.7C_1**	**1.7C_2**	**1.7C_3**
Actinobacteria	60.05	56.68	55.16	63.69	53.38	59.08	46.53	57.98	52.62	55.86	49.22
Proteobacteria	17.39	25.39	25.56	20.26	23.05	20.78	23.81	24.23	24.03	22.76	23.27
Firmicutes	15.15	0.19	2.04	1.80	0.31	0.04	18.22	0.35	8.42	0.06	0.05
Chloroflexi	1.43	5.50	4.59	3.77	6.15	5.63	2.77	4.77	5.23	6.14	4.45
Bacteroidetes	2.96	4.43	4.63	2.84	4.02	5.55	4.24	4.40	2.54	4.90	4.54
Cyanobacteria	0.42	0.80	0.44	2.27	1.32	1.12	1.60	1.20	1.03	0.73	12.67
Planctomycetes	0.59	1.99	2.49	1.02	3.27	2.48	0.77	1.88	1.32	2.67	1.46
Acidobacteria	0.56	1.61	1.50	1.31	2.62	1.39	0.87	1.26	1.61	2.29	1.21
Gemmatimonadetes	0.29	0.71	0.98	0.66	0.60	0.91	0.42	0.86	0.59	0.49	0.62
Verrucomicrobia	0.12	0.97	0.19	0.52	1.55	1.04	0.00	0.93	0.43	1.43	0.89
unclassified	0.09	0.27	0.45	0.34	0.14	0.21	0.09	0.69	1.04	0.56	0.29
Deinococcus-Thermus	0.16	0.48	0.09	0.22	1.15	0.66	0.00	0.50	0.00	0.58	0.39
Patescibacteria	0.16	0.13	0.75	0.40	0.63	0.12	0.02	0.20	0.23	0.28	0.19
BRC1	0.00	0.19	0.25	0.24	0.33	0.28	0.00	0.14	0.63	0.25	0.14
Thaumarchaeota	0.00	0.18	0.14	0.11	0.59	0.21	0.30	0.23	0.17	0.34	0.18
Armatimonadetes	0.45	0.25	0.10	0.17	0.46	0.25	0.00	0.19	0.00	0.39	0.18
Nitrospirae	0.00	0.02	0.04	0.00	0.00	0.00	0.36	0.01	0.00	0.00	0.01
Dadabacteria	0.00	0.07	0.14	0.00	0.13	0.06	0.00	0.12	0.00	0.06	0.08
Epsilonbacteraeota	0.10	0.00	0.00	0.23	0.00	0.00	0.00	0.00	0.00	0.02	0.00
Hydrogenedentes	0.00	0.04	0.11	0.03	0.08	0.02	0.00	0.00	0.00	0.00	0.04
Nitrospinae	0.00	0.02	0.17	0.00	0.03	0.02	0.00	0.02	0.00	0.03	0.05
Eukaryota	0.00	0.03	0.00	0.00	0.09	0.02	0.00	0.01	0.00	0.09	0.01
FBP	0.00	0.03	0.01	0.00	0.06	0.05	0.00	0.03	0.00	0.03	0.03

Fusobacteria	0.07	0.00	0.00	0.00	0.00	0.00	0.00	0.00	0.12	0.00	0.00
Chlamydiae	0.00	0.01	0.04	0.01	0.00	0.03	0.00	0.01	0.00	0.02	0.00
Elusimicrobia	0.00	0.01	0.00	0.04	0.02	0.01	0.00	0.00	0.00	0.00	0.01
Nanoarchaeaeota	0.00	0.00	0.07	0.01	0.01	0.00	0.00	0.00	0.00	0.01	0.00
Dependentiae	0.00	0.01	0.00	0.00	0.00	0.00	0.00	0.00	0.00	0.00	0.00
Diapherotrites	0.00	0.00	0.00	0.02	0.00	0.00	0.00	0.00	0.00	0.00	0.00
Euryarchaeota	0.00	0.00	0.01	0.00	0.00	0.00	0.00	0.01	0.00	0.00	0.02
Fibrobacteres	0.00	0.00	0.00	0.02	0.00	0.00	0.00	0.00	0.00	0.00	0.00
Omnitrophicaeota	0.00	0.00	0.00	0.02	0.00	0.00	0.00	0.00	0.00	0.00	0.00
PAUC34f	0.00	0.00	0.01	0.00	0.00	0.00	0.00	0.00	0.00	0.00	0.00
Spirochaetes	0.00	0.00	0.04	0.00	0.00	0.00	0.00	0.00	0.00	0.00	0.00
WOR-1	0.00	0.00	0.03	0.00	0.00	0.00	0.00	0.00	0.00	0.00	0.00

Supplementary Table 5. Bacterial classes of compacted bentonite at time 0 and their corresponding relative abundances (%) in each treatment.

Classes	Compacted bentonite at time 0			
	A1 (%)	A2 (%)	C1 (%)	C2 (%)
Actinobacteria	12.65	8.93	10.70	8.12
Gammaproteobacteria	1.95	2.76	2.19	2.11
Alphaproteobacteria	1.68	0.90	1.56	1.62
Betaproteobacteria	1.56	1.69	1.62	1.22
Cytophagia	0.56	0.72	0.55	0.60
Sphingobacteriia	0.41	0.72	0.41	0.42
Bacilli	0.08	0.18	0.79	1.15
Deltaproteobacteria	0.52	0.43	0.48	0.25
Bacteroidetes incertae sedis	0.35	0.26	0.23	0.30
Anaerolineae	0.32	0.24	0.26	0.28
Flavobacteriia	0.14	0.26	0.12	0.23
Thermoleophilia	0.39	0.21	0.33	0.13
Planctomycetia	0.24	0.33	0.27	0.12
Clostridia	0.22	0.25	0.24	0.12
Caldilineae	0.11	0.07	0.10	0.07
Gemmatimonadetes	0.13	0.07	0.12	0.05
Thermomicrobia	0.09	0.04	0.09	0.05
Chlamydiia	0.02	0.10	0.06	0.05
Acidobacteria	0.04	0.09	0.04	0.03
Verrucomicrobiae	0.04	0.09	0.06	0.02
Acidobacteria Gp6	0.05	0.03	0.05	0.03
Saccharibacteria_genera_incertae_sedis	0.03	0.07	0.04	0.05
Deinococci	0.06	0.03	0.05	0.04
Ignavibacteria	0.04	0.04	0.03	0.05
Synergistia	0.07	0.03	0.04	0.01
Spartobacteria	0.05	0.04	0.05	0.02
Nitrospira	0.06	0.03	0.03	0.02
Opitutae	0.03	0.03	0.03	0.04
Ardenticatenia	0.03	0.02	0.04	0.03
Verrucomicrobia Subdivision 3	0.04	0.04	0.03	0.03
Parcubacteria_incertae_sedis	0.04	0.04	0.03	0.02
Chloroplast	0.04	0.02	0.02	0.02
Chloroflexia	0.03	0.02	0.03	0.03
Halobacteria	0.06	0.01	0.03	0.00
Thermoplasmata	0.04	0.01	0.02	0.00
Armatimonadia	0.02	0.02	0.02	0.02
Bacteroidia	0.02	0.02	0.05	0.01
BRC1_incertae_sedis	0.01	0.03	0.02	0.01
Candidatus Hydrogenedens	0.03	0.01	0.02	0.01

Armatimonadetes	0.01	0.01	0.03	0.01
Thermodesulfobacteria	0.03	0.02	0.02	0.01
Negativicutes	0.01	0.03	0.02	0.01
Nitrososphaerales	0.02	0.01	0.01	0.01
WPS-1_genera_incertae_sedis	0.02	0.02	0.01	0.01
Acidobacteria Gp10	0.01	0.01	0.01	0.01
WPS-2_genera_incertae_sedis	0.01	0.02	0.02	0.01
Dehalococcoidia	0.01	0.01	0.01	0.01
Phycisphaerae	0.02	0.01	0.01	0.01
Epsilonproteobacteria	0.01	0.02	0.01	0.00
Microgenomates_genera_incertae_sedis	0.01	0.02	0.00	0.00
Aquificae	0.02	0.02	0.01	0.00
Mollicutes	0.00	0.00	0.02	0.03
Thermotogae	0.02	0.00	0.01	0.00
Chitinivibrionia	0.00	0.00	0.03	0.01
Deferribacteres	0.01	0.01	0.00	0.01
Methanopyri	0.02	0.01	0.02	0.00
Dehalococcoidetes	0.02	0.00	0.01	0.00
Thermoflexia	0.01	0.01	0.01	0.00
Nitrosopumilales	0.01	0.01	0.00	0.01
Omnitrophica_genera_incertae_sedis	0.00	0.00	0.01	0.00
Thermoprotei	0.01	0.00	0.00	0.00
Holophagae	0.00	0.01	0.00	0.00
Acidobacteria Gp1	0.00	0.00	0.00	0.00
Candidatus Calescibacterium	0.01	0.00	0.01	0.00
Elusimicrobia	0.01	0.00	0.01	0.00
Nitrospinia	0.00	0.01	0.00	0.01
Ktedonobacteria	0.00	0.00	0.00	0.00

Supplementary Table 6. Bacterial classes of compacted bentonite after 24 months of anaerobic incubation and their corresponding relative abundances (%) in each treatment.

Classes	Relative abundances in compacted bentonite after 24 months of incubation (%)										
	1.5A_1	**1.5A_2**	**1.5A_3**	**1.5C_1**	**1.5C_2**	**1.5C_3**	**1.7A_1**	**1.7A_3**	**1.7C_1**	**1.7C_2**	**1.7C_3**
Actinobacteria	56.50	52.52	49.49	58.86	49.62	54.55	44.42	52.80	49.11	51.78	44.41
Gammaproteobacteria	9.35	11.87	12.57	10.43	12.70	7.28	14.72	11.01	15.16	11.83	10.29
Alphaproteobacteria	7.56	12.89	12.52	9.35	9.87	12.92	9.09	12.53	8.58	10.31	12.38
Bacilli	15.15	0.13	1.86	1.55	0.26	0.04	17.07	0.22	8.42	0.02	0.01
Acidimicrobiia	2.81	3.62	4.92	4.21	3.45	3.94	1.70	4.41	2.74	3.44	3.98
Bacteroidia	1.03	4.34	4.04	2.75	3.92	5.49	0.77	4.33	1.88	4.85	4.45
Oxyphotobacteria	0.42	0.79	0.44	2.26	1.30	1.12	1.60	1.20	0.83	0.73	12.66
Gitt-GS-136	0.41	2.13	1.34	1.34	1.88	2.16	0.67	1.55	2.06	2.16	1.51
Planctomycetacia	0.59	1.81	2.03	0.94	2.92	2.15	0.00	1.68	1.21	2.35	1.31
Subgroup_6	0.46	1.30	1.14	1.02	2.14	1.13	0.81	1.01	1.61	1.84	1.03
Chloroflexia	0.44	1.13	0.73	0.70	1.57	1.39	1.48	1.06	0.45	1.56	0.88
Ignavibacteria	1.93	0.07	0.59	0.08	0.10	0.06	3.47	0.08	0.67	0.05	0.08
Verrucomicrobiae	0.12	0.97	0.19	0.52	1.55	1.04	0.00	0.93	0.43	1.43	0.89
KD4-96	0.11	0.66	0.45	0.42	0.75	0.66	0.00	0.48	1.15	0.65	0.50
Thermoleophilia	0.59	0.38	0.55	0.45	0.27	0.38	0.28	0.50	0.58	0.47	0.59
Anaerolineae	0.07	0.68	0.65	0.51	0.59	0.41	0.01	0.71	0.11	0.62	0.67
Unclassified	0.09	0.27	0.45	0.34	0.14	0.21	0.09	0.69	1.04	0.56	0.29
OLB14	0.00	0.47	0.42	0.40	0.61	0.41	0.41	0.37	0.35	0.51	0.44
Deltaproteobacteria	0.44	0.53	0.44	0.37	0.46	0.52	0.00	0.49	0.21	0.47	0.48
Gemmatimonadetes	0.10	0.38	0.59	0.40	0.33	0.55	0.18	0.50	0.38	0.27	0.36
Deinococci	0.16	0.48	0.09	0.22	1.15	0.66	0.00	0.50	0.00	0.58	0.39
Phycisphaerae	0.00	0.16	0.45	0.07	0.31	0.32	0.77	0.19	0.11	0.31	0.14

P2-11E	0.00	0.17	0.31	0.24	0.33	0.47	0.00	0.39	0.51	0.36	0.30
unclassified BRC1	0.00	0.19	0.25	0.24	0.33	0.28	0.00	0.14	0.63	0.25	0.14
Nitrososphaeria	0.00	0.18	0.14	0.11	0.59	0.21	0.30	0.23	0.17	0.34	0.18
JG30-KF-CM66	0.33	0.14	0.48	0.02	0.29	0.05	0.00	0.12	0.30	0.18	0.07
Longimicrobia	0.07	0.23	0.27	0.14	0.21	0.27	0.24	0.26	0.11	0.13	0.21
Clostridia	0.00	0.00	0.10	0.14	0.03	0.00	1.15	0.03	0.00	0.01	0.00
Armatimonadia	0.27	0.25	0.08	0.17	0.46	0.24	0.00	0.17	0.00	0.35	0.17
Nitriliruptoria	0.08	0.13	0.13	0.13	0.03	0.21	0.13	0.21	0.15	0.12	0.18
Blastocatellia_(Subgroup_4)	0.00	0.21	0.25	0.06	0.32	0.17	0.00	0.13	0.00	0.35	0.10
Saccharimonadia	0.00	0.04	0.22	0.09	0.53	0.09	0.02	0.12	0.18	0.19	0.09
Dehalococcoidia	0.00	0.06	0.09	0.09	0.06	0.02	0.19	0.04	0.29	0.05	0.06
unclassified Proteobacteria	0.04	0.11	0.03	0.12	0.02	0.06	0.00	0.20	0.08	0.16	0.13
ABY1	0.00	0.08	0.17	0.16	0.10	0.03	0.00	0.06	0.00	0.08	0.08
Dadabacteriia	0.00	0.07	0.14	0.00	0.13	0.06	0.00	0.12	0.00	0.06	0.08
Subgroup_17	0.00	0.04	0.08	0.19	0.16	0.05	0.00	0.10	0.00	0.07	0.05
BD2-11_terrestrial_group	0.02	0.10	0.07	0.06	0.05	0.03	0.00	0.08	0.09	0.04	0.03
Parcubacteria	0.05	0.01	0.27	0.10	0.00	0.00	0.00	0.01	0.00	0.00	0.00
Thermodesulfovibrionia	0.00	0.00	0.04	0.00	0.00	0.00	0.34	0.00	0.00	0.00	0.00
Campylobacteria	0.10	0.00	0.00	0.23	0.00	0.00	0.00	0.00	0.00	0.02	0.00
Hydrogenedentia	0.00	0.04	0.11	0.03	0.08	0.02	0.00	0.00	0.00	0.00	0.04
Melainabacteria	0.00	0.01	0.00	0.01	0.02	0.00	0.00	0.00	0.21	0.00	0.01
P9X2b3D02	0.00	0.02	0.17	0.00	0.03	0.02	0.00	0.02	0.00	0.02	0.05
TK10	0.07	0.02	0.05	0.04	0.06	0.05	0.00	0.04	0.00	0.05	0.00
unclassified Armatimonadetes	0.18	0.00	0.02	0.00	0.00	0.01	0.00	0.02	0.00	0.03	0.01
unclassified Firmicutes	0.00	0.07	0.08	0.05	0.02	0.00	0.00	0.09	0.00	0.03	0.05
Acidobacteriia	0.00	0.04	0.02	0.02	0.00	0.04	0.00	0.02	0.00	0.02	0.03

Fusobacteriia	0.07	0.00	0.00	0.00	0.00	0.00	0.00	0.00	0.12	0.00	0.00
Microgenomatia	0.11	0.00	0.01	0.02	0.00	0.00	0.00	0.02	0.05	0.01	0.01
Rubrobacteria	0.00	0.02	0.05	0.00	0.00	0.00	0.00	0.05	0.04	0.05	0.04
S0134_terrestrial_group	0.06	0.00	0.04	0.03	0.01	0.07	0.00	0.02	0.00	0.03	0.02
unclassified	0.00	0.03	0.00	0.00	0.09	0.02	0.00	0.01	0.00	0.09	0.01
unclassified FBP	0.00	0.03	0.01	0.00	0.06	0.05	0.00	0.03	0.00	0.03	0.03
0319-7L14	0.02	0.00	0.03	0.00	0.00	0.00	0.00	0.02	0.00	0.01	0.03
Chlamydiae	0.00	0.01	0.04	0.01	0.00	0.03	0.00	0.01	0.00	0.02	0.00
Elusimicrobia	0.00	0.01	0.00	0.03	0.02	0.02	0.00	0.00	0.00	0.00	0.01
Holophagae	0.10	0.01	0.00	0.00	0.00	0.00	0.00	0.00	0.00	0.00	0.00
Thermoanaerobaculia	0.00	0.01	0.01	0.00	0.00	0.00	0.06	0.00	0.00	0.02	0.00
unclassified Chloroflexi	0.00	0.03	0.08	0.00	0.00	0.00	0.00	0.00	0.00	0.00	0.02
unclassified Gemmatimonadetes	0.04	0.00	0.01	0.03	0.00	0.00	0.00	0.00	0.00	0.02	0.00
unclassified Patescibacteria	0.00	0.00	0.08	0.00	0.00	0.00	0.00	0.00	0.00	0.00	0.00
Woesearchaeia	0.00	0.00	0.07	0.01	0.01	0.00	0.00	0.00	0.00	0.01	0.00
4-29-1	0.00	0.00	0.00	0.00	0.00	0.00	0.02	0.00	0.00	0.00	0.00
Babeliae	0.00	0.01	0.00	0.00	0.00	0.00	0.00	0.00	0.00	0.00	0.00
Chitinivibrionia	0.00	0.00	0.00	0.02	0.00	0.00	0.00	0.00	0.00	0.00	0.00
Fimbriimonadia	0.00	0.00	0.00	0.00	0.00	0.00	0.00	0.01	0.00	0.00	0.00
Iainarchaeia	0.00	0.00	0.00	0.02	0.00	0.00	0.00	0.00	0.00	0.00	0.00
Kazania	0.00	0.00	0.00	0.03	0.00	0.00	0.00	0.00	0.00	0.00	0.00
Ktedonobacteria	0.00	0.00	0.00	0.00	0.00	0.01	0.00	0.00	0.00	0.00	0.01
Lineage_IIa	0.00	0.00	0.00	0.02	0.00	0.00	0.00	0.00	0.00	0.00	0.00
MB-A2-108	0.05	0.00	0.00	0.00	0.00	0.00	0.00	0.00	0.00	0.00	0.00
Negativicutes	0.00	0.00	0.00	0.06	0.00	0.00	0.00	0.00	0.00	0.00	0.00
Nitrospinia	0.00	0.00	0.00	0.00	0.00	0.00	0.00	0.01	0.00	0.01	0.00
Nitrospira	0.00	0.02	0.00	0.00	0.00	0.00	0.00	0.01	0.00	0.00	0.01

Supplementary Table 7. Bacterial genera of compacted bentonite at time 0 and their corresponding relative abundances (%) in each treatment.

Genera	Compacted bentonite at time 0			
	A1 (%)	A2 (%)	C1 (%)	C2 (%)
Arthrobacter	25.62	24.99	18.80	18.15
Nocardioides	5.85	5.90	9.45	4.82
Methylogaea	2.89	4.93	2.66	3.12
Candidatus Carsonella	0.84	3.84	2.28	4.16
Promicromonospora	2.38	2.55	2.73	2.66
Conexibacter	2.30	2.70	2.36	2.68
Dermabacter	3.88	1.00	1.76	2.89
Bacillus	0.11	0.43	2.78	3.81
Ohtaekwangia	1.57	1.31	1.08	1.62
Chitinimonas	1.34	2.08	1.26	0.87
Thermoleophilum	1.73	1.09	1.58	0.76
Aciditerrimonas	1.16	1.02	1.22	0.89
Gaiella	1.09	0.84	0.95	0.79
Thiobacillus	0.70	1.20	0.85	0.57
Pontibacter	0.75	0.84	0.70	1.02
Brooklawnia	0.79	0.61	0.80	0.77
Longilinea	0.81	0.73	0.58	0.92
Falsibacillus	0.00	0.00	0.78	2.35
Singularimonas	0.78	0.80	0.61	0.72
Mesorhizobium	0.63	0.33	0.63	1.07
Oxalicibacterium	0.41	0.85	0.65	0.59
Branchiibius	0.93	0.21	0.49	0.80
Sphingomonas	0.55	0.54	0.73	0.63
Acinetobacter	0.33	1.33	0.34	0.37
Olivibacter	0.37	0.80	0.57	0.56
Ramlibacter	0.53	0.57	0.61	0.49
Iamia	0.59	0.56	0.59	0.41
Xylanimonas	0.86	0.13	0.31	0.65
Rhodocytophaga	0.26	0.78	0.58	0.43
Rubellimicrobium	0.51	0.11	0.78	0.47
Adhaeribacter	0.36	0.62	0.42	0.49
Gemmatimonas	0.56	0.36	0.59	0.29
Marmoricola	0.37	0.31	0.78	0.29
Amycolatopsis	0.31	0.20	0.64	0.69
Jejuia	0.32	0.55	0.29	0.69
Streptomyces	0.36	0.20	0.50	0.75
Acidiferrobacter	0.46	0.38	0.52	0.31
Anaerolinea	0.38	0.39	0.46	0.44

Chelativorans	0.43	0.12	0.34	0.76
Haliangium	0.45	0.39	0.41	0.37
Paracoccus	0.43	0.54	0.32	0.30
Pseudomonas	0.22	0.34	0.62	0.38
Fodinicola	0.52	0.31	0.32	0.36
Litorilinea	0.45	0.31	0.41	0.29
Altererythrobacter	0.43	0.13	0.35	0.50
Massilia	0.18	0.54	0.44	0.29
Xylanimicrobium	0.55	0.11	0.22	0.44
Thermasporomyces	0.43	0.22	0.33	0.29
Nitriliruptor	0.33	0.30	0.28	0.36
Cesiribacter	0.26	0.25	0.22	0.50
Planctomyces	0.30	0.38	0.30	0.17
Azonexus	0.31	0.30	0.27	0.30
Glycomyces	0.30	0.13	0.23	0.46
Zhihengliuella	0.35	0.12	0.25	0.37
Roseivirga	0.23	0.51	0.17	0.20
Noviherbaspirillum	0.19	0.35	0.29	0.22
Solirubrobacter	0.22	0.27	0.31	0.16
Indibacter	0.19	0.48	0.22	0.06
Pseudosphingobacterium	0.28	0.15	0.13	0.41
Caldanaerovirga	0.22	0.38	0.24	0.10
Aquabacterium	0.11	0.12	0.37	0.38
Desulfoglaeba	0.28	0.31	0.23	0.11
Lysobacter	0.26	0.18	0.34	0.17
Panacagrimonas	0.37	0.11	0.23	0.22
Myceligenerans	0.27	0.09	0.29	0.26
Hymenobacter	0.26	0.31	0.18	0.15
Saccharibacteria_genera_i	0.14	0.34	0.18	0.28
Ilumatobacter	0.27	0.18	0.28	0.11
Arsenicicoccus	0.27	0.10	0.33	0.14
Pirellula	0.22	0.44	0.17	0.06
Orientia	0.00	0.00	0.42	0.50
Alicycliphilus	0.39	0.08	0.10	0.30
Gp6	0.23	0.17	0.25	0.18
Kinneretia	0.30	0.09	0.20	0.25
Bogoriella	0.18	0.14	0.16	0.32
Rubrobacter	0.15	0.12	0.30	0.23
Rudanella	0.04	0.11	0.21	0.48
Thermomicrobium	0.24	0.11	0.27	0.17
Syntrophaceticus	0.18	0.20	0.25	0.17
Ignavibacterium	0.18	0.23	0.14	0.26
Spartobacteria_genera_inc	0.22	0.20	0.24	0.11
Yonghaparkia	0.18	0.11	0.16	0.32
Granulicoccus	0.23	0.09	0.24	0.21
Saccharopolyspora	0.07	0.03	0.39	0.31
Flavisolibacter	0.15	0.31	0.10	0.21

Sediminibacterium	0.10	0.34	0.16	0.18
Guggenheimella	0.08	0.29	0.25	0.15
Afifella	0.24	0.02	0.13	0.40
Oceanibacterium	0.22	0.13	0.16	0.22
Sorangium	0.18	0.27	0.20	0.09
Kineococcus	0.29	0.05	0.20	0.15
Microcella	0.10	0.11	0.30	0.15
Kocuria	0.20	0.07	0.22	0.19
Millisia	0.24	0.02	0.17	0.22
Euzebya	0.15	0.15	0.21	0.16
Blastopirellula	0.16	0.24	0.15	0.14
Naxibacter	0.09	0.37	0.16	0.08
Jonquetella	0.30	0.16	0.13	0.07
Opitutus	0.13	0.18	0.14	0.23
Subdivision3_genera_incert	0.18	0.19	0.14	0.15
Luteolibacter	0.12	0.28	0.19	0.10
Kribbella	0.19	0.12	0.23	0.08
Terrimonas	0.08	0.28	0.13	0.20
Parcubacteria_genera_ince	0.20	0.19	0.15	0.11
Paucimonas	0.15	0.09	0.19	0.21
Sphaerotilus	0.14	0.21	0.18	0.09
Ardenticatena	0.15	0.10	0.17	0.18
Rhodopirellula	0.12	0.24	0.13	0.11
Sphingobium	0.13	0.08	0.20	0.21
Sulfuricella	0.20	0.10	0.12	0.17
Thioalbus	0.23	0.09	0.13	0.14

Supplementary Table 8. Bacterial genera of compacted bentonite after 24 months of anaerobic incubation and their corresponding relative abundances (%) in each treatment.

Genera	**Relative abundances in compacted bentonite after 24 months of incubation (%)**										
	1.5A_1	**1.5A_2**	**1.5A_3**	**1.5C_1**	**1.5C_2**	**1.5C_3**	**1.7A_1**	**1.7A_3**	**1.7C_1**	**1.7C_2**	**1.7C_3**
Pseudarthrobacter	38.85	36.38	25.39	29.99	28.50	33.00	26.98	32.78	23.37	27.69	23.94
Nocardioides	5.68	5.14	8.21	8.86	7.08	6.86	5.25	6.26	8.82	8.23	7.41
Arthrobacter	6.70	6.72	4.98	6.83	5.77	6.04	5.63	6.30	4.71	5.91	4.92
Marmoricola	2.60	0.79	3.87	4.64	3.30	3.68	2.32	3.19	3.95	4.23	3.90
Geobacillus	8.81	0.08	1.07	0.52	0.24	0.00	9.87	0.05	5.18	0.00	0.00
unclassified Gammaproteobacteria	1.55	3.68	4.24	2.58	2.90	2.70	0.99	4.56	3.30	2.85	3.45
Mesorhizobium	1.75	2.99	3.03	2.14	2.99	3.66	2.16	3.32	1.94	3.03	2.94
unclassified Actinomarinales	1.96	2.20	3.04	3.09	2.31	2.58	1.11	3.10	2.06	2.13	2.82
Ralstonia	0.49	2.61	1.78	1.86	5.20	0.24	0.08	1.60	3.45	4.72	2.41
Promicromonospora	1.00	1.40	2.98	3.44	1.94	2.02	1.45	1.44	2.58	2.46	1.48
unclassified Chloroplast	0.17	0.66	0.14	2.18	1.07	1.01	1.60	0.76	0.65	0.42	12.48
unclassified Gitt-GS-136	0.41	2.13	1.34	1.34	1.88	2.16	0.67	1.55	2.06	2.16	1.51
Delftia	1.47	0.07	0.66	0.45	0.00	0.09	4.73	0.11	2.26	0.00	0.00
unclassified Subgroup 6	0.46	1.25	1.06	1.02	2.06	1.13	0.81	0.98	1.61	1.77	0.98
Rubellimicrobium	0.27	1.14	1.32	1.12	1.15	1.73	0.64	1.29	0.50	1.20	1.34
Paracoccus	0.62	1.99	0.58	0.63	0.87	0.99	0.11	1.45	0.81	0.87	0.63
Sphingomonas	0.81	0.81	0.82	0.60	0.74	1.17	0.37	0.77	1.20	0.85	0.78
IheB3-7	1.93	0.00	0.44	0.06	0.00	0.00	2.94	0.00	0.65	0.00	0.01
unclassified Acidimicrobiia	0.53	0.82	1.04	0.69	0.74	0.79	0.55	0.80	0.48	0.81	0.68
Stenotrophomonas	0.46	0.06	0.25	0.08	0.00	0.05	3.70	0.09	0.81	0.06	0.06
unclassified JG30-KF-CM45	0.39	0.70	0.27	0.45	0.90	1.02	1.42	0.64	0.30	0.98	0.55
unclassified Chloroflexi	0.00	0.64	0.73	0.64	0.94	0.88	0.41	0.76	0.85	0.88	0.73
Thermicanus	1.86	0.01	0.25	0.04	0.00	0.00	2.70	0.02	0.25	0.00	0.00

Ochrobactrum	1.08	0.00	0.36	0.16	0.00	0.00	2.25	0.00	0.95	0.00	0.00
unclassified Mitochondria	0.11	0.53	0.52	0.37	0.08	0.19	0.62	1.11	0.19	0.47	2.14
Bacillus	1.71	0.00	0.07	0.14	0.00	0.04	2.17	0.08	0.46	0.00	0.00
unclassified *Microscillaceae*	0.15	0.79	0.84	0.42	0.56	0.87	0.05	1.00	0.07	0.83	0.94
Pontibacter	0.27	0.68	0.67	0.44	0.61	1.24	0.00	0.59	0.60	0.58	0.52
Streptomyces	0.14	0.37	0.67	0.95	0.42	0.33	0.61	0.39	0.88	0.42	0.42
unclassified *Sphingomonadaceae*	0.29	0.88	0.66	0.69	0.54	1.11	0.04	0.73	0.05	0.55	0.79
unclassified KD4-96	0.11	0.66	0.45	0.42	0.75	0.66	0.00	0.48	1.15	0.65	0.50
Hydrogenophilus	1.81	0.00	0.23	0.28	0.01	0.00	1.19	0.02	0.55	0.00	0.00
Olivibacter	0.14	0.76	0.38	0.29	0.45	0.75	0.27	0.50	0.17	0.64	0.75
Pseudomonas	0.19	0.86	0.16	1.63	0.44	0.30	0.18	0.35	0.69	0.27	0.32
Pararhizobium-Rhizobium	0.45	0.34	0.23	0.14	0.00	0.04	1.59	0.00	0.48	0.04	0.08
Noviherbaspirillum	0.17	0.56	0.52	0.29	0.53	0.59	0.10	0.38	0.49	0.43	0.49
unclassified	0.09	0.27	0.45	0.34	0.14	0.21	0.09	0.69	1.04	0.56	0.29
Amycolatopsis	0.22	0.25	0.38	0.66	0.19	0.34	0.05	0.29	0.96	0.49	0.34
MND1	0.23	0.42	0.42	0.34	0.38	0.34	0.43	0.44	0.29	0.40	0.41
Cesiribacter	0.05	0.45	0.32	0.32	0.60	0.69	0.00	0.52	0.28	0.76	0.50
Chthoniobacter	0.00	0.57	0.00	0.27	1.25	0.75	0.00	0.62	0.00	0.98	0.55
unclassified Frankiales	0.29	0.22	0.35	0.36	0.30	0.39	0.36	0.36	0.35	0.45	0.41
Robertkochia	0.00	0.43	0.46	0.38	0.51	0.37	0.00	0.56	0.21	0.64	0.53
Polycyclovorans	0.10	0.47	0.62	0.21	0.46	0.21	0.00	0.55	0.30	0.36	0.41
Chungangia	0.88	0.00	0.21	0.00	0.00	0.00	0.73	0.00	0.76	0.00	0.00
Herbaspirillum	0.39	0.27	0.43	0.13	0.23	0.00	0.70	0.00	0.40	0.27	0.16
unclassified Planctomycetales	0.00	0.37	0.33	0.14	0.49	0.59	0.00	0.33	0.61	0.48	0.29
Aminobacter	0.11	0.49	0.52	0.28	0.42	0.44	0.00	0.45	0.00	0.44	0.41
Truepera	0.16	0.46	0.09	0.20	1.09	0.66	0.00	0.47	0.00	0.55	0.39
Gaiella	0.38	0.25	0.37	0.27	0.19	0.22	0.20	0.33	0.26	0.27	0.39

Saccharopolyspora	0.05	0.00	0.25	0.80	0.12	0.25	0.11	0.17	0.88	0.28	0.18
unclassified *Anaerolineaceae*	0.04	0.48	0.59	0.42	0.25	0.18	0.01	0.47	0.08	0.34	0.39
unclassified Alphaproteobacteria	0.36	0.32	0.26	0.12	0.19	0.28	0.27	0.29	0.23	0.24	0.30
unclassified *Micrococcaceae*	0.08	0.33	0.45	0.42	0.31	0.53	0.02	0.33	0.29	0.39	0.00
unclassified *Burkholderiaceae*	0.09	0.34	0.33	0.22	0.23	0.30	0.00	0.32	0.59	0.32	0.25
Ellin6067	0.25	0.34	0.23	0.11	0.24	0.30	0.19	0.35	0.03	0.31	0.34
Planctopirus	0.00	0.33	0.35	0.12	0.60	0.45	0.00	0.38	0.00	0.50	0.28
Caldibacillus	0.45	0.00	0.04	0.08	0.00	0.00	0.74	0.00	0.51	0.00	0.00
Myceligenerans	0.07	0.06	0.44	0.29	0.21	0.13	0.21	0.27	0.16	0.25	0.36
Herpetosiphon	0.00	0.31	0.41	0.24	0.47	0.30	0.00	0.28	0.00	0.42	0.25
unclassified BRC1	0.00	0.19	0.25	0.24	0.33	0.28	0.00	0.14	0.63	0.25	0.14
unclassified Microtrichales	0.09	0.25	0.46	0.21	0.21	0.29	0.04	0.23	0.07	0.21	0.19
I-8	0.00	0.04	0.32	0.03	0.14	0.06	0.77	0.03	0.11	0.08	0.05
unclassified *Longimicrobiaceae*	0.07	0.23	0.27	0.14	0.21	0.27	0.24	0.26	0.11	0.13	0.21
unclassified *Gemmatimonadaceae*	0.05	0.16	0.33	0.18	0.15	0.27	0.12	0.21	0.29	0.17	0.17
Adhaeribacter	0.08	0.32	0.16	0.11	0.34	0.38	0.00	0.32	0.05	0.29	0.29
Lysobacter	0.42	0.20	0.10	0.12	0.29	0.39	0.00	0.21	0.00	0.23	0.28
unclassified *Gimesiaceae*	0.00	0.33	0.40	0.08	0.45	0.26	0.00	0.22	0.00	0.36	0.20
unclassified JG30-KF-CM66	0.33	0.14	0.48	0.02	0.29	0.05	0.00	0.12	0.30	0.18	0.07
unclassified *Pirellulaceae*	0.00	0.23	0.56	0.12	0.33	0.24	0.00	0.27	0.00	0.26	0.17
Glycomyces	0.03	0.17	0.23	0.28	0.25	0.16	0.16	0.17	0.26	0.21	0.14
Altererythrobacter	0.12	0.23	0.18	0.22	0.23	0.30	0.00	0.27	0.16	0.17	0.25
Ellin6055	0.20	0.15	0.15	0.12	0.00	0.13	0.53	0.18	0.00	0.09	0.11
Kocuria	0.14	0.18	0.12	0.14	0.16	0.22	0.20	0.17	0.25	0.13	0.16
Haliangium	0.00	0.27	0.21	0.21	0.31	0.27	0.00	0.22	0.07	0.27	0.26
Novosphingobium	0.00	0.25	0.30	0.13	0.21	0.32	0.00	0.28	0.07	0.20	0.21
Pseudorhizobium	0.17	0.20	0.18	0.24	0.35	0.18	0.00	0.27	0.00	0.21	0.39

unclassified Armatimonadales	0.27	0.25	0.08	0.17	0.46	0.24	0.00	0.17	0.00	0.35	0.17
unclassified Bacillales	0.43	0.00	0.00	0.23	0.00	0.00	0.31	0.00	0.53	0.00	0.00
Pseudonocardia	0.04	0.13	0.19	0.39	0.18	0.12	0.05	0.14	0.32	0.15	0.11
Gemmata	0.59	0.10	0.11	0.04	0.18	0.06	0.00	0.08	0.26	0.16	0.03
Flavisolibacter	0.00	0.32	0.11	0.12	0.30	0.21	0.02	0.23	0.00	0.33	0.28
Skermanella	0.03	0.19	0.24	0.11	0.17	0.27	0.00	0.26	0.13	0.12	0.23
Caenimonas	0.00	0.19	0.11	0.19	0.23	0.31	0.08	0.20	0.00	0.25	0.23
Porphyrobacter	0.00	0.16	0.31	0.20	0.00	0.24	0.00	0.23	0.12	0.14	0.21
oc32	0.04	0.14	0.13	0.07	0.19	0.16	0.09	0.23	0.15	0.18	0.18
Gemmatimonas	0.05	0.17	0.18	0.16	0.18	0.21	0.00	0.22	0.10	0.10	0.17
Ramlibacter	0.00	0.16	0.12	0.17	0.25	0.22	0.00	0.18	0.07	0.22	0.24
unclassified *Nitriliruptoraceae*	0.08	0.13	0.13	0.13	0.03	0.19	0.13	0.21	0.06	0.11	0.18
unclassified *Ilumatobacteraceae*	0.03	0.23	0.13	0.14	0.12	0.14	0.00	0.14	0.13	0.16	0.16
Rehaibacterium	0.11	0.09	0.29	0.09	0.05	0.06	0.07	0.07	0.12	0.06	0.12
Microvirga	0.03	0.21	0.21	0.14	0.05	0.14	0.00	0.10	0.08	0.17	0.11
unclassified *Caldilineaceae*	0.00	0.15	0.04	0.04	0.30	0.23	0.00	0.17	0.00	0.29	0.23
Pseudosphingobacterium	0.00	0.10	0.07	0.00	0.03	0.00	0.36	0.06	0.12	0.06	0.09
Pseudoxanthomonas	0.27	0.01	0.04	0.00	0.00	0.00	0.33	0.00	0.17	0.04	0.02
Belnapia	0.17	0.12	0.15	0.09	0.13	0.15	0.00	0.16	0.00	0.12	0.10
Cytophaga	0.05	0.05	0.07	0.14	0.11	0.29	0.00	0.14	0.00	0.22	0.17
Luteolibacter	0.12	0.10	0.00	0.04	0.09	0.11	0.00	0.15	0.25	0.16	0.12
Pirellula	0.00	0.09	0.04	0.06	0.24	0.09	0.00	0.11	0.34	0.19	0.09
Sulfurifustis	0.00	0.14	0.15	0.09	0.21	0.11	0.00	0.12	0.10	0.13	0.13
unclassified *Phormidiaceae*	0.25	0.04	0.10	0.03	0.03	0.04	0.00	0.17	0.17	0.12	0.04
TRA3-20	0.00	0.08	0.10	0.08	0.05	0.05	0.26	0.10	0.04	0.05	0.05
Ohtaekwangia	0.00	0.11	0.30	0.09	0.06	0.10	0.00	0.08	0.03	0.18	0.11

Acetobacterium	0.00	0.00	0.00	0.00	0.00	0.00	0.64	0.00	0.00	0.00	0.00
Bifidobacterium	0.00	0.00	0.00	0.00	0.00	0.00	0.46	0.00	0.14	0.00	0.00
unclassified S085	0.00	0.05	0.00	0.03	0.06	0.00	0.19	0.04	0.29	0.05	0.04
unclassified *Pseudonocardiaceae*	0.17	0.03	0.08	0.05	0.09	0.04	0.17	0.03	0.03	0.08	0.08
Oxalicibacterium	0.19	0.00	0.00	0.00	0.00	0.25	0.09	0.20	0.05	0.00	0.11
unclassified AKYG1722	0.05	0.09	0.05	0.00	0.17	0.03	0.06	0.11	0.15	0.13	0.05
Kribbella	0.05	0.05	0.10	0.07	0.05	0.06	0.02	0.08	0.25	0.06	0.08
Devosia	0.00	0.15	0.07	0.06	0.00	0.22	0.00	0.11	0.11	0.15	0.04
Massilia	0.00	0.16	0.05	0.13	0.06	0.04	0.00	0.10	0.21	0.05	0.06
Qipengyuania	0.07	0.06	0.17	0.14	0.17	0.09	0.00	0.04	0.00	0.16	0.14
Steroidobacter	0.00	0.10	0.16	0.10	0.21	0.11	0.00	0.18	0.00	0.07	0.10
Streptococcus	0.13	0.02	0.15	0.14	0.00	0.00	0.00	0.02	0.25	0.02	0.01
unclassified Proteobacteria	0.04	0.11	0.03	0.12	0.02	0.06	0.00	0.20	0.08	0.16	0.13
unclassified Saccharimonadales	0.00	0.00	0.22	0.00	0.31	0.05	0.00	0.07	0.18	0.11	0.02
unclassified WD2101_soil_group	0.00	0.10	0.08	0.04	0.13	0.25	0.00	0.15	0.00	0.21	0.09
Xylophilus	0.19	0.16	0.07	0.00	0.00	0.15	0.00	0.14	0.00	0.16	0.00
unclassified	0.00	0.00	0.00	0.00	0.00	0.00	0.54	0.00	0.00	0.00	0.00
Brucella	0.00	0.03	0.00	0.00	0.00	0.00	0.25	0.05	0.23	0.03	0.00
Rhodocytophaga	0.00	0.08	0.07	0.07	0.05	0.19	0.03	0.09	0.12	0.06	0.08
Candidatus_Nitrocosmicus	0.00	0.10	0.00	0.04	0.33	0.12	0.00	0.10	0.00	0.20	0.06
Arsenicitalea	0.04	0.06	0.09	0.08	0.23	0.05	0.00	0.06	0.05	0.06	0.17
SH-PL14	0.00	0.12	0.00	0.09	0.12	0.17	0.00	0.14	0.00	0.18	0.07

CHAPTER V

Impact of bentonite and its microbial communities on the biogeochemical cycle of selenium: Bioreduction of Se(IV) and the consequent structural biotransformation to Se(0)

Cristina Povedano-Priego, Fadwa Jroundi, Mohamed L. Merroun

Department of Microbiology, Faculty of Sciences, University of Granada, Granada, Spain. ppriego@ugr.es; fadwa@ugr.es; inesms@ugr.es; merroun@ugr.es.

1. ABSTRACT

Selenium 79 is one of the most critical radionuclides in future deep geological repository (DGR) as it was predicted by several safety assessment studies. This results from the long half-life activity and chemistry of this element controlled by its oxidation state (VI, IV, 0 and –II). In the present work, we described for the first time the impact of Se(IV) on the microbial diversity of the bentonites used as a reference material for the backfilling and sealing in the future DGR. Moreover, the effect of bentonite microbial populations on the reduction of Se(IV) and on the structure of the biogenic Se(0) is further assessed.

Microcosms of water-saturated Spanish bentonites were therefore treated with selenite, acetate, glycerol 2 phosphate (G2P), and spiked with a bacterial consortium including *Pseudomonas*, *Stenotrophomonas*, *Shewanella*, *Bacillus* and *Amycolatopsis*. After six months of anaerobic incubation at room temperature, DNA extractions and the derived next generation 16S rRNA gene sequencing were performed to study the microbial diversity of the different microcosms. The results obtained showed the occurrence of both Bacteria and Archaea, although the relative abundance of the latter, represented by *Methanosarcina*, highly decreased in the presence of Se(IV). Generally, the microbial community was mainly dominated by Firmicutes (Clostridia) and Proteobacteria (Gammaproteobacteria). *Pseudomonas* and *Stenotrophomonas* were also found in the non-spiked microcosms beside *Desulfosporosinus*, and unclassified genera affiliated to *Desulfuromonadaceae*, Clostridia, and Firmicutes, all of which are probably involved in the reduction of selenite to produce the elemental Se(0).

Along the incubation time, shifts in the color of bentonite, from transparent to black through an intermediate orange color were observed. Accordingly and using state-of-the-art microscopic and spectroscopic techniques, Se(0) nanostructures were found in the selenite-treated microcosms confirming the reduction of Se(IV) to the elemental Se. The analyzed orange layers corresponded to amorphous Se nanospheres or monoclinic crystalline phases of selenium, however the black precipitates showed the typical structure of the trigonal selenium (the most stable form of Se), when native and spiked bacteria were present.

In view of the obtained results, the present work highlighted the impact of the native bentonite microbial community on the reduction of toxic and soluble Se(IV),

which is critical for the safety of DGRs, to non-toxic and insoluble Se(0). New insights on the role of bentonite mineralogy in the immobilization of Se(IV) are also provided. In total, our finding confirmed a biotransformation process of amorphous Se nanospheres to stable trigonal Se in the Se(IV)-treated bentonites.

2. INTRODUCTION

Deep Geological Repository (DGR) is the internationally accepted option for the storage and management of the high-level radioactive wastes (HLW) (Grigoryan et al., 2018). This multi-barrier system consists of metal canisters (cast iron, stainless steel, or copper) containing spent fuel, surrounded by the backfilling and sealing material (e.g. highly compacted bentonite) and emplaced within a host rock (natural geological barrier) (Anderson et al., 2011; Bengtsson and Pedersen, 2017). All the evolution scenarios of the nuclear waste disposal suggest that the release of radionuclides over a long-term period of repository could be unavoidable.

The isotope Se^{79}, a 2.95×10^5 years long half-life element, is one of the radionuclides that may occur in the HLW (Kang et al., 2011). This isotope is generated by nuclear fuel reprocessing activities and could be problematic in the DGR system. The toxicity of selenium is mainly related to its oxidation state, being selenium oxyanions (selenate [Se(VI)] and selenite [Se(IV)]) are the most toxic forms due to their high solubility and mobility causing harmful effects on the environment (Avendaño et al., 2016; Garbisu et al., 1996; Nancharaiah and Lens, 2015). In addition, elemental selenium [Se(0)] and selenides [Se(-II)] are less soluble and immobile, exhibiting no or low toxicity in terrestrial and aquatic environments (Avendaño et al., 2016). In anaerobic conditions, Se(0) prevails and may exist in different allotropic forms such as amorphous, monoclinic, and trigonal (Nancharaiah and Lens, 2015). Therefore, it is necessary to study the impact of biotic and abiotic processes on the fate and mobility of selenium under DGR conditions, where the anaerobic and reducing environments would be prevalent few years after the closure of the galleries.

Bentonite has been selected as the best material for the sealing and backfilling in DGRs because of its suitable properties, among which is the radionuclide retardation capacity mainly due to its composition in montmorillonite (Montavon et al., 2009). Montavon et al. (2009) reported that the montmorillonite plays a key role in controlling the sorption of Se(IV) in bentonites beside calcite which could influence the Se(IV) sorption when pH is above 7. However, Se(IV) sorption to montmorillonite is a pH dependent process, being high sorption rates occurring at low pHs but they decrease with increasing pH (Shi et al., 2014). The reduction of Se(IV) to Se(0) by pyrite (FeS_2) is another selenite immobilization mechanism, which may occur in bentonite within the

DGR concept (Han et al., 2012; Kang et al., 2011). Se(IV) reduction by pyrite seems to be preceded by mineral surface adsorption of selenite, which is afterwards reduced to poorly soluble Se(0) or $FeSe_2$ due to electron transfer reactions (Hoving et al., 2019).

Additionally to the immobilization of selenium by abiotic factors, it has been reported that microbes are able to interact with this metalloid trough different processes such as reduction (Fresneda et al., 2018; Ruiz-Fresneda et al., 2019), oxidation (Eswayah et al., 2016; Nancharaiah and Lens, 2015) and volatilization (Ansede and Yoch, 1997; de Souza et al., 1999), affecting thus their speciation and in consequence their mobility in the environment (Fresneda et al., 2018; Nancharaiah and Lens, 2015; Ruiz-Fresneda et al., 2019). Bentonites have been characterized by a high microbial diversity and activity along the last years (Grigoryan et al., 2018; Lopez-Fernandez et al., 2014, 2015, 2018b; Povedano-Priego et al., 2019). In addition, bentonite microbial isolates were reported to have a great potential to interact with radionuclides (Fresneda et al., 2018; Lopez-Fernandez et al., 2018a; Povedano-Priego et al., 2019). For instance, *Stenotrophomonas bentonitica*, isolated from Spanish bentonite, was able to tolerate up to 200 mM of selenite reducing it to Se(0) (Fresneda et al., 2018). Grigoryan et al. (2018) studied the microbial diversity of microcosms containing uncompacted bentonite, identifying among the native bacteria the genus *Pseudomonas*, which has been described for its capacity to reduce selenate or selenite to elemental selenium (Avendaño et al., 2016; Gupta et al., 2010; Hunter, 2014). Different mechanisms have been described to explain Se(IV) bioreduction, such as the intracellular reduction mediated by molecules containing reduced thiols groups (-SH) (Fresneda et al., 2018; Li et al., 2014) or by enzymatic activity of reductases (Basaglia et al., 2007; Hunter, 2014; Li et al., 2014).

Elemental selenium resulted from biogenic Se(IV) reduction can exist in different allotropic forms including amorphous, monoclinic, and trigonal (Chen et al., 2010). Several bacteria, such as *Shewanella* sp. and *Stenotrophomonas* sp., have been reported to produce amorphous-Se(0) as intracellular and extracellular nanospheres (Fresneda et al., 2018; Tam et al., 2010). In addition, other bacterial strains are able to reduce Se(IV) forming intracellular monoclinic Se (e.g. *Ralstonia metallidurans*) (Oremland et al., 2004; Sarret et al., 2005). Monoclinic Se (m-Se) is metastable and could also eventually suffer a conversion to the trigonal form of Se (*t*-Se) (Goldan et al., 2016). These m-Se nanostructures can be found in three different allotropes (alfa, beta and gamma)

composed by 8 atoms of Se in polymer rings (Fernández-Martínez and Charlet, 2009). However, the trigonal Se (*t*-Se) is composed by polymeric helical chains of Se atoms parallel to each other and where every atom is connected by partially metallic bonds with four nearby Se atoms in the adjacent chains. This structure confers a high stability to *t*-Se in contrast to the weaker van der Waals forces linking the Se atoms in the m-Se (Fernández-Martínez and Charlet, 2009; Goldan et al., 2016). Biotransformation of amorphous/monoclinic Se into the most stable trigonal form of Se (*t*-Se) could be undertaken by several bacterial strains such as *S. bentonitica* and *Bacillus subtilis* (Fresneda et al., 2018; Wang et al., 2010).

Due to the great impact of the microbial processes on the mobilization/immobilization of radionuclides and the risk that Se may have on the safety of DGR, in the present study, microcosms of water-saturated bentonites were treated with selenite and spiked with a consortium containing bentonite natural bacteria. These strains (e.g. *Pseudomonas*, *Stenotrophomonas*, *Shewanella*, *Bacillus* and *Amycolatopsis)* were described for their capacities to interact with radionuclides (e.g. uranium and selenium). Therefore, the main aims of this work were 1) to investigate the potential effect of Se(IV) on the microbial community of bentonites, and identify tolerant bacterial strains involved in the transformation of the toxic Se(IV) into the less-toxic Se(0); and 2) to determine the impact of bentonite microbial community on the structure and chemical speciation of Se(IV) in such a complex system of water-saturated bentonite, by the use of state-of-the-art microscopic and spectroscopic techniques evidencing the transformation of amorphous/monoclinic Se into the more stable trigonal Se.

3. MATERIAL AND METHODS

3.1. Bentonite sample collection

Bentonite samples were collected from the clays formation in “El Cortijo de Archidona” (Almeria, Spain). These bentonites have been thoroughly characterized in their mineralogical, geochemical and mechanical properties (Villar et al., 2006). Sample collection was performed on January 2018 under aseptic conditions in previously sterilized containers and then the samples were stored at 4 ºC until further use.

3.2. Preparation of water-saturated bentonite microcosms

3.2.1. Preparation of the different solutions

Pore water (PW) for bentonite saturation was extracted by shaking 1 g of bentonite in 100 mL of sterile distilled water at 180 rpm for 24 h at 28 ºC. Then, the liquid phase was filtered using 0.45 µm pore-size sterile filters and autoclaved twice at 110 ºC for 20 min. Composition of major elements of the PW was described in Povedano-Priego et al. (2019).

PW was supplemented with 30 mM sodium acetate and 10 mM glycerol-2-phoshate (G2P). Sodium acetate and G2P was added as electron donors to stimulate the growth of bentonite bacterial communities. Stock solutions of 50 mM sodium acetate and of 50 mM G2P were prepared and sterilized by autoclave, and by using 0.22 µm pore-sized filters, respectively.

For the interaction experiments with selenium, a stock solution of 1 M sodium selenite (Na_2SeO_3) (Sigma-Aldrich) was prepared dissolving the suitable amount of solute in distilled water and sterilizing by filtration in 0.22 µm syringe filters (Sartorius).

3.2.2. Bacterial strains and growth conditions

A consortium of five bacterial strains was used in this study including genera affiliated to *Stenotrophomonas*, *Pseudomonas*, *Amycolatopsis*, *Shewanella* and *Bacillus* previously detected in the microbial community of Spanish bentonite (Lopez-Fernandez et al., 2018b, 2014; Povedano-Priego et al., 2019). This consortium consisted of *Stenotrophomonas bentonitica* BII-R7^T and *Bacillus* sp. BII-C3, which were previously isolated from Spanish bentonite (Lopez-Fernandez et al., 2014), in addition to *Pseudomonas putida* ATCC33015, *Amycolatopsis ruanii* NCIMB14711, and *Shewanella loihica* DSM17748, purchased from the culture collections: ATCC (https://www.lgcstandards-atcc.org/), NCIMB (https://www.ncimb.com/), and DSMZ (https://www.dsmz.de/), respectively. All bacterial strains were grown aerobically in Luria-Bertani (LB) broth medium (tryptone 10 g L^{-1}, yeast extract 5 g L^{-1}, and NaCl 10 g L^{-1}) with the exception of *A. ruanii* that was grown in yeast-malt broth (yeast extract 4 g L^{-1}, malt extract 10 g L^{-1}, glucose 4 g L^{-1}). The incubation conditions were 28 ºC and

180 rpm in a rotary shaker for 48 h. Initial biomass concentration was adjusted to the optical density (OD) of 0.4 (at a wavelength of 600 nm) for all bacterial consortium-containing treatments.

3.2.3. Experimental set-up

Bentonites were placed in a laminar flow cabinet for 72 h to air dry and also to facilitate the grinding of the samples (using a mortar). The water-saturated microcosms were prepared in sterile 250-mL borosilicate glass bottles consisting of 40 g of ground bentonite and 170 mL of PW, supplemented with sodium acetate and G2P solutions (with a final concentrations of 30 mM and 10 mM, respectively) reaching a final volume of 230 mL. In the case of selenite-treated microcosms, 460 µL of 1 M sodium selenite solution was added to each microcosm resulting in a final concentration of 2 mM. Finally, the bentonite microcosms were inoculated with the previously prepared bacterial consortium composed by *Bacillus* sp., *S. bentonitica*, *P. putida*, *A. ruanii*, and *S. loihica* (referred to hereafter as BSPAS). Microcosm controls without adding any bacteria, controls without adding selenium (Se) as well as controls using sterile bentonite were performed. Bentonite sterilization was performed by tyndallization because bentonite alteration could occur at higher temperatures such as those of the standard sterilization by autoclave (121 ºC for 15 min), thus bentonite was autoclaved at 100 ºC for 30 min during 3 or more consecutive days. All the experimental conditions are shown in Table 1. All treatments were performed in triplicates (three bottles per treatment), having a total of 24 bottles of saturated bentonite microcosms.

Once all components were placed in the 250-mL borosilicate glass bottle, these were sealed with the butyl-rubber stoppers (Fig. 1A) and bubbled with N_2 (for ~4 h) until saturation to create anaerobic conditions replacing the O_2 trapped inside each sealed bottle (Fig. 1B). After bubbling, microcosms were incubated for six months in dark at room temperature.

Table 1. Experimental conditions of the analyzed bentonite samples.

Sample ID	Bentonite	BSPAS consortium	Sodium selenite (2 mM)
BB	Non sterile	+	-
BBSe	Non sterile	+	+
B	Non sterile	-	-
BSe	Non sterile	-	+
BsB	Sterile	+	-
BsBSe	Sterile	+	+
Bs	Sterile	-	-
BsSe	Sterile	-	+

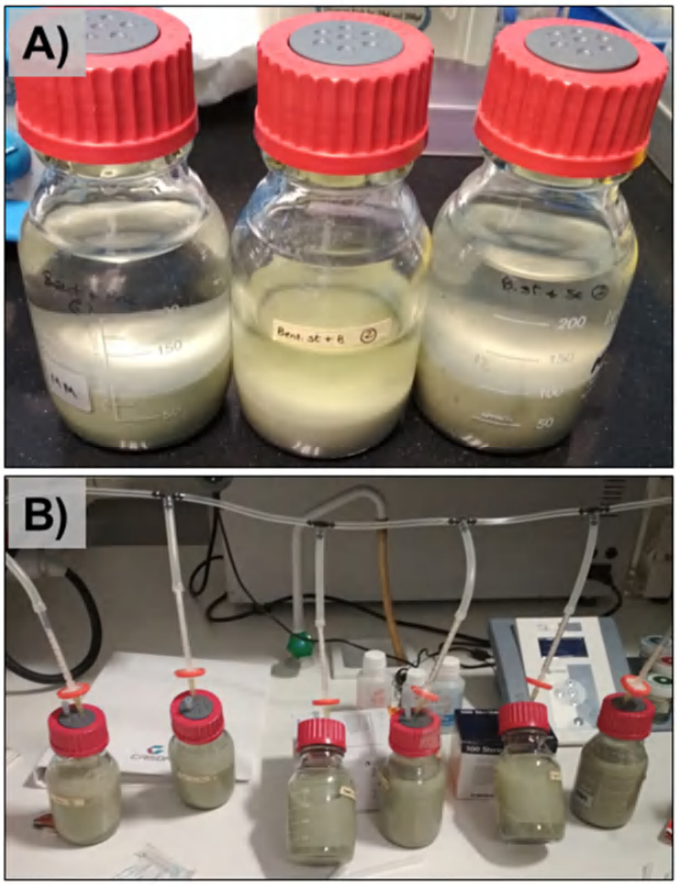

Figure 1. A) Water saturated microcosms composed of bentonite (sterile or non-sterile) and pore water (PW) amended with sodium acetate (30 mM) and G2P (10 mM) independently of the treatment. B) Bubbling nitrogen gas in the microcosms to eliminate the dissolved oxygen from the bottles.

3.3. Characterization of bacterial community in the water-saturated microcosms

3.3.1. DNA extraction from bentonite microcosms

DNA extraction of all treated microcosms were performed as was described in detail in Povedano-Priego et al. (2019). Pellets of DNA were stored at -20 ºC until used.

Concentration and cleaning of all extracted DNA samples were performed with 0.1 volumes of 20% sodium acetate and 2.5 volumes of ice-cold absolute ethanol. The tubes were frozen for one hour at -20 °C and then centrifuged at 12,000 × g for 10 min at 4 °C. The supernatants were discarded and the pellets were washed with 70% ethanol followed by centrifugation at the same conditions. Finally, pellets were air dried to be then dissolved with 30 µL of MilliQ water.

3.3.2. Library preparation and sequencing of the samples

Two consecutive PCR reactions were performed for each sample with the use of normal and bar code fusion primers for the library preparation. The primers used for amplification of variable V5 and V6 regions of 16S rRNA gene were 807F (5'-ACGACGCTCTTCCGATCTGGATTAGATACCCBRGTAGTC-3') and 1050R (5'-GACGTGTGCTCTTCCGATCTAGYTGDCGACRRCCRTGCA-3') (Bohorquez et al., 2012). The first PCR reaction was performed as follows: one cycle at 95 °C for 15 min; 35 cycles at 98 °C for 10 s, 55 °C for 10 s, and 72 °C for 45 s; and a final extension step at 72 °C for 2 min. The same conditions were performed for the barcoding (the second PCR reaction) by using only 10 PCR cycles. A gel-electrophoresis was used to check the quality of the library product. Libraries were sequenced by MiSeq Illumina platform (2 × 250 bp, Hayward, California, USA) for generating the fastQ files.

3.3.3. Bioinformatics and bacterial diversity analyses

The analyses of all FastaQ files were achieved using dada2 package in R (www.r-project.org) resulting in a unique table containing the sequence reads and abundances of all samples. All samples normalized using the "phyloseq" package and returning 354 phylotypes. Sequence reads were assigned to a taxonomic affiliation based on the naïve Bayesian classification, establishing a pseudo-bootstrap threshold of 80%. Relative

abundances in percentage of phylum, class, order, family and genus were obtained by Explicet 2.10.5 software (Robertson et al., 2013) and used for downstream analyses.

Alpha diversity (Shannon H index) was calculated to the lowest sample size (1006) and bootstrapped 100 times. Beta-diversity analyses were performed to evaluate the similarity between taxa as it was described in Chapter 2. At OTU level, microbial community composition was analyzed using PAST3 v. 3.18 and the output visualized with Principal Coordinate Analysis (PCoA).

3.4. Mineralogical and microscopic characterization of water-saturated bentonite microcosms and selenium nanoparticles

Selenium-treated microcosm samples were analyzed by Variable Pressure Field Emission Scanning Electron Microscopy (VP-FESEM) *ZeissSupra 40VP* equipped with SE (InLens) and BSE detectors to provide morphological and chemical characterizations. This microscope is coupled with a microanalysis system (*Aztec 2.2*) to deliver elemental composition data by Energy Dispersive X-ray (EDX). In addition, this model is equipped with Raman spectrometer *Renishaw In Via* fitted with a Nd:YAG 532 nm laser and a near infrared diode 785 nm laser, with 500 mW and 100 mW as maximum powers, respectively (Guerra and Cardell, 2015). Raman spectroscopy was used to determine the structure of Se nanoparticles (SeNPs).

Additional ultrastructural features on the SeNPs and water-saturated bentonite were determined using Scanning Transmission Electron Microscope (STEM; FEI TITAN G2 80-300) equipped with an EDX spectrometer working at 300 kV. High-Angle Annular Dark Field (HAADF) detector was used to determine the elemental composition of the SeNPs. The characterization of Se nanoparticles was performed by Selected-Area Electron Diffraction (SAED) and High-Resolution Transmission Electron Microscopy (HRTEM) combined with Fast Fourier Transform (FFT). Samples were prepared as described in Povedano-Priego et al. (2019).

4. RESULTS

4.1. Changes in microbial diversity of saturated-bentonite microcosms induced by sodium selenite

Total DNA of untreated and selenite treated bentonite microcosms was extracted and sequenced by Illumina approach, obtaining data relative to the diversity of the microbial community. The extracted DNA from sterile bentonite microcosms (Bs) failed in the PCR amplification step for the construction of the libraries, probably because of the low bacterial diversity of this sample as a consequence of the heating treatment. Moreover, one replicate of the samples BB2, BsB3 and B1 were discarded due to their great deviation with respect to the other two replicates of the same sample. After normalization, 1006 sequences per sample were annotated. Rarefaction curves (data not shown) and values of Good's coverage of >99% in all cases (Table 2) indicated the sequencing was adequately and deeply performed. Normalization by relative abundance final count values was used instead.

Table 2. Alpha-diversity indices of selenium-treated (BBSe, BsBSe, BSe, and BsSe) and untreated (BB, BsB, and B) saturated-bentonite microcosms. Richness index (S), diversity indices (ShannonD, and SimpsonD), evenness index (ShannonE), and Good's coverage values are shown.

	S	ShannonD	ShannonE	SimpsonD	Good's coverage
BB	120	3.90	0.56	0.81	0.992
BBSe	65	3.62	0.60	0.85	0.995
B	84	3.73	0.58	0.78	0.997
BSe	74	4.65	0.75	0.93	0.998
BsB	82	2.81	0.44	0.61	0.995
BsBSe	36	2.55	0.49	0.76	0.998
BsSe	49	3.59	0.64	0.82	0.998

A total of 355 OTUs were classified into phylum (97.9% of phylotypes), class (92% of phylotypes), order (91.1% of phylotypes), family (87.1% phylotypes) and genus (79.5% phylotypes) levels. Richness (S), evenness and diversity of all the sequenced samples at phylotype level were calculated using diversity indices (Shannon, Shannon's evenness, and Simpson) indicating a high bacterial diversity (ShannonD and SimpsonD) and a highly uniform distribution of OTUs (ShannonE) (Table 2). As expected, a decrease in the microbial diversity was observed in the "sterile" bentonite

microcosms although this diversity was not drastically reduced in the case of BsSe or even BsBSe and BsB.

Sequences belonging to Archaea and Bacteria kingdoms were identified in the untreated and selenite-treated water-saturated bentonite microcosms (Fig. 2). Although Bacteria was present in all the studied microcosms, distribution of Archaea seems to be dependent on the treatments, being almost or completely absent in Se(IV)-treated samples, except for the BBSe where they were represented by 21.9% of relative abundance and with a less extend in BsB represented by 1.1% of the total community.

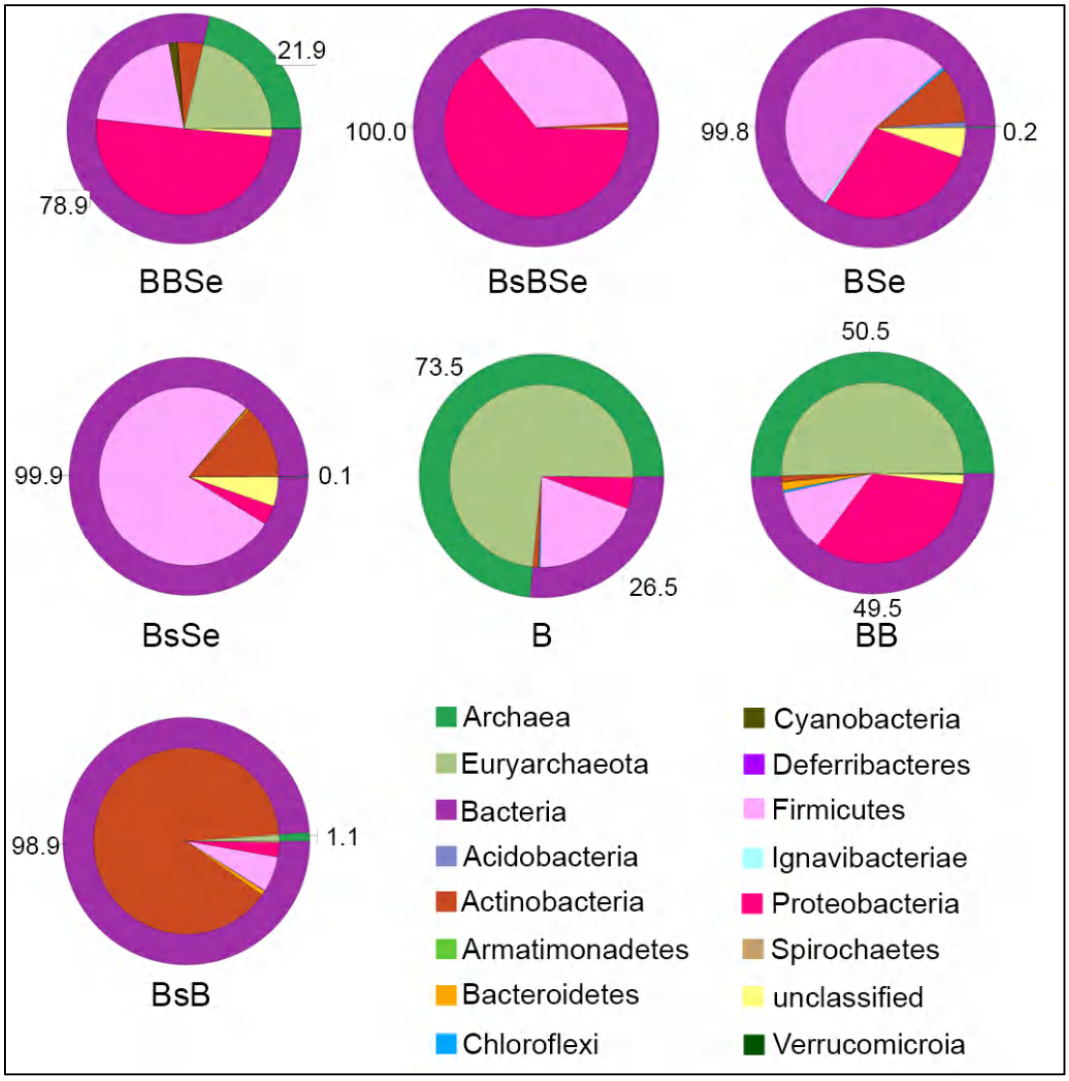

Figure 2. Pie chart representing the relative abundances of Bacteria and Archaea and their corresponding phyla in all the experimental bentonite microcosms averaging triplicates (except for BB, BsB, and B, in duplicates). B=bentonite, BB=bentonite spiked with BSPAS consortium, BsB=sterile bentonite spiked with BSPAS consortium, Se=sodium selenite treatment.

Thirteen different bacterial phyla were annotated including Firmicutes (33.1%), Proteobacteria (32.1%), Actinobacteria (13.5%), Cyanobacteria (0.5%), Bacteroidetes (0.3%), and Chloroflexi (0.15%), among others, in addition to the archaeal phylum Euryarchaeota (18.1%) (Fig. 2, Supplementary Table 1). The distribution of dominant bacterial phyla was different depending on the treatment, being Proteobacteria abundant in BsBSe (64%), BBSe (50.3%), and BB (33.4%); Firmicutes in BsSe (77.3%), BSe (53.5%), and B (19.5%); and Actinobacteria in BsB (89%) (Fig. 2, Supplementary Table 1). The high abundance of Proteobacteria in BsBSe, BBSe and BB could be explained by the fact that the BSPAS consortium used to inoculate these samples contained *Pseudomonas*, *Shewanella*, and *Stenotrophomonas*, which are affiliated to Proteobacteria, particularly Gammaproteobacteria. Interestingly, Euryarchaeota was highly abundant only in B, BB, and BBSe with 73.5, 50.5, and 22.5% of the total community, respectively (Fig. 2, Supplementary Table 1). However, this archaeal phylum was strongly reduced in BsB (1.1%), BSe (0.2%), and BsSe (0.1%) or completely absent in BsBSe, indicating that they might have hardly survived the heating treatment (tyndallization) as well as the potential toxic effect of the dissolved Se(IV).

Regarding the class level, within the Proteobacteria phylum, Gammaproteobacteria was dominant in BsBSe and BBSe with 64 and 50% of relative abundance, respectively (Fig. 3, Supplementary Table 2). The second more represented class was Clostridia mainly in BsSe (≈60%), BSe (≈40%), BsBSe (≈33%), which could indicate a high tolerance to selenium and/or to heating treatment. In addition, Actinobacteria class was remarkably abundant in BsB microcosms with a relative abundance of ≈89%, but also highly present with more than 4% in BsSe (≈13%), BSe (≈10%), and BBSe (≈5%). Moreover, the archaeal class Methanomicrobia was highly abundant only in B, BB, and BBSe (Fig. 3, Supplementary Table 2).

Accentuated differences between samples were observed at genus level showing an effect on the microbial diversity of the sterilization, the addition of BSPAS consortium, and the selenium treatments. Firstly, the heating treatment used to sterilize the bentonites had an effect on the bacterial diversity (as it was shown in Table 2) resulting in a different microbial community. Comparing BsSe with BSe, *Symbiobacterium* (50.4%), *Nitriliruptor* (9.5%) and *Bacillus* (1.66%) were more abundant in the “sterile” bentonite than in non-sterile ones (7.7, 2.2, 0%, respectively), however *Desulfosporosinus* and the unclassified *Desulfuromonadaceae* were absent in

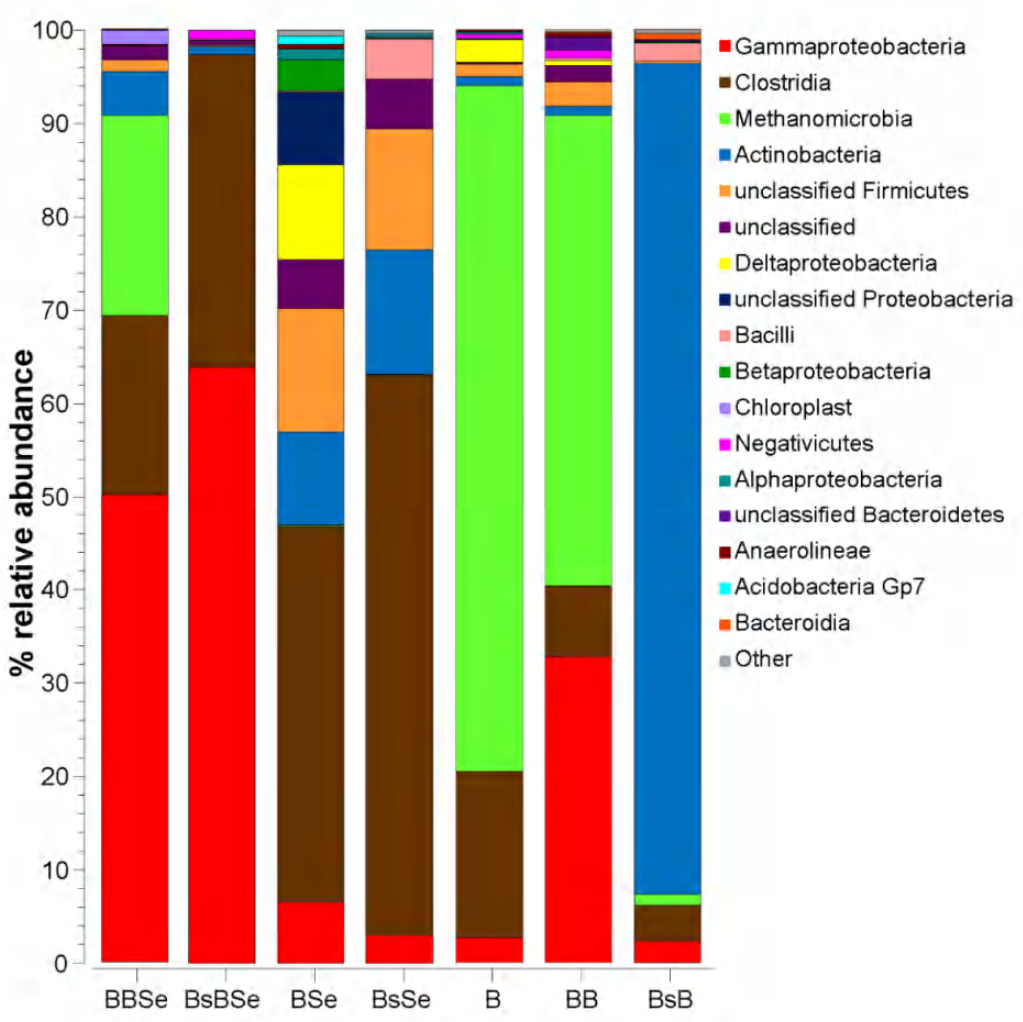

Figure 3. Relative abundances of Bacteria and Archaea at class level in all the water-saturated bentonite microcosms averaging triplicates (except for BB, BsB, and B, in duplicates) with a cut-off of 0.10% of the total community. B=bentonite, BB=bentonite spiked with BSPAS consortium, BsB=sterile bentonite spiked with BSPAS consortium, Se=sodium selenite treatment.

BsSe but highly abundant in BSe accounting for 22.4 and 10.1%, respectively (Fig. 4, Supplementary Table 3). Additionally, *Anaerosolibacter* (28.7%), and *Symbiobacterium* (2.4%) showed higher relative abundance in BsBSe than in BBSe microcosms (1.3, and 0.5%, respectively) which indicated high survival of these genera to the heating treatment (Fig. 4, Supplementary Table 3). The same behavior was observed for *Pseudomonas* and *Stenotrophomonas*, which despite being included in the BSPAS consortium, they accounted for 33.8% and 29% in BsBSe, and 2.5% and 25.1% in BBSe, respectively. However, *Brachybacterium* represented 89% of the community in the BsB microcosms in spite of the fact that genera of BSPAS consortium were expected to be the dominants.

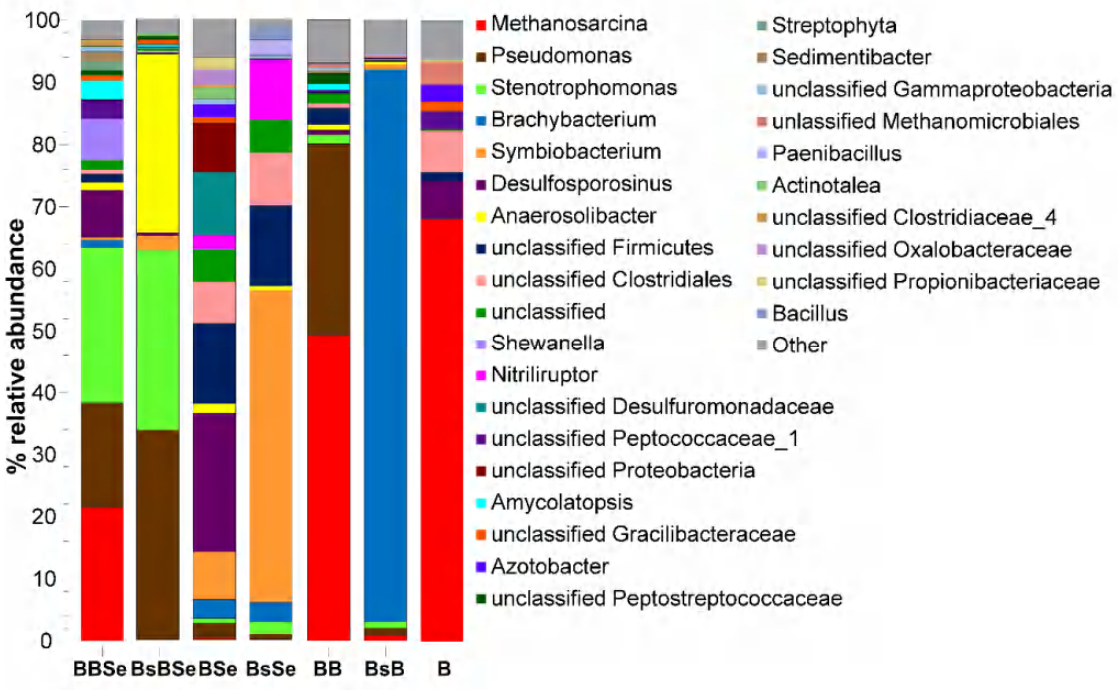

Figure 4. Relative abundances of Bacteria and Archaea at genus level in all the water-saturated bentonite microcosms averaging triplicates (except for BB, BsB, and B, in duplicates) with a cut-off of 0.27% of the total community. B=bentonite, BB=bentonite spiked with BSPAS consortium, BsB=sterile bentonite spiked with BSPAS consortium, Se=sodium selenite treatment.

The addition of BSPAS consortium affected the microbial diversity by shifting the indigenous bacterial community of the bentonite as it was observed in BBSe, BsBSe and BB, where members of the BSPAS were more abundant in comparison with the unspiked samples BSe, BsSe and B. For example, *Stenotrophomonas* and *Pseudomonas* were enriched in BBSe accounting for 25.1 and 16.9% of the bacterial community, respectively, while in BSe they were represented by only 0.7 and 2.5%, respectively (Fig. 4, Supplementary Table 3). However, in the uninoculated bentonite samples different genera were enriched in comparison with their controls such as *Desulfosporosinus* in BSe and B microcosms; unclassified genera affiliated to Firmicutes, Clostridiales, and *Nitriliruptor* in BSe and BsSe; unclassified genera related to Clostridiales, *Peptococcaceae*, *Gracillibacteraceae* and *Methanomicrobiales* in B samples (Fig. 4, Supplementary Table 3).

Interestingly, the impact of selenium on the microbial community in the water-saturated bentonite microcosms was remarkable. Mainly, the toxic effect of Se(IV) was observed on the archaeal genus *Methanosarcina* which was highly abundant in BB (49.2%) and B (68.2%) in comparison with selenium-treated samples BBSe (21.5%)

and BSe (0.2%) (Fig. 4, Supplementary Table 3). In view of this results, this genus could not tolerate the toxic effect of Se(VI) being unable to growth when this soluble selenium species was present in the environment. However, in BBSe sample *Methanosarcina* showed a relative high abundance, which could be due to the removal of Se(IV) through its enzymatic reduction to a less toxic Se(0) by the activity of natural bentonite bacterial communities and also the inoculated bacterial strains. Furthermore, *Stenotrophomonas* was represented by 25.1% of relative abundance in BBSe but only by 0.7% in BSe, where BSPAS was not added. In addition, other bacteria were enriched in the presence of Se(IV) such as *Desulfosporosinus* in BSe (22.4%) and BBSe (7.5%) in comparison with their controls B (6%) and BB (0.8%); *Anaerosolibacter* in BsBSe with 28.7% while in BsB it was represented by only 0.4% of relative abundance; and the unclassified genera affiliated to Firmicutes and *Desulfuromonadaceae* in BSe (13.2, and 10.1%, respectively) with respect to B (1.3, and 0%, respectively), among others (Fig. 4, Supplementary Table 3).

Considering the microbial diversity distribution along the communities of the Se-treated and untreated microcosms, samples were grouped in different clusters. PCoA analysis showed considerable differences between treatments, being the most different those of the control B microcosms (Fig. 5). One of the aggrupation was composed of

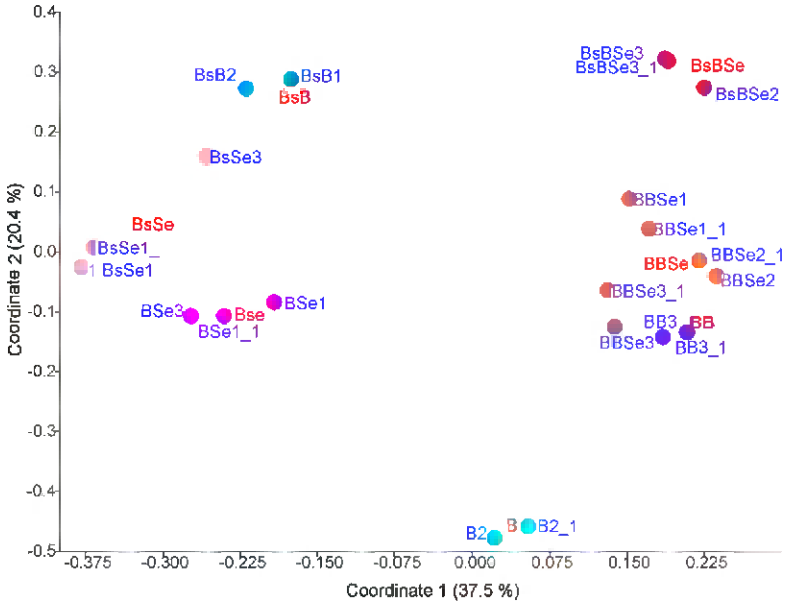

Figure 5. Principal Component Analysis (PCoA) plot comparing the microbial community structure at genus level of the different microcosms in triplicates (except for BB, BsB, and B, in duplicates). The percentage of variation explained by Coordinate 1 and Coordinate 2 is indicated in the axes.

BBSe and BB and clearly separated from the BSe and BsSe microcosms supporting the previously observed effect of the BSPAS addition. Moreover, a clear effect of Se(IV) was observed in BsBSe samples which were remarkably different from BsB control without selenium (Fig. 5). To identify which microorganisms were involved in these differences, a heatmap was constructed showing that *Methanosarcina*, *Pseudomonas*, *Stenotrophomonas*, *Brachybacterium*, *Symbiobacterium*, *Desulfosporosinus* and the unclassified genera affiliated to Firmicutes and Clostridiales were mainly responsible for this clustering (Fig. 6).

4.2. Electron microscopic and spectroscopic characterization of the resulting products from Se(IV) reduction in water-saturated anaerobic microcosms

During the anaerobic incubation, color changes in the Se(IV)-treated microcosms were observed as the incubation time increases (Fig. 7). In the first week of incubation, no changes occurred in the BSe and BsSe samples, whilst BBSe and BsBSe liquid phases (supernatants) turned orange, being more intense in BBSe samples. This orange color was probably due to the biotic/abiotic reduction of Se(IV) into elemental selenium and the formation of amorphous Se nanospheres (Fernández-Llamosas et al., 2017). The liquid phases (supernatant) of the samples BBSe, BsBSe, and BSe turned uncolored and an orange layer began to appear as the incubation time increase, forming at day 30 a thicker layer at the interface supernatant/bentonite. In BBSe sample, the whole bentonite sample acquired an orange tone, which after 60 days of incubation turned darker (gray) with an incipient black layer at the surface of the bentonite and the orange tone remained in a thin layer. The black/gray layer may probably contain trigonal Se nanostructures (Wang et al., 2010). Meanwhile, BsSe microcosms exhibited a thin orange layer until 6 months of incubation. From 60 to 180 days, the pigmented layers (orange in BSe and BsBSe, and black/gray in BBSe) increased in thickness. Lastly, spots appeared in the bentonite of the BSe microcosms at 30 days and their quantity and size increased along the incubation time (Fig. 7).

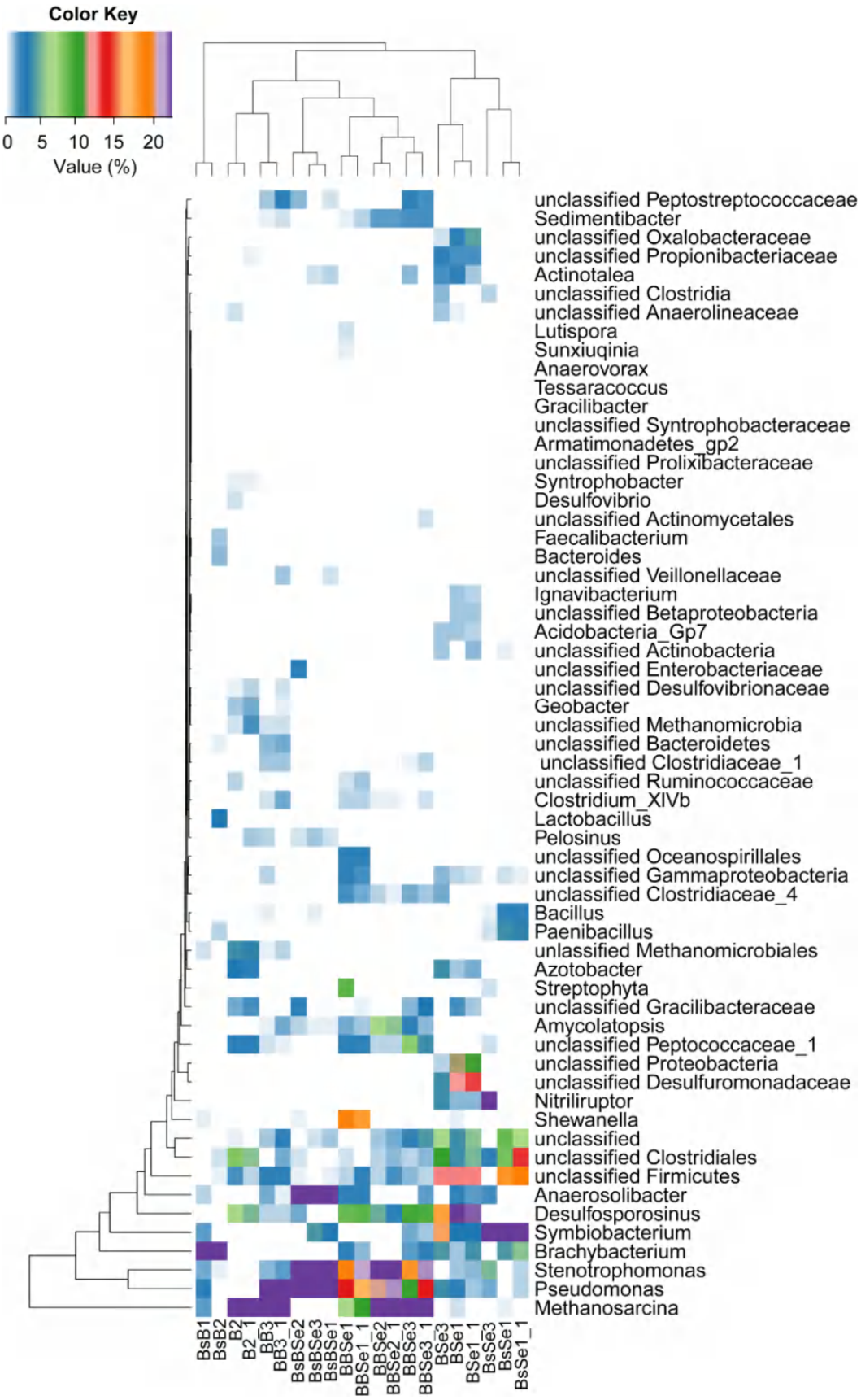

Figure 6. Heatmap of the relative abundance at the genus level, and the clustering based on Manhattan distance and average linkage for both columns and rows throughout the sample sets. The relative abundance of each genus was shown by different colors indicated in the color bar.

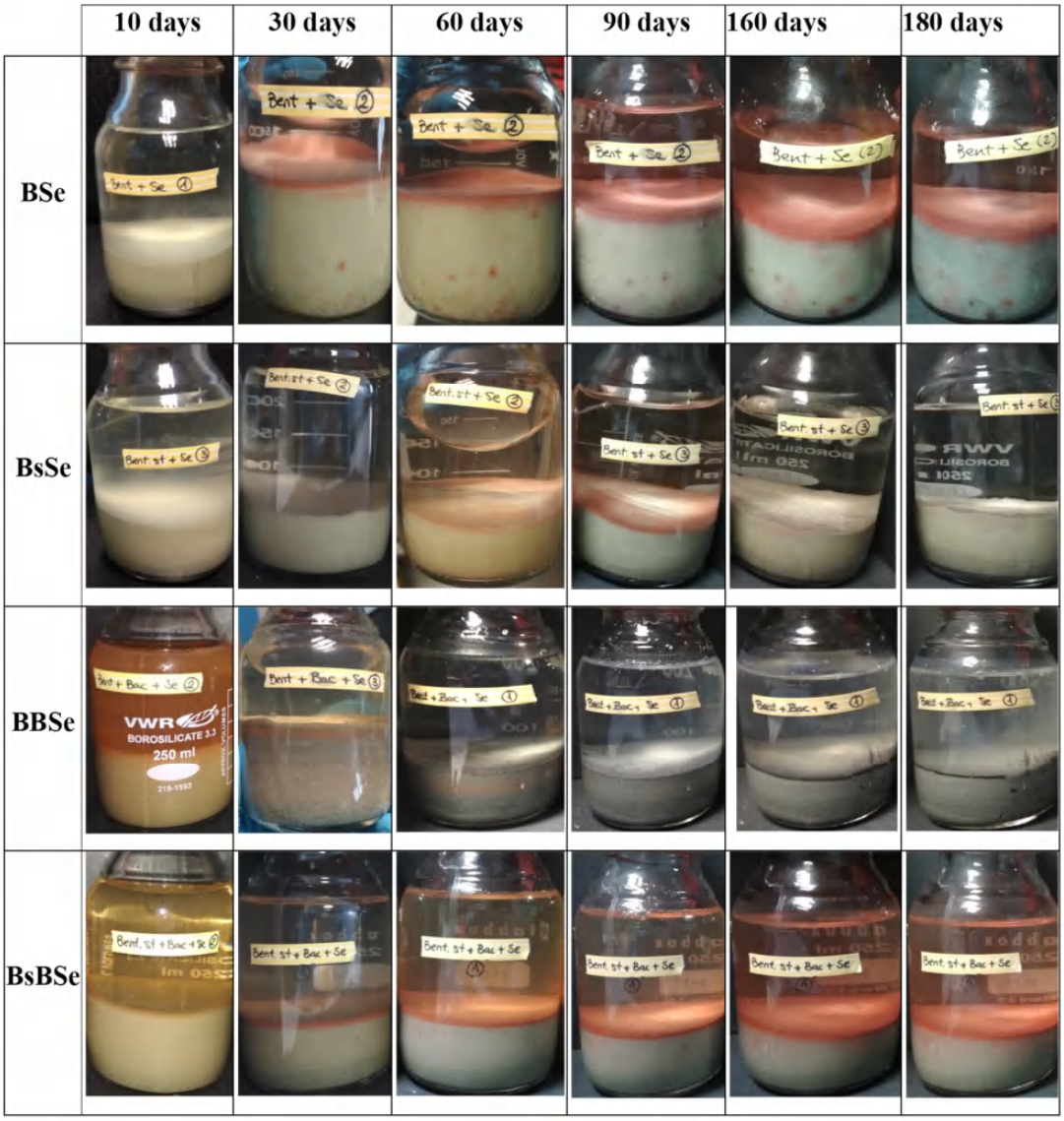

Figure 7. Water-saturated bentonite microcosms treated with sodium selenite along the anaerobic incubation period (from 10 to 180 days). B=bentonite, Bs=sterile bentonite, BB=bentonite spiked with BSPAS consortium, BsB=sterile bentonite spiked with BSPAS consortium, Se=sodium selenite treatment.

4.2.1. Se(IV)-treated bentonite (BSe)

The interface orange layers of the 6 month-BSe microcosms were recovered and prepared for their microscopic analyses. A combination of HAADF-STEM and FESEM coupled with Raman spectroscopy were used to characterize the structure, morphology and element composition of Se(IV) reduction products. HAADF-STEM micrographs of thin sections of the recovered orange layers showed the presence of electron-dense nanostructures (Figs. 8, 9, and 10). These Se-precipitates showed different

morphologies mainly composed by polymorphous aggregates (Fig. 8Ba), accumulates associated to bentonite (Fig. 9a), and nanowires of up to ≈2 µm in length (Fig. 10a).

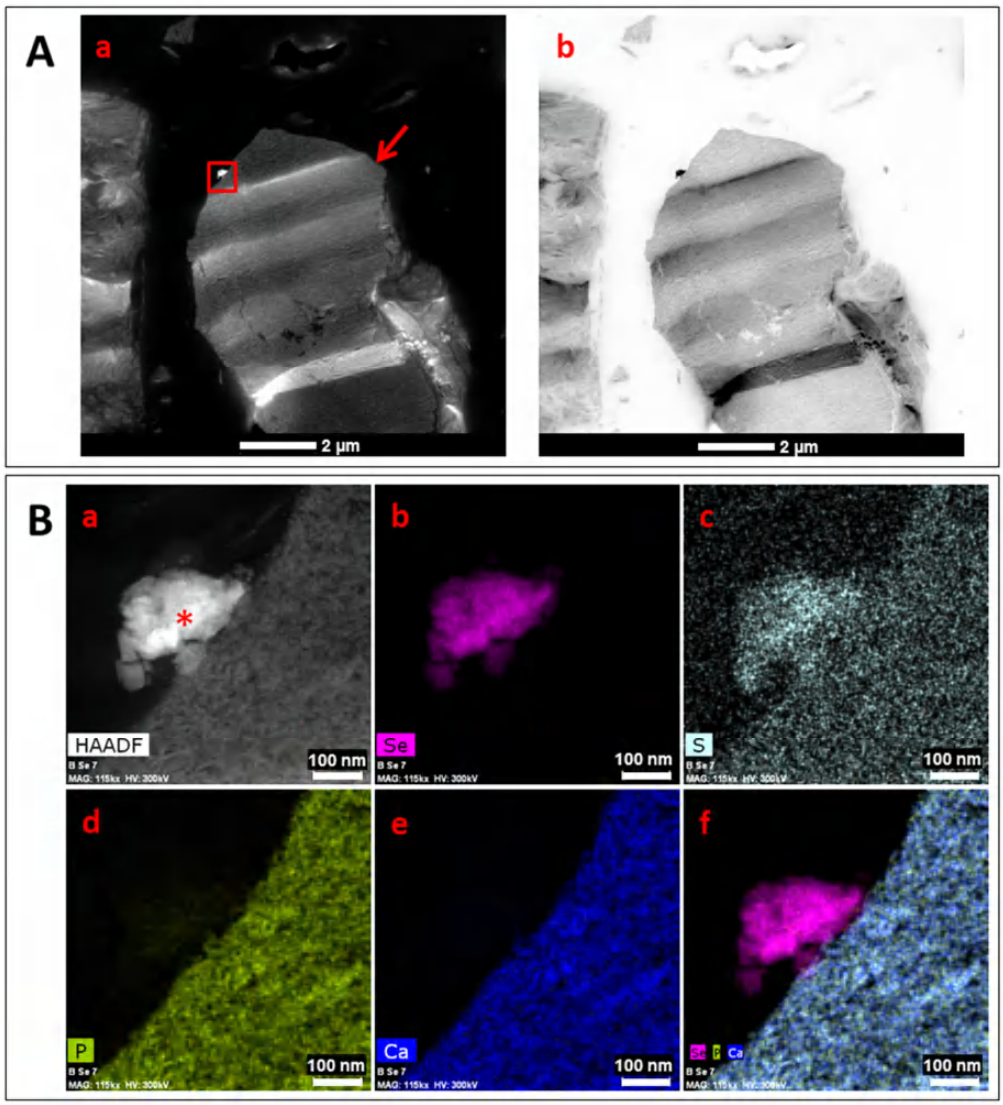

Figure 8. High-Angle Annular Dark-Field Scanning Transmission Electron Microscopy (HAADF-STEM) imaging of SeNPs associated with apatite in the BSe microcosms. A) Size comparison of SeNPs (red square) and the apatite mineral (arrow) in the HAADF mode (a) and inverse image (b). B) High-magnification HAADF-STEM micrograph of SeNPs and apatite (a), and their corresponding EDX elemental maps showing the distribution of Se (b), S (c), P (d), Ca (e), and a combination of Se+P+Ca (f).

In Fig. 8A, SeNPs seemed to be associated to a large mineral phase identified as apatite by EDX elemental mapping and showing the presence of Ca and P, the typical components of this mineral. In addition, apatite was surrounded by smectite layers. EDX maps also revealed the presence of Se and S within the electron-dense precipitates, in the nanowires and in the Se accumulates associated to the bentonite (Figs. 9b, 9c, 10b, and 10d). A representative EDX spectrum showing a high peak of Se and a less

contribution of S is presented in Fig. 10e. In addition, high signals of Fe were detected in Figs. 9 and 10 associated to the Si of smectite as shown in the EDX maps (Figs. 9d and 10c).

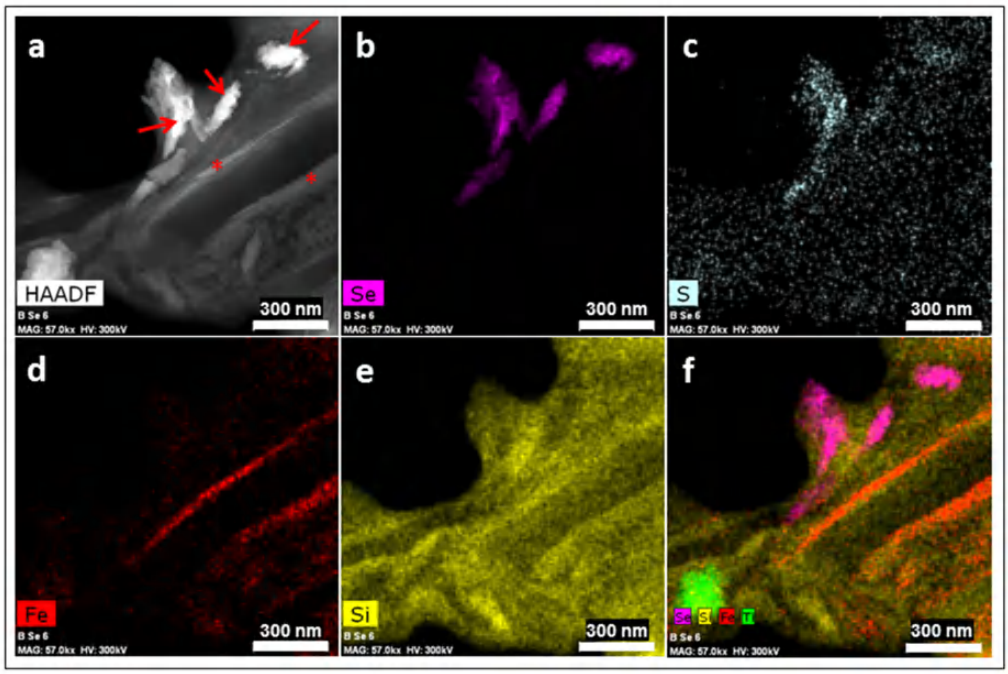

Figure 9. HAADF-STEM imaging of SeNPs associated to smectite in the BSe microcosms (a) and their corresponding EDX elemental maps with distribution of Se (b), S (c), Fe (d), Si (e), and a combination of Se+Si+Fe+Ti (f).

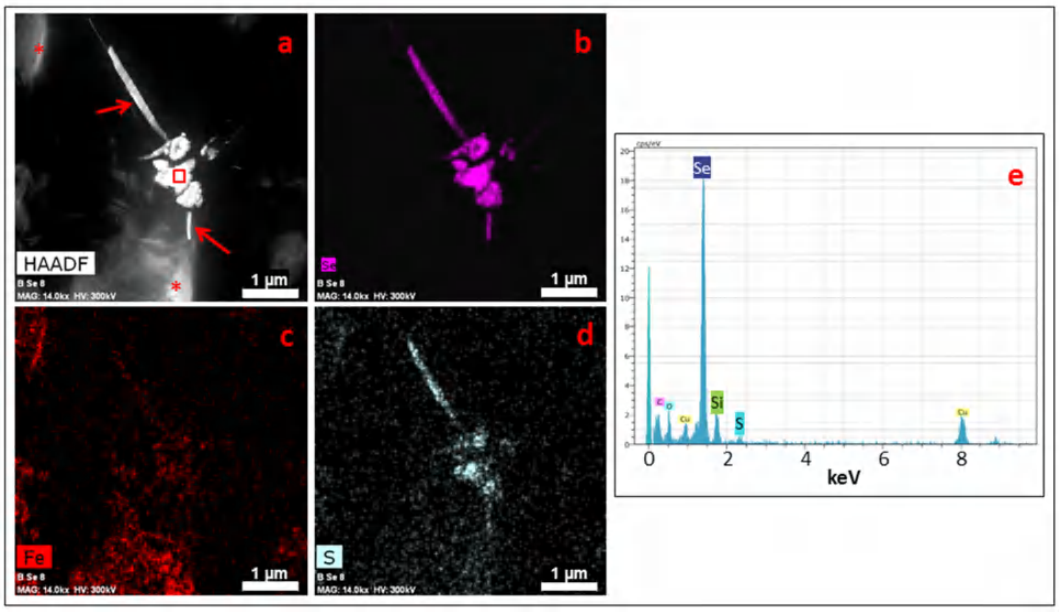

Figure 10. STEM-HAADF image of the SeNPs forming nanowires and polygonal particles in the BSe microcosms (a) and their corresponding EDX maps with the elemental distribution of Se (b), Fe (c), and S (d). e) Representative EDX spectrum of the polygonal SeNPs (selected area in a) indicating the presence of Se, S and Si.

The crystalline structure of the selenium nanowires were studied using Selected-Area Electron Diffraction (SAED), High-Resolution Transmission Electron Microscopy (HRTEM) and the associated Fast Fourier Transform (FFT). These techniques confirmed the crystalline nature of the Se-nanowires (Fig. 11B, C, and D). The SAED analyses indicated lattice spacings of 0.22 nm and 0.20 nm corresponding to the (111) plane of trigonal phase of Se (*t*-Se) (Fig. 11B). The HRTEM image of the nanowire showed a lattice spacing of 0.30 nm corresponding to the (101) plane of *t*-Se, confirmed by the FFT (Fig. 11C and D).

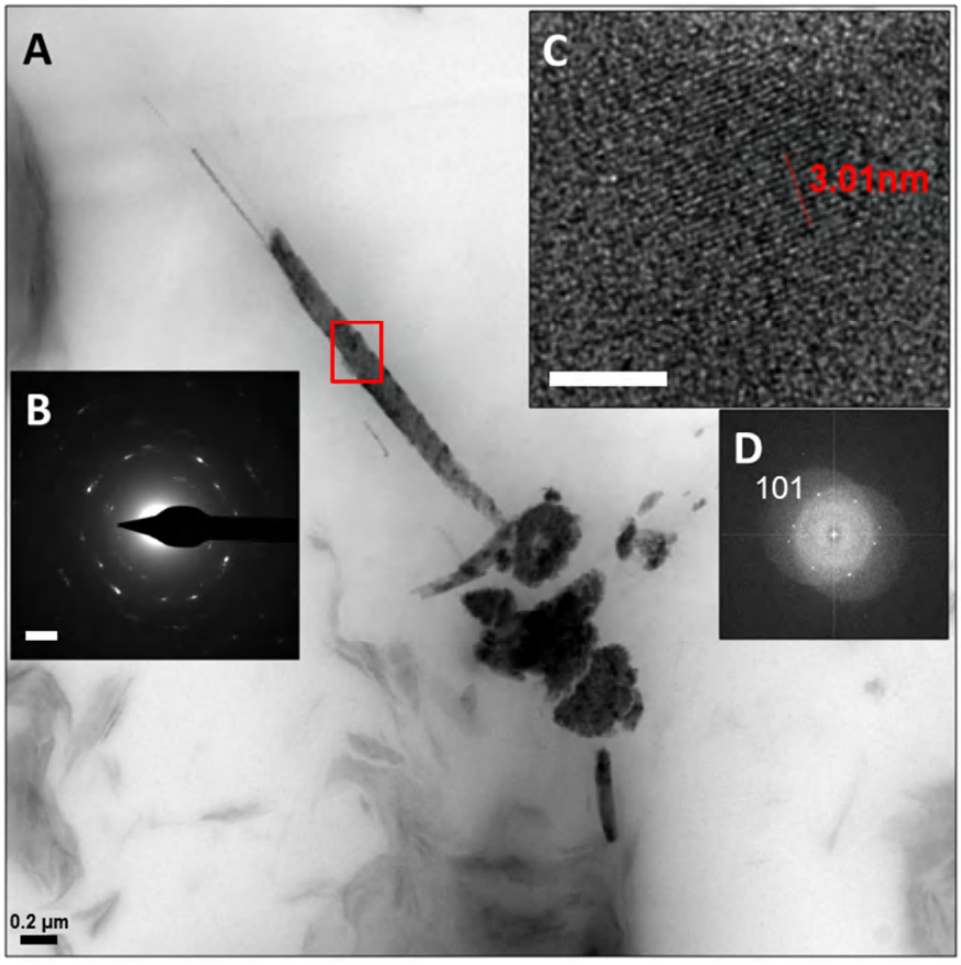

Figure 11. High-Resolution Transmission Electron Microscopy (HRTEM) image of the SeNPs forming nanowires and polygonal particles in the BSe microcosms (A). B) Selected-Area Electron Diffraction (SAED) pattern corresponding to the selected area in A. C) HRTEM image of the selenium nanowire with the measured spacing of 10 lines and D) their correspondent Fast Fourier Transform (FFT). Scale bars: 2 1 nm^{-1} (B), 5 nm (C).

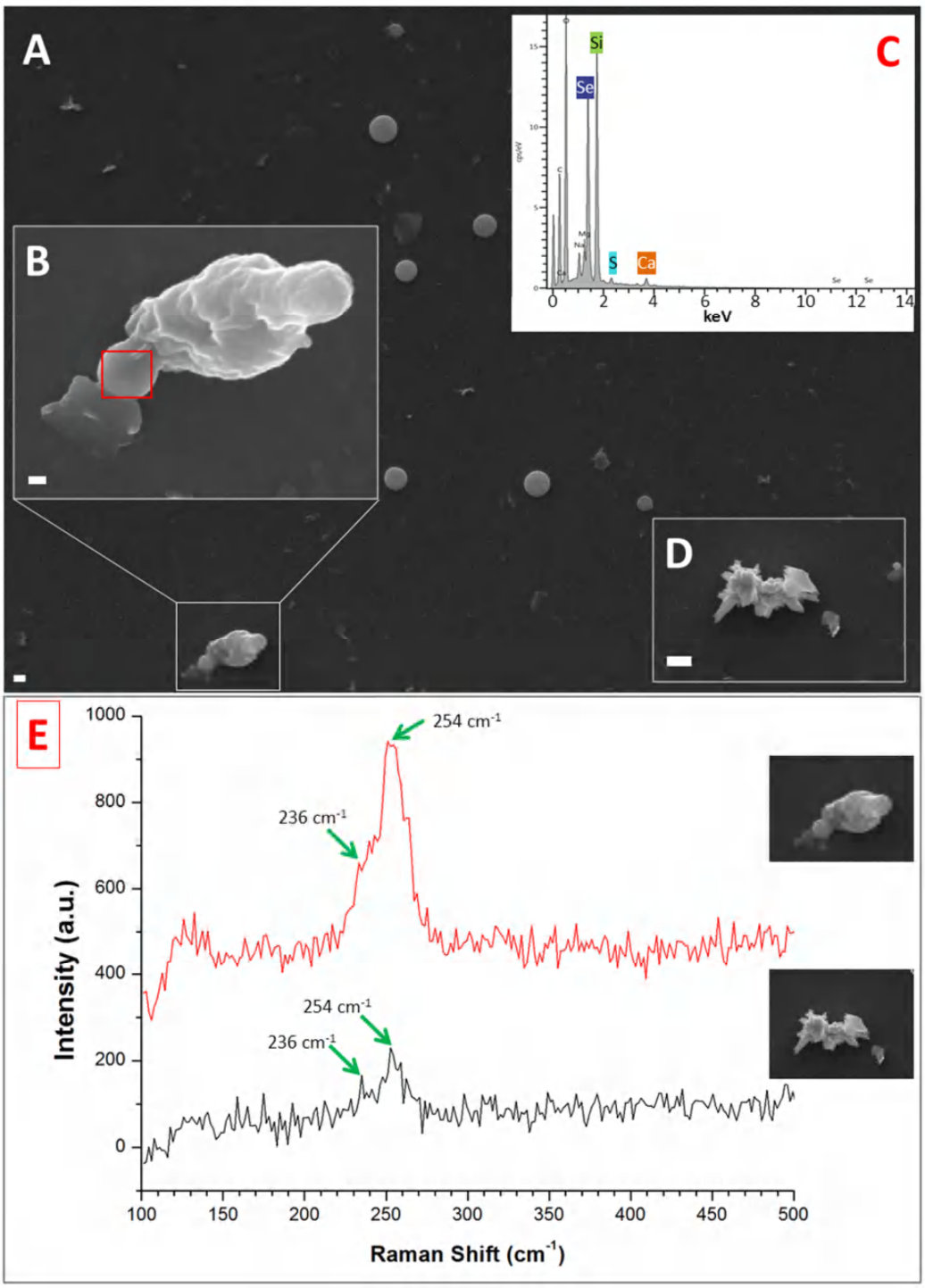

Figure 12. Variable Pressure Field Emission Scanning Electron Microscopy (VP-FESEM) images of the SeNPs formed in BSe microcosms (A, B, and D). Images are shown in secondary electrons with the InLens detector. C) Representative EDX spectrum of the selenium nanospheres (selected area in B) indicating the composition of Se, and S (Si and Ca are attributed to the background). E) Raman spectroscopy analyses derived from selenium nanosphere (red) and aggregates (black). Scale bar represents 200 nm in A, 100 nm in B, and 1 µm in D. Selected area in A is amplified in B.

VP-FESEM images indicated the presence of individual Se nanospheres and aggregates SeNPs (Fig. 12A and D). Interestingly, some Se nanospheres seemed to be released at the extracellular space as a consequence of cell lysis (Fig. 12B). Individual and aggregates of Se nanoparticles were composed of Se and S according to EDX analysis (Fig. 12C). Raman spectra derived from these two types of Se nanostructures revealed the presence of peaks at 254 cm^{-1} corresponding to amorphous SeNPs (*a*-Se), in addition to a small peak at 236 cm^{-1} corresponding to symmetric stretching mode of *t*-Se.

4.2.2. Se(IV)-treated sterile bentonite (BsSe)

At 6 months of incubation, a slightly orange layer was observed on the surface of the BsSe sample probably due to the formation of Se(0) as a result of Se(IV) reduction. HAADF-STEM micrographs of thin sections of the studied sample confirmed the presence of electron-dense nanostructures of different shapes and sizes such as polygonal aggregates growing longitudinally (Fig. 13A and B) or hexagonal nanoparticles (Fig. 13C and D) and sizing from approximately 100 to 700 nm. These nanostructures contained Se and S as it was shown by EDX analysis (Data not shown).

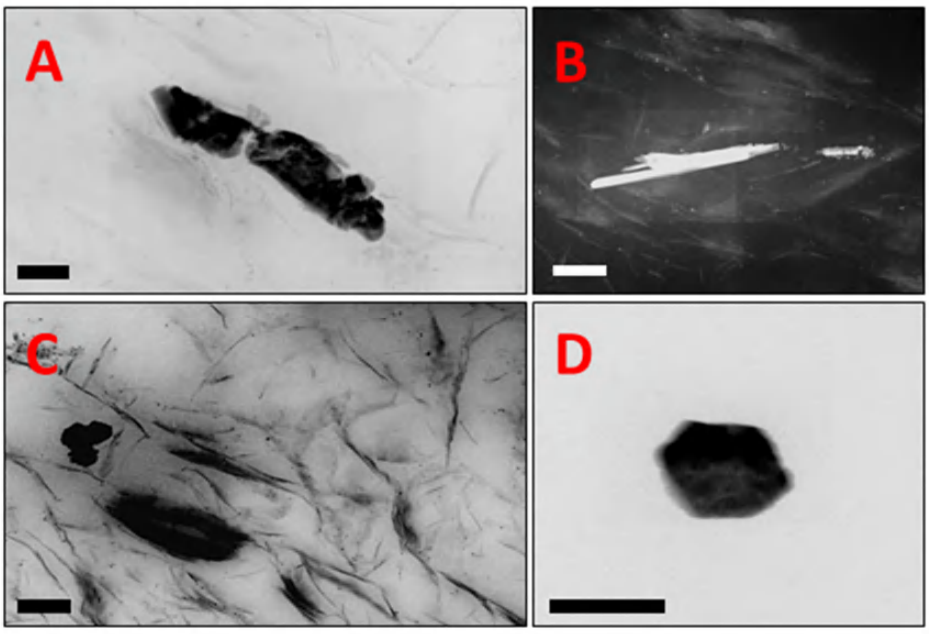

Figure 13. HAADF-STEM micrographs of SeNPs in the BsSe sample in the HAADF mode (B) and digital transformation of HAADF image (A, C, and D). Images of Se nanostructures with different morphologies: polygons (A, and B) hexagons as aggregates (C) or individual (D). Scale bars represent 100 nm in A and D, and 200 nm in B and C.

In some thin sections, Se nanostructures were located at the surface of smectite layers (Fig. 14A) as it was confirmed by EDX analysis (Fig. 14f). EDX spectrum of these electron-dense aggregates showed high peak of Se and a minor presence of S, confirming the composition of Se-S of the nanoparticles (Fig. 14e). EDX maps also revealed the composition and the distribution of Se (Fig. 14b). In addition, as expected high signals of Fe were detected in the smectite EDX spectrum, as it was also its distribution revealed by EDX map (Fig. 14c) associated to the Si of smectite. The superposition of Si and Se obtained in the EDX maps (Fig. 14d and Fig. 14e) indicated that these SeNPs may be probably associated to the smectites.

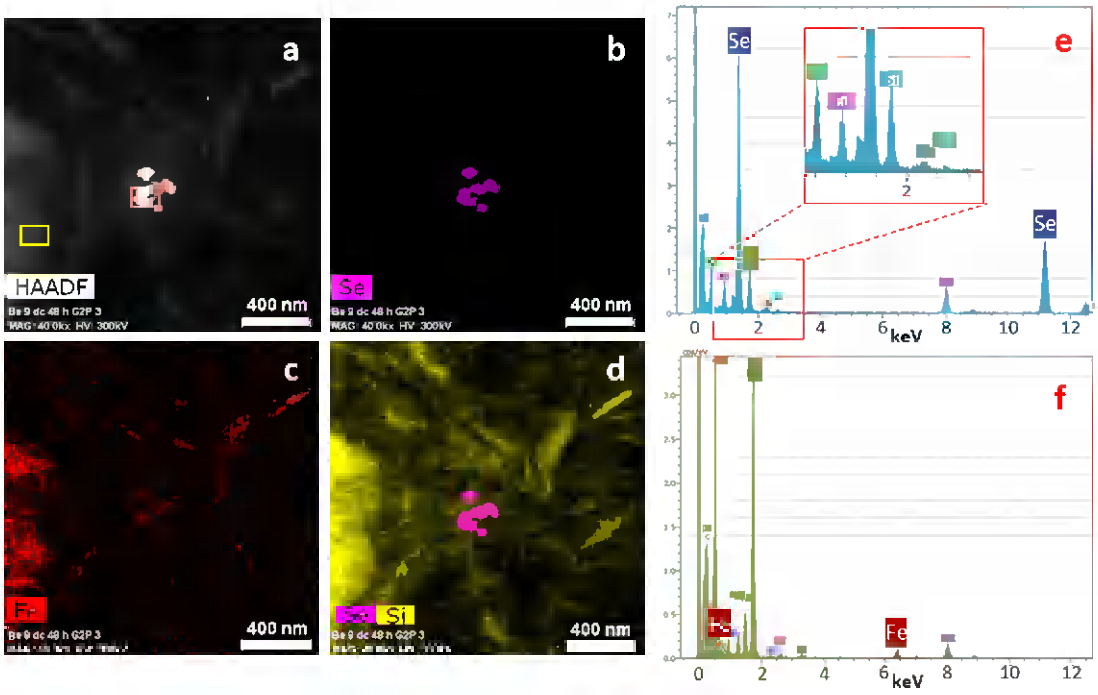

Figure 14. HAADF-STEM micrographs of SeNPs in the BsSe sample associated to smectites (a) and their corresponding EDX maps with the elemental distribution of Se (b), Fe (c), and a combination of Se and Si (d). e) Representative EDX spectrum of the polygonal SeNPs (red-selected area in a) indicating the presence of Se, S and Si. f) EDX spectrum of the smectites showing peaks of Fe (yellow-selected area in a).

The crystalline structure of the SeNPs formed in BsSe microcosms was studied using SAED and measuring the lattice spacing by HRTEM and the associated FFT (Fig. 14). SAED analysis of polygonal Se nanostructures showed lattice spacings of 0.30 nm and 0.21 nm both corresponding to the (101) and (111) planes of crystalline form *t*-Se (Fig. 15B). In addition, this trigonal structure was also confirmed by HRTEM and FFT

analyses where the lattice spacing corresponding to 0.38 nm related to the (100) plane of *t*-Se was obtained (Fig. 15C and D).

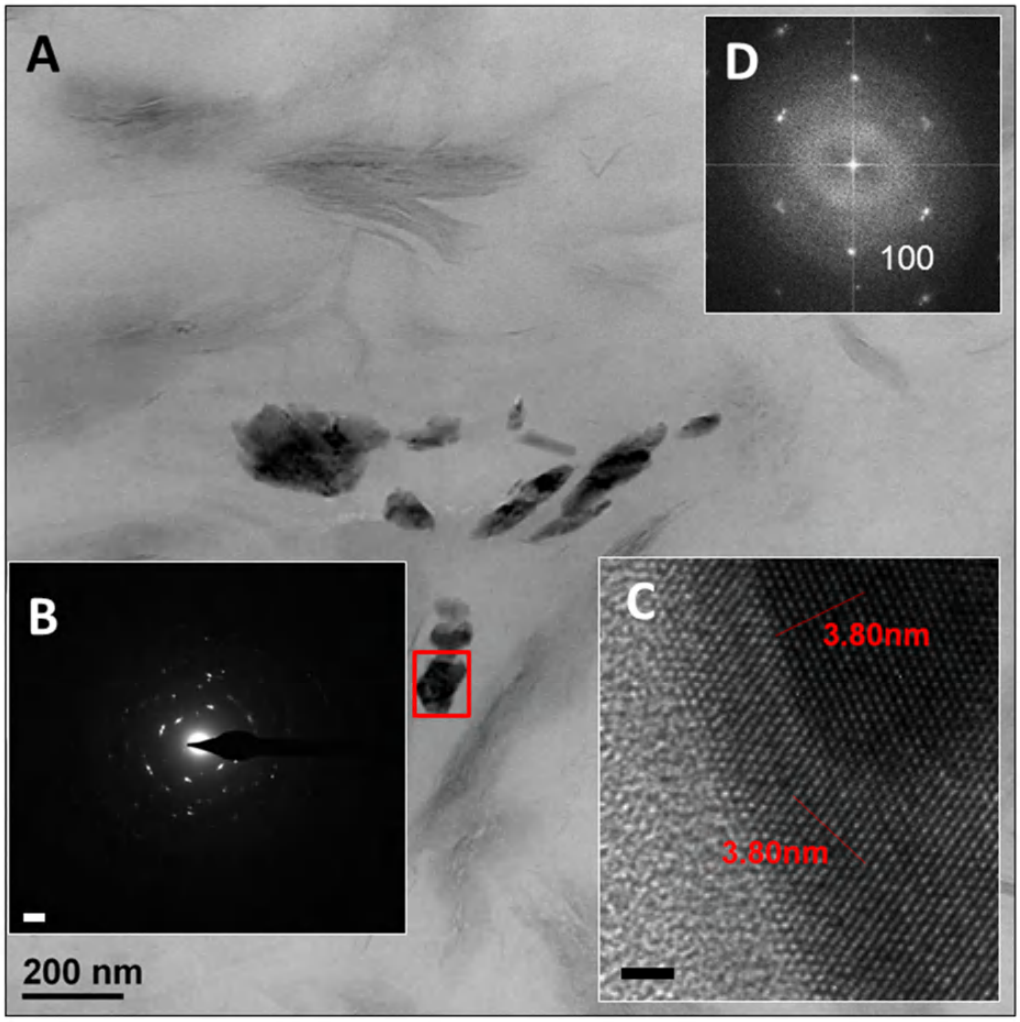

Figure 15. HRTEM image of the polygonal SeNPs formed in the BsSe microcosms (A). B) SAED pattern corresponding to the selected area in A. C) HRTEM image of the selected SeNP in A with the measured spacing of 10 lines, and D) their correspondent FFT showing a (100) crystallographic plane of the SeNP. Scale bars: 2 1 nm^{-1} (B) and 2 nm (C).

As in the case of BSe sample, numerous sphere-shaped SeNPs were observed in the BsSe microcosms (Fig. 16A, C and D). In addition, VP-FESEM analysis revealed other Se nanostructure morphologies similar to those obtained in the sample BSe (Fig. 12D). In these samples, nanowires were also identified (Fig. 16B, and E). All these selenium nanostructures were composed of Se and S according to their EDX spectra (Data not shown). The aggregated forms of SeNPs found in this sample (Fig. 16B) were apparently more crystalline than the individual nanospheres. Raman spectroscopy analyses were performed on the all types of SeNPs showing peaks at different Raman

shifts values. The Raman scattering spectrum derived from the individual Se nanospheres exhibited a peak at 252 cm^{-1} (Fig. 16F-A and F-C) which could be attributed to *a*-Se or crystalline monoclinic Se (*m*-Se) (Lucovsky et al., 1967). A peak at 235 cm^{-1} corresponding to *t*-Se was observed in the Raman spectra of the Se polygonal aggregate (Fig. 16F-B) and nanowires (Fig. 16F-E).

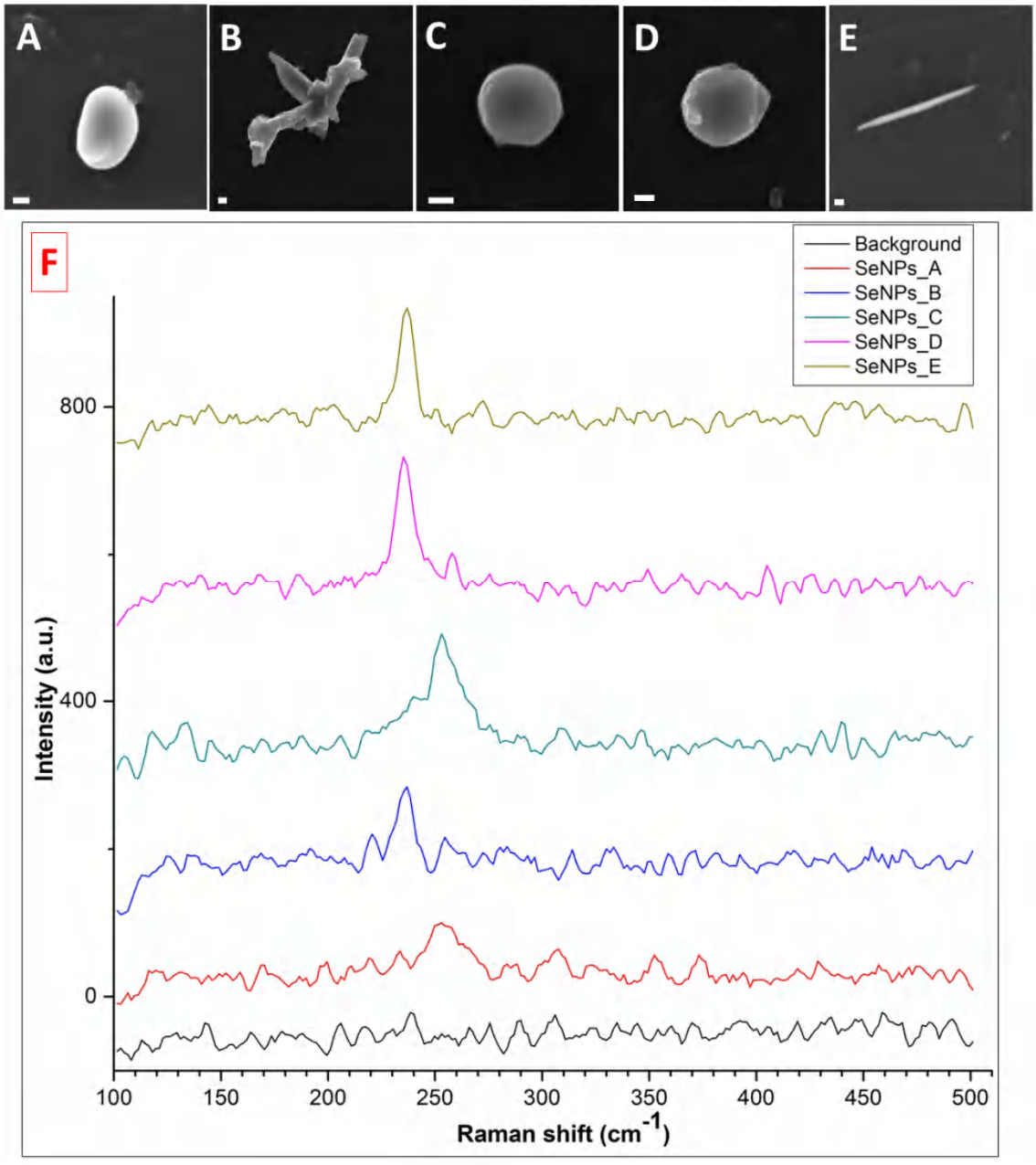

Figure 16. VP-FESEM images of the SeNPs formed in BsSe microcosms corresponding to nanospheres (A, C, D), polygonal aggregates (B) and nanowires (E). Images are shown in secondary electrons with the InLens detector performed at 5.00 kV (A, B, C, and D) and at 10.0 kV (E). F) Raman spectroscopy analyses derived from SeNPs in A (red), B (blue), C (green), D (pink), and E (brown) and a background signal (black). Scale bars represent 100 nm in A, B, C, and D; and 200 nm in E.

4.2.3. Se(IV)-treated bentonite spiked with BSPAS consortium (BBSe)

After six months of anaerobic incubation, BBSe microcosms presented a remarkable black layer on the top of the sedimented bentonite, probably due to the formation of SeNPs with different structure than those shown in the rest of the studied samples. HAADF-STEM and VP-FESEM micrographs confirmed the presence of SeNPs with different morphologies and sizes ranging from approximately 500 nm to 8 µm of diameter (Figs. 17, 18, 19 and 20). EDX spectra confirmed the Se and S composition of these precipitates (Data not shown).

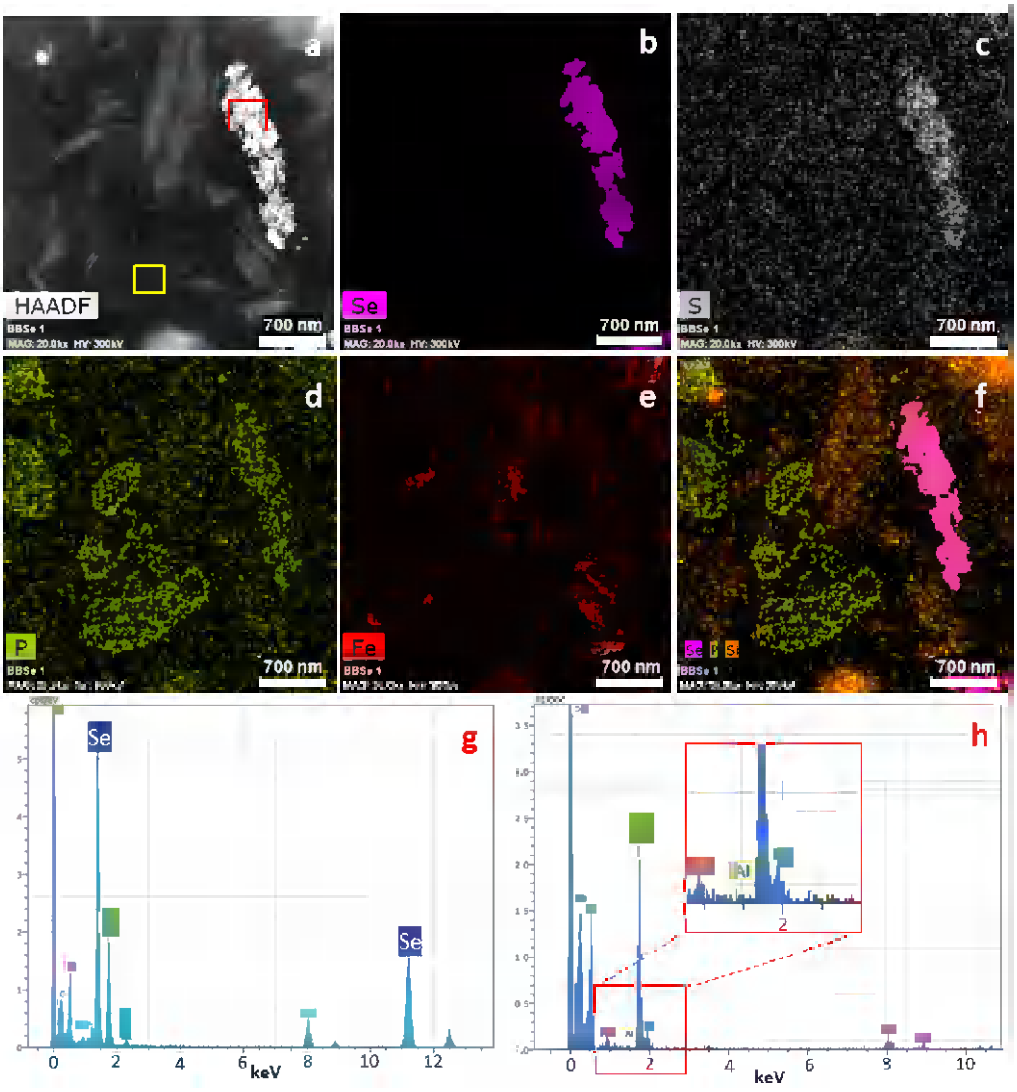

Figure 17. HAADF-STEM micrograph of extracellular SeNPs in the BBSe microcosms associated to smectites and bacterial cells (a). EDX maps with the elemental distribution of Se (b), S (c), P (d), Fe (e), and a combination of Se+P+Si (f, pink, green, and orange, respectively). Representative EDX spectrum of the polygonal SeNPs (red-selected area in a) indicating the presence of Se, S and Si (g). EDX spectrum of the cells (yellow-selected area in a) showing peaks of P (h).

HRTEM analyses of BBSe microcosms revealed the presence of bacterial cells surrounding the SeNPs (Fig. 17A) and confirmed by the presence of P in the EDX spectrum (Fig. 17h) and in the EDX map (Fig. 17d). As in the previous cases, SeNPs seemed to be associated to smectite detecting Si in the SeNPs beside peaks of Se and S (Fig. 17f) as confirmed by the EDX analysis. EDX maps also supported the composition and the distribution of Se (Fig. 17b) and S (Fig. 17c). In addition, high signals of Fe were detected in the smectite EDX spectrum and the distribution of Fe was revealed by the EDX map (Fig. 17e) to be associated to the Si of smectite.

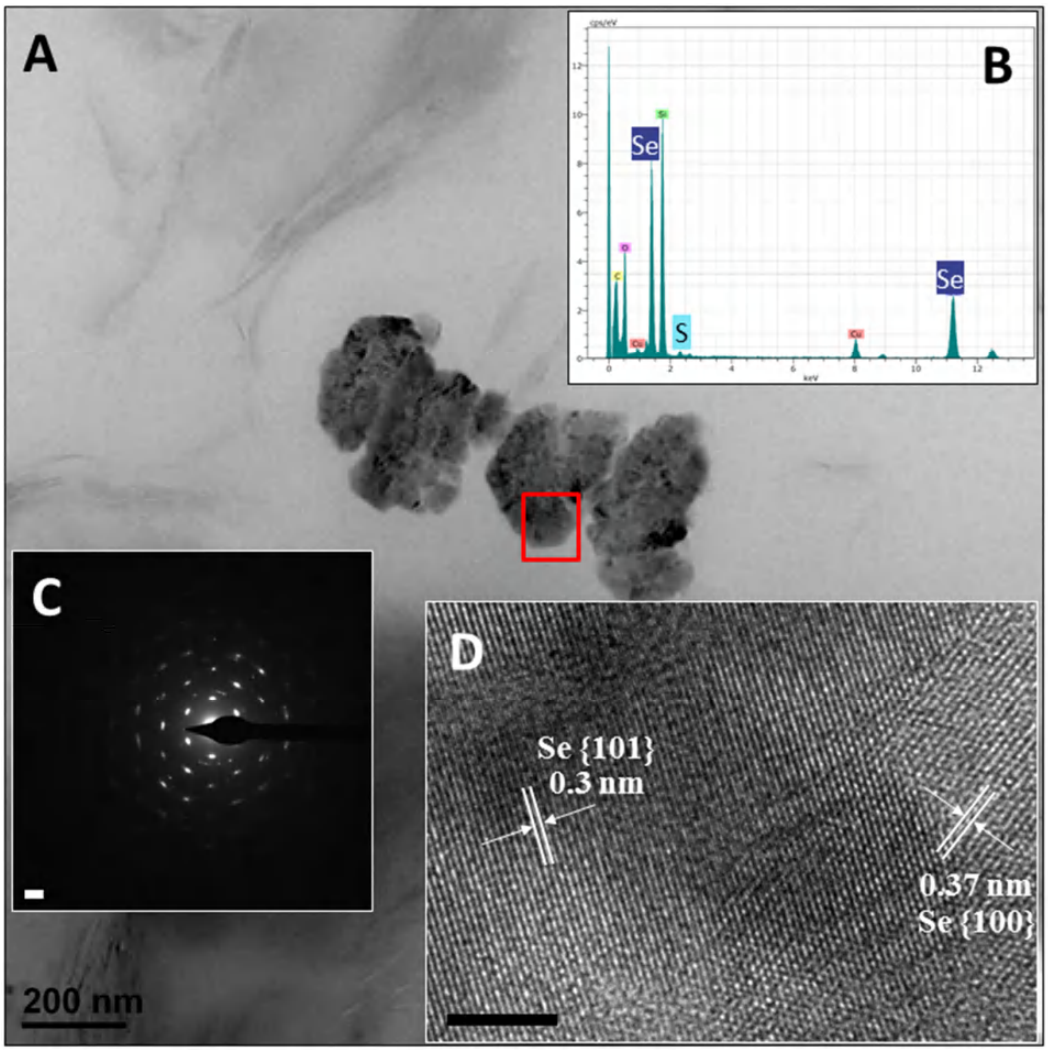

Figure 18. HRTEM image of the polygonal SeNPs formed in the BBSe microcosms (A). B) EDX spectrum of the polygonal SeNPs with peaks of Se and S. C) SAED pattern corresponding to the red-selected area in A. C) HRTEM image of the selected SeNP in A with the measured lattice spacing indicating the plane of crystalline Se. Scale bars: 2 1 nm^{-1} (C) and 2 nm (D).

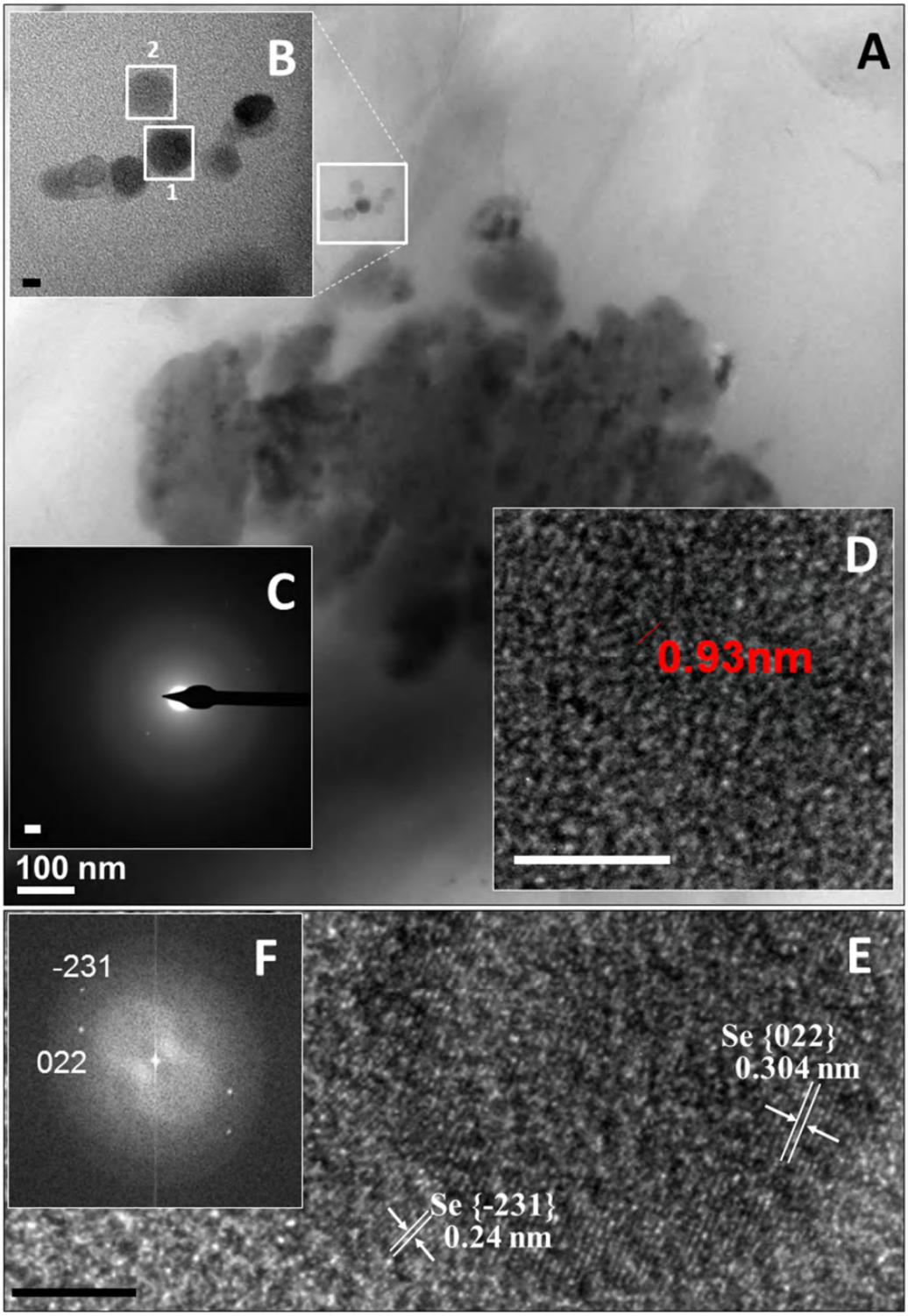

Figure 19. HRTEM image of the SeNPs formed in the BBSe microcosms (A). B) High magnitude HRTEM image of the selected area in A of the nanospheres. C) SAED pattern corresponding to the selected area 1 in B. D) HRTEM image of the selected area 1 in B with the measured spacing of 4 lines. E) HRTEM image of the selected area 2 in B with the measured lattice spacing, and F) their correspondent FFT. Scale bars: 2 1 nm^{-1} (C), 5 nm (D and E), and 10 nm (B).

Additionally, the structure of these aggregated SeNPs formed in BBSe microcosms were studied using SAED and HRTEM (Fig. 18). High number of nanoparticles was analyzed by EDX to determine the elemental composition resulting in peaks of Se and S (Fig. 18A and B). HRTEM analyses of these Se nanostructures showed two distinct lattice spacings of 0.37 and 0.30 nm, corresponding to the (100) and (101) planes of *t*-Se, respectively (Fig. 18D). SAED pattern indicated that these nanostructures were polycrystalline, which can be well indexed to *t*-Se (Fig. 18C). However, 20-30 nm Se nanospheres associated to bigger Se nanostructures were also observed (Fig. 19A and B) and exhibited poorer crystallinity as it was showed by the SAED pattern (Fig. 19C). HRTEM analyses and the associated FFT of these smaller NPs in the BBSe microcosms showed different lattice spacings of 0.24, 0.30, and 0.31 nm corresponding to the (-231), (022), and (-401) planes of the *m*-Se (Fig. 19D, E, and F). SAED pattern confirmed the low crystallinity of these nanospheres (Fig. 19C).

Interestingly, high number of big sized crystals of higher dimensions was observed in the BBSe sample using VP-FESEM in contrast to the previously described SeNPs obtained in BSe and BsSe microcosms (Fig. 20, A-F). All these selenium-crystals were composed of Se and S according to the EDX spectra (Data not shown). These microcrystals seemed to be formed by the aggregation of individual Se nanospheres as it was shown in Fig. 20D. After 6 months of incubation, these crystals were apparently growing both longitudinally and in height, as it was indicated by observing the edges and surface of the crystals. Raman scattering spectrum derived from these Se nanostructures exhibited peaks at 235-236 cm^{-1} (Fig. 20G), which could be attributed to *t*-Se (Lucovsky et al., 1967; Nagata et al., 1981). In addition, the crystal spectrum in Fig. 20G-F also contained a peak at 252 cm^{-1}, which could be attributed to *a*-Se or crystalline *m*-Se (Goldan et al., 2016; Lucovsky et al., 1967).

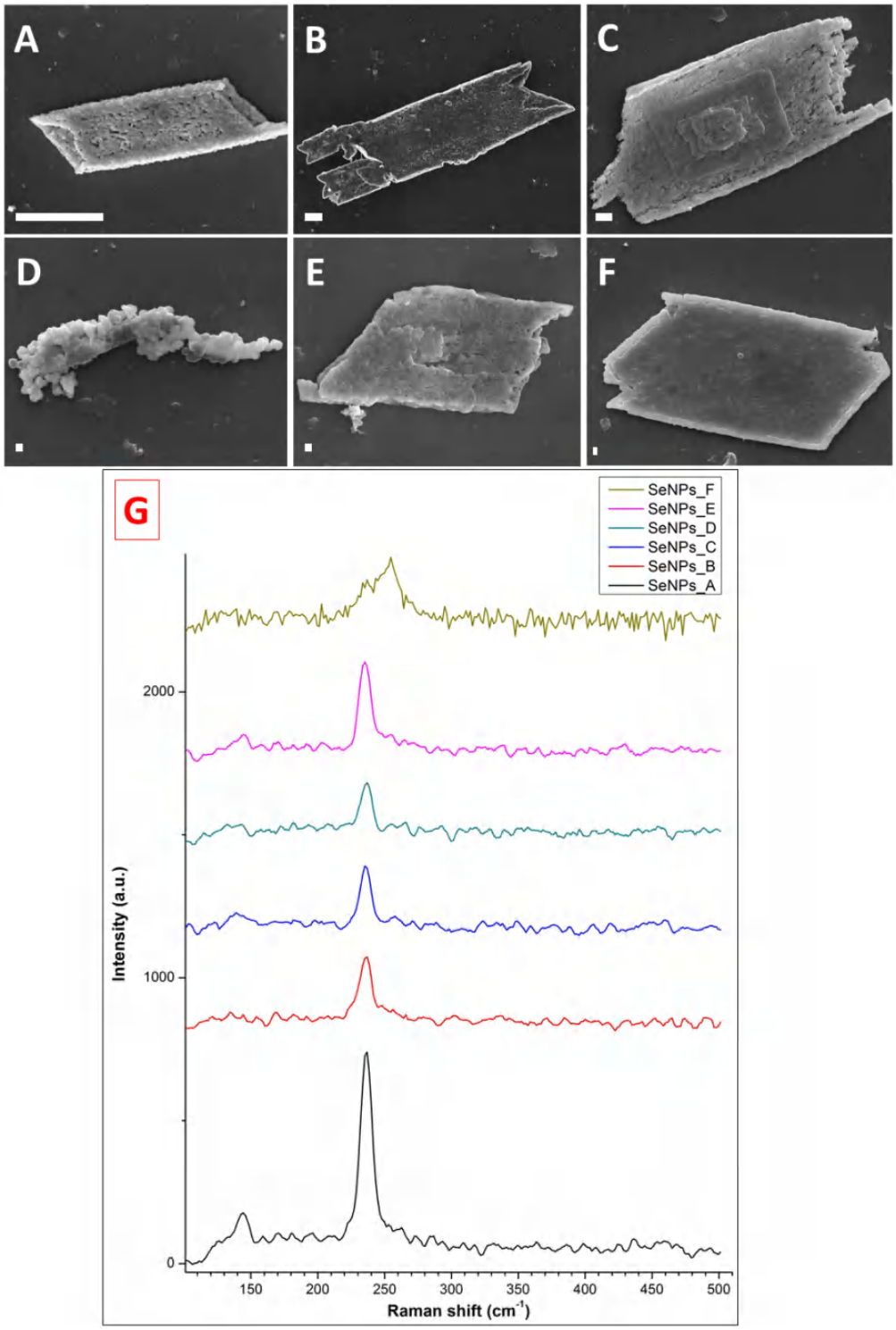

Figure 20. VP-FESEM images of the SeNPs formed in BBSe microcosms corresponding to growing selenium crystals (A, B, C, E, and F), and incipient in form of aggregated SeNPs (D). Images are shown in secondary electrons with the InLens detector performed at 5.00 kV (B) and 10.0 kV (A, C, D, E, and F). G) Raman spectroscopy analyses derived from crystals of SeNPs in A (black), B (red), C (blue), D (green), and E (pink) and F (brown). Scale bars represent 5 µm in A, 1 µm in B and C, and 200 nm in D, E and F.

4.2.4. Se(IV)-treated sterile bentonite spiked with BSPAS consortium (BsBSe)

BsBSe microcosms presented a remarkable orange layer on the surface of the bentonite as it was observed in the BSe sample. HAADF-STEM micrographs of thin sections of the recovered orange layers showed the presence of electron-dense nanostructures associated to bacterial cells (Figs. 21a, and 22A). In this case, cell surface- and intracellular-Se precipitates were observed (Fig. 21a). EDX element-distribution maps and EDX spectra of these Se nanostructures confirmed that they were

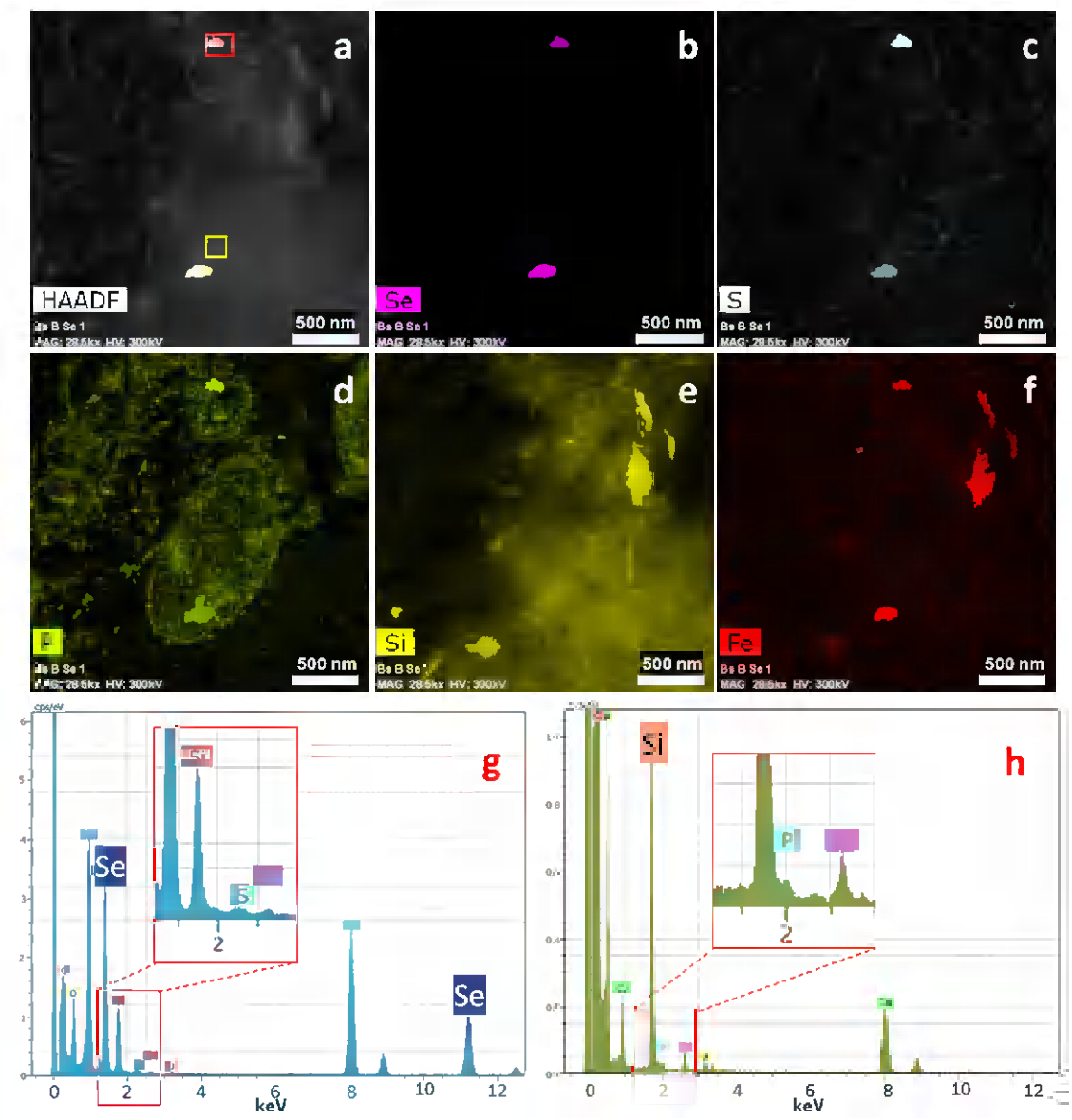

Figure 21. HAADF-STEM micrograph of intracellular SeNPs in the BsBSe microcosms (a). EDX maps with the elemental distribution of Se (b), S (c), P (d), Si (e), and Fe (f). EDX spectrum of the SeNP associated to bacterial cells (red-selected area in a) indicating the presence of Se, S and Si (g) and EDX spectrum of the cells showing peaks of P and Si (yellow-selected area in a).

mainly composed of Se and S (Fig. 21b; c; and g) in addition to P peak arising from cell biomass (Fig. 21d and 21h). As previously described, smectites were also present as it was shown by the EDX spectra (Fig. 21g and h) and the EDX maps of Si and Fe (Fig. 21e and f). Surprisingly, the signal of Fe in the EDX map overlapped with the Se signal but in the EDX spectrum of SeNPS, no peak of Fe was found (Fig. 21b, f, and g).

These SeNPs were quite smaller in size than those observed in the BBSe sample. In Fig. 22A, several intracellular SeNPs at the plasmatic membrane level are shown. HRTEM analyses and the associated FFT of the intracellular Se nanostructures showed two distinct lattice spacings of 0.33 and 0.34 nm corresponding to the (212) and (220) planes of *m*-Se (Fig. 22B, D and E). SAED pattern indicated that these nanostructures were crystalline, which could be well indexed to *m*-Se (Fig. 22C).

In order to determine if the SeNPs in the BsBSe microcosms were intra- or extracellular, VP-FESEM analyses were performed. The most abundant SeNPs found were the ones inside the bacterial cells (Figs. 23A-23C) or associated to cell debris (Figs. 23D-23I). These SeNPs were probably formed inside the cells and then released to the extracellular space to be aggregated afterwards. Backscattered electron images showed bright areas corresponding to Se and indicating the presence of individual Se nanospheres inside the cells (Fig. 22B) or interconnected to each other by the organic material (Fig. 23E, 23H). In the secondary electron detector performed at 1.0 kV, the association between nanospheres of selenium and the organic compounds resulting from cells was shown (Fig. 23C, F, and I). Raman spectroscopy analyses were performed for the intracellular Se-nanospheres showing peaks at 251-252 cm^{-1} (Fig. 23A), which could be ascribed to *a*-Se or crystalline *m*-Se.

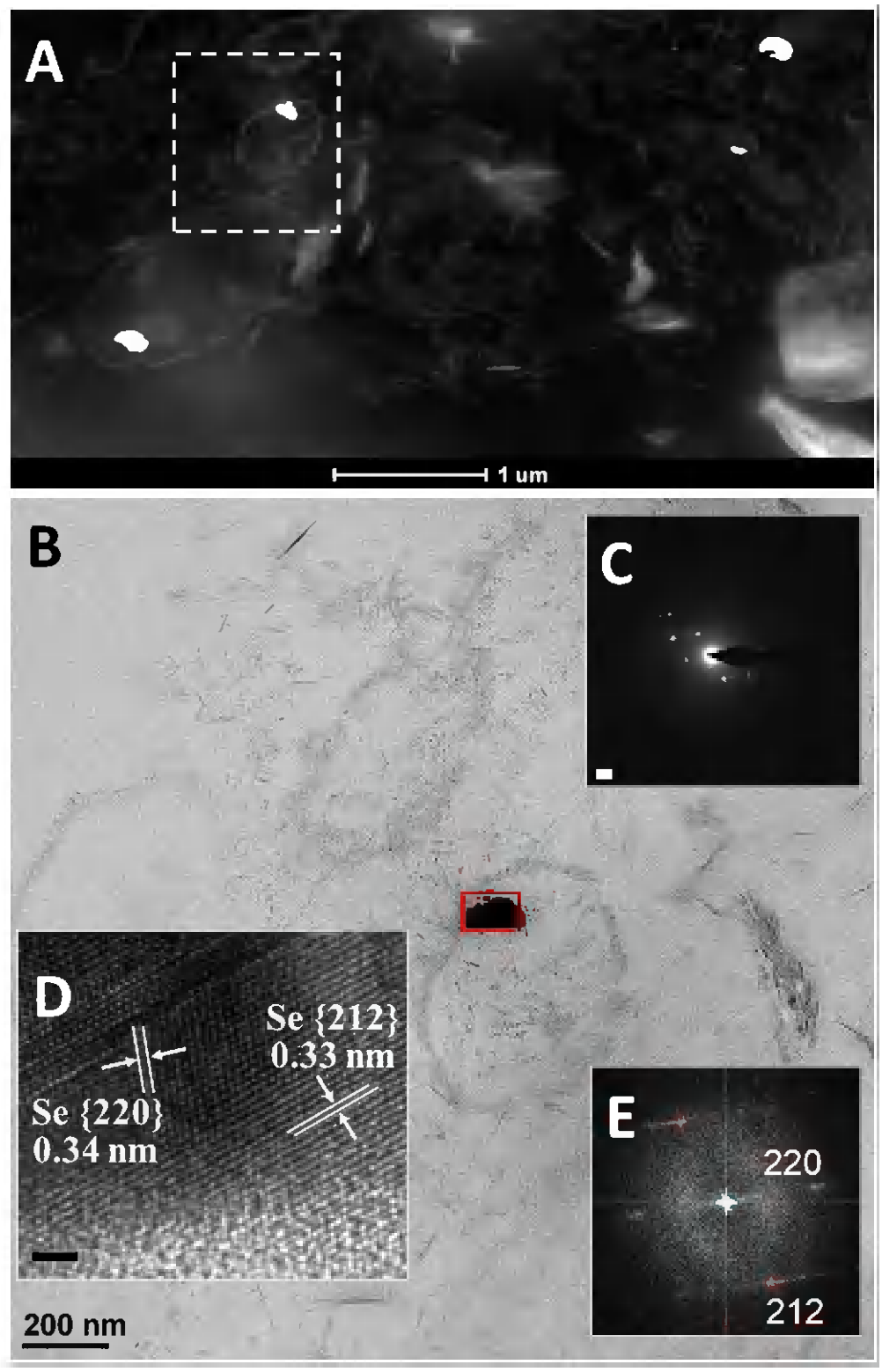

Figure 22. HAADF-STEM micrograph of intracellular SeNPs in the BsBSe microcosms associated to different bacterial cells (A) and the HRTEM image of the SeNP of the selected area in A (B). C) SAED pattern corresponding to the selected area in B. D) HRTEM image of the selected area in B with the measured lattice spacing and E) their correspondent FFT showing the plane of the crystalline Se. Scale bars: 2 1 nm^{-1} (C), and 2 nm (D).

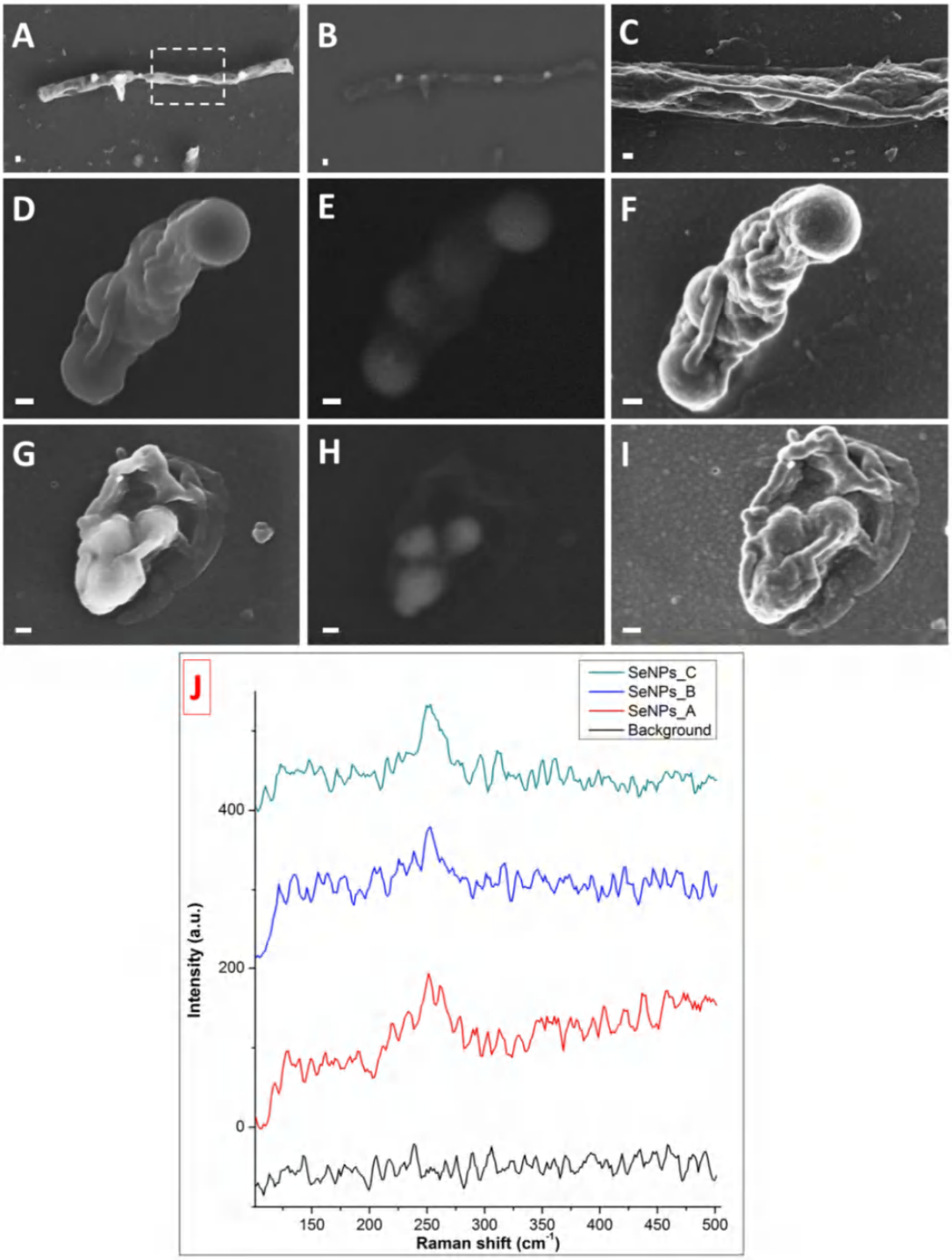

Figure 23. VP-FESEM images of the SeNPs formed in BsBSe microcosms corresponding to the selenium nanoparticles inside the bacterial cells (A, B, and C) and associated to cell debris (D, E, F, G, H, and I). The images are shown in secondary electrons with the InLens detector performed at 1.00 kV (C, F, and I), and 5.00 kV (D, and G). The images are shown in backscattered electrons with the AsB detector performed at 5.0 kV (E, and H), 10.0 kV (B). The image is shown in secondary-backscattered electron mixing mode at 10.0 kV (A). G) Raman spectroscopy analyses derived from SeNPs in A (red), B (blue), C (mint green), and background (black). Selected area in A is amplified in C. Scale bars represent 1 µm in A, and B; and 100 nm in C, D, E, F, G, J, and I.

5. DISCUSSION

The Se^{79} isotope generated by nuclear fission reactions is considered one of the critical radionuclides for the geological disposal due to its ability to emit β particles. Chemically, Selenium, existing in 4 oxidation states [Se(VI), Se(IV), elemental Se, Se(-II)], is widely distributed in nature, being the oxyanions selenate and selenite, the predominant forms of this element, able to produce harmful effects on the cell viability due to their high toxicity (Fernández-Llamosas et al., 2017). The present study aimed to shed light on the impact that has Se(IV) on the structure and composition of the bentonite microbial community in microcosms amended with acetate and G2P. In addition, the influence of bentonite microbial populations on the structure and chemical speciation of Se(IV) was also determined.

5.1. Impact of selenite on the microbial diversity of water-saturated bentonite

The results obtained in the present work indicated that Se(IV) affected the distribution of bacterial and archaeal communities, naturally present in the bentonites. In the case of archaea, the genus *Methanosarcina* was unable to grow in the presence of soluble Se(IV) as it was demonstrated by its low relative abundance in the selenite-treated microcosms (BBSe, BsBSe, BSe and BsSe). Although its abundance in BBSe (21.5%) was clearly lower than in the untreated control BB (49.2%), *Methanosarcina* seemed to be able to grow in bentonite microcosms inoculated with BSPAS consortium. The tolerance of this microorganism to Se(IV) could be enhanced by the total reduction of Se(IV) to Se(0) by members of the inoculated consortium (*Pseudomonas*, *Shewanella*, *Stenotrophomonas*, and *Amycolatopsis*). These bacterial strains were described for their ability to reduce soluble Se(IV) to Se(0), the much less toxic and insoluble form of selenium (Avendaño et al., 2016; Hunter, 2014; Ruiz-Fresneda et al., 2019, 2018). In addition, *Amycolatopsis,* also added to the bacterial consortium and detected in BBSe (3.1%), was found to be enriched in high-Se soils where this metalloid was present as a mixture of Se(IV) and Se(VI) at an average concentration of >30 mg/kg (Rosenfeld et al., 2018). Recently, Bueno-Galera (2019) reported the ability of pure culture of *A. ruanii* to tolerate high concentration of Se(IV) through its reduction to Se(0) forming intracellular nanospheres.

On the other hand, the presence of Se(IV) enhanced the occurrence of bacteria with Se-detoxification mechanisms such as *Pseudomonas* and *Stenotrophomonas*, which were more abundant in BsBSe microcosms accounting for 33.8 and 29% of the total bacterial community than in BsB (1.1 and 0.9%, respectively). Furthermore, sequences belonging to these bacteria were found in samples where BSPAS were not spiked (BSe and BsSe) indicating that both *Pseudomonas* and *Stenotrophomonas* were naturally occurring in the studied bentonites represented by approximately 3 and 1% of relative abundance in BSe. The relative abundance of these bacteria could have been enriched by the addition of sodium acetate in the microcosms since they are able to grow by the utilization of this organic acid as electron and carbon sources (Gonzalez-Gil et al., 2016; Sánchez-Castro et al., 2017; Yang et al., 2019).

In the same way, indigenous bacteria of bentonite such as *Desulfosporosinus* and unclassified *Desulfuromonadaceae* were found to be highly abundant in BSe microcosms than in the untreated samples (B) indicating their tolerance to the toxic selenite. These bacteria belong to the group of sulfate-reducing bacteria (SRB) whose capacities to reduce oxyanions of selenium to elemental selenium, utilizing lactate or acetate as electron donor, have been previously described (Hockin and Gadd, 2006, 2003; Nancharaiah and Lens, 2015).

Interestingly, unclassified genera affiliated to Firmicutes and Clostridiales were identified with high relative abundance in BSe and BsSe indicating that they were a naturally occurring bacteria in bentonites and showing a high resistance to the heat pressure and tolerance to selenite. Povedano-Priego et al. (2019) identified members of Clostridia in anaerobic microcosms treated with glycerol-2-phosphate revealing their ability to use this substrate as energy source. Also, their presence in the BsSe sample could be explained by their capacity to produce endospores as a resistant form to adverse conditions (e.g. heating) and afterwards these can germinate when favorable conditions reach the ecosystem (Xiao et al., 2011). For instance, favorable conditions like the availability of glycerol promoted the growth of *Clostridium* and other members of Clostridia in bentonite samples (Biebl, 2001; Patil et al., 2016). Gonzalez-Gil et al. (2016) also found that the abundance of Clostridia increased after 21 days of exposure to selenite in anaerobic sludge. In addition, several studies described the capacity of *Clostridium* to precipitate Se as Se(0) through an enzymatically active process (Bao et al., 2013; Gonzalez-Gil et al., 2016).

5.2. Effect of bentonite microbial communities on the chemical speciation of Se(VI)

5.2.1. Reduction of Se(IV) to Se(0) and the formation of SeNPs in the anaerobic water-saturated microcosms

In the different selenite-treated microcosms (BBSe, BsBSe, BSe and BsSe), the color changed depending on the treatment along the incubation, turning to orange or black. In general, an orange color was at first detected in all samples due to the generation of Se(0) as a consequence of Se(IV) reduction (Ruiz-Fresneda et al., 2018). In bentonites, selenite reduction could be mediated by abiotic and/or biotic processes. Several works stated that the retention of selenite in the bentonite happens through different processes: i) adsorption to bentonite mineral surfaces, or ii) reduction to Se(0) by pyrite (FeS_2), siderite minerals and even by the structural Fe(II) in smectites (Breynaert et al., 2010; Hoving et al., 2019; Kang et al., 2011). Hoving et al. (2018) showed that the Se(IV) reduction by pyrite seems to be headed by the adsorption of selenite which is transformed to Se(0) as a result of the electron transfer reactions. Accordingly, in the present study, EDX analysis of the BSe microcosms showed peaks of Se associated to smectite and adjacent to precipitates of Fe probably integrated in the bentonite structure. This finding could be related to the abiotic reduction of soluble selenite induced by the Fe(II) of pyrite.

In addition, by using microscopic techniques it was shown that Se was associated to different minerals. For instance, a big-sized apatite was found to be associated to this metalloid in the BSe sample. This apatite could be formed by the activity of bentonite indigenous microorganisms enriched by the addition of G2P in the pore water. Some of the native bentonite bacteria such as *Stenotrophomonas*, *Symbiobacterium* and *Brachybacterium* have been described for their phosphatase activity enabling them to release inorganic phosphate (P_i) from G2P (the organic source) (Hoang et al., 2014; Sánchez-Castro et al., 2017; Shiratori-Takano et al., 2014). This P_i could react with the Ca originated from the dissolution of calcite to induce the precipitation of apatite. Duc et al. (2003) showed the sorption of the selenite groups on the apatite surface. The sorbed selenium is embedded in the crystallographic sites where phosphorus is normally located, indicating that the Se sorption process on the apatite is commonly mediated by

an anionic exchange with phosphate groups. This could further explain the presence of SeNPs associated to the apatite in the BSe microcosms.

Biotic reduction of Se(IV) has been previously described in several works where the bacterial strains reduce oxyanions of Se to elemental selenium generating orange/reddish color of the medium under aerobic and anaerobic conditions (Avendaño et al., 2016; Dwivedi et al., 2013; Fernández-Llamosas et al., 2017; Ruiz-Fresneda et al., 2019, 2018). An orange layer on the surface of bentonite was observed in the Se(IV) treated bentonites. However, some differences were found between the studied samples. For instance, BsSe presented only a thin orange layer of SeNPs, which is probably due to the low bacterial density, as a result of the heating treatment (tyndallization), and the consequent low Se reduction rate in such microcosms.

A high number of works have described the reduction of Se(IV) by pure cultures of bacterial strains such as *Stenotrophomonas bentonitica* (Ruiz-Fresneda et al., 2019, 2018), *Pseudomonas seleniipraecipitans* (Hunter, 2014), *P. putida* (Avendaño et al., 2016), *P. aeruginosa* (Dwivedi et al., 2013), *Shewanella oneidensis* (Li et al., 2014) and *Pediococcus acidilactici* (Kousha et al., 2017), among others. Javed et al. (2015) investigated the selenite reduction by bacterial strains (*Bacillus subtilis*, *B. licheniformis*, *Exiguobacterium* sp., and *P. pseudoalcaligenes*) isolated from polluted environment. However, to the best of our knowledge this is the first work describing the reduction of Se(IV) within a ternary system containing microbe/bentonite/Se.

The obtained results indicated that the reduction of Se(IV) to Se(0) and the subsequent formation of SeNPs could be driven by the activity of the bentonite indigenous bacteria and/or the bacterial strains of the inoculated BSPAS consortium. Thus, in the BSe and BsBSe samples, SeNPs associated to bacterial cells were detected using state-of-the-art microscopic techniques (combination of HAADF-STEM, HRTEM/EDX and VP-FESEM). The location of Se nanostructures was determined by means of VP-FESEM. Interestingly, Se nanospheres seemed to be expelled out from the cells in BSe samples, while in the BsBSe microcosms, these nanospheres appeared associated to cell debris or inside the cells probably linked to the plasmatic membrane, as it was revealed by HAADF-STEM.

Different mechanisms have been proposed for explaining the bacterial Se reduction process. One of the best known is the intracellular reduction of selenite

mediated by molecules containing reduced thiols groups (-SH) such as the glutathione (GSH) that acts as selenite reducer. Selenite reacts with GSH producing selenodiglutathione (GS-Se-SG), which in turn is further reduced to selenopersulfide ($GS\text{-}Se^-$) by NADPH in presence of glutathione reductase (GS). The unstable selenopersulfide finally dismutates into GSH and Se(0) (Li et al., 2014; Ruiz-Fresneda et al., 2018). Hunter (2014) detected genes for GS and for the thioredoxin reductase (similar action to GS) in *P. seleniipraecipitans*, necessary for the intracellular selenite reduction. Other mechanism based on the activity of reductases that directly reduce Se(IV) to Se(0) such as nitrite reductase in *Rhizobium sullae* (Basaglia et al., 2007), fumarate reductase in *Shewanella oneidensis* (Li et al., 2014), and selenite reductase in *Bacillus selenitireducens* (Wells et al., 2019) is described in the literature. Fig. 24 depicts a schematic representation of the reduction process. Sarret et al. (2005) reported that the Se(IV) reduction resulted into intracellular granules of monoclinic Se(0) in the cells of *Ralstonia metallidurans*. Furthermore, Li et al. (2014) found that the fumarate

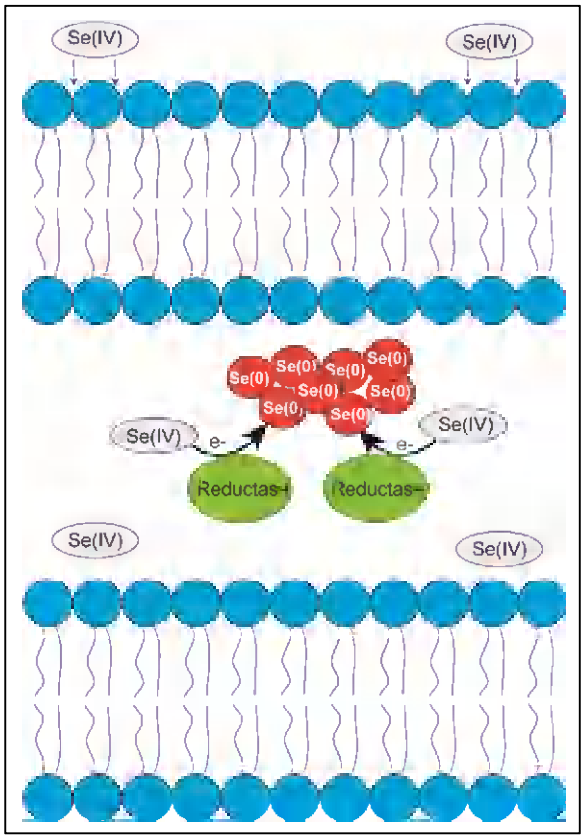

Figure 24. Graphical representation of the suggested potential mechanism for the production of elemental selenium in the plasmatic membrane mediated by reductase enzymes.

reductase could catalyze the reduction of selenite to elemental selenium in the periplasmic space of the bacteria, acquiring the electrons from the c-type cytochrome (CymA) (Fig. 24). This was in accordance with our results where SeNPs were observed at the plasmatic membrane of the bacterial cells in the BsBSe samples.

5.2.2. Biotransformation of amorphous Se nanospheres to trigonal Se

Selenium can exist in three different allotropes: amorphous (red *a*-Se), monoclinic (*m*-Se) and trigonal (grey/black *t*-Se). The amorphous Se is thermodynamically unstable and undergoes transformation to monoclinic Se at high temperatures. In the same way, monoclinic Se is metastable and could also eventually suffer conversion to the trigonal form of Se (Goldan et al., 2016). In addition, several bacterial strains are able to transform unstable amorphous Se nanospheres to the more stable trigonal Se nanostructures. Selenite-treated microcosms exhibited an orange/grey-black layer on the top bentonite microcosms depending on the treatment. SAED, HRTEM and Raman spectroscopy analyses revealed the extracellular and intracellular Se nanospheres of SeNPs turned to be monoclinic phases of crystalline selenium in the BSe, BsSe, and BsBSe samples.

The transformation of *a*-Se/*m*-Se into *t*-Se could be observed at macroscopic level by the shift in color of the deposited layer on the top of the bentonite. In the BBSe microcosms, an orange layer corresponding to the deposited Se(0) was detected in the first 30 days of anaerobic incubation, however along the time this orange color was gradually turning to dark grey/black layer corresponding to t-Se. This change in color was described by Wang et al. (2010) in a *Bacillus subtilis* culture after 24 h of incubation, being the orange color at time 0 corresponding to colloids of nanospheres of *a*-Se/*m*-Se but after 12 h a mixture of these m-Se and nanowires of t-Se were obtained. In our study, this mixture could be extrapolated to the described SeNPs detected in the BsSe samples by VP-FESEM and Raman spectroscopy. Therefore, in the BBSe sample, the orange layer turning to grey/black could be explained by structural transformation of the Se nanospheres from *a*-Se/*m*-Se (orange, reddish) to *t*-Se (grey/black).

The *m*-Se could be dissolved as a consequence of its low stability and the released Se would be deposited on the nanocrystals of *t*-Se acting as precursors and allowing the

uniform growth of nanowires, hexagonal or larger-sized crystals of *t*-Se (Wang et al., 2010). In contrast to what happens in *m*-Se where a weak van der Waals forces state between the eight-atom units, the *t*-Se (metallic gray color) consists of polymeric helical chains of Se atoms parallel to each other and where every individual atom is connected with partial metallic bonds to four nearby Se atoms in the adjacent chains, conferring thus high stability to the whole molecule (Fernández-Martínez and Charlet, 2009; Goldan et al., 2016). Additionally, Fresneda et al. (2018) hypothesized an analogous process in the pure culture of *Stenotrophomonas bentonitica*, a bacterium isolated from Spanish bentonites, which is also consistent with our experimental findings.

Based on all the above observations, we suggest that similarly to what it was previously described for the bacterial pure cultures, a Se transformation process takes place also in the bentonite microcosms. Firstly, a reduction of selenite into elemental selenium is conducted by the activity of potential periplasmic-reductase enzymes resulting in the accumulation of Se(0) in the periplasmic space. Secondly, the orange *a*-Se and *m*-Se nanoparticles are released to and aggregated in the extracellular environment. Finally, the unstable nature of the *m*-Se particles further leads to its solubilization and re-crystallization to the more stable form of *t*-Se, thus producing the growth of nanowires and large-polygonal crystals of Se(0).

6. REFERENCES

Anderson, C., Johnsson, A., Moll, H., Pedersen, K., 2011. Radionuclide Geomicrobiology of the Deep Biosphere. Geomicrobiology Journal 28, 540–561. https://doi.org/10.1080/01490451.2010.507644

Ansede, J.H., Yoch, D.C., 1997. Comparison of selenium and sulfur volatilization by dimethylsulfoniopropionate lyase (DMSP) in two marine bacteria and estuarine sediments. FEMS Microbiol Ecol 23, 315–324. https://doi.org/10.1111/j.1574-6941.1997.tb00412.x

Avendaño, R., Chaves, N., Fuentes, P., Sánchez, E., Jiménez, J.I., Chavarría, M., 2016. Production of selenium nanoparticles in Pseudomonas putida KT2440. Scientific Reports 6, 1–9. https://doi.org/10.1038/srep37155

Bao, P., Huang, H., Hu, Z.-Y., Häggblom, M.M., Zhu, Y.-G., 2013. Impact of temperature, CO2 fixation and nitrate reduction on selenium reduction, by a paddy soil Clostridium strain. Journal of Applied Microbiology 114, 703–712. https://doi.org/10.1111/jam.12084

Basaglia, M., Toffanin, A., Baldan, E., Bottegal, M., Shapleigh, J.P., Casella, S., 2007. Selenite-reducing capacity of the copper-containing nitrite reductase of Rhizobium sullae. FEMS Microbiol Lett 269, 124–130. https://doi.org/10.1111/j.1574-6968.2006.00617.x

Bengtsson, A., Pedersen, K., 2017. Microbial sulphide-producing activity in water saturated Wyoming MX-80, Asha and Calcigel bentonites at wet densities from 1500 to 2000kgm−3. Applied Clay Science 137, 203–212. https://doi.org/10.1016/j.clay.2016.12.024

Biebl, H., 2001. Fermentation of glycerol by Clostridium pasteurianum--batch and continuous culture studies. J. Ind. Microbiol. Biotechnol. 27, 18–26. https://doi.org/10.1038/sj/jim/7000155

Bohorquez, L.C., Delgado-Serrano, L., López, G., Osorio-Forero, C., Klepac-Ceraj, V., Kolter, R., Junca, H., Baena, S., Zambrano, M.M., 2012. In-depth Characterization via Complementing Culture-Independent Approaches of the Microbial Community in an Acidic Hot Spring of the Colombian Andes. Microb Ecol 63, 103–115. https://doi.org/10.1007/s00248-011-9943-3

Breynaert, E., Scheinost, A.C., Dom, D., Rossberg, A., Vancluysen, J., Gobechiya, E., Kirschhock, C.E.A., Maes, A., 2010. Reduction of Se(IV) in boom clay: XAS solid phase speciation. Environ. Sci. Technol. 44, 6649–6655. https://doi.org/10.1021/es100569e

Bueno-Galera, C., 2019. Caracterización espectroscópica y microscópica de la biosíntesis microbiana de SeNPs y el papel de las proteínas en su formación. Universidad de Granada.

Chen, H., Shin, D.-W., Nam, J.-G., Kwon, K.-W., Yoo, J.-B., 2010. Selenium nanowires and nanotubes synthesized via a facile template-free solution method. Materials Research Bulletin 45, 699–704. https://doi.org/10.1016/j.materresbull.2010.02.016

de Souza, M.P., Chu, D., Zhao, M., Zayed, A.M., Ruzin, S.E., Schichnes, D., Terry, N., 1999. Rhizosphere Bacteria Enhance Selenium Accumulation and Volatilization by Indian Mustard. Plant Physiol 119, 565–574.

Duc, M., Lefevre, G., Fedoroff, M., Jeanjean, J., Rouchaud, J.C., Monteil-Rivera, F., Dumonceau, J., Milonjic, S., 2003. Sorption of selenium anionic species on apatites and iron oxides from aqueous solutions. Journal of Environmental Radioactivity, International workshop on the mobility of iodine, technetium, selenium and uranium in the biosphere 70, 61–72. https://doi.org/10.1016/S0265-931X(03)00125-5

Dwivedi, S., AlKhedhairy, A.A., Ahamed, M., Musarrat, J., 2013. Biomimetic Synthesis of Selenium Nanospheres by Bacterial Strain JS-11 and Its Role as a Biosensor for Nanotoxicity Assessment: A Novel Se-Bioassay. PLOS ONE 8, e57404. https://doi.org/10.1371/journal.pone.0057404

Eswayah, A.S., Smith, T.J., Gardiner, P.H.E., 2016. Microbial Transformations of Selenium Species of Relevance to Bioremediation. Appl Environ Microbiol 82, 4848–4859. https://doi.org/10.1128/AEM.00877-16

Fernández-Llamosas, H., Castro, L., Blázquez, M.L., Díaz, E., Carmona, M., 2017. Speeding up bioproduction of selenium nanoparticles by using Vibrio natriegens as microbial factory. Scientific Reports 7, 1–9. https://doi.org/10.1038/s41598-017-16252-1

Fernández-Martínez, A., Charlet, L., 2009. Selenium environmental cycling and bioavailability: a structural chemist point of view. Rev Environ Sci Biotechnol 8, 81–110. https://doi.org/10.1007/s11157-009-9145-3

Fresneda, M.A.R., Martín, J.D., Bolívar, J.G., Cantos, M.V.F., Bosch-Estévez, G., Moreno, M.F.M., Merroun, M.L., 2018. Green synthesis and biotransformation of amorphous Se nanospheres to trigonal 1D Se nanostructures: impact on Se mobility within the concept of radioactive waste disposal. Environ. Sci.: Nano 5, 2103–2116. https://doi.org/10.1039/C8EN00221E

Garbisu, C., Ishii, T., Leighton, T., Buchanan, B.B., 1996. Bacterial reduction of selenite to elemental selenium. Chemical Geology, Chemical And Biological Control On Mineral Growth And Dissolution Kinetics, American Chemical Society Meeting 132, 199–204. https://doi.org/10.1016/S0009-2541(96)00056-3

Goldan, A.H., Li, C., Pennycook, S.J., Schneider, J., Blom, A., Zhao, W., 2016. Molecular structure of vapor-deposited amorphous selenium. Journal of Applied Physics 120, 135101. https://doi.org/10.1063/1.4962315

Gonzalez-Gil, G., Lens, P.N.L., Saikaly, P.E., 2016. Selenite Reduction by Anaerobic Microbial Aggregates: Microbial Community Structure, and Proteins Associated to the Produced Selenium Spheres. Front. Microbiol. 7. https://doi.org/10.3389/fmicb.2016.00571

Grigoryan, A.A., Jalique, D.R., Medihala, P., Stroes-Gascoyne, S., Wolfaardt, G.M., McKelvie, J., Korber, D.R., 2018. Bacterial diversity and production of sulfide in microcosms containing uncompacted bentonites. Heliyon 4. https://doi.org/10.1016/j.heliyon.2018.e00722

Guerra, I., Cardell, C., 2015. Optimizing use of the structural chemical analyser (variable pressure FESEM-EDX raman spectroscopy) on micro-size complex historical paintings characterization. Journal of Microscopy 260, 47–61. https://doi.org/10.1111/jmi.12265

Gupta, S., Prakash, R., Prakash, N.T., Pearce, C., Pattrick, R., Hery, M., Lloyd, J., 2010. Selenium Mobilization by Pseudomonas aeruginosa (SNT-SG1) Isolated from Seleniferous Soils from India. Geomicrobiology Journal 27, 35–42. https://doi.org/10.1080/01490450903232173

Han, D.S., Batchelor, B., Abdel-Wahab, A., 2012. Sorption of selenium(IV) and selenium(VI) onto synthetic pyrite (FeS2): Spectroscopic and microscopic analyses. Journal of Colloid and Interface Science 368, 496–504. https://doi.org/10.1016/j.jcis.2011.10.065

Hoang, V.-A., Kim, Y.-J., Nguyen, N.-L., Yang, D.-C., 2014. Brachybacterium ginsengisoli sp. nov., isolated from soil of a ginseng field. Int. J. Syst. Evol. Microbiol. 64, 3063–3068. https://doi.org/10.1099/ijs.0.058388-0

Hockin, S., Gadd, G.M., 2006. Removal of selenate from sulfate-containing media by sulfate-reducing bacterial biofilms. Environmental Microbiology 8, 816–826. https://doi.org/10.1111/j.1462-2920.2005.00967.x

Hockin, S.L., Gadd, G.M., 2003. Linked Redox Precipitation of Sulfur and Selenium under Anaerobic Conditions by Sulfate-Reducing Bacterial Biofilms. Appl Environ Microbiol 69, 7063–7072. https://doi.org/10.1128/AEM.69.12.7063-7072.2003

Hoving, A.L., Münch, M.A., Bruggeman, C., Banerjee, D., Behrends, T., 2019. Kinetics of selenite interactions with Boom Clay: adsorption–reduction interplay. Geological Society, London, Special Publications 482, 225–239. https://doi.org/10.1144/SP482-2018-60

Hunter, W.J., 2014. Pseudomonas seleniipraecipitans Proteins Potentially Involved in Selenite Reduction. Curr Microbiol 69, 69–74. https://doi.org/10.1007/s00284-014-0555-2

Javed, S., Sarwar, A., Tassawar, M., Faisal, M., 2015. Conversion of selenite to elemental selenium by indigenous bacteria isolated from polluted areas. Chemical Speciation & Bioavailability 27, 162–168. https://doi.org/10.1080/09542299.2015.1112751

Kang, M., Chen, F., Wu, S., Yang, Y., Bruggeman, C., Charlet, L., 2011. Effect of pH on Aqueous Se(IV) Reduction by Pyrite. Environ. Sci. Technol. 45, 2704–2710. https://doi.org/10.1021/es1033553

Kousha, M., Yeganeh, S., Keramat Amirkolaie, A., 2017. Effect of sodium selenite on the bacteria growth, selenium accumulation, and selenium biotransformation in Pediococcus acidilactici. Food Sci. Biotechnol. 26, 1013–1018. https://doi.org/10.1007/s10068-017-0142-y

Li, D.-B., Cheng, Y.-Y., Wu, C., Li, W.-W., Li, N., Yang, Z.-C., Tong, Z.-H., Yu, H.-Q., 2014. Selenite reduction by Shewanella oneidensis MR-1 is mediated by fumarate reductase in periplasm. Scientific Reports 4, 1–7. https://doi.org/10.1038/srep03735

Lopez-Fernandez, M., Cherkouk, A., Vilchez-Vargas, R., Jauregui, R., Pieper, D., Boon, N., Sanchez-Castro, I., Merroun, M.L., 2015. Bacterial Diversity in Bentonites, Engineered Barrier for Deep

Geological Disposal of Radioactive Wastes. Microb Ecol 70, 922–935. https://doi.org/10.1007/s00248-015-0630-7

Lopez-Fernandez, M., Fernández-Sanfrancisco, O., Moreno-García, A., Martín-Sánchez, I., Sánchez-Castro, I., Merroun, M.L., 2014. Microbial communities in bentonite formations and their interactions with uranium. Applied Geochemistry 49, 77–86. https://doi.org/10.1016/j.apgeochem.2014.06.022

Lopez-Fernandez, M., Romero-González, M., Günther, A., Solari, P.L., Merroun, M.L., 2018a. Effect of U(VI) aqueous speciation on the binding of uranium by the cell surface of Rhodotorula mucilaginosa, a natural yeast isolate from bentonites. Chemosphere 199, 351–360. https://doi.org/10.1016/j.chemosphere.2018.02.055

Lopez-Fernandez, M., Vilchez-Vargas, R., Jroundi, F., Boon, N., Pieper, D., Merroun, M.L., 2018b. Microbial community changes induced by uranyl nitrate in bentonite clay microcosms. Applied Clay Science, ACS - SI ICC 2017 XVI International Clay Conference – Clays, from the oceans to space 160, 206–216. https://doi.org/10.1016/j.clay.2017.12.034

Lucovsky, G., Mooradian, A., Taylor, W., Wright, G.B., Keezer, R.C., 1967. Identification of the fundamental vibrational modes of trigonal, α - monoclinic and amorphous selenium. Solid State Communications 5, 113–117. https://doi.org/10.1016/0038-1098(67)90006-3

Montavon, G., Guo, Z., Lützenkirchen, J., Alhajji, E., Kedziorek, M.A.M., Bourg, A.C.M., Grambow, B., 2009. Interaction of selenite with MX-80 bentonite: Effect of minor phases, pH, selenite loading, solution composition and compaction. Colloids and Surfaces A: Physicochemical and Engineering Aspects 332, 71–77. https://doi.org/10.1016/j.colsurfa.2008.09.014

Nagata, K., Ishibashi, K., Miyamoto, Y., 1981. Raman and Infrared Spectra of Rhombohedral Selenium. Jpn. J. Appl. Phys. 20, 463. https://doi.org/10.1143/JJAP.20.463

Nancharaiah, Y.V., Lens, P.N.L., 2015. Ecology and Biotechnology of Selenium-Respiring Bacteria. Microbiol. Mol. Biol. Rev. 79, 61–80. https://doi.org/10.1128/MMBR.00037-14

Oremland, R.S., Herbel, M.J., Blum, J.S., Langley, S., Beveridge, T.J., Ajayan, P.M., Sutto, T., Ellis, A.V., Curran, S., 2004. Structural and Spectral Features of Selenium Nanospheres Produced by Se-Respiring Bacteria. Appl Environ Microbiol 70, 52–60. https://doi.org/10.1128/AEM.70.1.52-60.2004

Patil, Y., Junghare, M., Müller, N., 2016. Fermentation of glycerol by Anaerobium acetethylicum and its potential use in biofuel production. Microb Biotechnol 10, 203–217. https://doi.org/10.1111/1751-7915.12484

Povedano-Priego, C., Jroundi, F., Lopez-Fernandez, M., Sánchez-Castro, I., Martin-Sánchez, I., Huertas, F.J., Merroun, M.L., 2019. Shifts in bentonite bacterial community and mineralogy in response to uranium and glycerol-2-phosphate exposure. Science of The Total Environment 692, 219–232. https://doi.org/10.1016/j.scitotenv.2019.07.228

Robertson, C.E., Harris, J.K., Wagner, B.D., Granger, D., Browne, K., Tatem, B., Feazel, L.M., Park, K., Pace, N.R., Frank, D.N., 2013. Explicet: graphical user interface software for metadata-driven management, analysis and visualization of microbiome data. Bioinformatics 29, 3100–3101. https://doi.org/10.1093/bioinformatics/btt526

Rosenfeld, C.E., James, B.R., Santelli, C.M., 2018. Persistent Bacterial and Fungal Community Shifts Exhibited in Selenium-Contaminated Reclaimed Mine Soils. Appl Environ Microbiol 84. https://doi.org/10.1128/AEM.01394-18

Ruiz-Fresneda, M.A., Gomez-Bolivar, J., Delgado-Martin, J., Abad-Ortega, M. del M., Guerra-Tschuschke, I., Merroun, M.L., 2019. The Bioreduction of Selenite under Anaerobic and Alkaline Conditions Analogous to Those Expected for a Deep Geological Repository System. Molecules 24, 3868. https://doi.org/10.3390/molecules24213868

Ruiz-Fresneda, M.A., Martín, J.D., Bolívar, J.G., Cantos, M.V.F., Bosch-Estévez, G., Moreno, M.F.M., Merroun, M.L., 2018. Green synthesis and biotransformation of amorphous Se nanospheres to trigonal 1D Se nanostructures: impact on Se mobility within the concept of radioactive waste disposal. Environ. Sci.: Nano 5, 2103–2116. https://doi.org/10.1039/C8EN00221E

Sánchez-Castro, I., Ruiz-Fresneda, M.A., Bakkali, M., Kämpfer, P., Glaeser, S.P., Busse, H.J., López-Fernández, M., Martínez-Rodríguez, P., Merroun, M.L., 2017. Stenotrophomonas bentonitica sp. nov., isolated from bentonite formations. Int. J. Syst. Evol. Microbiol. 67, 2779–2786. https://doi.org/10.1099/ijsem.0.002016

Sarret, G., Avoscan, L., Carrière, M., Collins, R., Geoffroy, N., Carrot, F., Covès, J., Gouget, B., 2005. Chemical forms of selenium in the metal-resistant bacterium Ralstonia metallidurans CH34 exposed to selenite and selenate. Appl. Environ. Microbiol. 71, 2331–2337. https://doi.org/10.1128/AEM.71.5.2331-2337.2005

Shi, K., Ye, Y., Guo, N., Guo, Z., Wu, W., 2014. Evaluation of Se(IV) removal from aqueous solution by GMZ Na-bentonite: batch experiment and modeling studies. J Radioanal Nucl Chem 299, 583–589. https://doi.org/10.1007/s10967-013-2807-1

Shiratori-Takano, H., Akita, K., Yamada, K., Itoh, T., Sugihara, T., Beppu, T., Ueda, K., 2014. Description of Symbiobacterium ostreiconchae sp. nov., Symbiobacterium turbinis sp. nov. and Symbiobacterium terraclitae sp. nov., isolated from shellfish, emended description of the genus Symbiobacterium and proposal of Symbiobacteriaceae fam. nov. International Journal of Systematic and Evolutionary Microbiology, 64, 3375–3383. https://doi.org/10.1099/ijs.0.063750-0

Tam, K., Ho, C.T., Lee, J.-H., Lai, M., Chang, C.H., Rheem, Y., Chen, W., Hur, H.-G., Myung, N.V., 2010. Growth mechanism of amorphous selenium nanoparticles synthesized by Shewanella sp. HN-41. Biosci. Biotechnol. Biochem. 74, 696–700. https://doi.org/10.1271/bbb.90454

Villar, M.V., Fernández-Soler, J.M., Delgado Huertas, A., Reyes, E., Linares, J., Jiménez de Cisneros, C., Huertas, F.J., Caballero, E., Leguey, S., Cuevas, J., Garralón, A., Fernández, A.M., Pelayo, M., Martín, P.L., Pérez Del Villar, L., Astudillo, J., 2006. The study of Spanish clays for their use as sealing materials in nuclear waste repositories: 20 years of progress. El estudio de arcillas españolas para su utilización como material de sellado en almacenamientos de residuos radiactivos: 20 años de progreso.

Wang, T., Yang, L., Zhang, B., Liu, J., 2010. Extracellular biosynthesis and transformation of selenium nanoparticles and application in H2O2 biosensor. Colloids and Surfaces B: Biointerfaces 80, 94–102. https://doi.org/10.1016/j.colsurfb.2010.05.041

Wells, M., McGarry, J., Gaye, M.M., Basu, P., Oremland, R.S., Stolz, J.F., 2019. Respiratory Selenite Reductase from Bacillus selenitireducens Strain MLS10. Journal of Bacteriology 201. https://doi.org/10.1128/JB.00614-18

Xiao, Y., Francke, C., Abee, T., Wells-Bennik, M.H.J., 2011. Clostridial spore germination versus bacilli: Genome mining and current insights. Food Microbiology 28, 266–274. https://doi.org/10.1016/j.fm.2010.03.016

Yang, S., Li, S., Jia, X., 2019. Production of medium chain length polyhydroxyalkanoate from acetate by engineered Pseudomonas putida KT2440. J Ind Microbiol Biotechnol 46, 793–800. https://doi.org/10.1007/s10295-019-02159-5

7. SUPPLEMENTARY TABLES

Supplementary Table 1. Bacterial phyla of water-saturated bentonite microcosms and their corresponding relative abundances (%) in each treatment.

Phlya	**Relative abundances in water-saturated bentonite microcosms (%)**						
	BB	**BBSe**	**B**	**BSe**	**BsB**	**BsBSe**	**BsSe**
Firmicutes	11.33	20.44	19.48	53.51	6.16	34.69	77.34
Proteobacteria	33.35	50.25	5.52	28.96	2.49	63.95	3.45
Euryarchaeota	50.45	21.49	73.51	0.17	1.14	0.00	0.10
Actinobacteria	0.99	4.64	0.99	10.07	89.07	0.89	13.29
unclassified Bacteria	1.69	1.52	0.20	5.27	0.00	0.46	5.30
Cyanobacteria	0.00	1.52	0.00	0.00	0.00	0.00	0.17
Bacteroidetes	1.49	0.10	0.05	0.00	0.80	0.00	0.36
Chloroflexi	0.40	0.03	0.25	0.53	0.00	0.00	0.00
Acidobacteria	0.00	0.00	0.00	0.89	0.00	0.00	0.00
Ignavibacteriae	0.00	0.00	0.00	0.60	0.00	0.00	0.00
Spirochaetes	0.00	0.00	0.00	0.00	0.25	0.00	0.00
Verrucomicrobia	0.20	0.00	0.00	0.00	0.00	0.00	0.00
Deferribacteres	0.00	0.00	0.00	0.00	0.10	0.00	0.00
Armatimonadetes	0.05	0.00	0.00	0.00	0.00	0.00	0.00
unclassified Archaea	0.05	0.00	0.00	0.00	0.00	0.00	0.00

Supplementary Table 2. Bacterial classes of water-saturated bentonite microcosms and their corresponding relative abundances (%) in each treatment.

Classes	**Relative abundances in water-saturated bentonite microcosms (%)**						
	BB	**BBSe**	**B**	**BSe**	**BsB**	**BsBSe**	**BsSe**
Gammaproteobacteria	32.75	50.18	2.73	6.59	2.29	63.95	3.02
Clostridia	7.60	19.10	17.74	40.16	3.88	33.40	60.07
Methanomicrobia	50.45	21.49	73.51	0.17	1.14	0.00	0.10
Actinobacteria	0.99	4.64	0.99	10.07	89.07	0.89	13.29
unclassified Firmicutes	2.63	1.29	1.29	13.19	0.25	0.20	12.99
unclassified	1.69	1.52	0.20	5.27	0.00	0.46	5.30
Deltaproteobacteria	0.60	0.03	2.44	10.11	0.00	0.00	0.00
unclassified Proteobacteria	0.00	0.03	0.00	7.82	0.00	0.00	0.00
Bacilli	0.25	0.05	0.00	0.17	1.94	0.13	4.27
Betaproteobacteria	0.00	0.00	0.15	3.31	0.15	0.00	0.10
Chloroplast	0.00	1.52	0.00	0.00	0.00	0.00	0.17
Negativicutes	0.84	0.00	0.45	0.00	0.00	0.96	0.00
Alphaproteobacteria	0.00	0.00	0.20	1.13	0.05	0.00	0.33
unclassified Bacteroidetes	1.34	0.02	0.00	0.00	0.15	0.00	0.00
Anaerolineae	0.40	0.03	0.25	0.53	0.00	0.00	0.00
Acidobacteria_Gp7	0.00	0.00	0.00	0.89	0.00	0.00	0.00
Bacteroidia	0.15	0.08	0.00	0.00	0.65	0.00	0.00
Ignavibacteria	0.00	0.00	0.00	0.60	0.00	0.00	0.00
Flavobacteriia	0.00	0.00	0.00	0.00	0.00	0.00	0.36
Spirochaetia	0.00	0.00	0.00	0.00	0.25	0.00	0.00
Subdivision3 (Verrucomicrobia)	0.20	0.00	0.00	0.00	0.00	0.00	0.00
Erysipelotrichia	0.00	0.00	0.00	0.00	0.10	0.00	0.00
Deferribacteres	0.00	0.00	0.00	0.00	0.10	0.00	0.00
unclassified Archaea	0.05	0.00	0.00	0.00	0.00	0.00	0.00
Armatimonadetes_gp2	0.05	0.00	0.00	0.00	0.00	0.00	0.00
Sphingobacteriia	0.00	0.00	0.05	0.00	0.00	0.00	0.00

Supplementary Table 3. Bacterial classes of water-saturated bentonite microcosms and their corresponding relative abundances (%) in each treatment.

Genera	Relative abundances in water-saturated bentonite microcosms (%)						
	BB	**BBSe**	**B**	**BSe**	**BsB**	**BsBSe**	**BsSe**
Methanosarcina	49.20	21.49	68.19	0.17	0.89	0.00	0.10
Pseudomonas	30.86	16.90	0.00	2.52	1.14	33.76	0.73
Stenotrophomonas	1.44	25.07	0.00	0.70	0.94	28.99	1.95
Brachybacterium	0.00	1.23	0.10	3.02	89.02	0.00	3.18
Symbiobacterium	0.00	0.46	0.00	7.69	0.84	2.42	50.43
Desulfosporosinus	0.75	7.54	6.01	22.40	0.00	0.50	0.00
Anaerosolibacter	0.89	1.28	0.00	1.42	0.40	28.66	0.66
unclassified Firmicutes	2.63	1.29	1.29	13.19	0.25	0.20	12.99
unclassified Clostridiales	0.75	0.76	6.76	6.59	0.25	0.27	8.45
unclassified	1.74	1.52	0.20	5.27	0.00	0.46	5.30
Shewanella	0.00	6.58	0.00	0.10	0.15	0.10	0.00
Nitriliruptor	0.00	0.00	0.00	2.15	0.00	0.00	9.51
unclassified Desulfuromonadaceae	0.00	0.03	0.00	10.11	0.00	0.00	0.00
unclassified Peptococcaceae_1	0.45	3.08	2.83	0.00	0.00	0.07	0.27
unclassified Proteobacteria	0.00	0.03	0.00	7.82	0.00	0.00	0.00
Amycolatopsis	0.94	3.06	0.00	0.03	0.05	0.43	0.00
unclassified Gracilibacteraceae	0.05	0.83	1.59	1.03	0.00	0.73	0.00
Azotobacter	0.00	0.00	2.73	2.05	0.00	0.00	0.00
unclassified Peptostreptococcaceae	1.69	0.80	0.00	0.00	0.00	0.60	0.00
Streptophyta	0.00	1.52	0.00	0.00	0.00	0.00	0.17
Sedimentibacter	0.45	1.39	0.00	0.00	0.00	0.00	0.00
unclassified Gammaproteobacteria	0.45	0.75	0.00	0.86	0.00	0.03	0.33
unlassified Methanomicrobiales	0.55	0.00	3.68	0.00	0.25	0.00	0.00
Paenibacillus	0.00	0.00	0.00	0.00	0.35	0.00	2.62
Actinotalea	0.00	0.22	0.00	1.82	0.00	0.46	0.00
unclassified Clostridiaceae_4	0.00	1.11	0.00	0.46	0.00	0.00	0.00
unclassified Oxalobacteraceae	0.00	0.00	0.00	2.45	0.00	0.00	0.00
unclassified Propionibacteriaceae	0.00	0.00	0.25	1.99	0.00	0.00	0.00
Bacillus	0.20	0.00	0.00	0.00	0.00	0.13	1.66
unclassified Oceanospirillales	0.00	0.84	0.00	0.00	0.00	0.07	0.00
Clostridium_XlVb	0.94	0.41	0.00	0.00	0.00	0.00	0.00
unclassified Methanomicrobia	0.60	0.00	1.29	0.00	0.00	0.00	0.00
Pelosinus	0.40	0.00	0.45	0.00	0.00	0.73	0.00
unclassified Clostridiaceae_1	0.99	0.23	0.00	0.00	0.00	0.00	0.00
unclassified Bacteroidetes	1.34	0.02	0.00	0.00	0.15	0.00	0.00
Lactobacillus	0.00	0.00	0.00	0.00	1.59	0.00	0.00
unclassified Actinobacteria	0.00	0.00	0.00	0.80	0.00	0.00	0.10
Acidobacteria_Gp7	0.00	0.00	0.00	0.89	0.00	0.00	0.00
Geobacter	0.15	0.00	1.19	0.00	0.00	0.00	0.00
unclassified Ruminococcaceae	0.15	0.28	0.40	0.00	0.00	0.00	0.00
unclassified Anaerolineaceae	0.20	0.00	0.25	0.53	0.00	0.00	0.00
unclassified Enterobacteriaceae	0.00	0.00	0.00	0.00	0.05	0.76	0.00
Alkaliphilus	0.00	0.40	0.00	0.00	0.00	0.00	0.00
unclassified Clostridia	0.00	0.00	0.00	0.43	0.10	0.00	0.27
unclassified Lachnospiraceae	0.25	0.00	0.00	0.00	0.55	0.17	0.00
unclassified Xanthomonadaceae	0.00	0.05	0.00	0.30	0.00	0.23	0.00
Arthrobacter	0.00	0.00	0.45	0.07	0.00	0.00	0.27

unclassified Betaproteobacteria	0.00	0.00	0.00	0.66	0.00	0.00	0.00
Ignavibacterium	0.00	0.00	0.00	0.60	0.00	0.00	0.00
unclassified Veillonellaceae	0.45	0.00	0.00	0.00	0.00	0.23	0.00
Ferrovibrio	0.00	0.00	0.00	0.50	0.00	0.00	0.03
unclassified Desulfovibrionaceae	0.35	0.00	0.50	0.00	0.00	0.00	0.00
Bacteroides	0.00	0.00	0.00	0.00	0.60	0.00	0.00
unclassified Actinomycetales	0.00	0.13	0.00	0.07	0.00	0.00	0.00
Brassicibacter	0.00	0.18	0.00	0.00	0.00	0.00	0.00
Faecalibacterium	0.00	0.00	0.00	0.00	0.50	0.00	0.00
Nocardioides	0.00	0.00	0.15	0.03	0.00	0.00	0.20
Tissierella	0.00	0.15	0.00	0.00	0.00	0.00	0.00
Methanocella	0.10	0.00	0.35	0.00	0.00	0.00	0.00
unclassified Rhodospirillaceae	0.00	0.00	0.00	0.27	0.00	0.00	0.00
Desulfovibrio	0.10	0.00	0.30	0.00	0.00	0.00	0.00
Rhizobium	0.00	0.00	0.00	0.17	0.00	0.00	0.13
Lutispora	0.00	0.12	0.00	0.00	0.00	0.00	0.00
Filifactor	0.00	0.00	0.00	0.00	0.35	0.00	0.00
unclassified Comamonadaceae	0.00	0.00	0.00	0.20	0.00	0.00	0.00
Syntrophobacter	0.00	0.00	0.35	0.00	0.00	0.00	0.00
Cloacibacterium	0.00	0.00	0.00	0.00	0.00	0.00	0.20
Anaerostipes	0.00	0.00	0.00	0.00	0.25	0.00	0.00
Treponema	0.00	0.00	0.00	0.00	0.25	0.00	0.00
Bergeyella	0.00	0.00	0.00	0.00	0.00	0.00	0.17
Desulfotomaculum	0.00	0.00	0.00	0.13	0.00	0.00	0.00
Lachnospiracea_incertae_sedis	0.00	0.00	0.00	0.00	0.20	0.00	0.00
Ornatilinea	0.20	0.00	0.00	0.00	0.00	0.00	0.00
Rhodoligotrophos	0.00	0.00	0.00	0.17	0.00	0.00	0.00
Romboutsia	0.20	0.00	0.00	0.00	0.00	0.00	0.00
Sporacetigenium	0.00	0.08	0.00	0.00	0.00	0.00	0.00
Subdivision3 (Verrucomicrobia)	0.20	0.00	0.00	0.00	0.00	0.00	0.00
Sunxiuqinia	0.00	0.08	0.00	0.00	0.00	0.00	0.00
unclassified Bacillales	0.00	0.00	0.00	0.17	0.00	0.00	0.00
Corynebacterium	0.00	0.00	0.00	0.10	0.00	0.00	0.00
unclassified Rhodocyclaceae	0.00	0.00	0.15	0.00	0.00	0.00	0.00
Mucispirillum	0.00	0.00	0.00	0.00	0.10	0.00	0.00
Azospirillum	0.00	0.00	0.15	0.00	0.00	0.00	0.00
unclassified Erysipelotrichaceae	0.00	0.00	0.00	0.00	0.10	0.00	0.00
Fusicatenibacter	0.00	0.00	0.00	0.00	0.10	0.00	0.00
Mesorhizobium	0.00	0.00	0.00	0.00	0.00	0.00	0.07
unclassified Prolixibacteraceae	0.10	0.00	0.00	0.00	0.00	0.00	0.00
Anaerolinea	0.00	0.03	0.00	0.00	0.00	0.00	0.00
Anaeromyxobacter	0.00	0.00	0.10	0.00	0.00	0.00	0.00
Desulfurispora	0.00	0.00	0.00	0.00	0.15	0.00	0.00
Exiguobacterium	0.00	0.03	0.00	0.00	0.00	0.00	0.00
Roseburia	0.00	0.00	0.00	0.00	0.10	0.00	0.00
Steroidobacter	0.00	0.00	0.00	0.07	0.00	0.00	0.00
Syntrophobotulus	0.00	0.00	0.15	0.00	0.00	0.00	0.00
Thiobacillus	0.00	0.00	0.00	0.00	0.00	0.00	0.10
unclassified Sphingomonadaceae	0.00	0.00	0.00	0.00	0.00	0.00	0.07
unclassified Microbacteriaceae	0.00	0.00	0.00	0.00	0.00	0.00	0.03
Blautia	0.00	0.00	0.00	0.00	0.05	0.00	0.00
unclassified Porphyromonadaceae	0.00	0.00	0.00	0.00	0.05	0.00	0.00
Sutterella	0.00	0.00	0.00	0.00	0.05	0.00	0.00

Paludibacter	0.05	0.00	0.00	0.00	0.00	0.00	0.00
Cupriavidus	0.00	0.00	0.00	0.00	0.05	0.00	0.00
unclassified Coriobacteriaceae	0.05	0.00	0.00	0.00	0.00	0.00	0.00
Armatimonadetes_gp2	0.05	0.00	0.00	0.00	0.00	0.00	0.00
Parvibaculum	0.00	0.00	0.00	0.03	0.00	0.00	0.00
unclassified Rhizobiales	0.00	0.00	0.00	0.00	0.00	0.00	0.03
Comamonas	0.00	0.00	0.00	0.00	0.05	0.00	0.00
Oscillibacter	0.00	0.00	0.00	0.00	0.05	0.00	0.00
Pseudolabrys	0.00	0.00	0.05	0.00	0.00	0.00	0.00
Sphingomonas	0.00	0.00	0.00	0.00	0.05	0.00	0.00
Staphylococcus	0.00	0.02	0.00	0.00	0.00	0.00	0.00
unclassified Bacilli	0.05	0.00	0.00	0.00	0.00	0.00	0.00
unclassified Chitinophagaceae	0.00	0.00	0.05	0.00	0.00	0.00	0.00
unclassified Clostridiales_Incertae_Sedis_XI	0.05	0.00	0.00	0.00	0.00	0.00	0.00
unclassified Nocardioidaceae	0.00	0.00	0.05	0.00	0.00	0.00	0.00

DISCUSIÓN GENERAL

Debido a que, en la actualidad, está ampliamente extendida la selección de las arcillas (concretamente las bentonitas) como material de relleno y sellado en el concepto de Almacenamiento Geológico Profundo (AGP) de residuos nucleares es necesario llevar a cabo un amplio estudio del comportamiento de estas arcillas tanto a nivel geofísico-químico como a nivel microbiológico.

En nuestro país, las bentonitas han sido seleccionadas y extensamente estudiadas como material de relleno y sellado para un futuro almacenamiento de residuos radiactivos, optándose por los yacimientos arcillosos en Almeria (concretamente las del Cortijo de Archidona) (Villar *et al.*, 2006). La alta capacidad de adsorción, gran área superficial, impermeabilidad, y el hinchamiento cuando se hidrata, son las propiedades que hacen idónea su utilización en la construcción de los almacenamientos de residuos radiactivos de alta actividad (ej. combustible gastado de las centrales nucleares) (Perdrial *et al.*, 2009). Por tanto, es necesario que la bentonita mantenga su estructura, es decir, que presente una gran estabilidad durante el tiempo en que el AGP esté en funcionamiento (hasta 100.000 años en algunos casos) para que estas propiedades no se vean alteradas (Anderson et al., 2011).

La estabilidad de la bentonita puede verse afectada por la actividad de los microorganismos presentes en ella (ej. reducción del hierro estructural de la esmectita), no solo de forma natural sino, también, por los que puedan ser introducidos durante la construcción, operación y mantenimiento del AGP. Debido a esta preocupación, a lo largo de los años se han realizado diversos estudios acerca de las comunidades microbianas que puedan estar presentes en las bentonitas (Bengtsson and Pedersen, 2017; Grigoryan et al., 2018; Haynes et al., 2018; Leupin et al., 2017; Lopez-Fernandez et al., 2018, 2015, 2014). La actividad microbiana podría afectar la integridad y el rendimiento del almacenamiento, a través de diferentes procesos: corrosión de los contenedores metálicos, alteración de las propiedades fisicoquímicas de la bentonita y afectar a la especiación y movilidad de radionucleidos (Liu et al., 2017; Pentráková et al., 2013; Stone et al., 2016; Stroes-Gascoyne et al., 2010). Este último proceso tendría un gran impacto en el caso de que se produjeran daños en los contenedores metálicos y, en consecuencia, se liberaran los radionucleidos contenidos. En esta hipotética situación, los microorganismos podrían interaccionar con ellos por diversos

mecanismos como la biosorción, la acumulación intracelular, la biomineralización y la biorreducción (Lopez-Fernandez *et al.*, 2018).

Por todo ello, en esta Tesis Doctoral se ha realizado un estudio de las comunidades bacterianas presentes en las bentonitas españolas que puedan tener un impacto en el correcto funcionamiento del AGP, bien por producir alteraciones negativas para el mismo o de forma positiva mediante la inmovilización de radionucleidos y metaloides peligrosos (ej. uranio y selenio) que puedan ser liberados de forma accidental. Para ello se ha empleado una metodología multidisciplinar en la que se combinan técnicas de microbiología, biología molecular, microscópicas y espectroscópicas.

En primer lugar, se propuso investigar el comportamiento de la bentonita y su comunidad bacteriana en el caso de una fuga de radionucleidos (mayoritariamente uranio) de los contenedores de residuos. Para este hipotético caso se elaboraron microcosmos de bentonita, procedente de El Cortijo de Archidona en Almería, tratados con uranio (nitrato de uranilo) y glicerol-2-fosfato (G2P) que fueron incubados aeróbicamente durante 6 meses. La adición de G2P tuvo doble finalidad: su utilización como fuente de carbono y fosfato para estimular el crecimiento bacteriano (Lopez-Fernandez et al., 2015); y la función de favorecer el proceso de biomineralización de uranio al estimular la actividad fosfatasa que poseen algunos microorganismos y, consecuentemente, la precipitación de fosfatos de uranio del grupo de la autunita (mineral de uranio muy estable) (Beazley et al., 2011; Jroundi et al., 2007; Martinez et al., 2014). Sin embargo, no se obtuvieron resultados relevantes a la hora de encontrar minerales de autunita en los microcosmos salvo algunos datos, de pequeña cuantía, de especiación de U en la muestra tratada conjuntamente con uranio y G2P (GU) usando para su detección HAADF-STEM. Tampoco se observaron cambios significativos en la mineralogía de la bentonita, lo que indica la alta estabilidad de estas arcillas a pesar de los cambios ocurridos en la estructura y composición de las poblaciones bacterianas.

Mediante los análisis bioinformáticos de las secuencias obtenidas (diversidad beta), se observó un gran efecto del G2P sobre la diversidad bacteriana en los microcosmos, distinguiéndose una agrupación marcada de los microcosmos tratados, por un lado, y no tratados con G2P, por otro. Estas diferencias venían determinadas por la alta presencia de *Azotobacter*, *Streptomyces, Rhizobium* y *Amycolatopsis*

principalmente cuando el G2P estaba presente (junto con nitrato de uranilo [GU], con nitrato sódico [GN], y solamente G2P [G]). *Azotobacter* sólo se encontró en los microcosmos tratados con G2P (G) con una abundancia relativa del 40% de la comunidad bacteriana, probablemente debido a su capacidad para utilizar el glicerol como fuente de carbono en condiciones libres de nitrógeno (Yoneyama et al., 2015). Como en *Azotobacter*, el G2P potenció el crecimiento de *Streptomyces* ya que el glicerol es considerado una de las mejores fuentes de carbono utilizadas para ello y para la producción de antibióticos (Lee et al., 2017). En el caso de *Rhizobium*, se identificó prácticamente sólo en los microcosmos tratados con G2P en el que estaba presente el nitrato (nitrato de uranilo y nitrato sódico), es decir las muestras denominadas GU y GN. Este hecho no es sorprendente ya que diversas especies de *Rhizobium*, son conocidas por su capacidad para reducir el nitrato a nitritos o nitrógeno molecular, pudiendo utilizar el glicerol como fuente de carbono (Safonov et al., 2018; Spain and Krumholz, 2012). En cualquier caso, el hecho más relevante fue la abundancia significativa del género *Amycolatopsis* en las muestras tratadas con uranio y G2P con respecto a las demás. Esta bacteria tiene un gran potencial en la biomineralización del uranio por su capacidad de degradar G2P gracias a su actividad fosfatasa, liberando fosfatos orgánicos que, en combinación con el uranio, precipitan en forma de fosfatos de uranio de gran estabilidad (Camas et al., 2013; Zucchi et al., 2012). Este proceso resulta de gran importancia en el AGP ya que reduce la movilidad y, por tanto, la biodisponibilidad del uranio en el medioambiente. Además, *Amycolatopsis* no es sólo capaz de llevar a cabo este proceso sino que también se ha descubierto, recientemente, la capacidad de adsorción de uranio en su superficie celular ya que están presentes grupos funcionales como ácido carboxílico, hidroxilo y amida que podrían interactuar con los iones de uranio (Celik et al., 2018).

En los microcosmos aerobios se detectaron otros géneros bacterianos que acompañan a *Amycolatopsis* en su interacción con el uranio, como es el caso de *Burkholderia*, *Bacillus* y *Desulfomicrobium.* En los dos primeros casos se produce una precipitación de uranio en forma de fosfatos de uranio (biomineralización) mientras que en el caso de *Desulfomicrobium* se produciría una reducción de U(VI) a especies de U(IV) menos móviles (Converse et al., 2013; Huang et al., 2017; Merroun et al., 2011; Pathak et al., 2017). La presencia de *Bacillus* en bentonitas tratadas con uranio se ha descrito previamente en un estudio llevado a cabo con bentonitas españolas que

provenían también del yacimiento localizado en Almería (Lopez-Fernandez et al., 2018).

Debido a la alta abundancia de *Amycolatopsis*, se quiso determinar el verdadero potencial de este género en cuanto a la inmovilización de uranio. Por ello, se llevó a cabo un estudio basado en la interacción de uranio con *Amycolatopsis ruanii* en presencia de un consorcio bacteriano procedente del agua de poro de la bentonita (*Bradyrhizobium-Rhizobium-Pseudomonas*). Con ello, se confirmó la participación de la actividad fosfatasa de esta bacteria para la formación de fosfatos de uranio, que se encontraron tanto en presencia como en ausencia de G2P, mediante los análisis de HAADF-STEM. Sin embargo, solamente en presencia de la fuente orgánica de fosfatos se observó una estructura intracelular compuesta por U y P, según confirmó el análisis por EDX. Por tanto, la presencia de *Amycolatopis* en las bentonitas puede tener un impacto positivo en el AGP teniendo en cuenta su capacidad de inmovilizar el uranio hacia formas menos solubles y, por tanto, menos móviles del radionucleido.

Durante la construcción del AGP, y el emplazamiento de los contenedores metálicos en los túneles, una gran cantidad de oxígeno puede ser introducido. No obstante, la presencia de oxígeno no se prolonga en el tiempo ya que se consumirá rápidamente debido a la actividad microbiana, a los procesos de corrosión o a la oxidación mineral (King et al., 2017; Payer et al., 2019). Por lo tanto, habrá una prevalencia de condiciones anóxicas a largo plazo, las cuales requieren un estudio más profundo y extenso. Por este motivo, se elaboraron los microcosmos de bentonita, pero, en esta ocasión, en condiciones anaeróbicas simulando las condiciones del AGP para así determinar la diversidad microbiana y las alteraciones en la mineralogía que se pudieran dar en ausencia de oxígeno.

Después de seis meses de incubación anaeróbica se encontraron depósitos de color marrón (tanto superficiales como en profundidad) en todos los microcosmos: de mayor tamaño en los microcosmos tratados con G2P y más pequeñas en su ausencia. Para dar explicación a su presencia, se realizaron análisis microscópicos y espectroscópicos de dichos depósitos y se observó que estaban compuestos de manganeso (Mn). Se podría tratar de óxidos de Mn adheridos a la bentonita, ya que previamente se había descrito la capacidad de la misma por adsorber Mn (Al-Jariri and Khalili, 2010; Dolinská et al., 2015; Iskander et al., 2011). Lo más probable es que se

trate de óxidos de Mn(IV) puesto que el color marrón oscuro es una característica propia de estos compuestos (Kitjanukit et al., 2019), los cuales se podrían producir tanto por la actividad de bacterias oxidadoras de Mn como por cierto tipo de hongos (Liu et al., 2018; Santelli et al., 2011).

Con respecto a la diversidad microbiana en condiciones anaérobicas, el hecho más notable observado fue la drástica disminución de Actinobacterias en comparación con su gran abundancia en los microcosmos aeróbicos. Este hecho es debido a que la gran mayoría de las Actinobacterias son bacterias aerobias, aunque un pequeño porcentaje de las mismas pueden llegar a adaptarse a condiciones anóxicas (Anandan et al., 2016). Considerando la distribución de la diversidad bacteriana en los distintos microcosmos anaeróbicos, los más diferentes con respecto a los demás fueron los tratados con uranio y G2P (GU) principalmente por la contribución de *Pseudomonas* y *Desulfovibrio. Pseudomonas* tiene una amplia repercusión en cuanto a la inmovilización del uranio, además al ser una bacteria desnitrificante es capaz de reducir los nitratos para obtener energía. Estas bacterias están descritas por su capacidad de interaccionar con uranio mediante diferentes mecanismos (bio-adsorción, acumulación intracelular, biomineralización y transformación por reducción) (Chabalala and Chirwa, 2010; D'Souza et al., 2006; Hu et al., 1996; Kazy et al., 2009, 2008; Newsome et al., 2014) lo que hace que la presencia de *Pseudomonas* en las bentonitas sea de gran interés por el potencial beneficio que podría aportar al AGP. En este sentido, dentro del grupo de las bacterias sulfato-reductoras, *Desulfovibrio* también contribuye a esta función ya que estas bacterias han demostrado, a través de numerosos estudios, su capacidad de reducir el uranio hexavalente al tetravalente mediante un mecanismo en el que interviene el citocromo $c_{3,}$ también llamado U(VI) reductasa (Heidelberg et al., 2004; Lovley et al., 1993; Payne et al., 2002; Stylo et al., 2015). Además, se determinó que el género *Clostridium* era significativamente abundante en los microcosmos tratados con uranio (sin G2P) con un 4.5% de la comunidad total. Se trata de un grupo de bacterias anaerobias estrictas de las que se ha descrito su capacidad de reducir U(VI) formando precipitados de U(IV), tanto sus células vegetativas como las esporas que producen (Francis and Dodge, 2008; Gao and Francis, 2008; Vecchia et al., 2010). Por lo tanto, bajo condiciones anaeróbicas también se da el crecimiento de bacterias, anaerobias estrictas o facultativas, que son capaces de contribuir positivamente al ciclo del uranio,

inmovilizándolo, preferentemente mediante su reducción, de manera que dificulta su dispersión hacia el medioambiente.

Para poder determinar la implicación de los microorganismos en las bentonitas en una situación más real se elaboraron bloques de bentonita compactada ya que, en este sistema, se dispondrán bloques compactados de dimensiones determinadas y densidades secas a lo largo de los túneles y galerías (Lopez-Fernandez et al., 2018). Como consecuencia se crearán condiciones adversas para la actividad y subsistencia de los microorganismos, tanto propios de la bentonita como de los introducidos, tales como la baja actividad de agua, presión de hinchamiento muy alta, y un tamaño de poro promedio de aproximadamente 0,02 µm (Pedersen et al., 2000; Ratto and Itavaara, 2012; Stroes-Gascoyne et al., 2011). Sin embargo, se espera que algunos microorganismos sean capaces de mantener la viabilidad celular y de subsistir en este ambiente adverso gracias a la formación de espacios entre los contenedores metálicos/roca hospedante y los bloques, entre un bloque y otro, e incluso en fracturas que podrían formarse dentro de cada bloque de bentonita compactada (Pedersen et al., 2000). Por ello, fue necesario el estudio de la comunidad bacteriana que pudiera coexistir en bentonitas compactadas para inferir el impacto que podrían tener estos microorganismos en el AGP a largo plazo. Las bentonitas españolas tratadas con acetato se compactaron a dos densidades secas diferentes (1,5 y 1,7 g/cm^3) y se incubaron anaeróbicamente durante 24 meses. El acetato se usó como donador de electrones para estimular el crecimiento de bacterias reductoras de hierro (BRH) y reductoras de sulfato (BRS).

Sin embargo, la extracción de ácidos nucleicos de bentonitas compactadas supone un reto, no solamente en nuestro laboratorio sino también a nivel global en la comunidad científica. Esto es debido a la baja biomasa microbiana que se espera que esté presente y, por tanto, a la poca cantidad de células que aporten moléculas de ADN. Otras razones que contribuyen a esa dificultad son: 1) la impermeabilidad y el hinchamiento de las bentonitas cuando se hidratan, ya que por un lado impiden que las soluciones penetren de forma uniforme en toda la muestra y, por otro lado, forman una mezcla muy compacta que dificulta la mezcla de las bentonitas con las soluciones químicas; 2) fuerte capacidad de adhesión de moléculas debido a su gran capacidad de intercambio iónico (Stone et al., 2016). Por ello, se requirió del desarrollo de un protocolo de extracción de ADN libre de inhibidores y de alta calidad que pudiera ser

amplificado por PCR, que se ha optimizado a partir del protocolo tradicional basado en el fenol-cloroformo.

Tras superar esta dificultad, la secuenciación de las muestras de ADN derivó en información sobre la diversidad bacteriana presente en los bloques de 1,5 y 1,7 g/cm^3. Esa diversidad fue inferior después de 24 meses de incubación en comparación con la presente al inicio del experimento. Esto respalda la hipótesis de que la alta compactación de la bentonita afecta el comportamiento de los microorganismos naturales y reduce la diversidad bacteriana en la comunidad, ya que sólo las bacterias que puedan ser albergadas en los espacios creados (fracturas y poros) en las bentonitas podrán sobrevivir en este ambiente. Los análisis usando VP-FESEM pusieron de manifiesto la presencia de fracturas y poros en los bloques de bentonita de ambas densidades. Algunas bacterias son capaces de adaptarse a espacios pequeños y falta de nutrientes para sobrevivir, como es el caso de *Sphingomonas* y *Pseudomonas* (Chien et al., 2012; Ghuneim et al., 2018; Monier and Lindow, 2003), ambas presentes tras 24 meses de incubación por lo que podrían haber hecho uso de esta capacidad para subsistir.

Una de las preocupaciones en el futuro AGP es la corrosión de los contenedores metálicos, pues deben permanecer intactos hasta que la radiactividad de los desechos decaiga a niveles de fondo naturales. Por lo tanto, es especialmente importante considerar la diversidad de bacterias reductoras de sulfato en la bentonita compactada. Las BRS son capaces de acoplar la oxidación de ácidos orgánicos (ej. acetato) con la reducción de sulfato a sulfuro que podría corroer los recipientes metálicos (Pedersen, 2010). En los bloques de bentonita estudiados por diversos autores se encontraron bacterias con potencial para producir ácido sulfhídrico que podría corroer los contenedores como pueden ser *Pseudomonas*, *Desulfosporosinus*, y *Desulfobacter* (Loka Bharathi, 2008; Timmers et al., 2018; van den Brand et al., 2014). En nuestro estudio, después de 24 meses de incubación, se encontraron varias bacterias oxidantes de azufre como *Delftia*, *Paracoccus*, *Mesorhizobium*, *Thiobacillus* y *Sulfurifustis,* que podrían contrarrestar la actividad de las bacterias reductoras de sulfato al oxidar el sulfuro producido por ellas y, de esta manera, paliar el efecto negativo que podría tener ese sulfuro (Huber et al., 2016; Poser et al., 2014; Quentmeier et al., 2003).

Otro de los grupos bacterianos clave en el AGP es el de las bacterias reductoras de hierro ya que uno de los aceptores de electrones más abundantes en la bentonita es el propio hierro estructural que se encuentra en la capa octaédrica de la esmectita (Esnault et al., 2010). Por tanto, las BRH podrían llegar a producir la alteración de la bentonita (ilitización) haciendo que se pierdan o reduzcan drásticamente las propiedades que la hacen idónea para su utilización en el AGP (como la capacidad de hinchamiento, alta capacidad de adsorción de iones, etc.) (Dong, 2012). En los bloques tratados con acetato, tras 24 meses de incubación, se encontraron géneros bacterianos con capacidad de reducir el Fe(III) utilizando el acetato como fuente de electrones tales como *Geobacillus*, *Pseudomonas*, *Stenotrophomonas*, *Bacillus* y *Thermicanus* (Brooke, 2012; Gößner et al., 1999; Valencia-Cantero and Peña-Cabriales, 2014).

Por tanto, los resultados de la diversidad bacteriana en bentonitas compactadas han puesto de manifiesto la presencia de grupos bacterianos relacionados con los ciclos biogeoquímicos de azufre y del hierro, que podrían enriquecerse con la adición de acetato. Sin embargo, no se han encontrado diferencias entre las distintas densidades de compactación. Esto podría explicarse por el corto tiempo de incubación (2 años), que podría resultar insuficiente para detectar un enriquecimiento de las comunidades BRH y BRS, además de por las condiciones poco propicias derivadas de la falta de humedad durante el experimento que frenaría el crecimiento de las bacterias. Por consiguiente, sería de un gran interés realizar este experimento a largo plazo para propiciar el enriquecimiento de estos grupos de bacterias, alterando la estabilidad de las bentonitas (por reducción estructural de hierro) y/o induciendo la corrosión del recipiente metálico (por la producción de sulfuro).

Por último, para completar un estudio exhaustivo de las comunidades bacterianas presentes en las bentonitas y su comportamiento frente a diferentes condiciones, se han elaborado microcosmos de bentonita en los que se han añadido diferentes fuentes de carbono y de fosfatos orgánicos (acetato y G2P). Estos microcosmos, a diferencia de los anteriores, se han elaborado de forma que la bentonita se encontraba saturada de agua para posibilitar el crecimiento bacteriano. En esta ocasión, el estudio de la interacción de la bentonita y su comunidad bacteriana con el posible contenido de los residuos radiactivos de alta actividad (RAA) se ha llevado a cabo añadiendo selenito [Se(IV)], ya que se trata de la forma predominante del selenio que se encuentra en los RAA. A diferencia de los otros experimentos, en este caso también se ha contemplado un nuevo

tratamiento consistente en la adición de un consorcio bacteriano (BSPAS) que lo conforman bacterias que han sido descritas por su capacidad de interaccionar con radionucleidos como el uranio y el selenio: *Stenotrophomonas* (Fresneda et al., 2018; Ruiz-Fresneda et al., 2019), *Pseudomonas* (Hunter, 2014), *Shewanella* (Li et al., 2014a), *Bacillus* (Javed et al., 2015) y *Amycolatopsis* (Bueno-Galera, 2019). Analizando la diversidad microbiana de estos microcosmos, se ha demostrado un efecto tóxico del selenito para algunos de los microorganismos presentes en las bentonitas, como es el caso de *Methanosarcina*. Esta arquea se ha encontrado abundantemente en aquellas muestras no tratadas con selenito (B y BB); sin embargo, en las muestras tratadas (BBSe, BsBSe, BSe and BsSe) está práctica o completamente ausente. Por otro lado, la presencia de Se(IV) promovió la abundancia de bacterias con mecanismos de desintoxicación de Se, como *Pseudomonas* y *Stenotrophomonas* (Fresneda et al., 2018; Hunter, 2014), las cuales, no solo forman parte del consorcio BSPAS sino que también son bacterias naturales de la bentonita ya que han sido identificadas también en aquellas muestras que no fueron inoculadas con las mismas. Además de estas bacterias, *Desulfosporosinus* y la familia *Desulfuromonadaceae* se encontraron más abundantes en los microcosmos de BSe que en las muestras no tratadas (B) indicando una alta tolerancia al selenito tóxico, ambas han sido previamente descritas por su habilidad para reducir los oxianiones de selenio a selenio elemental [Se(0)] (Hockin and Gadd, 2006, 2003; Nancharaiah and Lens, 2015). El Se(0) es una forma menos soluble que el selenito o el selenato y, por tanto, menos tóxico al presentar una menor biodisponibilidad. Por tanto, gracias a estos resultados, podemos determinar que en la microbiota de la bentonita se encuentran presentes diversas bacterias capaces de inmovilizar el selenio tóxico en formas menos solubles y, consecuentemente, menos móviles.

La reducción de Se(IV) se ha podido comprobar ya que, tras la incubación de 6 meses en condiciones anaérobicas, apareció un color rojo anaranjado en la superficie de la bentonita. Sin embargo, en la muestra tratada con selenio e inoculada con el consorcio BSPAS se presentó un color negro/gris oscuro a partir del segundo mes de incubación (Fig. 7 del Capítulo 5). Esta observación está estrechamente relacionado con la transformación de las distintas fases del Se(0): selenio amorfo (*a*-Se) y monoclínico (*m*-Se) presentan un color rojo anaranjado mientras que el selenio trigonal (*t*-Se) es de color gris oscuro/negro (Wang et al., 2010). El *a*-Se es termodinámicamente inestable y

se transforma en *m*-Se a altas temperaturas. Del mismo modo, el *m*-Se es metaestable y también podría sufrir la conversión a la forma *t*-Se (Goldan et al., 2016). Los análisis de HRTEM, SAED, y espectroscopía Raman revelaron que las nanopartículas de Se (SeNPs), en forma de nanoesferas tanto en el espacio extracelular como intracelular, pertenecían a la fase cristalina del *m*-Se en las muestras BSe, BsSe y BsBSe. El *m*-Se podría disolverse debido a la menor estabilidad y el Se liberado se depositaría en los nanocristales de *t*-Se permitiendo el crecimiento uniforme de nanotubos, cristales hexagonales o cristales poligonales de mayor tamaño compuestos por *t*-Se (Wang et al., 2010).

La formación del m-Se podría tener un origen bacteriano por reducción del Se(IV) a Se(0) ya que, en las muestras de BsBSe, encontramos SeNPs en el interior de las células a nivel de la membrana plasmática. Se han planteado diferentes mecanismos por los que la bacteria es capaz de producir estas nanopartículas de Se(0). Uno de ellos es la reducción intracelular de selenito mediada por moléculas que contienen grupos tioles reducidos (-SH) como el glutatión (GSH) (Fresneda et al., 2018; Li et al., 2014a). La otra estrategia consiste en la reducción enzimática del selenito para formar precipitados de Se(0), como la actividad de nitrito reductasa en *Rhizobium sullae* (Basaglia et al., 2007), fumarato reductasa en *Shewanella oneidensis* (Li et al., 2014b) o la selenito reductasa de *Bacillus selenitireducens* (Wells et al., 2019). El selenio reducido se acumulará en el citoplasma o a nivel de membrana que, en cierto momento, se liberarán por una lisis celular y quedarán en el espacio extracelular, dando lugar al color rojo anaranjado característico de las formas *a*-/*m*- Se (Fresneda et al., 2018). Finalmente, la naturaleza inestable de las partículas de *m*-Se conduce a su solubilización y recristalización en la forma más estable (*t*-Se), produciendo el crecimiento de nanotubos y cristales poligonales grandes de Se(0), lo que otorga el color negro/gris oscuro característico del *t*-Se.

Además de esta forma microbiológica de inmovilización del selenio, las bentonitas también tienen cierta capacidad de retención de selenio: por adsorción en su superficie, o bien por reducción abiótica de Se(IV) mediada por pirita, minerales de siderita e, incluso, el hierro estructural de las esmectitas (Breynaert et al., 2010; Hoving et al., 2019; Kang et al., 2011). En los microcosmos de BSe, se encontró un ejemplo de estos posibles mecanismos ya que el análisis EDX mostró picos de Se asociados a la esmectita adyacente a los precipitados de Fe. También se encontraron precipitados de

selenio asociados a apatita, pudiendo estar adsorbidos en la superficie del mineral. Esta asociación ya fue descrita por Duc y colaboradores (2003) tratándose, posiblemente, de un proceso mediado por un intercambio aniónico con grupos fosfato. Por tanto, el uso de la bentonita en el AGP, en cuanto a la presencia de selenio se refiere, es bastante positiva desde ambos puntos de vista: microbiológico y mineralógico, ya que tanto los propios minerales presentes en la bentonita como los microorganismos que habitan estas arcillas tienen la capacidad de inmovilizar selenio, impidiendo a diferentes niveles la dispersión de este elemento hacia el medioambiente.

Por todo lo expuesto anteriormente, cabe deducir que tanto la bentonita como las comunidades microbianas presentes en ella pueden resultar unos grandes aliados a la hora de preservar las condiciones de seguridad del AGP, gracias a la gran estabilidad que presenta a largo plazo y a la microbiota hallada en ella, la cual participaría de una manera beneficiosa en la inmovilización de elementos peligrosos para el medioambiente como son el uranio y el selenio. No obstante, estos trabajos han puesto de manifiesto la necesidad de seguir ahondando en el estudio de las bentonitas como material de relleno y sellado en la forma en que éstas serán empleadas en el AGP. Esto es debido fundamentalmente a que, en esta Tesis Doctoral, se ha encontrado la presencia de bacterias que podrían comprometer la seguridad del almacenamiento de RAA como es el caso de las bacterias sulfato-reductoras y las hierro-reductoras, estableciéndose precedentes para el desarrollo de investigaciones futuras.

1. REFERENCIAS

Al-Jariri, J.S., Khalili, F., 2010. Adsorption of Zn(II), Pb(II), Cr(III) and Mn(II) from water by Jordanian bentonite. Desalination and Water Treatment 21, 308–322. https://doi.org/10.5004/dwt.2010.1623

Anandan, R., Dharumadurai, D., Manogaran, G.P., 2016. An Introduction to Actinobacteria. Actinobacteria - Basics and Biotechnological Applications. https://doi.org/10.5772/62329

Anderson, C., Johnsson, A., Moll, H., Pedersen, K., 2011. Radionuclide Geomicrobiology of the Deep Biosphere. Geomicrobiology Journal 28, 540–561. https://doi.org/10.1080/01490451.2010.507644

Anderson, C., Pedersen, K., Jakobsson, A.-M., 2006. Autoradiographic Comparisons of Radionuclide Adsorption Between Subsurface Anaerobic Biofilms and Granitic Host Rocks. Geomicrobiology Journal 23, 15–29. https://doi.org/10.1080/01490450500399946

Baños, S., Pérez-Redondo, R., Koekman, B., Liras, P., 2009. Glycerol Utilization Gene Cluster in Streptomyces clavuligerus. Appl. Environ. Microbiol. 75, 2991–2995. https://doi.org/10.1128/AEM.00181-09

Basaglia, M., Toffanin, A., Baldan, E., Bottegal, M., Shapleigh, J.P., Casella, S., 2007. Selenite-reducing capacity of the copper-containing nitrite reductase of Rhizobium sullae. FEMS Microbiol Lett 269, 124–130. https://doi.org/10.1111/j.1574-6968.2006.00617.x

Beazley, M.J., Martinez, R.J., Webb, S.M., Sobecky, P.A., Taillefert, M., 2011. The effect of pH and natural microbial phosphatase activity on the speciation of uranium in subsurface soils. Geochimica et Cosmochimica Acta 75, 5648–5663. https://doi.org/10.1016/j.gca.2011.07.006

Bengtsson, A., Pedersen, K., 2017. Microbial sulphide-producing activity in water saturated Wyoming MX-80, Asha and Calcigel bentonites at wet densities from 1500 to 2000kgm−3. Applied Clay Science 137, 203–212. https://doi.org/10.1016/j.clay.2016.12.024

Breynaert, E., Scheinost, A.C., Dom, D., Rossberg, A., Vancluysen, J., Gobechiya, E., Kirschhock, C.E.A., Maes, A., 2010. Reduction of Se(IV) in boom clay: XAS solid phase speciation. Environ. Sci. Technol. 44, 6649–6655. https://doi.org/10.1021/es100569e

Brooke, J.S., 2012. Stenotrophomonas maltophilia: an Emerging Global Opportunistic Pathogen. Clinical Microbiology Reviews 25, 2–41. https://doi.org/10.1128/CMR.00019-11

Bueno-Galera, C., 2019. Caracterización espectroscópica y microscópica de la biosíntesis microbiana de SeNPs y el papel de las proteínas en su formación. Universidad de Granada.

Camas, M., Sahin, N., Sazak, A., Spröer, C., Klenk, H.-P., 2013. Amycolatopsis magusensis sp. nov., isolated from soil. Int. J. Syst. Evol. Microbiol. 63, 1254–1260. https://doi.org/10.1099/ijs.0.042770-0

Celik, F., Camas, M., Kyeremeh, K., Sazak Camas, A., 2018. Microbial Sorption of Uranium Using Amycolatopsis sp. K47 Isolated from Uranium Deposits. Water Air Soil Pollut 229, 112. https://doi.org/10.1007/s11270-018-3766-5

Chabalala, S., Chirwa, E.M.N., 2010. Uranium(VI) reduction and removal by high performing purified anaerobic cultures from mine soil. Chemosphere 78, 52–55. https://doi.org/10.1016/j.chemosphere.2009.10.026

Chien, A.-C., Hill, N.S., Levin, P.A., 2012. Cell size control in bacteria. Curr. Biol. 22, R340-349. https://doi.org/10.1016/j.cub.2012.02.032

Converse, B.J., Wu, T., Findlay, R.H., Roden, E.E., 2013. U(VI) Reduction in Sulfate-Reducing Subsurface Sediments Amended with Ethanol or Acetate. Appl. Environ. Microbiol. 79, 4173–4177. https://doi.org/10.1128/AEM.00420-13

Dolinská, S., Schütz, T., Znamenáčková, I., Lovas, M., Vaculíková, L., 2015. Bentonite modification with manganese oxides and its characterization. Inzynieria Mineralna 2015, 213–218.

Dong, H., 2012. Clay–Microbe Interactions and Implications for Environmental Mitigation. Elements 8, 113–118. https://doi.org/10.2113/gselements.8.2.113

D'Souza, S.F., Sar, P., Kazy, S.K., Kubal, B.S., 2006. Uranium Sorption by Pseudomonas Biomass Immobilized in Radiation Polymerized Polyacrylamide Bio-Beads. Journal of Environmental Science and Health, Part A 41, 487–500. https://doi.org/10.1080/10934520500428377

Duc, M., Lefevre, G., Fedoroff, M., Jeanjean, J., Rouchaud, J.C., Monteil-Rivera, F., Dumonceau, J., Milonjic, S., 2003. Sorption of selenium anionic species on apatites and iron oxides from aqueous solutions. Journal of Environmental Radioactivity, International workshop on the mobility of iodine, technetium, selenium and uranium in the biosphere 70, 61–72. https://doi.org/10.1016/S0265-931X(03)00125-5

Esnault, L., Libert, M., Bildstein, O., Jullien, M., Mustin, C., 2010. Clay-iron reducing bacteria interaction in deep geological environment: Experimental and modeling approach. Presented at the Water-Rock Interaction - Proceedings of the 13th International Conference on Water-Rock Interaction, WRI-13, pp. 939–942.

Francis, A.J., Dodge, C.J., 2008. Bioreduction of Uranium(VI) Complexed with Citric Acid by Clostridia Affects Its Structure and Solubility. Environ. Sci. Technol. 42, 8277–8282. https://doi.org/10.1021/es801045m

Fresneda, M.A.R., Martín, J.D., Bolívar, J.G., Cantos, M.V.F., Bosch-Estévez, G., Moreno, M.F.M., Merroun, M.L., 2018. Green synthesis and biotransformation of amorphous Se nanospheres to trigonal 1D Se nanostructures: impact on Se mobility within the concept of radioactive waste disposal. Environ. Sci.: Nano 5, 2103–2116. https://doi.org/10.1039/C8EN00221E

Gao, W., Francis, A.J., 2008. Reduction of Uranium(VI) to Uranium(IV) by Clostridia. Appl. Environ. Microbiol. 74, 4580–4584. https://doi.org/10.1128/AEM.00239-08

Ghuneim, L.-A.J., Jones, D.L., Golyshin, P.N., Golyshina, O.V., 2018. Nano-Sized and Filterable Bacteria and Archaea: Biodiversity and Function. Front Microbiol 9. https://doi.org/10.3389/fmicb.2018.01971

Goldan, A.H., Li, C., Pennycook, S.J., Schneider, J., Blom, A., Zhao, W., 2016. Molecular structure of vapor-deposited amorphous selenium. Journal of Applied Physics 120, 135101. https://doi.org/10.1063/1.4962315

Gößner, A.S., Devereux, R., Ohnemüller, N., Acker, G., Stackebrandt, E., Drake, H.L., 1999. Thermicanus aegyptius gen. nov., sp. nov., Isolated from Oxic Soil, a Fermentative Microaerophile That Grows Commensally with the Thermophilic Acetogen Moorella thermoacetica. Appl Environ Microbiol 65, 5124–5133.

Grigoryan, A.A., Jalique, D.R., Medihala, P., Stroes-Gascoyne, S., Wolfaardt, G.M., McKelvie, J., Korber, D.R., 2018. Bacterial diversity and production of sulfide in microcosms containing uncompacted bentonites. Heliyon 4. https://doi.org/10.1016/j.heliyon.2018.e00722

Groth, I., Tan, G.Y.A., González, J.M., Laiz, L., Carlsohn, M.R., Schütze, B., Wink, J., Goodfellow, M., 2007. Amycolatopsis nigrescens sp. nov., an actinomycete isolated from a Roman catacomb. Int. J. Syst. Evol. Microbiol. 57, 513–519. https://doi.org/10.1099/ijs.0.64602-0

Haynes, H.M., Pearce, C.I., Boothman, C., Lloyd, J.R., 2018. Response of bentonite microbial communities to stresses relevant to geodisposal of radioactive waste. Chemical Geology 501, 58–67. https://doi.org/10.1016/j.chemgeo.2018.10.004

Heidelberg, J.F., Seshadri, R., Haveman, S.A., Hemme, C.L., Paulsen, I.T., Kolonay, J.F., Eisen, J.A., Ward, N., Methe, B., Brinkac, L.M., Daugherty, S.C., Deboy, R.T., Dodson, R.J., Durkin, A.S., Madupu, R., Nelson, W.C., Sullivan, S.A., Fouts, D., Haft, D.H., Selengut, J., Peterson, J.D., Davidsen, T.M., Zafar, N., Zhou, L., Radune, D., Dimitrov, G., Hance, M., Tran, K., Khouri, H., Gill, J., Utterback, T.R., Feldblyum, T.V., Wall, J.D., Voordouw, G., Fraser, C.M., 2004. The genome sequence of the anaerobic, sulfate-reducing bacterium Desulfovibrio vulgaris Hildenborough. Nat Biotechnol 22, 554–559. https://doi.org/10.1038/nbt959

Hockin, S., Gadd, G.M., 2006. Removal of selenate from sulfate-containing media by sulfate-reducing bacterial biofilms. Environmental Microbiology 8, 816–826. https://doi.org/10.1111/j.1462-2920.2005.00967.x

Hockin, S.L., Gadd, G.M., 2003. Linked Redox Precipitation of Sulfur and Selenium under Anaerobic Conditions by Sulfate-Reducing Bacterial Biofilms. Appl Environ Microbiol 69, 7063–7072. https://doi.org/10.1128/AEM.69.12.7063-7072.2003

Hoving, A.L., Münch, M.A., Bruggeman, C., Banerjee, D., Behrends, T., 2019. Kinetics of selenite interactions with Boom Clay: adsorption–reduction interplay. Geological Society, London, Special Publications 482, 225–239. https://doi.org/10.1144/SP482-2018-60

Hu, M.Z.-C., Norman, J.M., Faison, B.D., Reeves, M.E., 1996. Biosorption of uranium by Pseudomonas aeruginosa strain CSU: Characterization and comparison studies. Biotechnology and

Bioengineering 51, 237–247. https://doi.org/10.1002/(SICI)1097-0290(19960720)51:2<237::AID-BIT14>3.0.CO;2-J

Huang, W., Cheng, W., Nie, X., Dong, F., Ding, C., Liu, M., Li, Z., Hayat, T., Alharbi, N.S., 2017. Microscopic and Spectroscopic Insights into Uranium Phosphate Mineral Precipitated by Bacillus Mucilaginosus. ACS Earth Space Chem. 1, 483–492. https://doi.org/10.1021/acsearthspacechem.7b00060

Huber, B., Herzog, B., Drewes, J.E., Koch, K., Müller, E., 2016. Characterization of sulfur oxidizing bacteria related to biogenic sulfuric acid corrosion in sludge digesters. BMC Microbiol 16. https://doi.org/10.1186/s12866-016-0767-7

Hunter, W.J., 2014. Pseudomonas seleniipraecipitans Proteins Potentially Involved in Selenite Reduction. Curr Microbiol 69, 69–74. https://doi.org/10.1007/s00284-014-0555-2

Ilić, S.B., Konstantinović, S.S., Gojgić Cvijović, G.Đ., Savić, D.S., Veljković, V.B., 2013. The impact of glycerol and some carbohydrates on antibiotic production by Streptomyces hygroscopicus CH-7. Med Chem Res 22, 934–937. https://doi.org/10.1007/s00044-012-0088-9

Iskander, A.L., Khald, E.M., Sheta, A.S., 2011. Zinc and manganese sorption behavior by natural zeolite and bentonite. Annals of Agricultural Sciences 56, 43–48. https://doi.org/10.1016/j.aoas.2011.05.002

Javed, S., Sarwar, A., Tassawar, M., Faisal, M., 2015. Conversion of selenite to elemental selenium by indigenous bacteria isolated from polluted areas. Chemical Speciation & Bioavailability 27, 162–168. https://doi.org/10.1080/09542299.2015.1112751

Jroundi, F., Merroun, M.L., Arias, J.M., Rossberg, A., Selenska-Pobell, S., González-Muñoz, M.T., 2007. Spectroscopic and Microscopic Characterization of Uranium Biomineralization in Myxococcus xanthus. Geomicrobiology Journal 24, 441–449. https://doi.org/10.1080/01490450701437651

Kang, M., Chen, F., Wu, S., Yang, Y., Bruggeman, C., Charlet, L., 2011. Effect of pH on Aqueous Se(IV) Reduction by Pyrite. Environ. Sci. Technol. 45, 2704–2710. https://doi.org/10.1021/es1033553

Kaur, N., Kumar, S., Mayilraj, S., 2013. Genome sequencing and annotation of Amycolatopsis vancoresmycina strain DSM 44592T. Genom Data 2, 16–17. https://doi.org/10.1016/j.gdata.2013.10.006

Kazy, S.K., D'Souza, S.F., Sar, P., 2009. Uranium and thorium sequestration by a Pseudomonas sp.: Mechanism and chemical characterization. Journal of Hazardous Materials 163, 65–72. https://doi.org/10.1016/j.jhazmat.2008.06.076

Kazy, S.K., Sar, P., D'Souza, S.F., 2008. Studies on Uranium Removal by the Extracellular Polysaccharide of a Pseudomonas aeruginosa Strain. Bioremediation Journal 12, 47–57. https://doi.org/10.1080/10889860802052870

King, F., Hall, D.S., Keech, P.G., 2017. Nature of the near-field environment in a deep geological repository and the implications for the corrosion behaviour of the container. Corrosion Engineering, Science and Technology 52, 25–30. https://doi.org/10.1080/1478422X.2017.1330736

Kitjanukit, S., Takamatsu, K., Okibe, N., 2019. Natural Attenuation of Mn(II) in Metal Refinery Wastewater: Microbial Community Structure Analysis and Isolation of a New Mn(II)-Oxidizing Bacterium Pseudomonas sp. SK3. Water 11, 507. https://doi.org/10.3390/w11030507

Lee, B.-R., Bhatia, S.K., Song, H.-S., Kim, J., Kim, W., Park, H., Yoon, J.-J., Park, S.-H., Hwang, D., Kim, B.-G., Yang, Y.-H., 2017. The role of NdgR in glycerol metabolism in Streptomyces coelicolor. Bioprocess Biosyst Eng 40, 1573–1580. https://doi.org/10.1007/s00449-017-1813-z

Leupin, O.X., Bernier-Latmani, R., Bagnoud, A., Moors, H., Leys, N., Wouters, K., Stroes-Gascoyne, S., 2017. Fifteen years of microbiological investigation in Opalinus Clay at the Mont Terri rock laboratory (Switzerland). Swiss J Geosci 110, 343–354. https://doi.org/10.1007/s00015-016-0255-y

Li, D.-B., Cheng, Y.-Y., Wu, C., Li, W.-W., Li, N., Yang, Z.-C., Tong, Z.-H., Yu, H.-Q., 2014a. Selenite reduction by Shewanella oneidensis MR-1 is mediated by fumarate reductase in periplasm. Sci Rep 4, 1–7. https://doi.org/10.1038/srep03735

Li, D.-B., Cheng, Y.-Y., Wu, C., Li, W.-W., Li, N., Yang, Z.-C., Tong, Z.-H., Yu, H.-Q., 2014b. Selenite reduction by Shewanella oneidensis MR-1 is mediated by fumarate reductase in periplasm. Scientific Reports 4, 1–7. https://doi.org/10.1038/srep03735

Liu, G., Qiu, S., Liu, B., Pu, Y., Gao, Z., Wang, J., Jin, R., Zhou, J., 2017. Microbial reduction of Fe(III)-bearing clay minerals in the presence of humic acids. Scientific Reports 7, 45354. https://doi.org/10.1038/srep45354

Liu, W., Langenhoff, A.A.M., Sutton, N.B., Rijnaarts, H.H.M., 2018. Biological regeneration of manganese (IV) and iron (III) for anaerobic metal oxide-mediated removal of pharmaceuticals from water. Chemosphere 208, 122–130. https://doi.org/10.1016/j.chemosphere.2018.05.097

Loka Bharathi, P.A., 2008. Sulfur Cycle, in: Jørgensen, S.E., Fath, B.D. (Eds.), Encyclopedia of Ecology. Academic Press, Oxford, pp. 3424–3431. https://doi.org/10.1016/B978-008045405-4.00761-8

Lopez-Fernandez, M., Cherkouk, A., Vilchez-Vargas, R., Jauregui, R., Pieper, D., Boon, N., Sanchez-Castro, I., Merroun, M.L., 2015. Bacterial Diversity in Bentonites, Engineered Barrier for Deep Geological Disposal of Radioactive Wastes. Microb Ecol 70, 922–935. https://doi.org/10.1007/s00248-015-0630-7

Lopez-Fernandez, M., Fernández-Sanfrancisco, O., Moreno-García, A., Martín-Sánchez, I., Sánchez-Castro, I., Merroun, M.L., 2014. Microbial communities in bentonite formations and their interactions with uranium. Applied Geochemistry 49, 77–86. https://doi.org/10.1016/j.apgeochem.2014.06.022

Lopez-Fernandez, M., Vilchez-Vargas, R., Jroundi, F., Boon, N., Pieper, D., Merroun, M.L., 2018. Microbial community changes induced by uranyl nitrate in bentonite clay microcosms. Applied Clay Science, ACS - SI ICC 2017 XVI International Clay Conference – Clays, from the oceans to space 160, 206–216. https://doi.org/10.1016/j.clay.2017.12.034

Lovley, D.R., Roden, E.E., Phillips, E.J.P., Woodward, J.C., 1993. Enzymatic iron and uranium reduction by sulfate-reducing bacteria. Marine Geology, Marine Sediments, Burial, Pore Water Chemistry, Microbiology and Diagenesis 113, 41–53. https://doi.org/10.1016/0025-3227(93)90148-O

Martinez, R.J., Wu, C.H., Beazley, M.J., Andersen, G.L., Conrad, M.E., Hazen, T.C., Taillefert, M., Sobecky, P.A., 2014. Microbial Community Responses to Organophosphate Substrate Additions in Contaminated Subsurface Sediments. PLOS ONE 9, e100383. https://doi.org/10.1371/journal.pone.0100383

Merroun, M.L., Nedelkova, M., Ojeda, J.J., Reitz, T., Fernández, M.L., Arias, J.M., Romero-González, M., Selenska-Pobell, S., 2011. Bio-precipitation of uranium by two bacterial isolates recovered from extreme environments as estimated by potentiometric titration, TEM and X-ray absorption spectroscopic analyses. Journal of Hazardous Materials 197, 1–10. https://doi.org/10.1016/j.jhazmat.2011.09.049

Monier, J.-M., Lindow, S.E., 2003. Pseudomonas syringae Responds to the Environment on Leaves by Cell Size Reduction. Phytopathology 93, 1209–1216. https://doi.org/10.1094/PHYTO.2003.93.10.1209

Nancharaiah, Y.V., Lens, P.N.L., 2015. Ecology and Biotechnology of Selenium-Respiring Bacteria. Microbiol. Mol. Biol. Rev. 79, 61–80. https://doi.org/10.1128/MMBR.00037-14

Newsome, L., Morris, K., Trivedi, D., Atherton, N., Lloyd, J.R., 2014. Microbial reduction of uranium(VI) in sediments of different lithologies collected from Sellafield. Applied Geochemistry 51, 55–64. https://doi.org/10.1016/j.apgeochem.2014.09.008

Pathak, A., Chauhan, A., Stothard, P., Green, S., Maienschein-Cline, M., Jaswal, R., Seaman, J., 2017. Genome-centric evaluation of Burkholderia sp. strain SRS-W-2-2016 resistant to high concentrations of uranium and nickel isolated from the Savannah River Site (SRS), USA. Genom Data 12, 62–68. https://doi.org/10.1016/j.gdata.2017.02.011

Payer, J.H., Finsterle, S., Apps, J.A., Muller, R.A., 2019. Corrosion Performance of Engineered Barrier System in Deep Horizontal Drillholes. Energies 12, 1491. https://doi.org/10.3390/en12081491

Payne, R.B., Gentry, D.M., Rapp-Giles, B.J., Casalot, L., Wall, J.D., 2002. Uranium Reduction by Desulfovibrio desulfuricans Strain G20 and a Cytochrome c3 Mutant. Appl Environ Microbiol 68, 3129–3132. https://doi.org/10.1128/AEM.68.6.3129-3132.2002

Pedersen, K., 2010. Analysis of copper corrosion in compacted bentonite clay as a function of clay density and growth conditions for sulfate-reducing bacteria. J. Appl. Microbiol. 108, 1094–1104. https://doi.org/10.1111/j.1365-2672.2009.04629.x

Pedersen, K., Motamedi, M., Karnland, O., Sandén, T., 2000. Mixing and sulphate-reducing activity of bacteria in swelling, compacted bentonite clay under high-level radioactive waste repository conditions. Journal of Applied Microbiology 89, 1038–1047. https://doi.org/10.1046/j.1365-2672.2000.01212.x

Pentráková, L., Su, K., Pentrák, M., Stucki, J.W., 2013. A review of microbial redox interactions with structural Fe in clay minerals. Clay Minerals 48, 543–560. https://doi.org/10.1180/claymin.2013.048.3.10

Perdrial, J.N., Warr, L.N., Perdrial, N., Lett, M.-C., Elsass, F., 2009. Interaction between smectite and bacteria: Implications for bentonite as backfill material in the disposal of nuclear waste. Chemical Geology 264, 281–294. https://doi.org/10.1016/j.chemgeo.2009.03.012

Poser, A., Vogt, C., Knöller, K., Ahlheim, J., Weiss, H., Kleinsteuber, S., Richnow, H.-H., 2014. Stable Sulfur and Oxygen Isotope Fractionation of Anoxic Sulfide Oxidation by Two Different Enzymatic Pathways. Environ. Sci. Technol. 48, 9094–9102. https://doi.org/10.1021/es404808r

Quentmeier, A., Hellwig, P., Bardischewsky, F., Grelle, G., Kraft, R., Friedrich, C.G., 2003. Sulfur oxidation in Paracoccus pantotrophus: interaction of the sulfur-binding protein SoxYZ with the dimanganese SoxB protein. Biochem. Biophys. Res. Commun. 312, 1011–1018. https://doi.org/10.1016/j.bbrc.2003.11.021

Rao, N.S.S., 2016. Advances in Agricultural Microbiology. Elsevier.

Ratto, M., Itavaara, M., 2012. Microbial activity in bentonite buffers. Literature study (No. VTT-TECHNOLOGY--20). VTT Technical Research Centre of Finland.

Ruiz-Fresneda, M.A., Gomez-Bolivar, J., Delgado-Martin, J., Abad-Ortega, M. del M., Guerra-Tschuschke, I., Merroun, M.L., 2019. The Bioreduction of Selenite under Anaerobic and Alkaline Conditions Analogous to Those Expected for a Deep Geological Repository System. Molecules 24, 3868. https://doi.org/10.3390/molecules24213868

Safonov, A.V., Babich, T.L., Sokolova, D.S., Grouzdev, D.S., Tourova, T.P., Poltaraus, A.B., Zakharova, E.V., Merkel, A.Y., Novikov, A.P., Nazina, T.N., 2018. Microbial Community and in situ Bioremediation of Groundwater by Nitrate Removal in the Zone of a Radioactive Waste Surface Repository. Front. Microbiol. 9. https://doi.org/10.3389/fmicb.2018.01985

Santelli, C.M., Webb, S.M., Dohnalkova, A.C., Hansel, C.M., 2011. Diversity of Mn oxides produced by Mn(II)-oxidizing fungi. Geochimica et Cosmochimica Acta 75, 2762–2776. https://doi.org/10.1016/j.gca.2011.02.022

Spain, A.M., Krumholz, L., 2012. Cooperation of Three Denitrifying Bacteria in Nitrate Removal of Acidic Nitrate- and Uranium-Contaminated Groundwater. Geomicrobiology Journal 29, 830–842. https://doi.org/10.1080/01490451.2011.635757

Stone, W., Kroukamp, O., Moes, A., McKelvie, J., Korber, D.R., Wolfaardt, G.M., 2016a. Measuring microbial metabolism in atypical environments: Bentonite in used nuclear fuel storage. J. Microbiol. Methods 120, 79–90. https://doi.org/10.1016/j.mimet.2015.11.006

Stone, W., Kroukamp, O., Moes, A., McKelvie, J., Korber, D.R., Wolfaardt, G.M., 2016b. Measuring microbial metabolism in atypical environments: Bentonite in used nuclear fuel storage. J. Microbiol. Methods 120, 79–90. https://doi.org/10.1016/j.mimet.2015.11.006

Stroes-Gascoyne, S., Hamon, C.J., Maak, P., 2011. Limits to the use of highly compacted bentonite as a deterrent for microbiologically influenced corrosion in a nuclear fuel waste repository. Physics and Chemistry of the Earth, Parts A/B/C, Clays in Natural & Engineered Barriers for Radioactive Waste Confinement 36, 1630–1638. https://doi.org/10.1016/j.pce.2011.07.085

Stroes-Gascoyne, S., Hamon, C.J., Maak, P., Russell, S., 2010. The effects of the physical properties of highly compacted smectitic clay (bentonite) on the culturability of indigenous microorganisms. Applied Clay Science, Advanced smectitic clay research 47, 155–162. https://doi.org/10.1016/j.clay.2008.06.010

Stylo, M., Neubert, N., Roebbert, Y., Weyer, S., Bernier-Latmani, R., 2015. Mechanism of Uranium Reduction and Immobilization in Desulfovibrio vulgaris Biofilms. Environ. Sci. Technol. 49, 10553–10561. https://doi.org/10.1021/acs.est.5b01769

Timmers, P.H.A., Vavourakis, C.D., Kleerebezem, R., Damsté, J.S.S., Muyzer, G., Stams, A.J.M., Sorokin, D.Y., Plugge, C.M., 2018. Metabolism and Occurrence of Methanogenic and Sulfate-Reducing Syntrophic Acetate Oxidizing Communities in Haloalkaline Environments. Front Microbiol 9, 3039. https://doi.org/10.3389/fmicb.2018.03039

Valencia-Cantero, E., Peña-Cabriales, J.J., 2014. Effects of iron-reducing bacteria on carbon steel corrosion induced by thermophilic sulfate-reducing consortia. J. Microbiol. Biotechnol. 24, 280–286. https://doi.org/10.4014/jmb.1310.10002

van den Brand, T.P.H., Roest, K., Brdjanovic, D., Chen, G.H., van Loosdrecht, M.C.M., 2014. Influence of acetate and propionate on sulphate-reducing bacteria activity. J. Appl. Microbiol. 117, 1839–1847. https://doi.org/10.1111/jam.12661

Vecchia, E.D., Veeramani, H., Suvorova, E.I., Wigginton, N.S., Bargar, J.R., Bernier-Latmani, R., 2010. U(VI) reduction by spores of Clostridium acetobutylicum. Research in Microbiology, Special issue on the biology of spore-formers 161, 765–771. https://doi.org/10.1016/j.resmic.2010.08.001

Villar, M.V., Cuevas, J., Leguey, S., Caballero, E., Huertas, F.J., Delgado, A., Fernández-Soler, J.M., Astudillo, J., 2006. The study of Spanish clays for their use as sealing materials in nuclear waste repositories: 20 years of progress. Journal of Iberian Geology 32, 15–36.

Wang, T., Yang, L., Zhang, B., Liu, J., 2010. Extracellular biosynthesis and transformation of selenium nanoparticles and application in H2O2 biosensor. Colloids and Surfaces B: Biointerfaces 80, 94–102. https://doi.org/10.1016/j.colsurfb.2010.05.041

Wells, M., McGarry, J., Gaye, M.M., Basu, P., Oremland, R.S., Stolz, J.F., 2019. Respiratory Selenite Reductase from Bacillus selenitireducens Strain MLS10. Journal of Bacteriology 201. https://doi.org/10.1128/JB.00614-18

Whitman, W.B., Goodfellow, M., Kämpfer, P., Busse, H.-J., Trujillo, M.E., Ludwig, W., Suzuki, K., 2012. Bergey's Manual of Systematic Bacteriology: Volume 5: The Actinobacteria. Springer Science & Business Media.

Yoneyama, F., Yamamoto, M., Hashimoto, W., Murata, K., 2015. Production of polyhydroxybutyrate and alginate from glycerol by Azotobacter vinelandii under nitrogen-free conditions. Bioengineered 6, 209–217. https://doi.org/10.1080/21655979.2015.1040209

Zucchi, T.D., Tan, G.Y.A., Bonda, A.N.V., Frank, S., Kshetrimayum, J.D., Goodfellow, M., 2012. Amycolatopsis granulosa sp. nov., Amycolatopsis ruanii sp. nov. and Amycolatopsis thermalba sp. nov., thermophilic actinomycetes isolated from arid soils. Int. J. Syst. Evol. Microbiol. 62, 1245–1251. https://doi.org/10.1099/ijs.0.031039-0

CONCLUSIONES

En relación con los resultados obtenidos, las principales conclusiones de esta Tesis Doctoral son:

1. La optimización del protocolo de extracción de ADN, a partir de muestras de bentonita, ha dado lugar a un método eficaz, reproducible y aplicable a diferentes tipos de bentonita (no compactada, compactada, saturada con agua, etc.).

2. Los análisis mineralógicos de la bentonita (compactada y no compactada) realizados antes y después de la incubación aeróbica y anaeróbica no mostraron cambios significativos en su composición, lo que indica su gran estabilidad a lo largo del tiempo en el marco del Almacenamiento Geológico Profundo (AGP).

3. Las diferentes muestras de bentonita empleadas en esta Tesis Doctoral (compactada, no compactada y saturada con agua), tratadas con diferentes fuentes de carbono, fueron estudiadas, mediante métodos moleculares, y caracterizadas por presentar una alta diversidad microbiana, principalmente representada por Actinobacteria, Proteobacteria, Firmicutes y Bacteroidetes.

4. El uranio y el glicerol-2-fosfato (G2P) ejercieron un efecto sobre la diversidad bacteriana de los microcosmos aeróbicos y anaeróbicos produciendo el enriquecimiento de bacterias con capacidad de afectar la especiación química del uranio como *Bacillus* y *Amycolatopsis* en microcosmos aeróbicos y *Pseudomonas* y *Desulfovibrio* en microcosmos anaérobicos.

5. La presencia de G2P influye en el proceso de biomineralización llevado a cabo por *Amycolatopsis ruanii*, produciéndose la acumulación intracelular de fosfatos de uranio, además de los extracelulares, indicando que la adición de G2P en la bentonita tendría un impacto positivo sobre la inmovilización de radionucleidos como el uranio.

6. La compactación de la bentonita hizo disminuir la diversidad microbiana. Esto podría tener repercusiones positivas para el AGP, ya que se dificultaría la subsistencia de microorganismos que, por un lado, afectan a la seguridad del AGP

por medio de la alteración de la bentonita o por la corrosión de los contenedores metálicos (bacterias hierro-reductoras y sulfato-reductoras, respectivamente).

7. No se observaron diferencias significativas entre los distintos tratamientos en las bentonitas compactadas (acetato y densidad de compactación). Esto se puede atribuir al corto periodo de incubación.

8. La presencia de selenito ejerce un efecto sobre la diversidad microbiana, produciendo tanto el enriquecimiento de microorganismos tolerantes, *Stenotrophomonas*, y *Pseudomonas*, entre otras, como la inhibición de aquellos que son susceptibles a su toxicidad (p. ej. la arquea metanógena *Methanosarcina*).

9. Por primera vez, se ha observado la reducción de selenito [Se(IV)] a selenio metálico [Se(0)] en un sistema complejo formado por bentonita, microorganismos y selenio. El Se(0), formado en el interior de las células, sería liberado al medio extracelular sufriendo una transformación desde nanoesferas de Se amorfo o monoclínico a nanoestructuras más estables de Se trigonal cristalino.

CONCLUSIONS

Regarding the obtained results, the main conclusions of this PhD Thesis are:

1. The optimization of the DNA extraction protocol from bentonite samples has resulted in an effective, reproducible and applicable method for different types of bentonite (non-compacted, compacted, saturated with water, etc.).

2. Mineralogical analyses of bentonite (compacted and non-compacted), performed before and after aerobic and anaerobic incubation, showed no significant changes in its composition, indicating the high stability of bentonite over time in the concept of Deep Geological Repository (DGR).

3. Different samples of bentonite used in this Doctoral Thesis (compacted, non-compacted, saturated with water, and treated with different carbon sources) studied using molecular methods, revealed a high microbial diversity, mainly represented by Actinobacteria, Proteobacteria, Firmicutes and Bacteroidetes.

4. Uranium and glycerol-2-phosphate (G2P) amendment had an effect on the bacterial diversity of aerobic and anaerobic microcosms, leading to the enrichment of bacteria with the ability to affect the chemical speciation of uranium, such as *Bacillus* and *Amycolatopsis* in aerobic microcosms, and *Pseudomonas* and *Desulfovibrio* in anaerobic microcosms.

5. The presence of G2P influences the U biomineralization process performed by *Amycolatopsis ruanii*, resulting in the intracellular accumulation of uranium phosphates, besides the extracellular ones. This indicates that the addition of G2P in bentonite would have a positive impact on the immobilization of radionuclides such as uranium.

6. The bentonite compaction decreased the microbial diversity. This could have positive consequences for the DGR: the prevention of the subsistence of microorganisms that prejudice the safety of the DGRs in terms of bentonite alteration (by iron-reducing bacteria) and/or the corrosion of metallic containers (by sulfate-reducing bacteria).

7. No significant differences were observed between the different treatments in compacted bentonites (acetate and compaction density). This can be attributed to the short incubation period.

8. The presence of selenite promotes an effect on microbial diversity, leading to the enrichment of Se tolerant microorganisms, *Stenotrophomonas* and *Pseudomonas*, among others; and the inhibition of those that are sensitive to the toxicity towards this metalloid (e.g. the methanogenic archaea *Methanosarcina*).

9. For the first time, the reduction of selenite [Se(IV)] to metallic selenium [Se(0)] has been reported for the complex system of bentonite-microorganisms-selenium. The Se(0), formed inside the cells, would be released into the extracellular space undergoing a transformation from amorphous/monoclinic nanospheres to more stable nanostructures composed of crystalline trigonal Se.